Università degli Studi di Ferrara

DOTTORATO DI RICERCA IN "SCIENZE CHIMICHE"

CICLO XXXIV

COORDINATORE Prof. Cavazzini Alberto

Exploring the potential of Pd-catalyzed C–H activation reaction for the synthesis of non-natural amino acid 2,6-dimethyl tyrosine-like (Dmt-like) analogues

Settore Scientifico Disciplinare CHIM/08

Dottorando
Dott. Illuminati Davide

_____

(firma)

Tutore
Prof. Guerrini Remo

_____

(firma)

Tutore
Prof. Trapella Claudio

_____

(firma)

Anni 2018/2021

Ai miei nonni,
Giorgio e Anna

Abstract

The opioid system (OS) is involved in the modulation of multiple biological functions, including stress, anxiety, cough, locomotor activity, emotional responses, feeding, learning and memory processes, reward, addiction and, above all, pain behavior.

The OS consists of four different families of opioid receptors (ORs) which have been identified thus far, namely, MOP (μ), KOP (κ), DOP (δ) and NOP (ORL-1). All of these are $G_{\alpha i}/G_{\alpha 0}$ protein coupled receptors (GPCRs) expressed throughout the spinal axis and pain related pathways. A series of endogenous peptides with different selectivity for ORs are known to exert effects resembling those of opiate drugs. The activation of ORs by an agonist induces cell hyperpolarization and ion channels opening, regulating the release of second messengers and promoting signaling cascades which converge to cell desensitization and, ultimately, to analgesia.

The most potent analgesic effect is known to be exerted by the activation of MOP receptor, which is the main target of morphine and clinically relevant opioid analgesics. Unfortunately, the strong antinociceptive action of opiate drugs is associated to important side effects which represent the major limitation for their clinical use, such as constipation, cough, itch, respiratory depression, tolerance and addiction. While the selective activation of MOP receptor is related to these undesired effects, the co-activation of different OR subtypes is emerging as a safer therapeutic strategy to promote analgesia. At this regard, the simultaneous activation of MOP and NOP receptors has been suggested as an interesting pharmacological approach to treat pain with potentially reduced side effects. Dual MOP/NOP ligands have been obtained through subtle changes of the *N*-terminal part of the NOP ligand Nociceptin/Orphanin FQ (N/OFQ) or, more recently, modifying also the threonine residue in position five. The most important substitution which confers such interesting behavior is the replacement of phenylalanine residue at the *N*-terminal position (Phe^1) of N/OFQ with the non-canonical amino acid 2,6-dimethyl tyrosine (Dmt).

The importance of Dmt as non-natural aromatic amino acid, in the field of opioid peptides is underlined by the huge amounts of papers and reviews focused on its synthesis and applications. Of note, some Dmt-modified opioid peptides exhibited increased biological activity and extended half-life with unexpected affinity and selectivity patterns.

This thesis has been focused on the development of different synthetic strategies for the synthesis of Dmt and Dmt-like analogues in which the OH phenol function was replaced with different substituents. In particular, through proper modifications of a previously

described synthetic route, we were able to functionalize the 4-position of the phenyl ring of the target residues after an *ortho-ortho* C(sp^2)–H alkylation reaction (Scheme 1). Some of these analogues were successfully employed as building blocks in solid phase peptide synthesis (SPPS) for the synthesis of N/OFQ(1-13)-NH_2 derivatives modified at the *N*-terminal message domain. This allowed the extension of structure activity relationship (SAR) studies around this endogenous peptide evaluating the effect of previously unexplored chemical modification on its biological activity.

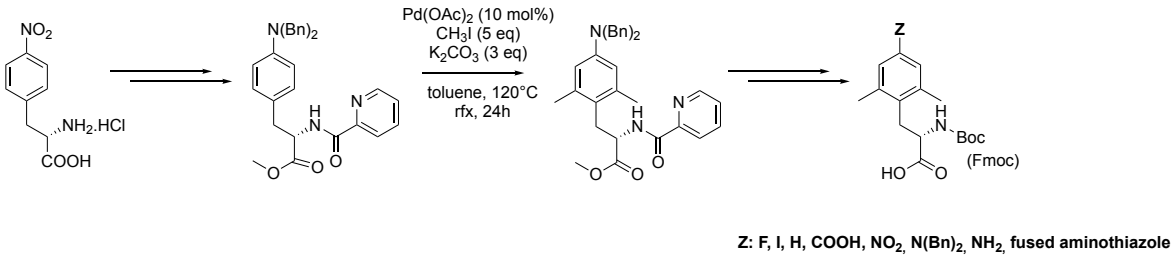

Scheme 1: Brief synthesis to obtain a small library of 4-substituted Dmt-like non-natural aromatic amino acids

Moreover, the Pd-catalyzed C(sp^2)–H activation chemistry was successfully applied for the regioselective synthesis of the non-natural amino acid monomethyl-tyrosine (Mmt) in which 3-nitro-(*L*)-tyrosine was employed as starting material. (Scheme 2).

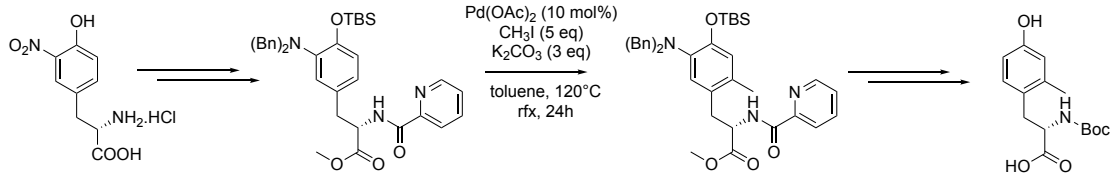

Scheme 2: Brief synthesis of Mmt

Another innovative Pd-catalyzed synthesis described in this thesis is focused on a β C(sp^3) –H activation of a properly functionalized alanine precursor which led to obtain 3,5-Dmt as well as the bis-arylated analogues of Tyr and of 3,5-Dmt. (Scheme 3).

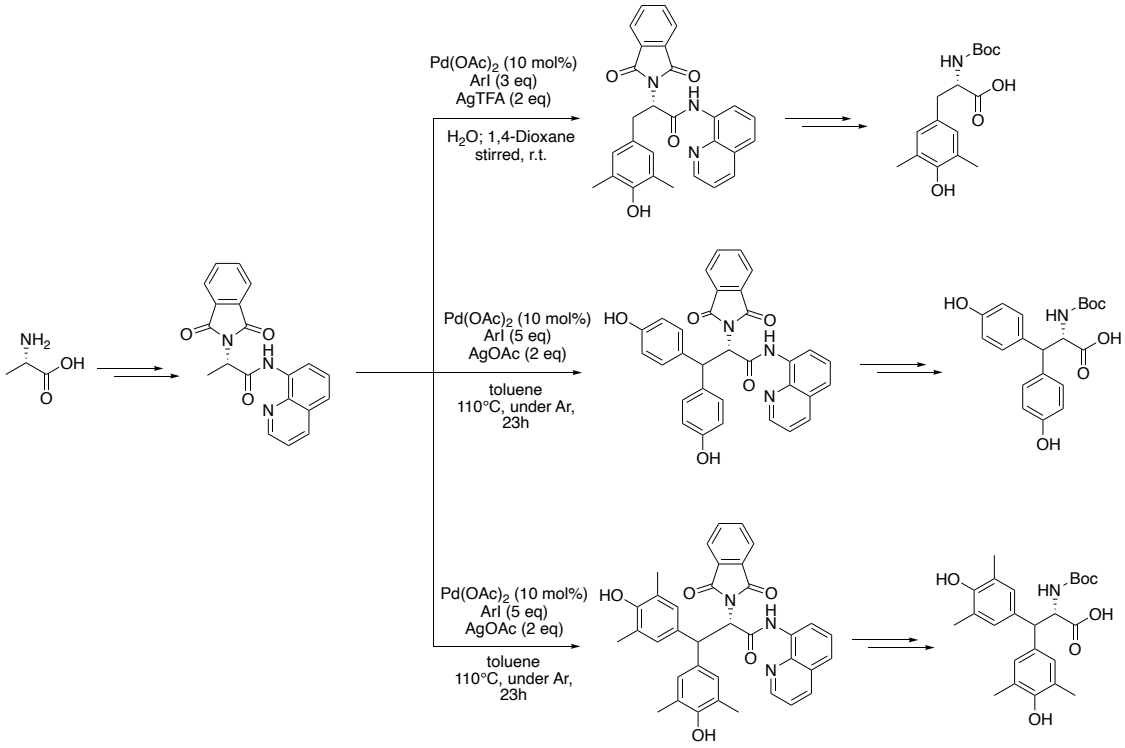

Scheme 3: Brief synthesis through β-C(sp3)–H activation on (*L*)-Ala

The innovative synthetic methodology reported in this work led us to obtain the Fmoc-protected Dmt in hundred milligrams scale. This non-natural amino acid was applied for assembling bifunctional (NOP/MOP) heterotetrabranched ligands. Peptide clustering is indeed emerging as an innovative tool to enhance the pharmacokinetic profile of therapeutic peptides *in vivo*, particularly by increasing their half-life. Specifically, we synthesized the heteromultimeric peptide conjugate H-PWT1-N/OFQ-[Dmt^{1}]dermorphin (Scheme 4) to target NOP and MOP opioid receptors, observing similar and high agonist potency compared to the parent peptides. The synthetic approach is extremely versatile and virtually applicable to different peptide sequences whose pharmacological activity could be combined to generate dual acting multimeric compounds.

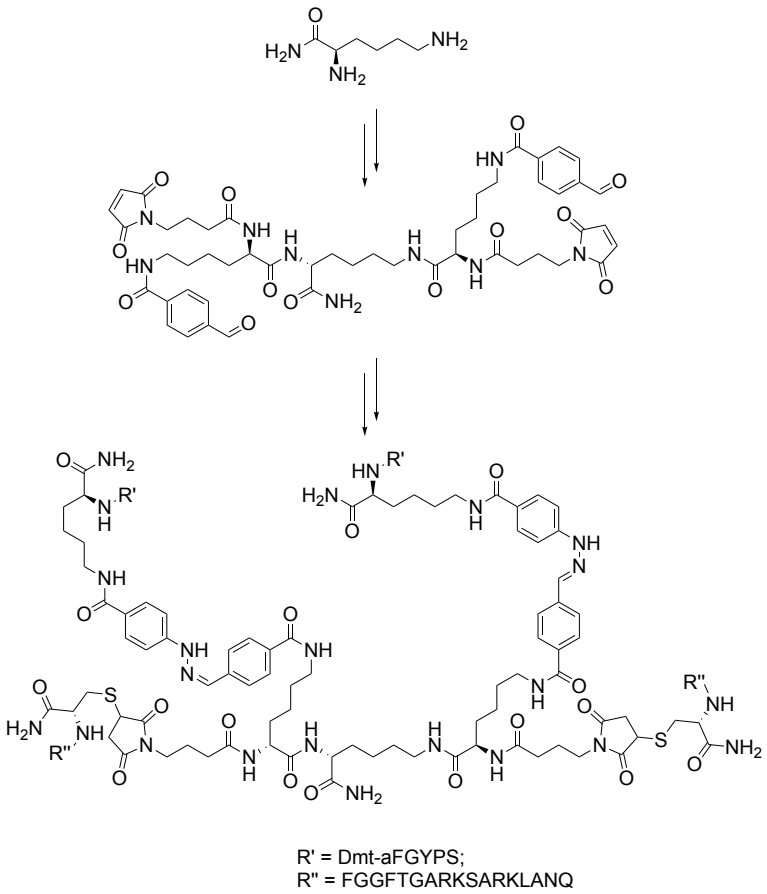

Scheme 4: Brief synthesis of bivalent heterotetrabranched PWT-1

Finally, with the aim to identify novel mixed NOP/opioid receptor peptide agonists, Dmt was employed as Fmoc-precursor in SPPS to build a series of linear peptides with the general sequence [Tyr/Dmt[1],Xaa[5]]N/OFQ(1-13)-NH_2. The best results in terms of NOP *versus* MOP opioid receptor potency were obtained by substituting both Tyr[1] and Thr[5] at the *N*-terminal portion of N/OFQ(1-13)-NH_2 with Dmt. Indeed, [Dmt[1,5]]N/OFQ(1-13)-NH_2 has been identified as the most potent dual NOP/MOP receptor peptide agonist so far described in literature.

LIST OF CONTENTS

1. INTRODUCTION 1

1.1 The opioid system 1

1.2 Mixed MOP/NOP ligands 2

1.3 Nocicepetin/orphanin FQ, an overview 3

1.5 Dmt and opioid peptides 7

1.6 Dmt synthesis: an overview 9

2. C–H ACTIVATION / FUNCTIONALIZATION AND THE SYNTHESIS OF NON-NATURAL AMINO ACIDS 12

2.1 Introduction 12

2.2 Mechanistic considerations 12

2.3 Directed C-H activation/functionalization: historical background 13

3. A SMALL LIBRARY OF PARA-SUBSTITUTED 2,6-DMT-LIKE AMINO ACIDS 18

3.1 Results and discussion 19

3.2 Pd-catalyzed methylations 20

3.3 Post-functionalizations 23

3.4 Solid phase peptide synthesis (SPPS), brief overview 26

3.5 Conclusions and pharmacological results 28

4. INNOVATIVE SYNTHESIS OF MONO-METHYL TYROSINE (MMT) 31

4.1 Aim and objectives 31

4.2 Results and discussion 33

4.3 Conclusions 35

5. SYNTHESIS OF NON-NATURAL AROMATIC AMINO ACIDS VIA PD-CATALYZED β C-H ACTIVATION 38

5.1 Aim and objectives 38

5.2 Results and discussion 42

5.3 Conclusions 51

6. FURTHER APPLICATION OF 2,6-DMT, VIA PEPTIDE WELDING TECHNOLOGY (PWT) 52

6.1 Aim and objectives **52**

6.2 Results and discussion **55**

6.3 Conclusions and pharmacological results **58**

FINAL CONCLUSIONS 62

7. EXPERIMENTAL SECTION 63

7.1 Chemicals and methods **63**

7.2 Synthesis of *para*-substituted 2,6-Dmt-like amino acids **64**

7.3 Innovative synthesis of mono-methyl Tyrosine (Mmt) **122**

7.4 Synthesis of non-natural aromatic amino acids via Pd-catalyzed β C-H activation **139**

7.5 Further application of 2,6-Dmt, via peptide welding technology (PWT) **180**

8. REFERENCES 191

1. Introduction

1.1 The opioid system

The opioid system in human beings is characterized by a series of short peptides as endogenous ligands, produced in the Central Nervous System (CNS) and throughout other glands (i.e. pituitary and adrenal glands), and their respective receptors.[1] MOP (μ or Mu), KOP (κ or Kappa) and DOP (δ or Delta) opioid receptors (ORs) represent the originally classified receptor subtypes, with opioid receptor like-1, also known as nociceptin/orphanin FQ receptor (ORL-1 or NOP), being the last characterized of this family. All ORs are seven-transmembrane G-protein coupled receptors, each one encoded by unique gene, respectively *Oprm1*, *Oprd1*, *Oprk1*, *Oprl1*.[2] Despite this, ORs share up to the 60% of the structural composition and, importantly, there is a distinct expression pattern throughout the nervous system for each receptor.[3,4] The inactive state structure of all OR subtypes have been characterized at atomic-level unravelling in detail the mechanism of ligand interactions in the binding pocket (Figure 1).[5,6,7,8]

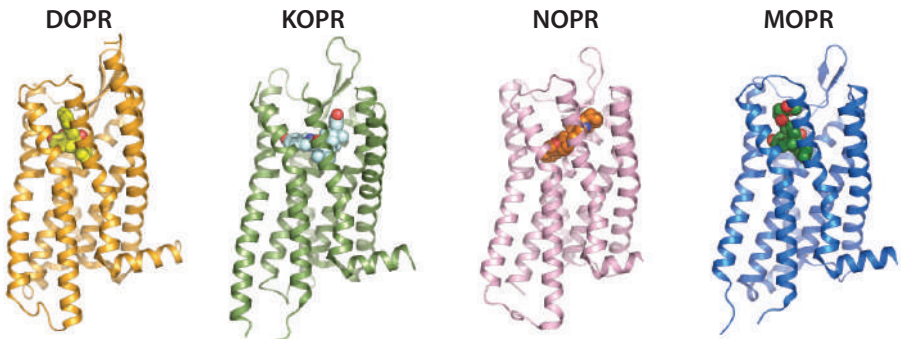

Figure 1: Inactive state conformation of the four opioid receptors

The four major classes of endogenous opioid peptides are β-endorphins, dynorphins, enkephalins and nocicepetin/orphanin FQ, respectively selective for MOP, KOP, DOP and NOP-ORs. These ligands and their receptors are expressed through the spinal axis, in pain related pathways such as medulla, locus coeruleus, periaqueductal grey area, limbic, midbrain and cortical structures.[9,10]

Since the opioid system plays a major role in the neuronal routes regulating pain processing/perception and nociceptive behavior, opioids are the most widely used and effective analgesics for the treatment of severe pain and related disorders. Besides such

indications, opioids are frequently used in the treatment of numerous other disorders including diarrhoea, cough, post-operative pain and cancer.

Common opioid agonists used to manage pain addressing MOP receptor system. Even though the analgesic response mediated by MOP receptors is the most effective, this is also related to important side effects such as dopamine reward pathway, euphoria, respiratory depression, nausea, constipation and itch. One of the main issues of MOP receptor activation by morphine-like agonists is the insurgence of tolerance and abuse behaviours. In this frame, a lot of work has been focused on the identification of opioid ligands with similar analgesic profiles to those of morphine and phentanyl, which are standard drugs in the clinical treatment of pain, but with reduced side effects.

1.2 Mixed MOP/NOP ligands

One of the possible strategies aimed to improve the antinociceptive potential and the clinical utility of opioid receptor ligands is the development of compounds capable of bi- or multiple target interaction.[11] Bi- or multifunctional opioid compounds are innovative pharmaceuticals since they have been demonstrated to be potentially effective in reducing undesirable side effects.[12] As mentioned above, morphine and MOP opioid analgesics display a potent antinociceptive effect, but their activity is related also to important side effects including respiratory depression, gastrointestinal motility inhibition, tolerance, addiction and abuse, which represent a strong limitation for the clinical use of these substances. Along with MOP agonists, KOP ligands demonstrated a potent analgesic potential, but their use is strongly discouraged because of typical dysphoric, sedative and psychotomimetic effects. Moreover, DOP ligands are reported to elicit less strong physical dependence, respiratory depression and constipation compared to morphine, but they do not show the same analgesic potential and, in some cases, the administration of DOP agonists has been associated to the onset of seizures in animals.[11] As far as NOP receptor, its selective agonists promoted anxiolytic effects and analgesia lacking reinforcement in primates.[13,14,15]

Several dual ligands targeting different OR subtypes have been studied. Mixed MOP agonists/DOP antagonists have been demonstrated to induce analgesic responses in vivo, with reduced abuse liability,[16,17] stipsi and respiratory depression[18] compared to morphine. KOP agonist/MOP partial agonist ligands have been studied to treat cocaine and drug abuse, because the dysphoric effect of KOP agonist might balance the euphoric effect due to MOP

receptor activation.[19,20] KOP agonists/MOP antagonists might have therapeutic potential for the treatment of drug abuse, as both are able to inhibit dopamine release in the nucleus accumbens, associated to fewer side effects than pure KOP agonists.[21,22]

Several examples of NOP/MOP bifunctional peptides were synthesized and described in literature.[23,24] In particular, it has been demonstrated how the co-activation of MOP and NOP receptors produces a strong analgesic effect without eliciting the classical opioid side effects.[25,26,27] Of note, NOP/MOP heterodimers were observed to be associated with *N*-type Ca^{2+} channels, whose internalization is triggered by MOP receptor, but only if also the NOP one is associated to them too. Furthermore, the inhibition of *N*-type channels is attenuated by their heterodimerization. This may have profound implications in receptor signaling and trafficking, relevant in nociceptive transmissions.[28]

1.3 Nocicepetin/orphanin FQ, an overview

Nociceptin/orphanin FQ (N/OFQ) is a heptadecapeptide discovered in 1995[29,30] as the endogenous agonist of the orphan receptor isolated just one year before and initially called opioid receptor like-1 (ORL-1) because of its inability to bind opioids despite the highly conserved structural homology. ORL-1, then renamed as NOP, is highly conserved in mammalian species and the receptor gene has been localized in the distal region of mice chromosome 2, and in the q13.2-13.3 region of human chromosome 20.[31]

N/OFQ sequence, Phe-Gly-Gly-Phe-Thr-Gly-Ala-Arg-Lys-Ser-Ala-Arg-Lys-Leu-Ala-Asn-Gln, (fig. 2) is characterized by the presence of an *N*-terminal tetrapeptide (FGGF sequence) which is considered as the "message domain" responsible for NOP activation, while the *C*-terminal sequence, from residue 7 to 17, identifies the so called "address domain" which guides NOP binding affinity and receptor selectivity.[32,33] The central dipeptide Thr^5Gly^6 constitutes a hinge region between message and address sequences.

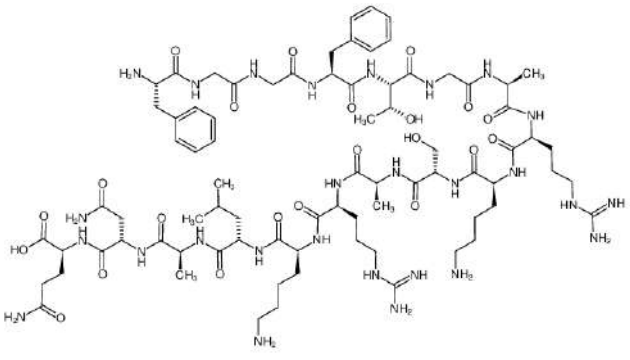

Figure 2: Nociceptin Orphanin FQ peptide structure

The main difference, in the message domain, between nociceptin and other endogenous opioid peptides is the replacement of Tyr[1] with Phe[1], hence, the canonical, conserved sequence is known to be Tyr-Gly-Gly-Phe. This simple modification at the 1-position importantly affects N/OFQ selectivity, being able to preclude NOP/ORs cross activation.[34] It has been observed that the phenol moiety in Tyr[1] may be involved in a hydrogen bond interaction with a His residue located in position 52 of TM VI of opioid receptors, while Phe[1] would undergo hydrophobic bonding with the receptor pocket.[34] A 3D conformational analysis has been recently performed through molecular dynamics (MD) and docking studies to compare the interactions between MOP receptor and small peptide ligands, such as N/OFQ, [Dmt[1,5]]N/OFQ(1-9)-NH_2 and DAMGO (H-Tyr[1]-*D*-Ala[2]-Gly[3]-*N*-Me-Phe[4]-Gly-ol-Enkephalin). Of note for this thesis work, the model suggests that Dmt[1] of [Dmt[1,5]]N/OFQ(1-9)-NH_2 would interact with Asp[147], a residue common to all the opioid receptor, through salt bridge/hydrogen bond contacts, confirming the crucial role of this non-natural residue in order to handle mixed ORs profiles.[35] (Figure 3).

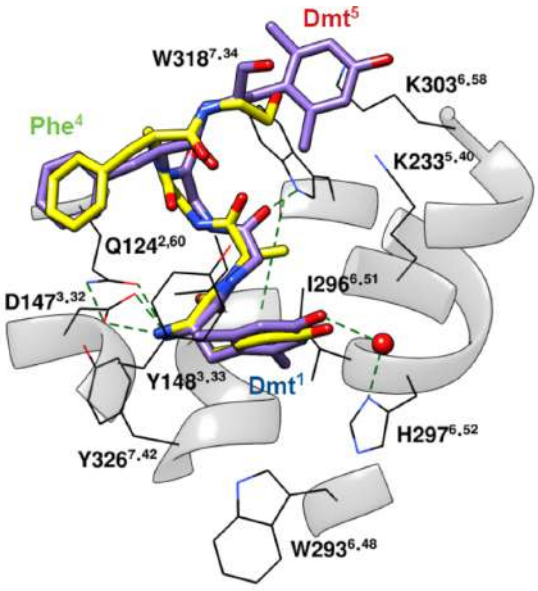

Figure 3: Orthosteric site of [Dmt[1,5]]N/OFQ(1-9)-NH_2 (in purple) in the MOP receptor active state, according to 'in silico' docking and MD[35]

It has also been observed that the presence of constrained non-natural amino acids, such as Dmt and Dmp, in peptide domains leads to conformational and stereo-electronic properties modifications. Particularly, the replacement of Phe residue in aspartame dipeptide, with both Dmp and Dmt, result in a lack of ligand/receptor interaction, due to incompatible conformational changes.[36]

1.4 Brief SAR of N/OFQ peptide studies

Key results from structure-activity relationship (SAR) studies performed on the linear peptide structure of N/OFQ and/or its fragments are reported in figure 4.

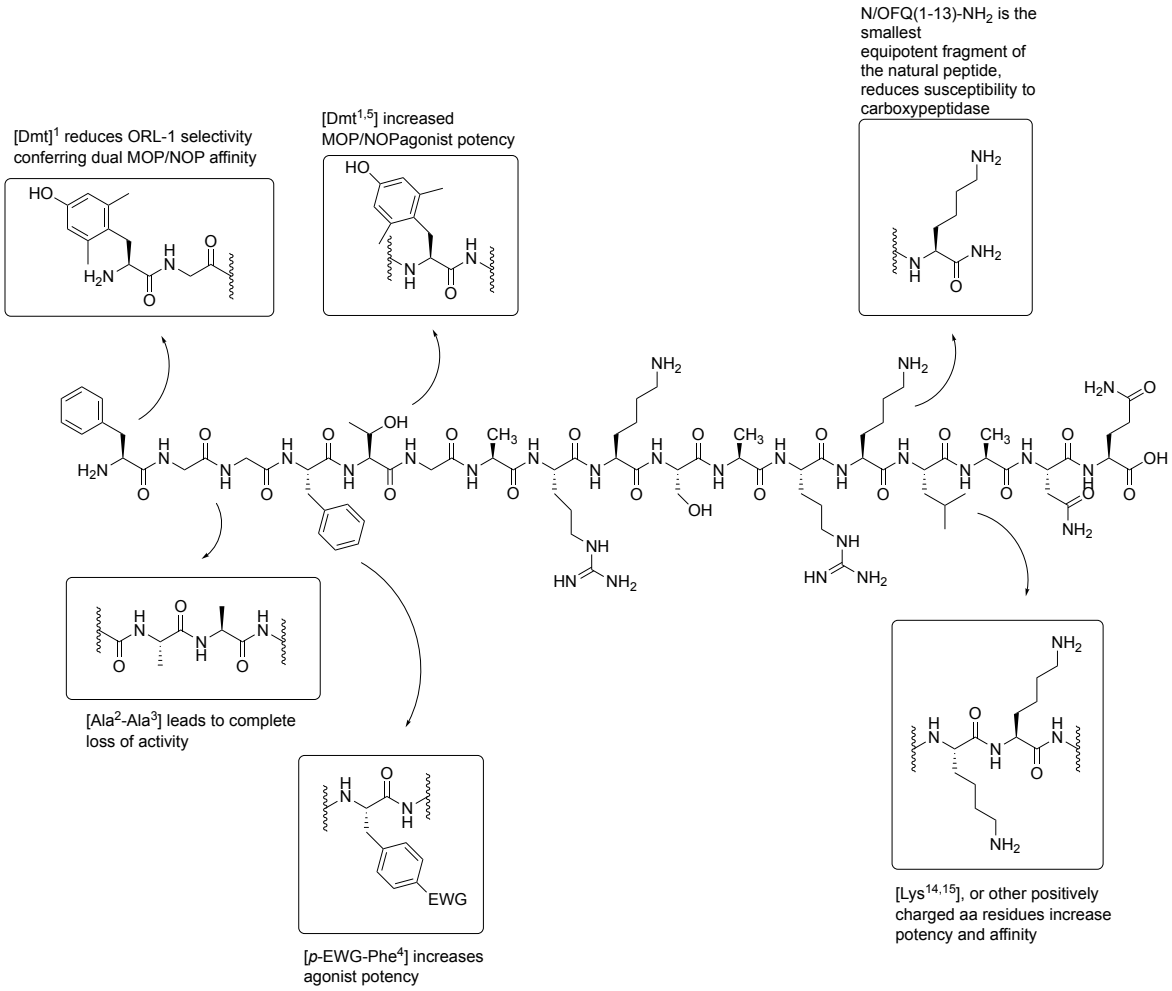

Figure 4: Possible structure modification on Nociceptin from SAR studies

Considering the entire peptide structure, it has been demonstrated that the minimum peptide chain which maintains the biological activity is N/OFQ-(1-13)[37,38] whose *C*-terminal amidation (N/OFQ-(1-13)-NH_2) is known to reduce the susceptibility to carboxypeptidases, prolonging the half time of the peptide.[39]

One of the most important amino acidic residues, strongly involved in NOP binding, selectivity and activation is Phe[1]. Even if the aromaticity of the side chain at the 1-position is not mandatory, a bulky and lipophilic residue is required to sustain biological activity. Moreover, the inversion of the chiral configuration is not tolerated, in fact, the replacement of (*L*)-Phe[1] with (*D*)-Phe[1] determined the complete loss of biological activity.[40]

Noteworthy, the replacement of Phe^1 with Tyr^1 led to a diminished selectivity toward NOP, combined to an increased binding affinity towards classical opioid receptors, especially MOP and KOP;[41] this behavior is further enhanced by the insertion of the non-natural 2,6-dimethyl tyrosine residue (Dmt).[42] This observation led to the discovery of [Dmt^1]N/OFQ-NH_2 and [Dmt^1]-N/OFQ(1-13)-NH_2 as potent mixed opioid/NOP agonists, as promising innovative spinal analgesics.

Moving forward from position 1, the dipeptide spacer Gly^2-Gly^3 is also crucial for biological activity. Indeed, according to X-ray and docking studies,[43,44] it would be necessary to maintain the right distance between Phe^1 and Phe^4, and to provide a high conformational flexibility. The substitution with (*D*)-Ala^2-(*D*)-Ala^3 led to a complete loss of activity. In addition, it permits ionic bond between the *N*-terminal sequence and Asp^{130} in NOP receptor pocket.[39,45]

The Phe^4 residue has been demonstrated to be crucial for NOP receptor occupation and activation, it is characterized by strictly chemical requirements: the substitution with Tyr or Leu are, indeed, tolerated in position 1 but not in position 4. The removal of the aromaticity leads to a complete inactive ligand, while the enhancement in aromaticity character, e.g. the presence of naphthyl or fused rings, is also related with decreased or no biological activity at all (the steric bulkiness results detrimental for peptide/receptor interaction). It is also remarkable that the insertion of electron withdrawing groups (EWG) in *para* position of the aromatic ring has been proved to enhance the biological activity of the entire peptide. As a matter of fact, the derivative [(pF)Phe^4]NC(1-13)-NH_2 is 4 times more potent than the natural peptide.[46] It has also been suggested that Phe^4 may interact with Phe^{220} (TM V) and Tyr^{131} (TM III), and the EWG electronic influence may facilitate the aromatic hydrophobic interaction between ligand and receptor pocket.[47,48]

A series of N/OFQ analogues in which the Thr^5 residue was substituted with both natural and non-natural amino acids has been recently investigated. These analogues behaved as NOP full agonists with highly variable potency thus suggesting that Thr^5 would contribute to the binding to the receptor more than to its activation. Yet, neither the size of X^5 side chain nor its lipo/hydrophilic nature and hydrogen bond capability seemed of significant relevance for receptor binding.[49]

According to NMR studies, the *C*-terminal "address" portion of N/OFQ would assume a typical alpha helix conformation in physiological conditions. This region is characterized by the presence of two couples of Arg-Lys dipeptide units at 8-9 and 12-13 positions, which are important for receptor affinity/selectivity properties of the peptide because of the capability to promote the α-helix bioactive motif as well as to interact with negative residues in the

second extracellular loop of the NOP receptor. It has been observed that the introduction of a an additional Arg^{14}-Lys^{15} couple (or similar combination of positively charged residues) in the address domain led to an agonist with higher potency and affinity compared to the natural peptide.[50,51]

1.5 Dmt and opioid peptides

The development of a unique analogue of Tyr, achieved by methylation of the 2- and 6-positions of the aromatic ring (2,6-dimethyl tyrosine, Dmt), furnished a possible strategy to achieve highly bioactive small peptides.[52,53] The insertion of this non-natural aromatic amino acid instead of tyrosine in the dipeptide H-Tyr-Tic-OH, a DOP selective antagonist, led to an important increase in receptor binding affinity.[54] (Figure 5). This discovery revolutionized the opioid field by clearly demonstrating how a single amino acid substitution may have huge effects in terms of bioactivity, selectivity and binding receptor properties.

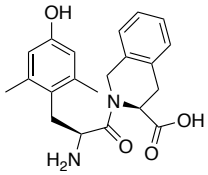

Figure 5: *H*-Dmt-Tic-OH, H-2,6-dimethyl-*L*-tyrosine-1,2,3,4-tetrahydroisoquinoline-3-carboxylic acid, DOP opioid antagonist

Noteworthy, the replacement of Dmt, instead of Tyr, in the *N*-terminal sequence of various opioid peptides produced a broad range of biological effects.[55] For example, a high affinity mixed MOP/DOP agonist was achieved by introducing Dmt^1 in Deltorphin B (H-Dmt-D-Ala-Phe-Glu-Val-Val-Gly-NH_2), an exogenous opioid peptide derived from frog skins secretions.[56,57] Moreover, the introduction of Dmt in the sequence of Enkephalin (DOP-selective endogenous analogue), increased its biological activity and stability against endopeptidases.[58,59] Specifically, both the *L* and *D* enantiomers of Dmt have been inserted at the 1-position of Leu-Enkephalin (Tyr-Gly-Gly-Phe-Leu) and YRFB (Tyr-*D*-Arg-Phe-βAla-NH_2). The results showed that (*L*)-Dmt decreased the susceptibility to endopeptidases enhancing MOP *versus* DOP affinity in Enk, and DOP versus MOP affinity in YRFB, while (*D*)-Dmt led to diminished bioactivity and reduced affinity at both DOP and MOP receptors.[60] Furthermore, Dmt^1 insertion in endomorphin-1 (Tyr-Pro-Trp-Phe-NH_2) and

endomorphin-2 (Tyr-Pro-Phe-Phe-NH_2), led to increased MOP receptor binding affinity and bioactivity, compared to parent compounds.[61]

Dmt was also inserted in some peptidomimetic ligands, such as the tetrapeptide DALDA (H-Tyr-*D*-Arg-Phe-Lys-NH_2), a selective agonist for MOP receptor.[62] The insertion of Dmt^1 in TIPP-NH_2 (Tyr-Tic-Phe-Phe-NH_2) led to the identification of MOP agonist/DOP antagonist derivatives which are potentially characterized by reduced side effects such as tolerance and physical dependence.[63]

Anti-nociceptive and anti-inflammatory effects were also exerted by mixed MOP/KOP ligands, Dmt-c[*D*-Lys-Phe-Phe-Asp]-NH_2 and Dmt-c[*D*-Lys-Phe-*p*-CF_3-Phe-Asp]-NH_2, with reduced side effects.[64]

As reported above, mixed MOP/NOP receptor agonists are under investigation as possible opioid analgesics with reduced side effects. Noteworthy, the beneficial 'selectivity loss' effect due to the insertion of Dmt^1 in N/OFQ peptide or in its shorter amidated fragments led to potent non selective, mixed MOP/NOP highly bioactive agonists.[42]

Of note, [$Dmt^{1,5}$]N/OFQ(1-13)-NH_2 has been recently identified as one of the most potent NOP/MOP receptor agonist so far available and *in vivo* studies are under investigation to estimate its potential as a mixed opioid antitussive with less typical opioid side effects.[35]

The great enhancement of activity toward opioid receptors promoted by the presence of methyl groups at the 2- and 6-positions of Tyr^1, is supported by the evidence that also the corresponding dimethyl-phenylalanine (Dmp) residue, has been identify as an interesting aromatic amino acid surrogate for opioids.[65,66] In particular, the introduction of Dmp^1 in the message domain of peptides such as Endomorphin-2, Leu-Enkephalin, Dermorphin, YRFB, [*D*-Ala^2]-Deltorphin-2, Dynorphin and Nocicepetin F/Q, led to similar or slightly reduced biological activity and binding affinity, compared to what has been observed with the insertion of Dmt^1. In all these examples, the opioid receptor selectivity of the parent peptides was conserved, despite the lack of phenolic function at the 1-position.[67,68]

In conclusion, the Dmt^1/Tyr^1 replacement in opioid peptides produces an important increase of peptide potency associated with a moderate reduction of peptide selectivity. No other residue is known to play such a crucial role on the effectiveness of opioid peptides, except for the corresponding surrogate of Phe, Dmp.[55,69]

1.6 Dmt synthesis: an overview

Since Dmt has been discovered, due to the crucial implications observed about its application in opioid field, research has been boosted to synthesize this unnatural amino acid in many different ways.

Here are briefly reported the most important synthetic pathways described to date in literature. A large part of the work reported in this thesis was inspired particularly by one of them, the Pd-catalyzed C–H activation described by Zhang and Ma, in 2017.

Two different approaches have been developed to obtain Dmt through stereo controlled alkylation of Gly or diketopiperazine derivative. The former one was performed through the alkylation of a Ni(^{II}) complex of the chiral Schiff base obtained from Gly and (*S*)-o-[*N*-(*N*-benzylpropyl)amino]benzophenone with a properly functionalized benzyl halide.[70] (Scheme 5).

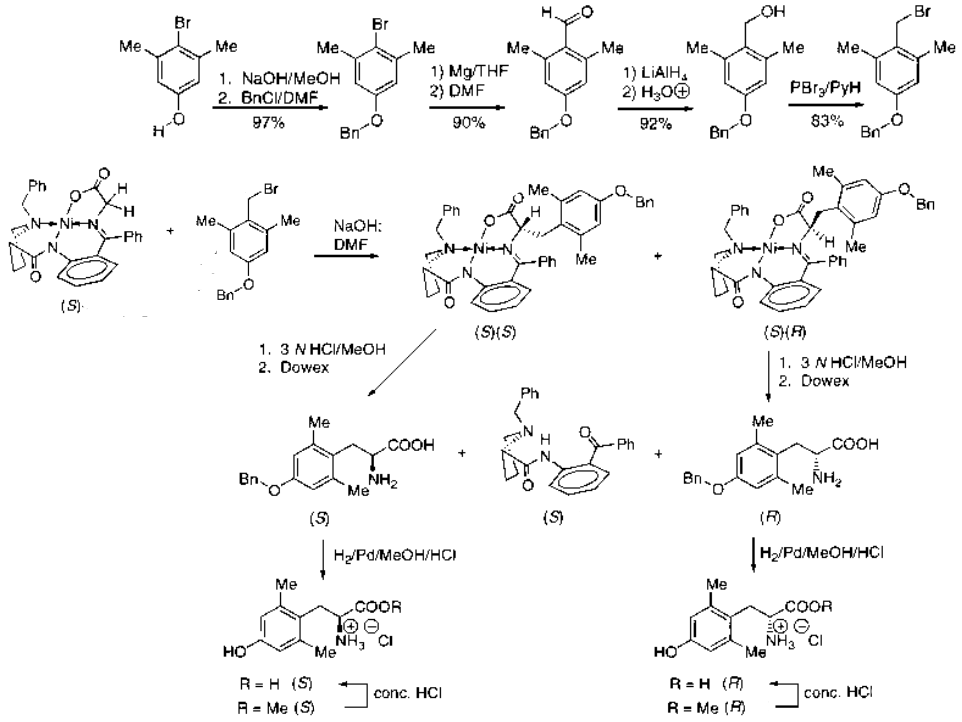

Scheme 5: 2,6-Dmt synthesis via alkylation of chiral nucleophilic Gly[70]

The other method was characterized by the diastereoselective alkylation of a 2,5-diketopiperazine (DKP). The first synthon has been obtained from chloro-acetyl chloride and (*S*)-phenylethylamine through acylation/dimerization. Following diastereoselective

alkylation with two equivalents of properly functionalized benzyl halide followed by DKP hydrolysis gave the desired enantiomerically pure 2,6-DKP derivative[71] (Scheme 6).

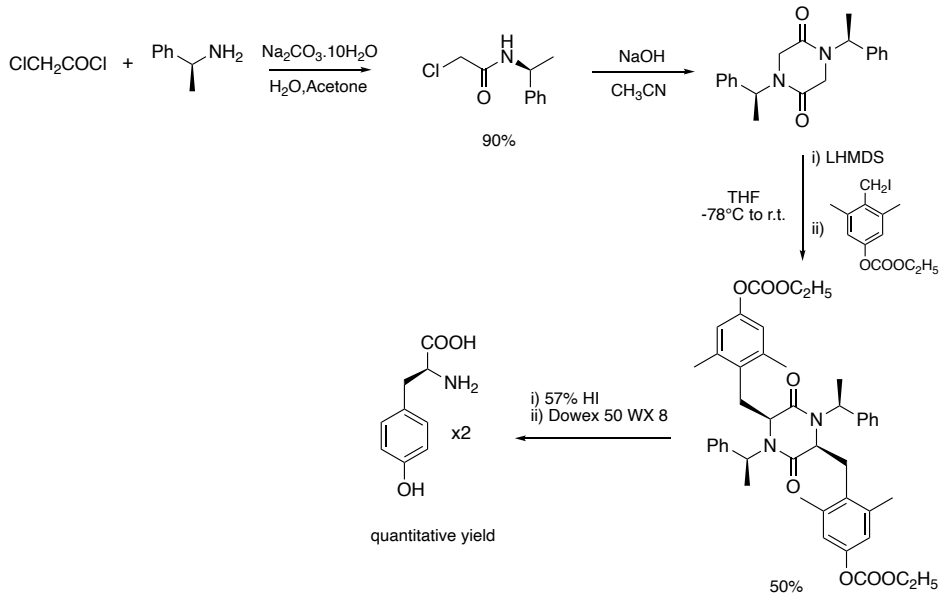

Scheme 6: Synthesis of 2,6-Dmt via diastereoselective alkylation of diketopiperazine derivative[71]

Otherwise, hydrogenation of *N*-acetyl (*Z*) unsaturated DKP derived from Boc-Val and *O*Me-Gly(HCl) coupling, took place preferentially at the more accessible side (*Re face*) of the prostereogenic center. Subsequent hydrolysis gave the desired enantiomerically pure 2,6-Dmp and 2,6-Dmt (Scheme 7).[72]

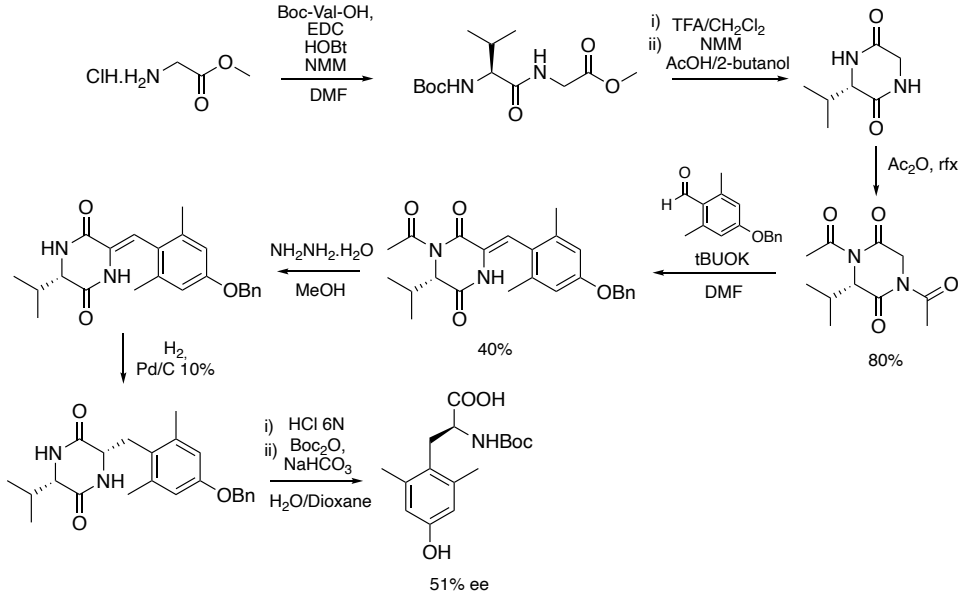

Scheme 7: Synthesis of 2,6-Dmt via asymmetric hydrogenation of DKP derivative[72]

In addition, an enzymatic hydrolysis of α-*N*-acetyl-(*D*,*L*)-2,6-dimethyltyrosine methyl ester via α-chymotrypsin has also been reported.[73]

Furthermore, (*L*)-Dmt, was also obtained through enantioselective hydrogenation of methyl (*Z*)-2-acetamido-3-(4-acetoxy-2,6-dimethylphenyl)-prop-2-enoate, with the chiral catalyst [Rh(1,5-COD)(*R,R*-DIPAMP)]BF_4.[74] The substrate was prepared via Heck reaction between 4-iodo-3,5-dimethylphenyl acetate and methyl-2-acetamido acrylate, synthesized in situ from Ser-*O*Me. The high cost of the chiral catalyst required for the enantio-selective double bond hydrogenation led researchers to use a less expensive catalyst, [Rh-(1,5-COD)(*S,S*-Et-FerroTANE)]BF_4 in reduced loading.[75] (Scheme 8). The cost of the catalyst required for the hydrogenation, and the drastic reaction conditions (less than 5 ppm of oxygen) make this approach non-ideal.

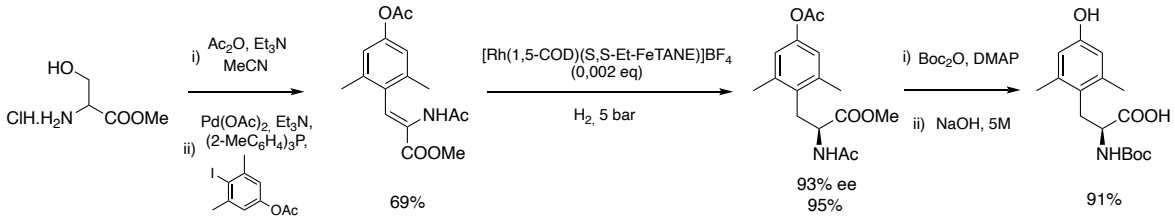

Scheme 8: Synthesis of 2,6-Dmt via asymmetric hydrogenation of the dimethyl-phenyl-acetamido acrylate derivative[75]

Another synthetic strategy to yield (*L*)-Dmt made use of a Negishi cross-coupling between the organozinc reagent derived from 3-iodoalanine *N*-Boc methyl ester (in turn derived from (*L*)-*N*-Boc-Serine methyl ester under Appel conditions), and 3,5-dimethyl-4-iodo phenol, catalyzed by the catalytic system [$Pd_2(dba)_3$ / SPhos] under microwave irradiation at 110°C. (Scheme 9). This synthetic route has the merit to get the obtainment of the enantiomerically pure target starting from a chiral pool substrate.[76]

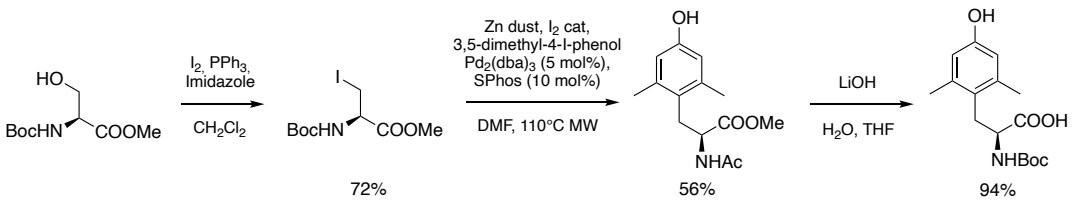

Scheme 9: Synthesis of 2,6-Dmt via Negishi cross coupling reaction[76]

2. C–H activation / functionalization and the synthesis of non-natural amino acids

2.1 Introduction

Over the last few years, the concept of step-economical and environmentally friendly synthesis emerged as a topic of much interest.[77,78] One of the simplest ways to render more straightforward a given coupling strategy is to decrease the overall number of functional group manipulations, and directly perform key C–H to C–C carbon-carbon (or carbon-heteroatom) bond formations (scheme 10).

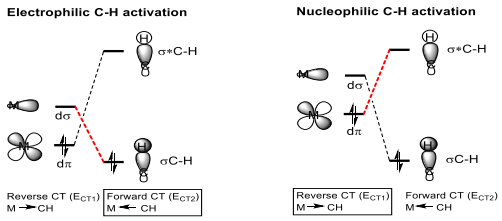

Scheme 10: C-H activation/functionalization strategy as opposed to the classical approach involving a pre-oxidation step.

Indeed, the direct functionalization of a non-acidic C–H bond, the unfunctional group by definition, enables the direct use of the cheapest and most abundant feedstock for the synthesis of more complex organic molecules, thus adding the C–H bond to the catalogue of the classical functional groups, such as halides, alcohols, carbonyls, etc.

As described above, non-natural α amino acids (αAAs) represent key structural motifs in peptide, peptidomimetics and many other pharmaceutical compounds of interest. They often display outstanding biological activity and enzymatic stability, compared to the parent ones. Since amino acids are abundant natural carbon-based resources, it is not surprising that the direct C–H bond activation/functionalization of natural amino acids represents a topic of utmost interest. Accordingly, the next section makes a brief introduction of the fundaments of directed transition-metal C–H activation/functionalization.

2.2 Mechanistic considerations

Several modes to activate an otherwise unreactive C–H bond exist. In particular, the one based on the action of transition metals is very powerful. We can in turn categorize a metal-based C–H activation/functionalization processes into two main classes. One class involves

the initial insertion of a C–H bond into the ligand of a transition metal (TM) complex (outer sphere mechanism), while the other involves coordination of the C–H bond to the metal center to create an organometallic complex wherein the (C–H)-bearing substrate stays in the inner-sphere during the C–H cleavage step. In this context, we can further classify these processes according to the main direction of the charge transfer involved in the C–H activation step. Indeed, interaction of a C–H bond with a transition metal takes place through a two-path charge transfer (CT): (i) from a metal-based occupied dπ orbital to the σ* orbital of the coordinated C–H bond (reverse CT), and (ii) from the filled $\sigma_{(C-H)}$ bond to an empty metal-based dσ orbital (forward CT). These charge transfers synergistically participate to weaken and ultimately break the C–H bond. Thus, according to the nature of the transition state of a C–H activation process, we can identify *nucleophilic* or *electrophilic* processes. For example, electron-deficient, including cationic, late transition metals such as Pd(^{II}) complexes are expected to possess low-energy dπ and dσ electrons. Therefore, in their interaction with a C–H bond, the forward CT dominates over the reverse CT and such transition metal complexes are defined as electrophilic. Contrariwise, electron-rich transition metal complexes are expected to have high energy dπ and dσ orbitals. In this case, the dominant frontier orbital interaction will be the reverse CT, which defines a nucleophilic C–H activation (figure 6).

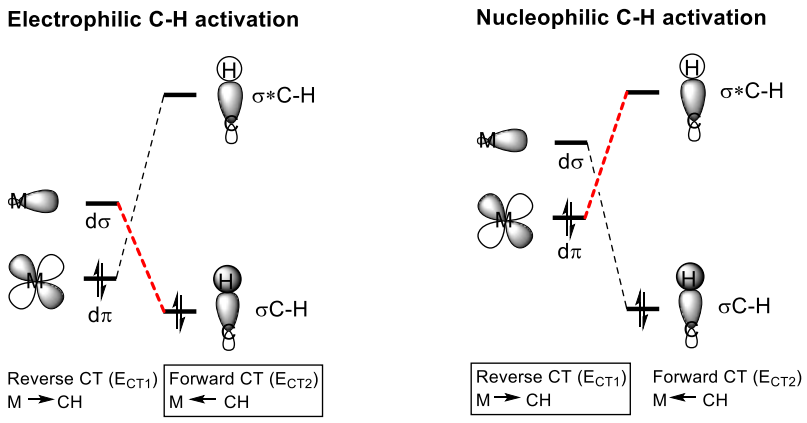

Figure 6: Frontier orbital interactions for electrophilic (left) and nucleophilic (right) mechanisms. Red dashed lines refer to the most contributive interactions[77]

2.3 Directed C-H activation/functionalization: historical background

Presently, the most widely used methods in C–H functionalization are based on directed C–H activation. Such a substrate-control based strategy exploits the action of Lewis bases

covalently linked to the substrate that are able to induce approach of the transition metal in the vicinity of a specific, otherwise inactivated C–H position. Although C–H bonds do not form stable σ-adducts with transition metals, Lewis-base/transition metal pre-organization is a mandatory step preceding its metalation, which is often the first step in a C–H functionalization process. In particular, cyclometalation is the classical path for this type of C–H activation, whose first examples date back to the seminal work of Murahashi in 1955 on the cobalt-catalyzed imine carbonylation, and of Cope and Kleiman on the azo-directed ortho-cyclonickelation (scheme 11).[79,80]

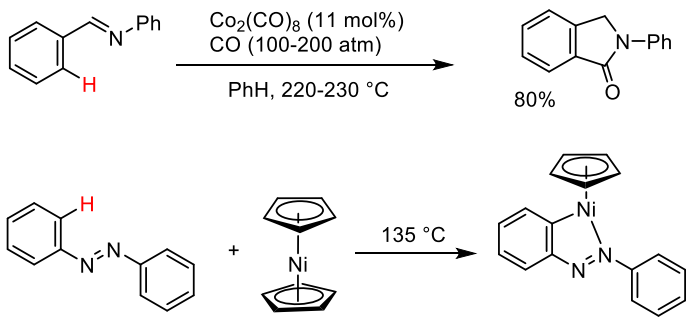

Scheme 11: First examples of C–H activation via TM-promoted cyclometallation.

The chemistry of cyclopalladations is very rich,[81,82] and was pioneered by Cope starting from 1965 using azobenzene as the substrate.[83,84] In particular, in 1984, Tremont and Rahman[85,86] reported that treatment of acetanilides with stoichiometric amounts of $Pd(OAc)_2$ brought about an ortho-cyclopalladation, and treatment of the resulting palladacycle with excess MeI afforded the methylation of the palladated position (Scheme 12).

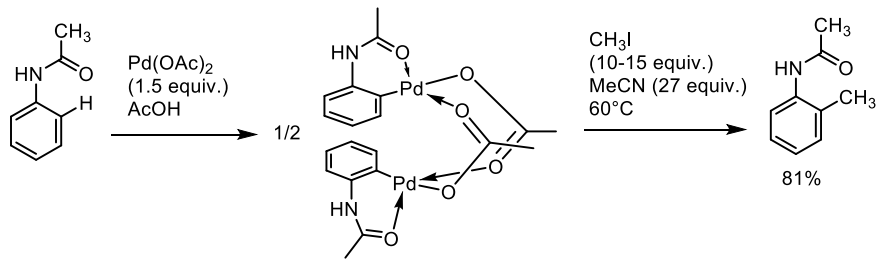

Scheme 12: Ortho alkylation of acetanilide using methyl iodide and stoichiometric $Pd(OAc)_2$.

More than twenty years later, Daugulis and Zaitsev[87] revisited the topic and showed that anilides could be arylated with aryl iodides by treatment with catalytic amounts of $Pd(OAc)_2$ in the presence of 1 equivalent of AgOAc per coupled aryl moiety (scheme 13).

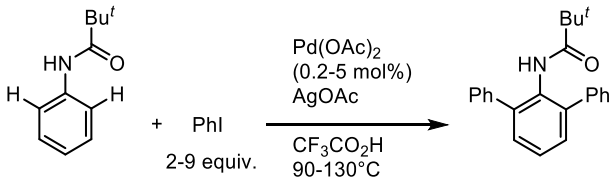

Scheme 13: Ortho arylation of anilides using aryl iodides and catalytic $Pd(OAc)_2$

Still in 2005, Daugulis *et al.*[88] developed bidentate monoanionic removable auxiliaries for carboxylic acids and amines, which allowed the Pd-catalyzed C(sp^3)–H arylation at the β position in the case of the former substrates, and the γ-position in the case of amines.[89,90] This breakthrough was obtained derivatizing the substrates as 8-aminoquinoline amides and picolinamides, respectively (scheme 14).

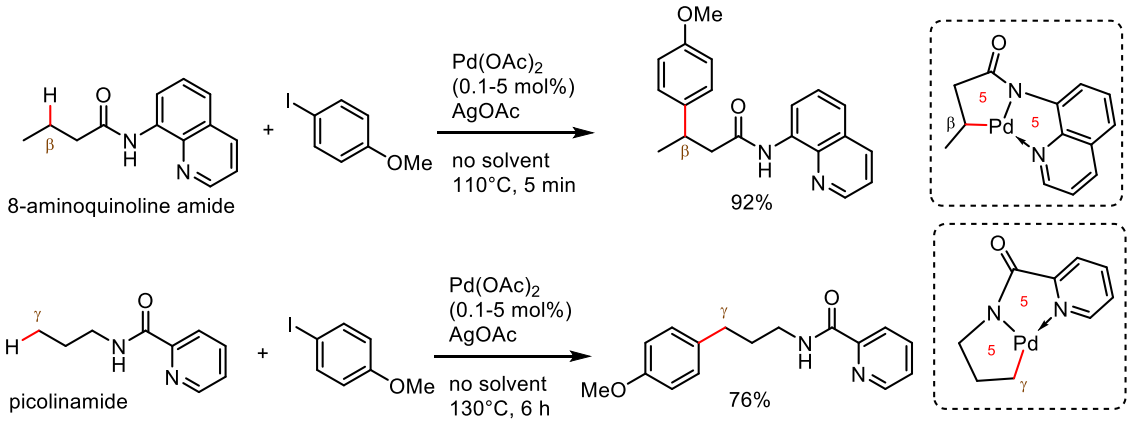

Scheme 14: Pd-catalyzed β- and γ-C(sp^3)-H arylation of carboxylic acid and amine derivatives. In the boxes the respective postulated cyclopalladacycles involved.

Several points deserve to be considered: a) the mechanism of the above Pd-catalyzed arylations is expected to involve the initial chelation of PdX_2 by the directing group with ligand exchange, followed by a cyclopalladation, and the resulting Pd(^{II}) complex can undergo oxidative addition by the aryl halide, to afford a transient Pd(^{IV}) complex, as postulated by Catellani[91] in the eponymous reaction; b) an anionic/dative chelating auxiliary helps in stabilizing the high-energy high-valent palladium species; c) a removable directing group greatly increases the synthetic applicability of C-H bond functionalization reactions. The postulated catalytic cycle in the case of the arylation of a carboxylic acid AQ is described in Scheme 15.[92]

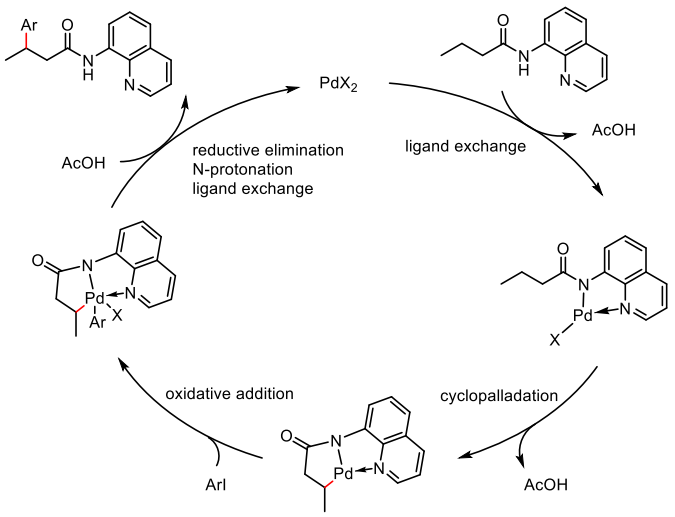

Scheme 15: Postulated mechanism for the Pd-catalyzed β-arylation of carboxylic acids AQ amides.

The chemistry of aminoquinoline, picolinic acid, and related directing auxiliaries was further extended by several authors in many variants, allowing the activation/functionalization not only of unactivated C(sp^3)-H bonds under palladium catalysis, but also of several C(sp^2)-H bonds, under iron, cobalt, nickel, copper, ruthenium, and rhodium catalysis, enabling, among other transformations, direct arylation, alkylation, fluorination, sulfenylation, amination, etherification, carbonylation, and alkenylation of carbon−hydrogen bonds.[93,94,95]

Furthermore, the direct C-H activation/functionalization of amino acid derivatives and peptides using this strategy has been particularly studied.

Along this line, in 2008, Yu et al.[96] showed that *L*-phenylalanine methyl ester *N*-triflate could be either *ortho-ortho'*-diiodinated or alkenylated under palladium catalysis, which implies a C(sp^2)-H activation at the remote δ position with respect to the directing nitrogen atom, and the consequent involvement of a 6-membered palladacycle (scheme 16).

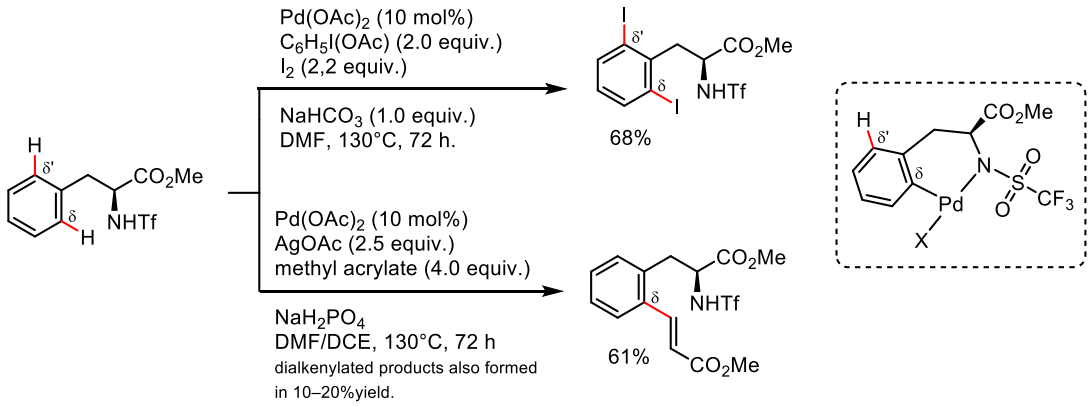

Scheme 16: Pd-catalyzed *ortho-ortho'*-diiodination of *L*-phenyl alanine methyl ester *N*-triflate. In the box on the right, the putative palladacycle involved.

In 2011, Chen *et al.*[97,98] reported that under specific conditions β-arylethylamine derivatives underwent alkylation at the δ-C(sp^2)-H bond, which implies the involvement of a 6-membered palladacycle fused to the picolinamide-based 5-membered palladacycle. Thus, for example, treatment of phenylalanine methyl ester *N*-picolinamide with CH_3I, at 110°C, in the presence of catalytic amounts of $Pd(OAc)_2$, dibenzyl phosphate, NaI, and of stoichiometric amounts of Ag_2CO_3 brought about its *ortho-ortho*-dimethylation in high yield (scheme 17).

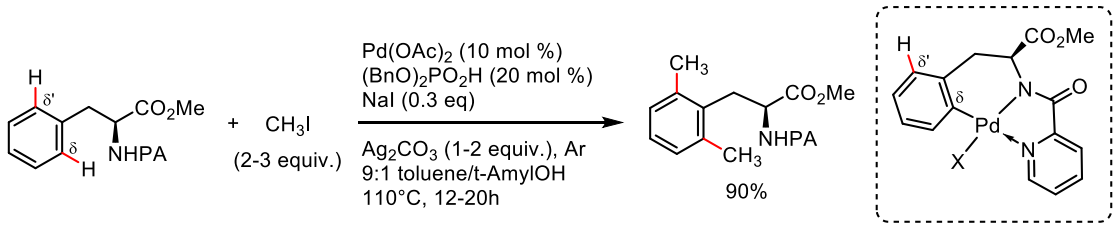

Scheme 17: Pd-catalyzed *ortho-ortho*-dimethylation of phenylalanine methyl ester *N*-PA. In the box on the right, the putative palladacycle involved.

In this context, in 2017 Ma and Zhang[99] reported the successful Pd-catalyzed *ortho-ortho*-dimethylation of *O*-TBDMS-(*L*)-tyrosine methyl ester picolinamide, which, after removal of the protecting/directing groups and *N*-reprotection gave (*S*)-*N*-Boc-2,6-dimethyltyrosine ((*L*)-Boc-Dmt,), ready to be inserted in solid phase peptide synthesis (SPPS). The dimethylation worked in a very good yield, and could be carried out on gram scale. Furthermore, the sequence from *S*-tyrosine is not racemizing (scheme 18).

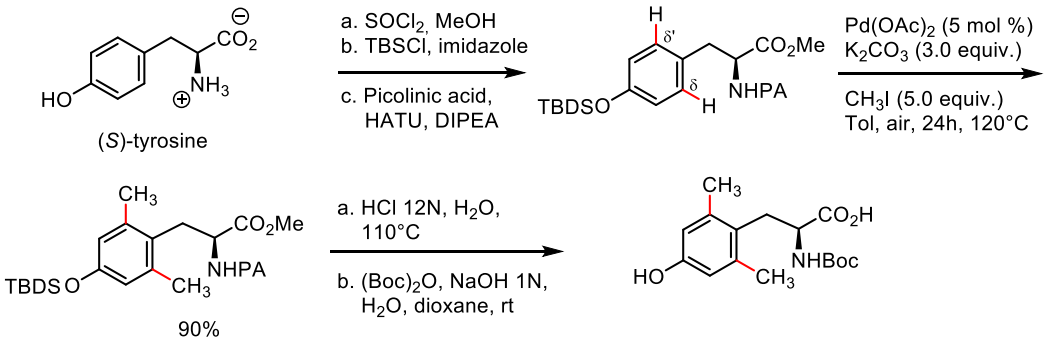

Scheme 18: Synthesis of (*L*)-Boc-Dmt via C-H alkylation Pd catalyzed[99]

Summing up, (*L*)-Dmt has been so far accessed via the following synthetic strategies, as reported below, scheme 19.

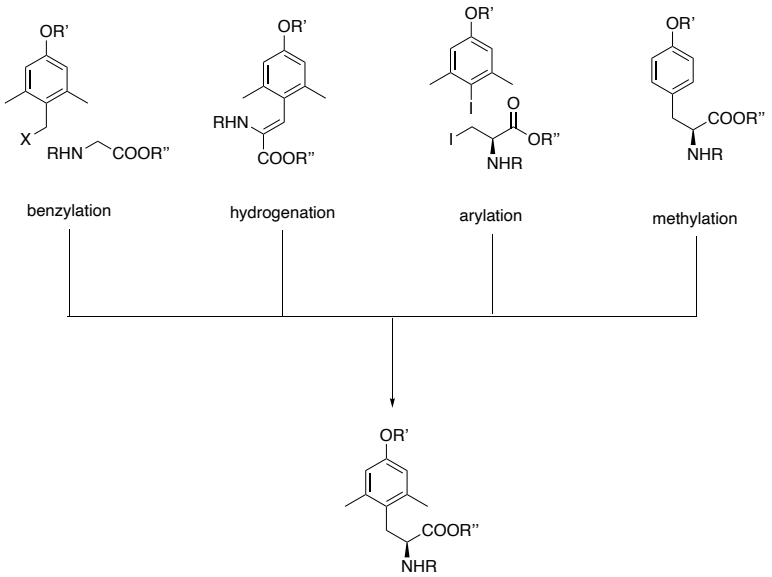

Scheme 19: General synthetic routes reported in literature to obtain (*L*)-Dmt

3. A Small library of para-substituted 2,6-Dmt-like amino acids

In view of the interest of non-natural amino acids for incorporation in peptides in conjunction with the relevance of new synthetic methods relying on directed C-H activation/functionalization, we started a long-term project aimed at developing new C-H activation-based methods to access unnatural amino acids derived from modification of proteinogenic ones, for incorporation into peptides via SPPS. Specifically, we planned, starting from (*L*)-phenylalanine, to access an appropriate 4-aza-substituted and DG-armed derivative, so as to allow a Pd-catalyzed 2,6-dimethylation. Then, thanks to the rich chemistry of anilines, generate a library of 4-substituted 2,6-dimethyl analogs, ready to be incorporated in peptide chains, through solid phase peptide synthesis (SPPS) (scheme 20).

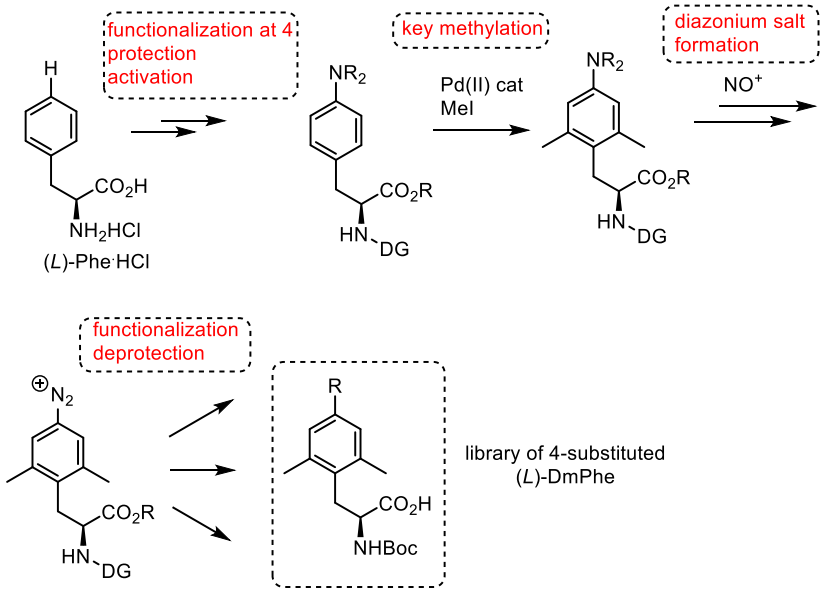

Scheme 20: General plan to transform (*L*)-phenylanine into a library of 4-substituted 2,6-dimethyl substituted, ready for incorporation in solid phase peptide synthesis (SPPS).

The purpose was trifold:

1) To validate a new synthetic route on a 4-substituted phenylalanine instead that on tyrosine.
2) To generate a small library of derivatives.
3) To study their biological activity.

In particular, we focused our attention on the smallest active fragment of N/OFQ peptide, N/OFQ (1-13)-NH_2, because of the interesting results already reported from SAR on the replacement of Phe[1] and Phe[4], with unnatural aromatic analogues.

3.1 Results and discussion

The above described Pd-catalyzed C(sp^2)-H activation reported by Ma and Zhang[99] captured our attention because of the easily accessible synthetic pathway, the absence of harsh condition to perform enantioselective hydrogenation on olefin derivatives, and the absence of expensive chiral catalysts.

3.2 Pd-catalyzed methylations

We decided to start our study from the commercially available 4-NO_2-Phe derivative **3**, in turn easily accessible by nitration of phenylalanine. The carboxylic acid function was transformed into the corresponding methyl ester by reaction with $SOCl_2$ in MeOH, while the resulting picolinamide derivative **4** was obtained by reaction with picolinic acid under classical amidic coupling.

Unfortunately, submission of **4** to the Pd-catalyzed methylation conditions reported by Ma and Zhang did not afford the desired dimethylated derivative, it was recovered indeed only starting material (scheme 21).

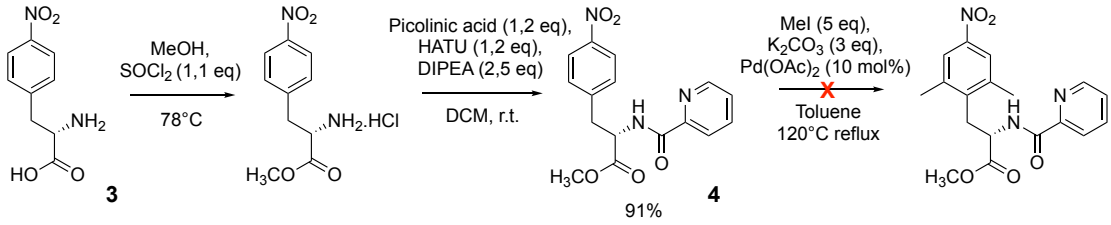

Scheme 21: Attempt of C-H alkylation on 4-NO_2-Phe PA-OMe

The failure of this reaction suggests that the electron-withdrawing effect exerted by the nitro group is detrimental for the C-H activation step. We then tested the methylation protocol on the 4-fluoro-phenylalanaine-PA-OMe, easily synthesized in turn 4-fluoro-phenylalanine via the same reaction sequence as previously described. Halogens are deactivators of the aromatic ring due to their strong electronegativity, which is anyway compensated by their mesomeric donor effect at ortho/para positions. However, in this case as well, the methylation failed (Scheme 22).

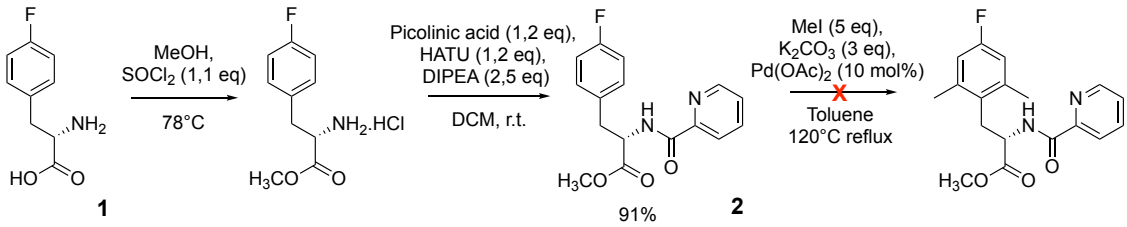

Scheme 22: C-H alkylation trial on 4-*F*-Phe derivative

At this point, we decided to reduce the nitro group of **4** to the corresponding aniline derivative. We reasoned that this transformation should enrich the aromatic ring and render it electronically closer to the silylated tyrosine of Ma and Zhang. Thus, treatment of the nitroamide **4** with Pd/C 10% and H_2 in AcOEt gave the corresponding aniline **5**, and

subsequent protection of the amine function as *N*-Boc derivative using tert-butoxy-carbonyl anhydride (Boc_2O) gave smoothly carbamate **6**. Unfortunately, subsequent submission of **6** to the Pd-catalyzed methylation, as reported above, failed again. We suspected that coordination between the carbamate oxygen atom and palladium may have halted the catalysis (Scheme 23).

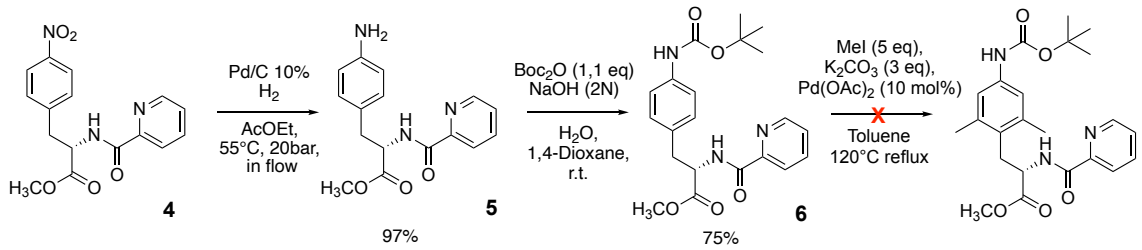

Scheme 23: C-H alkylation trial on aniline *N*-Boc- protected Phe derivative

In a final attempt, we submitted the primary aniline to **5** *N,N*-dibenzylation by reacting it with BnBr in the presence of K_2CO_3 in CH_3CN and the resulting tertiary aniline **7** was submitted to the Pd-catalyzed aromatic methylation. To our delight, the reaction afforded the expected 2,2'-dimethylated product **8** in 72% yield (Scheme 24).

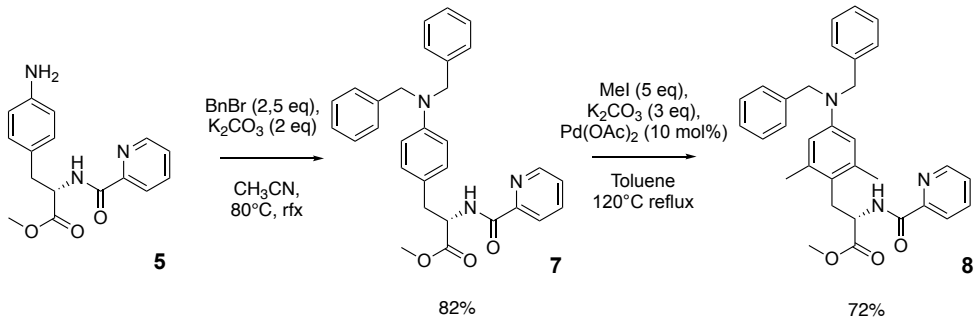

Scheme 24: Successful *ortho-ortho'*-dimethylation of of 4-methyl-phenylalanine-PA-OMe.

Unlike the reaction reported for Tyr derivative by Ma and Zhang, it was necessary to repeat 3 times the C-H alkylation to obtain the dimethylated product **8**. (Table 1). Indeed, the separation of the unreacted starting substrate from the mono- and the desired dimethylated product **8** turned out to be rather troublesome due to the very similar chromatographic mobility of the three compounds.

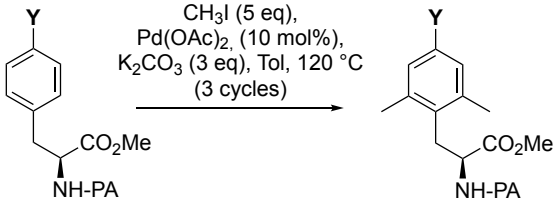

Y	Substrate	Product	Isolated yield (%)
F	2	-	-
NO_2	4	-	-
NHBoc	6	-	-
NBn_2	7	8	72%

Table 1: Summary of the Pd catalyzed C–H methylation tested

In accord with what is already reported in literature, we propose the following mechanism for this Pd-catalyzed dimethylation. Ligand exchange between the substrate **7** and $Pd(OAc)_2$ affords the chelated Pd-complex **I** with expulsion of AcOH that is scavenged by K_2CO_3. Following concerted metalation deprotonation (CMD) (alias: ambiphilic metal-ligand activation (AMLA)) accomplishes the palladation of the δ-C(sp^2)-H position, generating a fused bicyclic [6,5]-palladacycle intermediate **II** with expulsion of a second AcOH unit. Subsequent oxidative addition of MeI to **II** generates the high-energy $Pd(^{IV})$ (or corresponding dimeric $Pd(^{III})$) complex **III**, and following reductive elimination generates intermediate **IV** that carries the newly generated C-C bond. Subsequent ligand exchange by two acetate units affords the *ortho*-methylated product **V** in acid-base equilibrium with **VI** and regenerates the catalyst, ready to start a new cycle. The second methylation to afford **8** is expected to proceed via an analogous mechanism (Scheme 25).

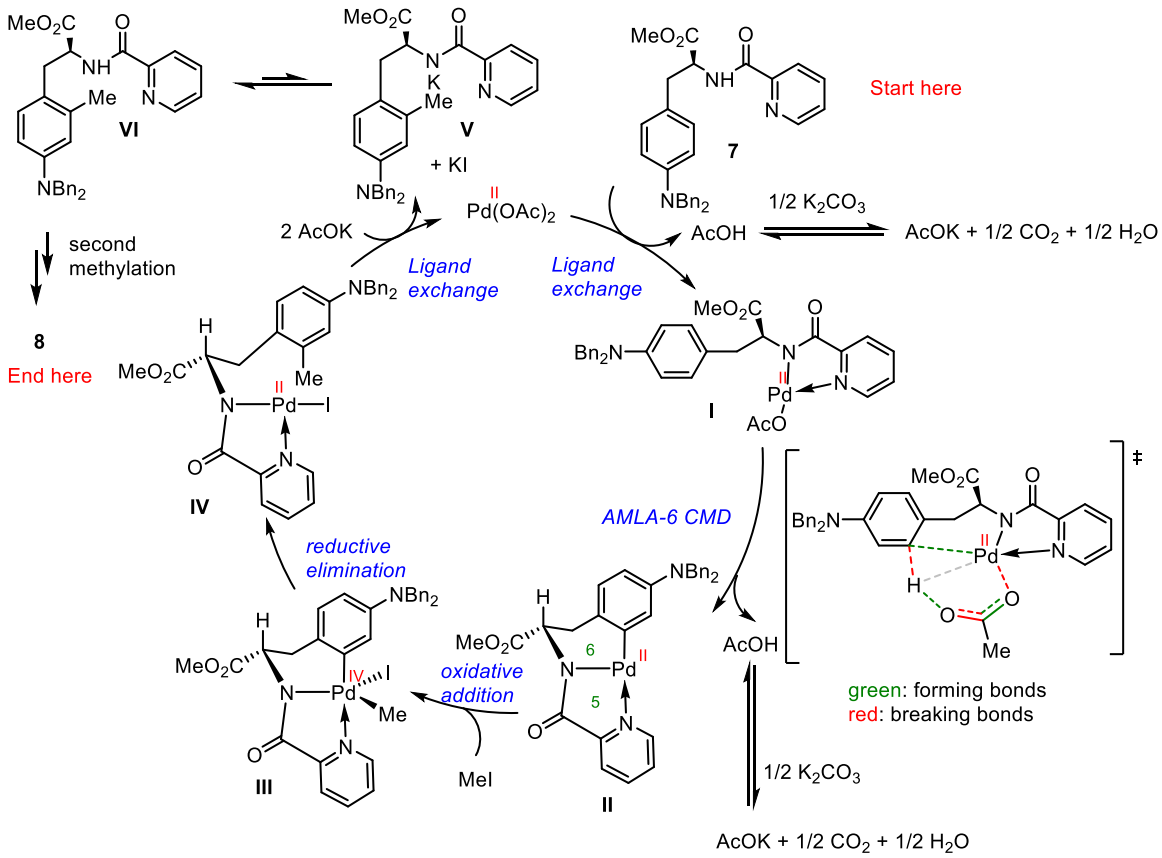

Scheme 25: Proposed full catalytical cycle for the Pd-catalyzed methylation of **8**. In the postulated transition state of the CMD step, green dashed bonds refer to forming bonds, red dashed bonds refer to breaking bonds, and the grey dashed refers to an agostic interaction.

3.3 Post-functionalizations

With the 2,2'-dimethylated *N,N*-dibenzyl derivative in hands, we focused our attention to its conversion into a number of other derivatives. Thus, submission of **8** to catalytic hydrogenation using Pd/C 10 mol% smoothly gave the corresponding 2,2'-dimethyl-4-amino phenylalanine-PA-*O*Me **9**. This latter was subsequently converted it into the corresponding diazonium salt **10** by reaction with tetrafluoroboric acid and isopentyl nitrite, and treated *in-situ* to obtain the corresponding 4-fluoro- (**11**), 4-iodo- (**12**), 4-cyano- (**14**) and 4-protio (unsubstituted)- (**13**) derivatives. (Scheme 26). Specifically, the 4-fluoro derivative **11**, was obtained by irradiating at 70°C the diazonium salt, in anhydrous THF, under microwave conditions,[100,101] while the 4-iodo derivative **12**, was secured via microwave irradiations in anhydrous acetone, in the presence of KI and CuI. The 4-cyano derivative **14**, was obtained by reaction with trimethyl silyl cyanide (TMSCN), and copper oxide (Cu_2O), in acetonitrile at 55°C.[102] The 4-unsubstituted derivative **13** was obtained through a radical protodeamination reaction, using $FeSO_4$ in DMF.[103]

For all the above described products, treatment with 6N HCl removed the picolinamide and methyl ester groups. Noteworthy, during this treatment, the cyano group was directly converted into the corresponding carboxylic acid. Finally, the resulting hydrochloride salts were readily protected as *N*-Boc or *N*-fluorenylmethyloxycarbonyl (*N*-Fmoc) derivatives, to be readily inserted in SPPS.

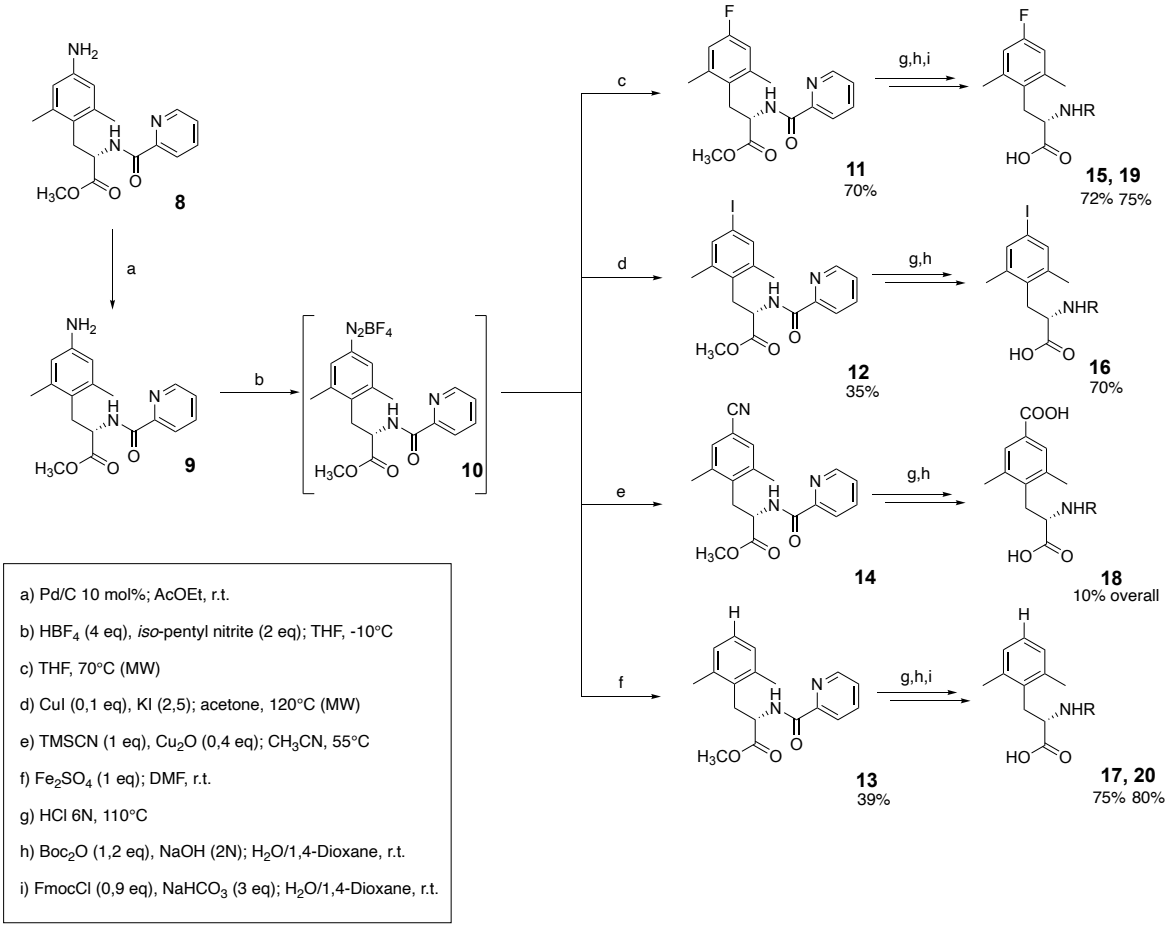

Scheme 26: General pathway to obtain *p*-F, *p*-I, *p*-COOH and Dmp per diazonium salt intermediate

It was also possible to convert the 2,2'dimethyl-4-*N,N*-dibenzyl-PA-OMe **8** into the corresponding *N*-Boc aniline amino acid **22** through mild acidic hydrolysis (HCl 3N, 60°C) followed by *N*-Boc protection, to give **21**, and final catalytic hydrogenation with Pd/C (10 mol%). (Scheme 27).

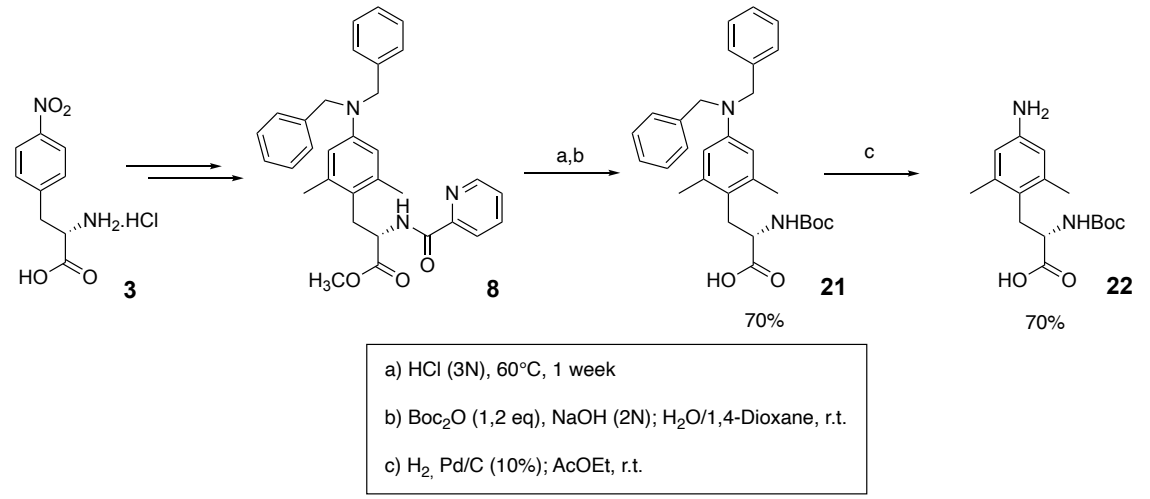

Scheme 27: Conversion of 2,2'dimethyl-4-*N,N*-dibenzyl-PA-OMe **8** into the corresponding *N*-Boc aniline amino acid **22**.

We also managed to take advantage of the aniline chemistry to synthesize more compounds, starting from the *p*-NH_2 PA-OMe derivative (**9**). For example, treatment of **9** with hydrogen peroxide gave the corresponding nitro derivative **23**,[104] and the subsequent removal of the protecting groups followed by *N*-Boc reprotection gave the *N*-Boc-4-NO_2-Dmt-like derivative **24**.

The primary aniline **9** could also be used to extend the aromaticity of the system, by building up an aminobenzothiazole derivative via cyclization with KSCN and bromine in acetic acid.[105] Again, the subsequent removal of the protecting groups followed by *N*-Boc reprotection gave the desired *N*-Boc derivative **26** (scheme 28).

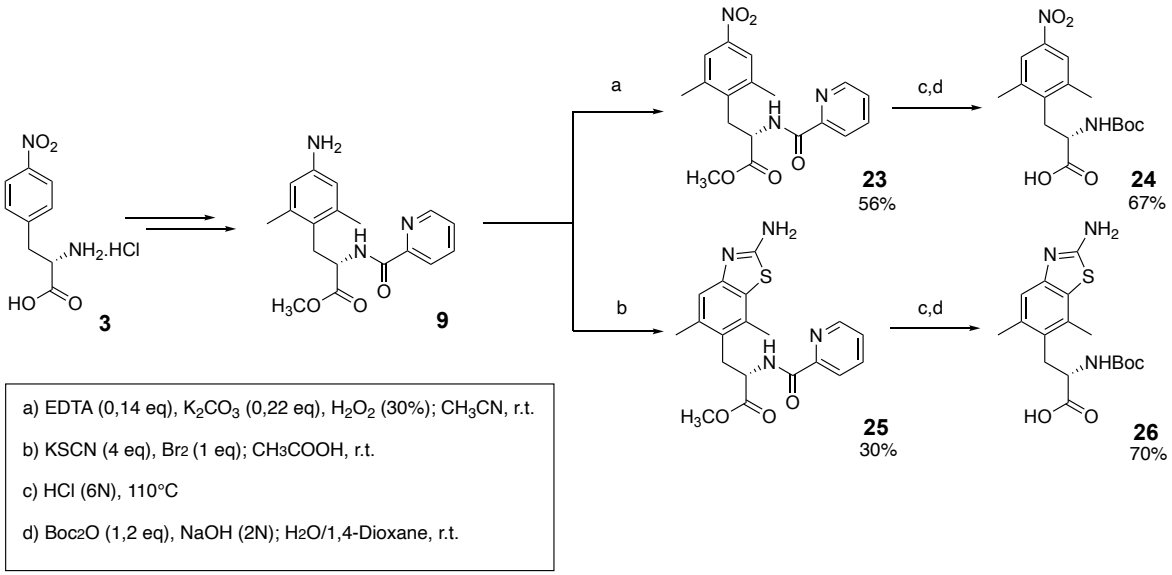

Scheme 28: General conditions to obtain *p*-NO_2 (**24**) and fused aminothiazole (**26**) derivatives as final products

In summary, we have developed an original synthetic strategy to obtain Dmt-like amino acids, dimethylated at position 2- and 6- of the aromatic ring, and differently functionalized at the 4-position. Specifically, it was possible to create a small library of 4-substituted phenylalanine derivatives characterized by different stereo-electronic properties. These include the EWG moieties such as 4-fluoro, 4-iodo, 4-nitro, 4-CO_2H functions, or EDG groups, such as 4-NH_2, and *N*$(Bn)_2$ to conclude with bulky *p*-*N,N*-dibenzylamine. We were also able to synthesize an original fused aminothiazole ring (fig. 7). The above library could be accessed thanks to the fact that the 4-*N,N*-dibenzylamino-phenylalanine-PA-OMe underwent successfully to the desired Pd-catalyzed the C(sp^2)-H 2,6-dimethylation, even though the reaction turned out to be more difficult than in the case of the tyrosine derivative developed by Zhang and Ma.

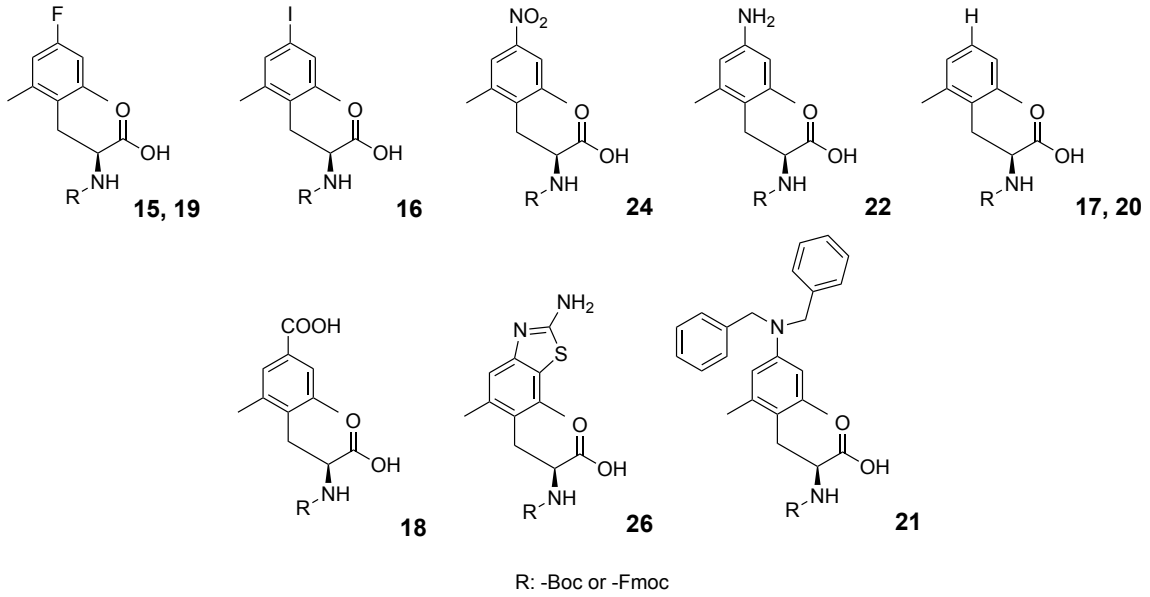

Figure 7: Final products obtained via C-H alkylation Pd-catalyzed from *p*-NO_2-Phe

3.4 Solid phase peptide synthesis (SPPS), brief overview

Some of the synthesized non-canonical aromatic residues above described were applied in SPPS for the replacement of Phe^1 and Phe^4 in the N/OFQ(1-13)-NH_2 peptide sequence. All the peptide were synthesized by taking advantage of the Fmoc/tBu strategy, using an automatic Synthesizer (XP Syro, Biotage Sweden).

Briefly, in SPPS the peptide chain is built up from the *C*-terminal amino acid, anchored to the resin, to the *N*-terminal one, through repeated cycles of alternate *N*-terminal deprotection and coupling reactions with activated *N*-Fmoc-*α*-amino acids. All the amino acids (aa) are

orthogonally protected: *N*-Fmoc in the aliphatic α amine and/or Boc, *tert*-butyl (tBu), trityl (Trt), 2,2,5,7,8-pentamethylcromane-6-sulfonyl (Pmc), benzyloxy carbonyl (Z or Cbz) in eventually side chain functional groups. The polystyrene resin Amispheres 20 RAM (20% of its weights is made of polyethylene glicole) was used as starting material. The resin is weighted into an empty syringe, then it is swelled in DMF, at room temperature.

Three steps are automatically repeated:

1. *N*-terminal deprotection: *N*-Fmoc is removed by suspending the resin in a solution of piperidine (40%) in DMF, which selectively removes the base-labile *N*-protecting group, in turn to be ready for the next amide coupling reaction.

2. Coupling: The free *N*-terminal residue of the growing peptide chain is coupled with the carboxylic group of the following *N*-Fmoc-*α*-amino acid of the sequence, upon proper activation using HOBt (0,5 M) and DIC (1,09 M) as coupling reagents in DMF.

3. Capping: an acetylation reaction with Ac_2O is usually performed to block the elongation of undesired peptide chains that can occur due to possible unsuccessful coupling reaction. This treatment allows to quench the reactivity of randomly uncoupled amine groups.

After each step the resin is washed: DMF previously used is filtered out, while the resin is hold into the syringe, refilled, washed with fresh solvent, then filtered again. The washing process is repeated for 3 times.

Once the last *α*-amino acid is inserted, the *N*-terminal Fmoc protection is removed, then a single acidic treatment is performed, allowing the removal of side chain protecting groups and the cleavage of the neo-synthesized peptide from the resin. Specifically, the 'cleavage cocktail' used to this aim is composed of trifluoroacetic acid (TFA), water and triethyl silane (Et_3SiH) in 9:0,5:0,5 proportion. The treatment is carried out at room temperature for 3 hours.
The exhausted resin is filtered off, TFA is removed from the filtrate under vacuum, and the neo-synthesized peptide is then precipitated in diethyl ether (Et_2O), isolated through centrifugation and finally purified via reverse phase preparative high performance liquid chromatography (RP-HPLC) then dried over lyophilization. (Scheme 29). RP-HPLC analytical gradients were run using a solvent system consisting of A (H_2O + 0.1% TFA) and

B (CH_3CN + 0.1% TFA. The conditions used to characterize pure peptides consisted of a linear gradient from 0% to 100% of B solution over 25 min).

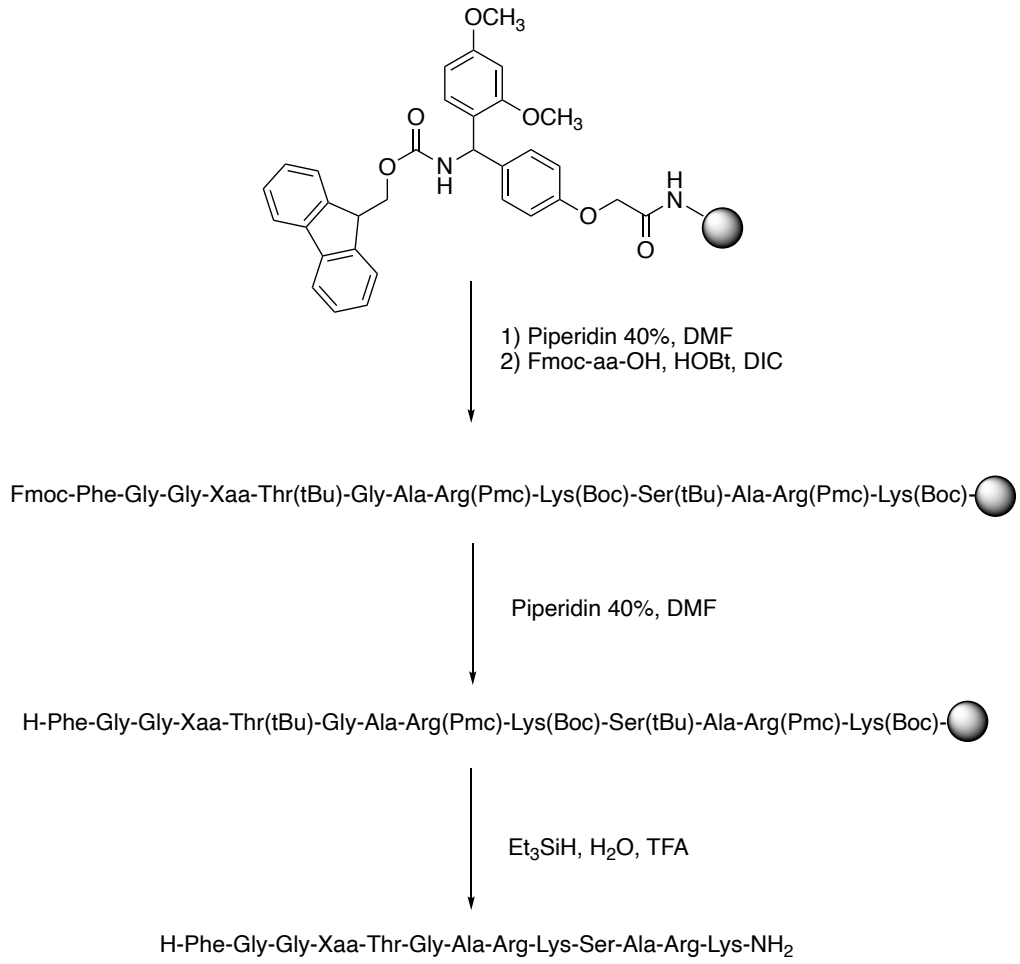

Scheme 29: Schematic overview of SPPS of N/OFQ(1-13)-NH_2 derivatives with different amino acid residues at the 4-position.

3.5 Conclusions and pharmacological results

The design and generation of a small library of *p*-substituted Dmt-like derivatives supported the synthetic strategy described above. Three of them, were inserted in N/OFQ(1-13)-NH_2 peptide, replacing Phe^4. Three different peptides were synthesized, particularly [(*p*-F)Dmp^4], [(*p*-NO_2)Dmp^4] and [Dmp^4]N/OFQ(1-13)-NH_2, whose *in vitro* biological activity was compared to that of their non-dimethylated cognates, [(*p*-F)Phe^4], [(*p*-NO_2)Phe^4] and N/OFQ(1-13)-NH_2. The pharmacological assay was performed by the research group of Prof. G. Calò at the Department of Medical Sciences of the University of Ferrara. All the compounds were evaluated in an intracellular Ca^{2+} mobilization assay on CHO cells,

transfected to express the recombinant NOP receptor, coupled to the chimeric protein $G\alpha_{qi5}$.[106,107] The results are represented by the dose-response curves in figure 8.

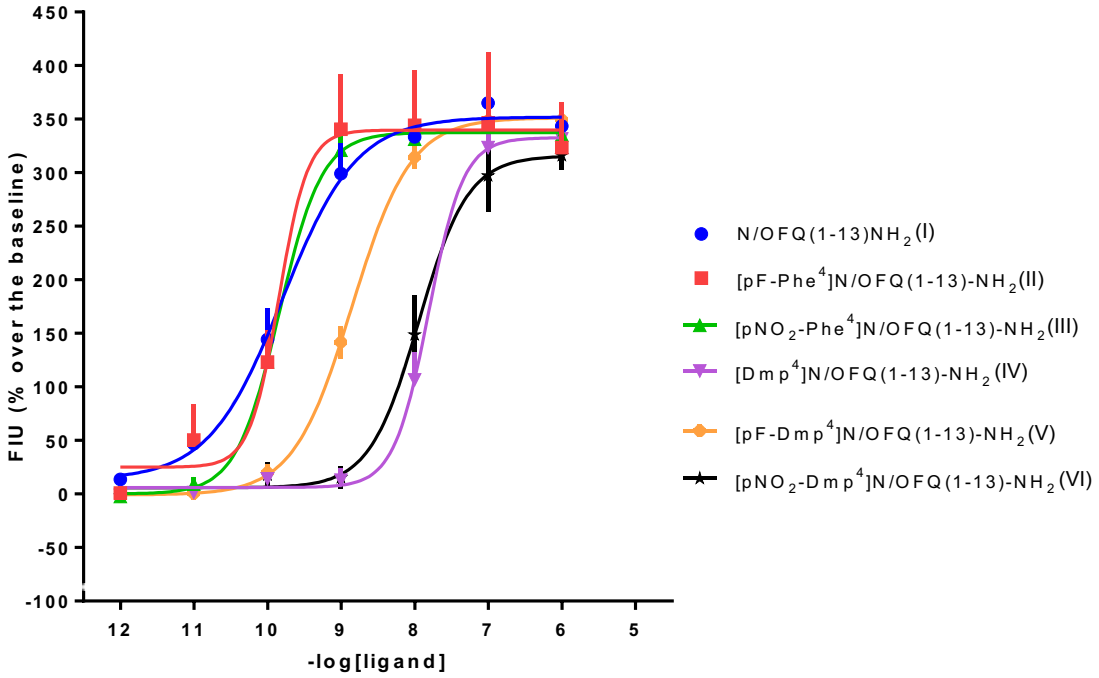

	I	II	III	IV	V	VI
Sigmoidal dose-response (variable slope) Best-fit values						
LogEC50	9.793	9.846	9.841	7.809	8.850	7.944

Figure 8: Dose-response curves of the synthetized peptides [aaX^4]N/OFQ(1-13)-NH_2 evaluated in an intracellular Ca^{2+} mobilization assay in transfected NOP/ $G\alpha_{qi5}$ CHO cells

This investigation confirmed a full agonist behavior for all the peptide derivatives, with variable potency depending on the amino acid introduced at the 4-position of the peptide chain. Noteworthy, as reported in literature,[46] it has been confirmed that [(*p*-F)Phe^4] and [(*p*-NO_2)Phe^4]N/OFQ(1-13)-NH_2 derivatives (**II**, **III**) display a higher potency compared to N/OFQ(1-13)-NH_2 (**I**), while the modification with Dmp^4 (**IV**) was detrimental for the activity. A loss of 100 times in potency was observed for the (*p*-NO_2)Dmp^4 analogue (**VI**). The same negative results were obtained with [Dmp-like^4] peptides except for [(*p*-F)Dmp^4] (**V**), whose *para*-fluorine substitution seems to partially balance the deleterious effect of the *ortho-ortho* methylation.

In conclusion, the substitution in 4-position, with *p*-substituted dimethylated non-natural aromatic amino acids, led to N/OFQ(1-13)-NH_2 analogues characterized by lower potency as NOP agonists if compared to the parent peptide.

Moreover, with the aim to identify novel mixed NOP/opioid receptor agonists able to elicit similar effects as strong opioids but with reduced side effects, Dmt was employed as Fmoc-precursor in SPPS to build a series of linear peptides with the general sequence [Tyr/Dmt^{1},Xaa^{5}]N/OFQ(1-13)-NH_2. The best results in terms of NOP *versus* MOP opioid receptor potency were obtained by substituting both Tyr^{1} and Thr^{5} at the *N*-terminal portion of N/OFQ(1-13)-NH_2 with Dmt. [Dmt^{1,5}]N/OFQ(1-13)-NH_2 has been identified as the most potent dual NOP/MOP receptor peptide agonist so far described in literature.[35]

To test the antitussive effect of [Dmt^{1,5}]N/OFQ(1-13)-NH_2 a model of cough induced by citric acid in guinea pigs was used. Data showed that the co-administration of [Dmt^{1,5}]N/OFQ(1-13)-NH_2 with citric acid did not affect the tussive response. On the contrary, the nebulization with [Dmt^{1,5}]N/OFQ(1-13)-NH_2 before the challenge with the tussive agent, significantly reduced the coughs number induced by citric acid (Fig. 9).

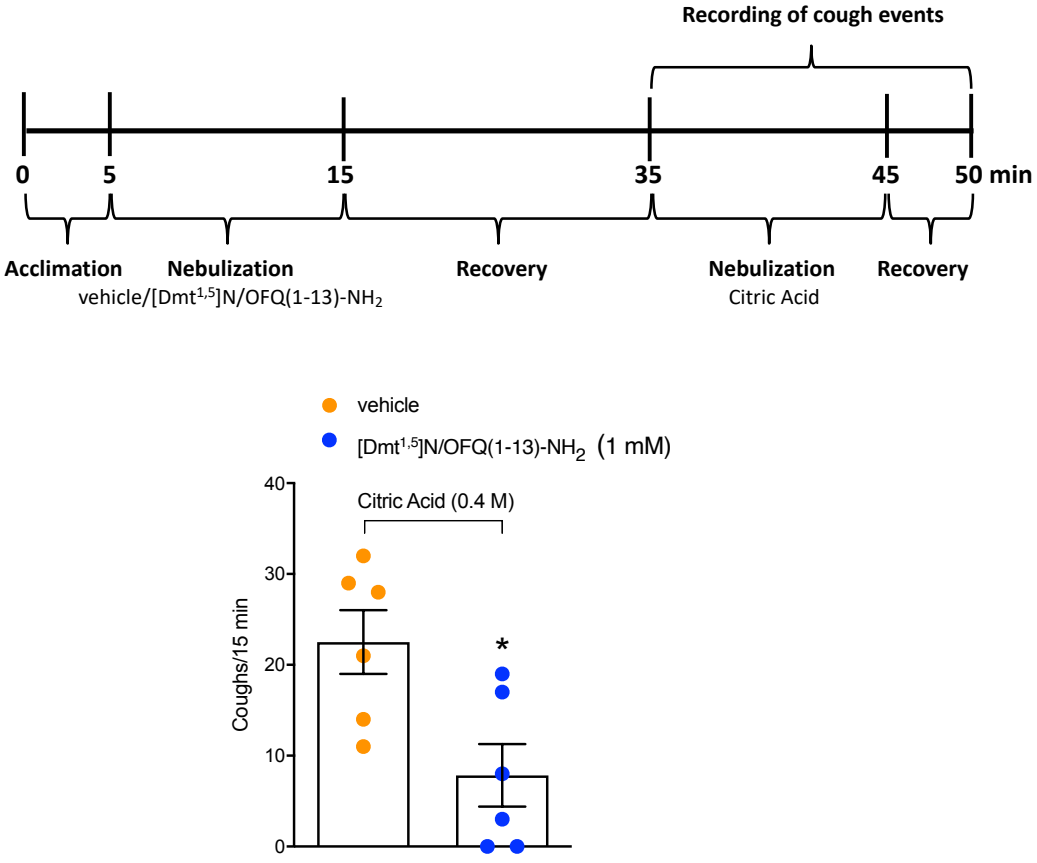

Figure 9: Effect of [Dmt^{1,5}]N/OFQ(1-13)-NH_2 on citric acid-induced cough in conscious guinea pigs. Schematic representation of the experimental procedure for coughs measurement in conscious guinea pigs and pooled data of coughs number after [Dmt^{1,5}]N/OFQ(1-13)-NH_2 (1 mM) or vehicle (0.9% NaCl) nebulization, 30 min before the nebulization of the tussive agent, citric acid (0.4 M). Values are mean ± SEM of the numbers of coughs/15 minutes, data points overlaid (n = 6 guinea pigs for each condition). *p< 0.05 vs vehicle, Student's t-test.

4. Innovative synthesis of mono-methyl Tyrosine (Mmt)

4.1 Aim and objectives

After having synthesized the small library of *p*-substituted Dmt-like amino acid derivatives, we decided to further extend the aniline synthesis reported above, to obtain tyrosine methylated at only one ortho position (*L*)-2-(Mmt).

Only a few syntheses are reported to access 2-Mmt, and none of them is based on C-H activation. In 1991, McDonald *et al.*[108] reported the synthesis of racemic monomethyl-tyrosine, in route toward the corresponding fluoromethyl and difluoromethyl derivatives. The synthesis started with the bromination of 3,4-dimethylanisole with NBS, to afford 4-Br-methyl-3-methyl anisole, and this latter was used to alkylate the anion of diethyl acetamido malonate. Treatment of the resulting adduct with HBr brought about decarboxylative ester hydrolysis. Finally, propylene oxide scavenged HBr, affording the free methylated amino acid (Scheme 30).

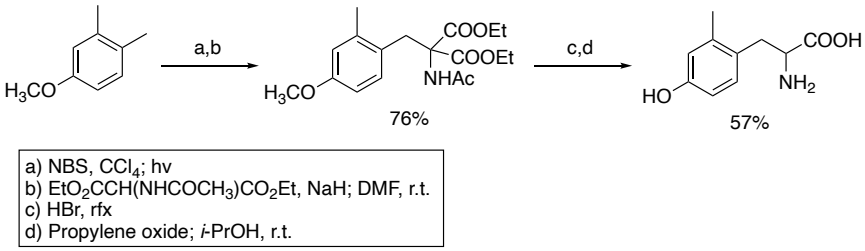

Scheme 30: Mmt synthesis from 3,4-dimethylanisole[108]

In 1994, Majer *et al.*[109] reported a synthesis of ortho-methyl phenyl alanine based on a Pictet-Spengler condensation between PheAla·HCl and formaldehyde. Submission of the resulting 1,2,3,4-tetrahydroisoquinoline-3-carboxylic acid (Tic) to catalytic hydrogenation in acetic acid cleaved the C–N bond affording the desired monomethylated amino acid. Unfortunately, the hydrogenation reaction conditions brought about partial racemization of the target, which could be mitigated by using milder hydrogenation conditions [Pd/C (10 mol%), H_2 (4 atm, 60°C)].[110] (Scheme 31).

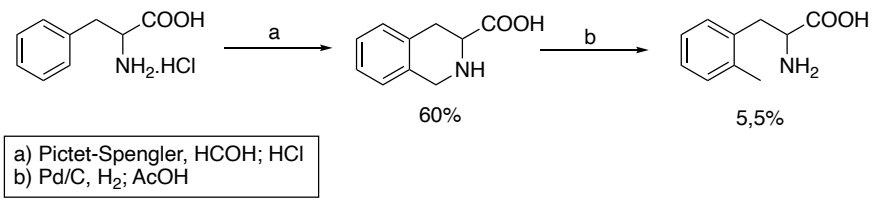

Scheme 31: Synthesis of Mmt from Phenylalanine via Pictet-Spengler Tic cyclization and subsequent hydrogenolysis[109]

In 2016, Kroutil *et al.* reported a biocatalytic one-pot two-step synthesis of para-coumaric acids staring from various phenols, pyruvate, and ammonia, wherein a series of tyrosine derivatives – including Mmt – where the intermediates. The first step required tyrosine phenol lyase (TLP), while the second one tyrosine ammonia lyase (TAL).[111] (Scheme 32)

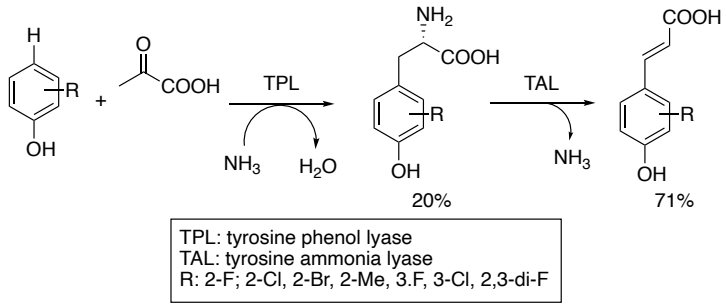

Scheme 32: Enzymatic coupling phenols with pyruvic acid.[111]

Moreover, the biological activity differences obtained by replacing Tyr^1 with non-natural aromatic amino acids, including Mmt^1, have been evaluated in DALDA, MOP selective agonist. From biological assays, Mmt^1 resulted more potent than the original peptide, though less potent than the [Dmt^1]DALDA analogue, while the receptor selectivity was similarly expressed.[58]

Given the paucity of reported synthetic methods to synthesize Mmt, we decided to investigate its synthesis, and possibly that of a library of related derivatives, via a Pd-catalyzed C-H activation strategy. Accordingly, we envisaged to exploit once more the above described Pd-catalyzed aromatic C(sp^2)–H methylation strategy, this time with a tyrosine picolinamide substrate *N,N*-dibenzylated at position 3 of the aromatic ring, in turn obtained from the commercially available 3-nitro-*L*-tyrosine. We reasoned that, in contrast to the previous studies of Ma and Zhang [99] wherein the monomethylation could not be controlled, such an additional substitution at the ring might have allowed only a single *ortho*-methylation, the second one being impeded for steric reasons (scheme 33).

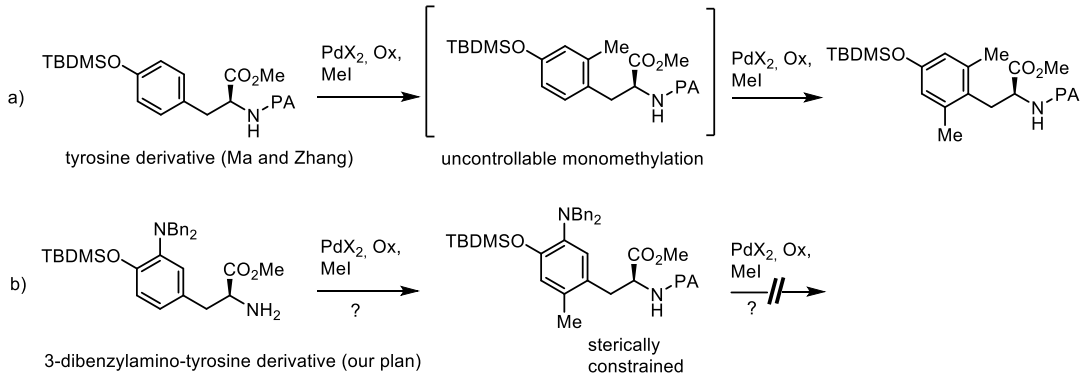

Scheme 33: Equation a) Ma and Zhang Pd-catalyzed approach toward *ortho-ortho* dimethylated tyrosine. Equation b) our *N,N*-dibenzyl substitution-based plan, to favor a single ortho-methylation.

4.2 Results and discussion

Accordingly, commercially available 3-nitro-*L*-tyrosine **27** was first protected at the carboxylic acid function as the corresponding methyl ester. Then, the amine function was converted into the picolinamide **28**, and subsequent silylation of the phenol function gave the corresponding TBDMS ether **29**. However, submission of this substrate to the previously optimized Pd-catalyzed methylation conditions failed (scheme 34).

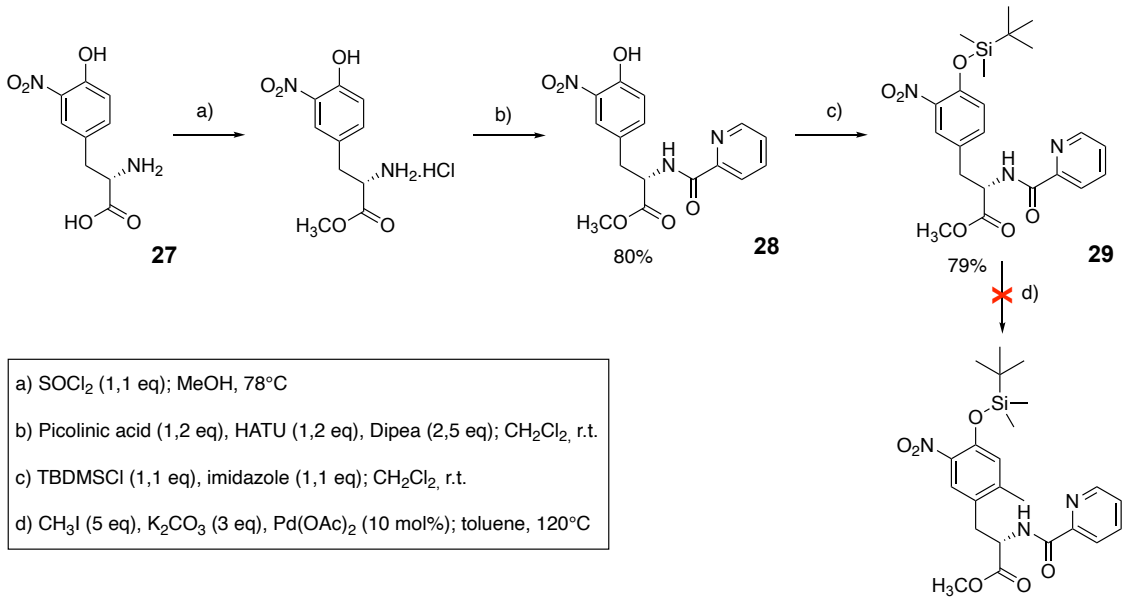

Scheme 34: Synthesis of the *m*-nitro derivative **29** and its attempted Pd-catalyzed C-H methylation.

The above failure was not so surprising. We believe that the presence of the nitro group renders the aromatic ring too electron poor to trigger the electrophilic component of the C–H activation step (scheme 35).

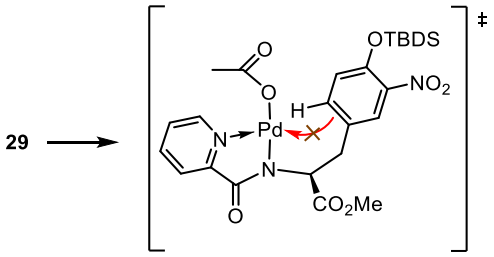

Scheme 35: Hypothesis for the non-reactivity toward the C–H methylation of the *m*-nitro derivative **29**

Accordingly, we submitted **29** to catalytic hydrogenation, to convert the nitro function into the corresponding amine **30**, and this latter was *N,N*-dibenzylated to afford **31**, following the same protocols as described above. This functional group modification had a double purpose: a) activation by resonance donation of the aromatic ring toward attack to palladium, b) inhibition, by steric reasons, of the second methylation step. Gratifyingly, submission of **31** to our standard Pd-catalyzed methylation conditions afforded the expected *ortho*-monomethylated product **32** in 91% yield. Having obtained the desired monomethylation, we then proceeded to the removal of the *N,N*-dibenzyl group, its role being completed. Accordingly, submission of **32** to catalytic hydrogenation afforded the corresponding primary amine **33**, which was deaminated to give **35** in a one-pot two-step procedure, passing through the corresponding diazonium salt **34**. Following treatment with 6N HCl removed all the protecting/directing groups (carboxylic ester, silyl ether and amide), and treatment of the resulting crude product with Boc anhydride gave the desired *N*-Boc protected monomethylated *L*-Mmt **36** ready to be used in SPPS. (Scheme 36).

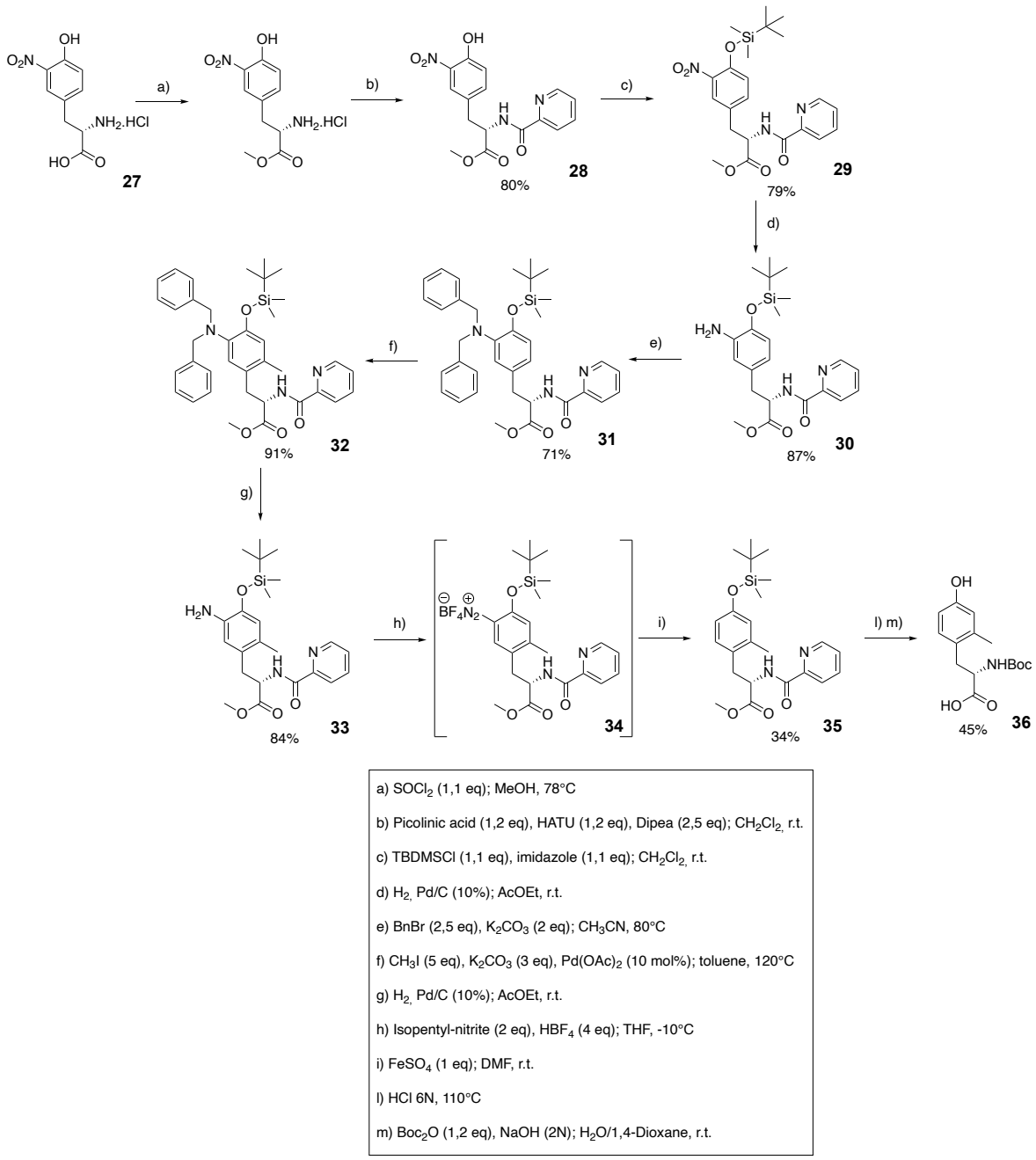

Scheme 36: Synthesis of Mmt via Pd-catalyzed C(sp^2)-H activation

4.3 Conclusions

By placing a removable *N,N*-dibenzyl moiety at the 3-position of the aromatic ring of tyrosine, we managed to obtain a selective Pd-catalyzed ortho monomethylation of the tyrosine derivative. This modification clearly enlarges the scope of the original method reported by Ma and Zhang of tyrosine ortho-methylation,[99] which suffered from an uncontrolled dimethylation. As in the case of Ma and Zhang the reaction conditions of the sequence are not racemizing, we expect that the final Mmt **36** is enantiopure.

Following the same strategies as reported for the *p*-substituted Dmt-like derivatives, in the future, it should be possible to take profit of the diazo intermediate to obtain a number of other 3-substituted monomethylated tyrosine derivatives such as halo, nitro, and carboxylic acid derivatives (Scheme 37).

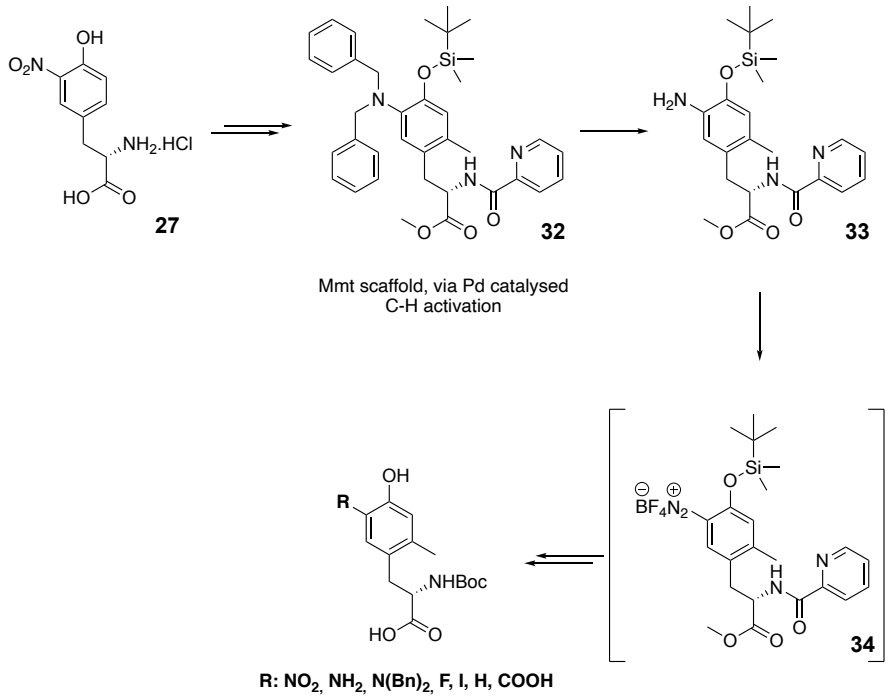

Scheme 37: Synthesis of *m*-substituted Mmt derivatives, through Pd-catalyzed C-H activation and subsequent functionalization of the aniline moiety in 3-position

Moreover, it should be possible to introduce two different alkyl groups, so as to obtain non-symmetrically *ortho-ortho'*-disubstituted tyrosine derivatives. In fact, after introduction of the first alkyl substituent and removal of the *N,N*-dibenzyl group through the diazonium salt as described above, a second Pd-catalyzed alkylation should allow to introduce a new alkyl group in the remaining free *ortho* position.

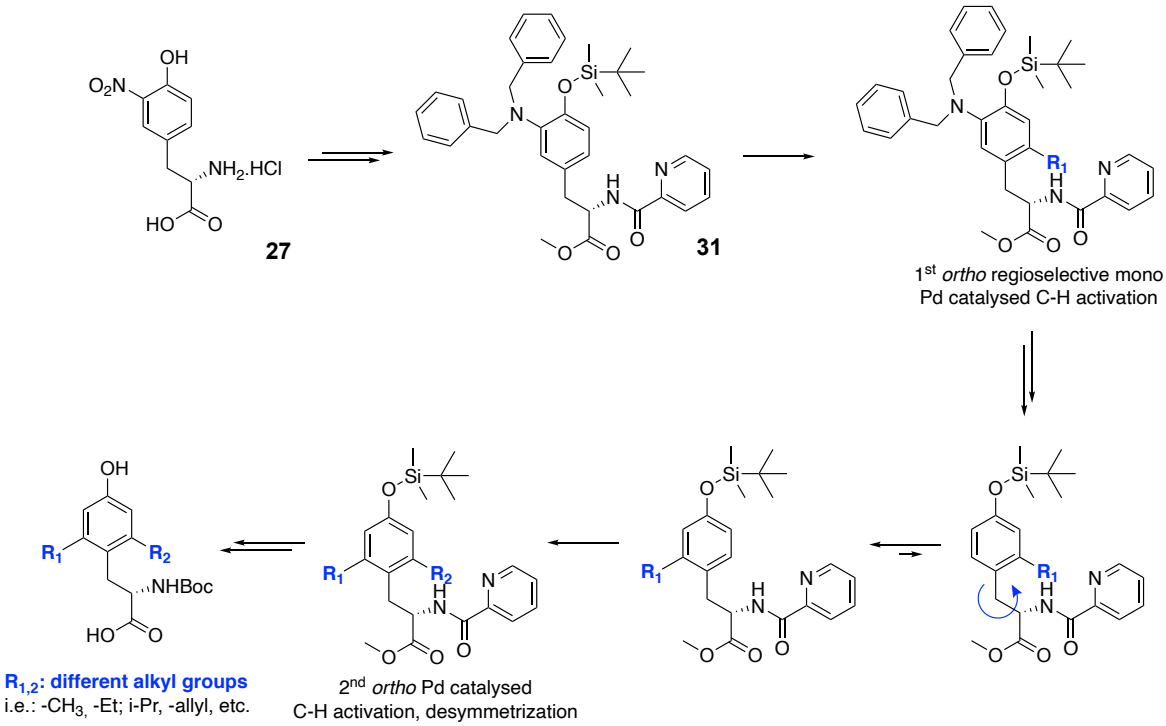

Scheme 38: Planned strategy to introduce two different ortho alkyl groups.

Finally, as reported for the *p*-substituted Dmp-like amino acid derivatives, it should be possible to scale up some of these syntheses, to obtain a new library of variously substituted, properly protected, non-natural amino acid derivatives, to be inserted in peptide chains through SPPS and evaluated in biological assays, as future perspectives.

To date, we successfully obtained the (*L*)-*N*-Boc-2-methyltyrosine (Mmt) **36** starting from (*L*)-3-nitro-tyrosine, which was the principal goal we aimed.

5. Synthesis of non-natural aromatic amino acids via Pd-catalyzed β C-H activation

5.1 Aim and objectives

Once accomplished the syntheses of *N*-Boc- and *N*-Fmoc-*ortho-ortho'*-dimethylated phenylalanine derivatives **15-22, 24, 26** and of *N*-Boc-2-methyltyrosine (Mmt) **36** exploiting the picolinamide-mediated Pd-catalyzed C(sp^2)–H *ortho* methylations of aromatic amino acids as key steps, we focused our attention toward the synthesis of non-natural aromatic amino acids, this time, exploiting the Pd-catalyzed C(sp^3)-H functionalization in β position of natural amino acids.

As already pointed out (vide infra), the AQ-based monoanionic bidentate auxiliaries pioneered by Daugulis[88] allowed the β-C(sp^3)-H arylation of carboxylic acids via the involvement of a fused [5,5]-palladacycle intermediate. This strategy inspired several following works. For example, soon after, Corey exploited the AQ directing group to achieve the β-acetoxylation and β-arylation of natural αAAs.[112] Other studies were conducted on the PA and AQ directing groups properties.[113] Further studies demonstrated the crucial role of the protection as phthalimide of the amine function of the amino acid. Moreover, alternative DGs, such as *N*-methoxyamides, [114] or perfluorinated arylamides,[115] and auxiliary ligands, to better control the mono- *vs* bis-arylation (2-picoline to stop to monoarylation, and 2,6-lutidine to access diarylated products) have been developed.[,] Monoarylation could be also controlled over diarylation by the incorporation of ArS-based auxiliary groups in Ala derivative,[116] or using 2-(pyridine-2yl)-isopropyl (PIP) DG.[117] Again, monoarylation of N-Phth/AQ Ala could be obtained in *t*-BuOH/DCE at 75°C in the presence of catalytic $Pd(OAc)_2$, and $AgBF_4$, as reported by Shi,[118] or in the presence of catalytic $Pd(OAc)_2$ and AgTFA in TCE/H_2O at room temperature, as published by Chen[119] (Scheme 39).

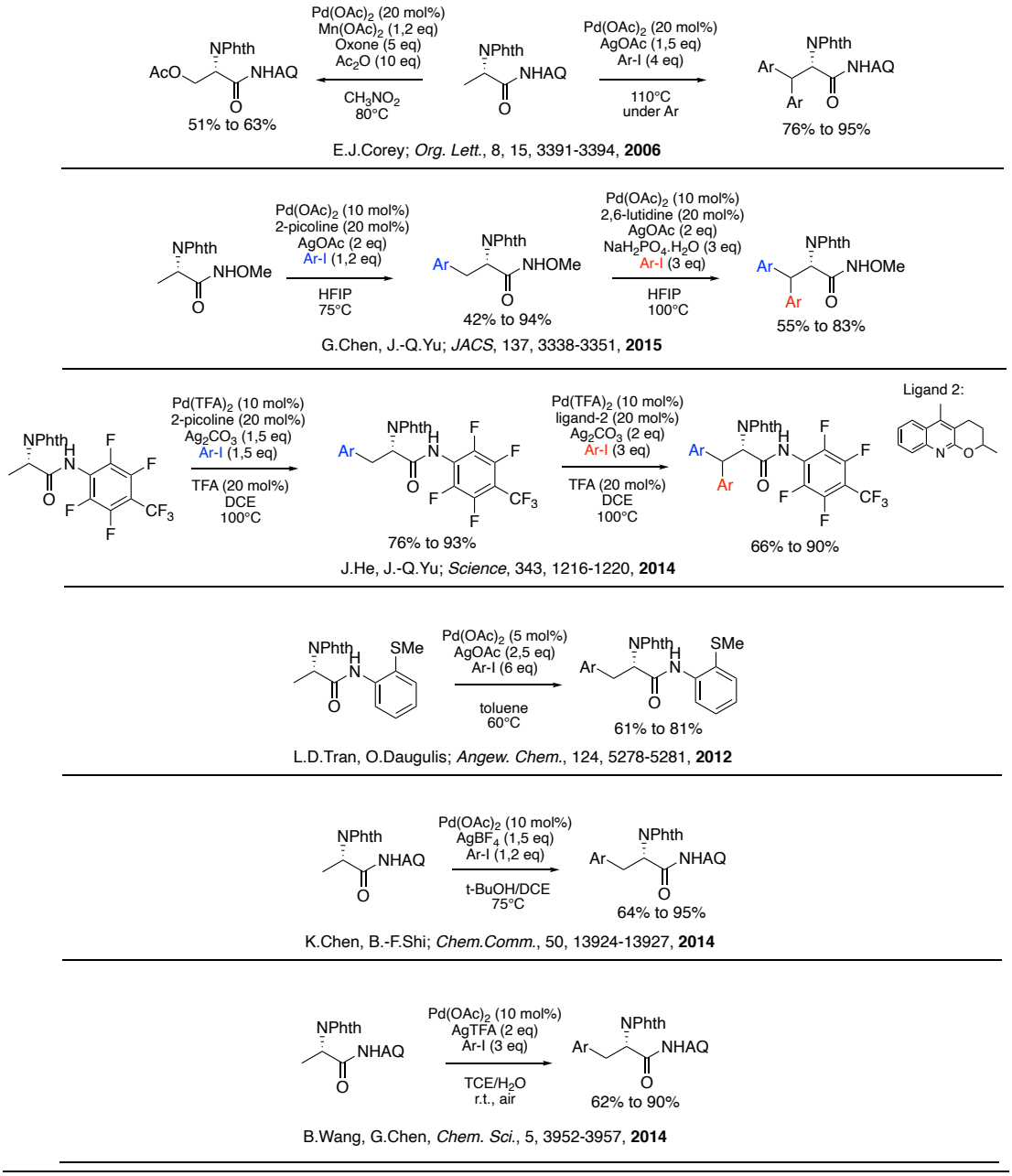

Scheme 39: Reported procedures to achieve Pd-catalyzed β-C(sp^3)-H mono- or di-arylation of alanine derivatives.

The group of Wang and Wang accomplished density functional theory (DFT) computational studies to support the mechanism of the β-C(sp^3)-H monoarylation of a perfluorinated arylamide of *N*-phthaloyl alanine with aryl iodides, obtained in the presence of $Pd(TFA)_2$ (10 mol%), picoline (20 mol%), and Ag_2CO_3 (1.5 equiv.) reported by the group of Yu (Scheme 31, equation 3, fig. 10).[115] After precatalyst initiation, substrate binds to the Pd(^{II}) center via the amidate, which directs the following rate-determining bicarbonate-assisted C(sp^3)−H bond activation, generating a five membered-ring cyclopalladate(^{II}). Subsequent oxidative addition by iodobenzene forms the corresponding Pd(^{IV}) complex. Reductive

elimination gives the final product.[120] 2-picoline ligand is present in every phase of the reaction.

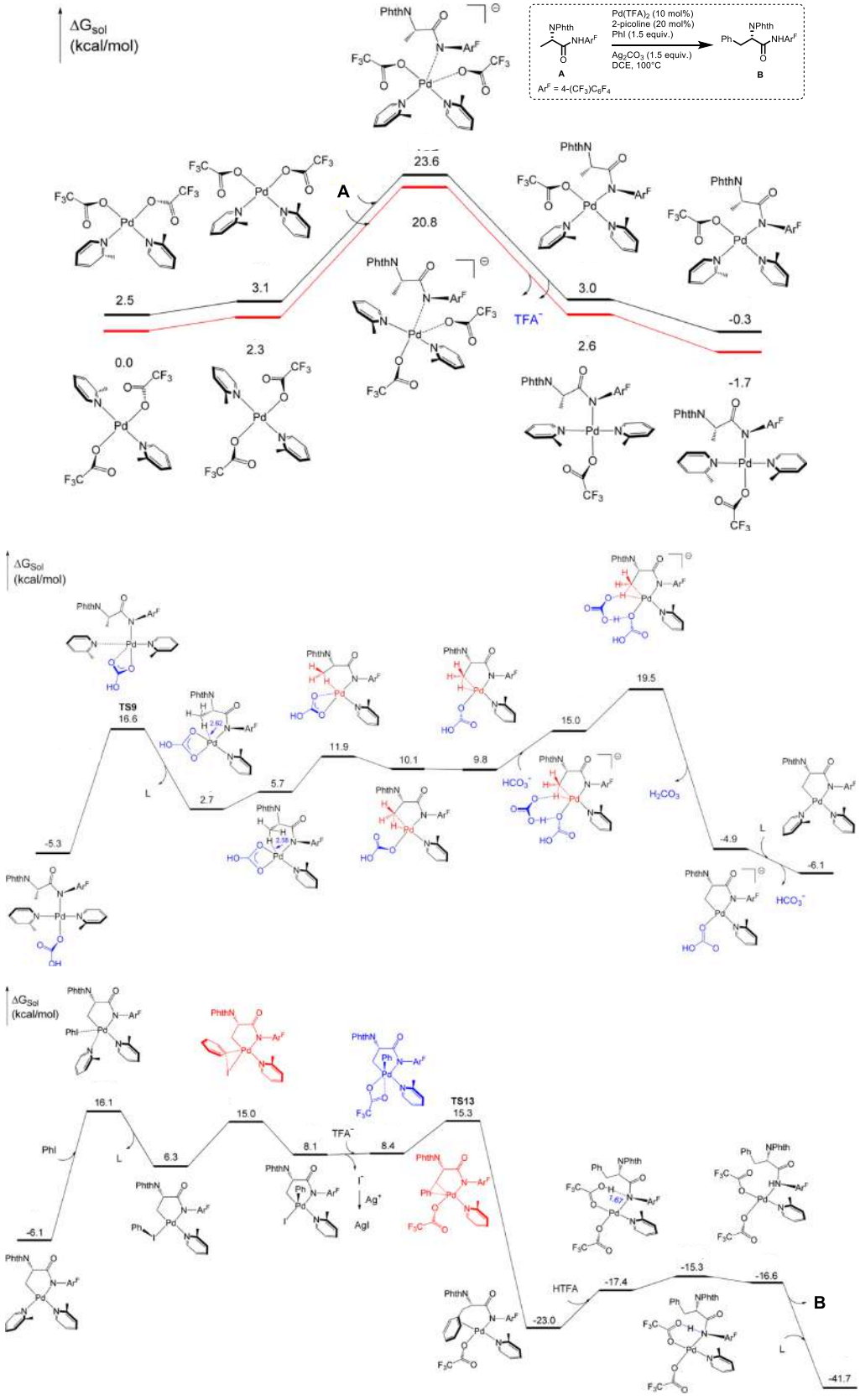

Figure 10: Adapted from ref 120. Free energy profile for the β-C(sp^3)-H monoarylation of a perfluorinated arylamide of *N*-phthaloyl alanine with phenyl iodide.

In light of the above studies, we aimed to contribute to this interesting topic by synthesizing new related compounds via the synthetic pathways reported above, starting from (*L*)-alanine, and under non-racemic conditions. Accordingly, we first attempted to synthesize 2,6-Dmt via Pd-catalyzed β-C–H dimethylation, using 4-iodo-3,5-dimethylphenol derivatives. We did not achieve this goal. Consequently, we decided to study the arylation of different iodophenol partners, using different directing groups. To our delight, we managed to obtain three different original β-arylated alanine derivatives, reported in scheme 31. In particular, starting from *N*-Phth (*L*)-alanine AQ, we were able to synthesize 3,5-Dmt (**52**), which carries the methyl groups *meta* positioned with respect to the amino acid chain, and thus represents a constitutional isomer of 2,6-Dmt. Furthermore, via β,β-diarylation, we managed to obtain the original bis-arylated analogs of Tyr (**53**) and of 3,5-Dmt (**54**). In all the cases, we managed to accomplish full deprotection of the products and *N*-reprotection, to obtain the corresponding *N*-Boc derivatives, ready for SPPS.

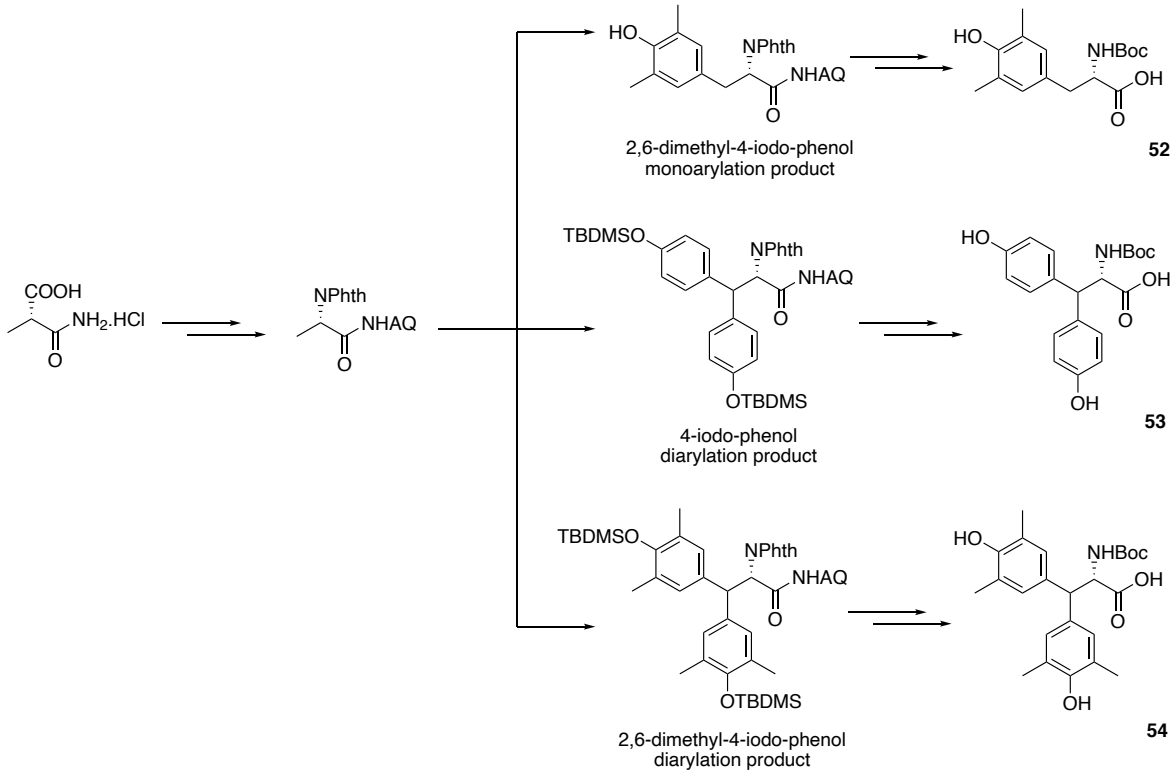

Scheme 40: General synthetic pathway to obtain non-natural arylated α amino acids

5.2 Results and discussion

We first synthesized the methoxy amide of *N*-phthaloyl-(*L*)-alanine following the protocol of Chen[114] and tried to access 3,5-Dmt via Pd-catalyzed arylation using 4-iodo-3,5-dimethylphenol. To this purpose, (*L*)-alanine was *N*-protected as phthaloyl derivative by reaction with phthalic anhydride (PhthO) and triethylamine (TEA), in toluene. Following standard amidic coupling with *O*-methylhydroxylamine gave the desired *N*-Phth (*L*)-alanine took place uneventfully (**39**). (Scheme 41).

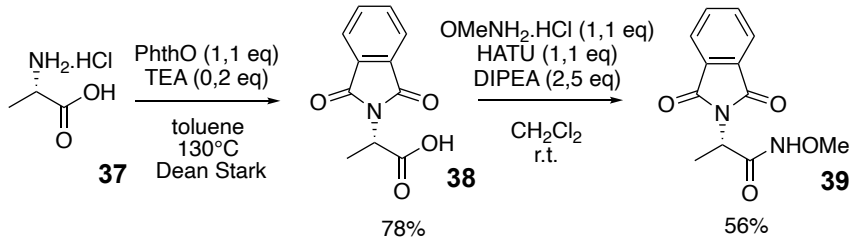

Scheme 41: Synthesis of N-Phth (*L*)-alanine in view to β C–H arylations

Unfortunately, submission of **39** to $Pd(OAc)_2$ (10 mol%), AgOAc (2 equiv.) and 2-picoline (20 mol%) in hexafluoro-2-propanol (HFIP), at 75°C, according to the protocol of Chen,[114] in the presence of 3,5-dimethyl-4-iodo-phenol (**44**) did not give the expected arylation product. Another analogous arylation attempt using the iodophenol protected as *O*-TBDMS (**45**) met with failure as well. Surmising that the failure of the arylation could be attributed to the steric hindrance brought by the two *ortho*-positioned methyl groups, we next tested 4-iodo-phenol *O*-TBDMS (**61**) as the aryl partner. This coupling gave the expected arylation product in 60 % yield. (Scheme 42).

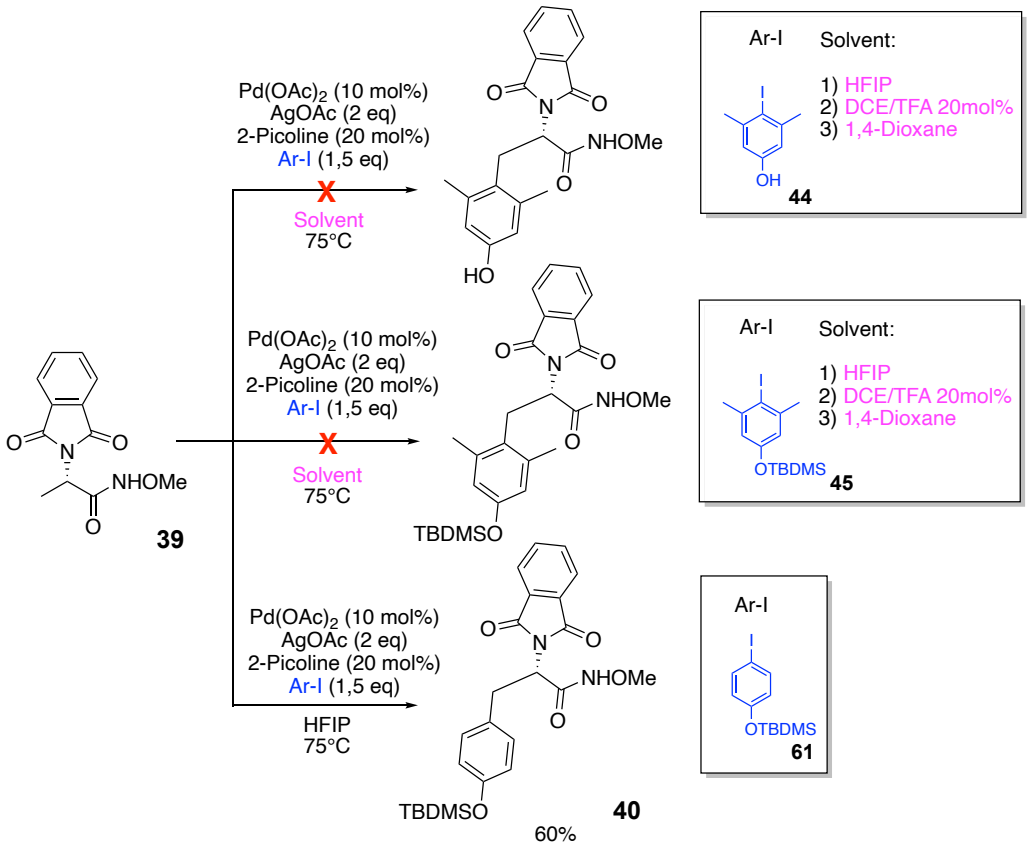

Scheme 42: Trials to obtain 2,6-Dmt through per β-C–H activation, it has been successful only when it was used 4-iodo-phenol as aromatic partner

At this point, we decided to change the directing group on alanine and test the *N*-Phth/*N*-AQ-(*L*)-Ala (**41**), adopting the mild protocol reported by Wang and Chen.[119] It has to be noted that the β-C(sp^3)−H activation of such a substrate would imply the generation of a fused bicyclic [5,5]-palladacycle intermediate. (Figure 11).

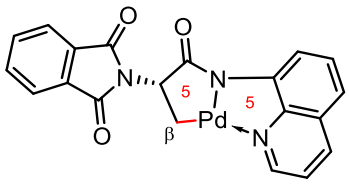

Figure 11: putative palladacycle intermediate involved from *N*-Phth/*N*-AQ-(*L*)-Ala (**41**)

Accordingly, *N*-Phth/*N*-AQ-(*L*)-Ala (**41**) was obtained by classical amidic coupling between **38** and 2-amino-quinoline, in the presence of HATU, DIPEA, in CH_2Cl_2 (Scheme 43).

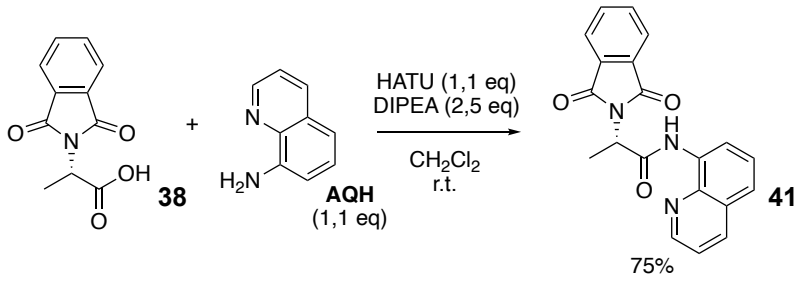

Scheme 43: Synthesis of *N*-Phth/*N*-AQ-(*L*)-Ala **41**.

With the new alanine AQ derivative **41** in hands, we repeated the same arylation tests as previously carried out with the methoxyamide derivative **39**. Again, using 4-iodo-3,5-dimethylphenol (**44**), we were unable to obtain the desired arylation product, either by working at room temperature, or by heating at 110°C (Scheme 35).[1] Here again, as previously observed with **39**, the use of 4-iodo-phenol gave the mono arylated desired product **42** in 78% yield. (Scheme 44).

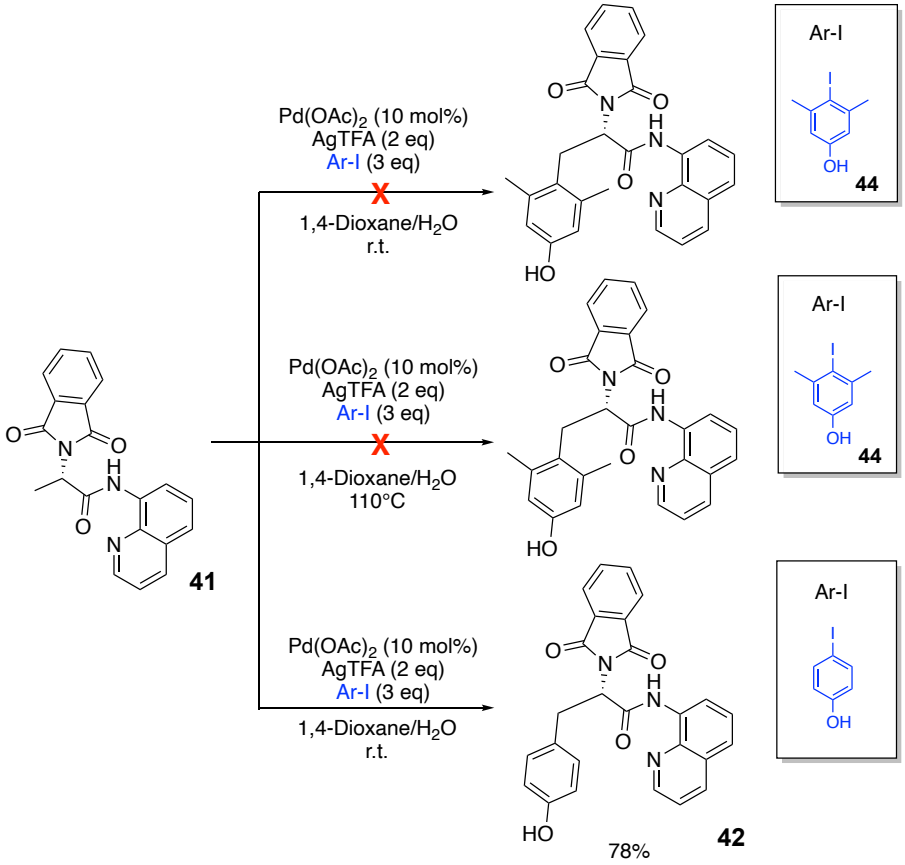

Scheme 44: Tests of β-C–H arylation on the Ala derivative **41**

[1] We adopted the reaction conditions of Wang and Chen (ref 119, see experimental part). Since we did not possess 1,1,2,2-tetrachloroethane, we used the mixture of 1,4-dioxane / water as solvent, which is reported to allow the arylation in good yields.

The above results support our hypothesis that the two ortho methyl groups of the iodoarene sterically prevent the arylation. This theory is also supported by the absence of reported examples in the literature of *ortho* functionalized iodoarenes in such arylations, only 2-methyl-4-iodo phenol having been observed to lead to the corresponding arylated product in traces. To prove this hypothesis, we synthesized the structural isomer of 3,5-dimethyl-4-iodo phenol (**44**), functionalized with 2 methyl groups in *meta-meta* position to iodine, simply by starting from 2,6-dimethyl phenol (**46**), rather than 3,5-dimethyl phenol (**43**), and proceeding by performing a iodination reaction with KIO_3 and KI in HCl and MeOH. In schemes 36 and 37 are reported the synthetic steps to obtain both of them.

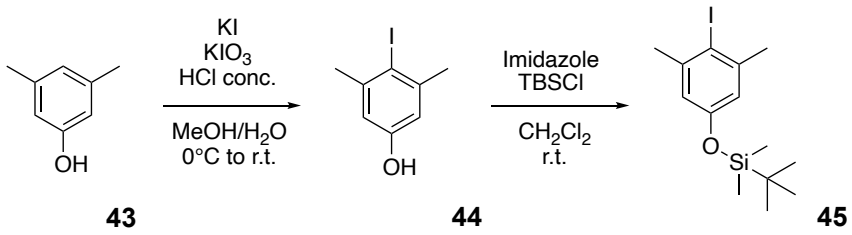

Scheme 45: Synthesis of 3,5-dimethyl-4-iodo phenol and its *O*-TBDMS protected analogue

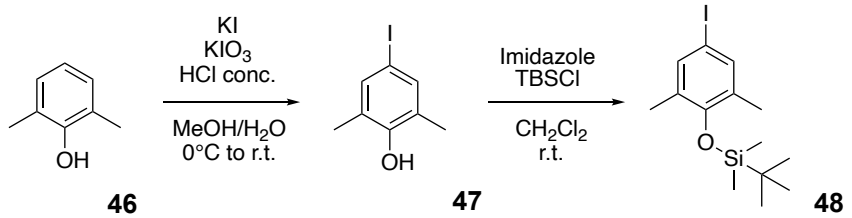

Scheme 46: Synthesis of 2,6-dimethyl-4-iodo phenol and its *O*-TBDMS protected analogue

Accordingly, we undertook the Pd-catalyzed β-C(sp^3)–H arylations using the three iodoarenes: 4-iodo-2,6-dimethylphenol (**47**), *O*-TBDMS-4-iodo-2,6-dimethylphenol (**48**), and *O*-TBDMS-4-iodophenol (**61**). In the event, reaction of **41** with iodoarene **47** using the mild conditions reported by Wang and Chen, allowed to afford the corresponding monoarylated product **49** in 82% yield. On the other hand, reacting **41** with iodoarenes **61** or **48**, and using the reaction conditions reported by Corey under argon atmosphere at 110°C,[112] allowed us to obtain the corresponding β,β'-diarylated products **50** and **51** in 48% and 40% yield, respectively. (Scheme 47).

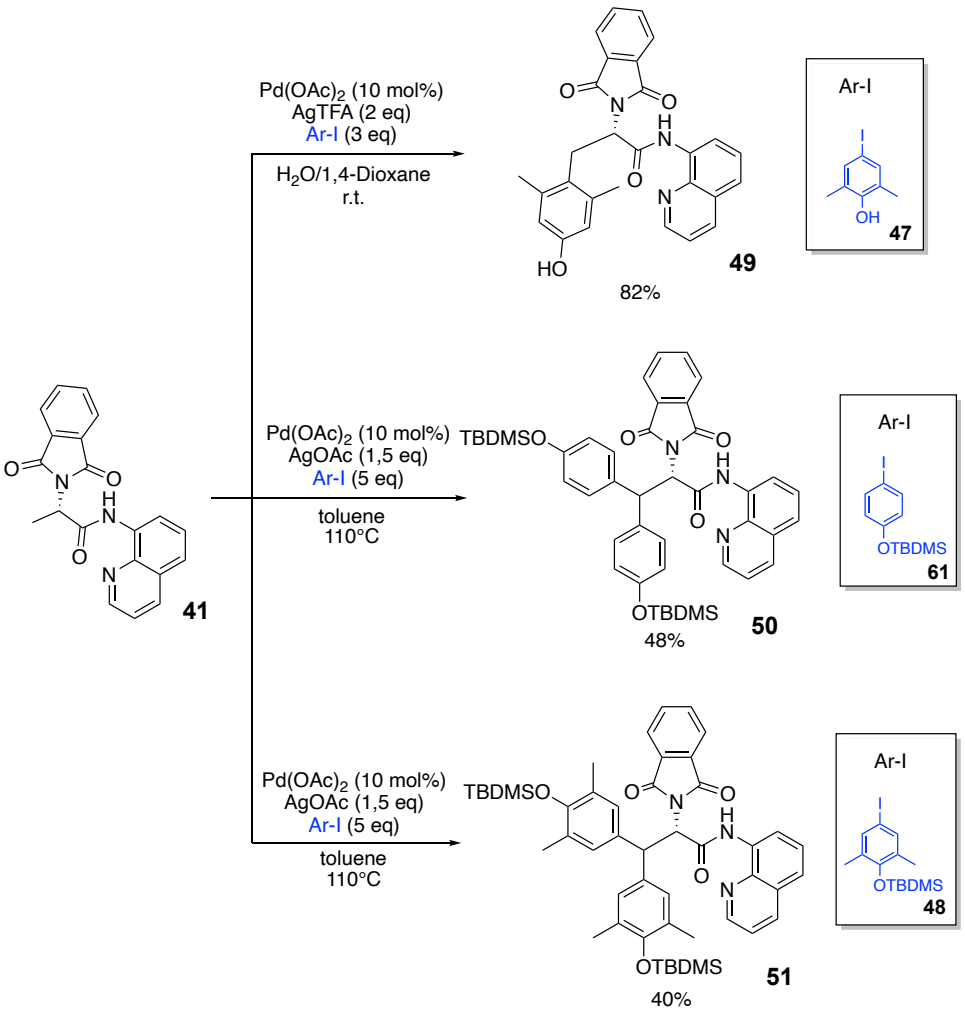

Scheme 47: Synthesis of 3,5-Dmt and its diarylated derivatives

Once obtained the desired β-arylated and β,β'-diarylated products **49-51**, removal of the protecting/directing groups through acid hydrolysis, followed by *N*-Boc protection under standard conditions gave the corresponding desired products **52-54**. These three products have been fully characterized, ready to be inserted in SPPS, once these procedures will be scaled up to gram scale. Scheme 48 summarizes the general conditions used to afford the final products. It has to be noted that **52** represents a constitutional isomer of Dmt *N*-Boc.

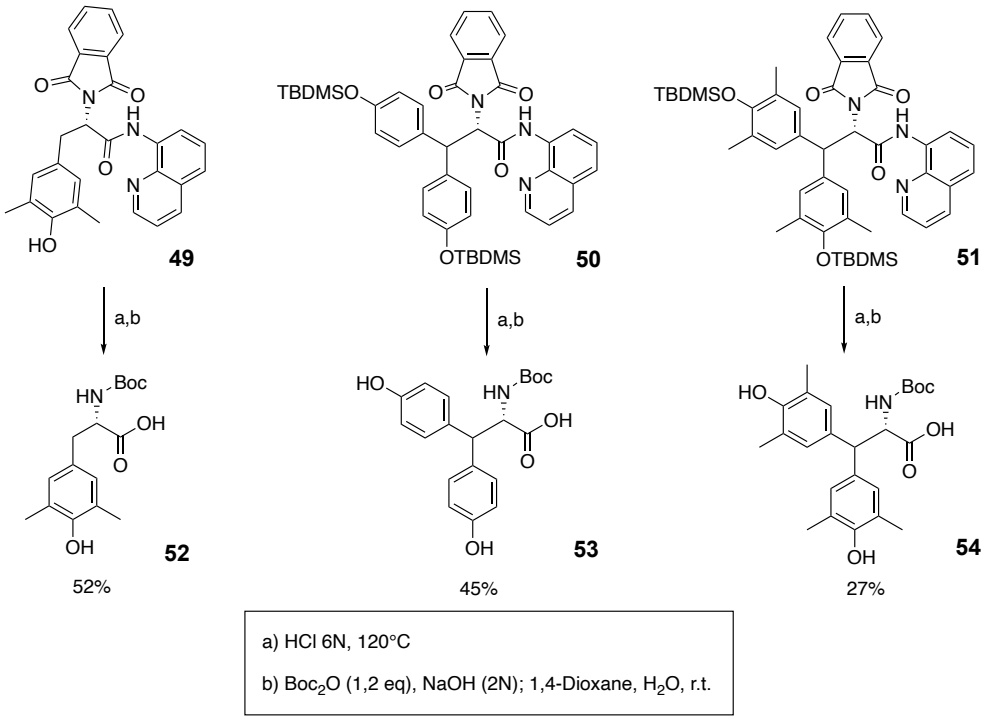

Scheme 48: General conditions to obtain **52-54** as final products

As, by this kind of metal-catalyzed β-C(sp^3)–H activation, we did not achieve the targeted 2,6-dimethyl tyrosine, we envisaged to test other directing groups, less sterically demanding and more flexible than the AQ amide **41**. Thus, similarly to our previous studies on the methylation of 4-substituted phenylalanine, we decided to synthesize (*L*)-alanine methyl ester *N*-picolinamide, and test it in the Pd-catalyzed arylation. This variation is not known for Pd-catalyzed β-C(sp^3)–H activation, and would involve a fused bicyclic [4,5]-palladacycle intermediate.

Accordingly, after conversion of (*L*)-alanine·HCl **37** into its methyl ester, a classical amidation reaction with 2-picolinic acid gave **55**. This latter was tested in arylation reactions with 4-iodo-3,5-dimethylphenol **44**, 4-iodophenol, and *O*TBDMS-4-iodophenol **61** using the modified Wang & Chen conditions for the first two iodoarenes, and the Corey conditions for the third iodoarene to access the diarylation (*vide supra*). Unfortunately, all the trials performed did not allow the generation of the desired arylation (scheme 49).

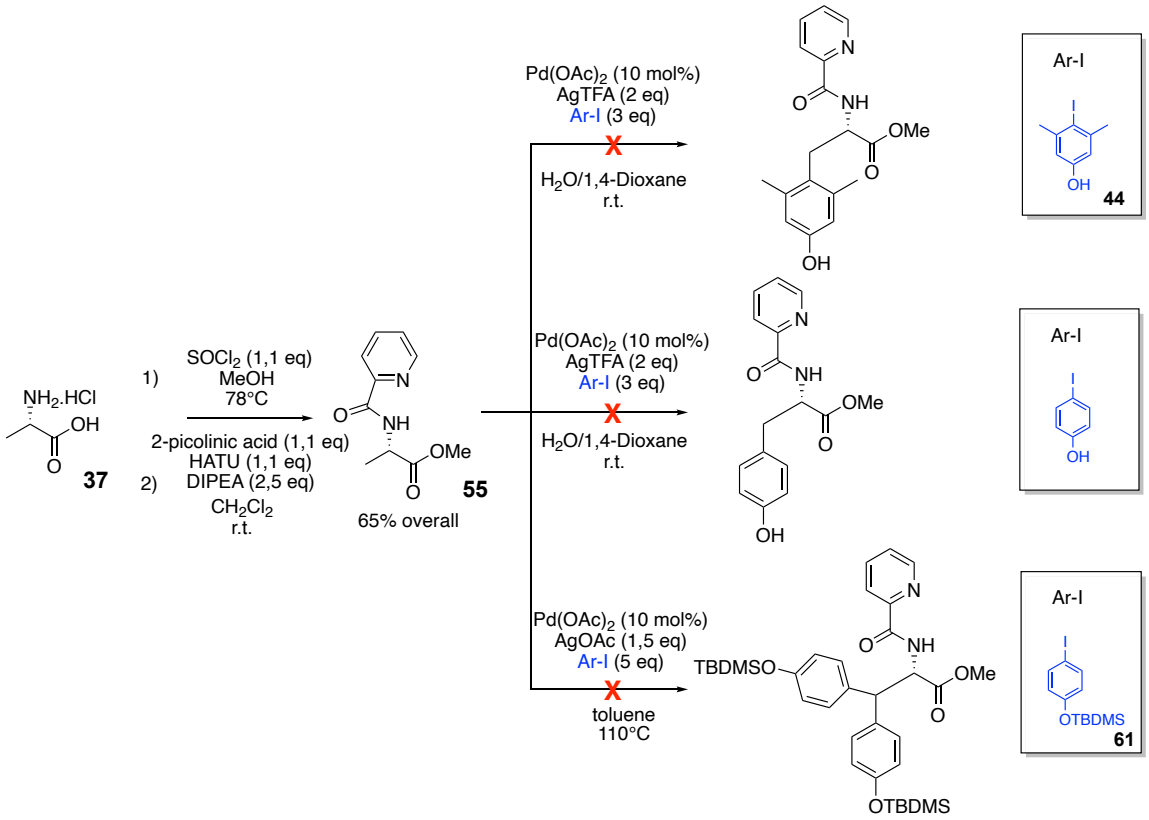

Scheme 49: Synthetic pathway to obtain derivative **55**, and subsequent Pd-catalyzed β arylation trials.

As a further modification, we decided to stick to an *N*-phthaloyl alanine, this time amidated with pyridin-2-amine instead of 8-aminoquinoline. The planned (*L*)-Ala N-Phth AQ **56** could be easily synthesized by standard amidation of (*L*)-Ala *N*-Phth **38** with 2-aminopyridine. Unfortunately, its submission to the Pd-catalyzed reaction conditions as described above, failed (scheme 50).

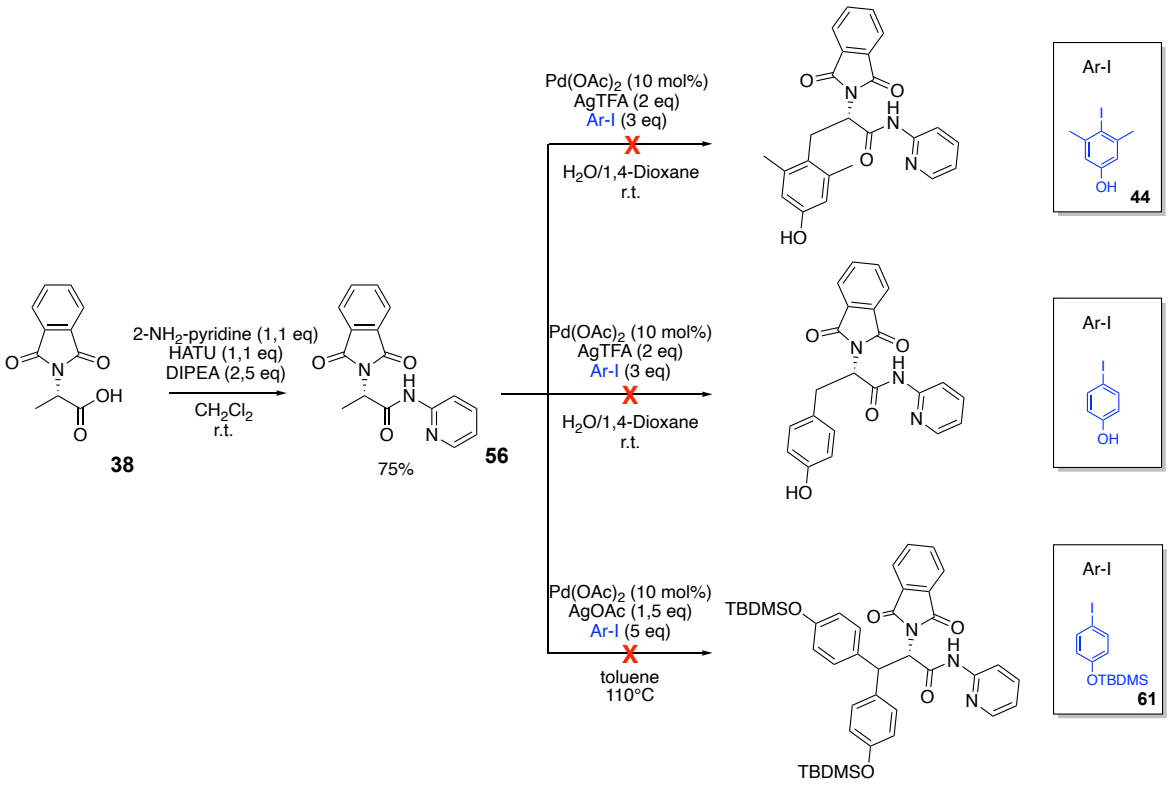

Scheme 50: Synthetic pathway to obtain *N*Phth/*N*-2-Pyr Ala derivative **56**, and subsequent metal catalyzed β arylation trials

We speculate that the four-membered cyclopalladated intermediates that should be involved according to the typical mechanism, are likely to be too strained to be generated (fig. 12).

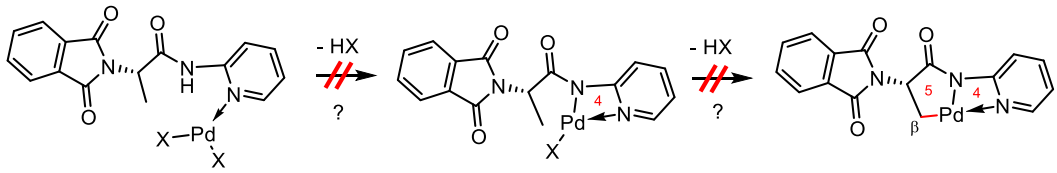

Figure **12**: putative palladacycle intermediates involved with (*L*)-Ala *N*-Phth AQ.

As the last trial, we decided to test *N*-phthaloyl alanine, amidated with 2-(aminomethyl)pyridine (AMP), **57**. We reasoned that with an extra methylene in the scaffold with respect to the previous substrate, the arylation mechanism would have implied a more reasonable fused bicyclic [5,5]-palladacycle intermediate. (Fig. 13).

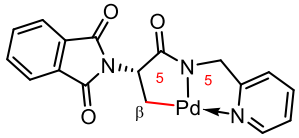

Figure 13: putative palladacycle intermediate involved with (*L*)-Ala *N*-Phth AMP

The synthesis of this new substrate was accomplished as above, and resulting (*L*)-Ala *N*-Phth AMP **57** was reacted with 4-iodo-3,5-dimethylphenol **44**, 4-iodophenol, and *O*TBDMS-4-iodophenol **61** using, as before, the modified Wang & Chen conditions for the first two iodoarenes, and the Corey conditions for the third iodoarene (*vide supra*). Although the reaction with 4-iodo-3,5-dimethylphenol failed again, that with 4-iodophenol gave the expected corresponding arylation product **58** in 38% yield. The reaction with *O*TBDMS-4-iodophenol worked too, affording a mixture of mono- and diarylated products **59** and **60**[2] in 35% and 5% yield, respectively.

In scheme 51 it is reported the synthetic strategy and the related obtained results.

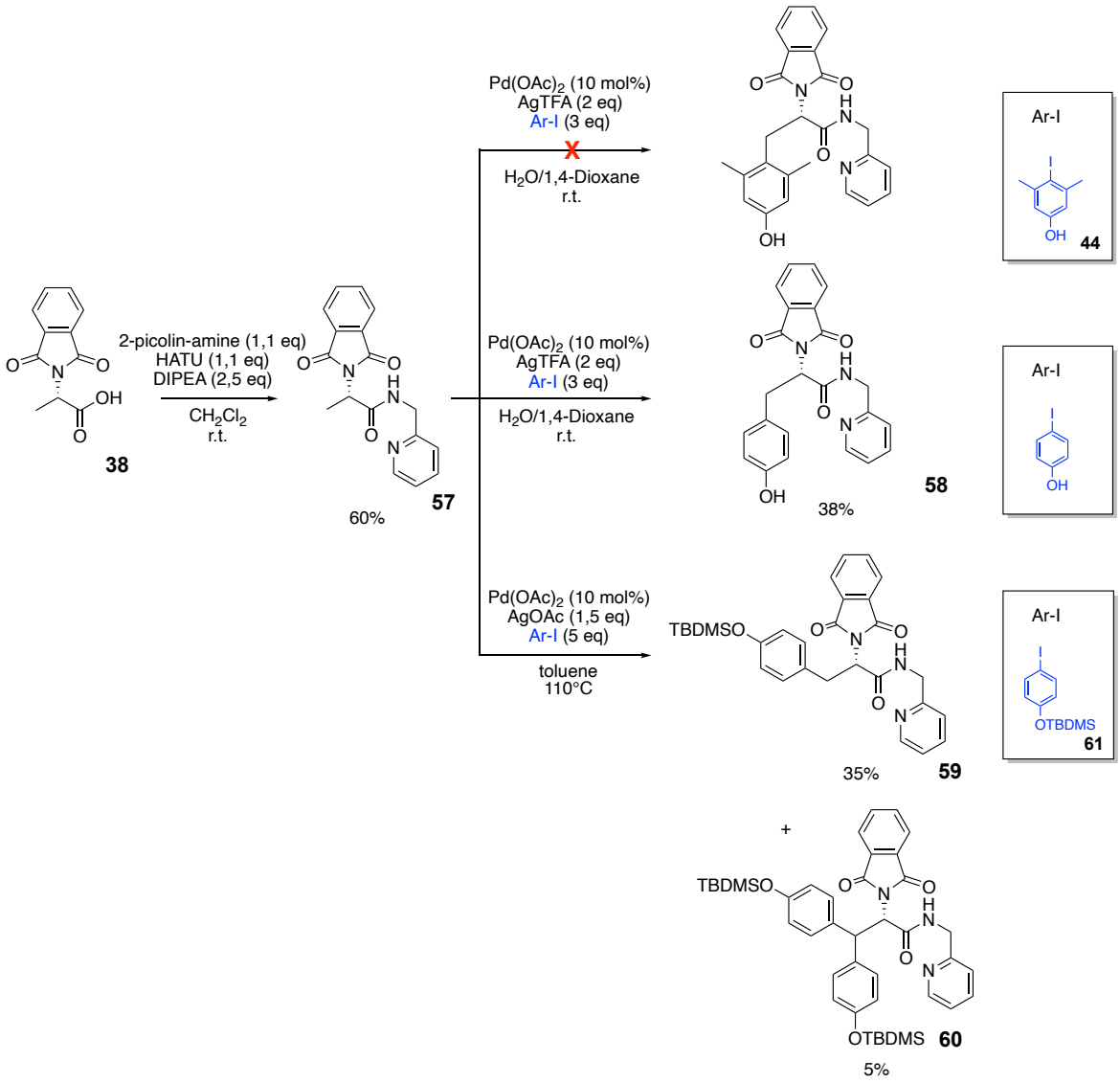

Scheme 51: Synthetic pathway to obtain *N*Phth/*N*-2-PA Ala derivative (**57**), and subsequent metal-catalyzed β arylation trials

[2] The product could not be obtained completely pure (see the experimental section).

5.3 Conclusions

Although we failed to obtain the initially targeted 2,6-Dmt via Pd-catalyzed β-C(sp^3)–H activation, we successfully achieved other non-natural aromatic amino acid analogs, structural isomers of Dmt.

To date, we have not attempted to scale up the syntheses described above, but we should be able to easily synthesize the aryl derivatives **52**, **53**, and **54** on a gram scale, insert them into peptides, and evaluate their behavior in comparison with the parent peptide and the Tyr- or Dmt-substituted peptides.

In summary, Pd-catalyzed β-C(sp^3)–H activation reveals to be a modern and very efficient strategy to obtain a number of non-natural arylated amino acid derivatives. In perspective, we plan to further extend the studies to different DGs and iodoarene partners, in search of non-racemizing and more straightforward routes allowing access to 2,6-Dmt, and/or other derivatives carrying more stereogenic centers.

If the peptides obtained incorporating these new non-natural amino acids will provide interesting results, we will synthesize additional monoarylated, homo-diarylated and hetero-diarylated derivatives, to evaluate their behavior. Furthermore, applying this arylation strategy to amino acids having a chain longer than alanine will generate product with a new stereogenic center that could be controlled. (Scheme 52).

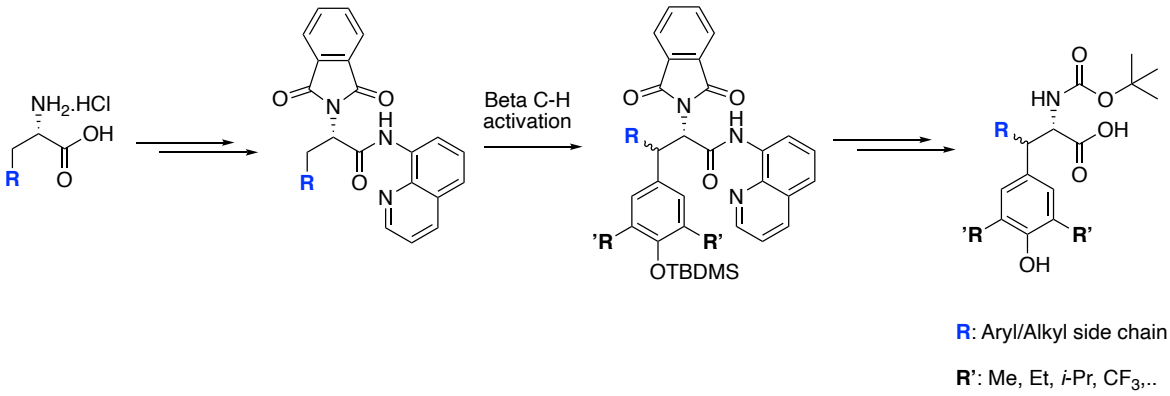

Scheme 52: Future perspectives starting from different functionalized amino acids to obtain different asymmetric products

To date, we were pleased of having obtained these Tyr di-aryl and 3,5-Dmt-aryl derivatives through this modern chemistry based on Pd-catalyzed C–H activation.

6. Further application of 2,6-Dmt, via peptide welding technology (PWT)

6.1 Aim and objectives

Only in recent years, the pharmaceutical industry has come to appreciate the role which therapeutic peptides may have in addressing unmet medical needs, hence this class of compounds could represent an excellent alternative to small molecule and biological therapeutics, in clinic.

Unfortunately, pharmacokinetic issues still represent a strict limitation to their use, indeed, peptides are characterized by short *in vivo* half-life, as they are rapidly recognized and metabolized by peptidases. Numerous strategies have been reported to overcome this limitation among which the insertion of non-natural α-(*D*)-amino acid in the peptide chain, peptide cyclization or *N*-methylation of peptide bonds.

In the last few years, the multimerization of bioactive peptides has been investigated as a further possible approach for extending their limited half-life. The first example of multimeric peptides was developed by Chang to generate antibodies against α_0 G protein subunits, called multiple antigen peptide.[121] Later on, in 2003, the synthesis of tetrabranched peptides has been reported, characterized by higher resistance in blood and serum, due to higher stability against proteases, with general retention of the biological activity.[122] Noteworthy, a novel strategy, the so-called peptide welding technology (PWT), has been reported in 2014 to obtain, in high yield and pure rate, multimerized bioactive peptides through a convergent synthetic route.[123] PWT compounds are generally characterized by the conjugation of three different clustering cores functionalized with four maleimide groups (PWT-1 with a tri-lysine motif, PWT-2 with a cyclam-based scaffold and PWT-3 which is a lysine-ethylendiamine derivative, as reported in figure 14) with four linear monomers of the desired target peptide.

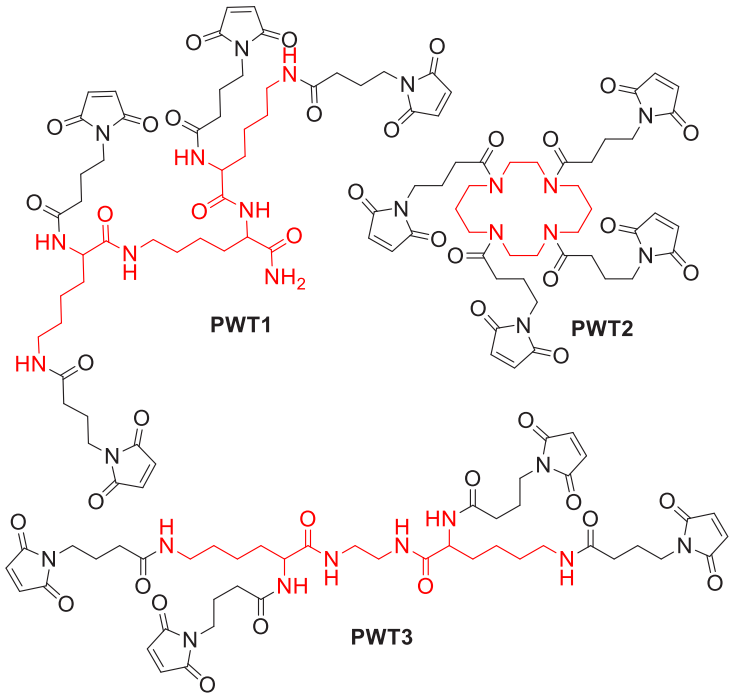

Figure 14: Chemical structures of the PWT-1, PWT-2 and PWT-3 cores

All PWT-derivatives reported to date have been efficiently prepared following a convergent synthetic approach based on the conjugation of the clustering core with four linear monomers of the same target peptide after their independent synthesis. The classical procedure consisted in a thiol-Michael reaction between the central reactive scaffold and the peptide of interest in which a key cysteine residue was conveniently introduced.

Due to the encouraging results obtained through the synthesis of the first PWT tetrabranched conjugated peptides in terms of pharmacokinetic and drug-likeness properties, the application of this strategy was extended to different bioactive compounds, such as N/OFQ, tackykinin, UFP-101 (NOP antagonist), neuropeptide S, dermorphin, to conclude with the unnatural [Dmt^{1}]N/OFQ(1-13)-NH_2.[124,125,126,127] In table 2 some *in vitro* data related to a series of PWT derivatives of bioactive peptides are reported.[127] Generally, PWT compounds showed the same pharmacological profile of the parent peptide monomers, with the advantage of a longer lasting effects *in vivo*, as reported below. (Tables 2 and 3).

PWT peptide	Test	Potency	Efficacy
PWT1-N/OFQ	receptor binding	+	
	[^{35}S]GTPγS binding	+	=
	Ca^{2+} mobilization	–	=
	mVD	+	=
PWT2-N/OFQ	receptor binding	+	
	[^{35}S]GTPγS binding	+	=
	Ca^{2+} mobilization	–	=
	BRET G protein	+	=
	BRET β-arrestin 2	–	=
	mVD	+	=
PWT3-N/OFQ	receptor binding	+	
	[^{35}S]GTPγS binding	+	=
	Ca^{2+} mobilization	–	=
	mVD	+	=
PWT1-NPS	Ca^{2+} mobilization	+	=
PWT2-SP	Ca^{2+} mobilization	–	=
	BRET G protein	=	=
	gpI	=	=
	rUB	=	=
PWT2-NKA	Ca^{2+} mobilization	–	=
PWT2-NKB	Ca^{2+} mobilization	=	=
PWT2-[Dmt^{1}]N/OFQ (1-13)	receptor binding	–	
	[^{35}S]GTPγS binding	=	=
	Ca^{2+} mobilization	–	=
	BRET G protein	=	=
	BRET β-arrestin 2	–	–
PWT2-UFP-101	BRET G protein	=	=
	mVD	–	=
PWT2-dermorphin	Ca^{2+} mobilization	–	=
	BRET G protein	–	=
	BRET β-arrestin 2	–	=
	gpI	–	=

Table 2: *In vitro* biological activities of PWT tetrabranched peptides, comparing PWT N/OFQ with 3 different scaffolds, neuropeptide S (NPS) the endogenous ligand for NPSR, tackykinins, Substance P (SP), neurokinin A and B (NKA, NKB), [Dmt^{1}]N/OFQ(1-13)-NH_2 derivative, UFP-101 and dermorphin[127]

Legend: +, -, = higher, lower or similar to linear peptide, mVD mouse vas deferens, gpI guinea pig ileum, rUB rat urinary bladder, BRET bioluminescence resonance energy transfer

	Species	Test	Potency	Duration of action
PWT1-N/OFQ	mouse	locomotor activity	+ +	+ + +
PWT2-N/OFQ	mouse	tail-withdrawal assay	+ +	+
	mouse	rotaroad	+ +	n.d.
	mouse	allodynia in CCI	+ +	+
	mouse	locomotor activity	+ +	+ + +
	mouse	food intake	+ +	n.d.
	rhesus monkey	tail-withdrawal assay	+ +	+ + +
PWT3-N/OFQ	mouse	locomotor activity	+ +	+ + +
PWT1-NPS	mouse	locomotor activity	+	=
	mouse	recovery of RR	+	+
PWT2-SP	mouse	SBL test	+	+
PWT2-[Dmt[1]]N/OFQ(1-13)	rhesus monkey	tail-withdrawal assay	+	+
PWT2-UFP−101[a]	mouse	forced swimming test	+	=

Table 3: *In vivo* activity of PWT tetrabranched peptides
Legend: +, = higher or similar to parent peptide, CCI chromic constriction injury, RR righting reflex, SBL scratching, biting, licking[127]

Inspired by these results, and with the aim to explore the concept of hetero multivalency, reported in Nature Chemistry[128] to better describe the simultaneous interaction of different receptors with different ligands, we decided to perform a synthetic strategy which allowed us to obtain a hetero multivalent PWT derivative. In this approach, the central PWT core was functionalized with two couples of different bioactive peptide analogues, capable to interact simultaneously with two different receptor systems. Particularly, the PWT core was conjugated with two peptides selective for NOP and two peptides selective for MOP receptors.

6.2 Results and discussion

The first example of mixed NOP/opioid PWT derivative was reported in 2017, by Cerelesi et al., who obtained the homotetrabranched PWT2-[Dmt[1]]N/OFQ(1-13)-NH_2. This compound behaved as NOP and opioid receptors agonist, eliciting robust antinociceptive effects after spinal administration in non-human primates.[129]

Worthy of note, we aimed to revisit the synthesis of the central core, making it capable to be conjugated to two couples of different peptide chains, one selective for MOP and one for NOP receptor.

To achieve this result, we firstly optimized the synthesis of the new H-PWT1 core, **65** (Scheme 53), bearing two maleimide and two benzaldehyde moieties. The central core was synthesized in liquid phase, by coupling Lys-NH_2 to two molecules of Z-Lys-(Boc)-OH to yield the tri-lysine scaffold (**63**), which underwent then to selective deprotection of Cbz via catalytic hydrogenation. The subsequent coupling with two equivalents of 4-

maleimidobutyrric acid provided the bis-functionalized core (**64**). Once the Boc groups were removed it was possible to perform a second amide coupling with 4-formyl benzoic acid, to obtain the desired H-PWT1 core (**65**).

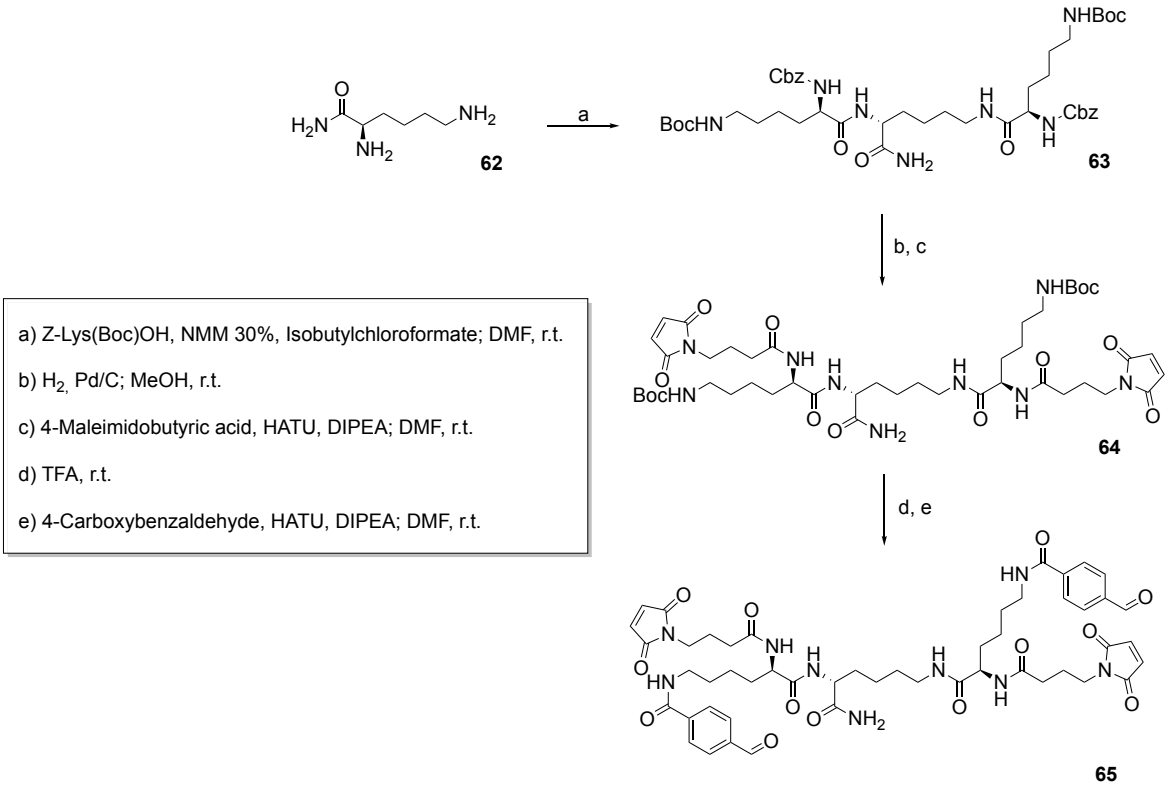

Scheme 53: Synthesis of the bis-functionalizable H-PWT1 tetrabranched core **65**

The peptides of interest were synthesized through SPPS. One of these was [Cys^{18}]N/OFQ, (FGGFTGARKSARKLANQC, **66**) in which the additional Cys residue was introduced in view of the subsequent thiol-Michael addition reaction on the maleimide moieties of H-PWT1. The chemoselectivity of the conjugation step was assured by the lack of other -SH side chain functional groups. The other peptide derivatives were three MOP targeting dermorphin (YaFGYPS-NH_2) analogues (**69a-c**, Scheme 54). In the first case, the native sequence of dermorphin was, functionalized with a hydrazine group on an additional *C*-terminal Lys residue (**69a**). A second example was characterized by the presence of a polioxyethylene $(O2Oc)_2$ spacer between the MOP pharmacophore and the *C*-terminal residue (**69b**), to evaluate the effects of a higher distance between the core and the message domain, with the additional advantage of improving water solubility. The third analogue (**69c**) was superimposable to the first one, but the *N*-terminal residue was replaced by [Dmt^1], in attempt to improve the opioid agonist activity, as reported in literature.[130,131,55]

To synthesize these compounds, we firstly elongated the *C*-terminal domain of dermorphin with a Lys (Dde) residue (**67a-c**). Compounds **68a-c**, obtained from the selective removal of the Dde protection, were coupled with 4-(2'-*N*-Boc-hydrazino) benzoic acid, then the target compounds were cleaved from the resin by acid hydrolysis.

Of note, it has been previously demonstrated for both dermorphin and N/OFQ that the *C*-terminal elongation with different functionalized residues does not alter the pharmacological profile of the entire peptides.[132,127]

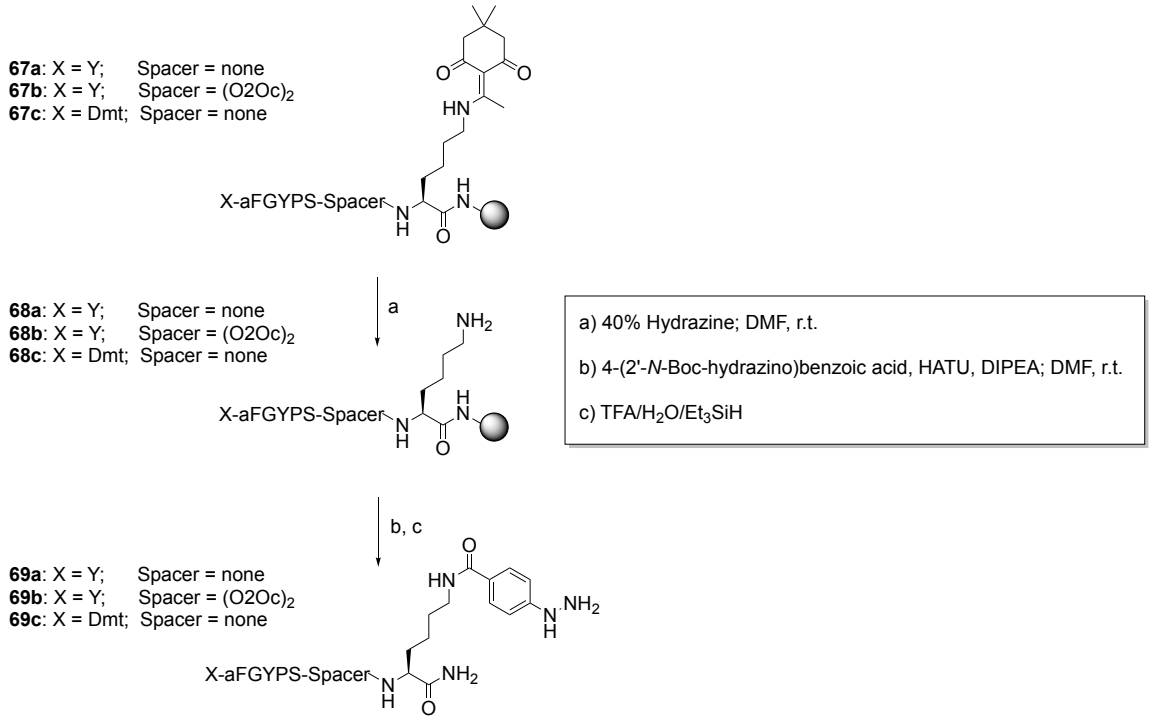

Scheme 54: Synthesis of hydrazine benzoic functionalized dermorphin derivatives

Finally, the properly functionalized peptides (**69a-c** and **66**) were selectively coupled to the H-PWT1 core **65**, as depicted in scheme 55. Firstly a thiol-Michael addition between 2 equivalents of [Cys^{18}]N/OFQ (**66**) and the maleimido moieties of **65** was performed, which was catalyzed by mild basic conditions, with $NaHCO_3$. Once the first conjugation reaction was completed, the pH was turned to acid values by adding CH_3COOH, and the dermorphin analogues were added, to obtain, in one pot, the final products **70a-c**, easily purified via preparative HPLC[133] (RP-HPLC analytical gradients were run using a solvent system consisting of A (H_2O + 0.1% TFA) and B (CH_3CN + 0.1% TFA)). The conditions used to characterize pure peptides consisted of a linear gradient from 0% to 100% of B solution in 25 min.

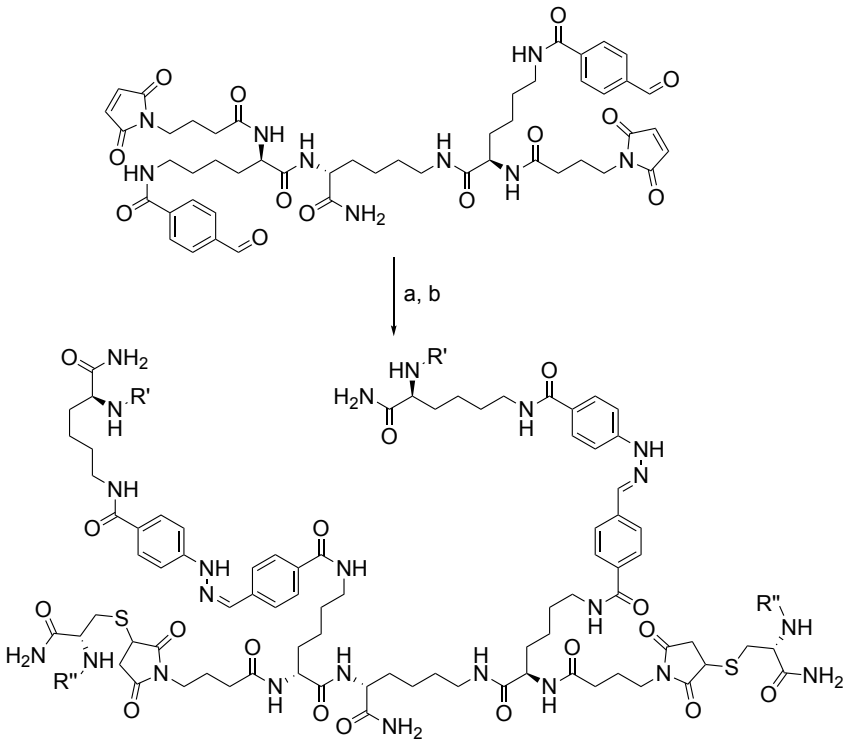

70a: R' = YaFGYPS; R'' = FGGFTGARKSARKLANQ
70b: R' = YaFGYPS(O2Oc)$_2$; R'' = FGGFTGARKSARKLANQ
70c: R' = Dmt-aFGYPS; R'' = FGGFTGARKSARKLANQ

a) [Cys$_{18}$]N/OFQ-NH$_2$, 5% NaHCO$_3$; DMF, r.t.

b) CH$_3$COOH; **69a-c**, DMF, r.t.

Scheme 55: Hetero tetrafunctionalization of H-PWT1 core in one pot reaction

6.3 Conclusions and pharmacological results

The final compounds were evaluated in calcium mobilization assays performed in CHO cells co-expressing either the recombinant human MOP or NOP receptors and the chimeric $G\alpha_{qi5}$ protein. The NOP and MOP potencies of the investigated compounds were expressed as pEC_{50} and compared to those of the respective parent monomer and the homotetrabranched derivatives investigated under the same experimental conditions.

	NOP		MOP		
	pEC_{50} ($CL_{95\%}$)	$\alpha \pm$ SEM	pEC_{50} ($CL_{95\%}$)	$\alpha \pm$ SEM	NOP/MOP
Linear Peptide Monomers					
N/OFQ	9.52 (8.97−10.06)	1	<6		>1000
dermorphin	<6		8.09 (7.44−8.74)	1	<0.01
dermorphin$(O2Oc)_2NH_2$	<6		7.74 (7.21−8.27)	0.94 ± 0.06	<0.1
[Dmt^1]dermorphin	<6		8.76 (8.42−9.10)	0.91 ± 0.07	<0.01
Homotetrameric PWT1 Derivatives					
PWT1-N/OFQ	8.44 (8.13−8.75)	1.08 ± 1.07	<6		>100
PWT1- dermorphin	<6		7.53 (7.23−7.84)	0.88 ± 0.05	<0.1
PWT1-dermorphin$(O2Oc)_2$	<6		7.34 (6.81−7.88)	0.80 ± 0.08	<0.1
PWT1-[Dmt^1]dermorphin	<6		9.64 (9.20−10.08)	1.04 ± 0.06	<0.001
Heterotetrameric H-PWT1 Derivatives					
H-PWT1-N/OFQ-dermorphin **(70a)**	8.09 (7.98−8.20)	0.99 ± 0.04	7.13 (6.90−7.37)	0.93 ± 0.03	0.11
H-PWT1-N/OFQ-dermorphin$(O2Oc)_2$ **(70b)**	8.21 (8.03−8.40)	1.09 ± 0.09	7.42 (7.25−7.59)	0.91 ± 0.03	0.16
H-PWT1-N/OFQ-[Dmt^1]dermorphin′ **(70c)**	8.35 (7.71−8.99)	0.88 ± 0.03	8.75 (8.32−9.19)	1.00 ± 0.04	2.5

Table 4: *In vitro* Ca^{2+} mobilization studies in CHO cells coexpressing either MOP or NOP receptors and the chimeric protein $G\alpha_{qi5}$[133]

The new heteromultimerization strategy did not compromise the pharmacological activity of the starting bioactive peptides, in line with what previously observed for most of PWT-based homotetramers. H-PWT1-N/OFQ-dermorphin (**70a**) displayed an interesting profile of mixed NOP/MOP full agonist, with 30-fold lower potency in activating the NOP receptor (pEC_{50} = 8.09) compared to that of N/OFQ. Likewise, **70a** was 10-fold less potent than dermorphin in stimulating the MOP receptor (pEC_{50} = 7.13). This would indicate that the H-PWT1-based assembling of the analysed bioactive sequences disfavours to some degree their interaction with the respective biological targets. The bifunctional profile of **70a** was considered suboptimal in view of the unbalanced NOP/MOP potency i.e. 10-fold higher potency for the NOP receptor. This prompted us to investigate suitable strategies for the structural modification of the dermorphin sequence with the aim to increase the MOP potency of the resulting heterotetrabranched derivatives. Firstly, we designed compound **70b** (H-PWT1-N/OFQ-dermorphin$(O2Oc)_2$) in which the MOP pharmacophore was spaced from the central PWT core through two polyoxyethylene units. We speculated about the possibility that a flexible linker of the proper length could facilitate the interaction of the message sequence of dermorphin with the binding pocket of the MOP receptor. Compared to **70a**, H-PWT1-N/OFQ-dermorphin$(O2Oc)_2$ displayed a substantial maintenance of NOP potency (pEC_{50} = 8.21) but only a marginal increase in MOP potency (pEC_{50} = 7.42). However, it has to be considered that the modification of the dermorphin sequence in the derivative dermorphin$(O2Oc)_2$-NH_2 resulted per se slightly detrimental for MOP potency. Thus, in the case of **70b** the H-PWT1-derivatization of the dermorphin component did not significantly affect the MOP potency of the linear precursor. This was also confirmed in the homotetrameric derivative PWT1-dermorphin$(O2Oc)_2$ displaying similar potency as PWT1-dermorphin.

In the last derivative, H-PWT1-N/OFQ-[Dmt^1]dermorphin (**70c**), the dermorphin component was directly linked to the core but modified at the *N*-terminal portion where the Tyr^1 residue was replaced with a 2,6-dimethyl tyrosine. The corresponding linear precursor [Dmt^1]dermorphin was shown to be 5-fold more potent than the native peptide analogue (pEC_{50} = 8.76) confirming the important effect of this chemical modification in promoting the interaction of opioid peptide ligands with the MOP receptor.

Of relevance for the aim of this work, the introduction of a Dmt^1 residue had also a positive impact on the pharmacological profile of compound **70c**. Indeed, the MOP potency of H-PWT1-N/OFQ-[Dmt^1]dermorphin was significantly incremented in comparison with **70a** and **70b** to such an extent that the NOP/MOP potency ratio was reversed (NOP pEC_{50} = 8.35, MOP pEC_{50} = 8.75). Thus, H-PWT1-N/OFQ-[Dmt^1]dermorphin exhibited a profile of dual acting full agonist with high and balanced potencies for NOP and MOP receptors.

This was also confirmed through Dynamic Mass Redistribution (DMR) studies performed on CHO cells expressing the human MOP or NOP receptors (figure 15). DMR is a non-invasive assay that allows to evaluate the receptor-dependent holistic cellular responses following the interaction with a ligand.

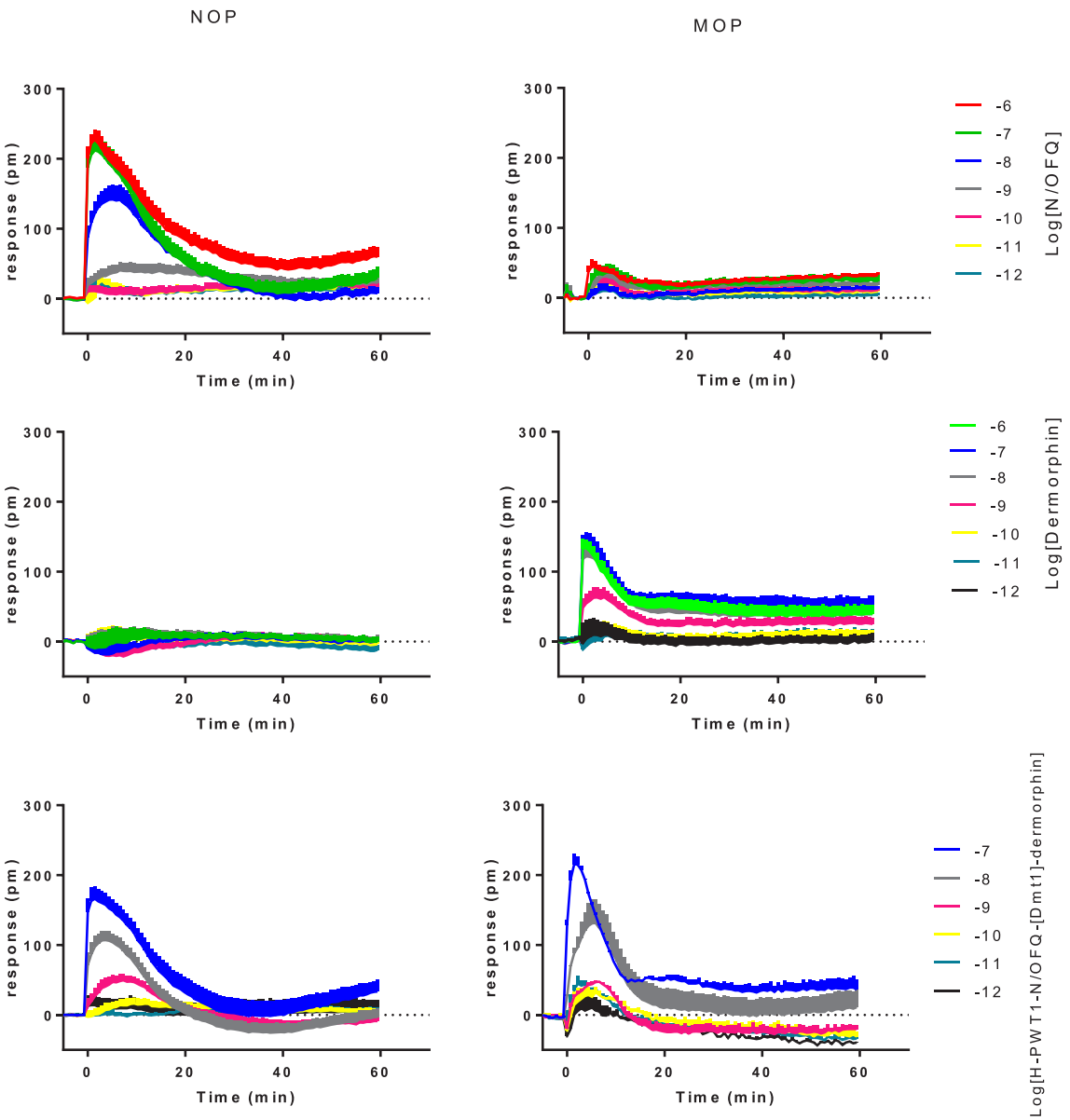

Figure 15: DMR studies on both MOP and NOP receptors[133]

In conclusion, it has been possible to identify a strategy for obtaining heterotetrabranched peptide derivatives through PWT methodology, which allowed us to synthesize some dual MOP/NOP full agonist derivatives. Compounds with this mixed profile could represent a possible therapeutic approach for the treatment of pain as non-addictive drugs.[40,134] It can be speculated that the developed compounds could exhibit improved pharmacokinetic properties, due to poor recognition and degradation by peptidases. Through this PWT synthetic strategy it was also possible to confirm the important role of Dmt: a single amino acid replacement could lead to important modification of the pharmacological behavior of a bioactive peptide.

Final Conclusions

To conclude, through this doctoral thesis it was possible to extend the knowledge about Pd-catalyzed C–H activation, specifically achieving some non-natural aromatic amino acids taking advantage of this modern and exciting topics. In detail, we were able to apply the Pd-catalyzed C(sp^2)–H activation on 4-NO_2-Phe, to obtain a small library of *p*-substituted Dmt-like derivatives, some of which were inserted in N/OFQ(1-13)-NH_2 peptide fragments, via SPPS. The resulting compounds were shown to exhibit interesting profiles on the basis of preliminary pharmacological evaluations.

In addition, it was possible to synthesize Mmt, the analogue of Dmt, characterized by only one *ortho* position functionalized via Pd-catalyzed C(sp^2)–H methylation, by controlling the insertion of the alkylating agent through an innovative regioselective synthetic route.

Moreover, a few derivatives of alkylated tyrosine derivatives were obtained via Pd-catalyzed β-C(sp^3)–H arylation of (*L*)-alanine derivatives, as opposed to δ-C(sp^2)–H methylation of (*L*)-Tyr derivatives. In particular, we managed to obtain 3,5-Dmt as well as the bis-arylated analogues of Tyr and of 3,5-Dmt, thus extending the current palette of methods allowing to access these targets.

The application of non-natural amino acids in SPPS, e.g. Dmt, was underlined by the encouraging results obtained by the insertion of these residues in opioid peptides. Particularly [$Dmt^{1,5}$]N/OFQ(1-13)-NH_2 has been identified as the most potent dual MOP/NOP agonist so far described in literature. In addition, an improvement of drug-likeness and stability was obtained through the application of PWT strategy, which represents an innovative and promising way for translating the advantageous properties of peptides in clinical use, as bivalent targeted clustered peptides.

7. Experimental Section

7.1 Chemicals and methods

Analytical RP-HPLC analyses were performed on a XBridge® C18 column (4.6 x 150 mm, 5 μm particle size) with a flow rate of 0.7 mL/min using a linear gradient of acetonitrile (0.1% TFA) in water (0.1% TFA) from 0% to 100% in 25 minutes. Retention times (Tr) from analytical RP-HPLC are reported in minutes. When necessary, compounds were purified on a reverse-phase Waters Prep 600 HPLC system equipped with a Jupiter column C18 (250 x 30 mm, 300 Å, 15 μm spherical particle size). Gradients used consisted of A (H_2O + 0.1% TFA) and B (40% H_2O in CH_3CN + 0.1% TFA) at a flow rate of 20 mL/min. UV detection wavelength for semi-preparative HPLC was 220 nm. For analytical controls Beckmann System Gold 168 HPLC have been used with LC column Kinetex 5μm EVO C18 100 A (250 X 4.6 mm) and a variable wavelength UV detector fixed to 220 nm. Analysis were conducted using two solution A and B containing, respectively, 100:0,1 H_2O:TFA and 40:60:0,1 of H_2O:CH_3CN:TFA with different gradients for the products. All final products showed a degree of purity >95% at 220 and 254 nm. The mass spectra were recorded with a MICROMASS ZMD 2000, after dissolution of compounds in a solution composed by 40:60:0,1 of H_2O:CH_3CN:TFA. High resolution mass spectrometry data were achieved using a ESI-Q-TOF 6520 instrument coupled with a nano HPLC with Chip Cube® technology (Agilent Tecnologies, USA). TLC were performed on pre-coated plates of silica gel F254 (Merck, Darmstadt, Germany). ^1H NMR and ^{13}C, DEPT NMR analysis were obtained at ambient temperature using a Varian 400 MHz spectrometer and were referenced to residual ^1H signals of the deuterated solvents respectively (δ ^1H 7.26 for $CDCl_3$, δ ^1H 2.50 for DMSO-d_6, δ ^1H 3.31, 4.87 for CD_3OD); the following abbreviations were used to describe the shape of the peaks: s: singlet; d: doublet; dd: double doublet; t: triplet; m: multiplet. Optical rotations were obtained on a Jasco P-2000 Polarimeter instrument with a path length of 1 dm (589 nm), and reported as follows: $[\alpha]_T^D$ (c = g/100 mL, solvent). Column chromatography was performed using Isolera One (Biotage Sweden) or traditional column chromatography with silica gel 60 (40-63 um). Melting point was measured with a Reichert Termovar (Austria). The infrared analyses were performed with a spectroscopy FT-IR spectrum 100 (Perkin Elmer Inc., Waltham, Massachusetts, USA). Hydrogenation reaction in AcOEt was performed under continuous-flow conditions in an H-Cube Pro™ setup (Thalesnano, Hungary) equipped with a module for automatic control of operational parameters (reaction temperature in °C and pressure in bar, flow rates of liquid feed in

mL/min and hydrogen). Reactions with microwave assistance were performed using a Biotage Initiator TM 2.0 apparatus (Biotage Sweden).

7.2 Synthesis of *para*-substituted 2,6-Dmt-like amino acids

Synthesis of *(S)-methyl-3-(4-fluorophenyl)-2-(picolinamido)propanoate* (**2**):

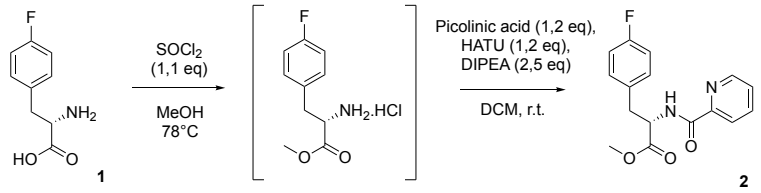

To a solution of 4-fluoro-*L*-phenylalanine (2.28 mmol, 0.500 g) in anhydrous MeOH (20 mL) was added $SOCl_2$ (2.50 mmol, 0.182 mL) in a dropwise manner. The reaction mixture was heated at reflux overnight. The volatile substances were removed under vacuum to give the crude methyl-4-fluoro-phenylalanine hydrochloride, which was washed with 10 mL of saturated sodium bicarbonate aqueous solution (to pH ~ 8) and extracted with DCM. The organic layers were combined and evaporated under vacuum to give the corresponding ester as white solid, which was used directly for the next step.

A mixture of the previous crude amino product, picolinic acid (2.70 mmol, 0.333 g), HATU (2.70 mmol, 1.02 g) and DIPEA (5.64 mmol, 0.98 mL) in DCM (40 mL) was stirred at room temperature overnight. The reaction was monitored through TLC and mass spectrometry, once completed it was quenched with a saturated NH_4Cl aqueous solution and the two layers were separated. The aqueous layer was extracted with DCM (3 times), and the organic layers were combined, dried over Na_2SO_4, filtered and concentrated in vacuum. The residue was purified by flash chromatography (1:1 petroleum ether/AcOEt) to afford compound **2** (0.618 g) as a white oil.

Compound **2**:

Yield: 91% overall

HRMS m/z: $[M+H]^+$ calcd for $C_{16}H_{16}N_2O_3F$ 303.1139; found 303.1137.

$[\alpha]_D^{22}$ = -37.22 (c=0.039, MeOH).

IR 3384, 1740, 1673, 1506, 1218 cm^{-1}.

^{1}H NMR (400 MHz, $CDCl_3$) δ 8.56 (ddt, J = 4.8, 1.8, 0.9 Hz, 1H), 8.48 (d, J = 8.4 Hz, 1H), 8.15 (dt, J = 7.8, 1.1 Hz, 1H), 7.84 (td, J = 7.7, 1.7 Hz, 1H), 7.43 (ddd, J = 7.6, 4.8, 1.2 Hz, 1H), 7.18 – 7.10 (m, 2H), 6.96 (dd, J = 9.2, 8.3 Hz, 2H), 5.05 (dt, J = 8.4, 6.1 Hz, 1H), 3.73 (d, J = 0.9 Hz, 3H), 3.25 (dd, J = 13.9, 7.2 Hz, 1H), 3.17 (dd, J = 13.9, 7.2 Hz, 1H).

^{13}C NMR (101 MHz, $CDCl_3$) δ 171.8, 164.1, 163.4, 160.9, 149.3, 148.4, 137.5, 131.9, 130.9, 126.6, 122.4, 115.7, 115.5, 53.6, 52.5, 37.6.

^{19}F NMR (376 MHz, $CDCl_3$) δ -115.8.

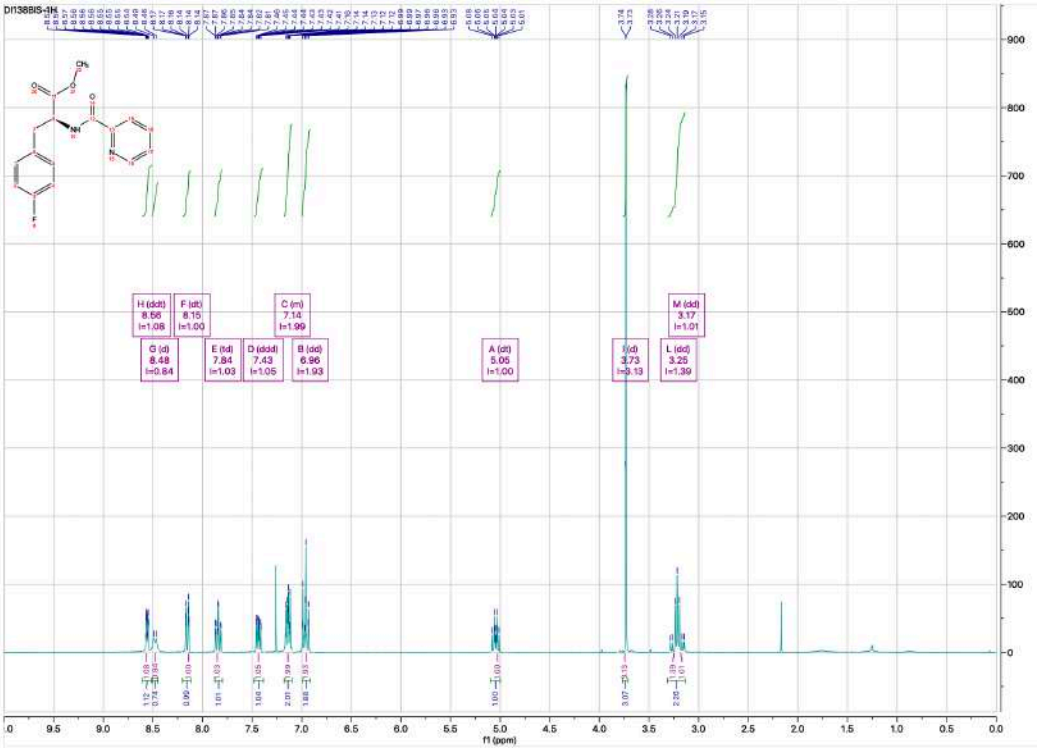

^{1}H NMR compound **2**

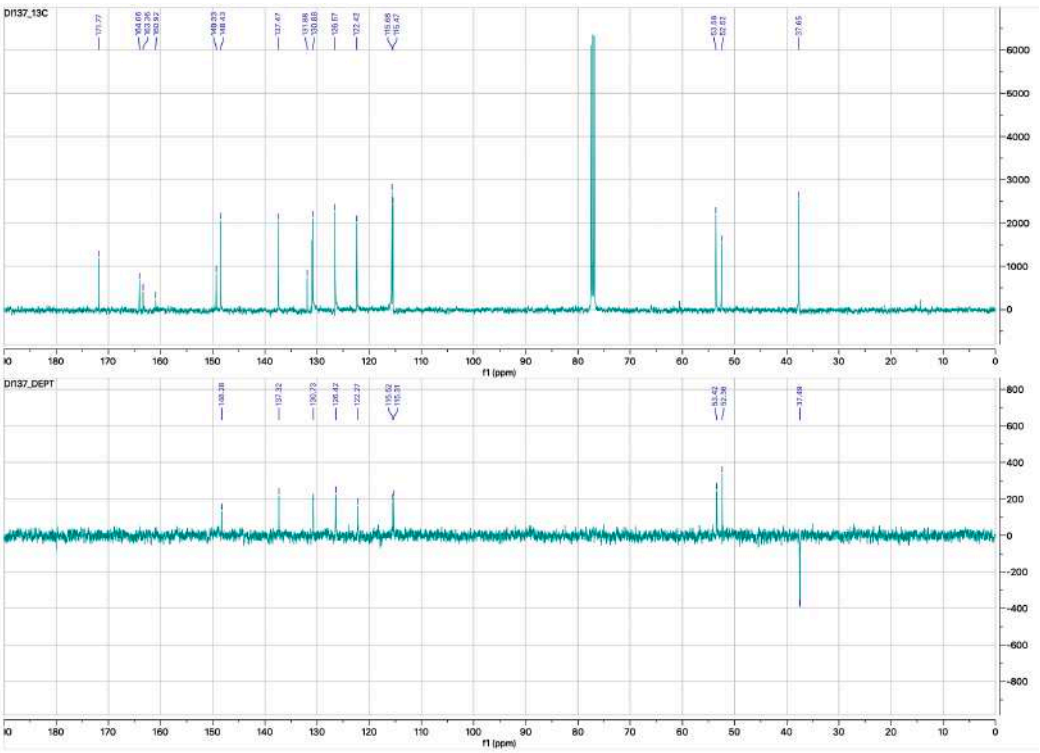

^{13}C and DEPT NMR compound **2**

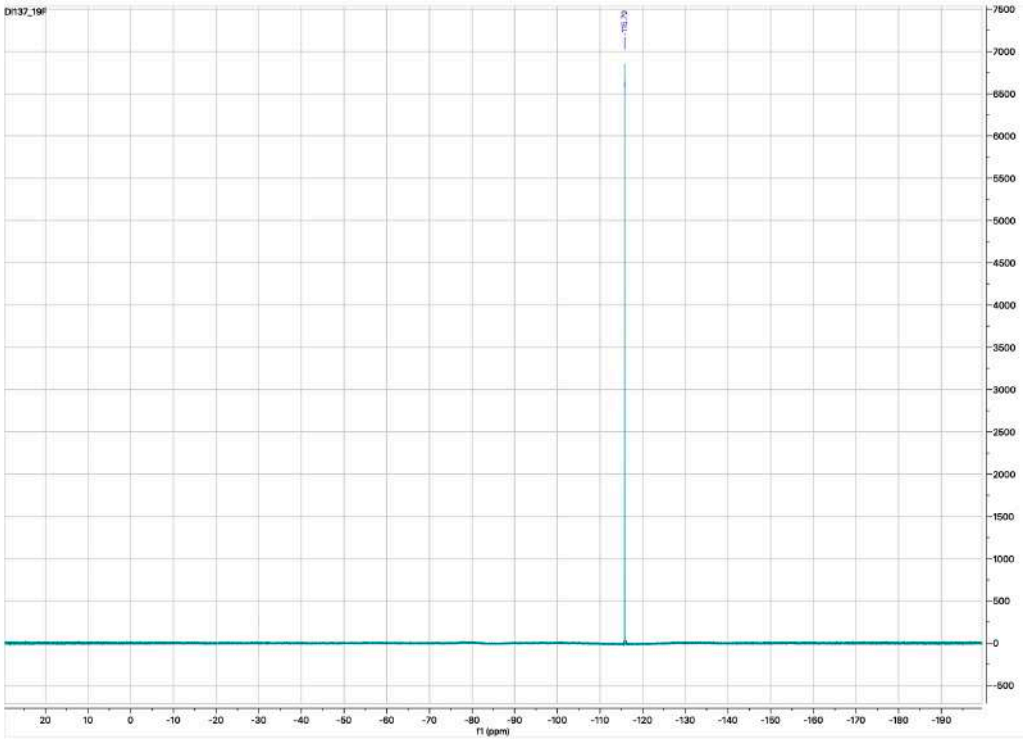

^{19}F NMR compound **2**

HRMS compound **2**

Synthesis of *(S)-methyl-3-(4-nitrophenyl)-2-(picolinamido)propanoate* (**4**):

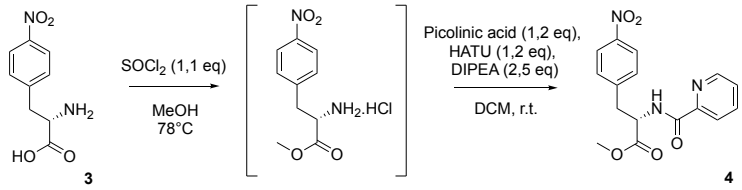

To a solution of 4-nitro-*L*-phenylalanine, **3** (23.81 mmol, 5.00 g) in anhydrous MeOH (100 mL) was added $SOCl_2$ (26.19 mmol, 1.91 mL) in a dropwise manner. The reaction mixture was heated at reflux overnight. The volatile substances were removed under vacuum to give the crude methyl-4-nitro-phenylalanine hydrochloride, which was washed with 30 mL of saturated sodium bicarbonate aqueous solution (to pH ~ 8) and extracted with DCM. The organic layers were combined and evaporated under vacuum to give the corresponding ester as yellowish solid (6.17 g, 99% yield), which was used directly for the next step.

A mixture of the previous crude amino product, picolinic acid (28.56 mmol, 3.51 g), HATU (28.56 mmol, 10.86 g) and DIPEA (59.52 mmol, 10.37 mL) in DCM (150 mL) was stirred at room temperature overnight. Then, the reaction was quenched with a saturated NH_4Cl aqueous solution and the two layers were separated. The aqueous layer was extracted with DCM, and the organic layers were combined, dried over Na_2SO_4, filtered and concentrated in vacuum. The residue was purified by flash chromatography (1:1 petroleum ether/AcOEt) to afford the compound **4** (7.12 g) as yellowish oil.

Compound **4**:

Yield: 91%

HRMS *m/z:* $[M+H]^+$ Calcd for $C_{16}H_{16}N_3O_5$ 330.1084; found 330.1087.

$[\alpha]_D^{23}$ = -23.14 (c=0.028, MeOH).

IR 3373, 1739, 1671, 1512, 1343 cm^{-1}.

^1H NMR (400 MHz, $CDCl_3$) δ 8.57 – 8.54 (m, 1H), 8.51 (d, J = 8.4 Hz, 1H), 8.22 – 8.03 (m, 3H), 7.85 (td, J = 7.7, 1.7 Hz, 1H), 7.49 – 7.41 (m, 1H), 7.35 (d, J = 8.7 Hz, 2H), 5.12 (dt, J = 8.4, 6.2 Hz, 1H), 3.76 (s, 3H), 3.41 (dd, J = 13.8, 5.8 Hz, 1H), 3.30 (dd, J = 13.8, 6.5 Hz, 1H).

^{13}C NMR (101 MHz, $CDCl_3$) δ 171.3, 164.1, 148.4, 144.1, 137.7, 130.4, 126.8, 123.9, 122.6, 53.2, 52.8, 38.2.

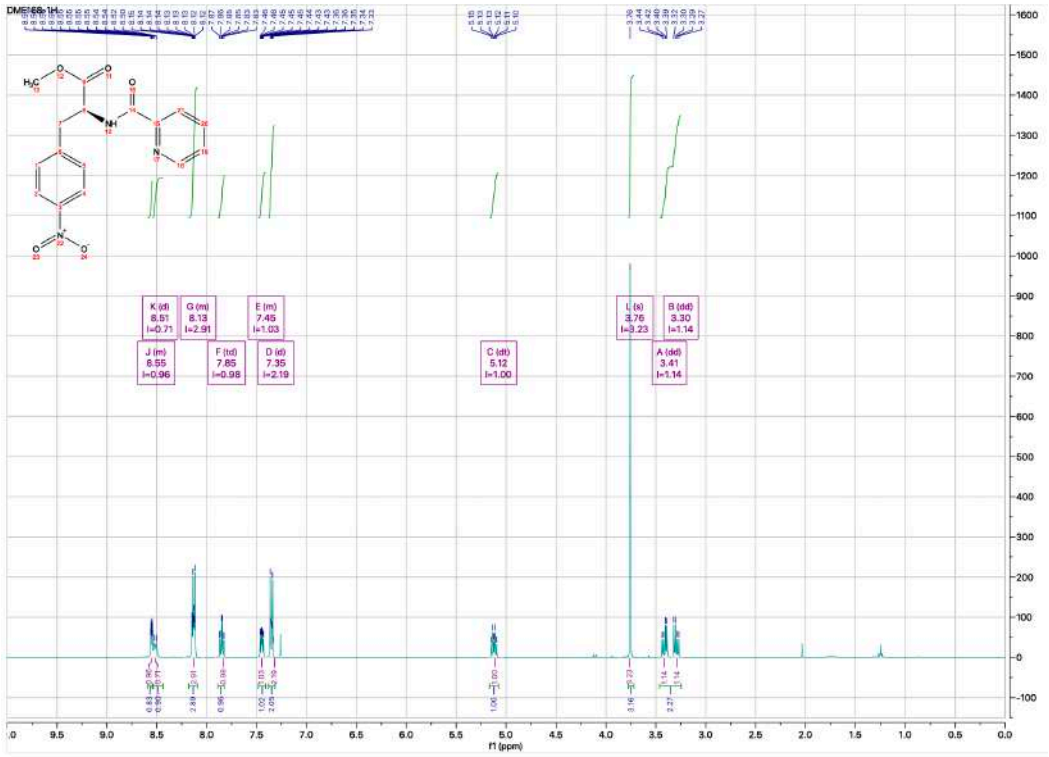

^1H NMR compound **4**

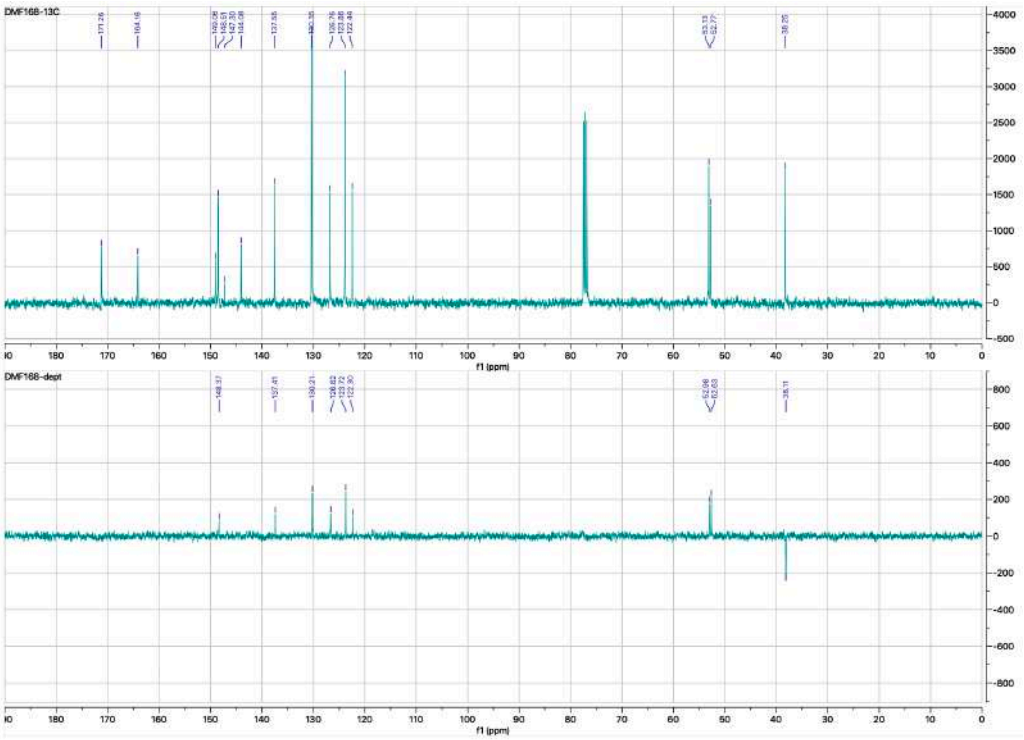

^{13}C and DEPT NMR compound **4**

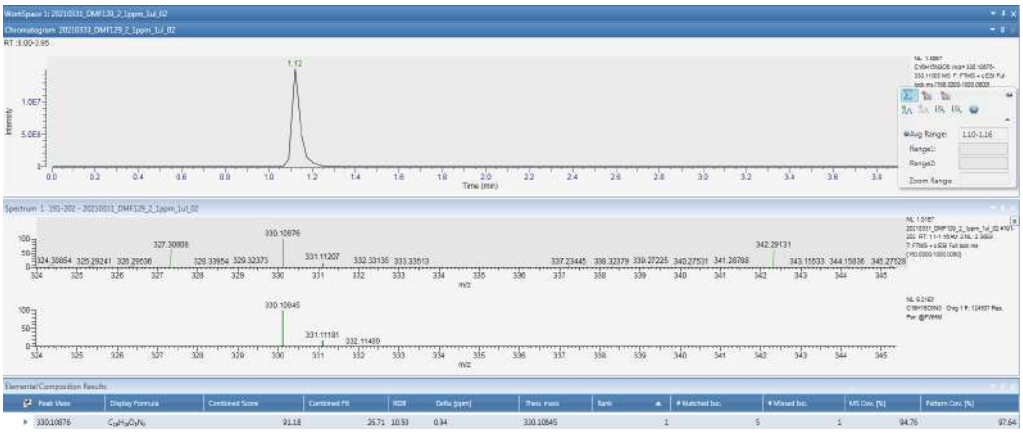

HRMS compound **4**

Synthesis of *(S)-methyl-3-(4-aminophenyl)-2-(picolinamido)propanoate* (**5**):

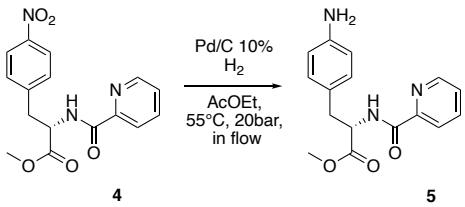

The compound **4** was dissolved in AcOEt (150 mL, 0.15 M) and set up in continuous-flow hydrogenator reactor H-Cube Pro Thales-Nano at 55 °C, 20 bar, in 0.3 mL/min flow, with Pd/C (10 mol%) as catalyst. When the reaction was completed, monitored via mass

spectrometry, the solvent was concentrated in vacuum to obtain the crude product **5** (6.70 g) as red-orange oil.

Compound **5**:

Yield: 97%

HRMS *m/z:* $[M+H]^+$ Calcd for $C_{16}H_{18}N_3O_3$ 300.1342; found 300.1341.

$[\alpha]_D^{22}$ = +3.98 (c=0.034, MeOH).

IR 3350, 1734, 1668, 1516, 831 cm^{-1}.

^1H NMR (400 MHz, DMSO-d6) δ 8.79 – 8.55 (m, 2H), 8.07 – 7.89 (m, 2H), 7.67 – 7.51 (m, 1H), 6.83 (d, J = 8.4 Hz, 2H), 6.45 (d, J = 8.4 Hz, 2H), 4.90 (s, 2H), 4.68 (ddd, J = 8.1, 7.1, 6.0 Hz, 1H), 3.65 (s, 3H), 3.05 – 2.92 (m, 2H).

^{13}C NMR (101 MHz, DMSO-d6) δ 171.8, 163.6, 149.1, 148.7, 147.3, 138.0, 129.6, 127.0, 123.5, 122.0, 114.0, 53.8, 52.1, 35.9.

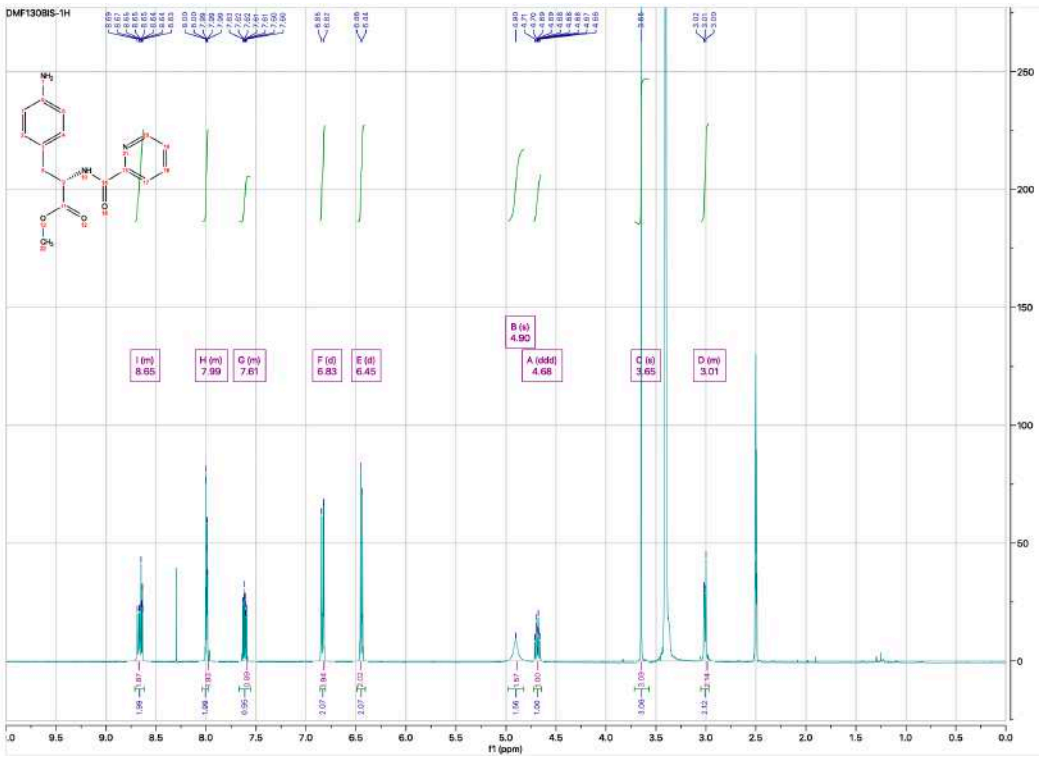

^1H NMR compound **5**

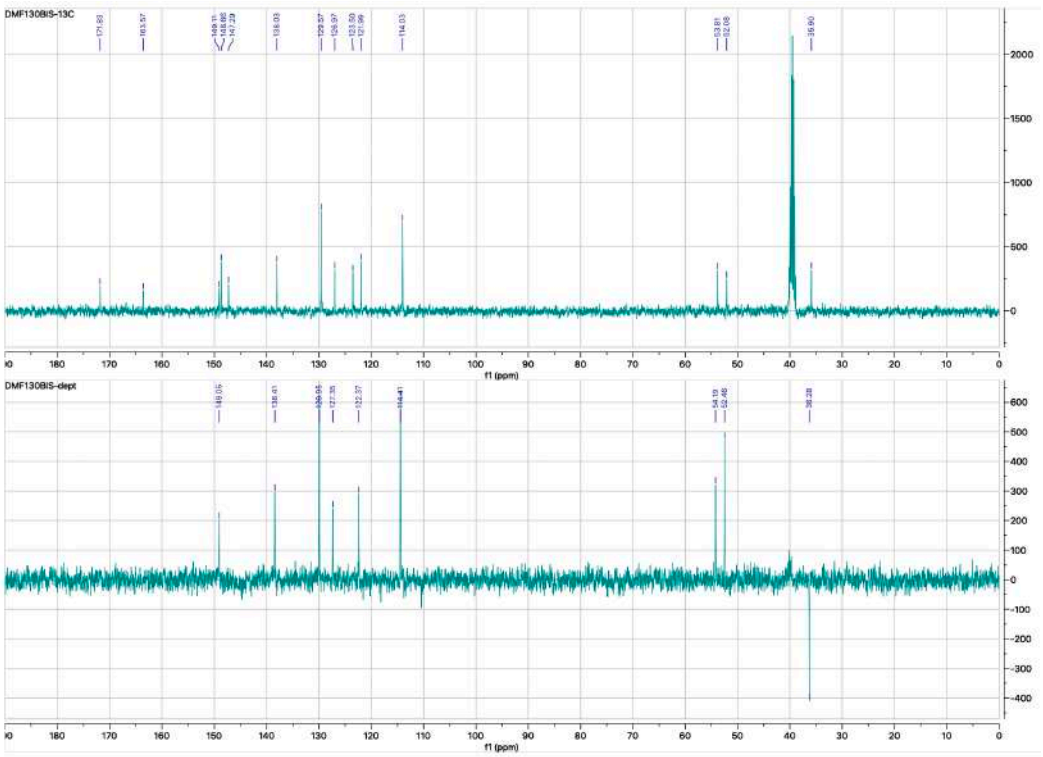

^{13}C NMR compound **5**

HRMS compounds **5**

Synthesis of *(S)-methyl-3-(4-((tert-butoxycarbonyl)amino)phenyl)-2-(picolinamido)propanoate* **(6):**

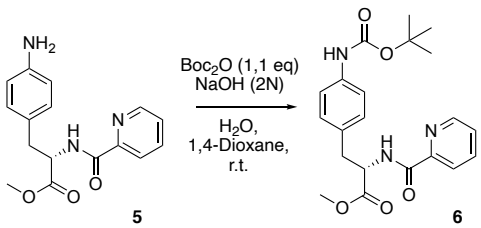

The compound **5** (1.13 mmol, 0.340 g) was solubilized in water/dioxane (1:2) solution (6 mL). The mixture was basified with NaOH 2N aqueous solution until pH 10/11 at 0 °C. Boc_2O (1.25 mmol, 0.273 g) was added and the reaction was left stirring at r.t. for 12 hours. The completion of the reaction was monitored per ESI mass spectrometry and TLC. The dioxane was removed under vacuum and HCl 1N aqueous solution was added at 0 °C to reach pH 1. The mixture was extracted with AcOEt (3 times) and the combined organic phases were dried over Na_2SO_4 and concentrated under vacuum. The crude was purified by flash chromatography (1:1 AcOEt/petroleum ether/1% acetic acid) and crystallized with 2:1 Et_2O/petroleum ether to obtain the compound **6** as a white solid (0.340 g).

Compound **6**:

Yield: 75%

HRMS *m/z:* $[M+H]^+$ Calcd for $C_{21}H_{26}N_3O_5$ 400.1867; found 400.1866.

$[\alpha]_D^{23}$ = +5.255 (c=0.0355, MeOH).

IR 3315, 1721, 1667, 1515, 1155 cm^{-1}.

MP 65-67 °C.

^1H NMR (400 MHz, $CDCl_3$) δ 8.55 (ddd, *J* = 4.8, 1.7, 0.9 Hz, 1H), 8.48 (d, *J* = 8.4 Hz, 1H), 8.15 (dt, *J* = 7.8, 1.1 Hz, 1H), 7.83 (td, *J* = 7.7, 1.7 Hz, 1H), 7.43 (ddd, *J* = 7.6, 4.8, 1.2 Hz, 1H), 7.27 (d, *J* = 8.3 Hz, 2H), 7.09 (d, *J* = 8.5 Hz, 2H), 6.47 (s, 1H), 5.03 (dt, *J* = 8.4, 6.0 Hz, 1H), 3.72 (s, 3H), 3.24 – 3.13 (m, 2H), 1.50 (s, 9H).

^{13}C NMR (101 MHz, $CDCl_3$) δ 171.9, 164.0, 152.9, 149.4, 148.4, 137.5, 130.7, 130.0, 126.5, 122.4, 118.7, 80.6, 53.7, 52.5, 37.7, 28.5, 27.6.

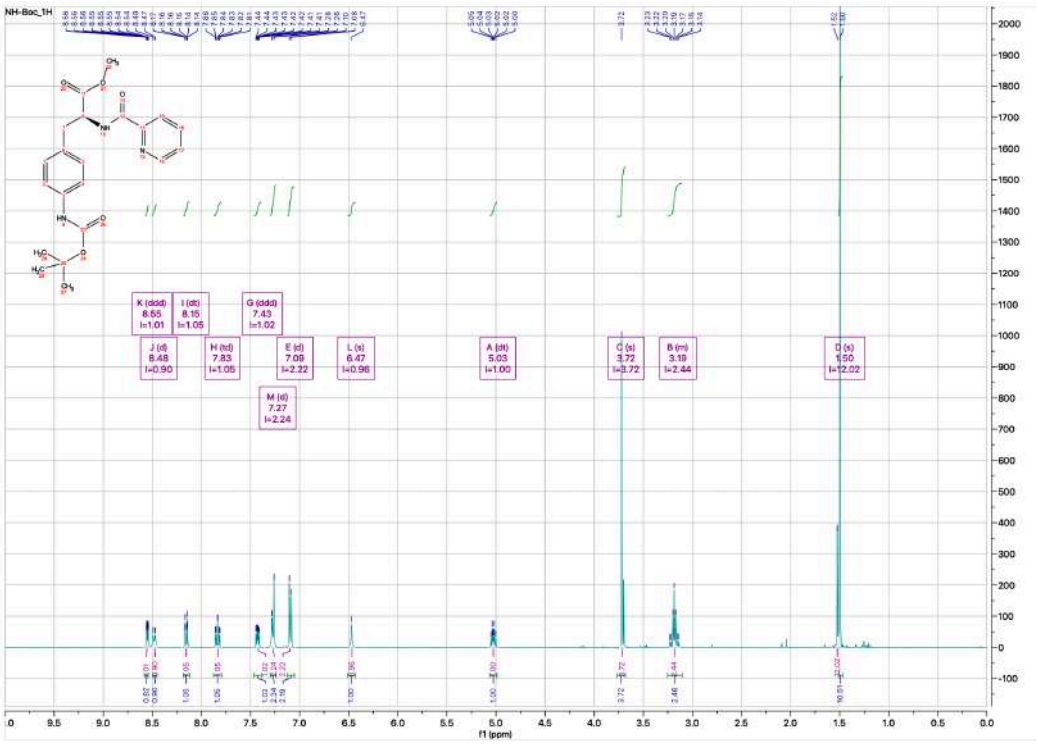

^{1}H NMR compound **6**

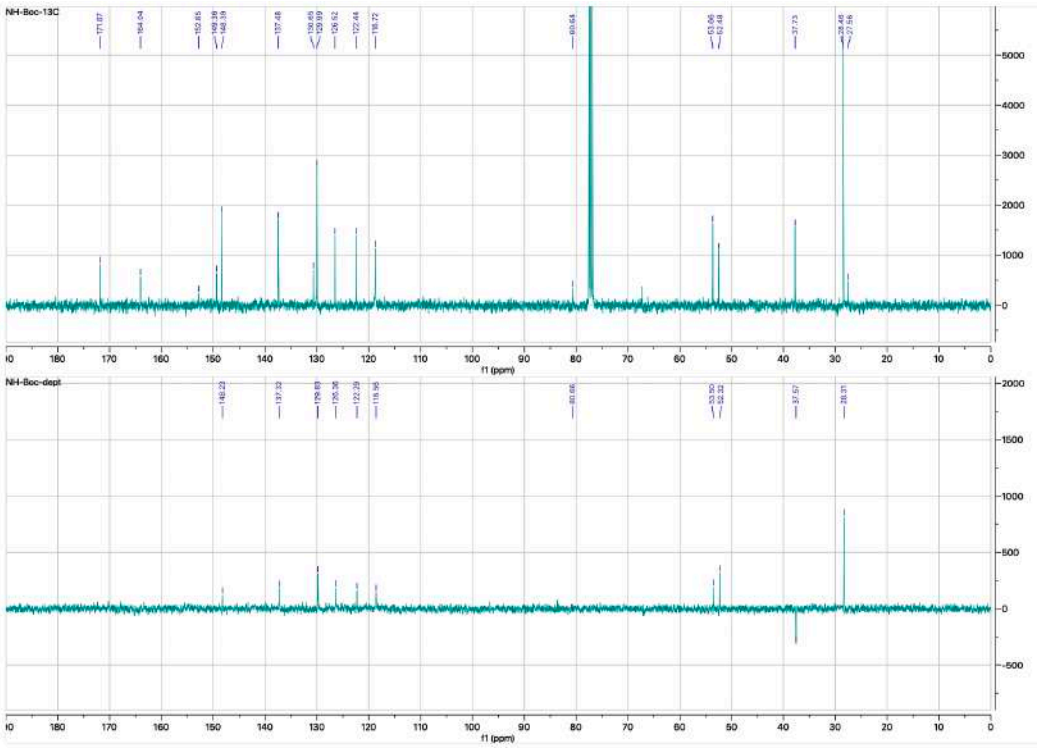

^{13}C and DEPT NMR compound **6**

HRMS compound **6**

Synthesis of *(S)-methyl-3-(4-(dibenzylamino)phenyl)-2-(picolinamido)propanoate* (**7**):

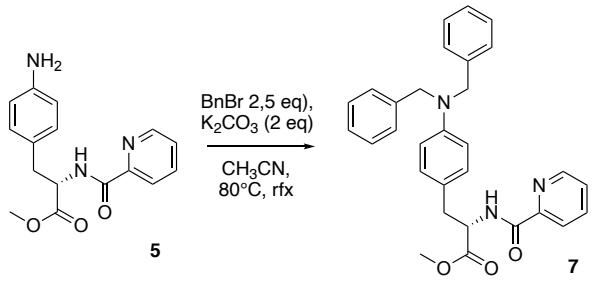

To a solution of the aniline derivative **5** (22.40 mmol, 7.32 g) in CH_3CN (150 mL) was added benzyl bromide (56.02 mmol, 6.66 mL) and potassium carbonate (44.81 mmol, 6.19 g). The mixture was stirred at 120 °C overnight. The crude mixture was purified by flash chromatography (2:3 AcOEt/petroleum ether) to afford **7** as an orange yellowish solid (8.76 g).

Compound **7**:

Yield: 82%

HRMS *m/z:* $[M+H]^+$ calcd for $C_{30}H_{30}N_3O_3$ 480.2281; found 480.2288.

$[\alpha]_D^{23}$ = -4.095 (c=0.0155, MeOH).

IR 3374, 1725, 1665, 1516, 837, 737 cm^{-1}.

MP 104-106 °C.

^1H NMR (400 MHz, $CDCl_3$) δ 8.54 (ddd, *J* = 4.8, 1.7, 0.9 Hz, 1H), 8.46 (d, *J* = 8.3 Hz, 1H), 8.15 (dt, *J* = 7.8, 1.1 Hz, 1H), 7.83 (td, *J* = 7.7, 1.7 Hz, 1H), 7.41 (ddd, *J* = 7.6, 4.8, 1.3 Hz, 1H), 7.35 – 7.28 (m, 4H), 7.27 – 7.20 (m, 6H), 6.98 (d, *J* = 8.7 Hz, 2H), 6.67 (d, *J* = 8.4 Hz, 2H), 4.97 (dt, *J* = 8.3, 6.0 Hz, 1H), 4.61 (s, 4H), 3.70 (s, 3H), 3.17 – 3.05 (m, 2H).

^{13}C NMR (101 MHz, $CDCl_3$) δ 171.9, 164.1, 149.5, 148.4, 137.4, 130.3, 130.1, 128.9, 128.8, 128.3, 127.9, 127.6, 127.1, 126.5, 122.4, 56.1, 53.7, 52.4, 37.5.

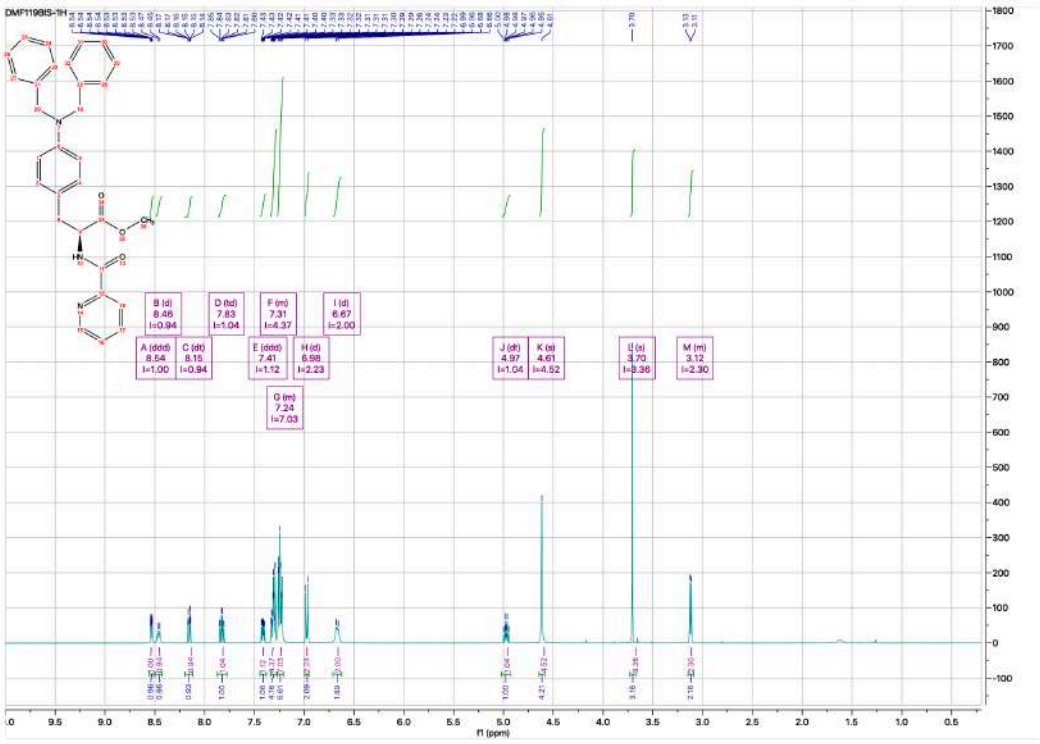

^{1}H NMR compound **7**

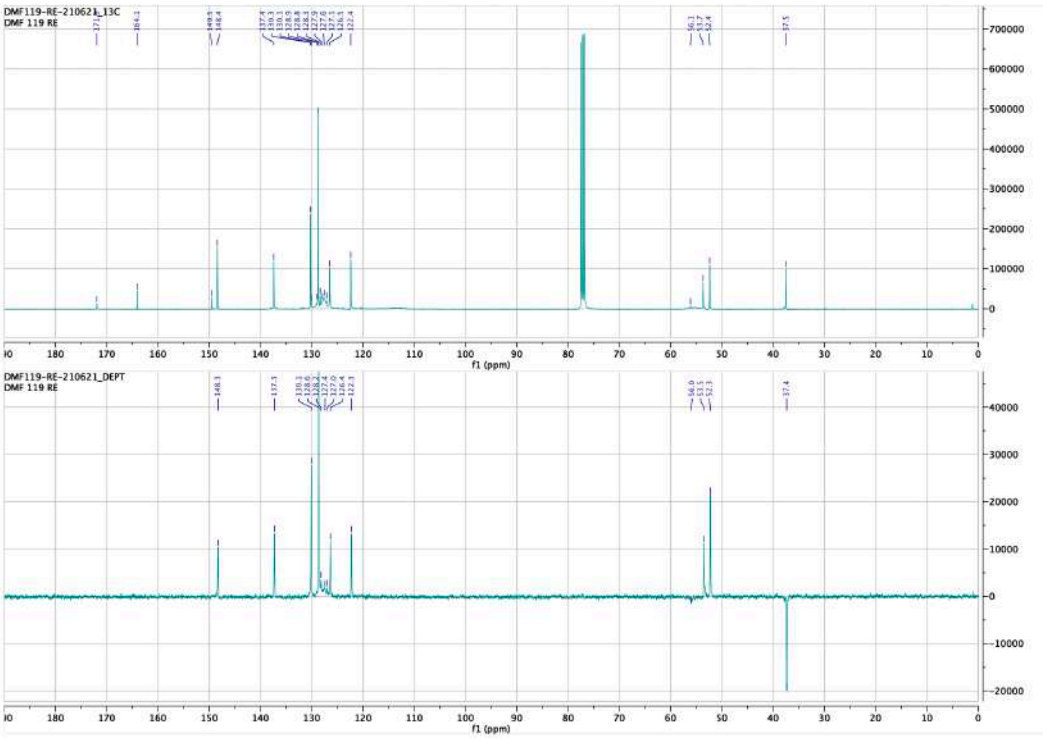

^{13}C and DEPT NMR compound **7**

HRMS compound **7**

Synthesis of *(S)-methyl-3-(4-(dibenzylamino)-2,6-dimethylphenyl)-2-(picolinamido)propanoate (**8**)*:

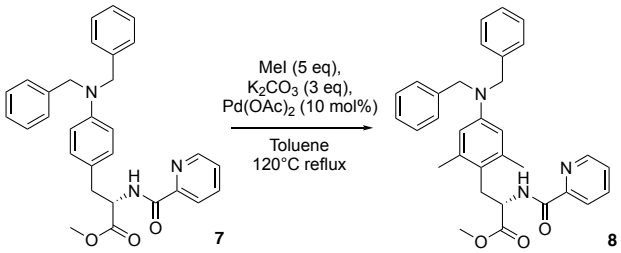

To a solution of compound **7** (18.30 mmol, 9.28 g) in toluene (150 mL) were added K_2CO_3 (54.86 mmol, 7.5 g), CH_3I (91.53 mmol, 5.69 mL), and $Pd(OAc)_2$ (1.83 mmol, 0.41 g). The mixture was stirred at 120 °C overnight. After 24 hours the reaction was cooled to r.t. and filtered through celite pad, washed with AcOEt (50 mL). The filtrate was concentrated under vacuum to obtain the crude product, which was then use for other two catalytic reaction at same conditions. The final crude product was purified by flash chromatography (3:7 AcOEt/petroleum ether), to afford **8** (6.76 g) as a yellowish solid.

Compound **8**:

Yield: 72%

HRMS *m/z:* $[M+H]^+$ calcd for $C_{32}H_{34}N_3O_3$ 508.2594; found 508.2597.

$[\alpha]_D^{22}$ = -8.82 (c=0.0085, MeOH).

IR 3384, 1738, 1676, 1602, 1494, 731, 700 cm^{-1}.

MP 77-79 °C.

^{1}H NMR (400 MHz, $CDCl_3$) δ 8.56 (ddd, J = 4.7, 1.7, 0.9 Hz, 1H), 8.13 (d, J = 7.8 Hz, 1H), 7.83 (td, J = 7.7, 1.7 Hz, 1H), 7.42 (ddd, J = 7.6, 4.8, 1.3 Hz, 1H), 7.33 – 7.26 (m, 4H), 7.26 – 7.20 (m, 6H), 6.44 (s, 2H), 4.89 (m, J = 7.9 Hz, 1H), 4.57 (s, 4H), 3.66 (s, 3H), 3.19 – 3.02 (m, 2H), 2.29 (s, 6H).

^{13}C NMR (101 MHz, $CDCl_3$) δ 173.0, 164.1, 149.5, 148.4, 148.0, 138.9, 138.1, 137.4, 128.9, 128.7, 128.2, 126.9, 126.4, 122.3, 112.6, 53.8, 52.7, 52.4, 32.4, 20.8.

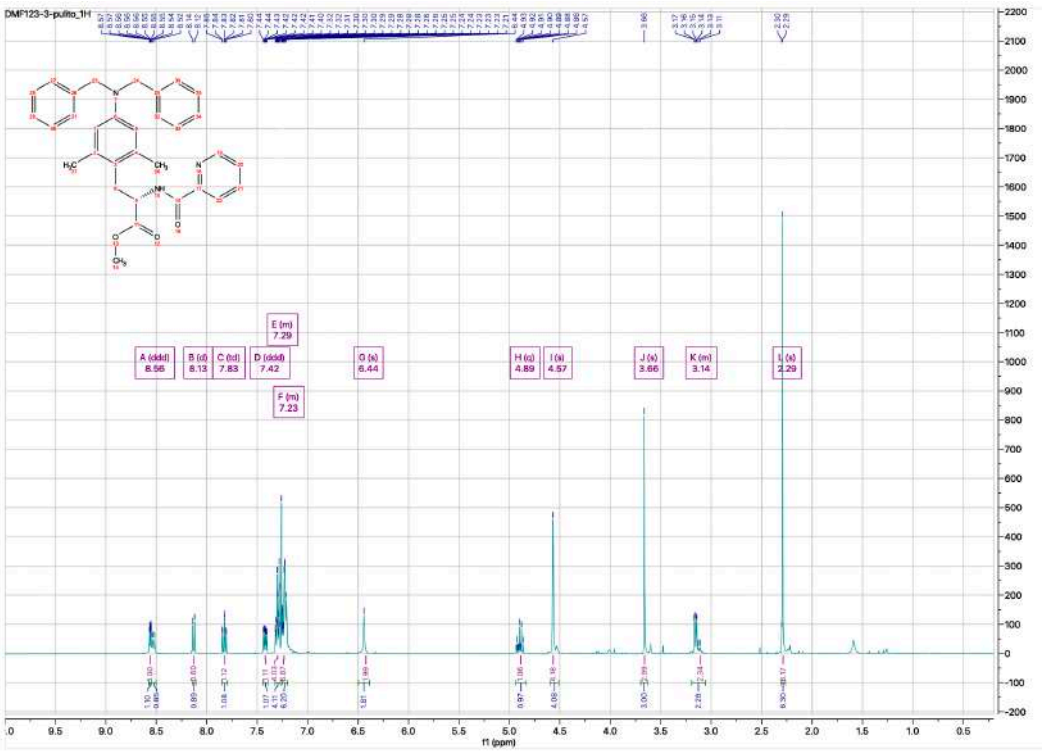

^{1}H NMR compound **8**

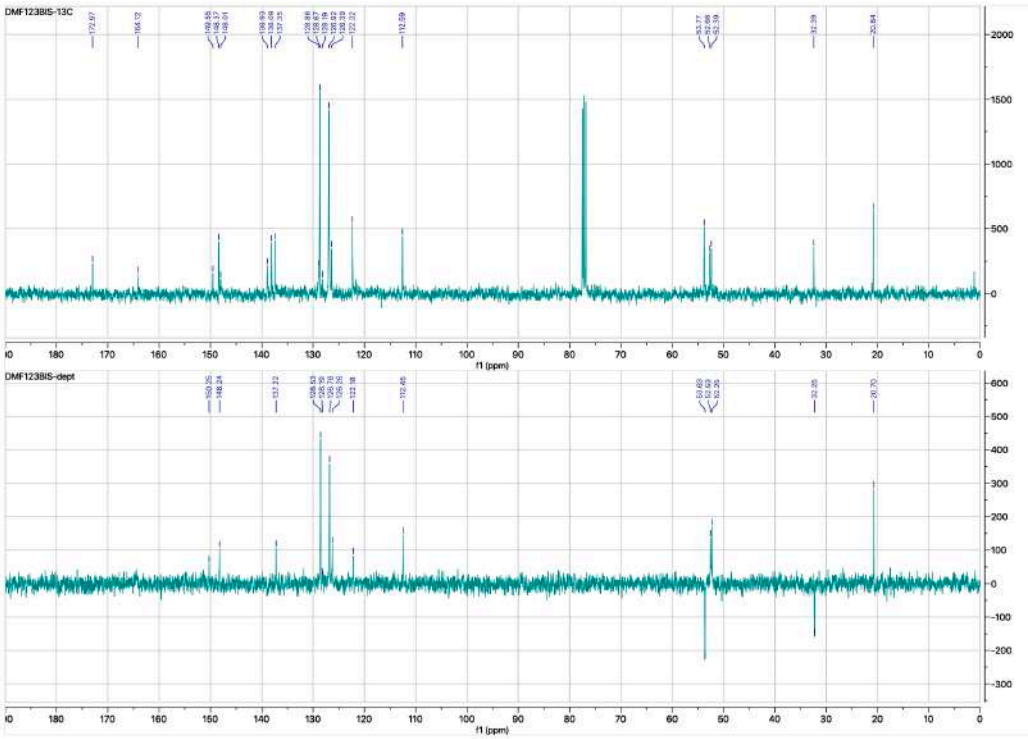

^{13}C and DEPT NMR compound **8**

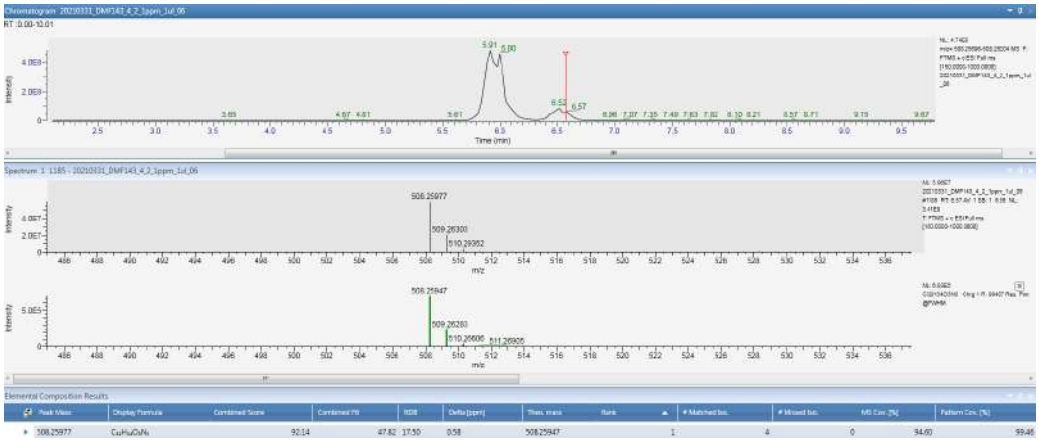

HRMS compound **8**

Synthesis of (*S)-methyl-3-(4-amino-2,6-dimethylphenyl)-2-(picolinamido)propanoate (**9**):*

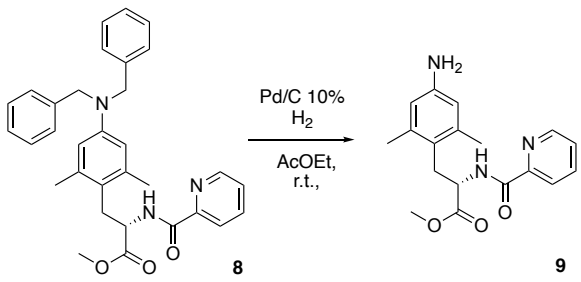

The compound **8** was dissolved in AcOEt (186 mL, 0.05 M) and set up in continuous-flow hydrogenator reactor H-Cube Pro Thales-Nano at 80 °C, 45 bar, flow 1 mL/min with Pd/C (10 mol%) as catalyst. When the reaction was completed, monitored via mass spectrometry,

the solvent was concentrated in vacuum to afford the crude product, which was purified by flash chromatography (1:1 AcOEt/petroleum ether) to obtain **9** (3.05 g) as a yellowish oil.

Compound **9**:

Yield: Quantitative

HRMS *m/z:* $[M+H]^+$ calcd for $C_{18}H_{22}N_3O_3$ 328.1655; found 328.1657.

$[\alpha]_D^{23}$ = -17.97 (c=0.011, MeOH).

IR 3360, 2952, 1734, 1670, 1511, 749 cm^{-1}.

^1H NMR (400 MHz, DMSO) δ 8.78 (d, *J* = 8.2 Hz, 1H), 8.67 (dt, *J* = 4.9, 1.2 Hz, 1H), 8.05 – 7.93 (m, 2H), 7.62 (tdd, *J* = 4.8, 2.5, 0.8 Hz, 1H), 6.19 (s, 2H), 4.72 (s, 2H), 4.61 (td, *J* = 8.4, 6.6 Hz, 1H), 3.61 (s, 3H), 3.19 – 2.03 (m, 2H), 2.14 (s, 6H).

^{13}C NMR (101 MHz, DMSO) δ 173.7, 165.6, 149.9, 149.3, 145.7, 139.4, 138.7, 128.5, 124.1, 123.3, 116.5, 53.6, 53.6, 31.5, 20.8.

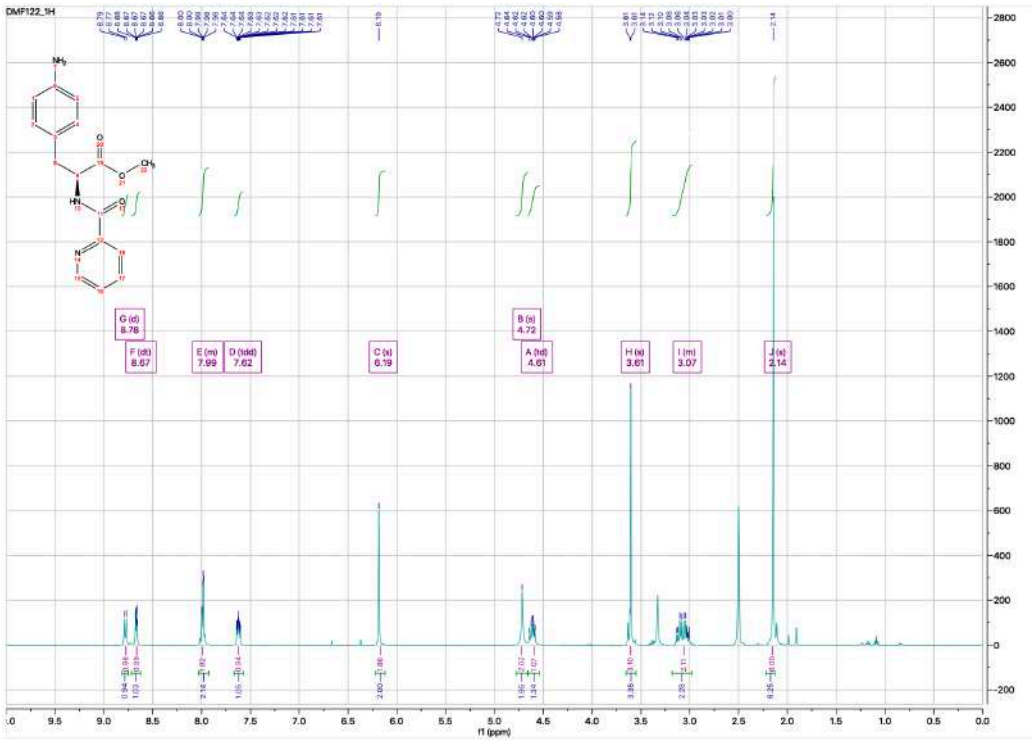

^1H NMR compound **9**

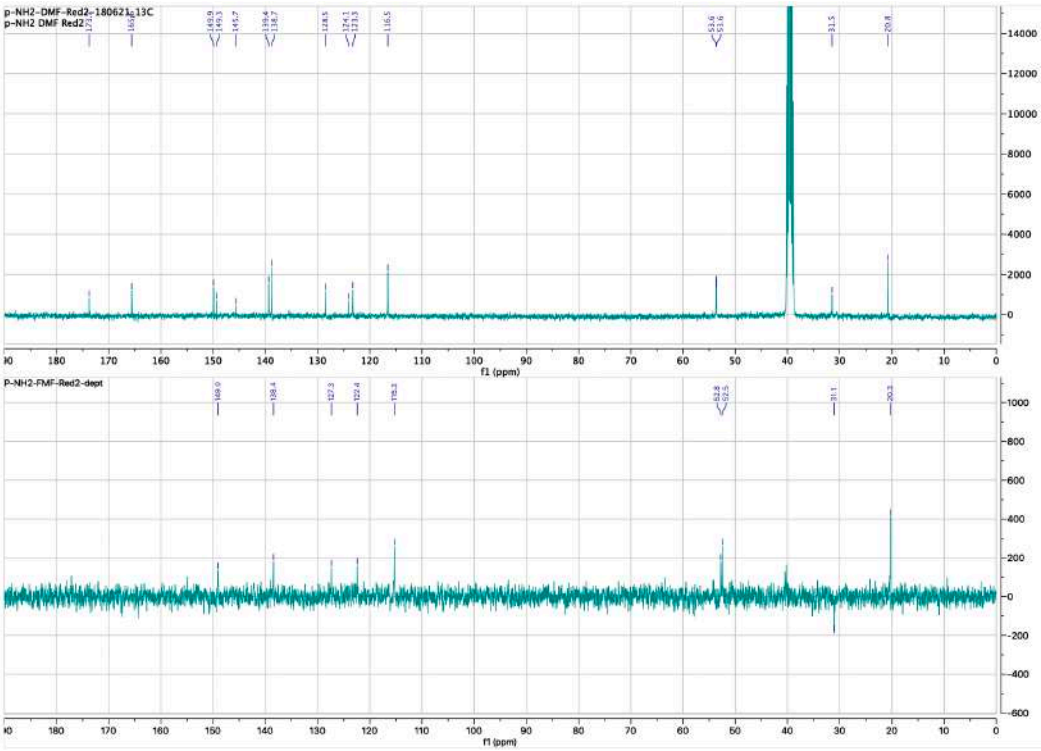

^{13}C and DEPT NMR compound **9**

HRMS compound **9**

Synthesis of *(S)-4-(3-methoxy-3-oxo-2-(picolinamido)propyl)-3,5-dimethylbenzenediazonium tetrafluoroborate (**10**):*

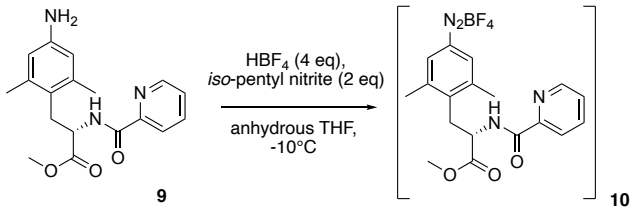

9 **10**

To a solution of compound **9** (2.41 mmol, 0.79 g) dissolved in anhydrous THF (15 mL), cooled to -10 °C, isoamyl nitrite (4.83 mmol, 0.643 mL) and HBF_4 (9.66 mmol, 1.31 mL) were added. The reaction was stirred for 4 hours at -10 °C and a yellow precipitate was formed, which was directly used as wet crude for the next step. An IR analysis and a diazocopulation assay were performed on the compound **10** with positive results. IR peaks referable to diazonium salt: 2274 cm^{-1}.

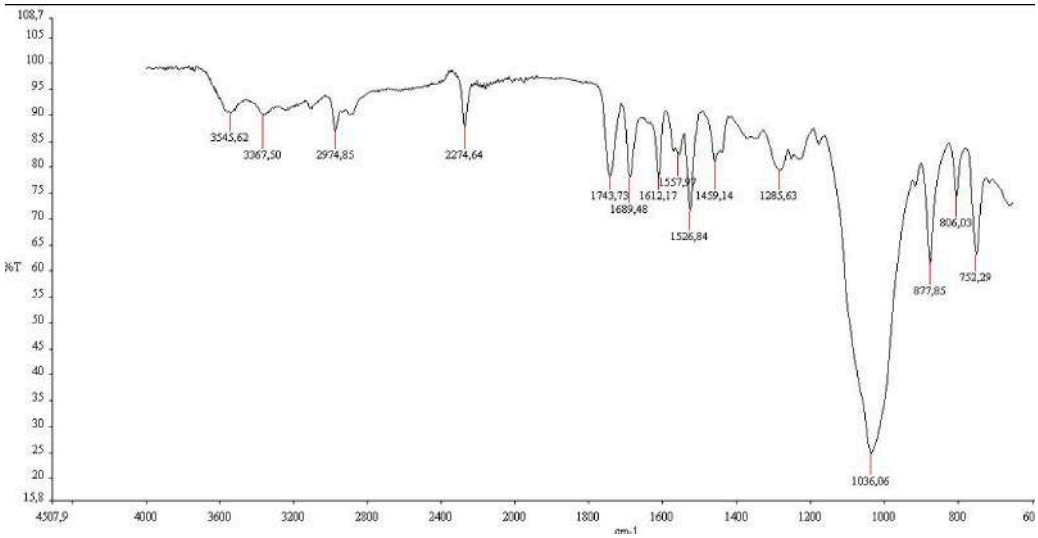

IR spectrum compound **10**

Synthesis of *(S)-methyl-3-(4-fluoro-2,6-dimethylphenyl)-2-(picolinamido)propanoate (**11**):*

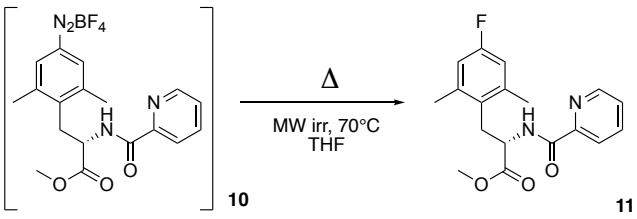

Compound **10** (2.41 mmol, 1.02 g) was used directly as crude dissolved in anhydrous THF (15 mL) in a sealed reaction vessel of 10-20 mL. The mixture was heated to 70 °C for 5 minutes under microwave irradiations. The resulting brown solution was evaporated under vacuum and the crude was solubilized in AcOEt, washed with H_2O and a saturated aqueous solution of $NaHCO_3$. The solvent of the organic phase was then removed under vacuum giving a crude product which was purified by flash chromatography (2:3 AcOEt/petroleum ether). The purified product **11** was obtained as white solid (0.556 g).

Compound **11**:

Yield: 70%

HRMS *m/z:* $[M+H]^+$ calcd $C_{18}H_{20}N_2O_3F$ 331.1452; found 331.1455.

$[\alpha]_D^{23}$ = -17.22 (c=0.01, MeOH).

IR 3365, 2956, 1731, 1658, 1514, 1018 cm^{-1}.

MP 117-119 °C.

^{1}H NMR (400 MHz, $CDCl_3$) δ 8.62 – 8.51 (m, 2H), 8.10 (dt, *J* = 7.8, 1.1 Hz, 1H), 7.83 (td, *J* = 7.7, 1.7 Hz, 1H), 7.43 (ddd, *J* = 7.6, 4.8, 1.3 Hz, 1H), 6.70 (d, *J* = 9.4 Hz, 2H), 5.04 – 4.92 (m, 1H), 3.68 (s, 3H), 3.25 – 3.15 (m, 2H), 2.39 (d, *J* = 0.6 Hz, 6H).

^{13}C NMR (101 MHz, $CDCl_3$) δ 172.6, 164.0, 161.3 (d, *J* = 244.2 Hz), 149.3, 148.4, 139.4 (d, *J* = 9Hz), 137.5, 129.0, 126.5, 122.4, 114.9 (d, *J* = 21Hz), 52.5, 52.0, 32.6, 20.5.

^{19}F NMR (376 MHz, $CDCl_3$) δ -117.20 (t, *J* = 9.4 Hz).

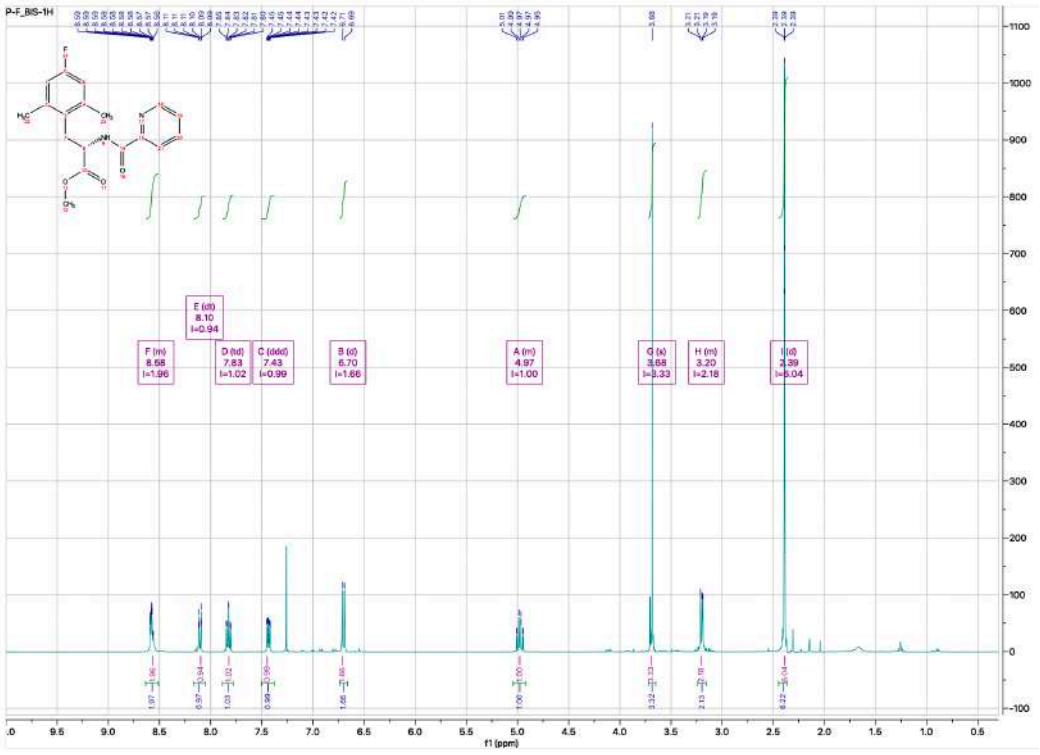

^{1}H NMR compound **11**

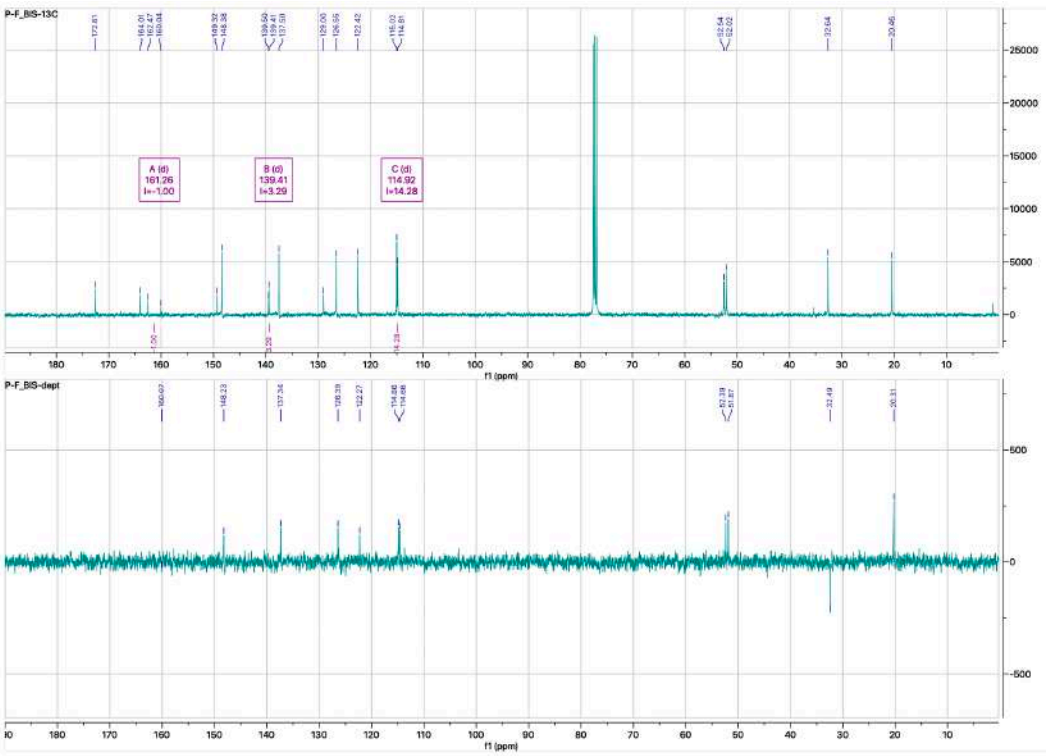

^{13}C and DEPT NMR compound **11**

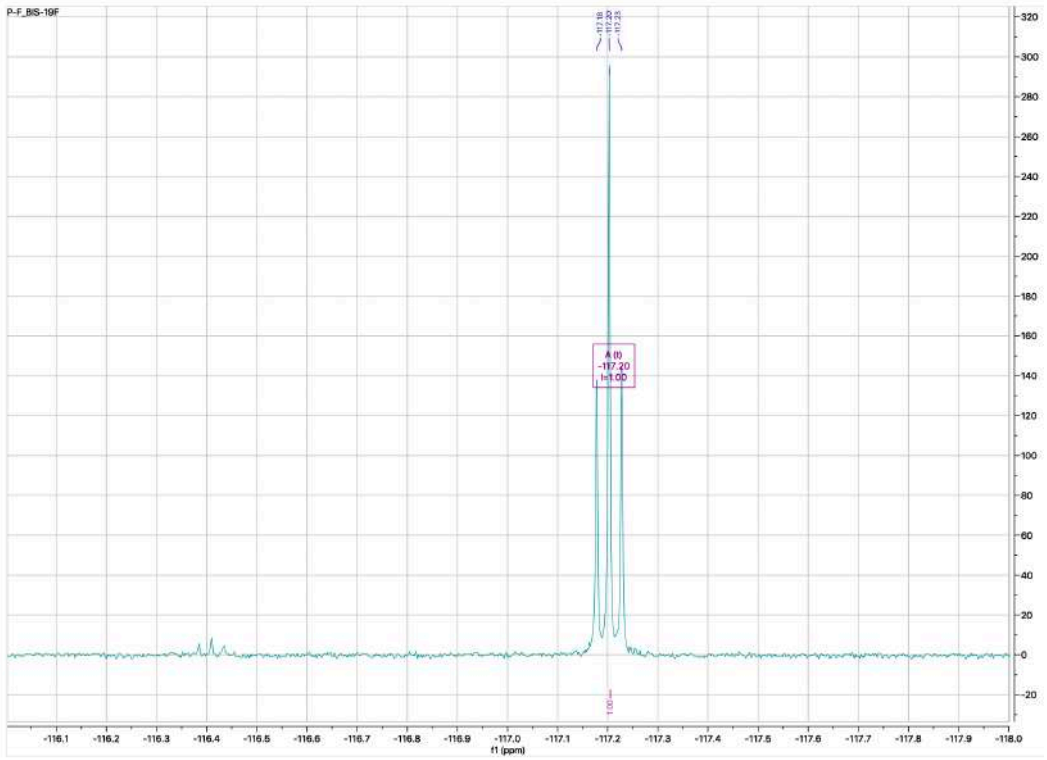

^{19}F NMR compound **11**

HRMS compound **11**

Synthesis of *(S)-methyl-3-(4-iodo-2,6-dimethylphenyl)-2-(picolinamido)propanoate (**12**):*

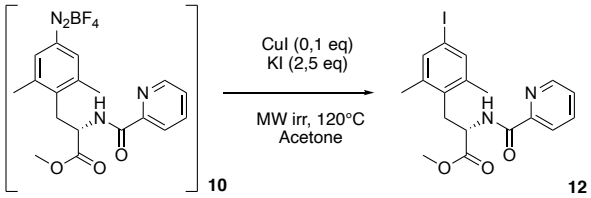

To a solution of crude compound **10** (0.704 mmol, 0.300 g) in anhydrous acetone (10 mL), CuI (0.070 mmol, 13.4 mg) and KI (1.76 mmol, 0.292 g) were added, in a sealed reaction vessel of 10-20 mL. The mixture was heated to 120 °C for 30 min under microwave irradiation. The resulting brown mixture was filtered through a celite pad and washed with acetone. The solvent was removed under vacuum until a dark solid was obtained, which was purified by flash chromatography (2:3 AcOEt/petroleum ether) to obtain compound **12** as a white oil (0.11 g).

Compound **12**:

Yield: 35%

HRMS *m/z:* $[M+H]^+$ calcd for $C_{18}H_{20}N_2O_3I$ 439.0513; found 439.0514.

$[\alpha]_D^{23}$ = -18.67 (c=0.0165, MeOH).

IR 3380, 2952, 1739, 1674, 1511, 1170 cm^{-1}.

^1H NMR (400 MHz, $CDCl_3$) δ 8.70 – 8.51 (m, 2H), 8.11 (d, *J* = 7.9 Hz, 1H), 7.91 – 7.78 (m, 1H), 7.50 – 7.43 (m, 1H), 7.35 (s, 2H), 4.98 (q, *J* = 8.1 Hz, 1H), 3.69 (s, 3H), 3.23 – 3.09 (m, 2H), 2.35 (s, 6H).

^{13}C NMR (101 MHz, $CDCl_3$) δ 172.4, 164.3, 149.0, 148.4, 139.5, 137.7, 137.1, 133.1, 126.8, 122.6, 92.7, 52.7, 51.9, 32.9, 19.9.

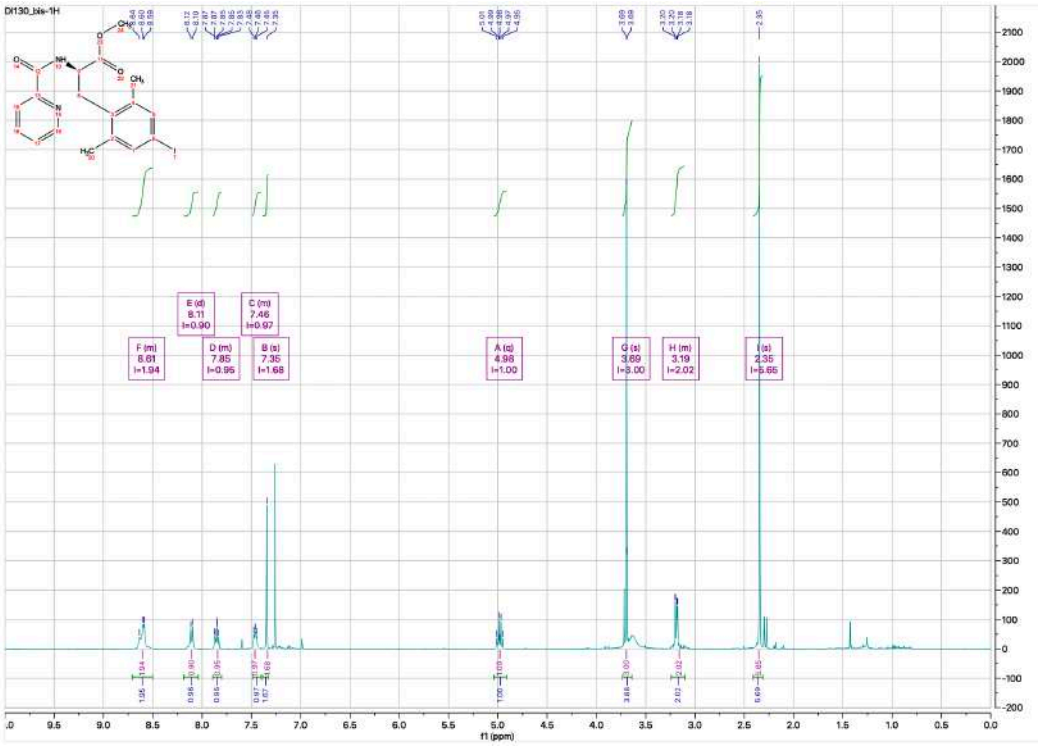

^{1}H NMR compound **12**

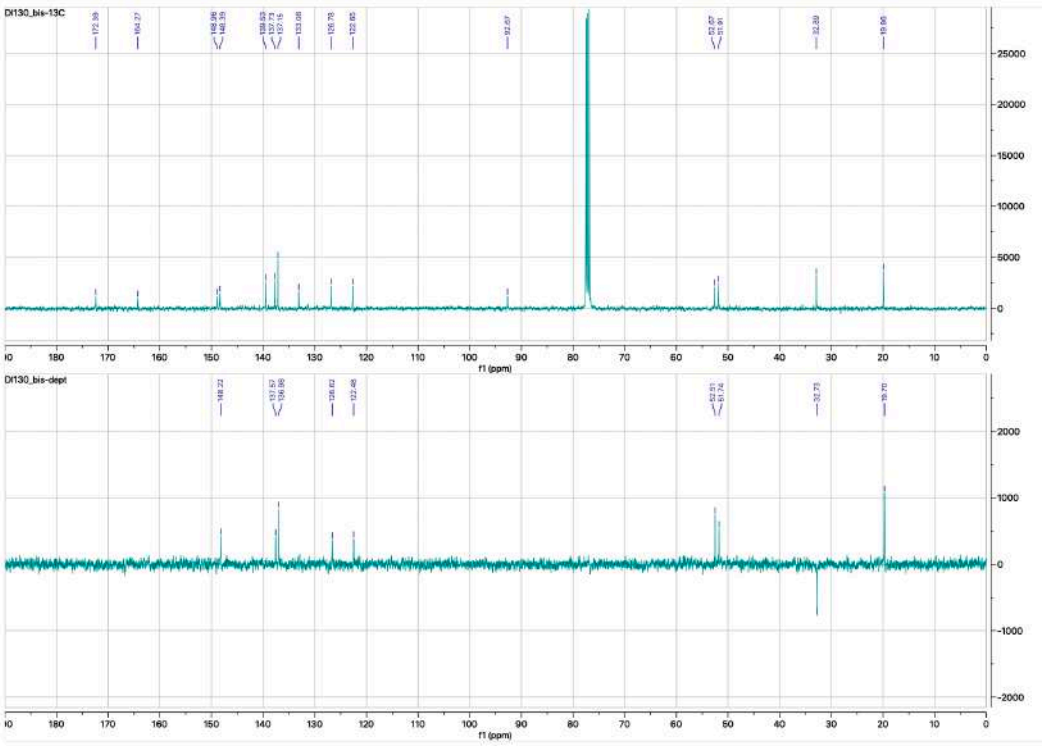

^{13}C and DEPT NMR compound **12**

HRMS compound **12**

Synthesis of *(S)-methyl-3-(2,6-dimethylphenyl)-2-(picolinamido)propanoate (**13**)*:

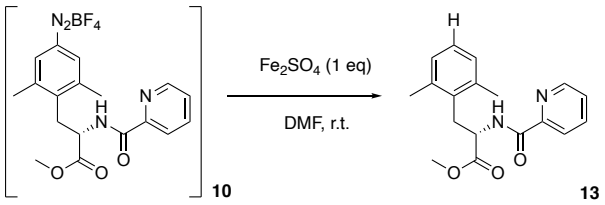

To a solution of Fe_2SO_4 (0.884 mmol, 0.246 g) in 6 mL of DMF was added dropwise to the compound **10** (0.884 mmol, 0.3 g) solubilized in DMF (1.51 mL). The reaction was stirred at r.t. overnight. The solvent was removed under vacuum and the residue was dissolved in DCM. The organic layer was washed with water, dried over Na_2SO_4, filtered and concentrated in vacuum. The crude orange oil was purified by flash chromatography (2:3 AcOEt/petroleum ether) obtaining the compound **13** as a yellow solid (0.107 g).

Compound **13**:

Yield: 39%

HRMS *m/z:* $[M+H]^+$ calcd for $C_{18}H_{21}N_2O_3$ 313.1546; found 313.1544.

$[\alpha]_D^{23}$ = -18.19 (c=0.0085, MeOH).

IR 3389, 1736, 1673, 1508, 746 cm^{-1}.

MP 94-96 °C.

^1H NMR (400 MHz, $CDCl_3$) δ 8.58 (ddd, *J* = 4.8, 1.8, 1.0 Hz, 2H), 8.11 (dt, *J* = 7.8, 1.1 Hz, 1H), 7.82 (td, *J* = 7.7, 1.7 Hz, 1H), 7.43 (ddd, *J* = 7.6, 4.8, 1.3 Hz, 1H), 7.06 – 6.94 (m, 3H), 5.00 (q, *J* = 8.1 Hz, 1H), 3.67 (s, 3H), 3.32 – 3.21 (m, 2H), 2.41 (s, 6H).

^{13}C NMR (101 MHz, $CDCl_3$) δ 172.8, 164.0, 149.4, 148.4, 137.4, 137.2, 133.3, 128.5, 126.9, 126.5, 122.4, 52.5, 52.1, 33.1, 20.3.

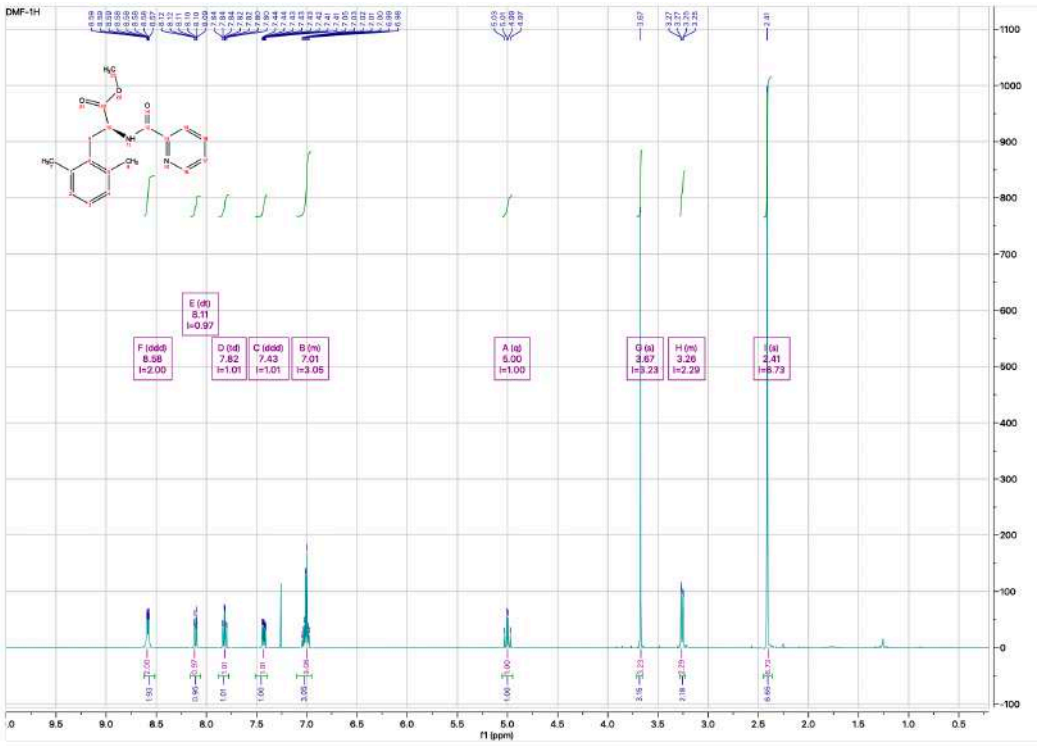

^{1}H NMR compound **13**

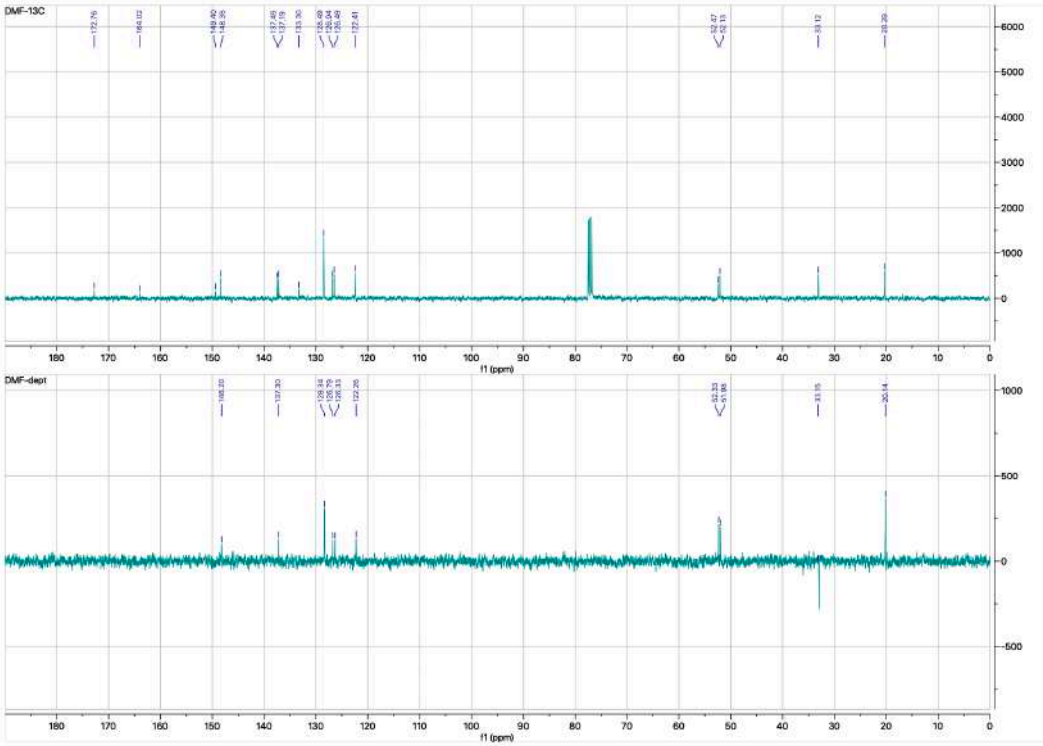

^{13}C and DEPT NMR compound **13**

HRMS compound **13**

Synthesis of *(S)-4-(2-((tert-butoxycarbonyl)amino)-2-carboxyethyl)-3,5-dimethylbenzoic acid (**18**)*:

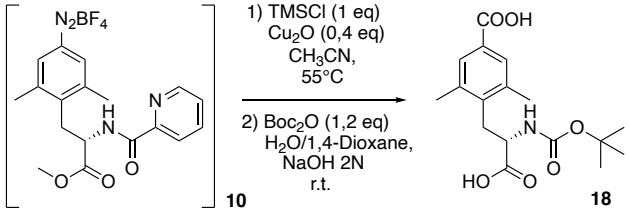

To a solution of compound **10** (1.76 mmol, 0.750 g) in acetonitrile (100 mL), were added trimethyl-silyl-cyanide (1.76 mmol, 0.220 mL) and Cu_2O (0.704 mmol, 0.100 g). The reaction was heated at 55 °C for 12 h leading to a crude orange solution. The solution was cooled to r.t, filtered through a celite pad and washed with DCM. The filtrate was concentrated under vacuum to reach an orange oil (**14**). The crude product was directly hydrolysed with HCl 6N aqueous solution at 110 °C to give the corresponding carboxylic acid. The crude was directly solubilized in water/dioxane (1:2) solution (30 mL), and basified with NaOH 2N aqueous solution until pH 10/11 at 0 °C. Boc_2O (2.11 mmol, 0.460 g) was added and the reaction was left stirring at r.t. for 12 hours. The completion of the reaction was monitored by ESI mass spectrometry and TLC. The dioxane was removed under vacuum and HCl 1N aqueous solution was added to the solution at 0 °C to pH 1. The mixture was extracted with ethyl acetate (3 times) and the organic phases were dried over Na_2SO_4 and concentrated under vacuum. The crude was purified per flash chromatography (1:1 AcOEt/petroleum ether/1% acetic acid) and crystallized with 2:1 Et_2O/petroleum ether to obtain compound **18,** as white solid (0.059 g).

Compound **18**:

Yield: 10% overall

T_R: 15.92 min.

HRMS *m/z:* $[M-H]^-$ calcd for $C_{17}H_{22}NO_6$ 336.1453; found 336.1456.

$[\alpha]_D^{22}$ = -33.1 (c=0.0145, MeOH).

IR 2924, 1687, 1163.

MP 80-82 °C.

^{1}H NMR (400 MHz, CD_3OD) δ 7.65 (s, 2H), 4.40 (dd, *J* = 9.5, 5.6 Hz, 1H), 3.30 – 3.02 (m, 2H), 2.43 (s, 6H), 1.34 (s, 7H), 1.18 (s, 2H).

^{13}C NMR (101 MHz, CD_3OD) δ 175.4, 170.2, 157.6, 141.4, 138.8, 130.4, 129.6, 80.5, 54.4, 33.6, 28.6, 28.1, 20.5.

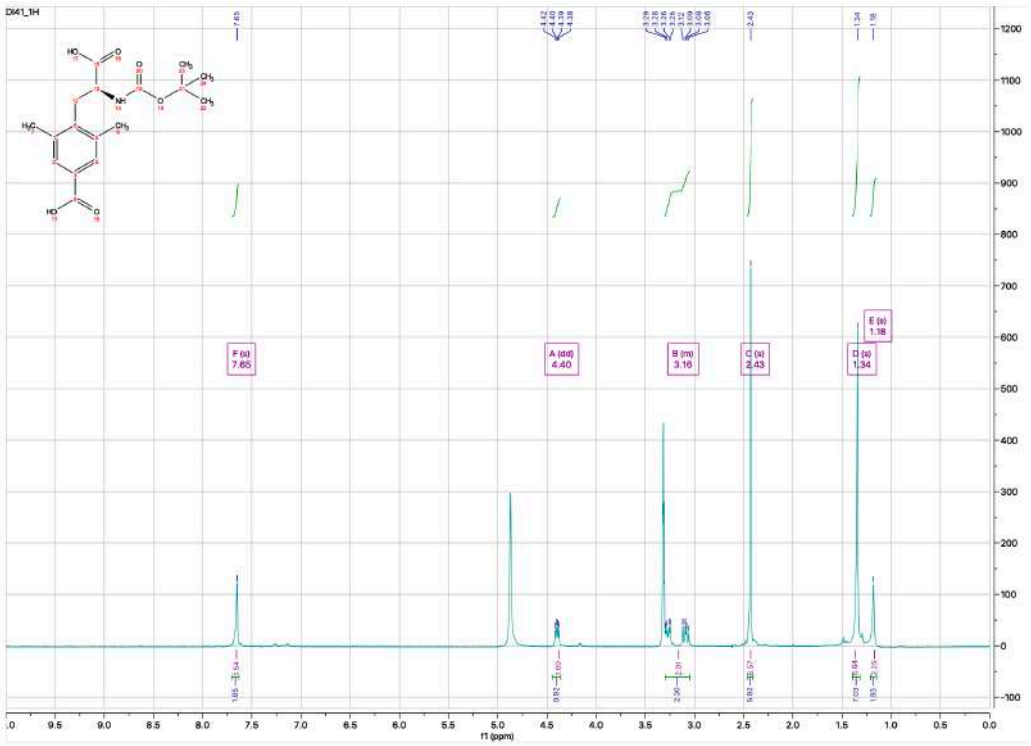

^{1}H NMR compound **18**

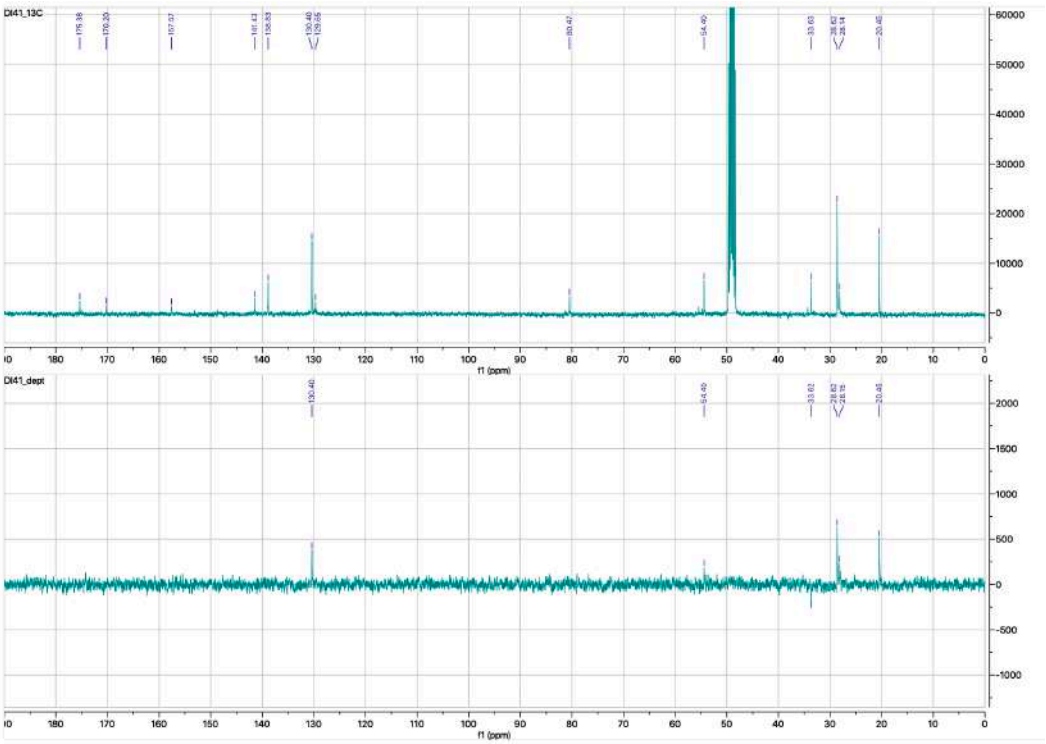

^{13}C and DEPT NMR compound **18**

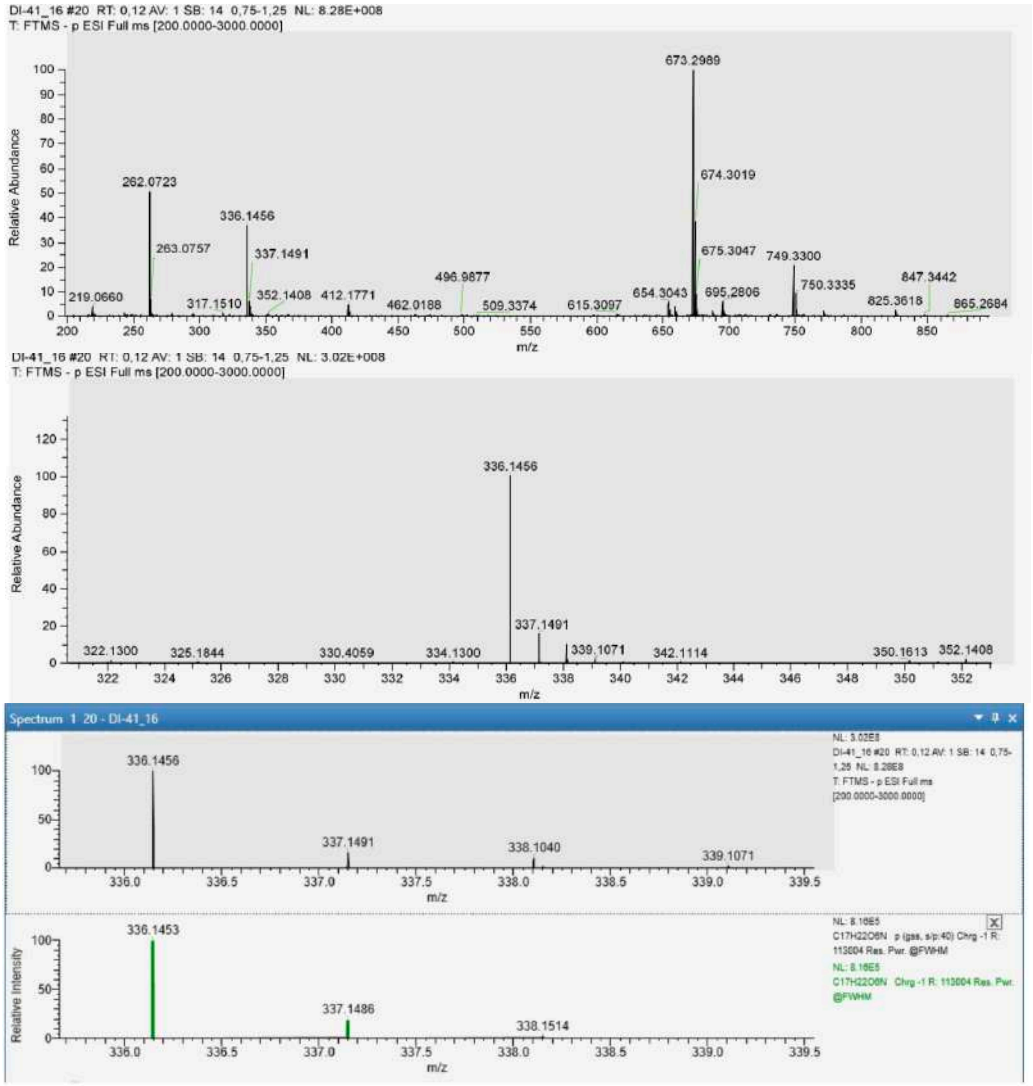

Peak Mass	Display Formula	Combined Fit	RDB	Delta [ppm]	Theo. mass	Rank	Combined Score	# Matched Iso.	# Missed Iso.	MS Cov. [%]	Pattern Cov. [%]
336.1456	$C_{17}H_{22}O_5N$	16.59	7.5	0.93	336.14526	1	85.32	2	3	89.14	97.95

HRMS compound **18**

Synthesis of *(S)-methyl-3-(2,6-dimethyl-4-nitrophenyl)-2-(picolinamido)propanoate propanoate* (**23**):

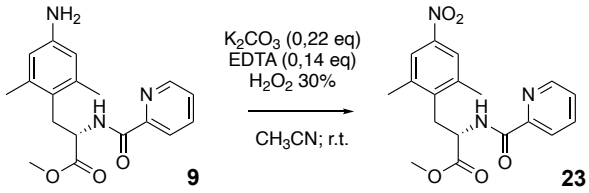

The amino compound **9** (4.78 mmol, 1.56 g) was solubilized in CH_3CN (3.5 mL). An aqueous buffer solution of K_2CO_3 (0.6 M, 1.05 mmol, 0.14 g) and EDTA disodium salt ($4x10^{-4}$ M; $0.7x10^{-3}$ mmol, 2.6 x 10^{-4} g) in 1.75 mL of H_2O was prepared and added to the mixture. Subsequently, 1.35 mL of H_2O_2 (30%) were added. The reaction was stirred at r.t. overnight, the formation of a yellow precipitate was observed. CH_3CN was removed under vacuum and the residue was dissolved in AcOEt. The organic layer was washed with water (10 mL x 3), dried over Na_2SO_4, filtered and concentrated in vacuum. The crude was purified by flash chromatography (1:1 AcOEt/petroleum ether) to obtain **23** (0.955 g), as a yellowish solid.

Compound **23**:

Yield: 56%

HRMS *m/z:* $[M+H]^+$ calcd for $C_{18}H_{20}N_3O_5$ 358.1397; found 358.1393.

$[\alpha]_D^{23}$ = -50.94 (c=0.0195, MeOH).

IR 3389, 1737, 1637, 1508, 1342, 745 cm^{-1}.

MP 132-134 °C.

^1H NMR (400 MHz, $CDCl_3$) δ 8.63 (d, *J* = 8.8 Hz, 1H), 8.61 – 8.54 (m, 1H), 8.07 (dt, *J* = 7.8, 1.1 Hz, 1H), 7.88 – 7.78 (m, 3H), 7.45 (ddd, *J* = 7.6, 4.7, 1.3 Hz, 1H), 5.07 (q, *J* = 8.2 Hz, 1H), 3.71 (s, 3H), 3.36 – 3.25 (m, 2H), 2.51 (s, 6H).

^{13}C NMR (101 MHz, $CDCl_3$) δ 172.0, 164.0, 149.0, 148.4, 146.4, 141.3, 139.1, 137.6, 126.7, 123.0, 122.5, 52.8, 51.4, 33.5, 20.6.

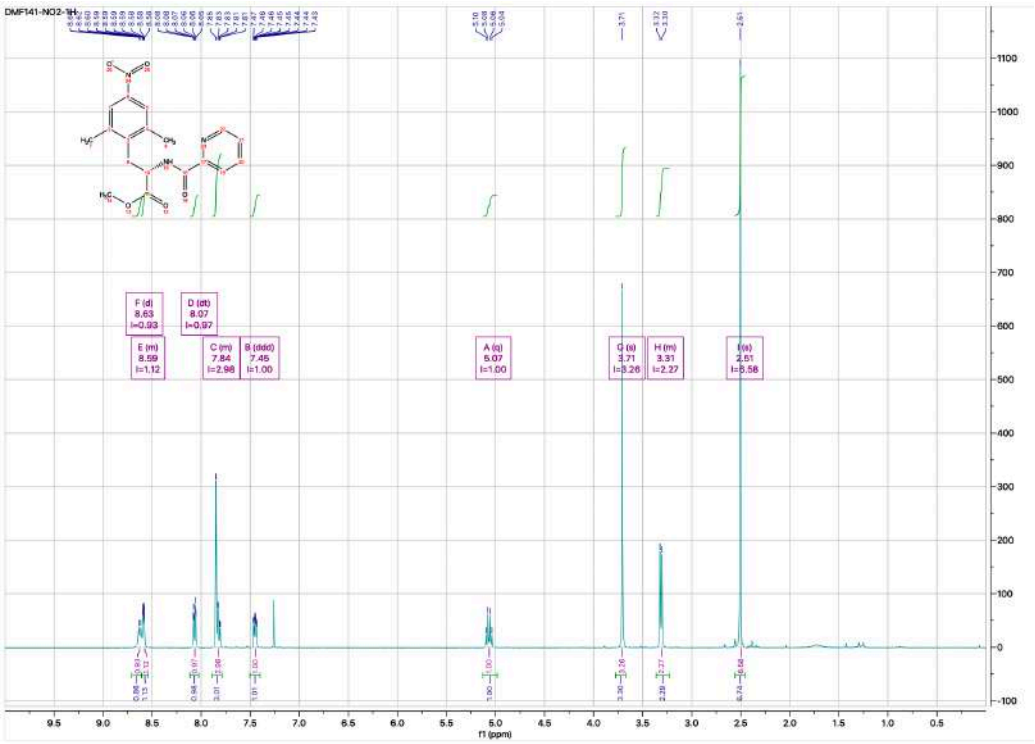

^{1}H NMR compound **23**

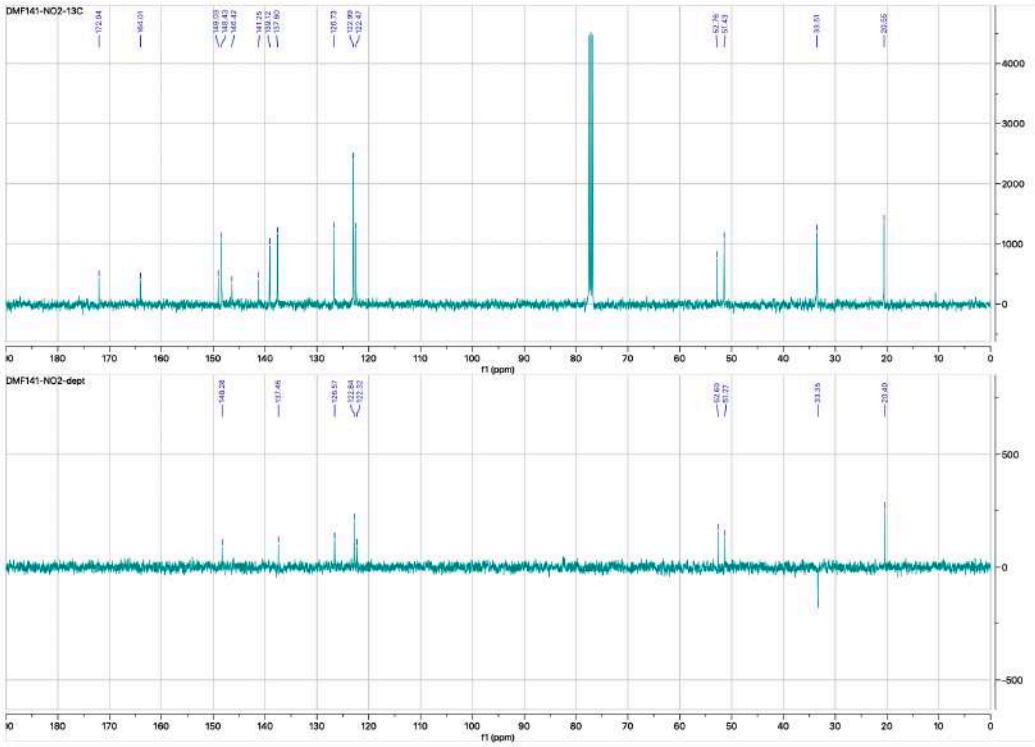

^{13}C and DEPT NMR compound **23**

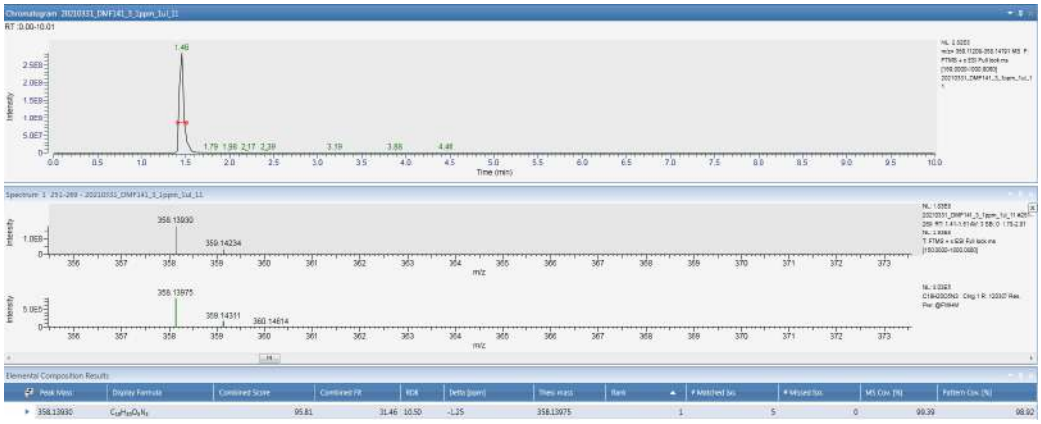

HRMS compound **23**

Synthesis of *(S)-methyl-3-(2-amino-5,7-dimethylbenzo[d]thiazol-6-yl)-2-(picolinamido) propanoate* (**25**):

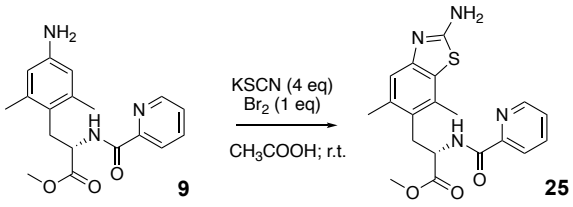

To a solution of compound **9** (1.07 mmol, 0.353 g) in AcOH (10 mL), KSCN (4.31 mmol, 0.419 g) and Br_2 (1.07mmol, 55.6 µl) were added. The reaction was stirred for 48 h at room temperature. The solvent was removed under vacuum leading to an orange compound that was extracted with $NaHCO_3$ sat. and AcOEt (3 times). The organic phases were collected and dried over Na_2SO_4, filtered and concentrated under vacuum. The crude was purified by preparative HPLC obtaining the compound **25** (0.123 g, 30% yield), as a white solid.

Compound **25**:

Yield: 30%

HRMS *m/z:* $[M+H]^+$ calcd for $C_{19}H_{21}N_4O_3S$ 385.1328; found 385.1329.

$[\alpha]_D^{22}$ = -2.67 (c=0.001, MeOH).

IR 2984, 1742, 1660, 1193, 1135 cm^{-1}.

MP 83-85 °C.

^1H NMR (400 MHz, DMSO) δ 8.94 (d, *J* = 8.3 Hz, 1H), 8.66 (dt, *J* = 4.8, 1.4 Hz, 1H), 8.06 – 7.89 (m, 2H), 7.62 (ddd, *J* = 6.8, 4.8, 2.0 Hz, 1H), 6.97 (s, 1H), 4.73 (td, *J* = 8.4, 5.8 Hz, 1H), 4.39 (s, 2H), 3.65 (s, 3H), 3.32 – 3.11 (m, 2H), 2.31 (s, 3H), 2.27 (s, 3H).

^{13}C NMR (101 MHz, DMSO) δ 171.6, 166.7, 163.7, 163.6, 149.1, 148.6, 137.9, 129.7, 129.2 (2CQ), 126.9, 126.6, 122.9, 122.0, 53.1, 52.1, 33.5, 17.9, 17.4.

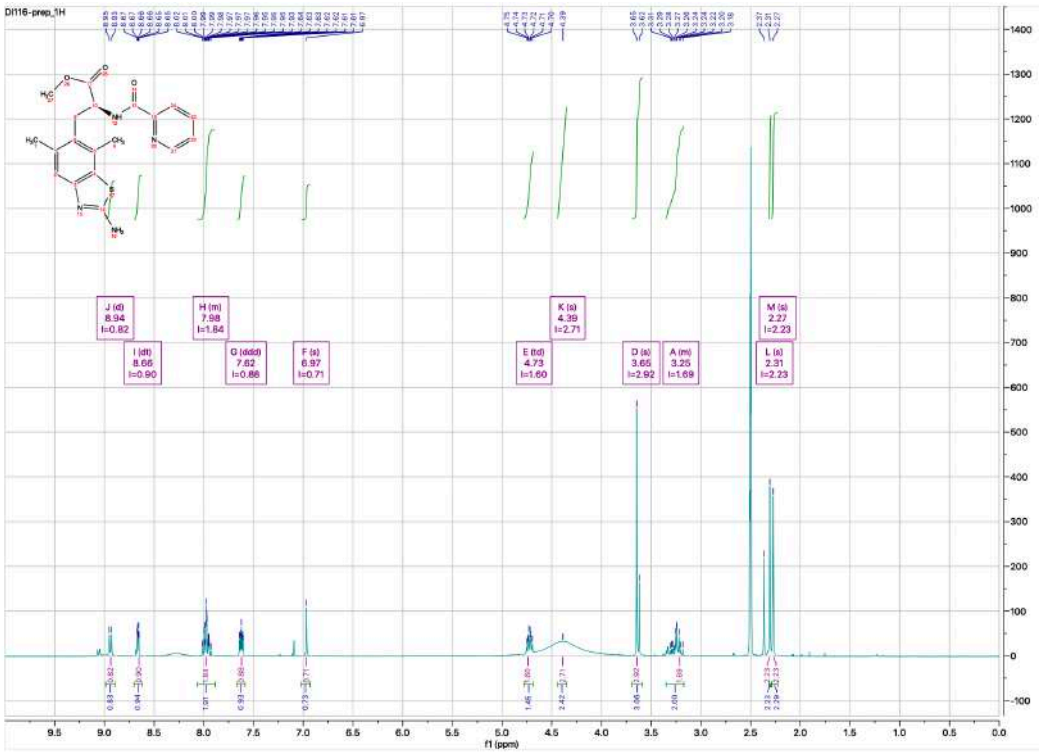

^{1}H NMR compound **25**

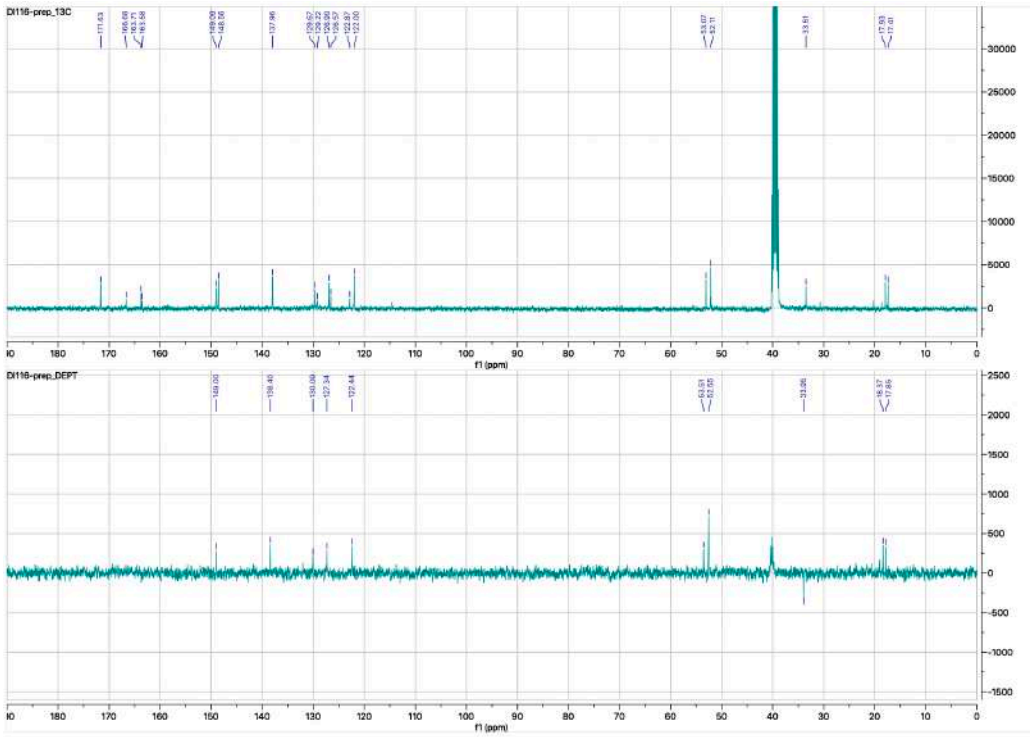

^{13}C and DEPT NMR compound **25**

HRMS compound **25**

Synthesis of *(S)-2-((tert-butoxycarbonyl)amino)-3-(4-(dibenzylamino)-2,6-dimethylphenyl)propanoic acid* (**21**):

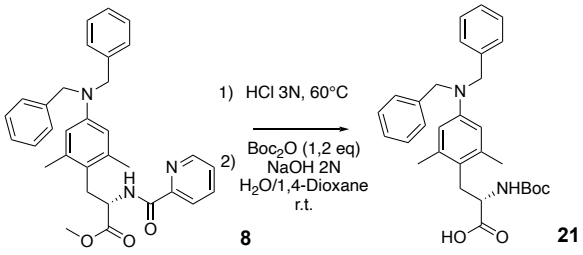

Compound **8** (1.97 mmol, 1.0 g) was hydrolyzed in a milder way than other acidic hydrolysis described in the hydrolysis general procedure (as reported below). It was solubilized in HCl 3N (11 mL) aqueous solution and maintained under reflux at 60 °C for 1 week. The solution was concentrated under vacuum to reduce the volume (about 3 mL) and the crude was used for the protection of the amine as Boc. The previous amine hydrochloride solution was diluted in water/dioxane (1:2) solution (21 mL). The solution was basified with NaOH 2N aqueous solution to reach pH 10 at 0 °C. Boc_2O (2.36 mmol, 0.516 g) was added and the reaction was stirred at r.t. for 12 hours. The completion of the reaction was monitored by ESI mass spectrometry and TLC, and the dioxane was removed under vacuum. HCl 1N aqueous solution was added at 0 °C to reach pH 1, then the mixture was extracted with ethyl acetate (3 times) and the organic phases combined were dried over Na_2SO_4 and concentrated under vacuum. The crude was purified per flash chromatography (1:1 AcOEt/petroleum ether/1% acetic acid) and crystallized with 2:1 Et_2O/petroleum ether to afford **21**, as a pale yellow solid (0.576 g).

Compound **21**:

Yield: 70%

T_R: 22.67 min.

HRMS *m/z:* $[M-H]^-$ calcd for $C_{30}H_{35}N_2O_4$ 487.2602; found 487.2606.

$[\alpha]_D^{23}$ = -133.6 (c=0.0515, MeOH).

IR 2980, 1713, 1603, 1494, 1158 cm^{-1}.

MP 82-84 °C.

^{1}H NMR (400 MHz, DMSO) (rotamers mixture) δ 7.36 – 7.27 (m, 4H), 7.26 – 7.17 (m, 6H), 7.04 (d, *J* = 8.6 Hz, 1H), 6.35 (s, 2H), 4.58 (s, 4H), 3.97 (td, *J* = 8.4, 5.2 Hz, 1H), 2.96 – 2.69 (m, 2H), 2.12 (s, 6H), 1.31 (s, 7H), 1.13 (s, 2H).

^{13}C NMR (101 MHz, DMSO) δ 173.9, 155.3, 146.5, 139.3, 137.2, 128.4, 126.7, 122.9, 112.1, 77.9, 53.9, 53.6, 30.6, 28.2, 27.6, 20.5. ^{1}H NMR (300 MHz, DMSO at 120 °C) δ 7.34 – 7.13 (m, 7H), 6.46 (s, 2H), 4.55 (s, 4H), 4.19 – 4.03 (m, 1H), 3.05 – 2.75 (m, 2H), 2.18 (s, 6H), 1.31 (s, 9H).

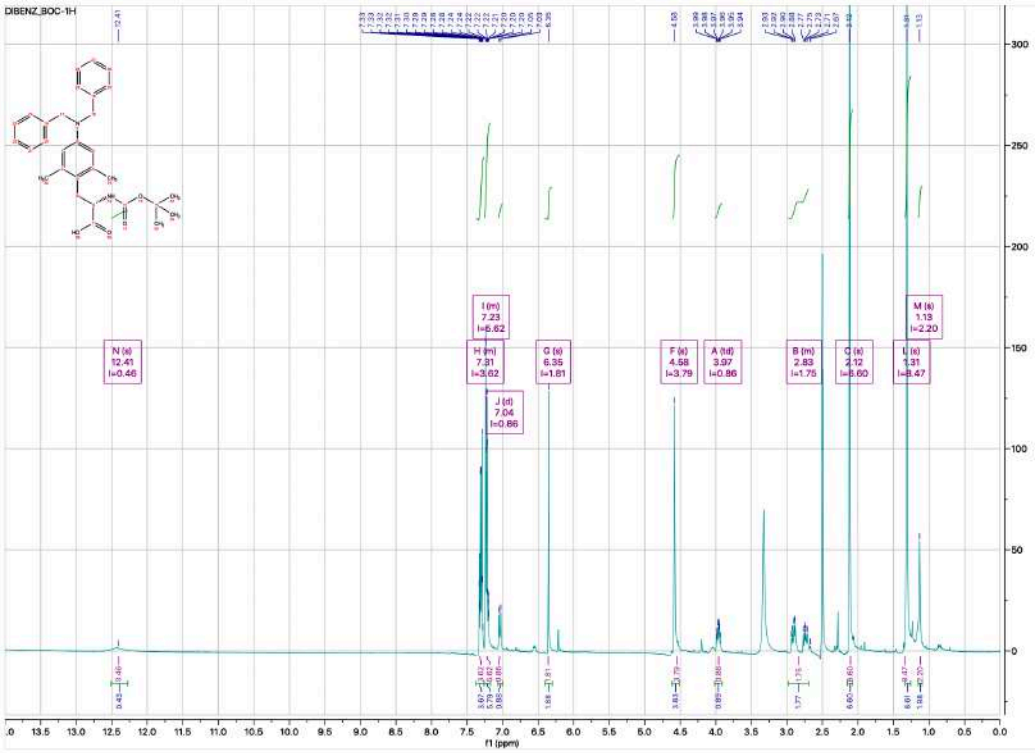

^{1}H NMR compound **21**

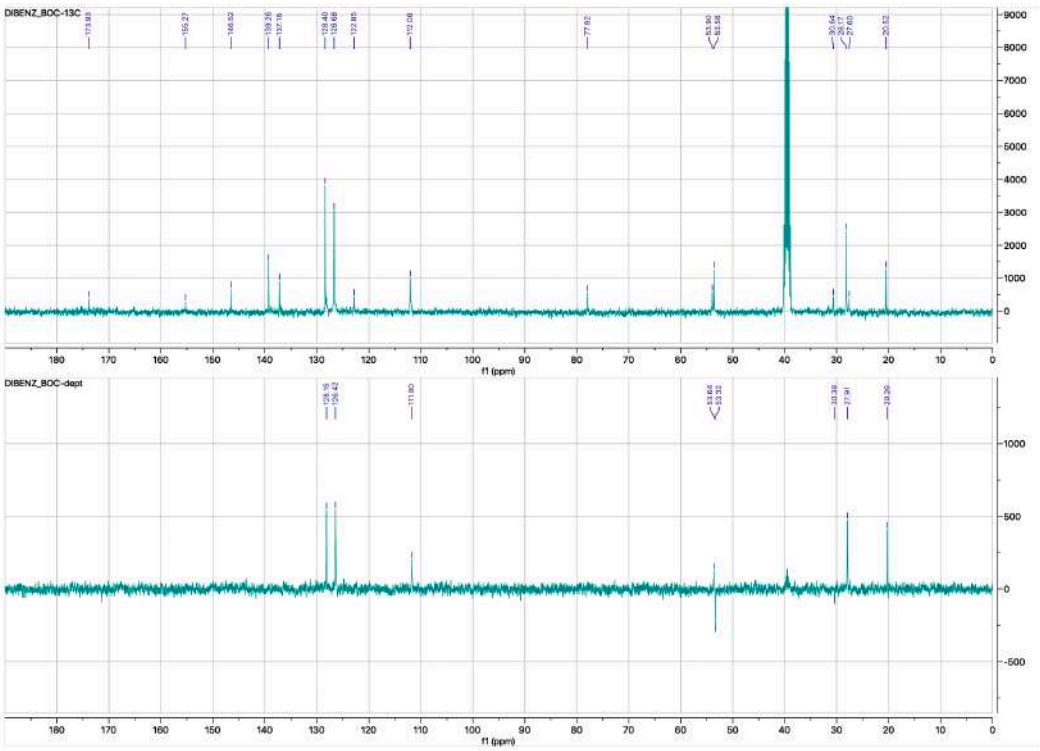

^{13}C and DEPT NMR compound **21**

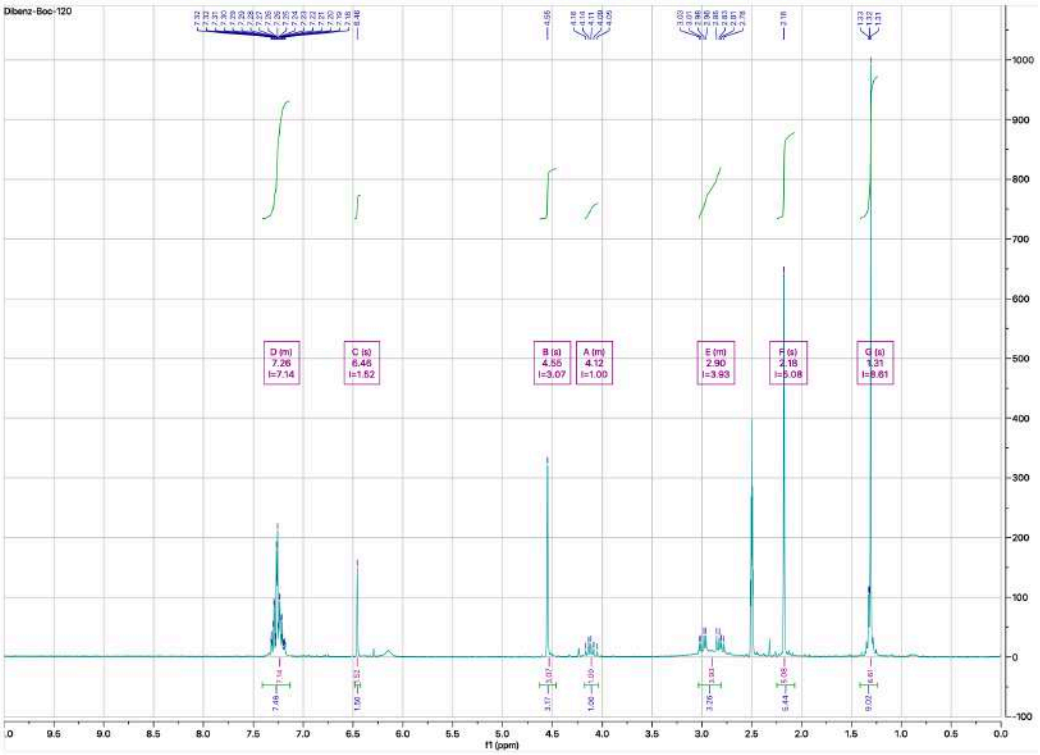

^{1}H NMR at 120°C compound **21**

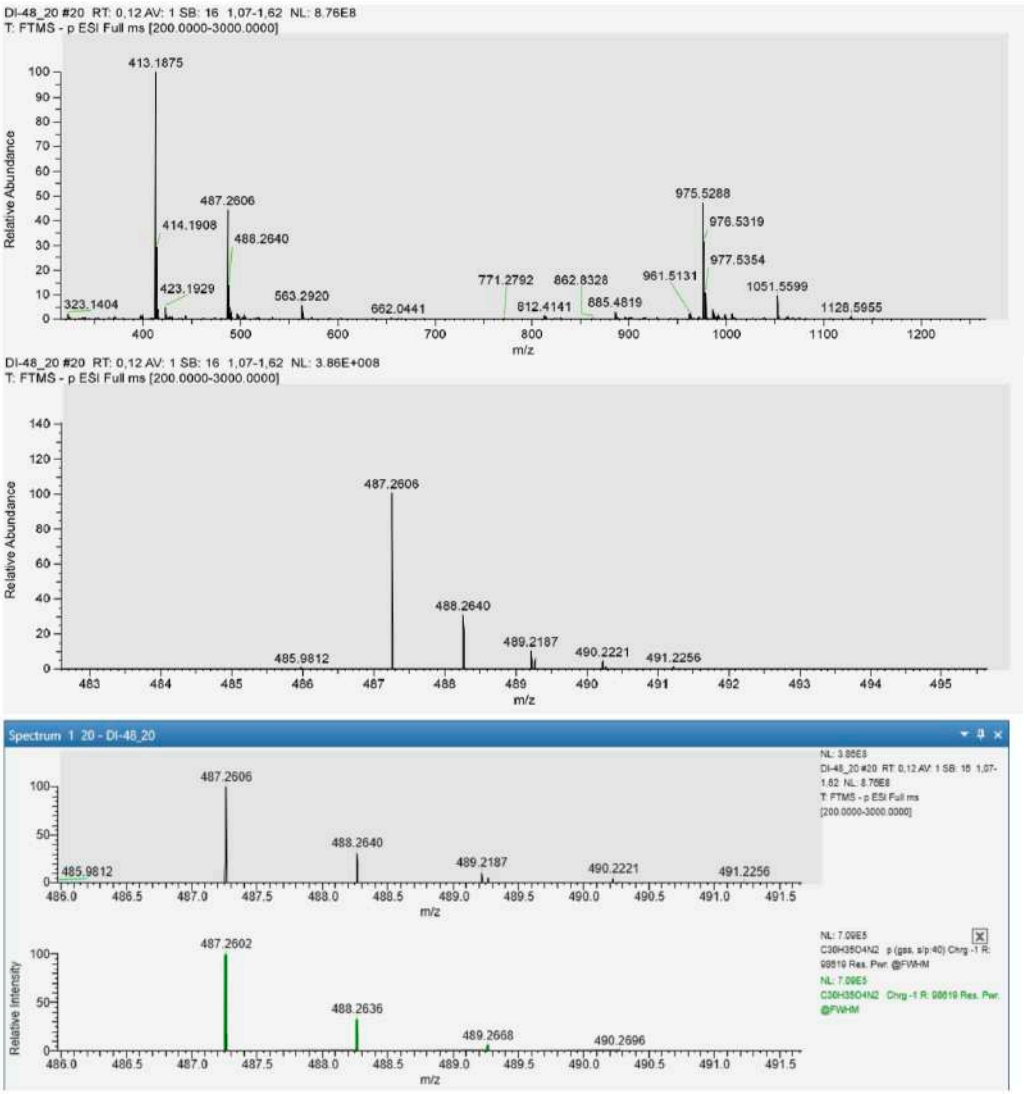

Peak Mass	Display Formula	Combined Fit	RDB	Delta [ppm]	Theo. mass	Rank	Combined Score	# Matched Iso.	# Missed Iso.	MS Cov. [%]	Pattern Cov. [%]
487.2606	$C_{30}H_{35}O_4N_2$	61.54	14.5	0.76	487.26023	1	89.41	4	0	90.96	100.00

HRMS compound **21**

Synthesis of *(S)-3-(4-amino-2,6-dimethylphenyl)-2-((tert butoxycarbonyl)amino)propanoic acid* (**22**):

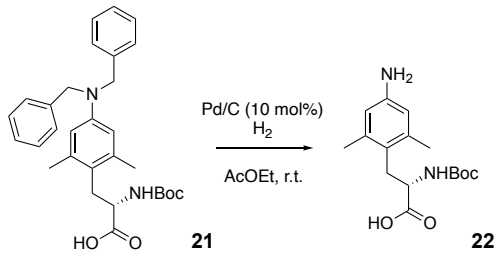

The benzyl removal reaction was performed by solubilizing compound **21** (0.246 mmol, 0.118 g) in AcOEt (10 mL) with Pd/C (10%), at r.t., under H_2 atmosphere. The reaction was left stirring until complete consumption of the starting material, controlled by ESI mass spectrometry and TLC. A yellow crude oil was obtained, then purified by flash

chromatography (4:1 AcOEt/Petroleum ether), then crystallized with 2:1 diethyl ether/petroleum ether until the compound **22** was obtained, as a white powder (0.052 g).

Compound **22**:

Yield: 70%

T_R: 12.60 min.

HRMS *m/z:* $[M-H]^-$ calcd for $C_{16}H_{23}N_2O_4$ 307.1663; found 307.1666.

$[\alpha]_D^{21}$ = +43.2 (c=0.009, MeOH).

IR 3361, 2984, 1694, 1363, 1171 cm^{-1}.

MP 160-162 °C.

^{1}H NMR (400 MHz, DMSO) (rotamers mixture) δ 7.03 (d, *J* = 8.4 Hz, 1H), 6.18 (s, 2H), 3.94 (q, *J* = 7.6 Hz, 1H), 2.99 – 2.62 (m, 2H), 2.12 (s, 6H), 1.33 (s, 7H), 1.20 (s, 2H).

^{13}C NMR (101 MHz, DMSO) δ 174.0, 155.3, 146.3, 136.9, 122.1, 113.9, 77.9, 54.1, 30.6, 28.2, 27.7, 20.0.

^{1}H NMR compound **22**

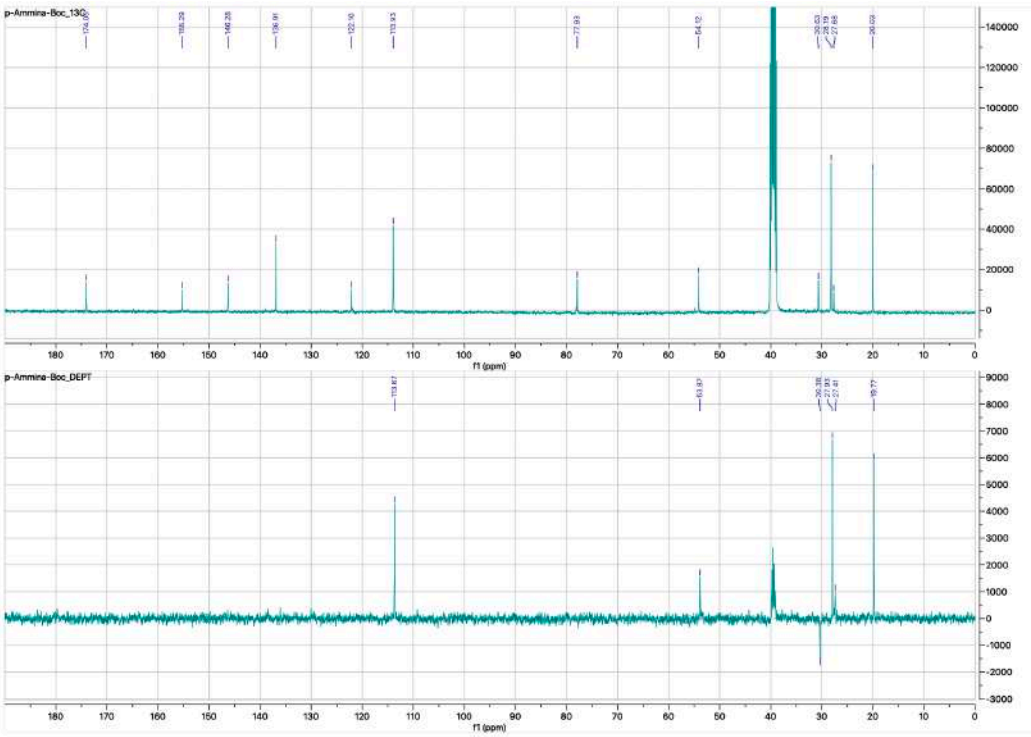

^{13}C and DEPT NMR compound **22**

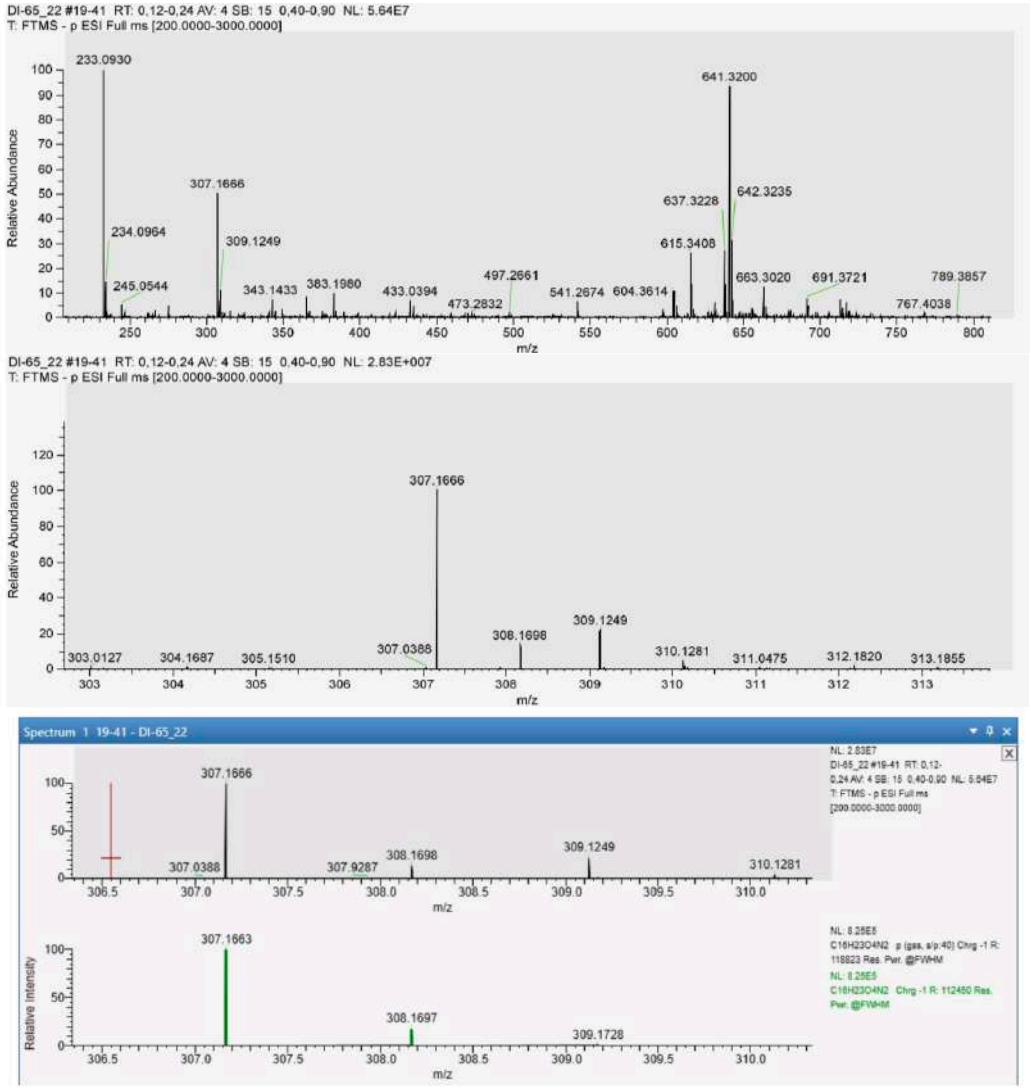

Peak Mass	Display Formula	Combined Fit	RDB	Delta [ppm]	Theo. mass	Rank	Combined Score	# Matched Iso.	# Missed Iso.	MS Cov. [%]	Pattern Cov. [%]
307.1666	$C_{16}H_{23}O_4N_2$	13.82	6.5	0.89	307.16633	1	73.75	4	2	77.08	97.88

HRMS compound **22**

General procedure for acidic hydrolysis and Boc protection (**15**, **16**, **17**, **24**, **26**):

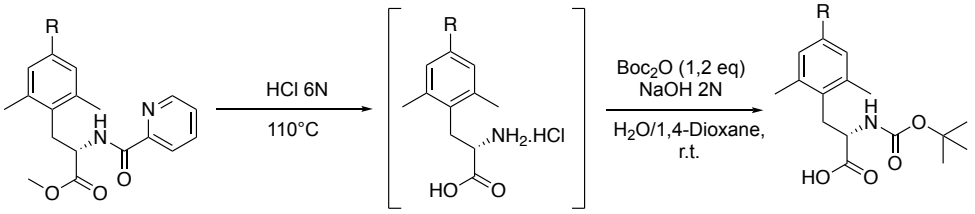

11: R = F
12: R = I
13: R = H
23: R = NO_2
25: R = aminothiazole

15: R = F
16: R = I
17: R = H
24: R = NO_2
26: R = aminothiazole

Once purified the compound was dissolved in HCl 6N aqueous solution (17 equiv.) and heated at 110 °C for 24 hours. The obtained hydrolyzed crude product was concentrated under vacuum to reduce the volume and the crude solution was used directly for the subsequent protection step.

The HCl salt synthesized was directly used as crude, and diluted in water/dioxane (1:2) solution (0.2 M). The mixture was basified with NaOH 2N aqueous solution until reachment of pH value of 10/11 at 0 °C. Boc_2O (1.2 equiv.) was added and the reaction was left stirring at r.t. for 12 hours. The completion of the reaction was monitored per ESI mass spectrometry and TLC. The dioxane was removed under vacuum and HCl 1N aqueous solution was added at 0 °C to pH 1. The mixture was extracted with ethyl acetate (3 times) and the organic phases combined were dried over Na_2SO_4 and concentrated under vacuum. The crude was purified by flash chromatography (AcOEt/petroleum ether/1% acetic acid) and crystallized with 2:1 Et_2O/petroleum ether.

(S)-2-((tert-butoxycarbonyl)amino)-3-(4-fluoro-2,6-dimethylphenyl)propanoic acid, compound **15**:

Yield: 72% white solid

T_R: 20.05 min.

HRMS *m/z:* $[M-H]^-$ calcd for $C_{16}H_{21}FNO_4$ 310.1460; found 310.1459.

$[\alpha]_D^{23}$ = -30.4 (c=0.025, MeOH).

IR 2974, 1721, 1651, 1164, 1021 cm^{-1}.

MP 133-135 °C.

^{1}H NMR (400 MHz, DMSO) (rotamers mixture) δ 12.61 (s, 1H), 7.16 (d, *J* = 8.7 Hz, 1H), 6.80 (d, *J* = 9.8 Hz, 2H), 4.06 (td, *J* = 8.8, 6.1 Hz, 1H), 3.07 – 2.80 (m, 2H), 2.28 (s, 6H), 1.31 (d, *J* = 4.3 Hz, 8H), 1.15 (s, 1H).

^{13}C NMR (101 MHz, DMSO) δ 173.5, 160.1 (d, *J* = 240 Hz), 155.2, 139.4, 131.1, 114.0 (d, *J* = 20 Hz), 78.0, 53.3, 30.7, 28.1, 27.6, 19.9.

^{19}F NMR (376 MHz, DMSO) δ -118.24 (t, *J* = 9.7 Hz).

^{1}H NMR (300 MHz, DMSO at 120 °C) δ 6.76 (d, *J* = 9.8 Hz, 2H), 4.17 (td, *J* = 8.6, 6.4 Hz, 1H), 3.18 – 2.85 (m, 2H), 2.32 (s, 6H), 1.32 (s, 9H).

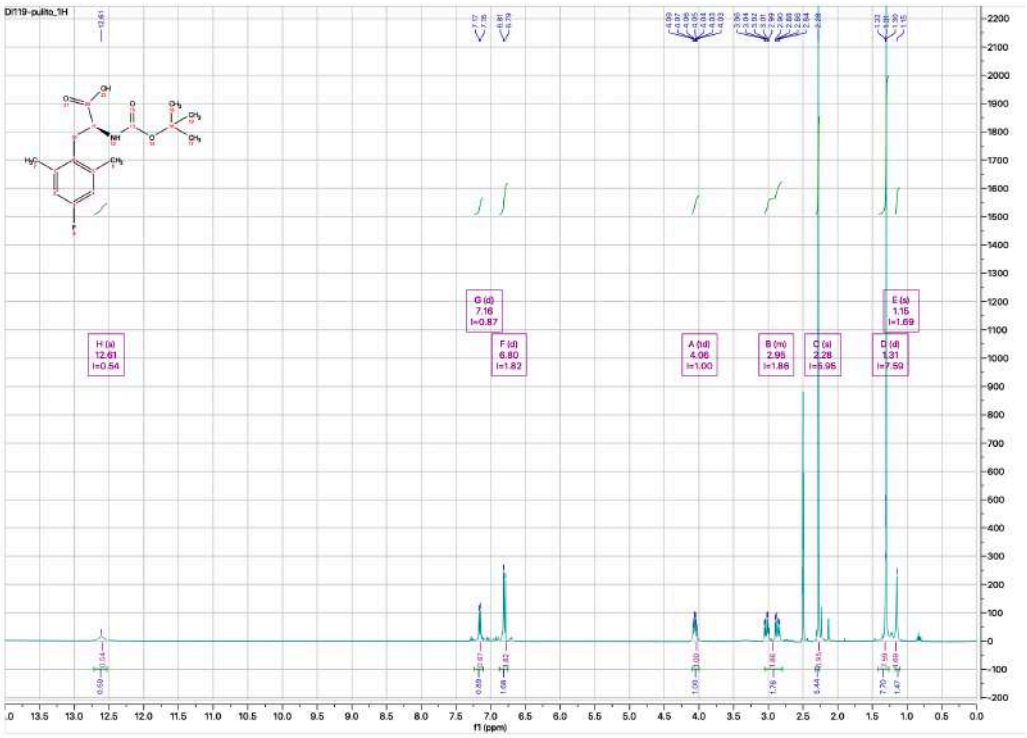

^{1}H NMR compound **15**

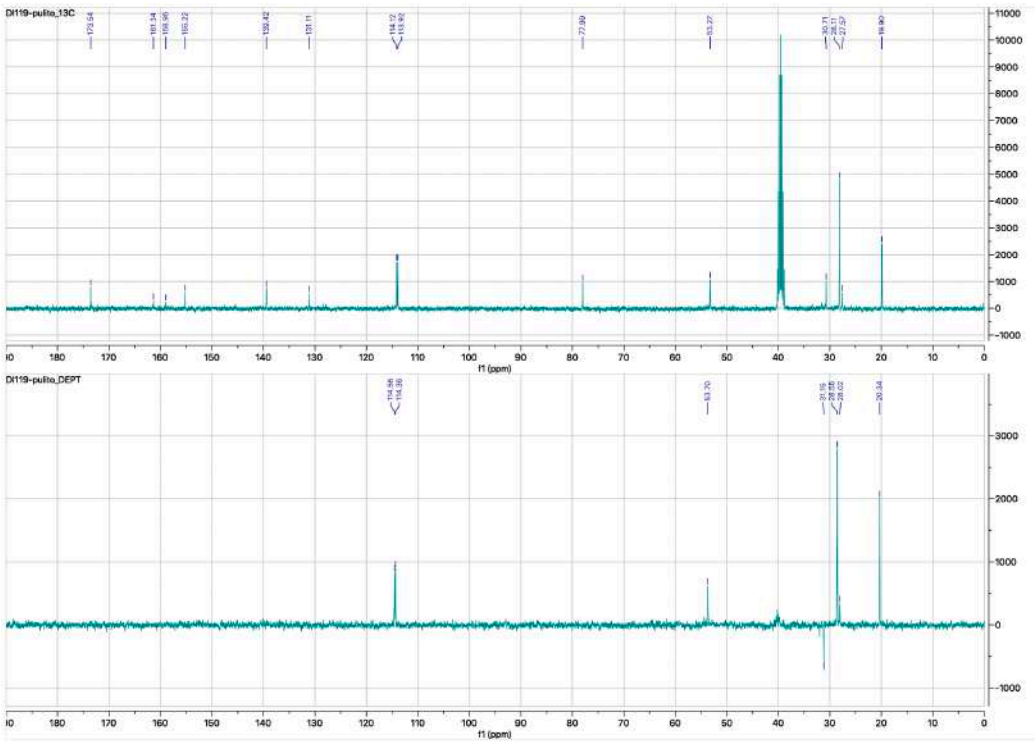

^{13}C and DEPT NMR compound **15**

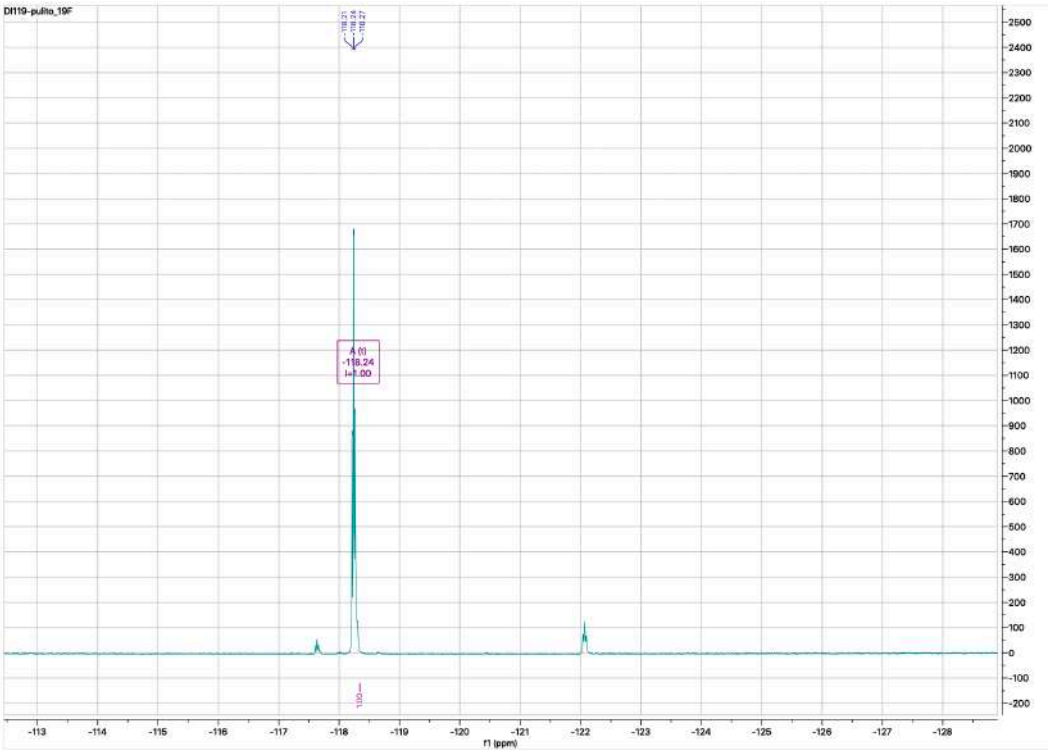

^{19}F NMR compound **15**

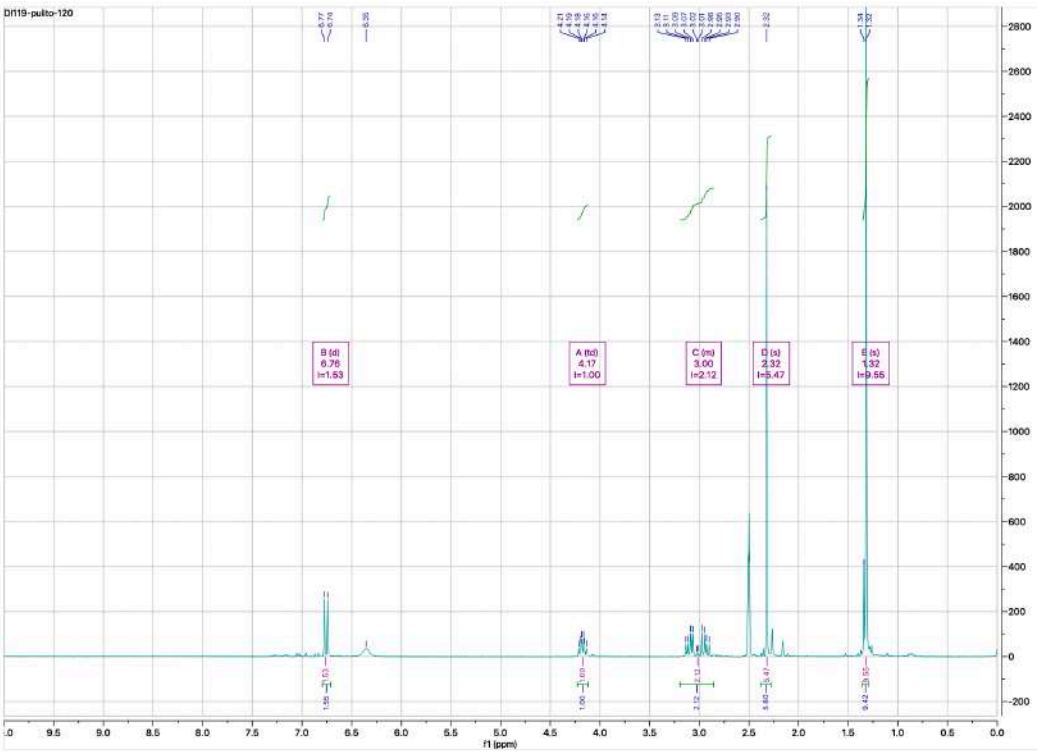

^{1}H NMR at 120 °C compound **15**

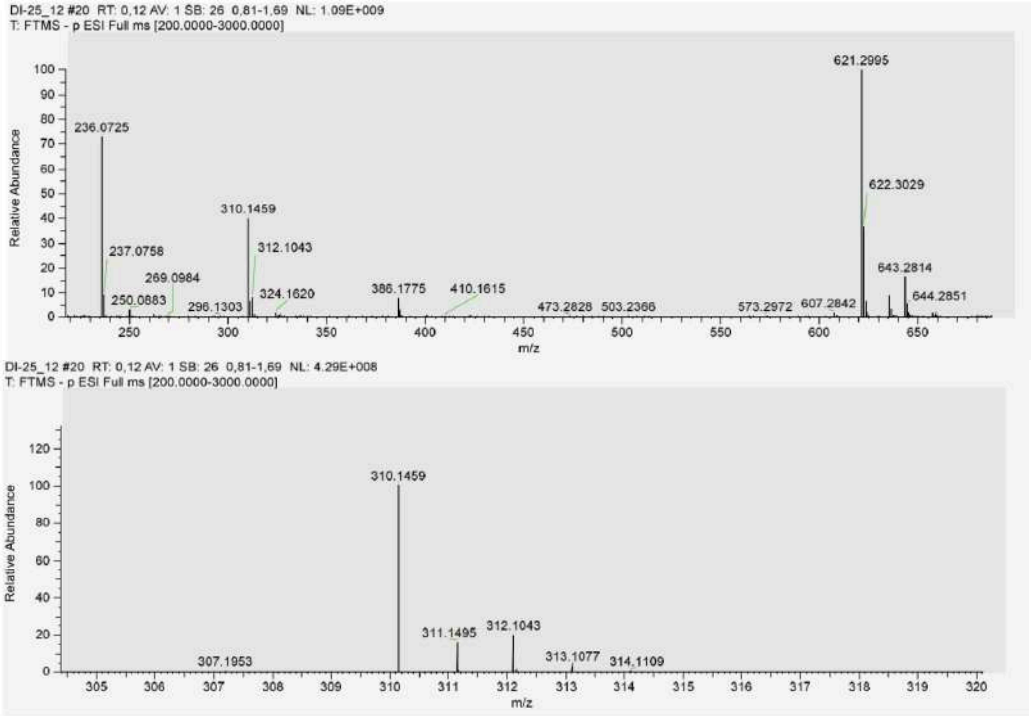

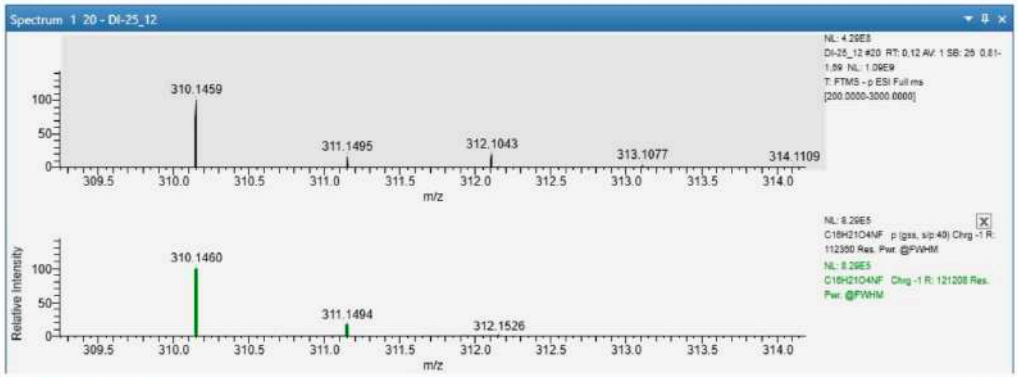

Peak Mass	Display Formula	Combined Fit	RDB	Delta [ppm]	Theo. mass	Rank	Combined Score	# Matched Iso.	# Missed Iso.	MS Cov. [%]	Pattern Cov. [%]
310.1459	$C_{16}H_{21}O_4NF$	21.15	6.5	-0.38	310.14601	1	79.81	3	2	83.07	98.31

HRMS compound **15**

(S)-2-((tert-butoxycarbonyl)amino)-3-(4-iodo-2,6-dimethylphenyl)propanoic acid, compound **16**:

Yield: 70%, white solid

T_R: 22.60 min.

HRMS *m/z:* $[M-H]^-$ calcd for $C_{16}H_{21}INO_4$ 418.0521; found 418.0524.

$[\alpha]_D^{21}$ = -82.7 (c=0.022, MeOH).

IR 3355, 2963, 1726, 1686, 1018, 793 cm^{-1}.

MP 128-130 °C.

^{1}H NMR (400 MHz, DMSO) (rotamers mixture) δ 12.53 (s, 1H), 7.34 (s, 2H), 7.15 (d, *J* = 8.6 Hz, 1H), 4.04 (q, *J* = 8.0, 7.5 Hz, 1H), 3.07 – 2.80 (m, 2H), 2.24 (s, 6H), 1.30 (s, 8H), 1.15 (s, 1H).

^{13}C NMR (101 MHz, DMSO) δ 173.4, 155.2, 139.6, 136.1, 135.1, 92.0, 78.0, 53.0, 31.0, 28.1, 19.3.

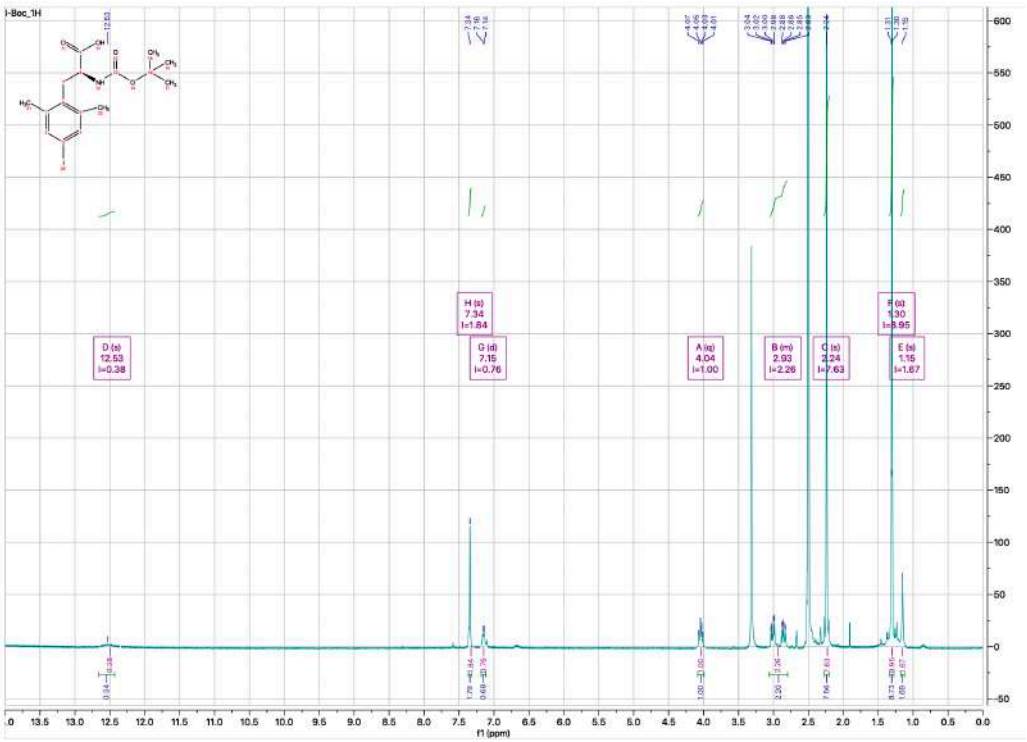

^{1}H NMR compound **16**

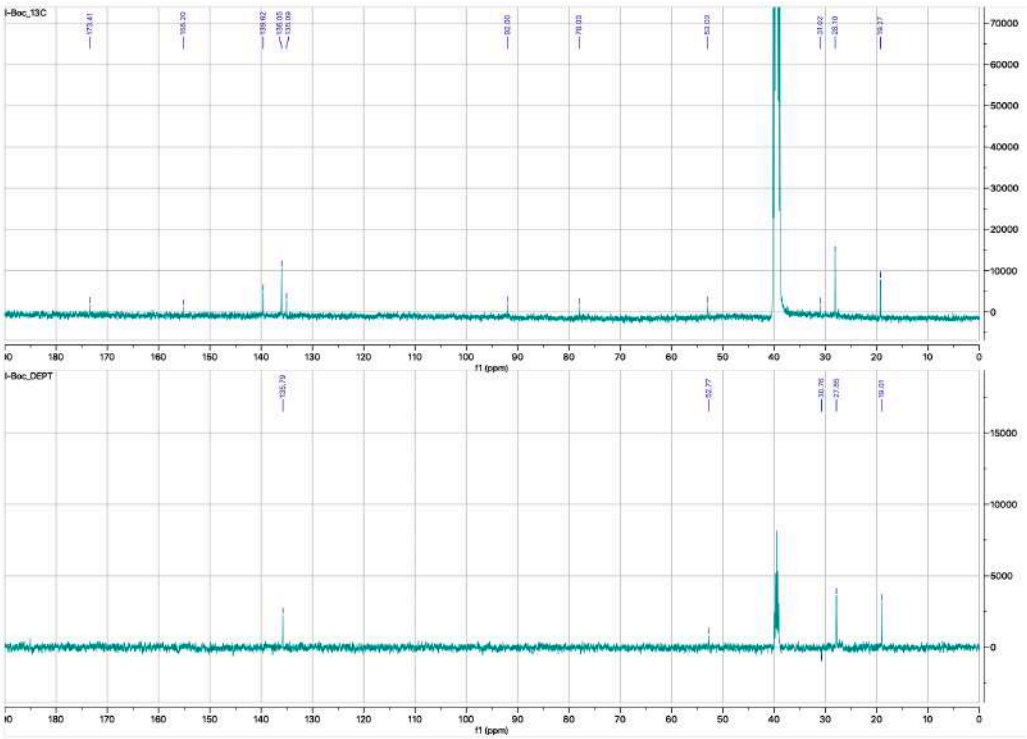

^{13}C and DEPT NMR compound **16**

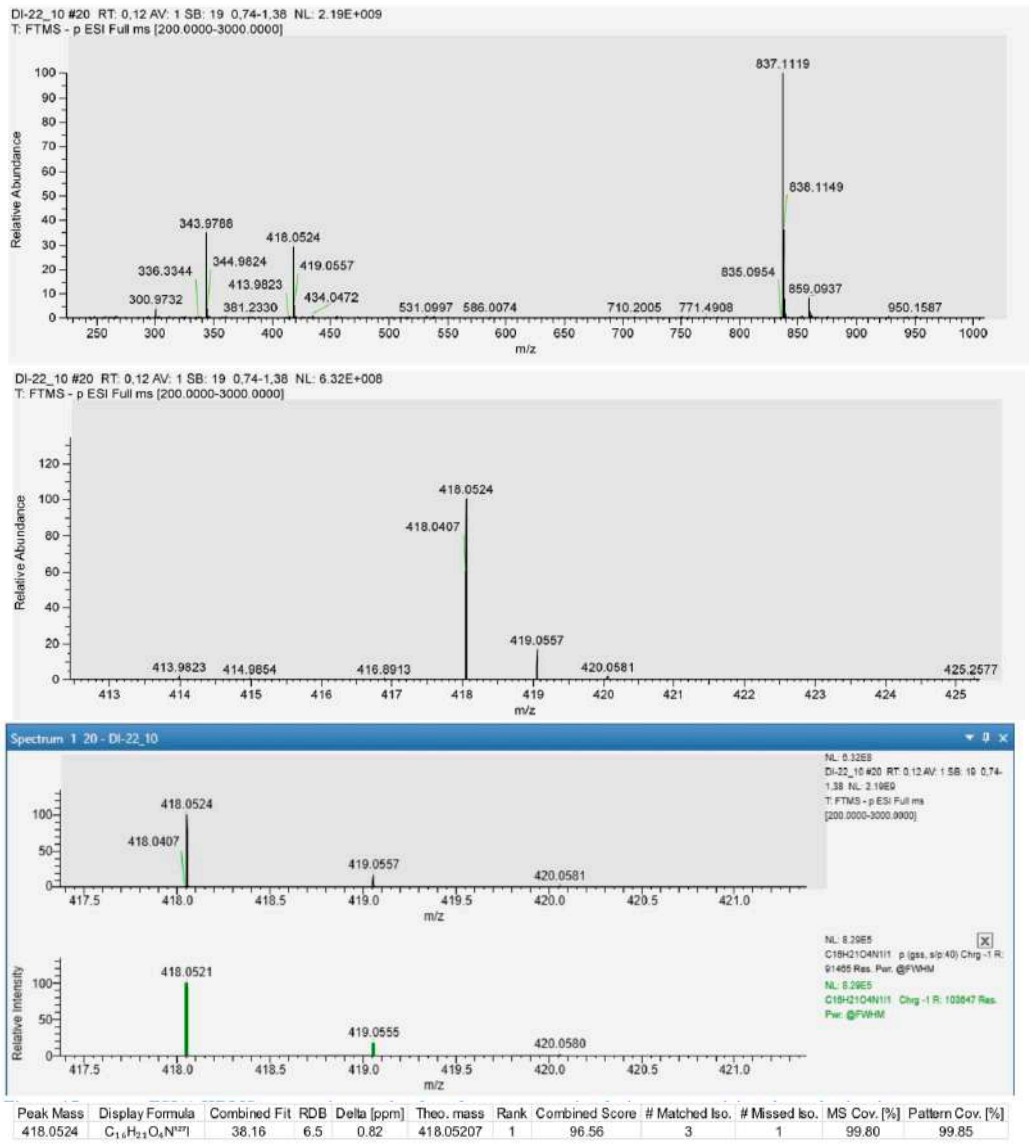

HRMS compound **16**

(S)-2-((tert-butoxycarbonyl)amino)-3-(2,6-dimethylphenyl)propanoic acid, compound **17**:

Yield: 75% white solid

T_R: 22.03. HRMS *m/z:*$[M-H]^-$ calcd for $C_{16}H_{22}NO_4$ 292.1543; found 292.1554.

$[\alpha]_D^{23}$ = +0,855 (c=0.0055, MeOH).

IR 3301, 2973, 1723, 1656, 1366, 1163, 765 cm^{-1}.

MP 65-67 °C.

^{1}H NMR (400 MHz, DMSO) δ 12.55 (s, 1H), 7.15 (d, *J* = 8.6 Hz, 1H), 6.96 (d, *J* = 1.7 Hz, 3H), 4.07 (td, *J* = 8.6, 6.1 Hz, 1H), 3.11 – 2.85 (m, 2H), 2.28 (s, 6H), 1.31 (s, 8H), 1.14 (s, 1H).

^{13}C NMR (101 MHz, DMSO) δ 173.7, 155.3, 136.7, 135.0, 127.9, 126.0, 78.0, 53.4, 31.3, 28.1, 27.6, 19.9.

^{1}H NMR compound **17**

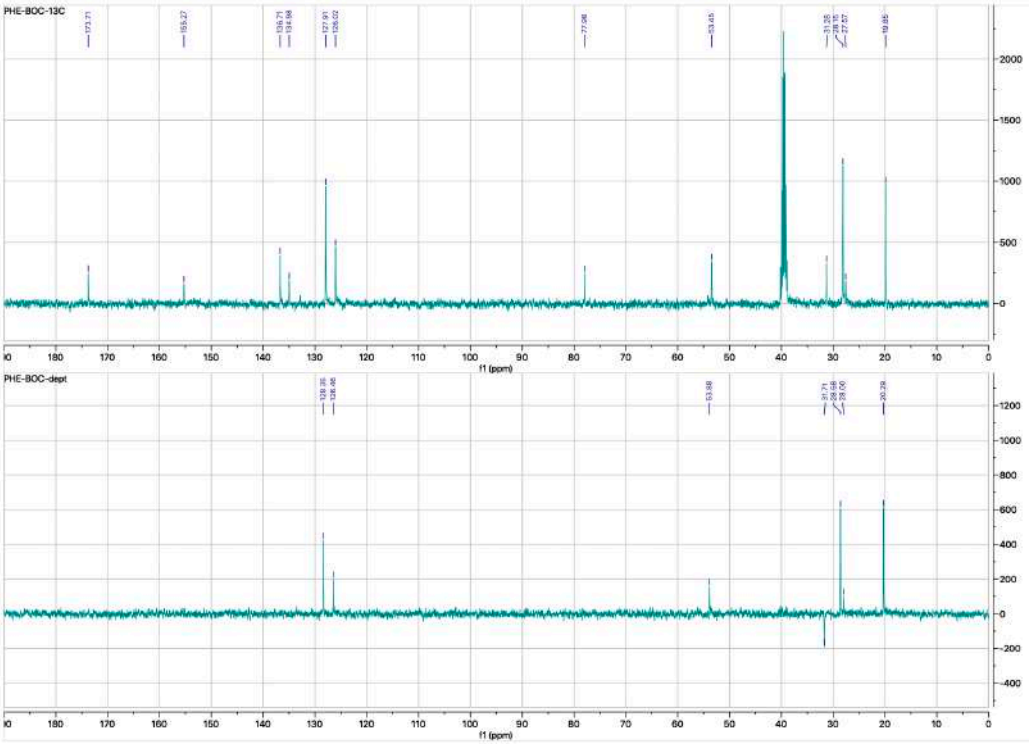

^{13}C and DEPT NMR compound **17**

HRMS compound **17**

(S)-2-((tert-butoxycarbonyl)amino)-3-(2,6-dimethyl-4-nitrophenyl)propanoic acid, compound **24**:

Yield: 67% pale yellow solid

T_R: 19.52 min.

HRMS *m/z:* $[M-H]^-$ calcd for $C_{16}H_{21}N_2O_6$ 337.1405; found 337.1405.

$[\alpha]_D^{23}$ = -164.2 (c=0.05, MeOH).

IR 3250, 2980, 1716, 1639, 1510, 1341, 1160 cm^{-1}.

MP 170-172 °C.

^{1}H NMR (400 MHz, DMSO) (rotamers mixture) δ 12.75 (s, 1H), 7.87 (s, 2H), 7.26 (d, *J* = 8.6 Hz, 1H), 4.16 (td, *J* = 9.1, 5.6 Hz, 1H), 3.19 – 2.97 (m, 2H), 2.42 (s, 6H), 1.27 (s, 7H), 1.13 (s, 2H).

^{13}C NMR (101 MHz, DMSO) δ 173.0, 155.2, 145.4, 143.8, 139.3, 122.1, 78.1, 52.6, 31.6, 28.0, 27.5, 19.8.

^{1}H NMR (300 MHz, 120 °C, DMSO) δ 7.82 (s, 2H), 6.53 (s, 1H), 4.25 (q, *J* = 8.2 Hz, 1H), 3.31 – 3.02 (m, 2H), 2.45 (s, 6H), 1.37 – 1.25 (m, 9H).

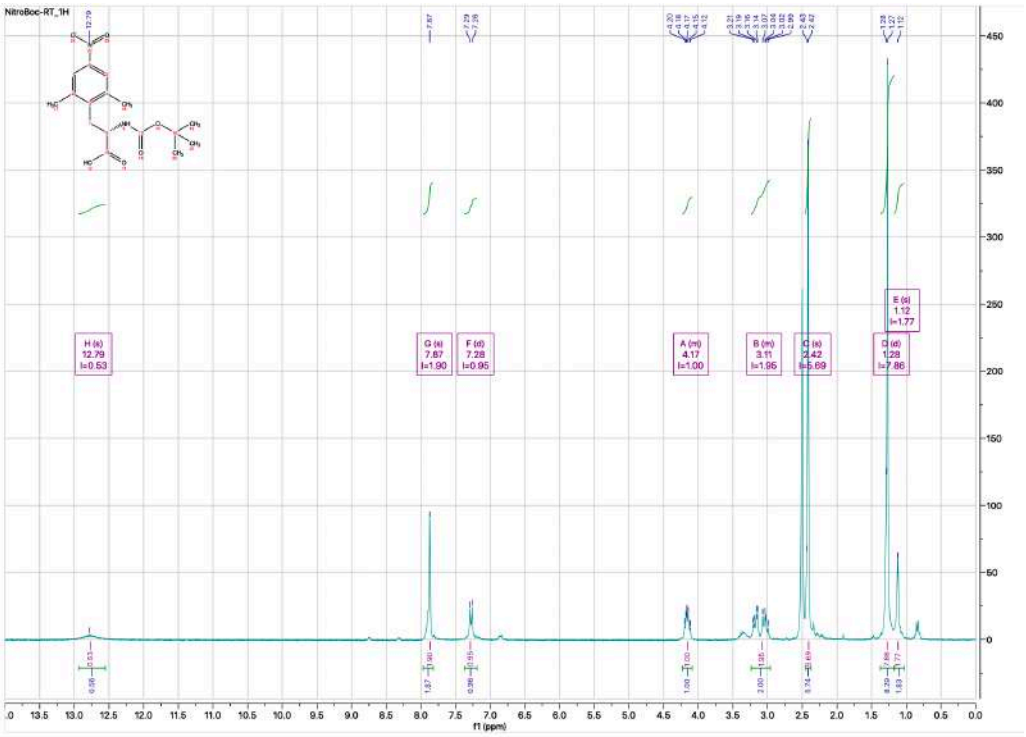

^{1}H NMR at r.t. compound **24**

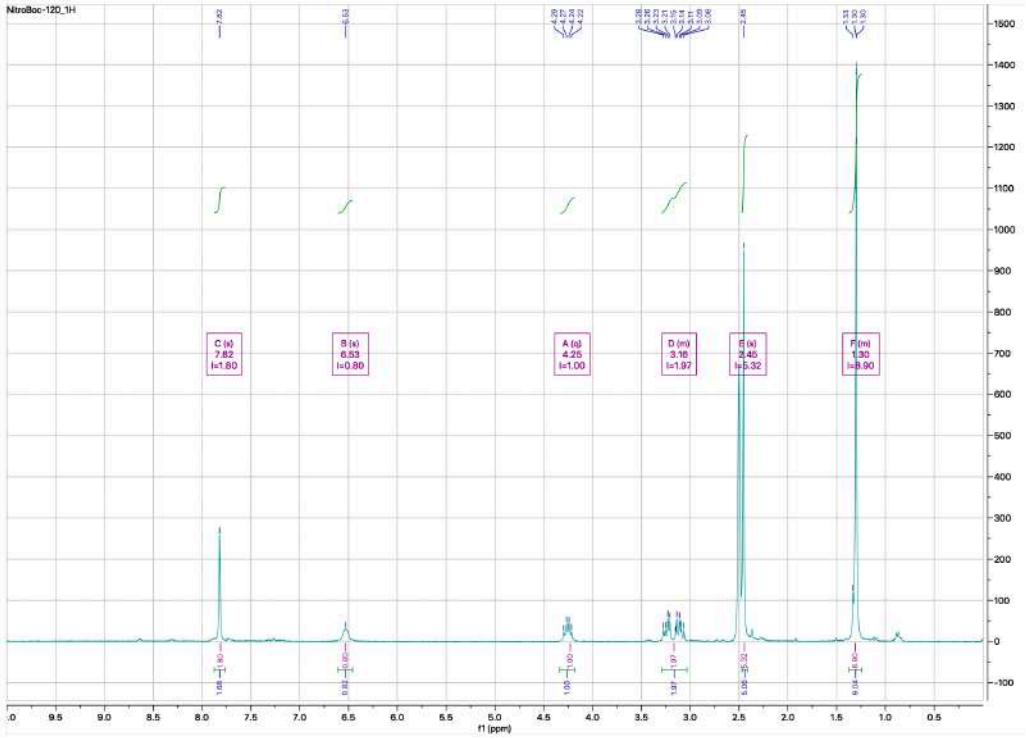

^{1}H NMR at 120 °C compound **24**

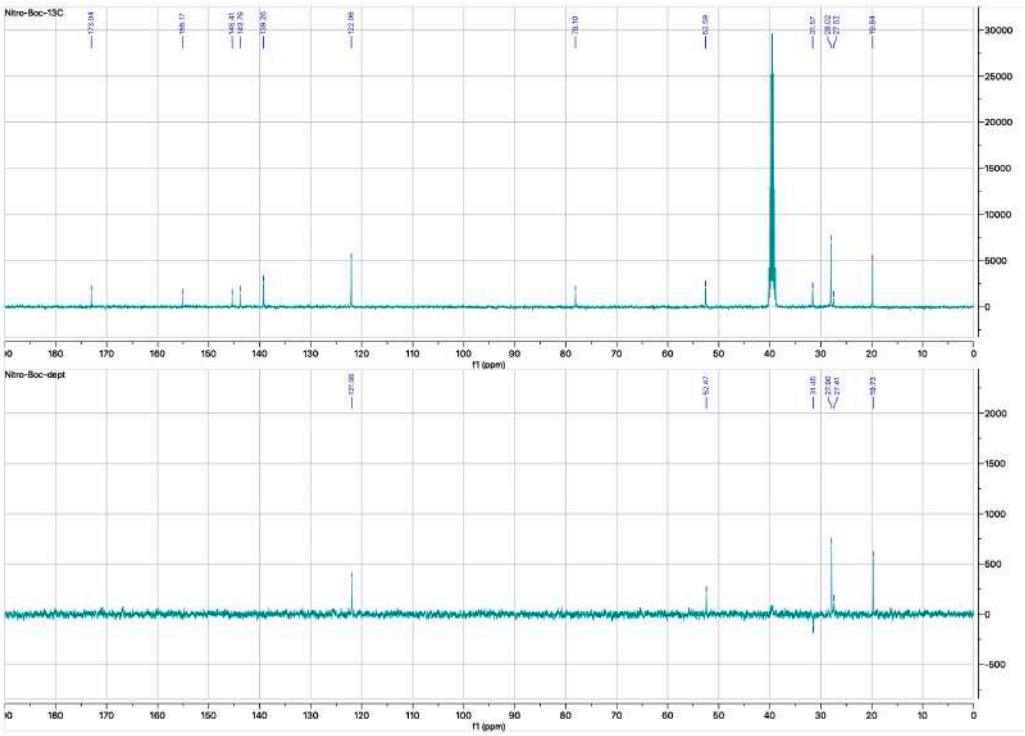

^{13}C and DEPT NMR compound **24**

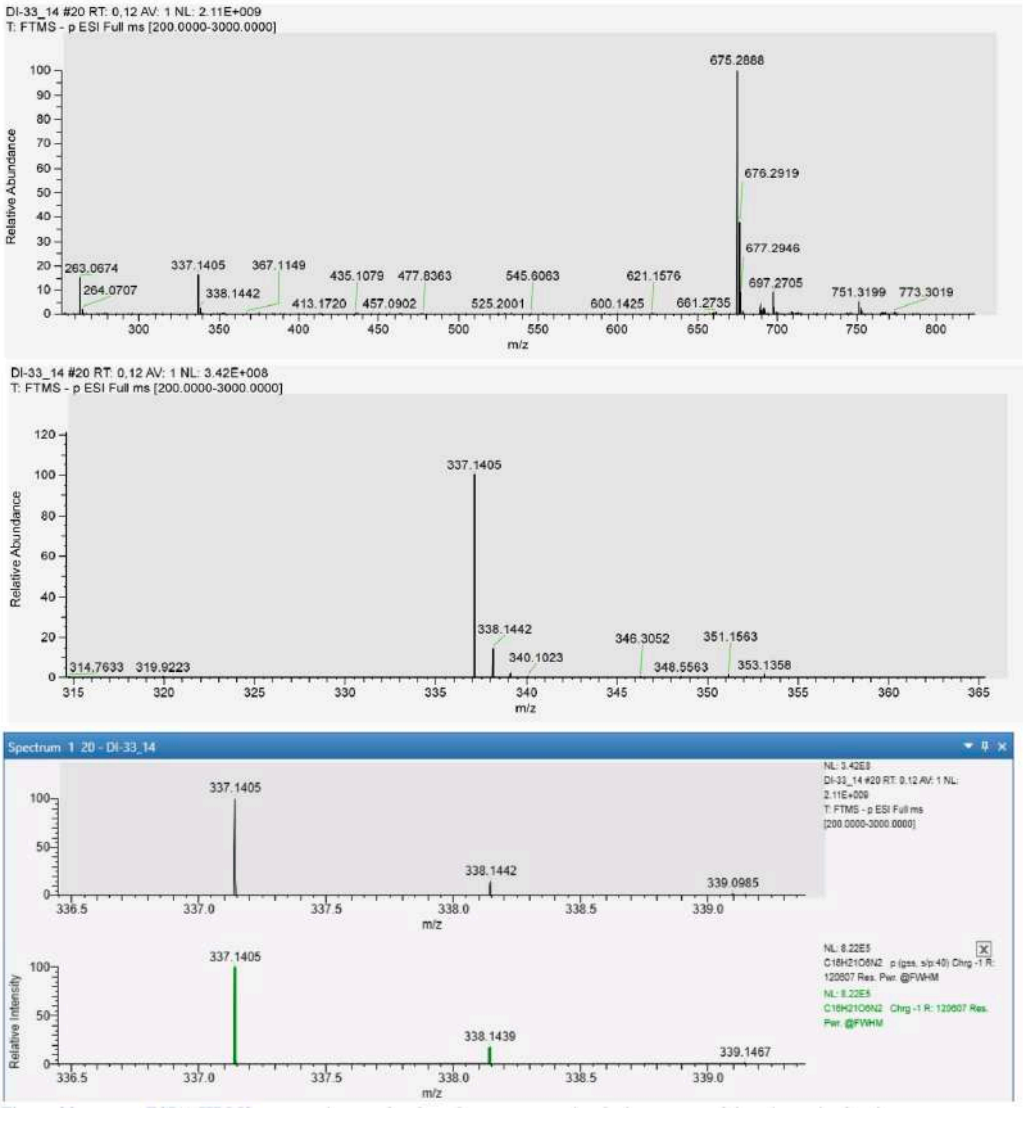

Peak Mass	Display Formula	Combined Fit	RDB	Delta [ppm]	Theo. mass	Rank	Combined Score	# Matched Iso.	# Missed Iso.	MS Cov. [%]	Pattern Cov. [%]
337.1405	$C_{15}H_{21}O_6N_2$	19.12	7.5	0.07	337.14051	1	92.87	3	2	96.96	97.84

HRMS compound **24**

(S)-3-(2-amino-5,7-dimethylbenzo[d]thiazol-6-yl)-2-((tert butoxycarbonyl)amino)propanoic acid, compound **26**:

Yield: 70%, white solid

T_R: 13.64 min. HRMS *m/z:*

$[M-H]^-$ calcd for $C_{17}H_{22}N_3O_4S$ 364.1336; found 364.1339.

$[\alpha]_D^{23}$ = -41.1 (c=0.009, MeOH).

IR 2927, 1692, 1513, 1158 cm^{-1}.

MP 190-192 °C.

^1H NMR (400 MHz, CD_3OD) (rotamers mixture) δ 7.08 (s, 1H), 4.35 (dd, *J* = 9.1, 6.0 Hz, 1H), 3.29 – 2.99 (m, 2H), 2.43 (s, 3H), 2.42 (s, 3H), 1.33 (s, 7H), 1.11 (s, 2H).

^{13}C NMR (101 MHz, CD_3OD) δ 175.8, 169.4, 157.6, 149.6, 137.0, 130.9, 130.0, 129.6, 118.1, 80.4, 55.2, 33.3, 28.6, 28.1, 20.9, 19.6.

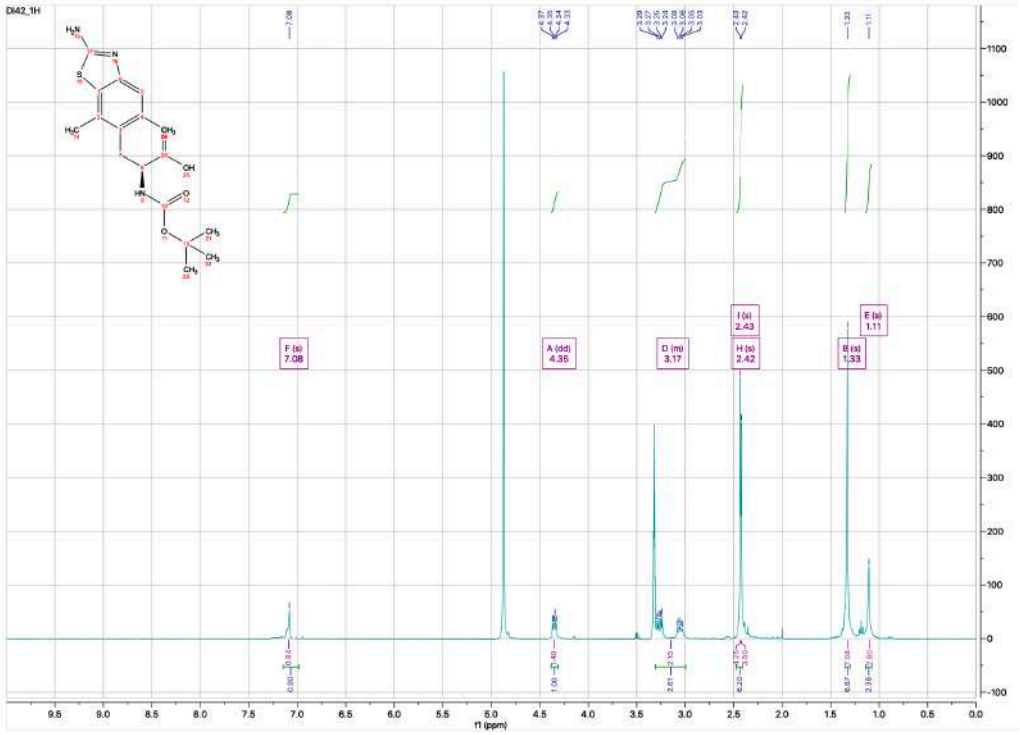

^1H NMR compound **26**

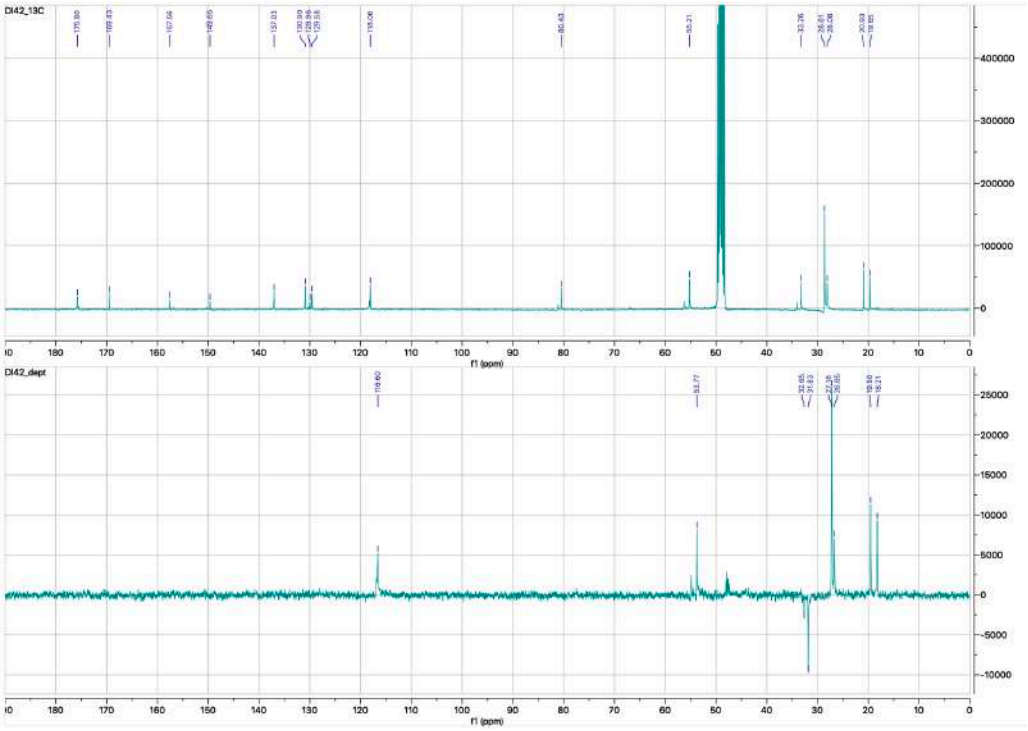

^{13}C and DEPT NMR compound **26**

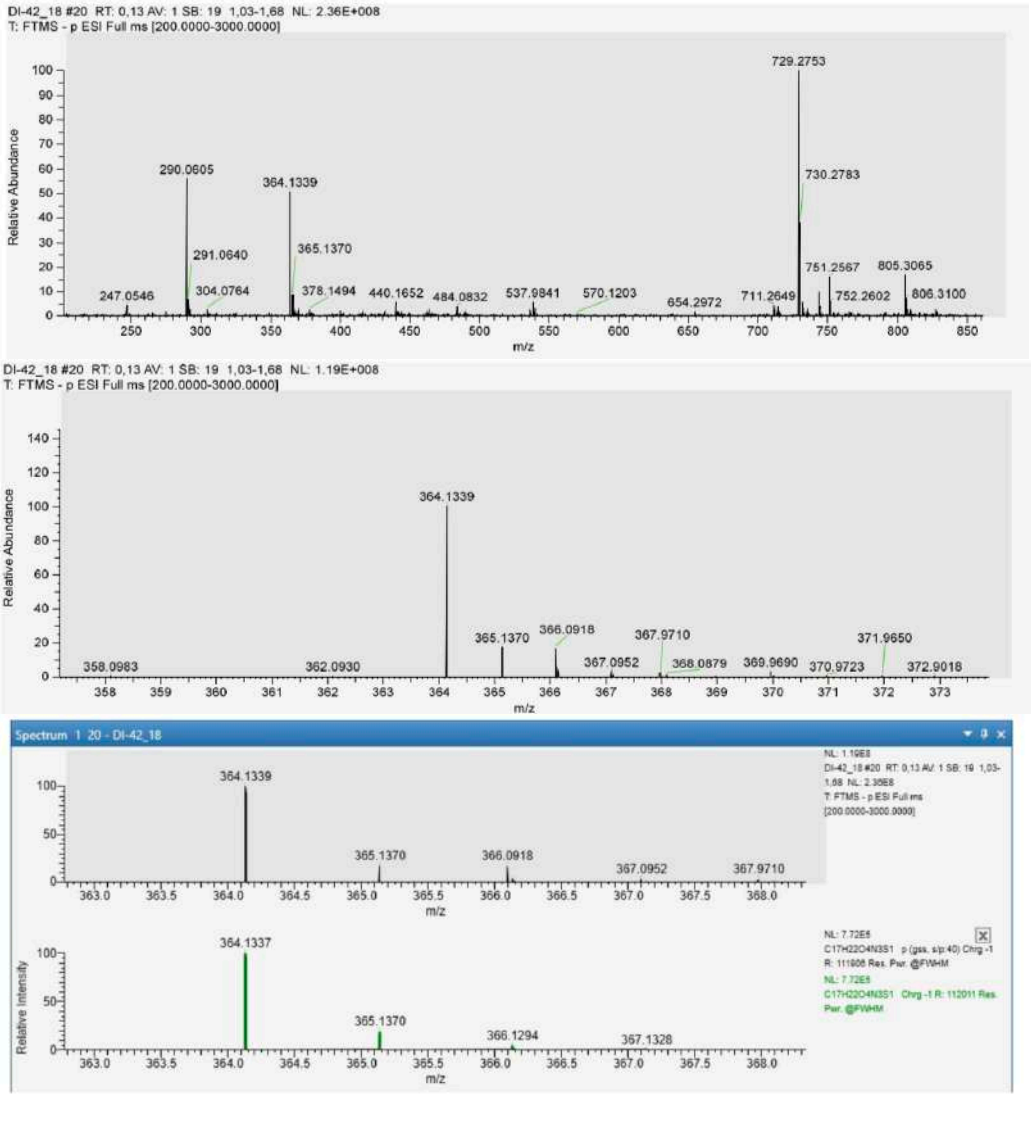

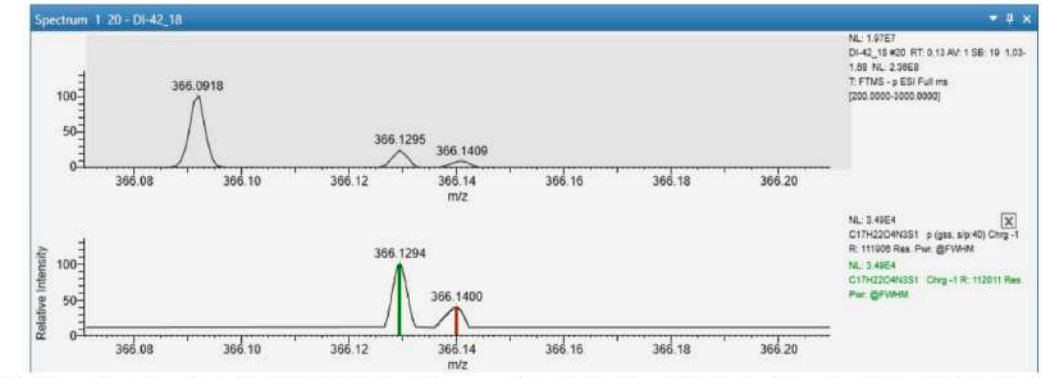

Peak Mass	Display Formula	Combined Fit	RDB	Delta [ppm]	Theo. mass	Rank	Combined Score	# Matched Iso.	# Missed Iso.	MS Cov. [%]	Pattern Cov. [%]
364.1339	$C_{17}H_{22}O_4N_3{}^{32}S$	28.00	8.5	0.58	364.13365	1	79.20	4	3	82.04	97.35

HRMS compound **26**

General procedure for acidic hydrolysis and Fmoc protection (**19**, **20**):

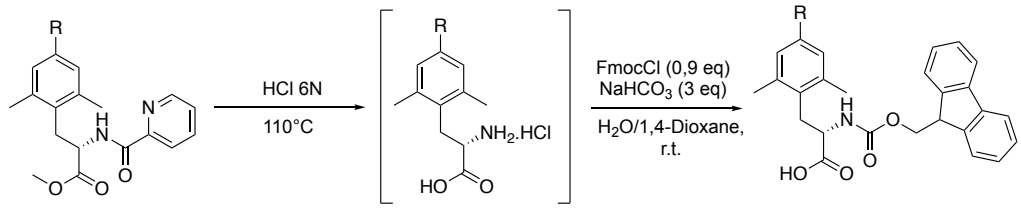

11: R = F
13: R = H

19: R = F
20: R = H

Once purified, the compound was dissolved in HCl 6N aqueous solution (17 equiv.) and heated at 110 °C for 24 hours. The obtained hydrolyzed crude product was concentrated under vacuum to reduce the volume and the crude solution was used directly for the subsequent protection step.

The HCl salt synthesized was used as crude. It was diluted in water/dioxane (1:2) solution (0.2 M) and basified with $NaHCO_3$ (3 eq) aqueous solution until pH 10/11 at 0 °C. FmocCl (0,9 eq) was added and the reaction was left stirring at r.t. for 2 hours. The reaction was monitored by ESI mass spectrometry and TLC, at the complete consumption of starting material. The dioxane was then removed under vacuum and HCl 1N aqueous solution was added at 0 °C to pH 1. The mixture was extracted with ethyl acetate (3 times) and the organic phases combined were dried over Na_2SO_4 and concentrated under vacuum. The crude was purified by flash chromatography (1:1 AcOEt/petroleum ether/1% acetic acid) and crystallized with 2:1 Et_2O/petroleum ether.

(S)-2-((((9H-fluoren-9-yl)methoxy)carbonyl)amino)-3-(4-fluoro-2,6-dimethylphenyl)propanoic acid, compound **19**:

Yield: 75% white solid

T_R: 23.33 min.

HRMS *m/z:* $[M+H]^+$ calcd for $C_{26}H_{25}NO_4F$ 434.1762; found 434.1762.

$[\alpha]_D^{22}$ = -3.32 (c=0.006, MeOH).

IR 3313, 1716, 1696, 1533, 730 cm^{-1}.

MP 197-199 °C.

^{1}H NMR (400 MHz, CD_3OD) δ 7.79 (d, *J* = 7.5 Hz, 2H), 7.60 (d, *J* = 4.2 Hz, 2H), 7.38 (t, *J* = 6.9 Hz, 2H), 7.30 (q, *J* = 6.9 Hz, 2H), 6.70 (d, *J* = 9.6 Hz, 2H), 4.42 – 4.36 (m, 1H), 4.26 (dd, *J* = 10.3, 6.9 Hz, 2H), 4.14 (t, *J* = 6.7 Hz, 1H), 3.28 – 2.90 (m, 2H), 2.35 (s, 6H).

^{13}C NMR (101 MHz, CD_3OD) δ 175.3, 162.4 (d, *J* = 243 Hz), 158.3, 145.2, 142.5, 140.8, 131.5, 128.7, 128.1, 126.2, 120.9, 115.4 (d, *J* = 21 Hz), 67.9, 55.2, 46.9, 32.6, 20.5.

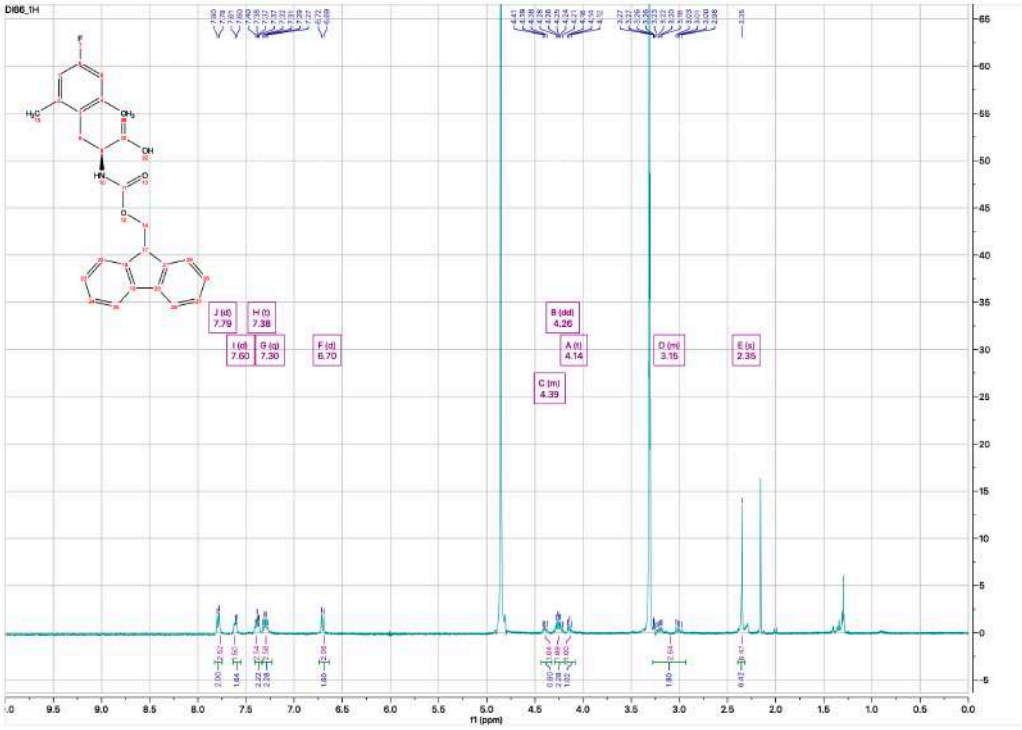

^{1}H NMR compound **19**

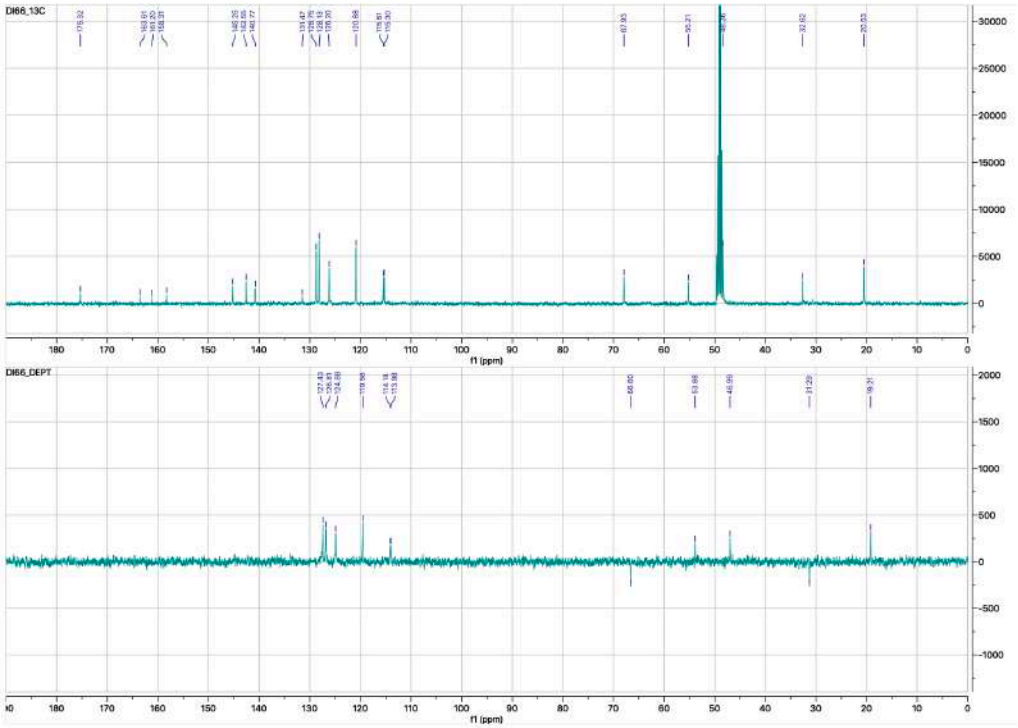

^{13}C and DEPT NMR compound **19**

HRMS compound **19**

(S)-2-((((9H-fluoren-9-yl)methoxy)carbonyl)amino)-3-(2,6-dimethylphenyl)propanoic acid, compound **20**:

Yield: 80%, white solid.

T_R: 23.30 min.

HRMS *m/z:* $[M-H]^-$ calcd for $C_{26}H_{24}NO_4$ 414.1711; found 414.1715. $[2M-H]^-$ calcd for $C_{52}H_{49}N_2O_8$ 829.3494; found 829.3503.

$[\alpha]_D^{23}$ = -284.7 (c=0.04, MeOH).

IR 3319, 2962, 1726, 1702, 1258, 1016, 794, 737 cm^{-1}.

MP 153-155 °C.

^{1}H NMR (400 MHz, DMSO) δ 12.65 (s, 1H), 7.88 (d, *J* = 7.6 Hz, 2H), 7.83 (d, *J* = 8.8 Hz, 1H), 7.72 – 7.61 (m, 2H), 7.49 – 7.36 (m, 2H), 7.32 (td, *J* = 7.5, 1.2 Hz, 2H), 6.98 – 6.89 (m, 3H), 4.24 – 4.07 (m, 4H), 3.16 – 2.91 (m, 2H), 2.30 (s, 6H).

^{13}C NMR (101 MHz, DMSO) δ 173.5, 155.9, 143.8, 140.7, 136.7, 134.9, 128.0, 127.6, 127.0, 126.1, 125.3, 120.1, 65.7, 53.9, 46.5, 31.3, 19.9.

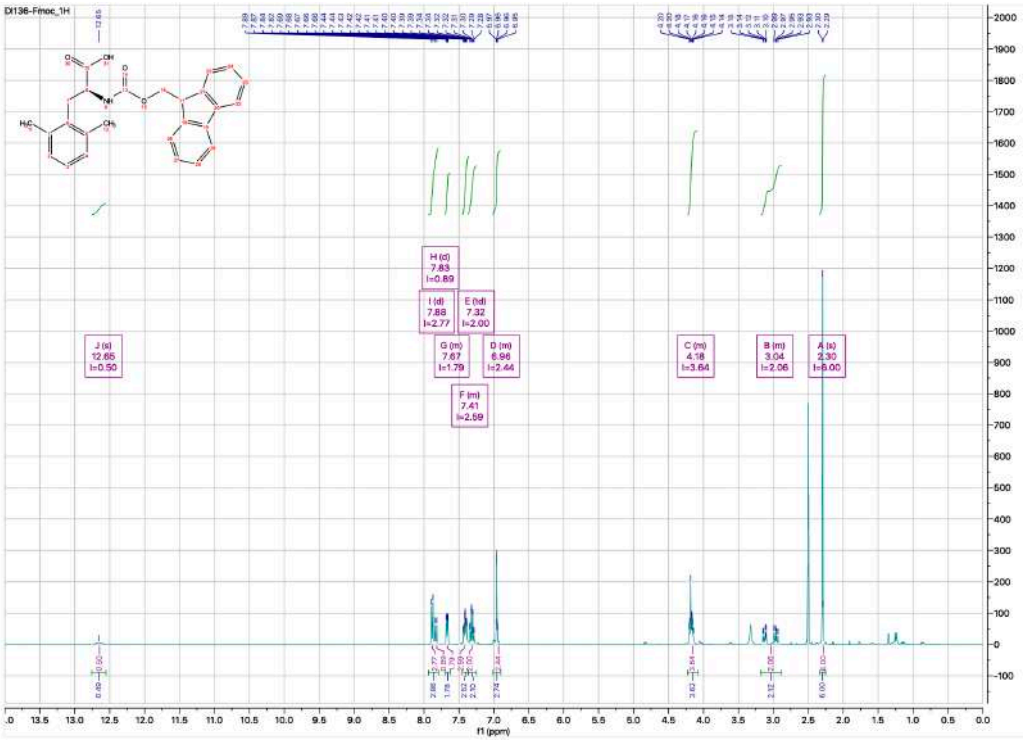

^{1}H NMR compound **20**

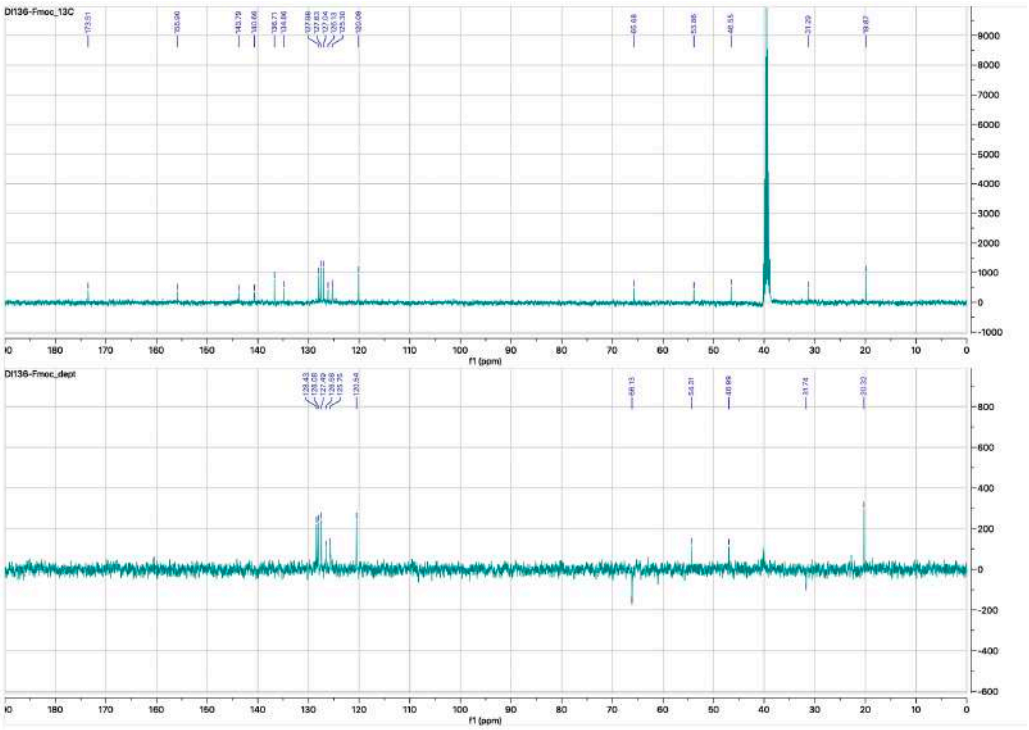

^{13}C and DEPT NMR compound **20**

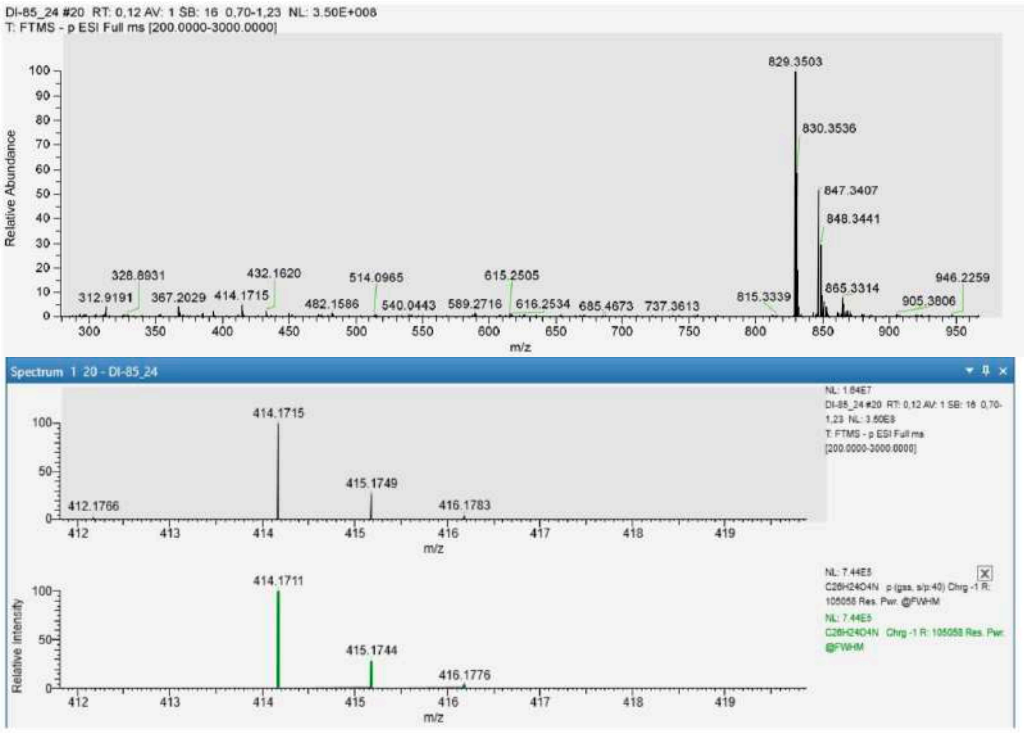

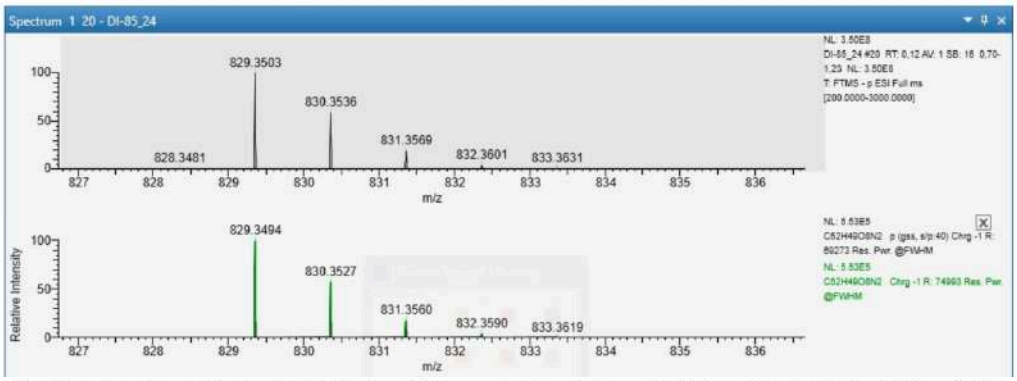

Peak Mass	Display Formula	Combined Fit	RDB	Delta [ppm]	Theo. mass	Rank	Combined Score	# Matched Iso.	# Missed Iso.	MS Cov. [%]	Pattern Cov. [%]
414.1715	$C_{7n}H_{2+}O_4N$	49.29	15.5	0.96	414.17108	1	97.33	3	0	100.00	100.00
Peak Mass	Display Formula	Combined Fit	RDB	Delta [ppm]	Theo. mass	Rank	Combined Score	# Matched Iso.	# Missed Iso.	MS Cov. [%]	Pattern Cov. [%]
829.3503	$C_{53}H_{45}O_8N_2$	41.02	29.5	1.07	829.34944	4	96.63	5	0	99.72	99.65

HRMS compound **20**

Analytical HPLC and masses of peptides [Dmp^4]N/OFQ(1-13)-NH_2 (**IV**), [(*p*-F)Dmp^4]N/OFQ(1-13)-NH_2 (**V**) and [(*p*-NO_2)Dmp^4]N/OFQ(1-13)-NH_2 (**VI**).

Molecular Weight (**IV**): 1409,64

MS (ESI): **IV**: m/z calcd for $C_{61}H_{100}N_{22}O_{15}$ $[M+2H]^{2+}$ 705.82; found 706.19

T_R: 12,3

Molecular Weight (**V**): 1427.65

MS (ESI): **V**: m/z calcd for $C_{63}H_{103}FN_{22}O_{15}$ $[M+2H]^{2+}$ 714.82; found 714.99

T_R: 13,1

Molecular Weight (**V**): 1454.64

MS (ESI): **VI**: m/z calcd for $C_{63}H_{103}N_{23}O_{17}$ $[M+2H]^{2+}$ 728.32; found 728.50

T_R: 12,3

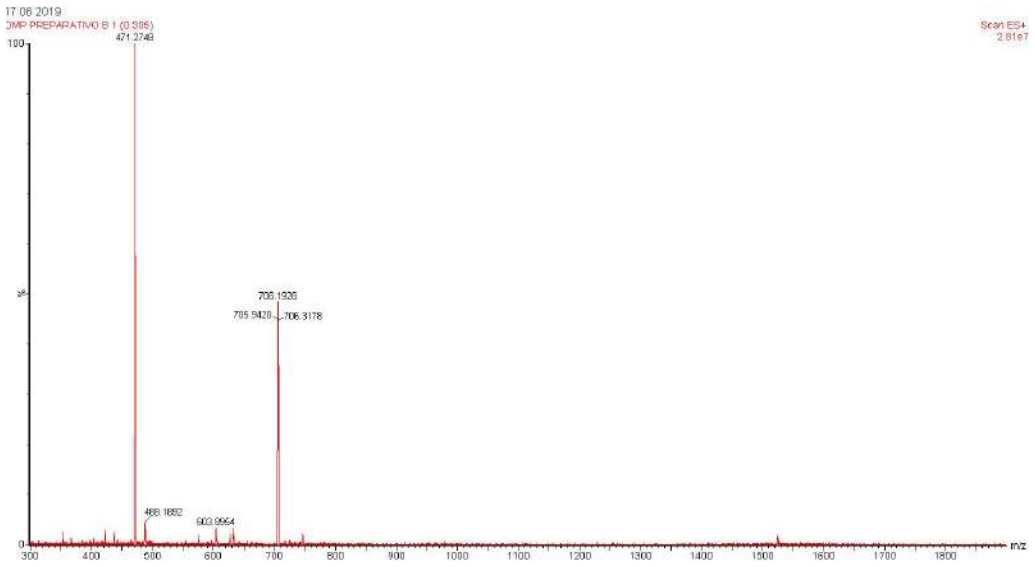

MS(ESI) m/z $[M+2H]^{2+}$ **IV**

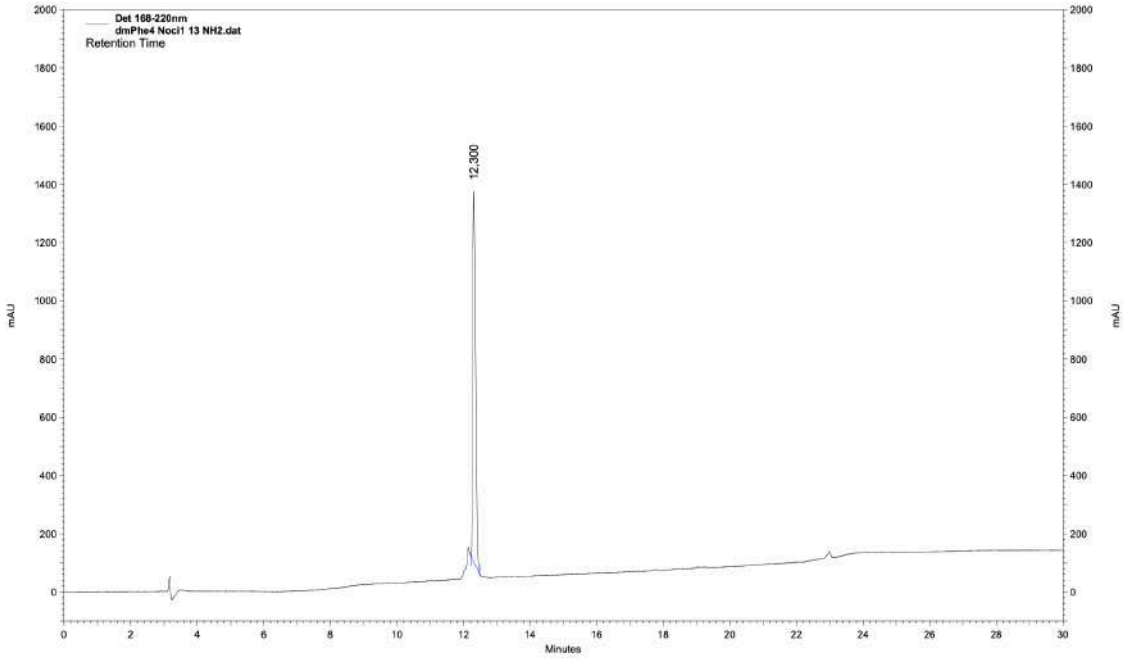

Analytical HPLC **IV**

MS(ESI) m/z $[M+2H]^{2+}$ **V**

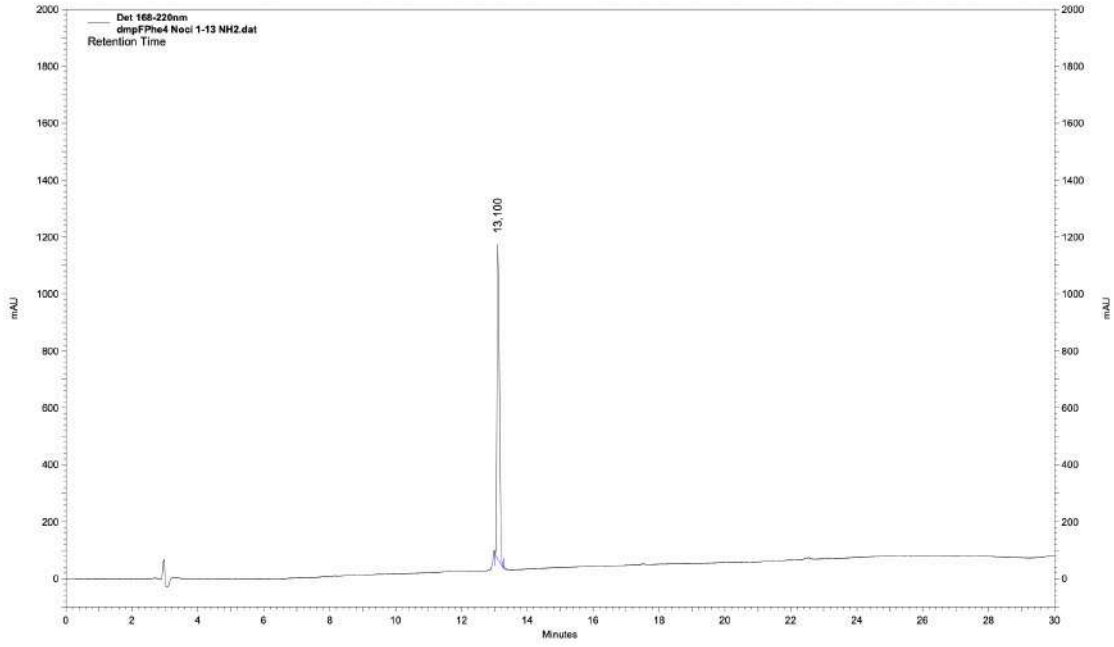

Analytical HPLC **V**

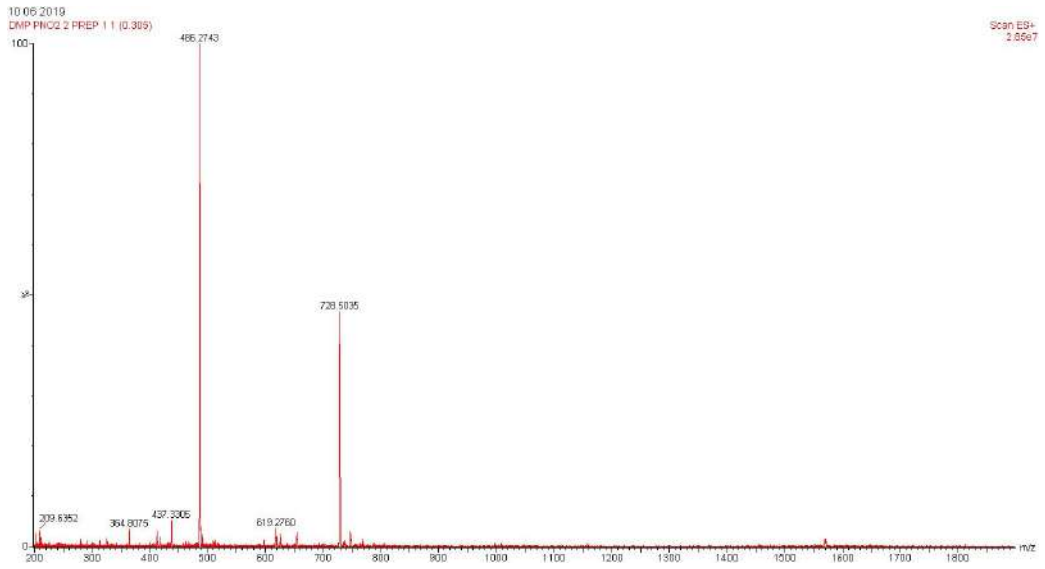

MS(ESI) m/z $[M+2H]^{2+}$ **VI**

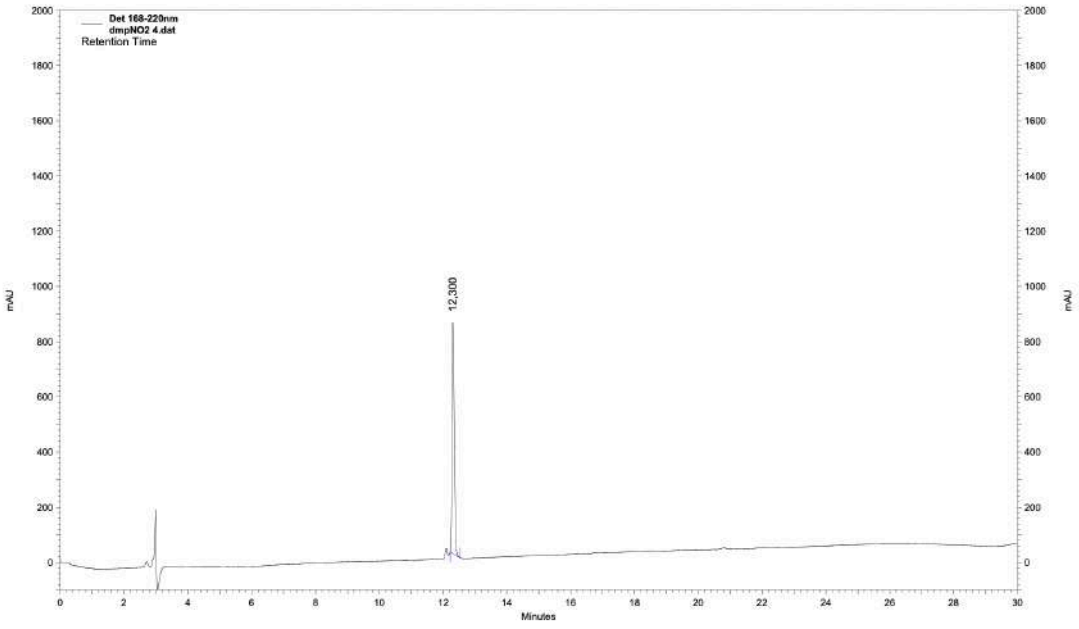

Analytical HPLC **VI**

7.3 Innovative synthesis of mono-methyl Tyrosine (Mmt)

Synthesis of *methyl (S)-3-(4-hydroxy-3-nitrophenyl)-2-(picolinamido)propanoate* (**28**):

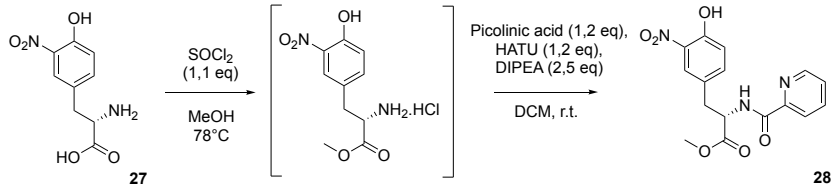

To a solution of 4-fluoro-*L*-phenylalanine (13.26 mmol, 3.00 g) in anhydrous MeOH (100 mL) was added $SOCl_2$ (14.58 mmol, 1.06 mL) in a dropwise manner. The reaction mixture was heated at reflux overnight. The solvent was removed under vacuum to give the crude methyl-4-hydroxy-3-nitro phenylalanine hydrochloride, which was washed with 50 mL of saturated sodium bicarbonate aqueous solution (to pH ~ 8) and extracted with DCM. The organic layers were combined and evaporated under vacuum to give the corresponding ester as yellowish solid, which was used directly for the next step.

A mixture of the previous crude amino product, picolinic acid (15.39 mmol, 1.89 g), HATU (15.39 mmol, 5.85 g) and DIPEA (32.07 mmol, 5.59 mL) in 150 mL of DCM was stirred at room temperature overnight. Then, the reaction was quenched with a saturated NH_4Cl aqueous solution and the two layers were separated. The aqueous layer was extracted with DCM (3 times), and the organic layers were combined, dried over Na_2SO_4, filtered and concentrated in vacuum. The residue was purified by flash chromatography (1:1 petroleum ether/AcOEt) to afford compound **28** (3.54 g) as an orange oil.

Compound **28**:

Yield: 80% overall

MS (ESI): m/z $[M+H]^+$ 346,31

^{1}H NMR (400 MHz, Chloroform-*d*) δ 10.47 (d, *J* = 0.4 Hz, 1H), 8.61 – 8.44 (m, 2H), 8.14 (dt, *J* = 7.8, 1.1 Hz, 1H), 7.91 (d, *J* = 2.2 Hz, 1H), 7.85 (td, *J* = 7.7, 1.7 Hz, 1H), 7.50 – 7.36 (m, 2H), 7.06 (d, *J* = 8.6 Hz, 1H), 5.06 (dt, *J* = 8.3, 6.0 Hz, 1H), 3.78 (s, 3H), 3.33 – 3.14 (m, 2H).

^{13}C NMR (101 MHz, Chloroform-*d*) δ 171.39, 164.18, 154.31, 149.13, 148.52, 138.82, 137.53, 133.48, 128.74, 126.73, 125.42, 122.42, 120.34, 53.30, 52.77, 37.26.

^{1}H NMR compound **28**

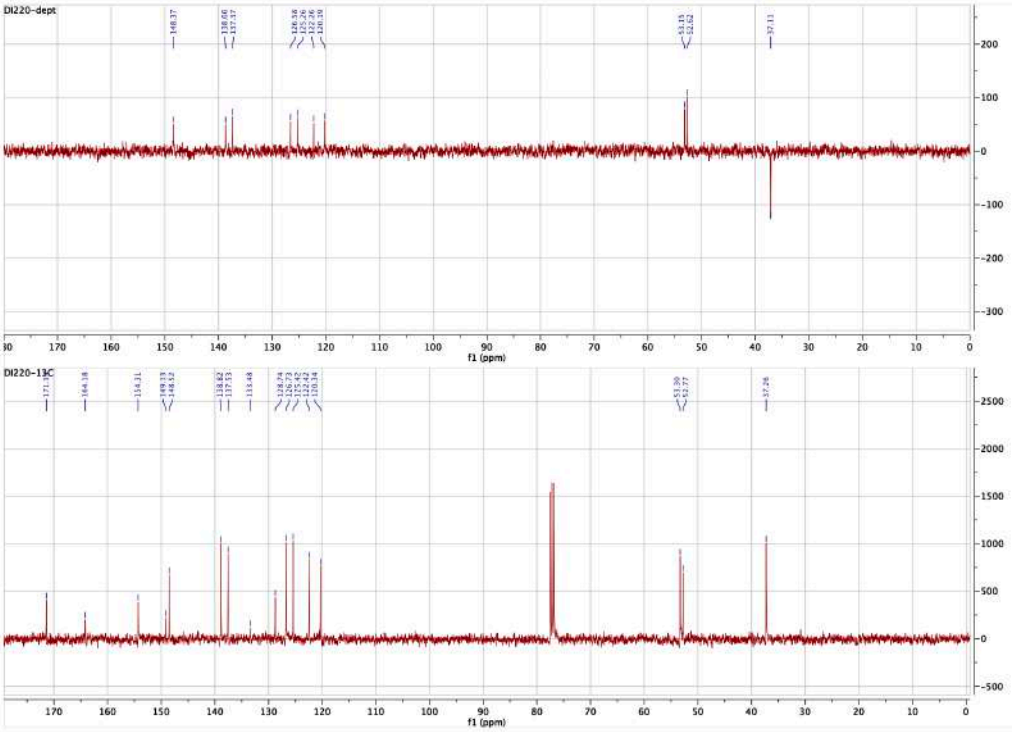

^{13}C and DEPT NMR compound **28**

Synthesis of *methyl (S)-3-(4-((tert-butyldimethylsilyl)oxy)-3-nitrophenyl)-2-(picolinamido)propanoate* (**29**):

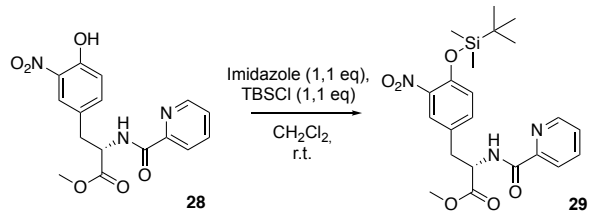

To a solution of **28** (10.25 mmol, 3.54g) in DCM (150 mL), were added imidazole (11.27 mmol, 0.76g) and TBSCl (11.27 mmol, 1.69 g). The reaction mixture was stirred at room temperature overnight before the reaction was quenched by adding saturated $NaHCO_3$. The organic layer was separated and the aqueous layer was extracted (3 times) with DCM. The reunited organic layers were dried over Na_2SO_4, filtered and concentrated under vacuum to give the TBS-ether as a yellowish oil, the crude was purified by flash chromatography (3:2 petroleum ether/AcOEt) to afford compound **29** (3.72 g) as a yellowish oil.

Compound **29**:

Yield: 79%

MS (ESI): m/z $[M+H]^+$ 460,57

^{1}H NMR (400 MHz, Chloroform-*d*) δ 8.56 (ddd, *J* = 4.8, 1.8, 1.0 Hz, 2H), 8.16 (dt, *J* = 7.8, 1.1 Hz, 1H), 7.86 (td, *J* = 7.7, 1.7 Hz, 1H), 7.62 (d, *J* = 2.3 Hz, 1H), 7.46 (ddd, *J* = 7.6, 4.8, 1.2 Hz, 1H), 7.31 – 7.23 (m, 1H), 6.88 (d, *J* = 8.5 Hz, 1H), 5.04 (dt, *J* = 8.3, 6.1 Hz, 1H), 3.76 (s, 3H), 3.31 – 3.14 (m, 2H), 0.98 (s, 9H), 0.22 (d, *J* = 1.3 Hz, 6H).

^{13}C NMR (101 MHz, Chloroform-*d*) δ 171.42, 163.97, 149.01, 148.44, 148.28, 141.75, 137.76, 134.79, 129.46, 126.75, 126.27, 122.59, 122.40, 53.39, 52.71, 37.21, 25.64, 18.30, -4.26.

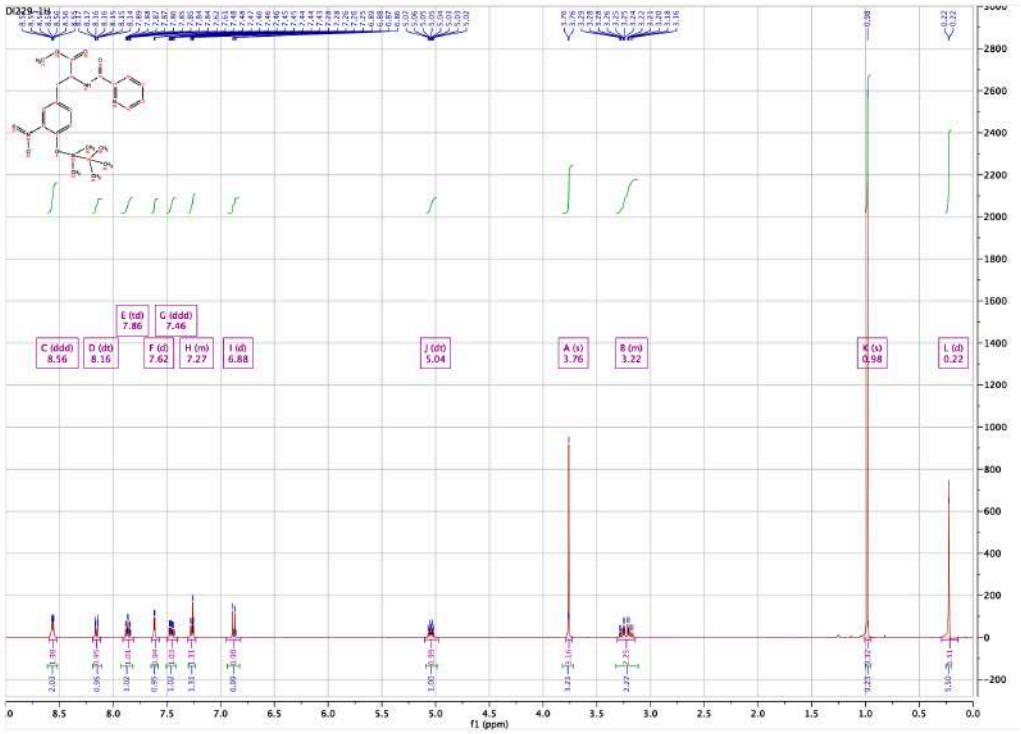

^{1}H NMR compound **29**

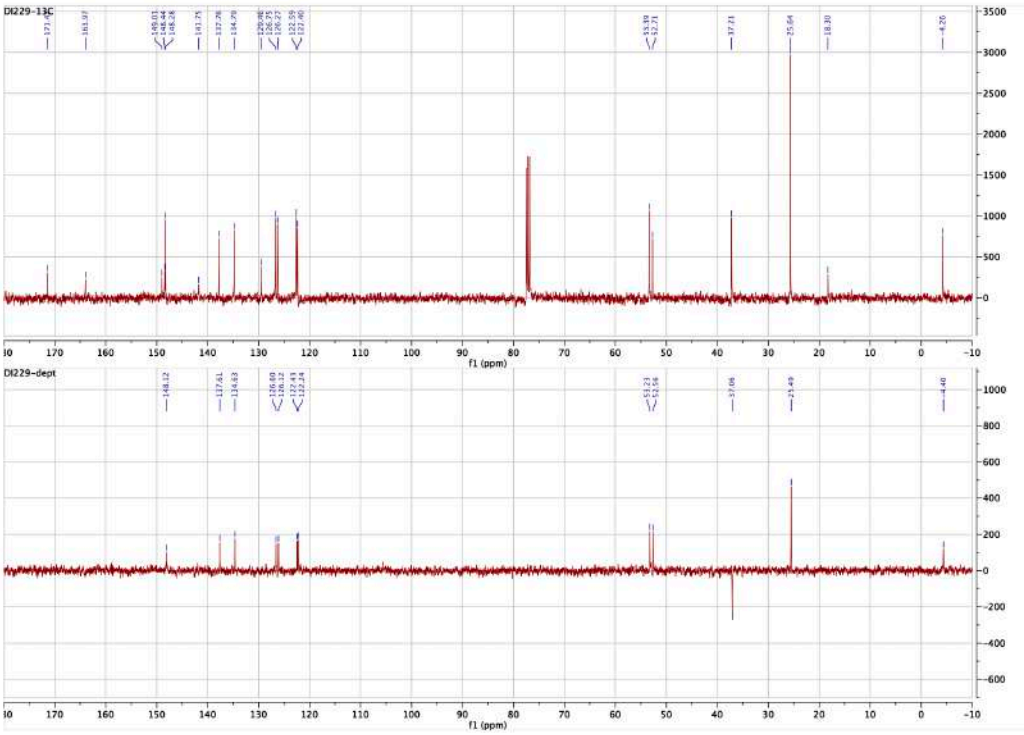

^{13}C and DEPT NMR compound **29**

Synthesis of *methyl (S)-3-(3-amino-4-((tert-butyldimethylsilyl)oxy)phenyl)-2-(picolinamido)propanoate* (**30**):

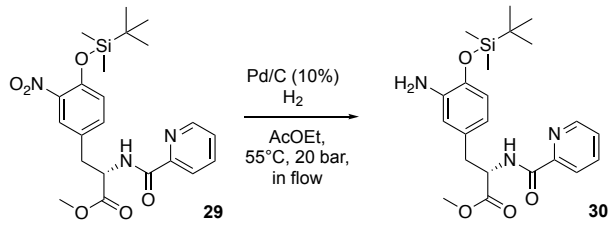

The compound **29** (8.09 mmol, 3.72g) was dissolved in AcOEt (53.96 mL, 0.15 M) and set up in continuous-flow hydrogenator reactor H-Cube Pro Thales-Nano at 55 °C, 20 bar, in 0.5 mL/min flow, with Pd/C (10 mol%) as catalyst. When the reaction was completed, monitored via mass spectrometry, the solvent was concentrated in vacuum to obtain the crude product **30** as red-orange oil which was purified by flash chromatography (1:1 petroleum ether/AcOEt) to afford compound **30** (3.02 g) as an orange oil.

Compound **30**:

Yield: 87%

MS (ESI): m/z $[M+H]^+$ 430,59

^{1}H NMR (400 MHz, Chloroform-*d*) δ 8.54 (ddd, *J* = 4.8, 1.7, 0.9 Hz, 1H), 8.45 (d, *J* = 8.4 Hz, 1H), 8.15 (dt, *J* = 7.9, 1.1 Hz, 1H), 7.82 (td, *J* = 7.7, 1.7 Hz, 1H), 7.41 (ddd, *J* = 7.6, 4.8, 1.2 Hz, 1H), 6.64 (d, *J* = 8.0 Hz, 1H), 6.59 (d, *J* = 2.2 Hz, 1H), 6.45 (dd, *J* = 8.1, 2.2 Hz, 1H), 4.98 (dt, *J* = 8.3, 6.2 Hz, 1H), 3.71 (s, 3H), 3.32 (s, 2H), 3.08 (d, *J* = 6.3 Hz, 2H), 1.05 – 0.95 (m, 9H), 0.21 (s, 6H).

^{13}C NMR (101 MHz, Chloroform-*d*) δ 172.15, 164.11, 149.51, 148.40, 142.26, 137.85, 137.35, 129.48, 126.42, 122.38, 119.54, 118.55, 116.74, 53.65, 52.39, 37.87, 25.95, 18.36, -4.13.

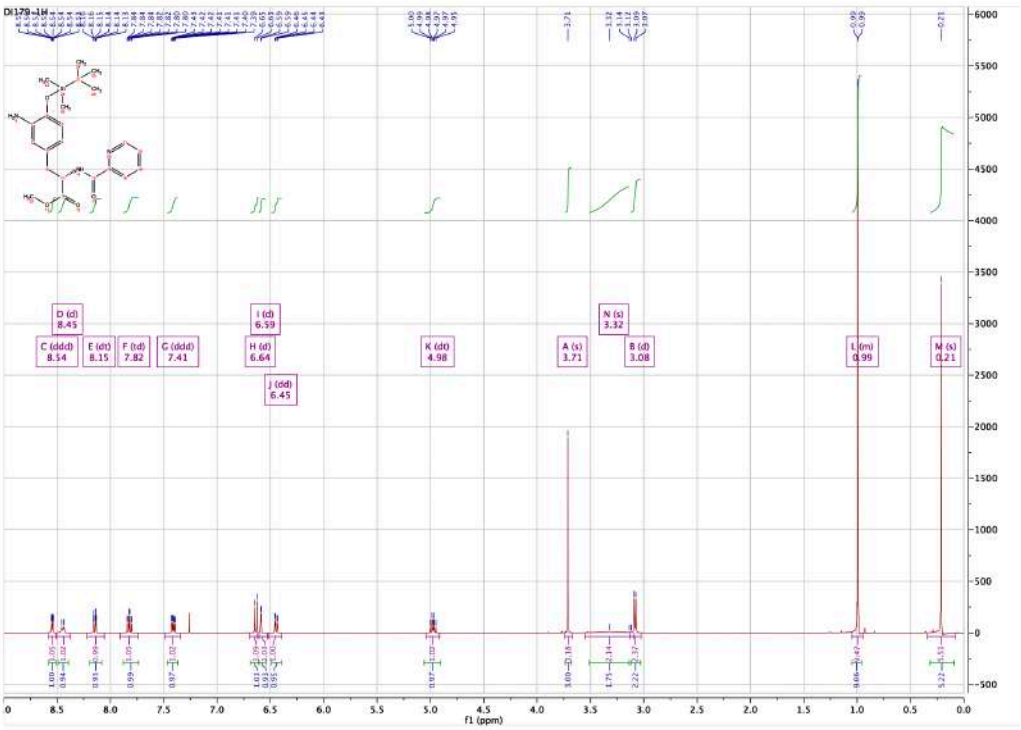

^{1}H NMR compound **30**

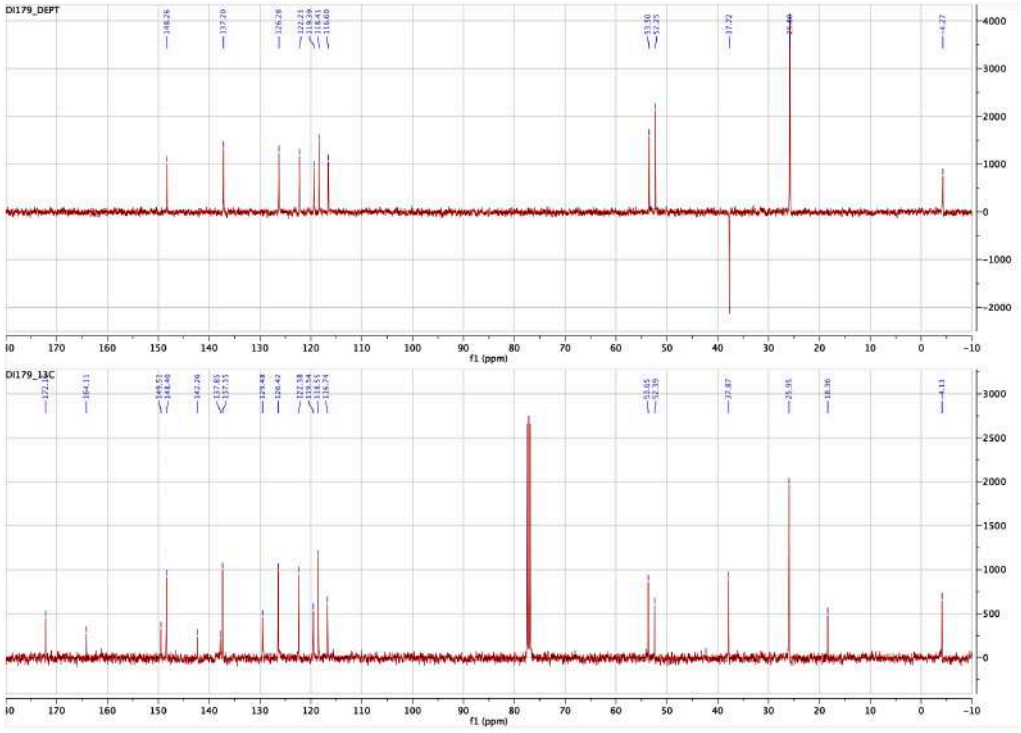

^{13}C and DEPT NMR compound **30**

Synthesis of methyl (*S*)-3-(4-((*tert*-butyldimethylsilyl)oxy)-3-(dibenzylamino)phenyl)-2-(picolinamido)propanoate (**31**):

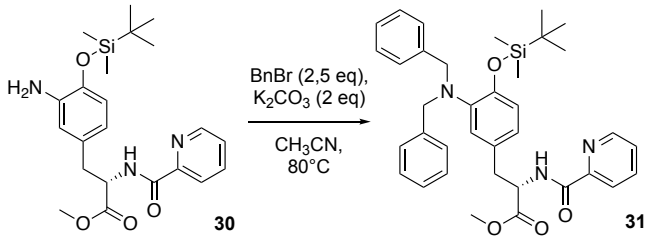

To a solution of the aniline derivative **30** (7.03 mmol, 3.02 g) in CH_3CN (100 mL) was added benzyl bromide (17.57 mmol, 2.09 mL) and potassium carbonate (14.06 mmol, 1.94 g). The mixture was stirred at 80°C overnight. The crude mixture was purified by flash chromatography (1:1 AcOEt/petroleum ether) to afford **31** as an orange oil (3.04 g).

Compound **31**:

Yield: 71%

MS (ESI): m/z $[M+H]^+$ 610,84

^{1}H NMR (400 MHz, Chloroform-*d*) δ 8.44 (d, *J* = 8.4 Hz, 1H), 8.38 (d, *J* = 4.8 Hz, 1H), 8.14 (dt, *J* = 7.8, 1.1 Hz, 1H), 7.80 (td, *J* = 7.7, 1.7 Hz, 1H), 7.34 (t, *J* = 6.3 Hz, 1H), 7.26 – 7.14 (m, 6H), 7.09 (d, *J* = 6.4 Hz, 4H), 6.78 (d, *J* = 8.0 Hz, 1H), 6.68 (d, *J* = 8.2 Hz, 1H), 6.56 (s, 1H), 4.93 (q, *J* = 6.5 Hz, 1H), 4.18 (d, *J* = 14.3 Hz, 2H), 4.08 (d, *J* = 14.3 Hz, 2H), 3.62 (s, 3H), 3.16 – 2.91 (m, 2H), 1.04 (s, 9H), 0.25 (s, 6H).

^{13}C NMR (101 MHz, Chloroform-*d*) δ 171.90, 163.98, 149.53, 148.38, 147.88, 142.63, 138.24, 137.31, 129.21, 128.78, 128.17, 126.99, 126.38, 123.09, 122.34, 120.19, 54.19, 53.57, 52.31, 37.85, 26.11, 18.52, -3.89.

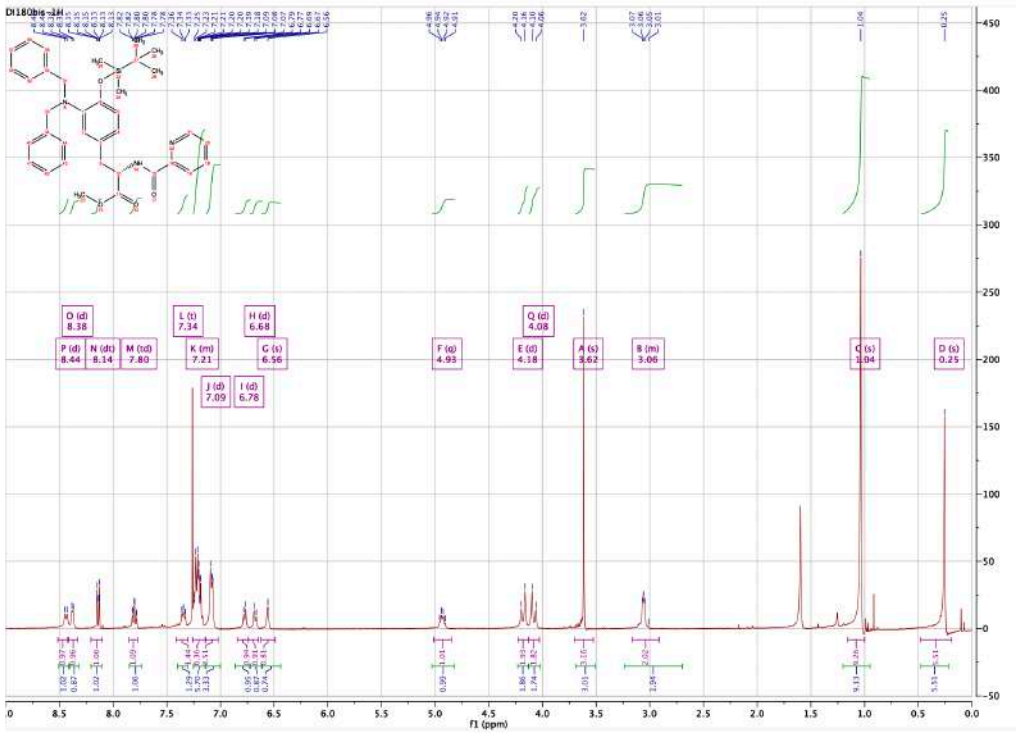

^{1}H NMR compound **31**

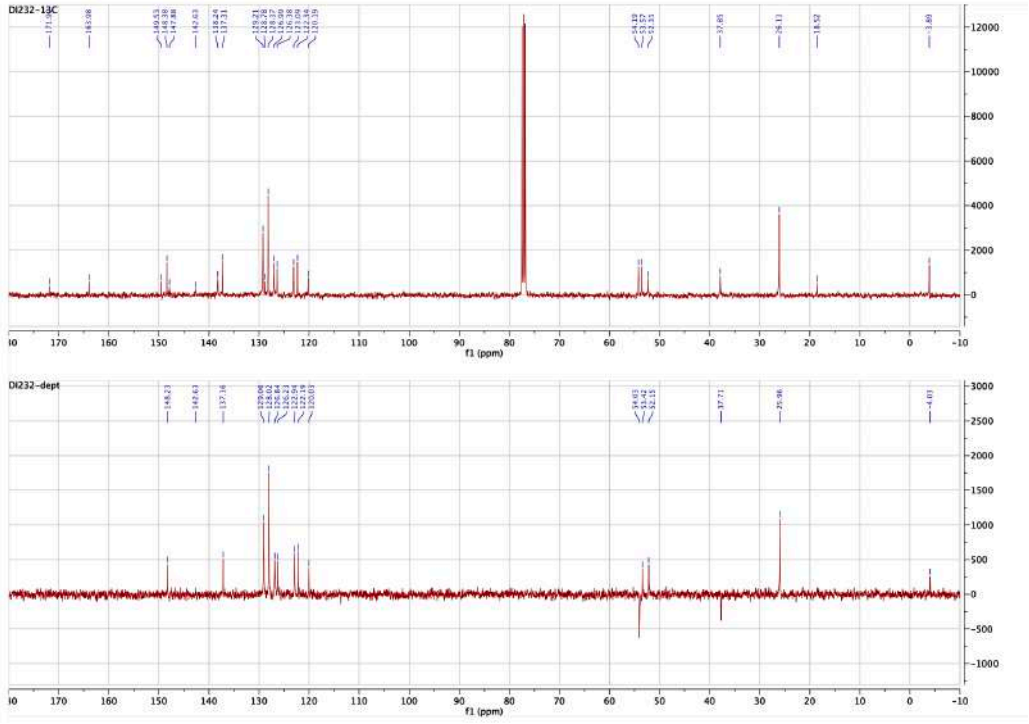

^{13}C and DEPT NMR compound **31**

Synthesis of *methyl (S)-3-(4-((tert-butyldimethylsilyl)oxy)-5-(dibenzylamino)-2-methylphenyl)-2-(picolinamido)propanoate* (**32**):

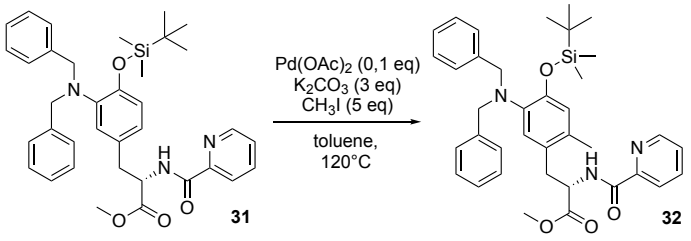

To a solution of compound **31** (4.98 mmol, 3.04 g) in toluene (90 mL) were added K_2CO_3 (14.95 mmol, 2.06 g), CH_3I (24.92 mmol, 1.55 mL), and $Pd(OAc)_2$ (0.49 mmol, 0.11 g). The mixture was stirred at 120 °C overnight. After 24 hours the reaction was cooled to r.t. and filtered through celite pad, washed with AcOEt (50 mL). The filtrate was concentrated under vacuum to obtain the crude product. The crude product was purified by flash chromatography (3:7 AcOEt/petroleum ether), to afford **32** (2.83 g) as a yellowish solid.

Compound **32**:

Yield: 91%

MS (ESI): m/z $[M+H]^+$ 624,87

^{1}H NMR (400 MHz, Chloroform-*d*) δ 8.43 (s, 1H), 8.39 (s, 1H), 8.12 (dt, *J* = 7.8, 1.1 Hz, 1H), 7.78 (td, *J* = 7.7, 1.7 Hz, 1H), 7.38 – 7.28 (m, 1H), 7.20 (ddd, *J* = 12.6, 7.7, 5.9 Hz, 6H), 7.13 – 7.04 (m, 4H), 6.65 (s, 1H), 6.51 (s, 1H), 4.87 (q, *J* = 7.2 Hz, 1H), 4.10 (d, *J* = 10.8 Hz, 4H), 3.59 (s, 3H), 3.09 (dd, *J* = 14.1, 6.4 Hz, 1H), 3.00 (dd, *J* = 14.1, 7.3 Hz, 1H), 2.25 (s, 3H), 1.03 (s, 9H), 0.25 (d, *J* = 2.3 Hz, 6H).

^{13}C NMR (101 MHz, Chloroform-*d*) δ 172.36, 164.01, 149.41, 148.33, 147.66, 140.28, 138.40, 137.33, 130.56, 129.48, 129.20, 128.31, 128.10, 126.91, 126.82, 126.39, 123.93, 122.34, 54.36, 52.96, 52.34, 35.34, 26.11, 18.95, -3.88.

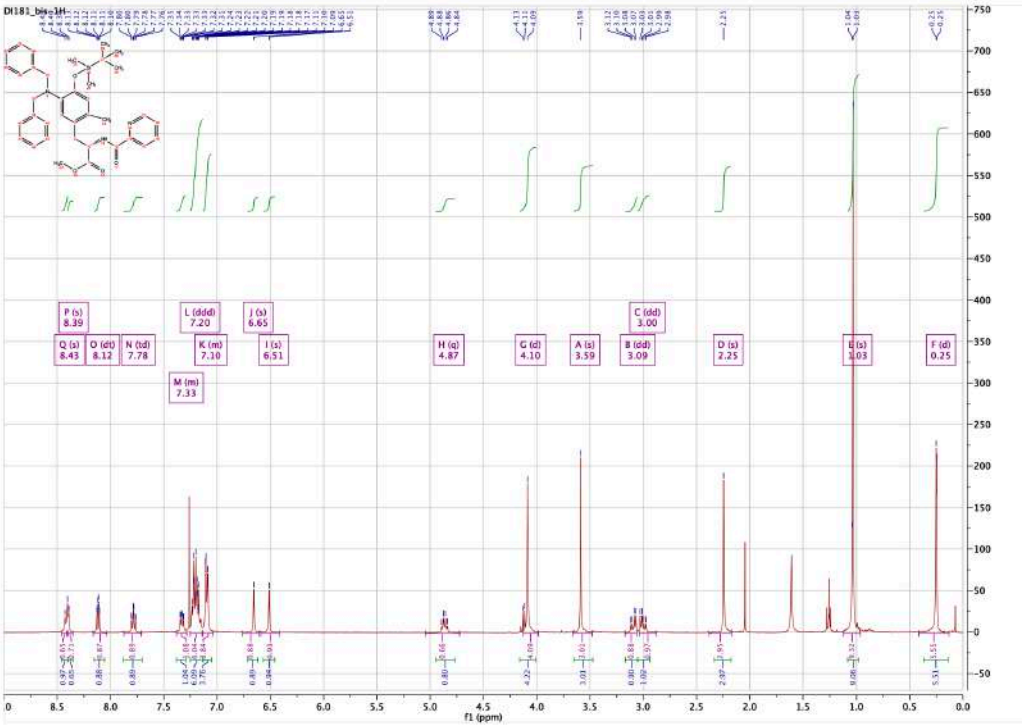

^{1}H NMR compound **32**

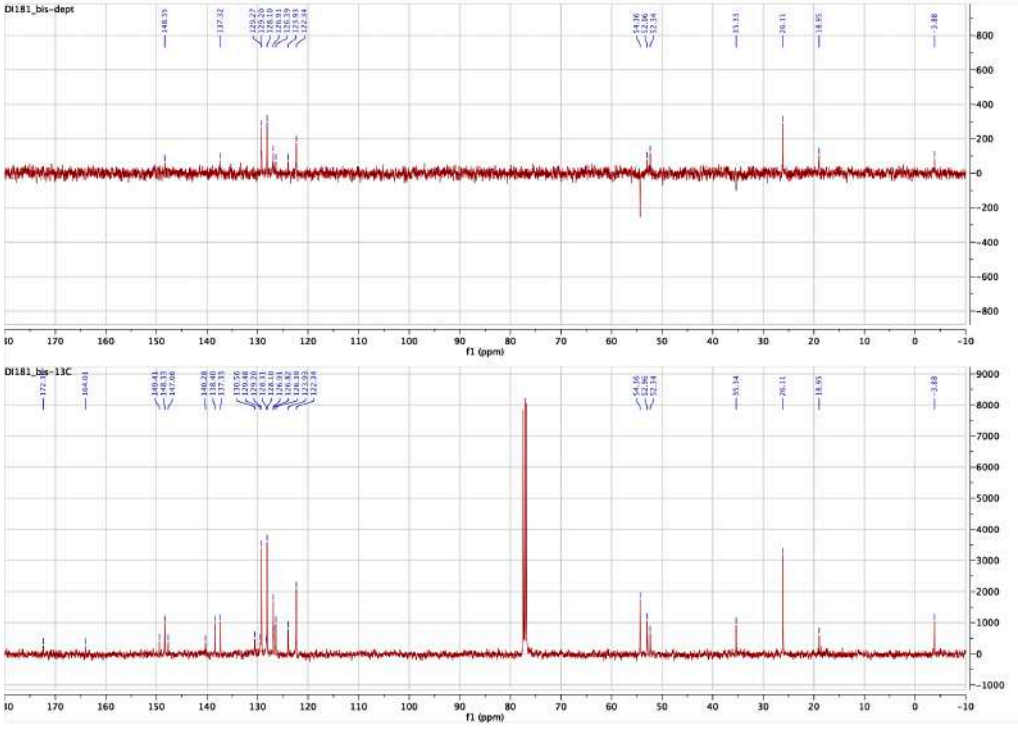

^{13}C and DEPT NMR compound **32**

Synthesis of *methyl (S)-3-(5-amino-4-((tert-butyldimethylsilyl)oxy)-2-methylphenyl)-2-(picolinamido)propanoate* (**33**):

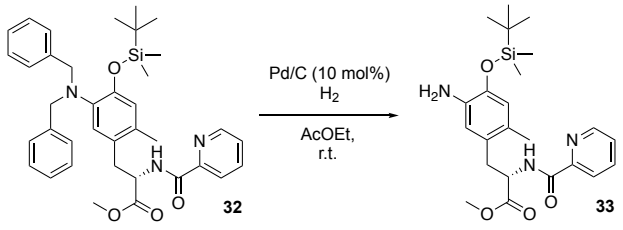

The compound **32** (4.53 mmol, 2,83g) was dissolved in AcOEt (100 mL) and the reductive hydrogenation was performed by the addition of Pd/C (10 mol%) under H_2 atmosphere. Once the reaction was completed, monitored via mass spectrometry, the solvent was concentrated in vacuum to afford the crude product, which was purified by flash chromatography (1:1 AcOEt/petroleum ether) to obtain **33** (1.69 g) as a yellowish oil.

Compound **33**:

Yield: 84%

MS (ESI): m/z $[M+H]^+$ 444,62

^{1}H NMR (400 MHz, Chloroform-*d*) δ 8.54 (ddd, *J* = 4.8, 1.7, 0.9 Hz, 1H), 8.45 (d, *J* = 8.3 Hz, 1H), 8.12 (dt, *J* = 7.8, 1.1 Hz, 1H), 7.81 (td, *J* = 7.7, 1.7 Hz, 1H), 7.40 (ddd, *J* = 7.6, 4.7, 1.2 Hz, 1H), 6.57 (s, 1H), 6.56 – 6.48 (m, 1H), 4.93 (dt, *J* = 8.3, 7.0 Hz, 1H), 3.69 (s, 3H), 3.63 (d, *J* = 20.4 Hz, 2H), 3.10 (dd, *J* = 14.1, 6.9 Hz, 1H), 3.04 (dd, *J* = 14.0, 7.3 Hz, 1H), 2.21 (s, 3H), 0.99 (s, 9H), 0.21 (s, 6H).

^{13}C NMR (101 MHz, Chloroform-*d*) δ 172.52, 164.10, 149.43, 148.34, 142.21, 137.34, 135.25, 127.49, 127.02, 126.41, 122.36, 120.72, 117.76, 53.04, 52.34, 35.47, 25.91, 18.84, 18.33, -4.13.

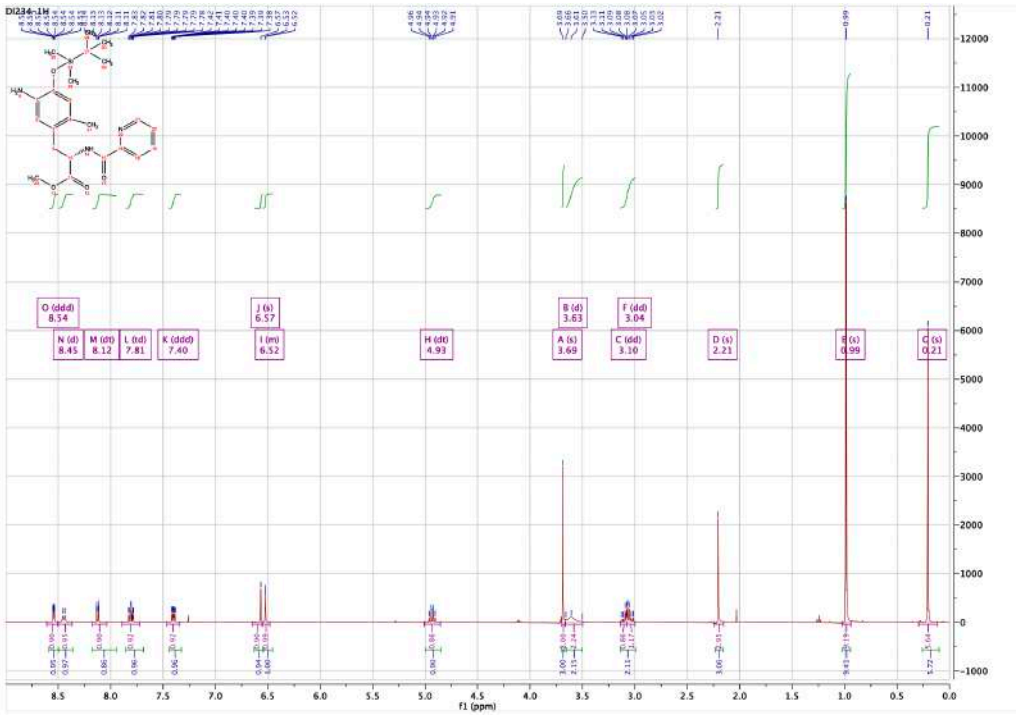

^{1}H NMR compound **33**

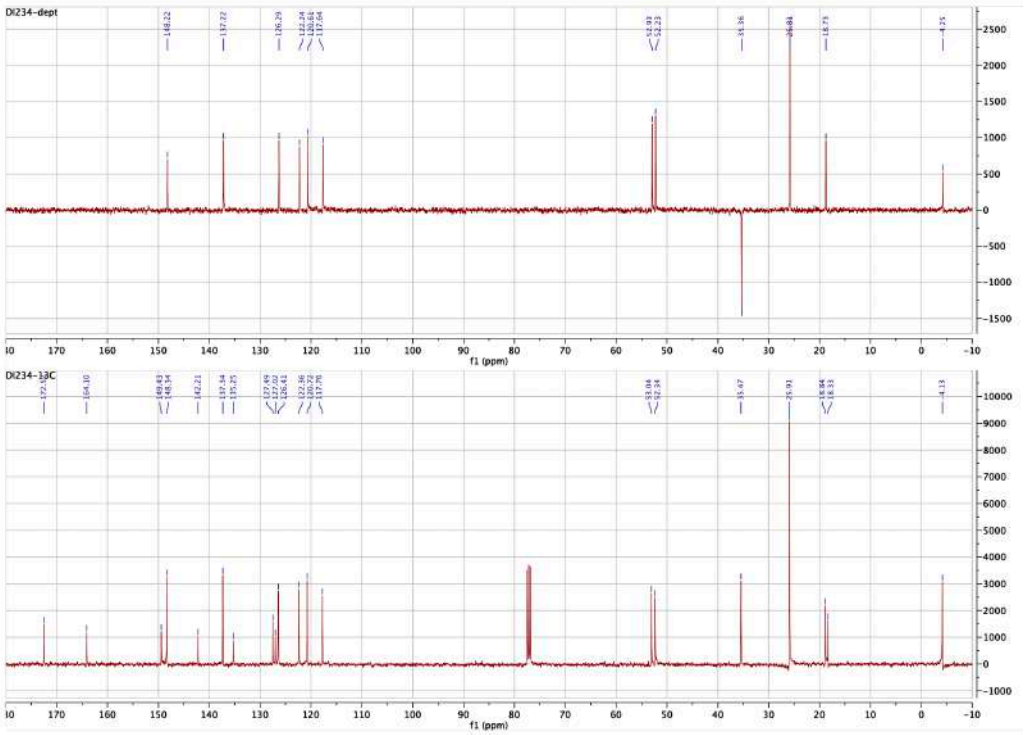

^{13}C and DEPT NMR compound **33**

Synthesis of *(S)-2-((tert-butyldimethylsilyl)oxy)-5-(3-methoxy-3-oxo-2-(picolinamido)propyl)-4-methylbenzenediazonium* (**34**):

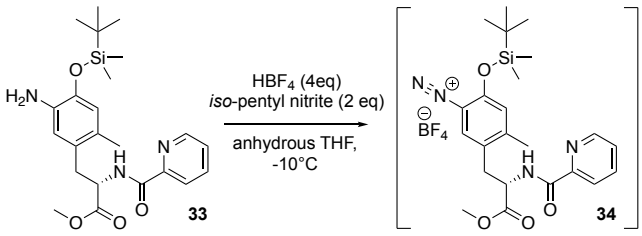

To a solution of compound **33** (3.81 mmol, 1.69 g) dissolved in anhydrous THF (30 mL), cooled to -10 °C, *iso*-pentyl nitrite (7.61 mmol, 1.02 mL) and HBF_4 (15.23 mmol, 0.95 mL) were added. The reaction was stirred for 4 hours at -10 °C and a orange precipitate was formed, which was directly used as wet crude for the next step. It was performed a diazocopulation assay on the crude **34**, with positive result.

Synthesis of *methyl (S)-3-(4-((tert-butyldimethylsilyl)oxy)-2-methylphenyl)-2-(picolinamido)propanoate* (**35**):

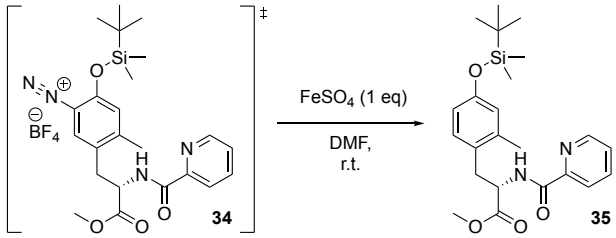

To a solution of Fe_2SO_4 (3.81 mmol, 0.57 g) in 15 mL of DMF was added dropwise to the crude compound **10** (3.71 mmol, 1.73 g) solubilized in DMF (5.00 mL). The reaction was stirred overnight, at r.t. The solvent was removed under vacuum and the residue was dissolved in DCM. The organic layer was washed with water, dried over Na_2SO_4, filtered and concentrated in vacuum. The crude orange oil was purified by flash chromatography (3:7 AcOEt/petroleum ether) obtaining the compound **35** as a yellow solid (0.55 g).

Compound **35**:

Yield: 34%

MS (ESI): m/z $[M+H]^+$ 429,60

^{1}H NMR (400 MHz, Chloroform-*d*) δ 8.56 (ddd, *J* = 4.8, 1.9, 0.9 Hz, 1H), 8.49 (d, *J* = 8.4 Hz, 1H), 8.14 (dt, *J* = 7.8, 1.2 Hz, 1H), 7.89 – 7.77 (m, 1H), 7.48 – 7.38 (m, 1H), 6.96 (d, *J* = 8.3 Hz, 1H), 6.65 (d, *J* = 2.6 Hz, 1H), 6.57 (dd, *J* = 8.2, 2.6 Hz, 1H), 4.97 (dt, *J* = 8.5, 7.2 Hz, 1H), 3.68 (s, 3H), 3.18 (dd, *J* = 14.1, 6.9 Hz, 1H), 3.12 (dd, *J* = 14.1, 7.3 Hz, 1H), 2.31 (s, 3H), 0.96 (s, 9H), 0.16 (s, 6H).

^{13}C NMR (101 MHz, Chloroform-*d*) δ 172.28, 163.63, 154.50, 149.02, 147.87, 137.98, 137.64, 130.80, 127.17, 126.41, 122.52, 122.10, 117.45, 52.89, 52.21, 35.38, 25.66, 19.49, 18.17, -4.44.

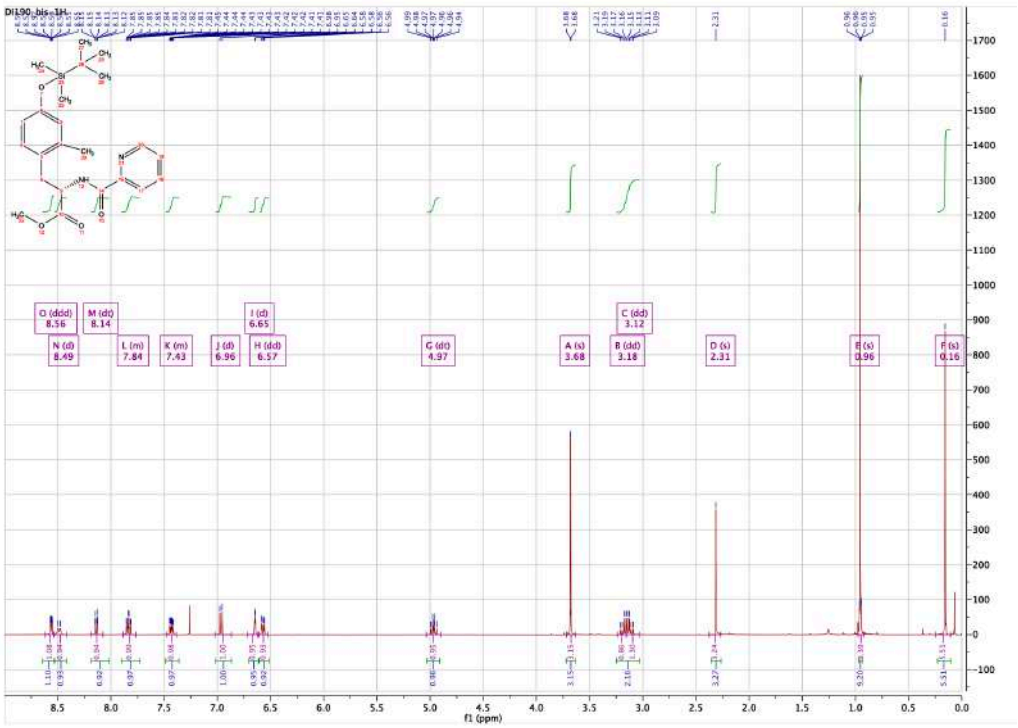

^{1}H NMR compound **35**

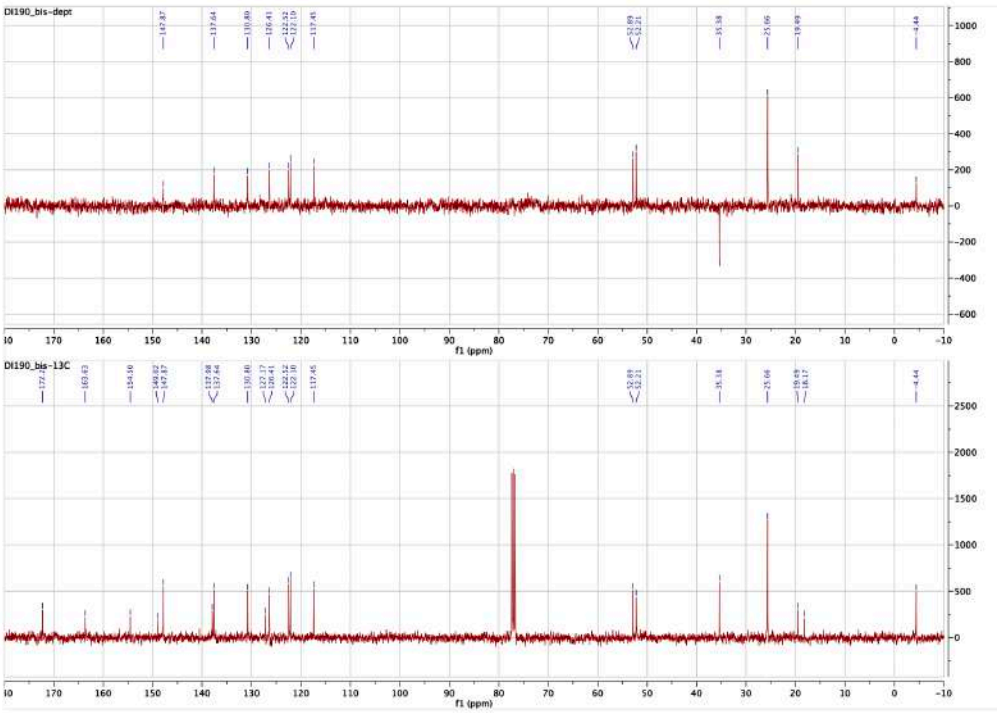

^{13}C and DEPT NMR compound **33**

Synthesis of *(S)-2-((tert-butoxycarbonyl)amino)-3-(4-hydroxy-2-methylphenyl)propanoic acid* (**36**) :

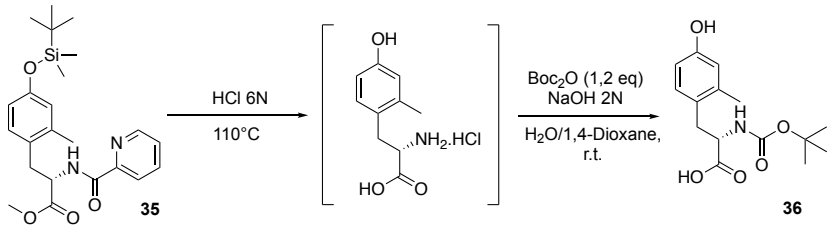

Once purified compound **35** was dissolved in HCl 6N aqueous solution (21.81 mmol, 1.81 mL) and heated at 110 °C for 24 hours. The obtained hydrolyzed crude product was concentrated under vacuum to reduce the volume and the crude solution was used directly for the subsequent protection step.

The HCl salt just synthesized was directly used as crude, and diluted in water/dioxane (1:2) solution (0.2 M). The mixture was basified with NaOH 2N aqueous solution until reachment of pH value of 10/11 at 0 °C. Boc_2O (1.53 mmol, 0.33 g) was added and the reaction was left stirring at r.t. for 12 hours. The completion of the reaction was monitored per ESI mass spectrometry and TLC. The dioxane was removed under vacuum and HCl 1N aqueous solution was added at 0 °C to pH 1. The mixture was extracted with ethyl acetate (3 times)

and the organic phases combined were dried over Na_2SO_4 and concentrated under vacuum. The crude was purified by flash chromatography (7:3 AcOEt/petroleum ether/1% acetic acid) and crystallized with 2:1 Et_2O/petroleum ether, obtaining a white solid as final product, **36**.

Compound **36**:

Yield: 45% (0,17g white solid)

MS (ESI): m/z $[M+H]^+$ 296,34

^{1}H NMR (400 MHz, DMSO-d_6) δ 12.47 (s, 1H), 9.06 (s, 1H), 7.06 (d, J = 8.4 Hz, 1H), 6.95 (d, J = 8.2 Hz, 1H), 6.54 (d, J = 2.6 Hz, 1H), 6.47 (dd, J = 8.2, 2.6 Hz, 1H), 3.99 (ddd, J = 10.0, 8.4, 4.6 Hz, 1H), 2.91 (dd, J = 14.2, 4.7 Hz, 1H), 2.67 (dd, J = 14.2, 10.0 Hz, 1H), 2.19 (s, 3H), 1.32 (s, 9H).

^{13}C NMR (101 MHz, dmso) δ 174.37, 156.17, 155.93, 137.49, 131.17, 126.78, 117.22, 112.79, 78.42, 54.59, 33.78, 28.62, 19.47.

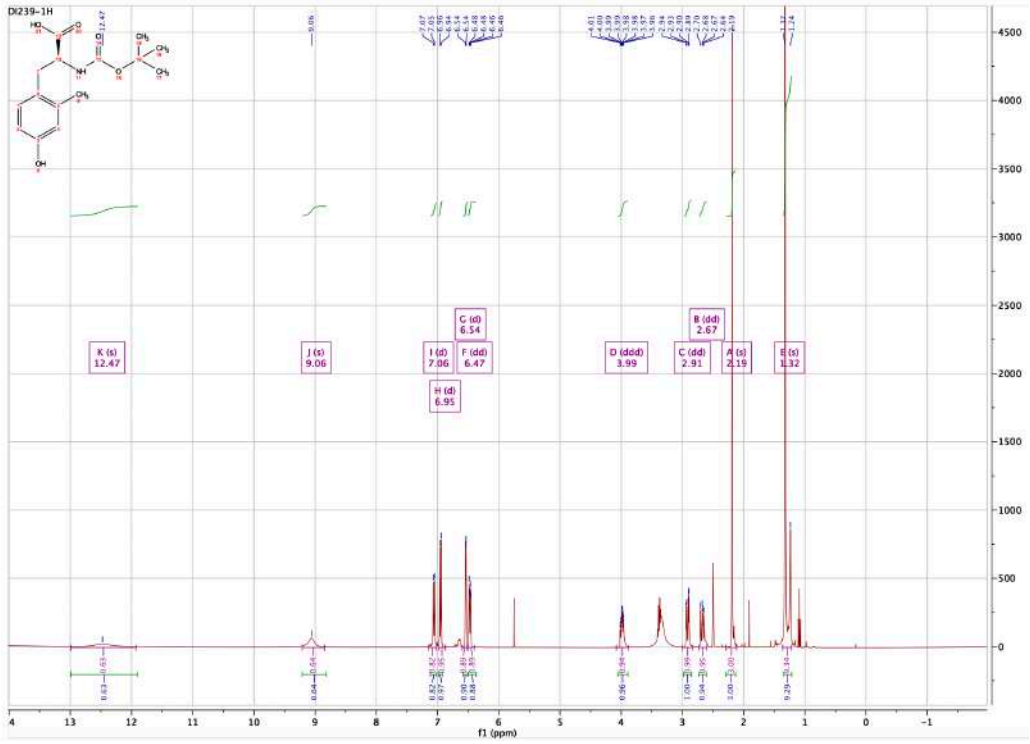

^{1}H NMR compound **36**

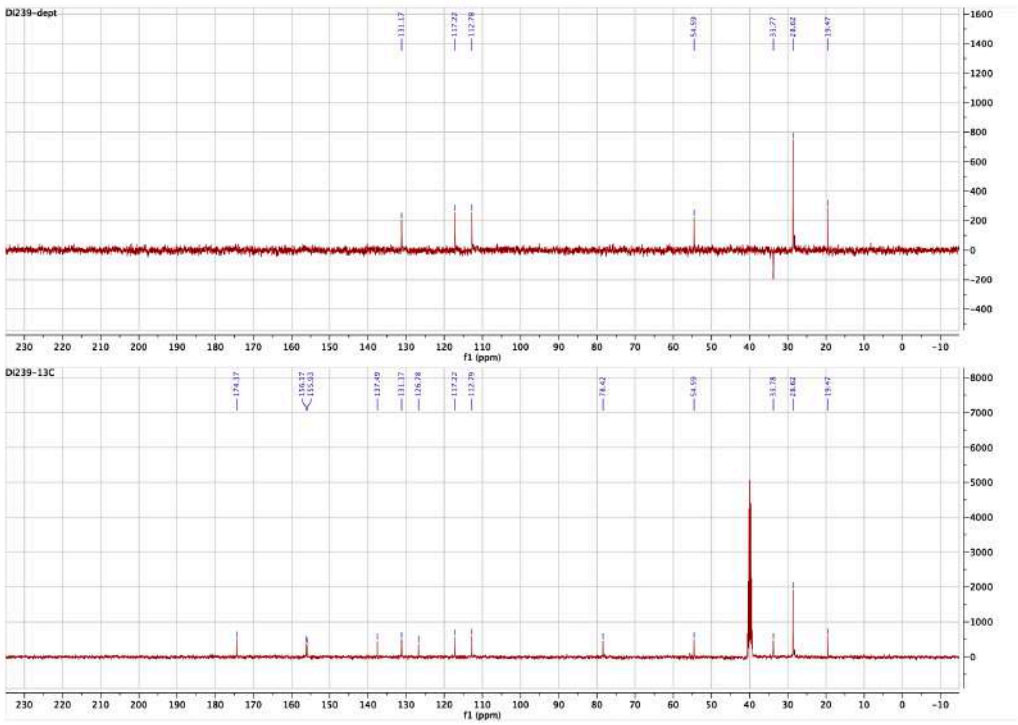

^{13}C and DEPT NMR compound **36**

7.4 Synthesis of non-natural aromatic amino acids via Pd-catalyzed β C-H activation

Synthesis of *(S)-2-(1,3-dioxoisoindolin-2-yl)propanoic acid* (**38**):

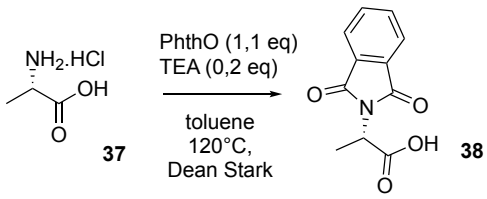

To a solution of *L*-alanine, **37** (10.10 mmol, 0.900 g) in toluene (100 mL) was added phthalic anhydride (PhthO) (10.10 mmol, 1.49 g) and triethylamine (TEA) (2.02 mmol, 0.28 mL). The reaction was performed adding molecular sieves, 4 Å and a Dean Stark apparatus to separate water. It was left stirred at 120°C for 24 h. The reaction was monitored through TLC. Once completed, it was cooled to r.t. and the solvent was removed under vacuum. The crude was dissolved in DCM and filtrated through celite pad to remove molecular sieves. The filtrate was washed with HCl 1N (2x30 mL) and Brine (1x30 mL), the organic layer was dried over Na_2SO_4 filtered and concentrated in vacuum. It was obtained **38** (1.74 g) as a white solid, directly used for the next step with no further purification.

Compound **38**:

Yield: 78%

^{1}H NMR (400 MHz, Chloroform-*d*) δ 7.86 (dd, *J* = 5.4, 3.0 Hz, 2H), 7.73 (dd, *J* = 5.5, 3.1 Hz, 2H), 5.04 (q, *J* = 7.4 Hz, 1H), 1.72 (d, *J* = 7.4 Hz, 3H).

^{13}C NMR (101 MHz, Chloroform-*d*) δ 175.40, 167.48, 134.38, 131.97, 123.73, 47.35, 15.16.

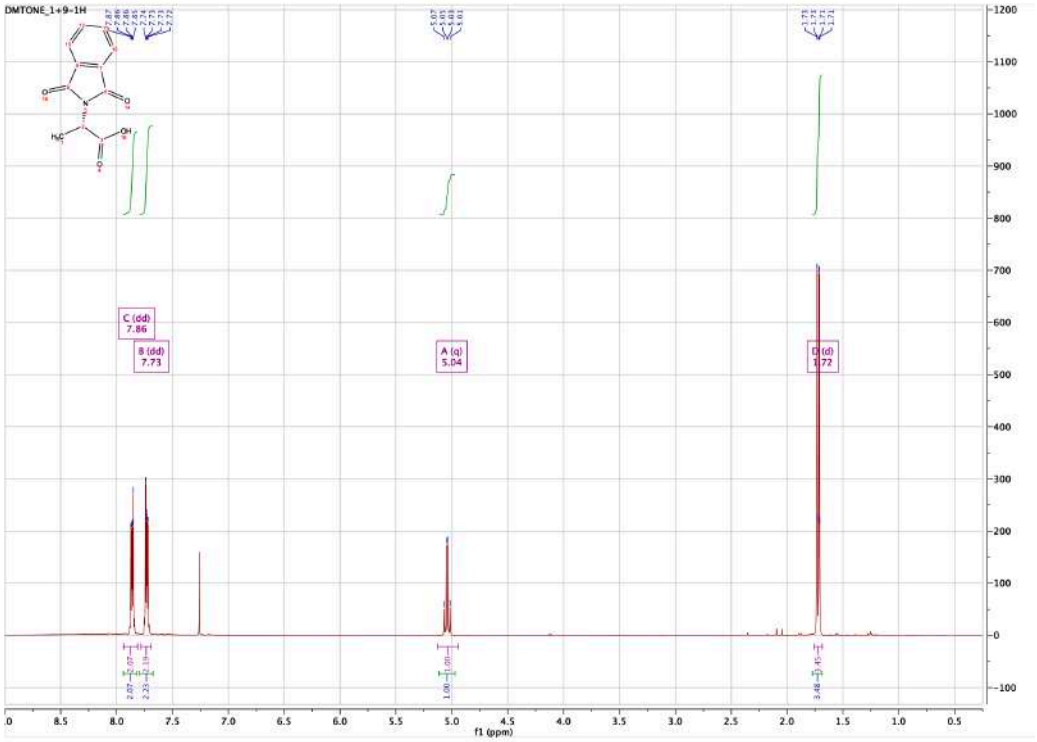

^{1}H NMR compound **38**

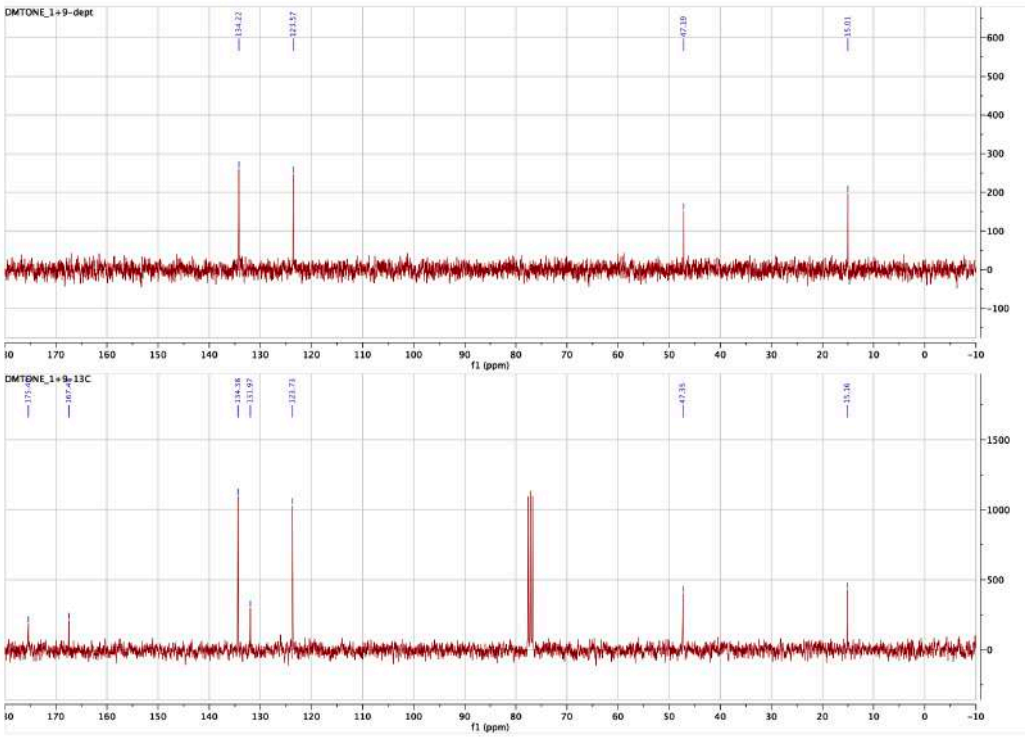

^{13}C and DEPT NMR compound **38**

Synthesis of *(S)-2-(1,3-dioxoisoindolin-2-yl)-N-methoxypropanamide* (**39**):

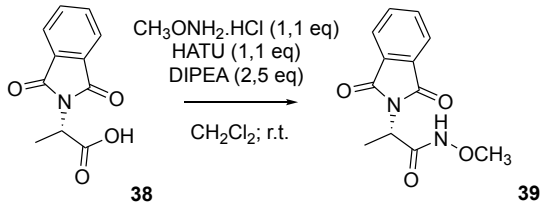

A mixture of the previous crude derivative **38** (7.93 mmol, 1.74g), methoxy amine hydrochloride (8.73 mmol, 0.72 mL), HATU (8.73 mmol, 3.32 g) and DIPEA (19.84 mmol, 3.45 mL) in DCM (100 mL) was stirred at room temperature overnight, monitored via TLC and mass spectrometry. Once completed, the reaction was quenched with a saturated NH_4Cl aqueous solution and the two layers were separated. The aqueous layer was extracted with DCM, and the organic layers were combined, dried over Na_2SO_4, filtered and concentrated in vacuum. The residue was purified by flash chromatography (1:4 petroleum ether/AcOEt) to afford compound **39** (1.10 g) as white yellowish solid.

Compound **39**:

Yield: 56%

MS (ESI): m/z $[M+H]^+$ 285,24

^{1}H NMR (400 MHz, Chloroform-*d*) δ 9.63 (s, 1H), 7.83 – 7.77 (m, 2H), 7.74 – 7.67 (m, 2H), 4.85 (s, 1H), 3.69 (s, 3H), 1.62 (d, J = 7.3 Hz, 3H).

^{13}C NMR (101 MHz, Chloroform-*d*) δ 167.77, 134.41, 131.79, 123.60, 64.35, 47.86, 15.13.

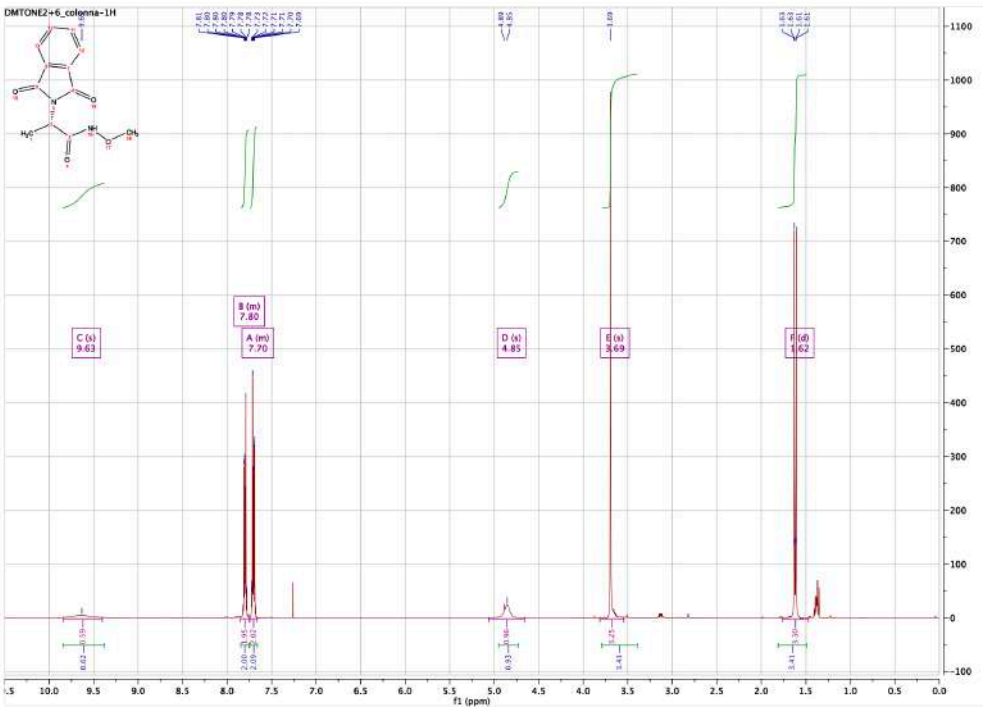

^{1}H NMR compound **39**

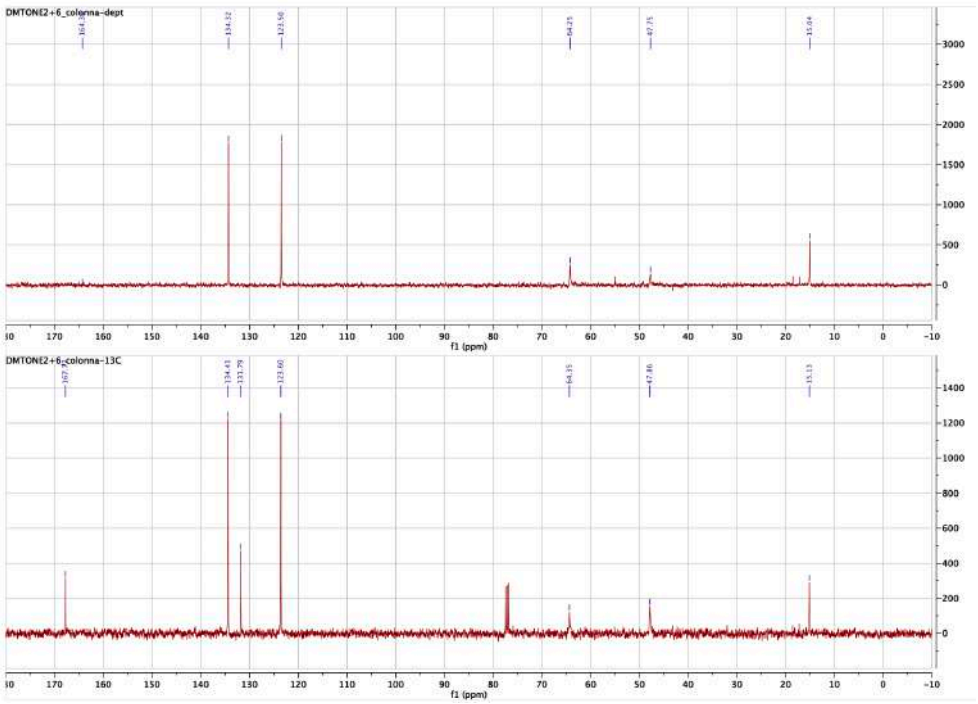

^{13}C and DEPT NMR compound **39**

Synthesis of *(S)-3-(4-((tert-butyldimethylsilyl)oxy)phenyl)-2-(1,3-dioxoisoindolin-2-yl)-N-methoxypropanamide* (**40**)

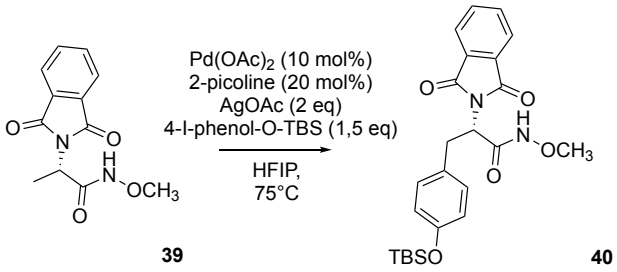

39 **40**

The compound **39** (0.10 mmol, 0.025g), $Pd(OAc)_2$ (0.01 mmol, 2.26 mg), AgOAc (0.20 mmol, 33.6 mg), were weighted and inserted in a microwave tube. It was added 4-I-phenol-*O*-TBS (0.15 mmol, 50.5 mg), 2-picoline (0.02 mmol, 1.98 μL) and the solvent hexafluoro *iso*-propanol (HFIP), (1 mL). The reaction mixture was stirred at r.t. for 10 min, then heated at 75°C for 24h.

The reaction was monitored per mass spectrometry and TLC, once completed it was filtered through celite pad, washed with DCM. The filtrate was concentrated under vacuum, obtaining a yellowish oil as crude, which was purified by flash chromatography (1:1 petroleum ether/AcOEt) to afford the compound **40** (27.46 mg) as white solid.

Compound **40:**

Yield: 60%

MS (ESI): m/z $[M+H]^+$ 455,60

^{1}H NMR (400 MHz, Chloroform-*d*) δ 9.16 (s, 1H), 7.80 – 7.74 (m, 2H), 7.72 – 7.68 (m, 2H), 7.02 – 6.95 (m, 2H), 6.66 – 6.60 (m, 2H), 5.06 (s, 1H), 3.75 (s, 3H), 3.44 (q, J = 9.0, 8.4 Hz, 2H), 0.89 (s, 9H), 0.21 – -0.03 (m, 6H).

^{13}C NMR (101 MHz, Chloroform-*d*) δ 168.08, 154.79, 138.45, 134.52, 131.38, 130.05, 128.80, 123.73, 120.55, 64.73, 54.96, 34.22, 25.76, 18.30, -4.41.

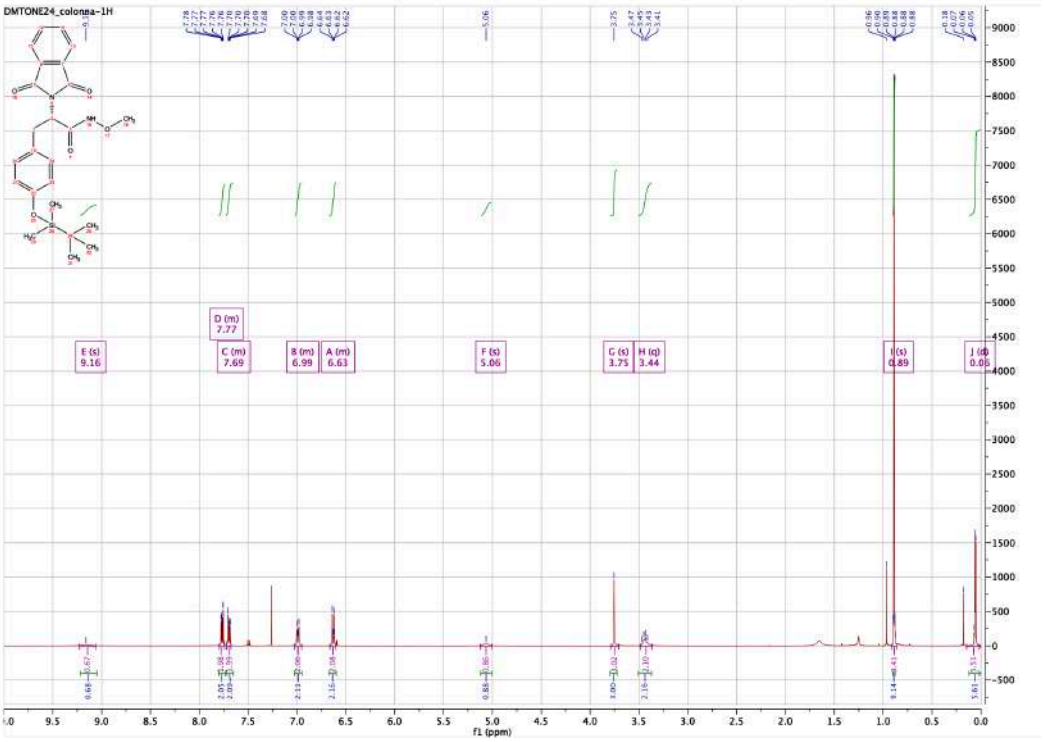

^{1}H NMR compound **40**

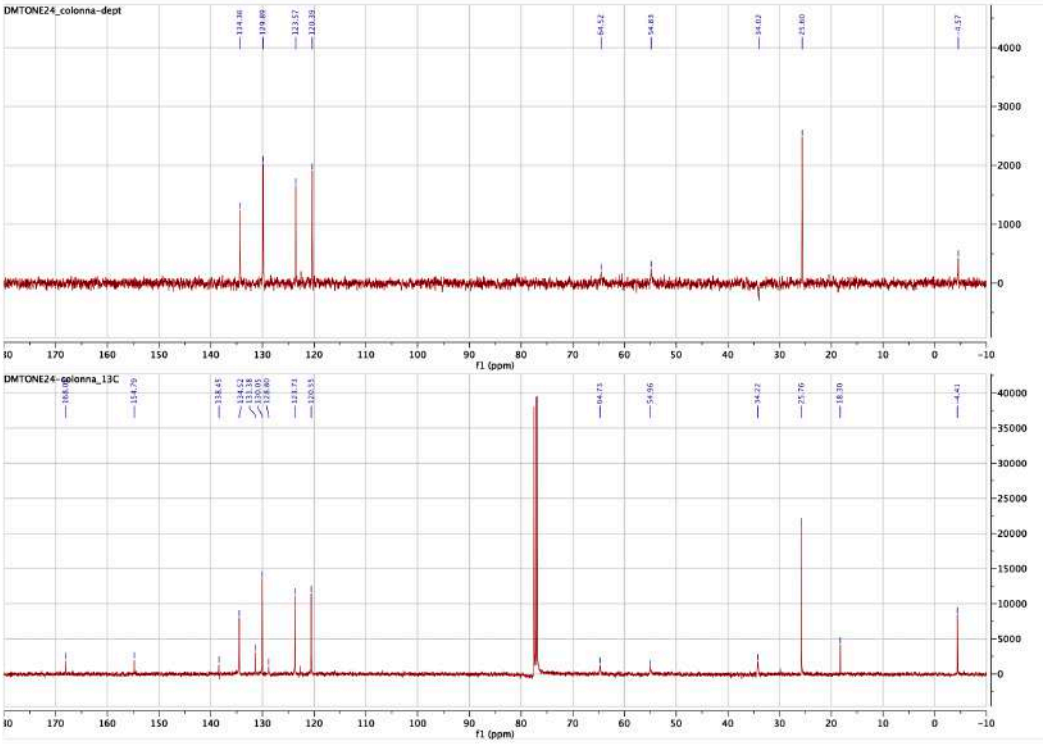

^{13}C and DEPT NMR compound **40**

Synthesis of *(S)-2-(1,3-dioxoisoindolin-2-yl)-N-(quinolin-8-yl)propanamide* (**41**)

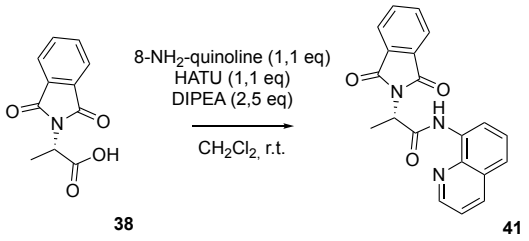

A mixture of the previous crude derivative **38** (4.56 mmol, 1.00g), 8-aminoquinoline (5.02 mmol, 0.72 g), HATU (5.02 mmol, 1.91 g) and DIPEA (11.40 mmol, 1.98 mL) in DCM (150 mL) was stirred at room temperature overnight, monitored through mass spectrometry and TLC. Once completed, the reaction was quenched with a saturated NH_4Cl aqueous solution and the two layers were separated. The aqueous layer was extracted with DCM, and the organic layers were combined, dried over Na_2SO_4, filtered and concentrated in vacuum. The residue was purified by flash chromatography (3:2 petroleum ether/AcOEt) to afford the compound **39** (1.18 g) as orange powder.

Compound **41**:

Yield: 75%

MS (ESI): m/z $[M+H]^+$ 346,36

^{1}H NMR (400 MHz, Chloroform-*d*) δ 10.34 (s, 1H), 8.73 (dd, *J* = 5.6, 3.5 Hz, 1H), 8.69 (dd, *J* = 4.3, 1.7 Hz, 1H), 8.16 (dd, *J* = 8.3, 1.7 Hz, 1H), 7.90 (dd, *J* = 5.5, 3.0 Hz, 2H), 7.75 (dd, *J* = 5.5, 3.1 Hz, 2H), 7.58 – 7.49 (m, 2H), 7.43 (dd, *J* = 8.3, 4.3 Hz, 1H), 5.27 (q, *J* = 7.3 Hz, 1H), 1.98 (d, *J* = 7.4 Hz, 3H).

^{13}C NMR (101 MHz, Chloroform-*d*) δ 167.98, 167.42, 148.33, 138.49, 136.66, 134.32, 133.97, 132.17, 128.05, 127.55, 123.72, 122.08, 121.75, 117.02, 50.25, 15.55.

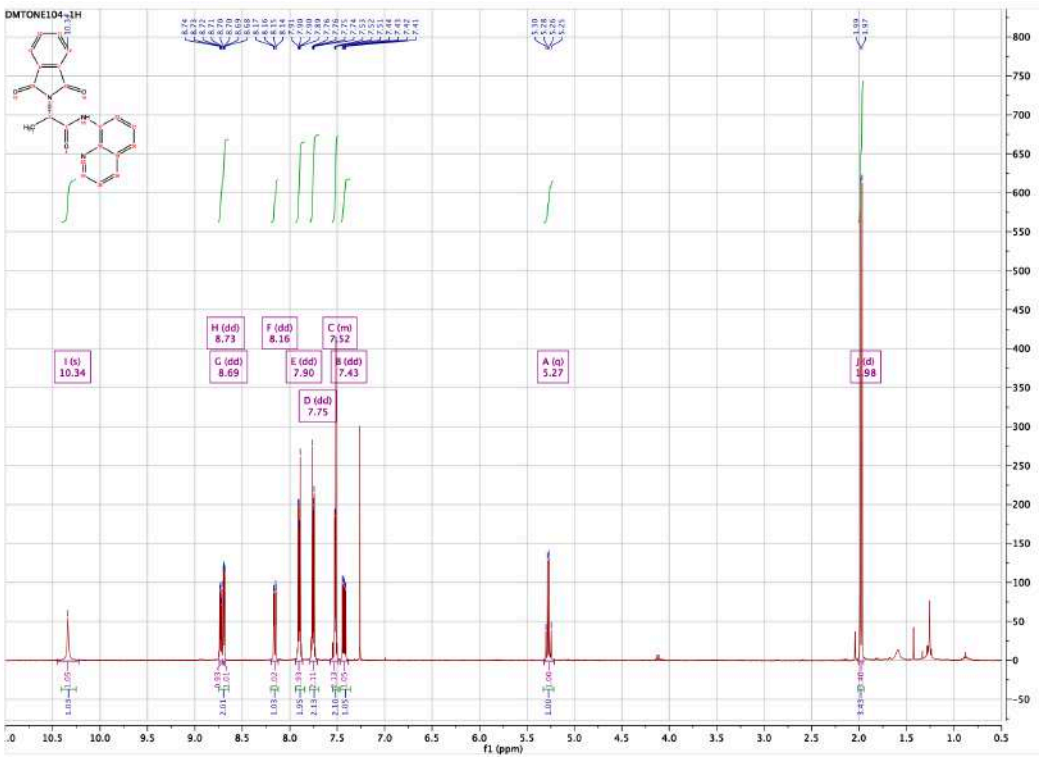

^{1}H NMR compound **41**

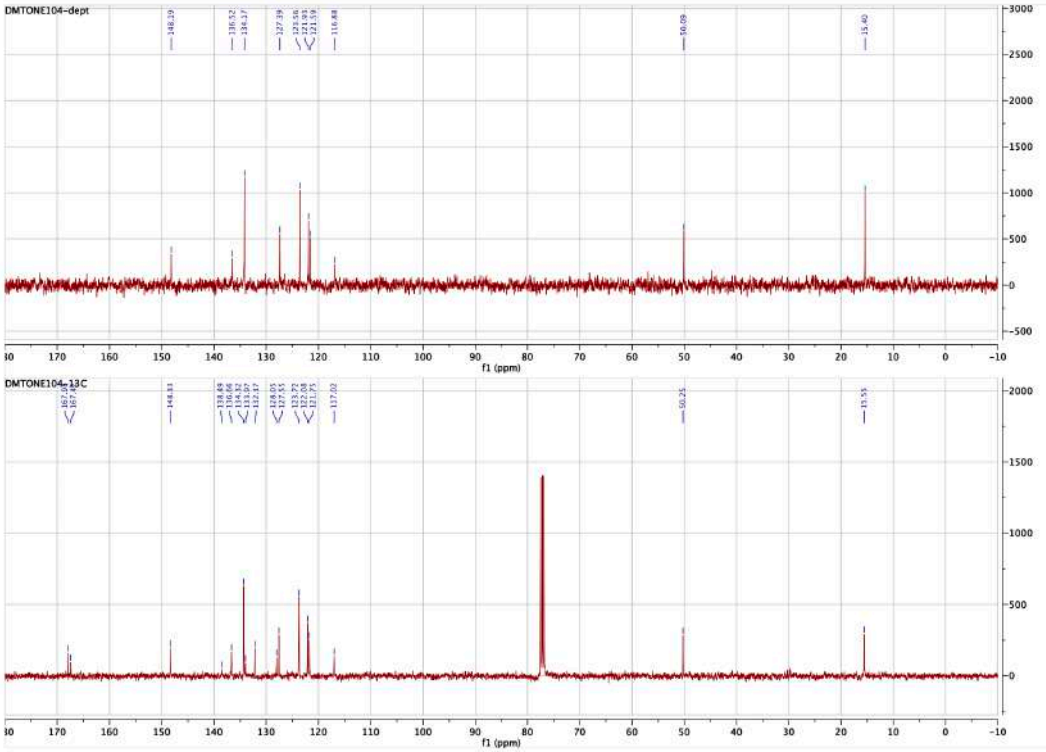

^{13}C and DEPT NMR compound **41**

Synthesis of *(S)-2-(1,3-dioxoisoindolin-2-yl)-3-(4-hydroxyphenyl)-N-(quinolin-8-yl)propanamide* (**42**)

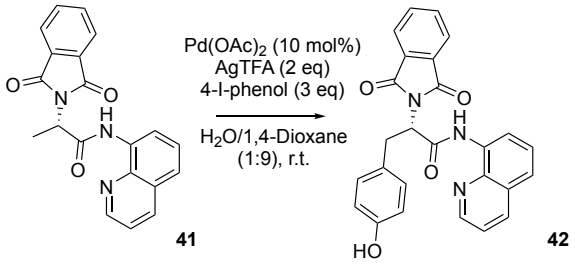

The compound **41** (0.14 mmol, 0.050g), $Pd(OAc)_2$ (0.014 mmol, 3.24 mg), AgTFA (0.289 mmol, 63.9 mg), and 4-Iodo-phenol (0.43 mmol, 95.5 mg) were inserted in a microwave tube. 1,4-Dioxane/H_2O (0.9 mL/0.1 mL) were used as mixed solvents. The reaction mixture was stirred at r.t. for 24h.

The reaction was monitored per mass spectrometry, once completed it was filtered through celite pad, washed with DCM. The filtrate was concentrated under vacuum, obtaining a crude oil, which was purified by flash chromatography (3:2 petroleum ether/AcOEt) to afford compound **42** (0.049 g) as white solid.

Compound **42**:

Yield: 78%

MS (ESI): m/z $[M+H]^+$ 437,46

^{1}H NMR (400 MHz, Chloroform-*d*) δ 10.33 (s, 1H), 8.72 (dd, *J* = 5.5, 3.5 Hz, 1H), 8.63 (dd, *J* = 4.2, 1.7 Hz, 1H), 8.13 (dd, *J* = 8.3, 1.7 Hz, 1H), 7.82 (dd, *J* = 5.5, 3.1 Hz, 2H), 7.70 (dd, *J* = 5.5, 3.0 Hz, 2H), 7.56 – 7.45 (m, 2H), 7.39 (dd, *J* = 8.3, 4.2 Hz, 1H), 7.20 – 7.04 (m, 2H), 6.74 – 6.62 (m, 2H), 5.39 (dd, *J* = 9.7, 7.0 Hz, 1H), 5.32 (s, 1H), 3.81 – 3.63 (m, 2H).

^{13}C NMR (101 MHz, Chloroform-*d*) δ 168.16, 166.68, 154.81, 148.44, 138.61, 136.42, 134.35, 133.95, 131.73, 130.33, 128.63, 127.99, 127.44, 123.73, 122.20, 121.77, 116.99, 115.77, 56.55, 34.09.

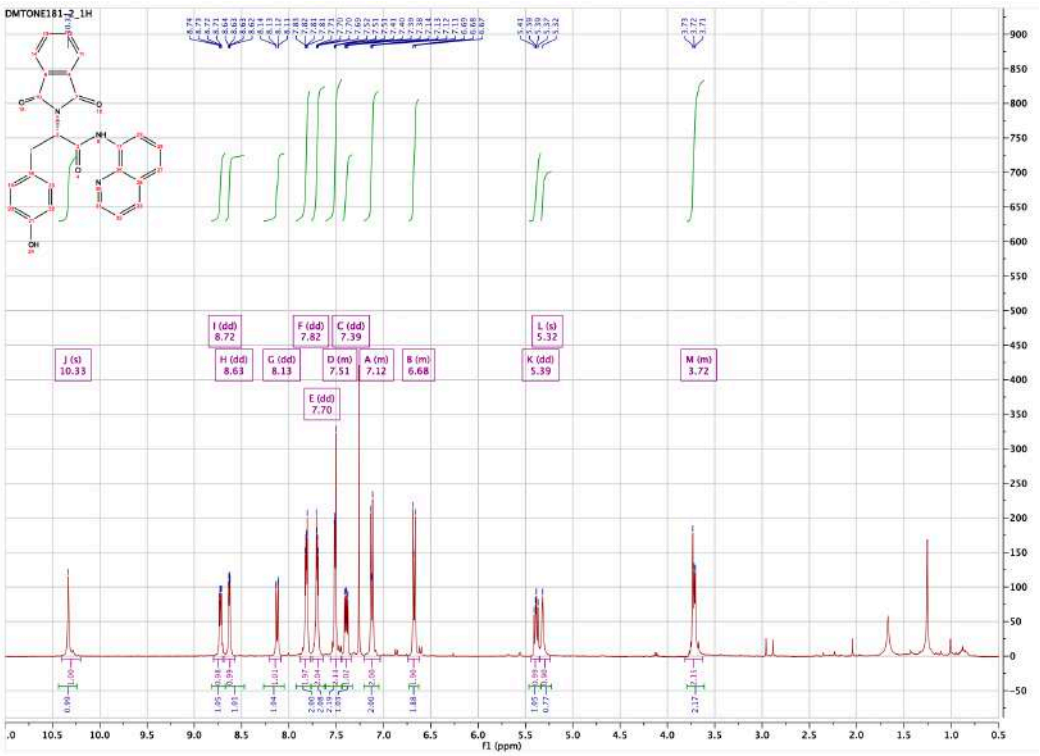

^{1}H NMR compound **42**

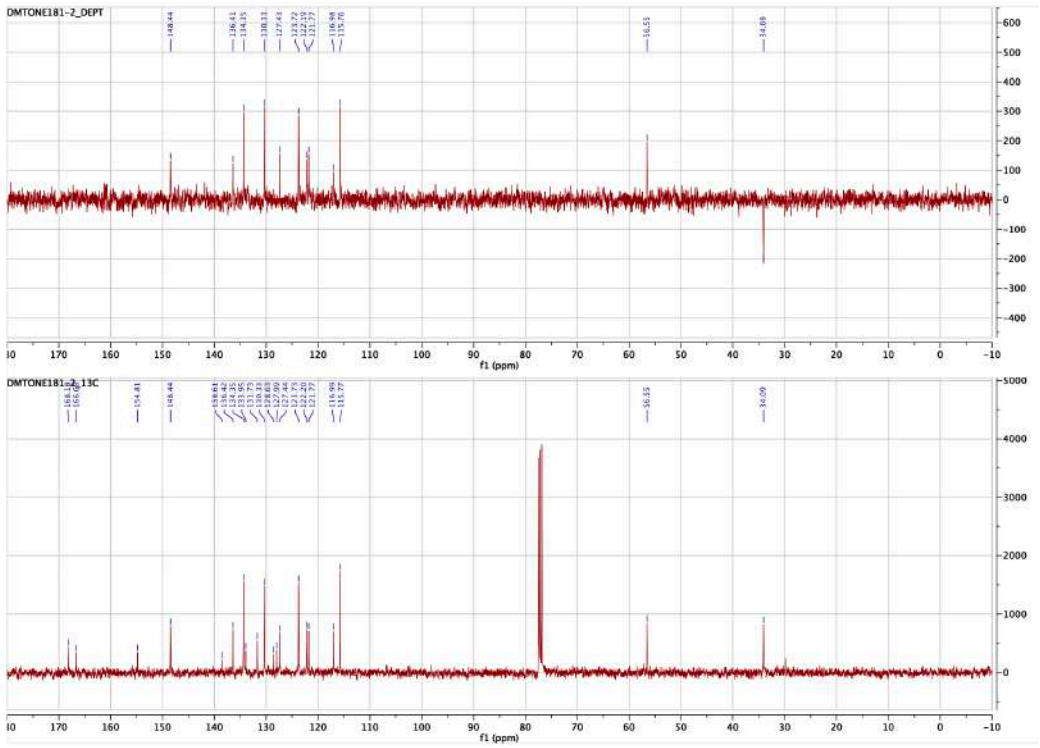

^{13}C and DEPT NMR compound **42**

Synthesis of *tert-butyl(4-iodophenoxy)dimethylsilane* (**61**):

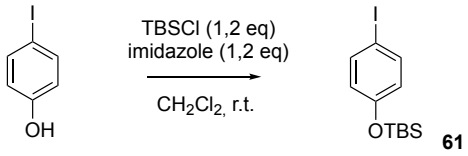

61

To a solution of 4-Iodo phenol (4.53 mmol, 1.00 g) in DCM (100 mL), were added imidazole (5.43 mmol, 0.37 g) and TBSCl (5.43 mmol, 0.82 g). The reaction mixture was stirred at room temperature overnight before the reaction was quenched by adding saturated $NaHCO_3$. The organic layer was separated and the aqueous layer was extracted (3 times) with DCM. The reunited organic layers were dried over Na_2SO_4, filtered and concentrated under vacuum to give a crude yellowish oil which was purified by flash chromatography (9,5:0,5 petroleum ether/AcOEt) to afford compound **61** (1.31 g) as a yellowish oil.

Compound **61**:

Yield: 87%

^{1}H NMR (400 MHz, Chloroform-*d*) δ 7.64 – 7.43 (m, 2H), 6.72 – 6.51 (m, 2H), 0.97 (d, *J* = 0.9 Hz, 9H), 0.18 (d, *J* = 0.9 Hz, 6H).

^{13}C NMR (101 MHz, Chloroform-*d*) δ 155.46, 138.13, 122.37, 83.53, 25.45, 18.03, -4.66.

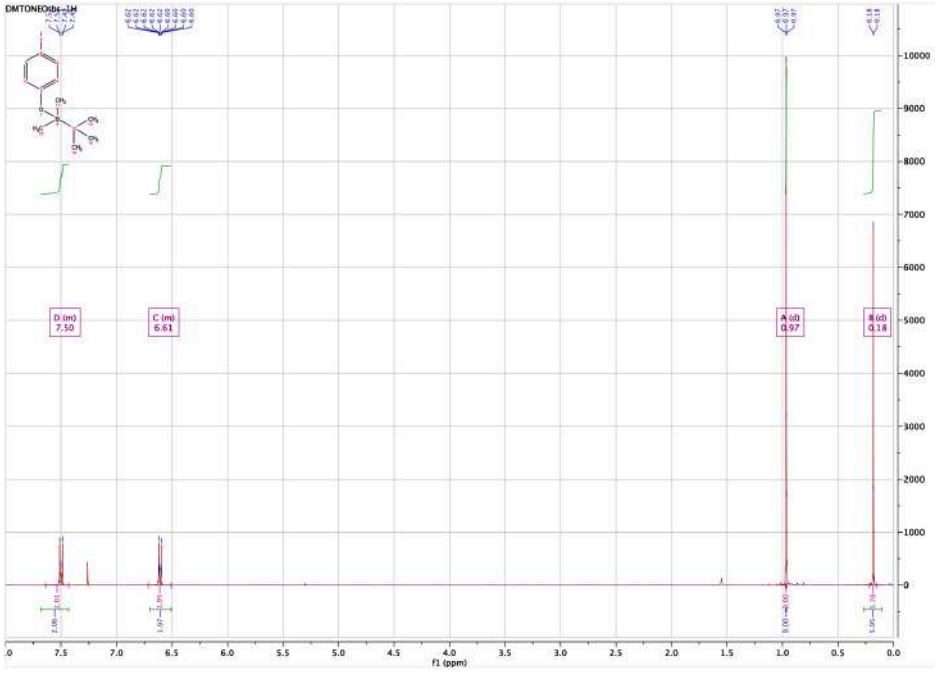

^{1}H NMR compound **61**

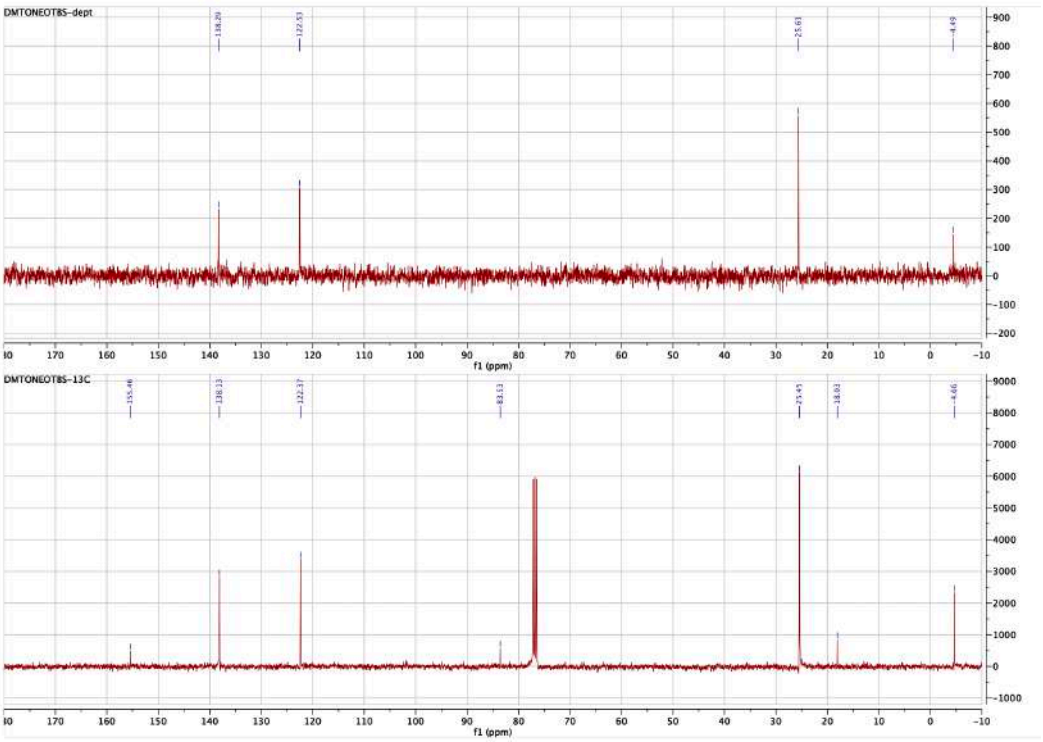

^{13}C and DEPT NMR compound **61**

Synthesis of *4-iodo-3,5-dimethylphenol* (**44**)

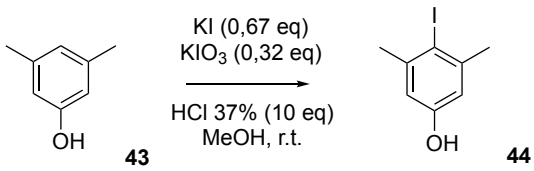

43 **44**

3,5-dimethyl phenol **43**, (20.5 mmol, 2.50 g) was solubilized in MeOH (42 mL), HCl 37% (0.205 mol, 17.08 mL) was added in a dropwise manner at 0°C. In the meanwhile, KI (13.7 mmol, 2.27g) and KIO_3 (6.55 mmol, 1.40 g) were solubilized in 21 mL of water. The aqueous solution was added to the former one, the ice bath was removed and the reaction was stirred at r.t. for 12h. Once the product was precipitated, the reaction was quenched by adding $Na_2S_2O_3$ saturated solution, the aqueous phase was extracted with AcOEt (3x40mL), the organic layers were combined, dried over Na_2SO_4, filtered and concentrated under vacuum. The crude oil obtained was purified by flash chromatography (8,5:1,5 petroleum ether/AcOEt) to afford compound **44** (3.04 g) as white yellowish solid.

Compound **44**:

Yield: 60%

^{1}H NMR (400 MHz, Chloroform-*d*) δ 6.61 (d, *J* = 0.6 Hz, 2H), 5.92 (s, 1H), 2.46 – 2.38 (m, 6H).

^{13}C NMR (101 MHz, Chloroform-*d*) δ 155.31, 143.31, 114.39, 97.05, 29.67.

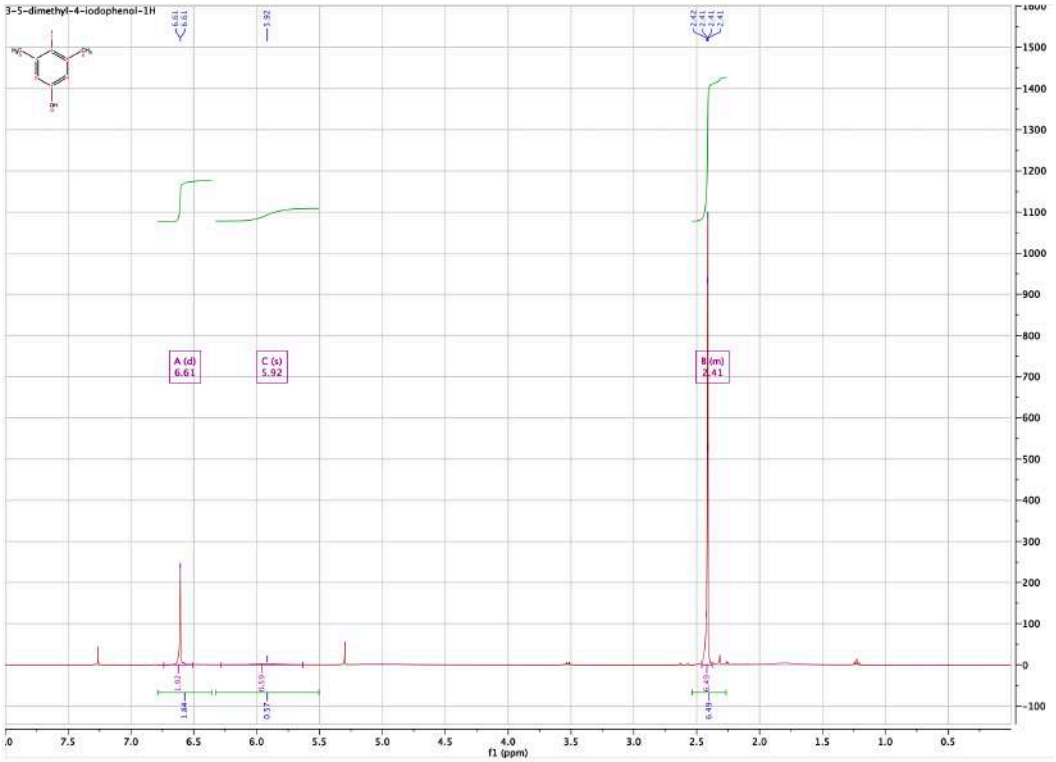

^{1}H NMR compound **44**

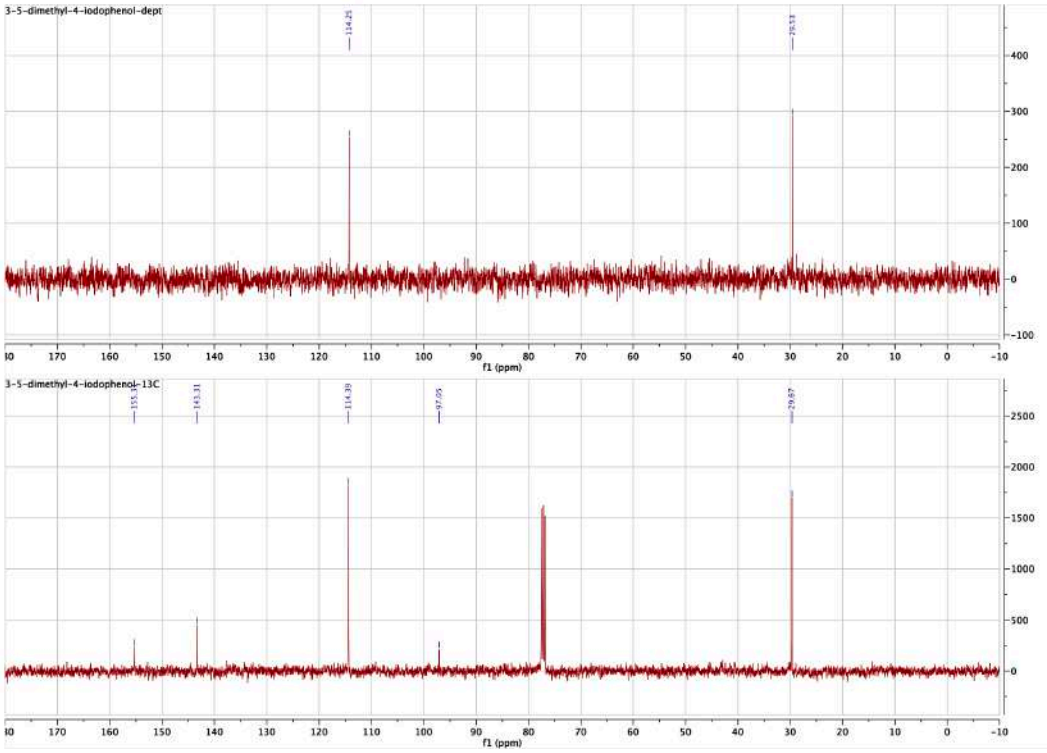

^{13}C and DEPT NMR compound **44**

Synthesis of *tert-butyl(4-iodo-3,5-dimethylphenoxy)dimethylsilane* (**45**):

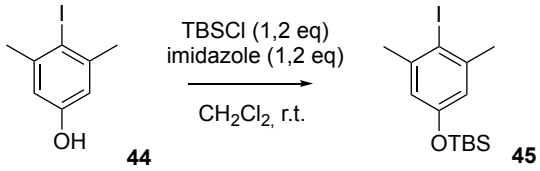

To a solution of **44** (4.03 mmol, 1.00 g) in DCM (100 mL), were added imidazole (4.83 mmol, 0.32 g) and TBSCl (4.83 mmol, 0.73 g). The reaction mixture was stirred at room temperature overnight and monitored through TLC. Once completed it was quenched by adding saturated $NaHCO_3$. The organic layer was separated and the aqueous layer was extracted (3 times) with DCM. The reunited organic layers were dried over Na_2SO_4, filtered and concentrated under vacuum to give the TBS-ether as a yellowish oil, the crude was purified by flash chromatography (8,5:1,5 petroleum ether/AcOEt) to afford compound **45** (1.35 g) as a yellowish oil.

Yield: 93%

^{1}H NMR (400 MHz, Chloroform-*d*) δ 6.59 (d, *J* = 0.8 Hz, 2H), 2.40 (d, *J* = 0.7 Hz, 6H), 0.97 (s, 9H), 0.18 (d, *J* = 0.9 Hz, 6H).

^{13}C NMR (101 MHz, Chloroform-*d*) δ 155.41, 142.93, 119.08, 98.18, 29.70, 25.81, 18.33, -4.28.

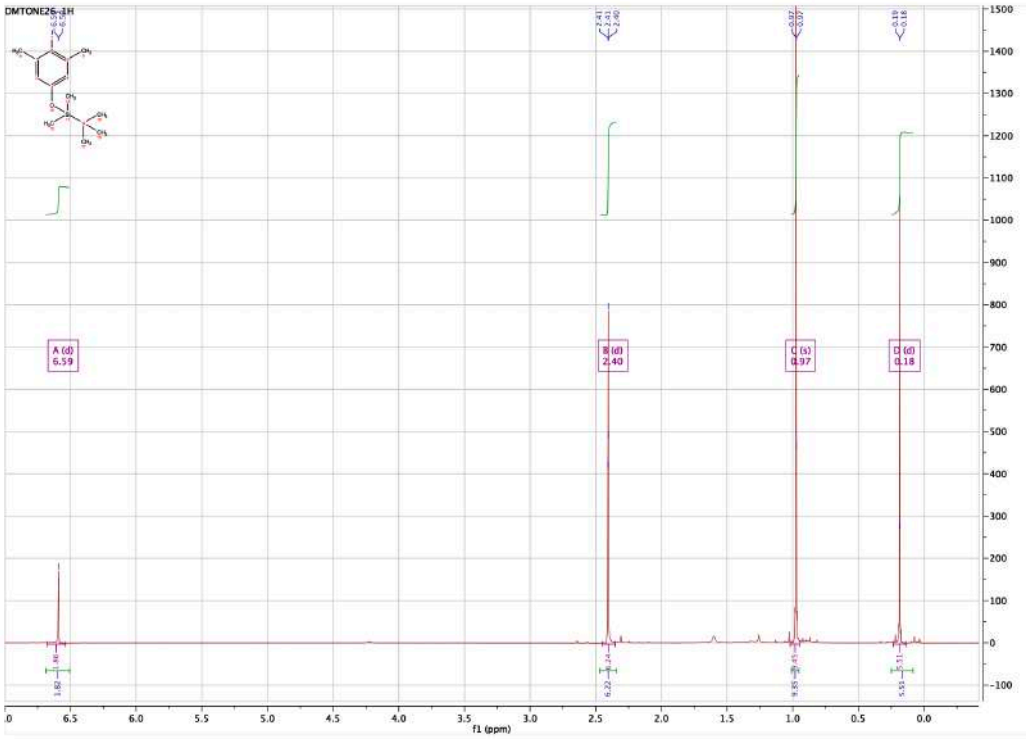

^{1}H NMR compound **45**

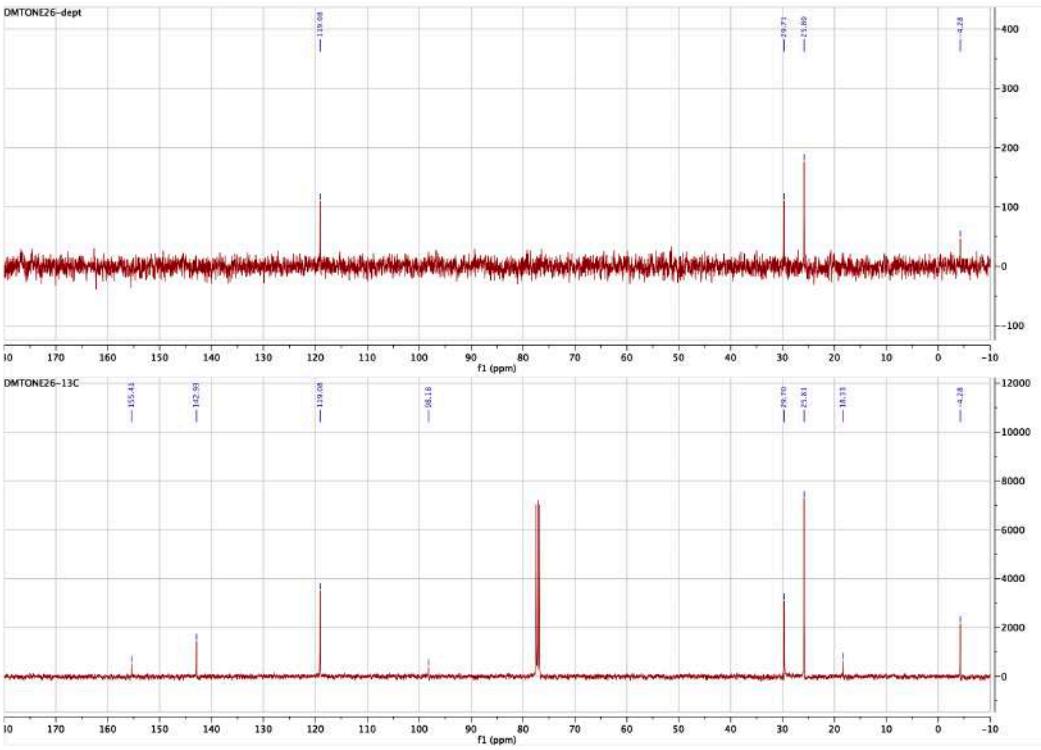

^{13}C and DEPT NMR compound **45**

Synthesis of *4-iodo-2,6-dimethylphenol* (**47**)

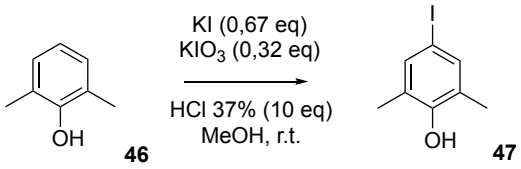

46 **47**

2,6-dimethyl phenol **46**, (28.6 mmol, 3.50 g) was solubilized in MeOH (58 mL), HCl 37% (0.286 mol, 23.87 mL) was added in a dropwise manner at 0°C. In the meanwhile, KI (19.2 mmol, 3.18g) and KIO_3 (9.20 mmol, 1.96 g) were solubilized in 29 mL of water. The aqueous solution was added to the former one, the ice bath was removed and the reaction was stirred at r.t. for 12h. Once the product was precipitated, the reaction was quenched by adding $Na_2S_2O_3$ saturated solution, the aqueous phase was extracted with AcOEt (3x40mL), the organic layers were combined, dried over Na_2SO_4, filtered and concentrated under vacuum. The crude oil obtained was purified by flash chromatography (8,5:1,5 petroleum ether/AcOEt) to afford compound **47** (3.98 g) as yellowish solid.

Compound **47**:

Yield: 56%

^{1}H NMR (400 MHz, Chloroform-*d*) δ 7.29 (q, *J* = 0.7 Hz, 2H), 4.58 (s, 1H), 2.20 (t, *J* = 0.7 Hz, 6H).

^{13}C NMR (101 MHz, Chloroform-*d*) δ 152.31, 137.16, 125.79, 82.42, 15.66.

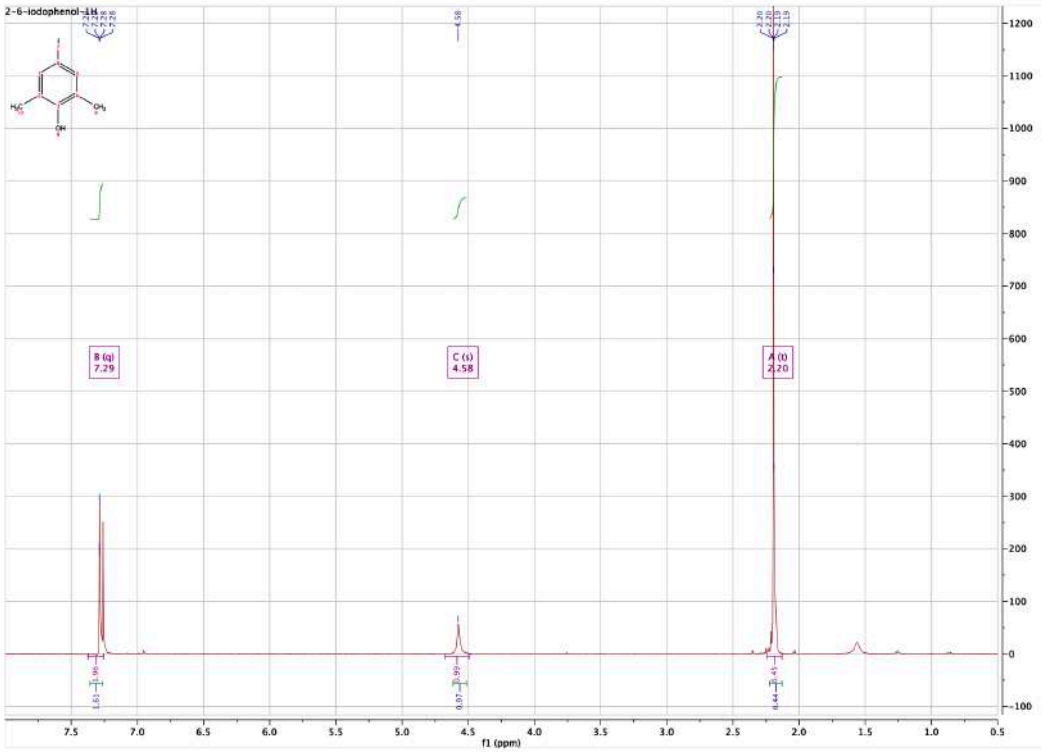

^{1}H NMR compound **47**

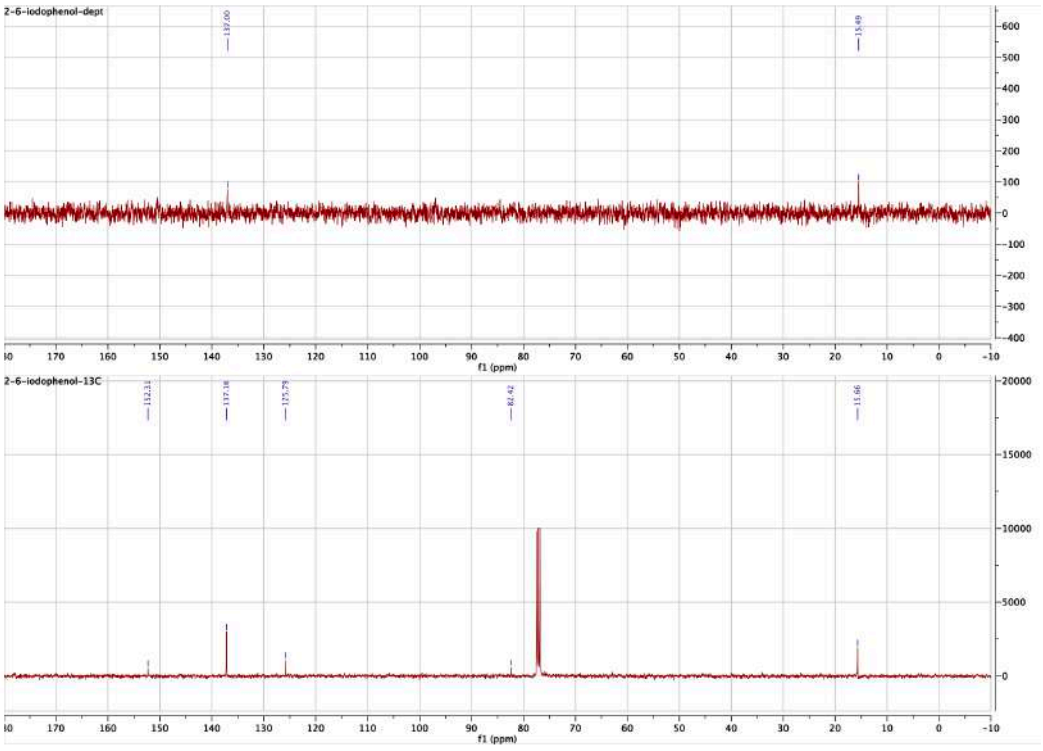

^{13}C and DEPT NMR compound **47**

Synthesis of *tert-butyl(4-iodo-2,6-dimethylphenoxy)dimethylsilane* (**48**):

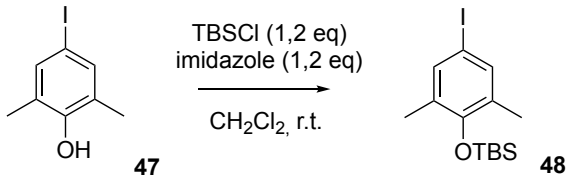

To a solution of **47** (6.04 mmol, 1.50 g) in DCM (150 mL), were added imidazole (7.26 mmol, 0.49 g) and TBSCl (7.26 mmol, 1.09 g). The reaction mixture was stirred at room temperature overnight and monitored through TLC. Once completed, it was quenched by adding saturated $NaHCO_3$. The organic layer was separated and the aqueous layer was extracted (3 times) with DCM. The reunited organic layers were dried over Na_2SO_4, filtered and concentrated under vacuum to give the TBS-ether as a yellowish oil, the crude was purified by flash chromatography (8,5:1,5 petroleum ether/AcOEt) to afford compound **48** (1.79 g) as a yellowish oil.

Compound **48**:

Yield: 82%

^{1}H NMR (400 MHz, Chloroform-*d*) δ 7.28 (dt, *J* = 1.4, 0.7 Hz, 2H), 2.16 (p, *J* = 0.7 Hz, 6H), 1.09 – 0.99 (m, 9H), 0.24 – 0.13 (m, 6H).

^{13}C NMR (101 MHz, Chloroform-*d*) δ 152.41, 137.42, 131.48, 84.27, 26.20, 18.89, 17.57, -2.83.

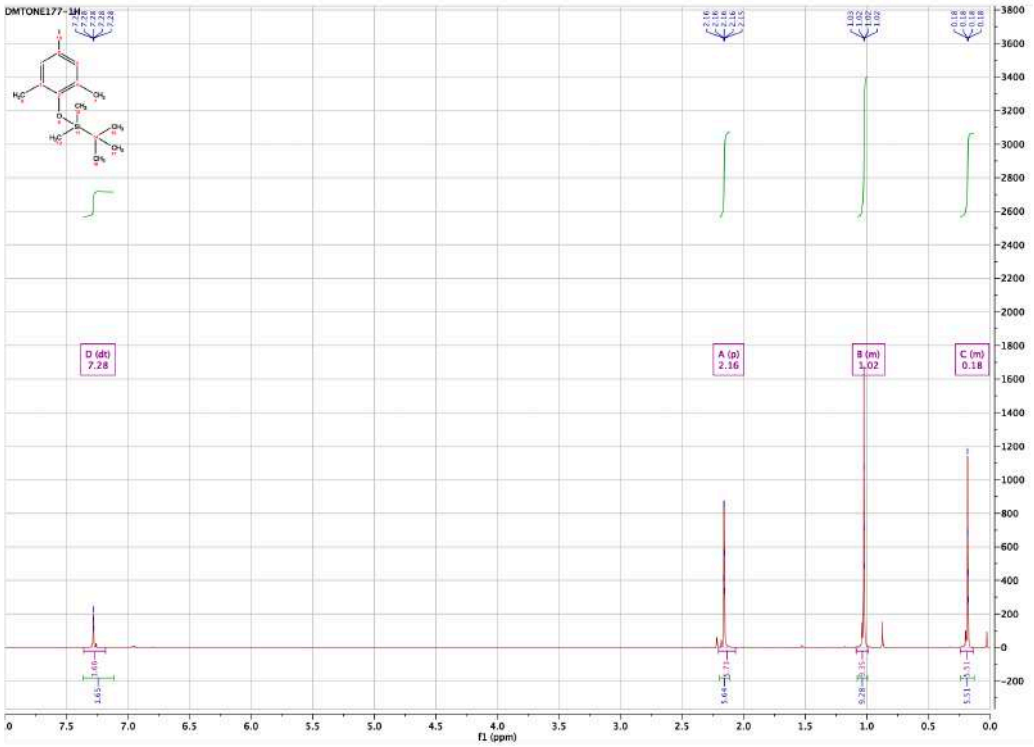

^{1}H NMR compound **48**

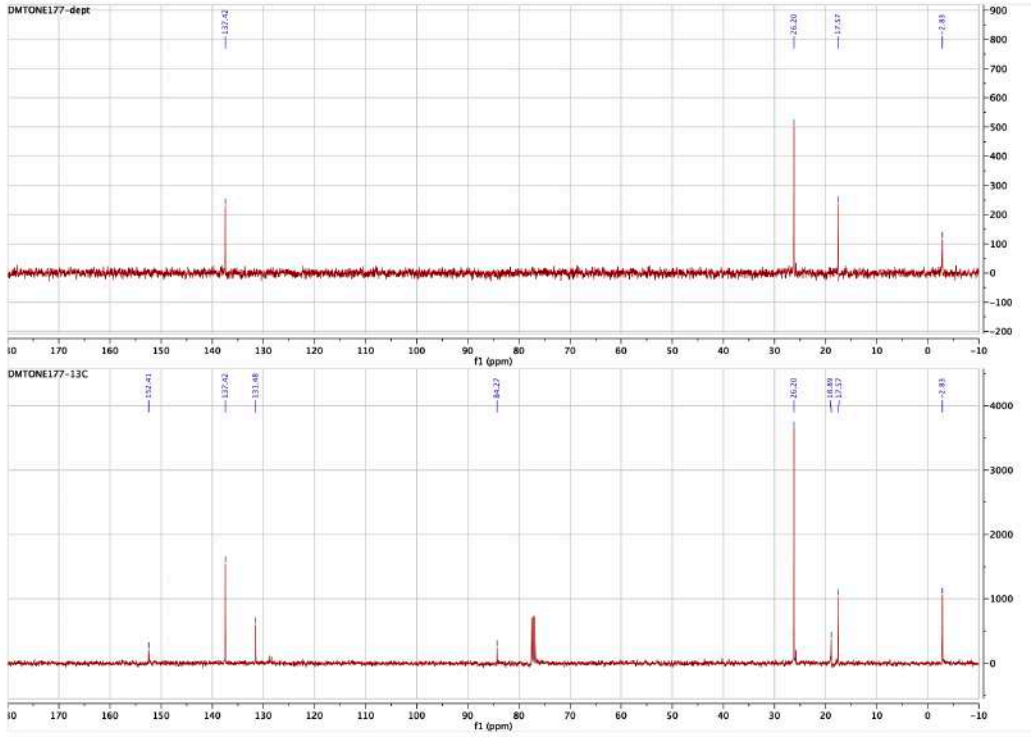

^{13}C and DEPT NMR compound **48**

Synthesis of *(S)-2-(1,3-dioxoisoindolin-2-yl)-3-(4-hydroxy-3,5-dimethylphenyl)-N-(quinolin-8-yl)propanamide* (**49**)

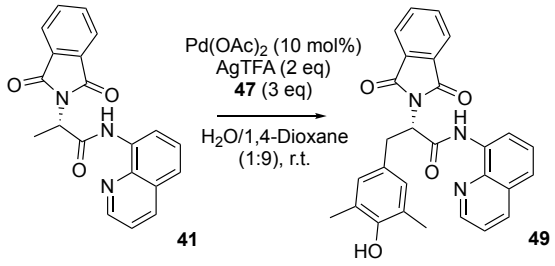

The compound **41** (0.58 mmol, 0.200g), $Pd(OAc)_2$ (0.058 mmol, 12.99 mg), AgTFA (1.16 mmol, 0.26 g), and 4-Iodo-2,6-dimethyl phenol **47** (1.73 mmol, 0.43 g) were inserted in a microwave tube. A mixtoure of 1,4-Dioxane/H_2O (0.9 mL/0.1 mL) was used as solvent. The reaction mixture was stirred at r.t. for 24h, it was monitored per mass spectrometry and TLC. Once completed, the crude was filtered through celite pad and washed with DCM. The filtrate was concentrated under vacuum, obtaining a crude oil, which was purified by flash chromatography (3:2 petroleum ether/AcOEt) to afford the compound **49** (0.220 g) as orange solid powder.

Compound **49**:

Yield: 82%

MS (ESI): m/z $[M+H]^+$ 466,51

^{1}H NMR (400 MHz, DMSO-d_6) δ 10.49 (s, 1H), 8.83 (dd, J = 4.3, 1.7 Hz, 1H), 8.52 (dd, J = 7.6, 1.4 Hz, 1H), 8.42 (dd, J = 8.4, 1.7 Hz, 1H), 8.00 (s, 1H), 7.91 – 7.81 (m, 4H), 7.71 (dd, J = 8.3, 1.3 Hz, 1H), 7.65 – 7.55 (m, 2H), 6.82 (s, 2H), 5.48 (dd, J = 10.9, 5.7 Hz, 1H), 3.58 – 3.41 (m, 2H), 2.00 (s, 6H).

^{13}C NMR (101 MHz, DMSO-d_6) δ 168.09, 167.35, 152.16, 149.54, 138.77, 137.09, 135.33, 134.36, 131.43, 129.07, 128.30, 127.69, 127.35, 124.53, 123.77, 122.98, 122.68, 117.62, 56.34, 33.67, 16.97.

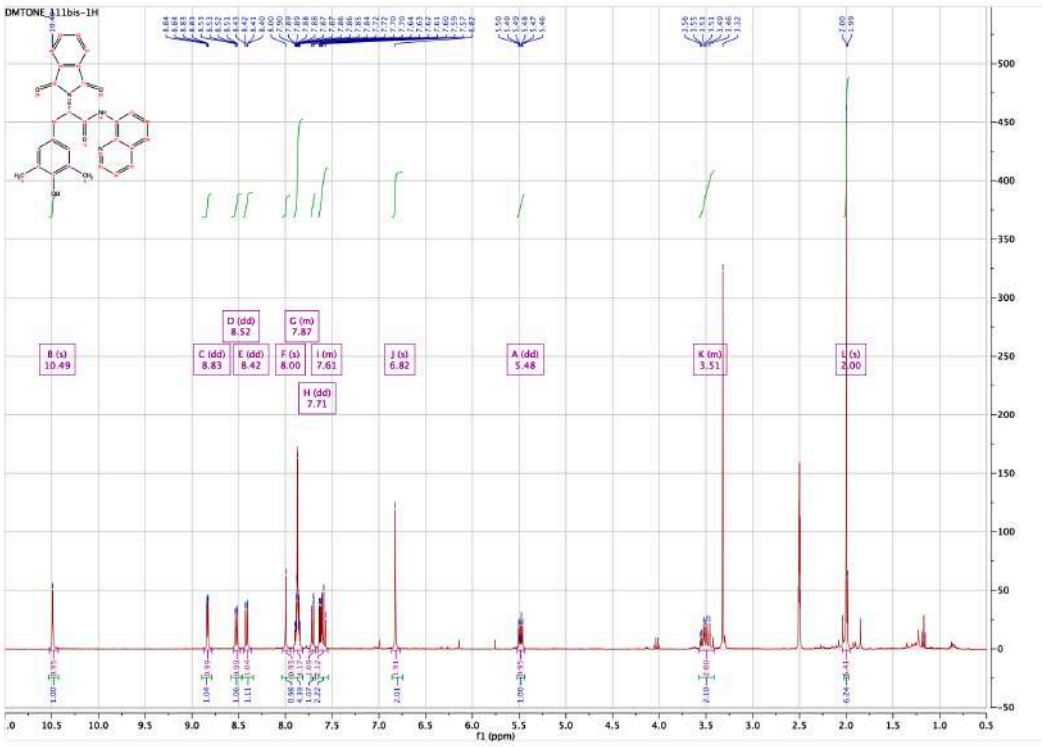

^{1}H NMR compound **49**

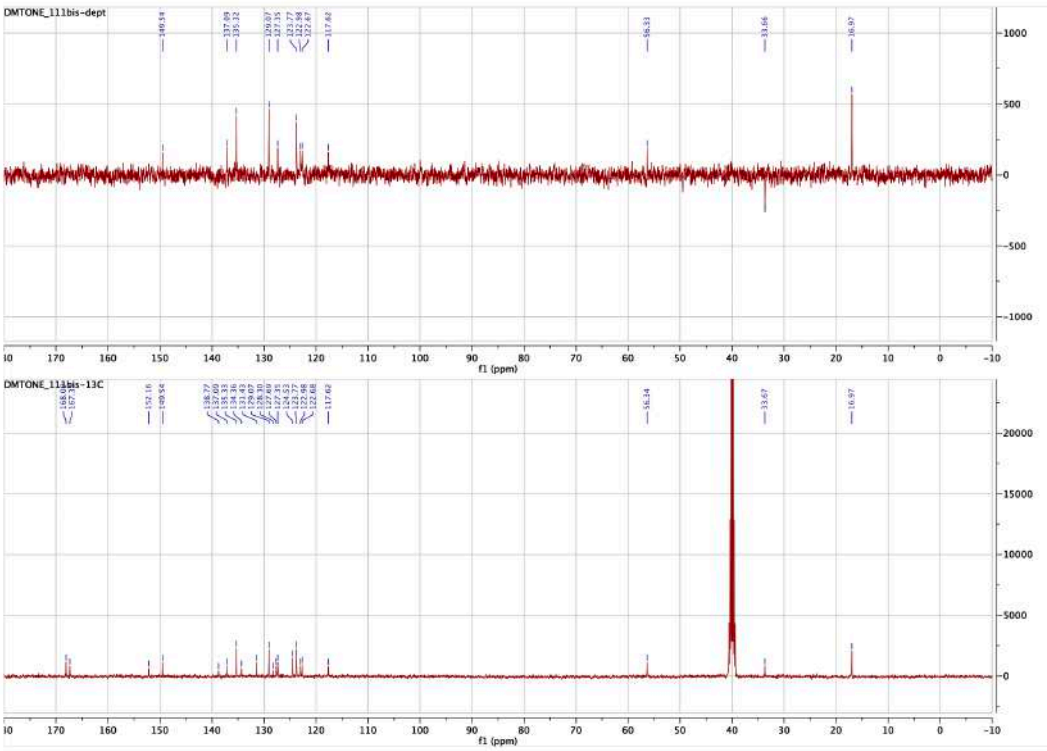

^{13}C and DEPT NMR compound **49**

Synthesis of *(S)-3,3-bis(4-((tert-butyldimethylsilyl)oxy)phenyl)-2-(1,3-dioxoisoindolin-2-yl)-N-(quinolin-8-yl)propanamide* (**50**)

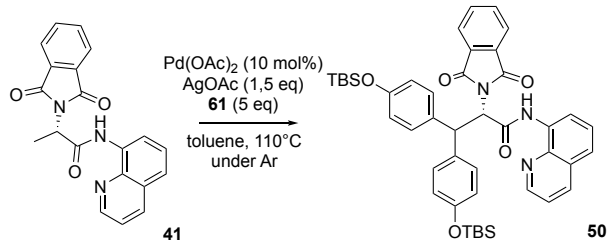

The compound **41** (0.86 mmol, 0.300g), $Pd(OAc)_2$ (0.086 mmol, 19.49 mg), AgOAc (1.32 mmol, 0.21 g), and 4-Iodo phenol *O*-TBS **61** (1.73 mmol, 0.43 g) were inserted in a microwave tube, and solubilized in toluene. The reaction mixture was stirred at r.t. for 10 min, bubbling Ar into the vial, then it was left stirred at 110°C for 24h, monitored per mass spectrometry and TLC. Once completed, the crude was filtered through celite pad and washed with DCM. The filtrate was concentrated under vacuum, obtaining a crude oil, which was purified by flash chromatography (7:3 petroleum ether/AcOEt) to afford the compound **50** (0.316 g) as white crystals.

Compound **50**:

Yield: 48%

MS (ESI): m/z $[M+H]^+$ 759,08

^{1}H NMR (400 MHz, Chloroform-*d*) δ 10.16 (s, 1H), 8.71 (dd, *J* = 4.2, 1.7 Hz, 1H), 8.63 (dd, *J* = 6.1, 2.9 Hz, 1H), 8.07 (dd, *J* = 8.3, 1.7 Hz, 1H), 7.81 – 7.66 (m, 2H), 7.61 (dd, *J* = 5.5, 3.0 Hz, 2H), 7.51 – 7.45 (m, 2H), 7.45 – 7.40 (m, 2H), 7.37 (dd, *J* = 8.2, 4.2 Hz, 1H), 7.24 – 7.16 (m, 2H), 6.81 – 6.73 (m, 2H), 6.66 – 6.57 (m, 2H), 5.83 (d, *J* = 12.3 Hz, 1H), 5.47 (d, *J* = 12.3 Hz, 1H), 0.90 (s, 9H), 0.83 (s, 9H), 0.13 – 0.03 (m, 6H), -0.02 (s, 6H).

^{13}C NMR (101 MHz, Chloroform-*d*) δ 168.18, 166.22, 155.19, 154.63, 148.42, 136.38, 134.47, 134.26, 133.69, 131.84, 129.55, 129.19, 128.09, 127.50, 123.69, 122.18, 121.78, 120.89, 120.51, 117.30, 59.55, 49.36, 25.93, 18.40, -4.19, -4.25.

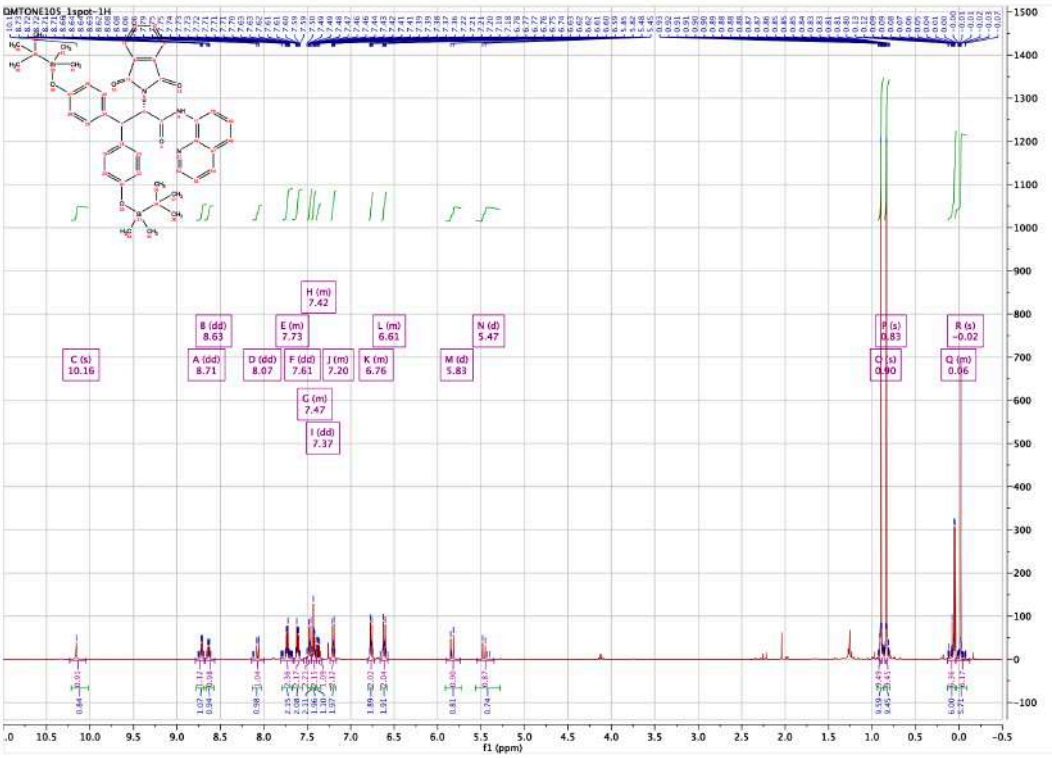

^{1}H NMR compound **50**

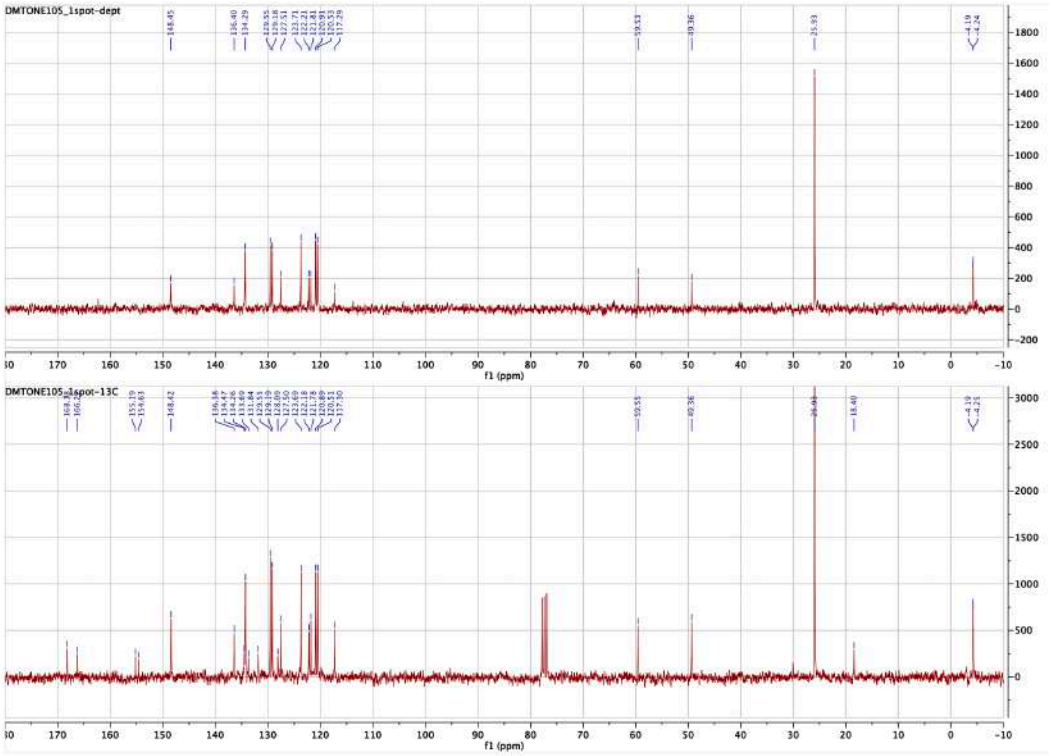

^{13}C and DEPT NMR compound **50**

Synthesis of *(S)-3,3-bis(4-((tert-butyldimethylsilyl)oxy)-3,5-dimethylphenyl)-2-(1,3-dioxoisoindolin-2-yl)-N-(quinolin-8-yl)propanamide* (**51**)

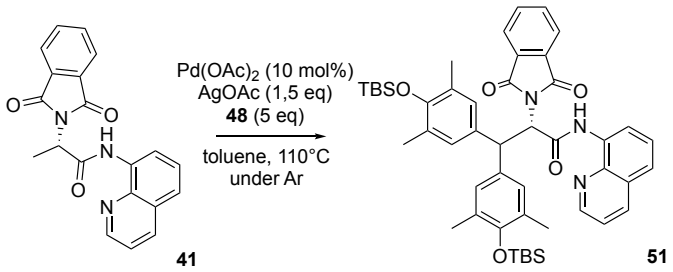

The compound **41** (0.43 mmol, 0.150 g), $Pd(OAc)_2$ (0.043 mmol, 9.74 mg), AgOAc (0.65 mmol, 0.109 g), and 4-I-2,6-dimethyl phenol *O*-TBS **48** (2.12 mmol, 0.78 g) were inserted in a microwave tube, and solubilized in toluene. The reaction mixture was stirred at r.t. for 10 min, bubbling Ar into the vial, then it was left stirred at 110°C for 24h, monitored per mass spectrometry and TLC. Once completed, the crude was filtered through celite pad and washed with DCM. The filtrate was concentrated under vacuum, obtaining a crude oil, which was purified by flash chromatography (7:3 petroleum ether/AcOEt) to afford the compound **51** (0.141 g) as yellowish solid.

Compound **51**:

Yield: 40%

MS (ESI): m/z $[M+H]^+$ 815,19

^{1}H NMR (400 MHz, DMSO-d_6) δ 10.14 (s, 1H), 8.79 (dd, J = 4.3, 1.7 Hz, 1H), 8.43 (dd, J = 7.8, 1.3 Hz, 1H), 8.35 (dd, J = 8.4, 1.7 Hz, 1H), 7.79 (d, J = 1.5 Hz, 4H), 7.64 – 7.56 (m, 2H), 7.49 (t, J = 8.0 Hz, 1H), 7.30 (s, 2H), 6.91 (s, 2H), 5.82 (d, J = 12.2 Hz, 1H), 5.14 (d, J = 12.2 Hz, 1H), 2.07 (s, 6H), 1.96 (s, 6H), 0.88 – 0.86 (m, 9H), 0.74 (s, 9H), -0.01 (s, 3H), -0.03 (s, 6H), -0.07 (s, 3H).

^{13}C NMR (101 MHz, DMSO-d_6) δ 167.26, 165.62, 158.63, 150.60, 150.25, 148.70, 137.79, 136.48, 134.82, 133.73, 133.69, 133.10, 128.36, 128.28, 127.82, 127.65, 127.56, 126.82, 123.23, 122.25, 122.12, 116.18, 58.28, 48.35, 25.84, 25.70, 18.33, 18.29, 17.55, 17.39, -3.18, -3.28.

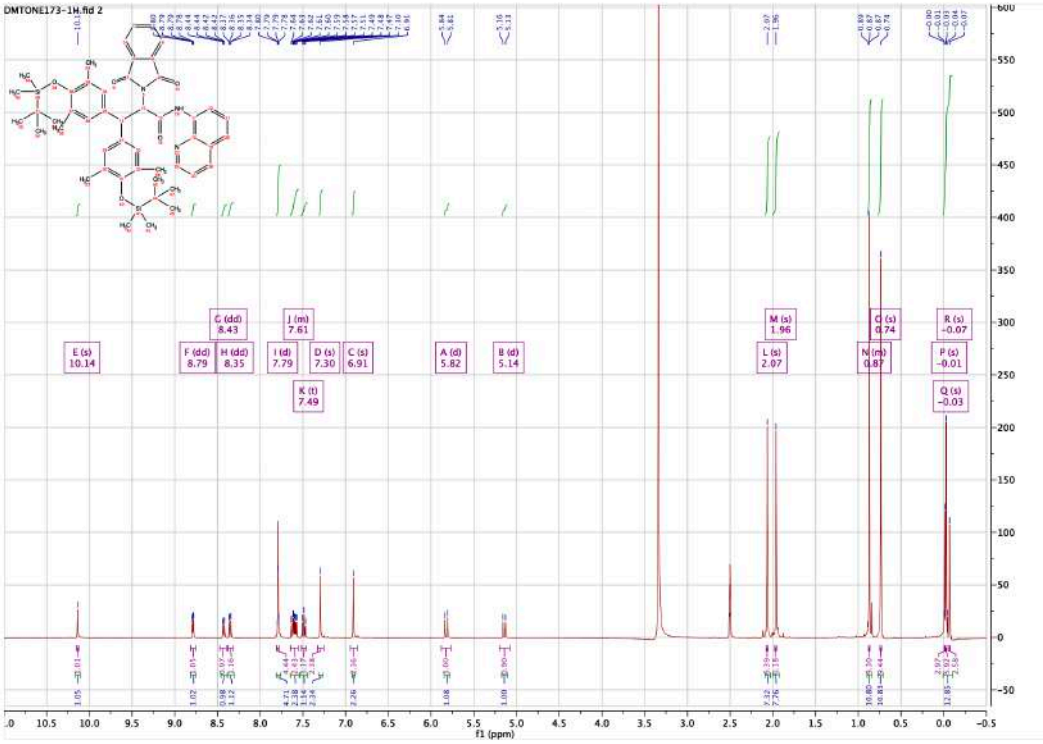

^{1}H NMR compound **51**

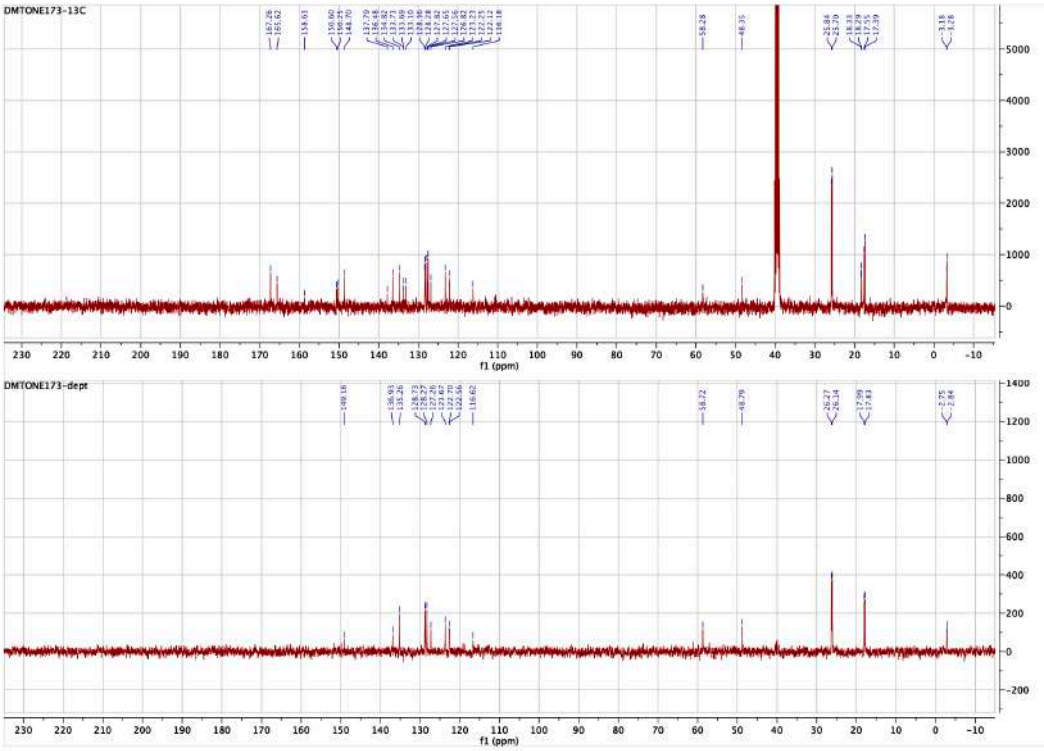

^{13}C and DEPT NMR compound **51**

Synthesis of *methyl picolinoyl-L-alaninate* (**55**):

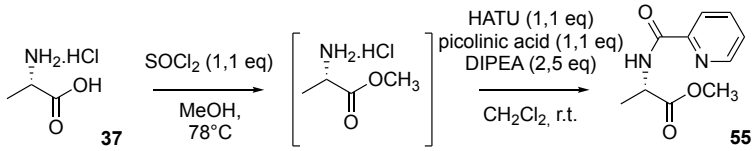

To a solution of *L*-alanine **37** (2.81 mmol, 0.250 g) in anhydrous MeOH (50 mL) was added $SOCl_2$ (3.08 mmol, 0.23 mL) in a dropwise manner. The reaction mixture was heated at reflux overnight. The solvent was removed under vacuum to give the crude *L*-Ala methyl-ester hydrochloride, which was washed with 20 mL of saturated sodium bicarbonate aqueous solution (to pH ~ 8) and extracted with DCM. The organic layers were combined and evaporated under vacuum to give the corresponding ester as yellowish crude oil, which was used directly for the next step.

A mixture of the previous crude amino product, picolinic acid (3.08 mmol, 0.38 g), HATU (3.08 mmol, 1.17 g) and DIPEA (7.01 mmol, 1.22 mL) in 50 mL of DCM was stirred at room temperature overnight. Then, the reaction was quenched with a saturated NH_4Cl aqueous solution and the two layers were separated. The aqueous layer was extracted with DCM (3 times), and the organic layers were combined, dried over Na_2SO_4, filtered and concentrated in vacuum. The residue was purified by flash chromatography (3:7 petroleum ether/AcOEt) to afford compound **55** (0.38 g) as yellowish oil.

Compound **55**:

Yield: 65% overall

MS (ESI): m/z $[M+H]^+$ 210,22

^{1}H NMR (400 MHz, Chloroform-*d*) δ 8.57 (ddt, *J* = 4.1, 2.4, 1.1 Hz, 1H), 8.48 (d, *J* = 7.7 Hz, 1H), 8.17 (dq, *J* = 8.2, 1.2 Hz, 1H), 7.90 – 7.76 (m, 1H), 7.43 (ddt, *J* = 7.4, 5.0, 1.3 Hz, 1H), 4.87 – 4.71 (m, 1H), 3.80 – 3.73 (m, 3H), 1.59 – 1.51 (m, 3H).

^{13}C NMR (101 MHz, Chloroform-*d*) δ 173.32, 164.01, 149.52, 148.32, 137.50, 126.51, 122.43, 52.61, 48.23, 18.56.

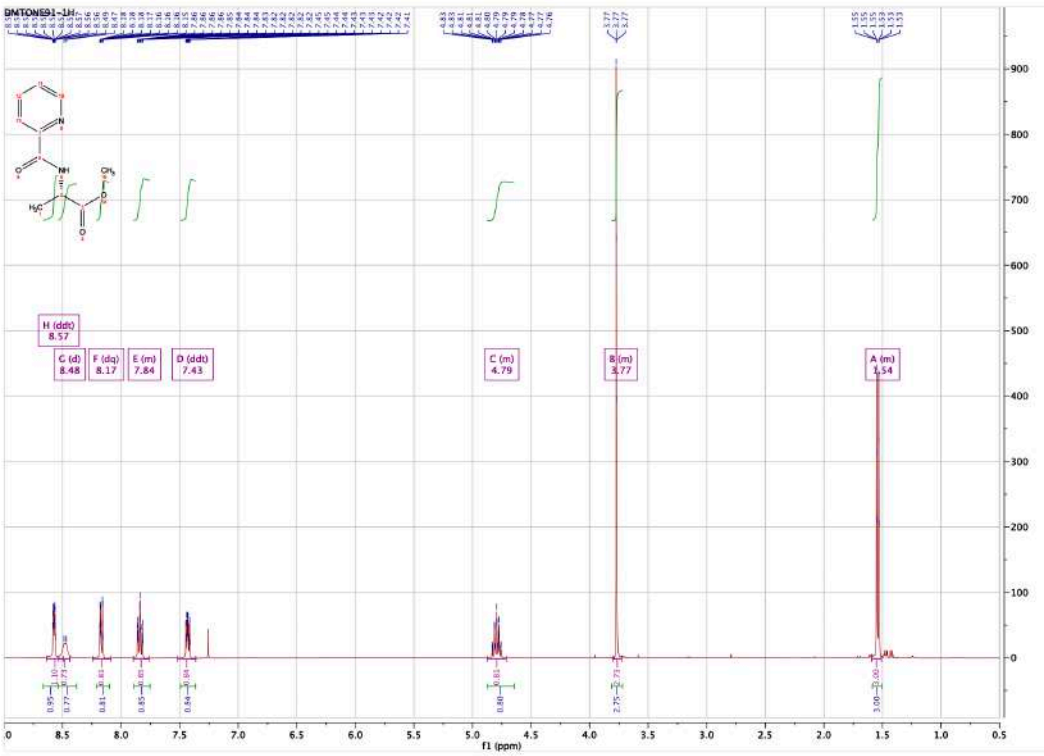

^{1}H NMR compound **55**

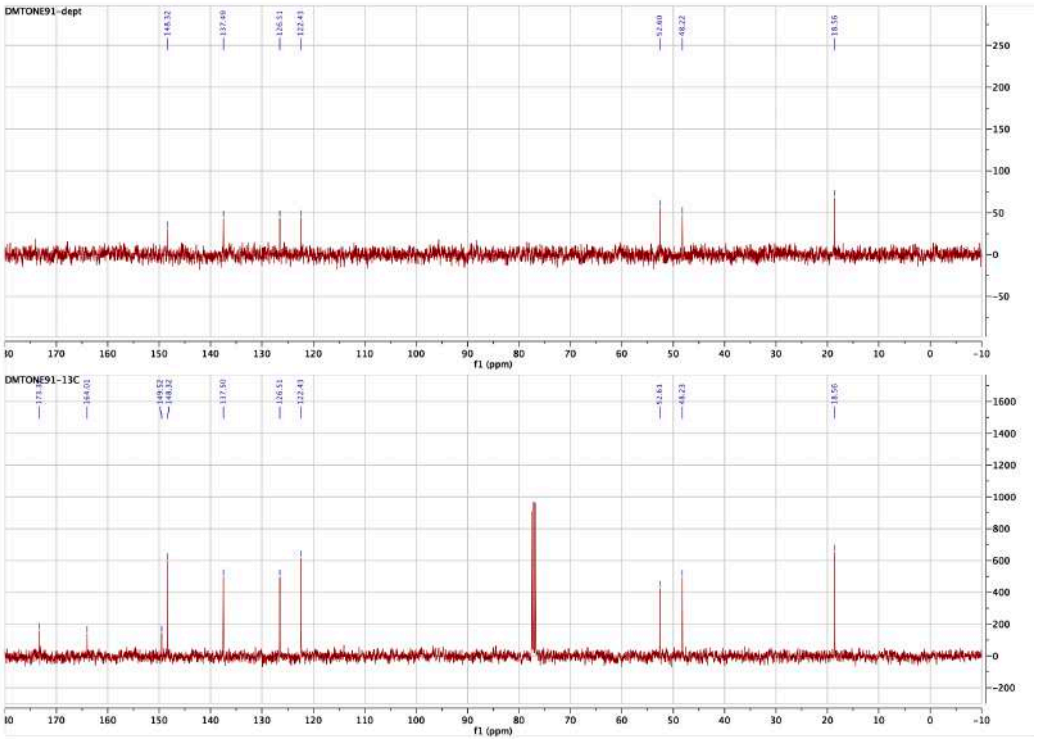

^{13}C and DEPT NMR compound **55**

Synthesis of *(S)-2-(1,3-dioxoisoindolin-2-yl)-N-(pyridin-2-yl)propanamide* (**56**)

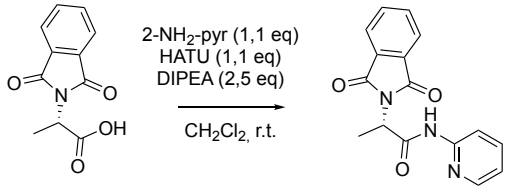

38 **56**

A mixture of the previous synthesized derivative **38** (0.45 mmol, 0.10 g), 2-aminopyridine (0.51 mmol, 0.047 g), HATU (0.51 mmol, 0.19 g) and DIPEA (1.14 mmol, 0.19 mL) in DCM (25 mL) was stirred at room temperature overnight, monitored through mass spectrometry and TLC. Once completed, the reaction was quenched with a saturated NH_4Cl aqueous solution and the two layers were separated. The aqueous layer was extracted with DCM, and the organic layers were combined, dried over Na_2SO_4, filtered and concentrated in vacuum. The residue was purified by flash chromatography (1:1 petroleum ether/AcOEt) to afford the compound **39** (0.101 g) as yellowish solid.

Compound **56**:

Yield: 75%

MS (ESI): m/z $[M+H]^+$ 296,30

^{1}H NMR (400 MHz, Chloroform-*d*) δ 8.97 (s, 1H), 8.30 – 8.15 (m, 2H), 7.87 (dd, *J* = 5.4, 3.1 Hz, 2H), 7.81 – 7.66 (m, 3H), 7.05 (ddd, *J* = 7.4, 5.0, 1.1 Hz, 1H), 5.11 (q, *J* = 7.3 Hz, 1H), 1.81 (d, *J* = 7.3 Hz, 3H).

^{13}C NMR (101 MHz, Chloroform-*d*) δ 167.94, 167.84, 150.93, 146.84, 139.34, 134.50, 131.96, 123.83, 120.20, 114.71, 50.13, 15.30.

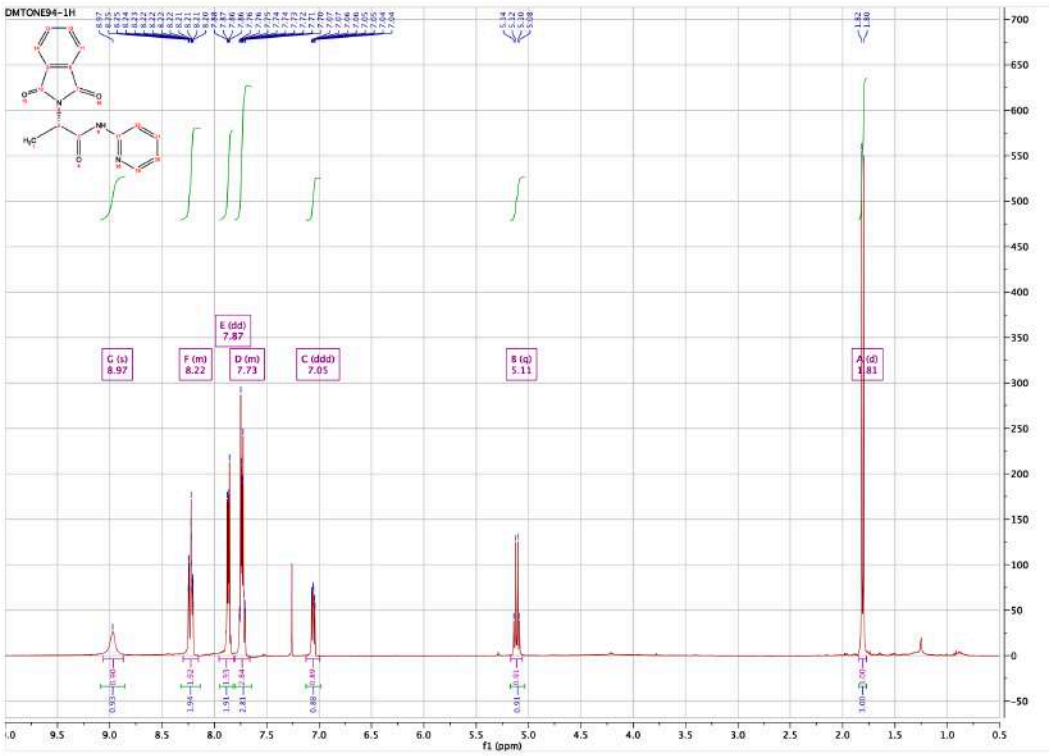

^{1}H NMR compound **56**

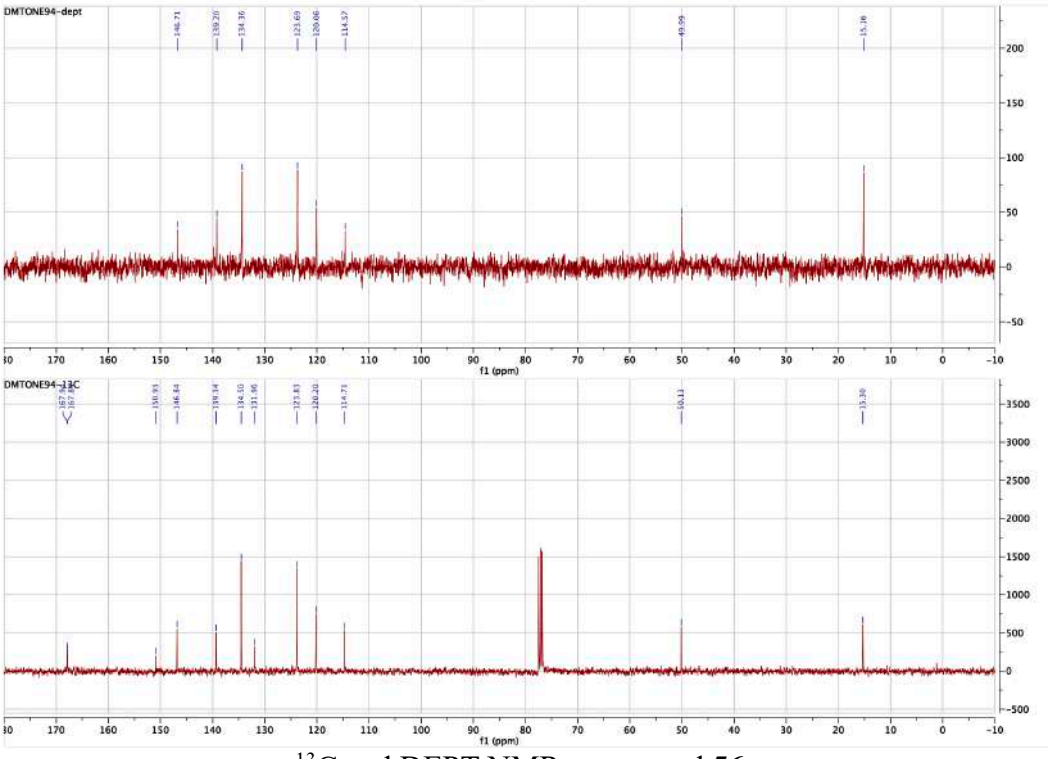

^{13}C and DEPT NMR compound **56**

Synthesis of *(S)-2-(1,3-dioxoisoindolin-2-yl)-N-(pyridin-2-ylmethyl)propanamide* (**57**)

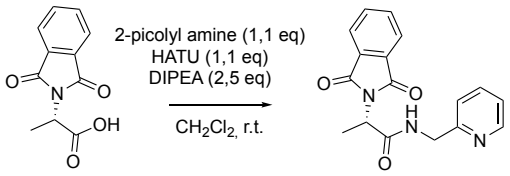

38 **57**

A mixture of the previous synthesized derivative **38** (1.37 mmol, 0.30 g), 2-picolyl amine (1.51 mmol, 0.15 mL), HATU (1.51 mmol, 0.57 g) and DIPEA (3.42 mmol, 0.59 mL) in DCM (50 mL) was stirred at room temperature overnight, monitored per TLC and mass spectrometry. Once completed, the reaction was quenched with a saturated NH_4Cl aqueous solution and the two layers were separated. The aqueous layer was extracted with DCM, and the organic layers were combined, dried over Na_2SO_4, filtered and concentrated in vacuum. The residue was purified by flash chromatography (0,5:9,5 petroleum ether/AcOEt) to afford the compound **57** (0.254 g) as yellow oil.

Compound **57**:

Yield: 60%

MS (ESI): m/z $[M+H]^+$ 309,33

^{1}H NMR (400 MHz, Chloroform-*d*) δ 8.45 (ddt, *J* = 5.1, 1.8, 0.9 Hz, 1H), 7.84 (ddd, *J* = 5.5, 3.1, 0.8 Hz, 2H), 7.76 – 7.67 (m, 3H), 7.41 (s, 1H), 7.33 (dd, *J* = 7.9, 1.1 Hz, 1H), 7.26 – 7.19 (m, 1H), 4.99 (q, *J* = 7.3 Hz, 1H), 4.59 (d, *J* = 5.1 Hz, 2H), 1.75 (dd, *J* = 7.4, 0.8 Hz, 3H).

^{13}C NMR (101 MHz, Chloroform-*d*) δ 169.40, 167.95, 155.91, 148.15, 137.95, 134.31, 132.06, 123.62, 122.83, 122.69, 49.23, 44.38, 15.39.

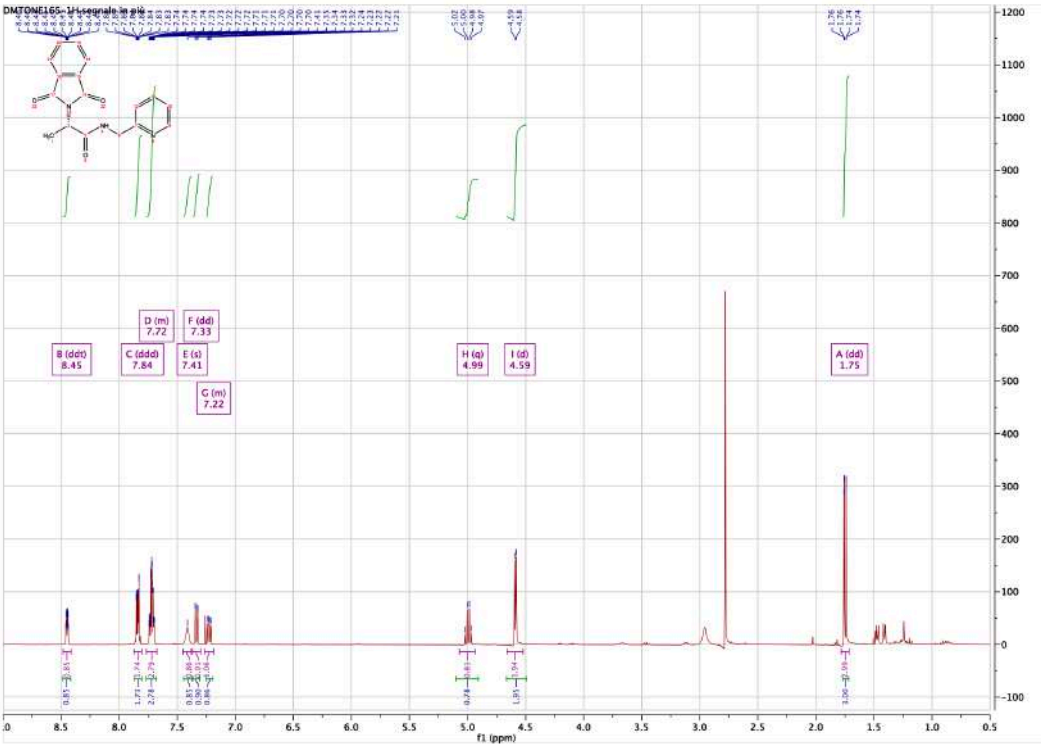

^{1}H NMR compound **57**

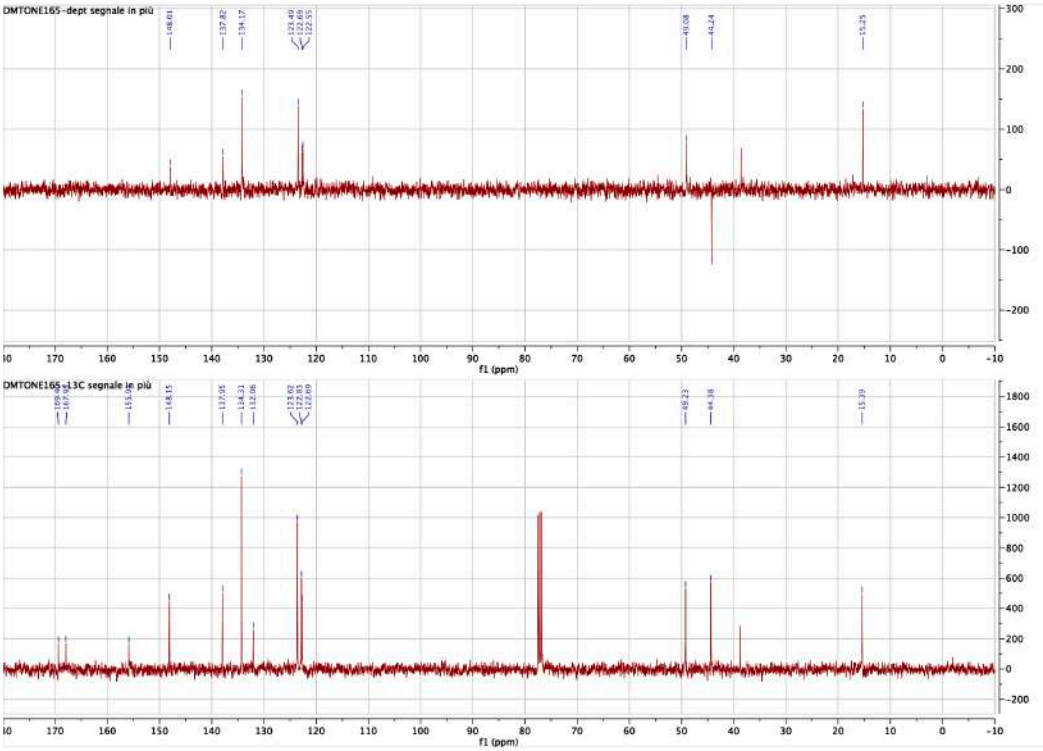

^{13}C and DEPT NMR compound **57**

Synthesis of *(S)-2-(1,3-dioxoisoindolin-2-yl)-3-(4-hydroxyphenyl)-N-(pyridin-2-ylmethyl)propanamide* (**58**)

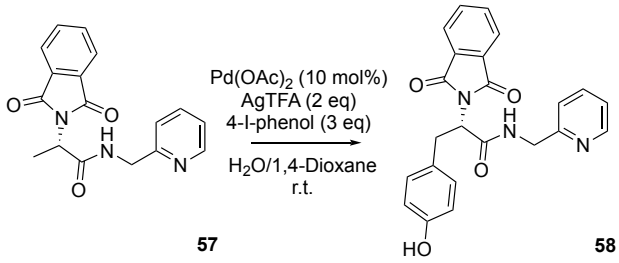

The compound **57** (0.19 mmol, 0.06 g), $Pd(OAc)_2$ (0.019 mmol, 4.35 mg), AgTFA (0.38 mmol, 0.85 g), and 4-iodo phenol (0.58 mmol, 0.128 g) were inserted in a microwave tube. A mixture of 1,4-Dioxane/H_2O (0.9 mL/0.1 mL) was used as solvent. The reaction mixture was stirred at r.t. for 24h, it was monitored per mass spectrometry and TLC. Once completed, the crude was filtered through celite pad and washed with DCM. The filtrate was concentrated under vacuum, obtaining a crude oil, which was purified by flash chromatography (1:9 petroleum ether/AcOEt) to afford the compound **49** (0.029 g) as yellowish solid.

Compound **58**:

Yield: 38%

MS (ESI): m/z $[M+H]^+$ 402,42

^{1}H NMR (400 MHz, DMSO-d_6) δ 9.12 (s, 1H), 8.85 (t, J = 5.9 Hz, 1H), 8.52 (ddd, J = 4.9, 1.8, 0.9 Hz, 1H), 7.87 (td, J = 7.7, 1.8 Hz, 1H), 7.81 (d, J = 1.0 Hz, 4H), 7.43 – 7.26 (m, 2H), 6.95 – 6.81 (m, 2H), 6.50 (d, J = 8.5 Hz, 2H), 4.98 (dd, J = 11.9, 4.6 Hz, 1H), 4.54 – 4.26 (m, 2H), 3.45 (dd, J = 14.0, 4.6 Hz, 2H).

^{13}C NMR (101 MHz, DMSO-d_6) δ 168.31, 167.51, 158.08, 155.73, 147.92, 137.79, 134.49, 131.36, 129.62, 127.41, 123.08, 122.44, 121.11, 115.09, 54.56, 44.09, 32.96.

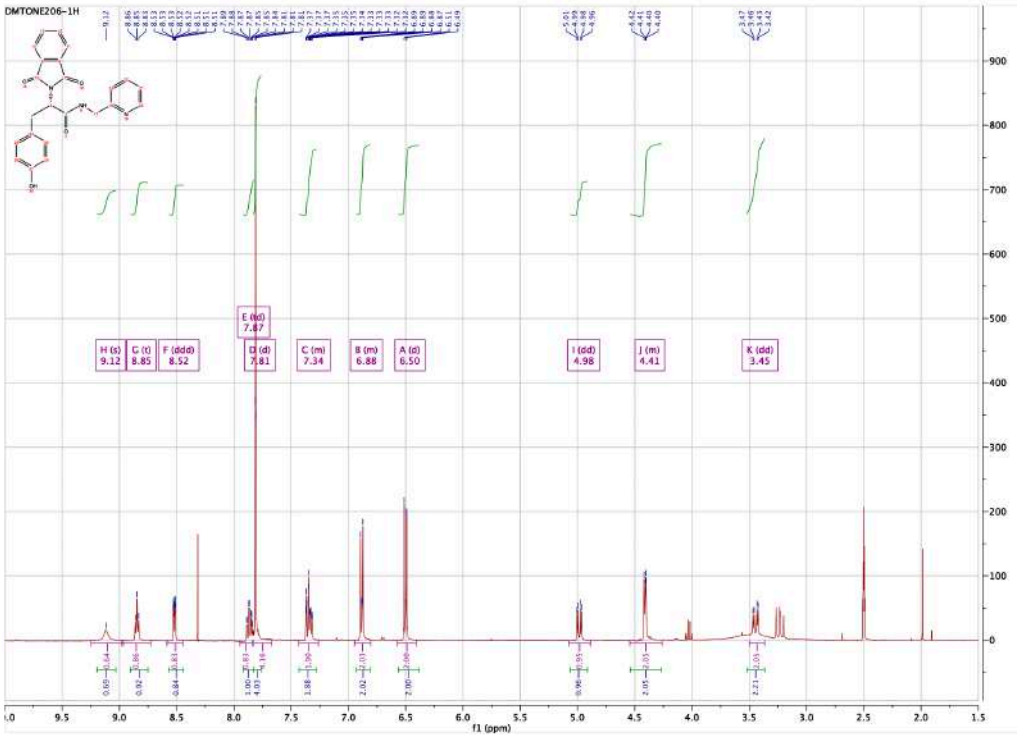

^{1}H NMR compound **58**

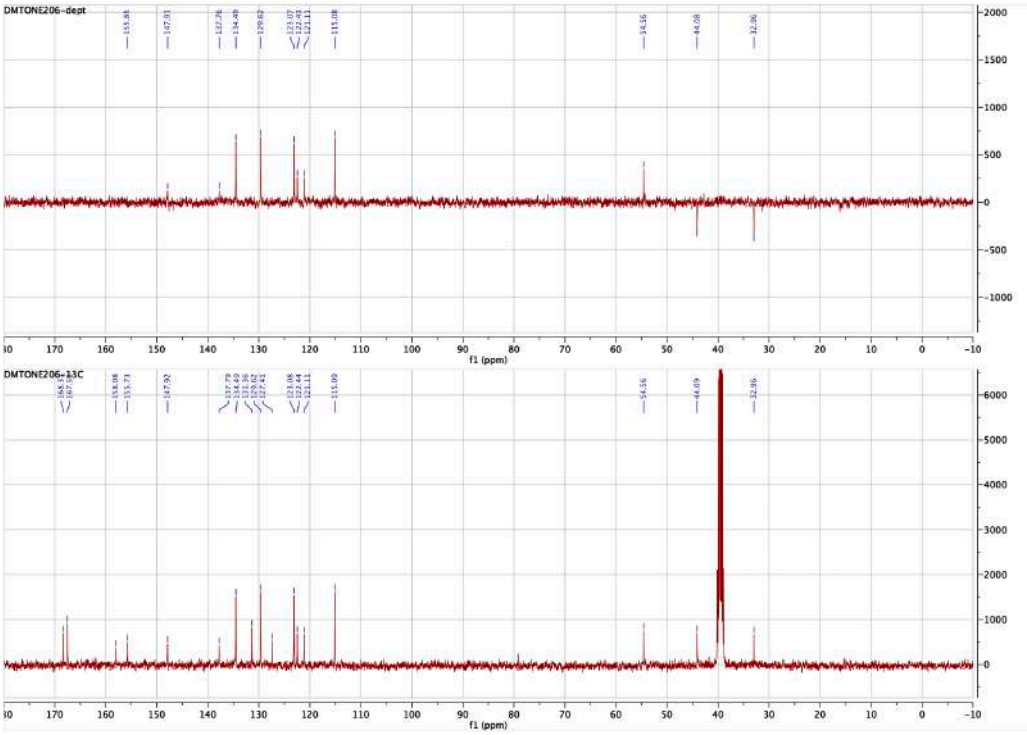

^{13}C and DEPT NMR compound **58**

Synthesis of *(S)-3-(4-((tert-butyldimethylsilyl)oxy)phenyl)-2-(1,3-dioxoisoindolin-2-yl)-N-(pyridin-2-ylmethyl)propanamide* and *(S)-3,3-bis(4-((tert-butyldimethylsilyl)oxy)phenyl)-2-(1,3-dioxoisoindolin-2-yl)-N-(pyridin-2-ylmethyl)propanamide* (**59**+**60**)

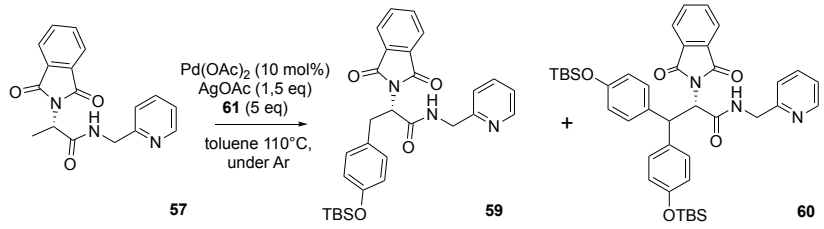

The compound **41** (0.19 mmol, 0.060g), $Pd(OAc)_2$ (0.019 mmol, 4.35 mg), AgOAc (1.32 mmol, 0.21 g), and 4-Iodo phenol *O*-TBS **61** (0.58 mmol, 0.194 g) were inserted in a microwave tube, and solubilized in toluene. The reaction mixture was stirred at r.t. for 10 min, bubbling Ar into the vial, then it was left stirred at 110°C for 24h, monitored per mass spectrometry and TLC. Once completed, the crude was filtered through celite pad and washed with DCM. The filtrate was concentrated under vacuum, obtaining a crude oil, which was purified by flash chromatography (0,5:9,5 petroleum ether/AcOEt) to afford the compound **59** (0.035 g) and **60**, only in traces.

Compound **59**:

Yield: 35%

MS (ESI): m/z $[M+H]^+$ 516,69

^{1}H NMR (400 MHz, Chloroform-*d*) δ 8.44 (dt, *J* = 5.1, 1.2 Hz, 1H), 7.74 (dt, *J* = 5.7, 2.8 Hz, 3H), 7.66 (dd, *J* = 5.5, 3.1 Hz, 2H), 7.45 (t, *J* = 5.2 Hz, 1H), 7.34 (d, *J* = 7.9 Hz, 1H), 7.26 – 7.20 (m, 1H), 7.03 – 6.96 (m, 2H), 6.64 – 6.58 (m, 2H), 5.13 (dd, *J* = 10.5, 6.4 Hz, 1H), 4.61 (t, *J* = 5.3 Hz, 2H), 3.61 – 3.41 (m, 2H), 0.89 (s, 9H), 0.05 (d, *J* = 2.6 Hz, 6H).

^{13}C NMR (101 MHz, Chloroform-*d*) δ 168.85, 168.05, 155.89, 154.57, 148.06, 138.10, 134.24, 131.64, 130.04, 129.49, 123.56, 122.87, 122.71, 120.43, 55.68, 44.37, 34.09, 25.76, 18.28, -4.42.

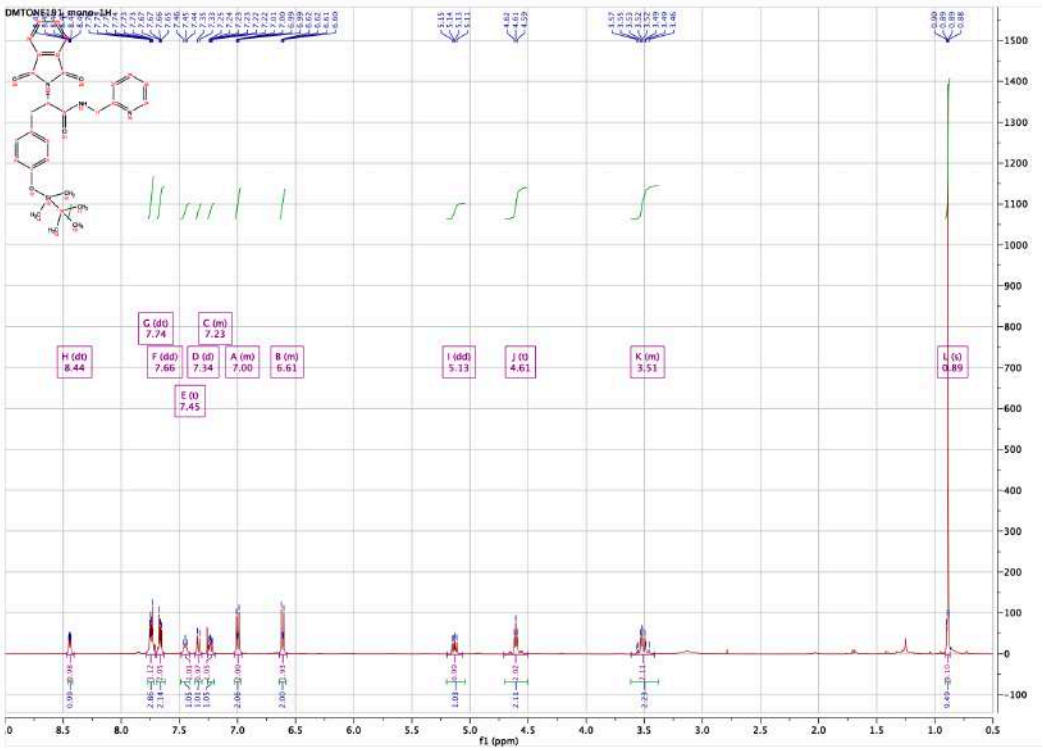

^{1}H NMR compound **59**

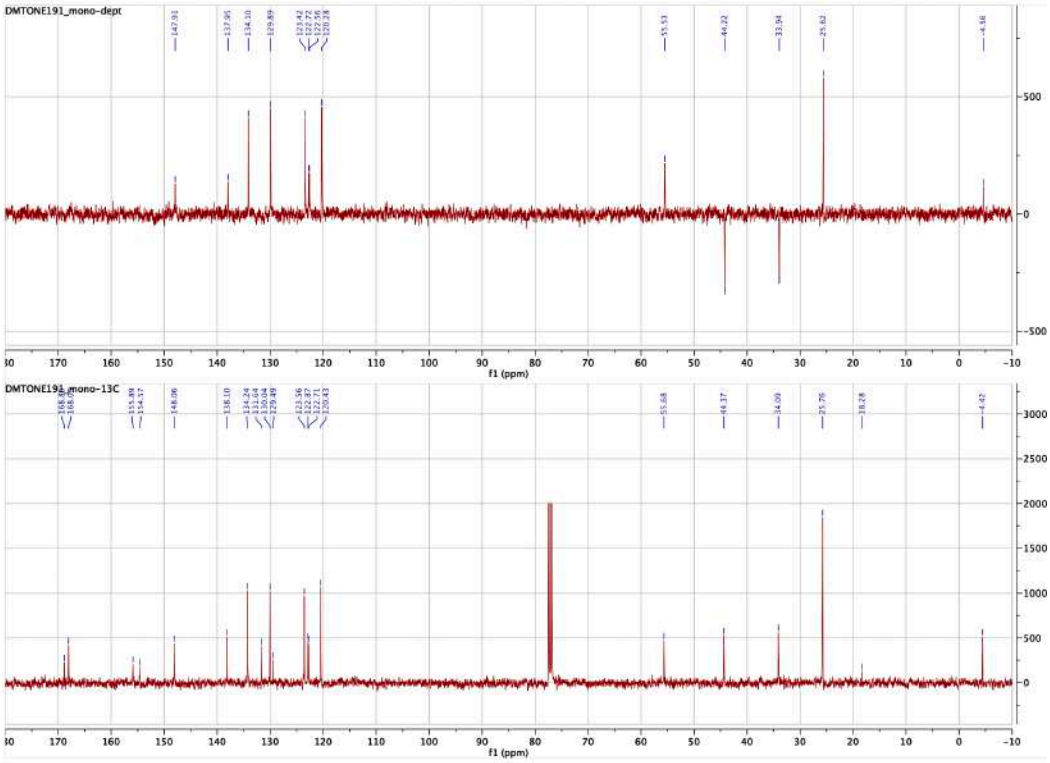

^{13}C and DEPT NMR compound **59**

Compound **60**:

Yield: 5%

MS (ESI): m/z $[M+H]^+$ 723,05

^{1}H NMR (400 MHz, Chloroform-*d*) δ 8.50 (d, *J* = 5.8 Hz, 1H), 8.25 (t, *J* = 7.9 Hz, 1H), 7.75 – 7.68 (m, 3H), 7.64 (dd, *J* = 5.6, 3.2 Hz, 3H), 7.52 (d, *J* = 8.1 Hz, 1H), 7.39 (d, *J* = 8.4 Hz, 2H), 7.06 (d, *J* = 8.5 Hz, 2H), 6.78 (d, *J* = 8.4 Hz, 2H), 6.53 (d, *J* = 8.4 Hz, 2H), 5.64 (d, *J* = 12.0 Hz, 1H), 5.11 (d, *J* = 11.9 Hz, 1H), 4.65 (d, *J* = 5.7 Hz, 2H), 0.97 (s, 9H), 0.83 (s, 9H), 0.18 (s, 6H), 0.07 (s, 6H).

^{13}C NMR (101 MHz, Chloroform-*d*) δ 169.55, 154.81, 154.61, 153.70, 134.38, 133.16, 132.89, 131.19, 129.94, 129.25, 129.01, 124.99, 123.64, 120.60, 120.50, 120.25, 76.78, 57.51, 55.78, 48.89, 41.67, 25.71, 25.64, 18.15, 1.10, -4.34, -4.55.

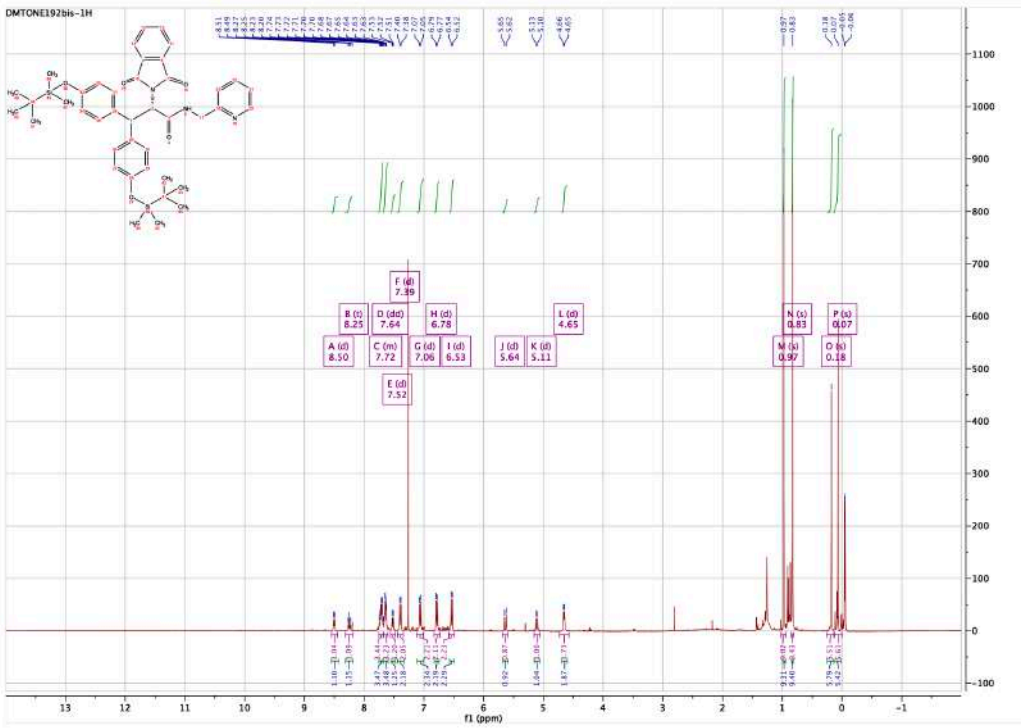

^{1}H NMR compound **60**

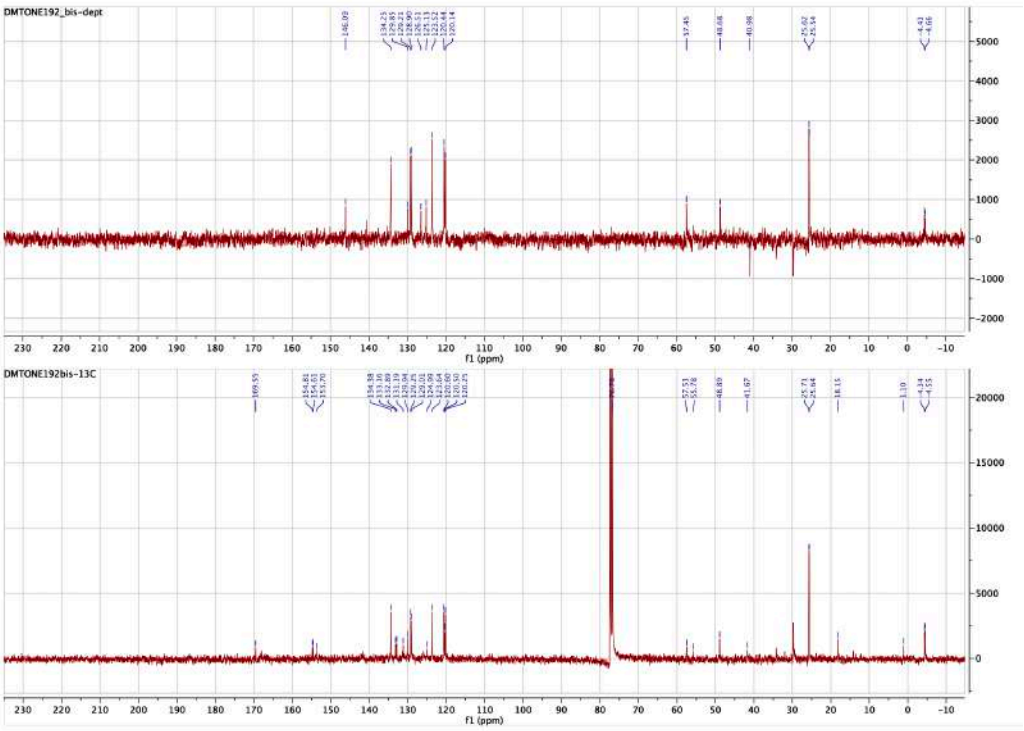

^{13}C and DEPT NMR compound **60**

General procedure for Boc protection (**52**, **53**, **54**):

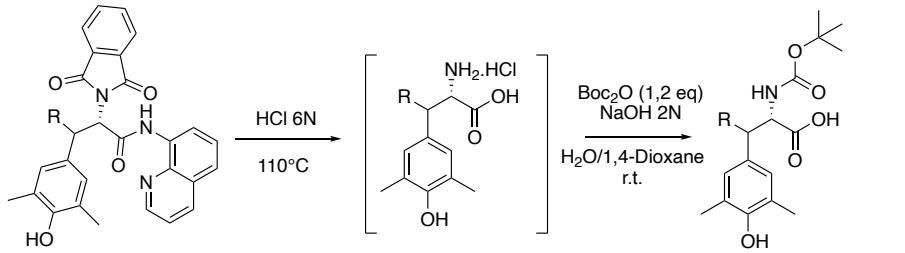

49 R: H
50 R: 4-phenol
51 R: 3,5-dimethyl-4-phenol

52 R: H
53 R: 4-phenol
54 R: 3,5-dimethyl-4-phenol

Once purified the compounds (**49**, **50**, **51**) were dissolved in HCl 6N aqueous solution (17 equiv.) and heated at 110 °C for 24 hours. The obtained hydrolyzed crude products were concentrated under vacuum to reduce the volume and the crudes were used directly for the subsequent protection step.

The HCl salts previously synthesized were directly used as crude, and diluted in water/dioxane (1:2) solution (0.2 M). The mixtures were basified with NaOH 2N aqueous solution until reachment of pH value of 10/11 at 0 °C. Boc_2O (1.2 equiv.) was added and the reaction was left stirring at r.t. for 12 hours. The completion of the reaction was monitored

per ESI mass spectrometry and TLC. The dioxane was removed under vacuum and HCl 1N aqueous solution was added at 0 °C to pH 1. The mixtures were extracted with ethyl acetate (3 times) and the organic phases combined were dried over Na_2SO_4 and concentrated under vacuum. The crudes were purified by flash chromatography (7:3 AcOEt/petroleum ether/1% acetic acid) and crystallized with 2:1 Et_2O/petroleum ether, to afford **52**, **53**, **54**.

Compound *(S)-2-((tert-butoxycarbonyl)amino)-3-(4-hydroxy-3,5-dimethylphenyl)propanoic acid* (**52**):

Yield: 52%

MS (ESI): m/z $[M+H]^+$ 310,36

^{1}H NMR (400 MHz, DMSO-d_6) δ 12.50 (s, 1H), 8.00 (s, 1H), 6.93 (d, J = 8.2 Hz, 1H), 6.75 (s, 2H), 3.99 (ddd, J = 9.7, 8.1, 4.8 Hz, 1H), 2.82 (dd, J = 13.9, 4.8 Hz, 1H), 2.65 (dd, J = 13.9, 9.7 Hz, 1H), 2.11 (s, 6H), 1.33 (s, 9H).

^{13}C NMR (101 MHz, DMSO-d_6) δ 173.75, 155.39, 151.64, 128.80, 128.21, 123.75, 77.97, 55.49, 39.73, 35.72, 28.17, 16.65.

^{1}H NMR compound **52**

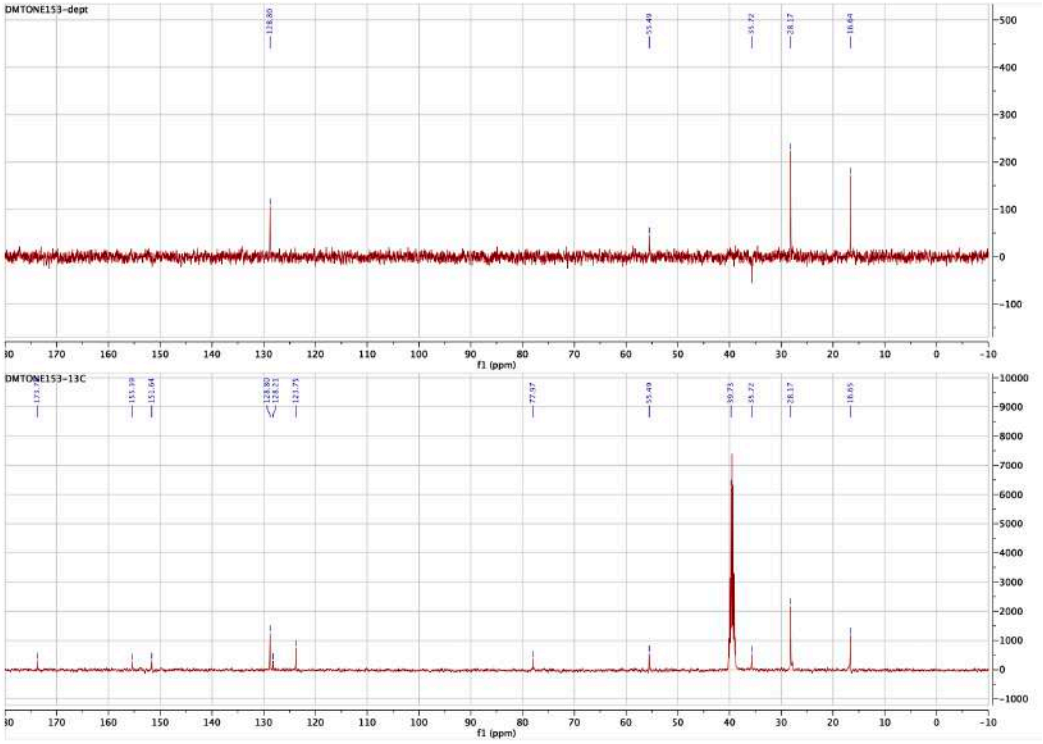

^{13}C and DEPT NMR compound **52**

Compound *(S)-2-((tert-butoxycarbonyl)amino)-3,3-bis(4-hydroxyphenyl)propanoic acid* (**53**):

Yield: 45%

MS (ESI): m/z $[M+H]^+$ 374,41

^{1}H NMR (400 MHz, DMSO-d_6) δ 9.18 (s, 1H), 7.19 – 6.98 (m, 4H), 6.89 (d, J = 8.9 Hz, 1H), 6.70 – 6.54 (m, 4H), 4.60 (dd, J = 11.0, 8.9 Hz, 1H), 4.06 (d, J = 11.1 Hz, 1H), 1.28 (s, 9H).

^{13}C NMR (101 MHz, DMSO-d_6) δ 172.98, 155.74, 155.57, 155.08, 132.33, 132.28, 129.05, 129.05, 114.90, 114.78, 77.98, 57.49, 51.03, 28.11.

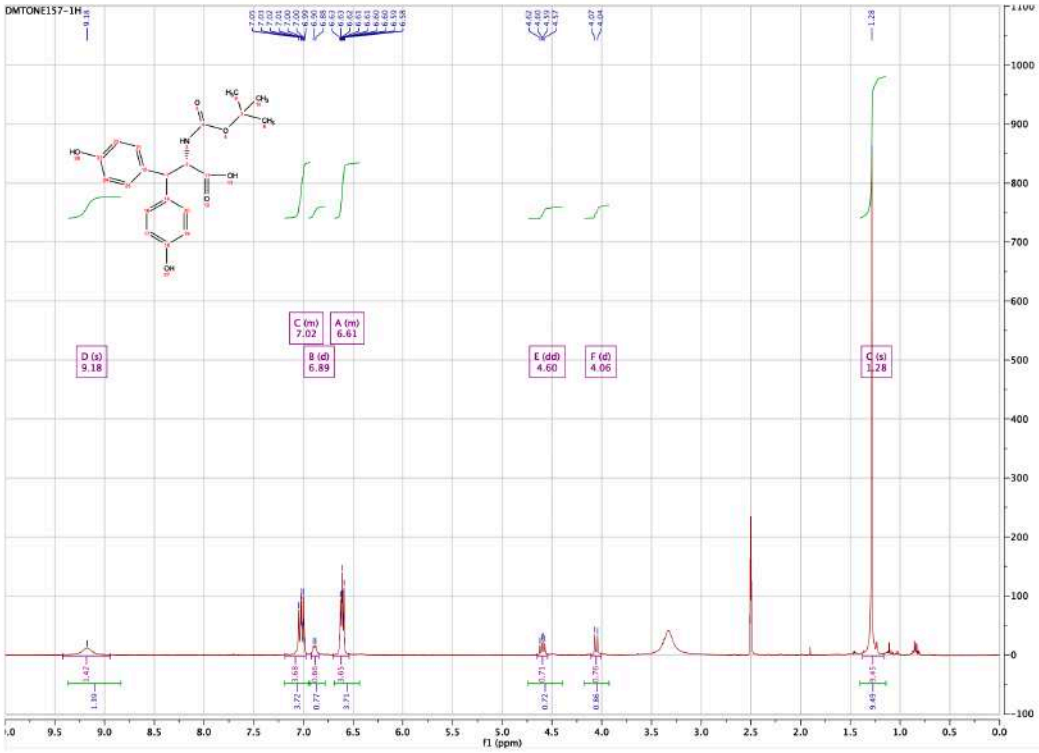

^{1}H NMR compound **53**

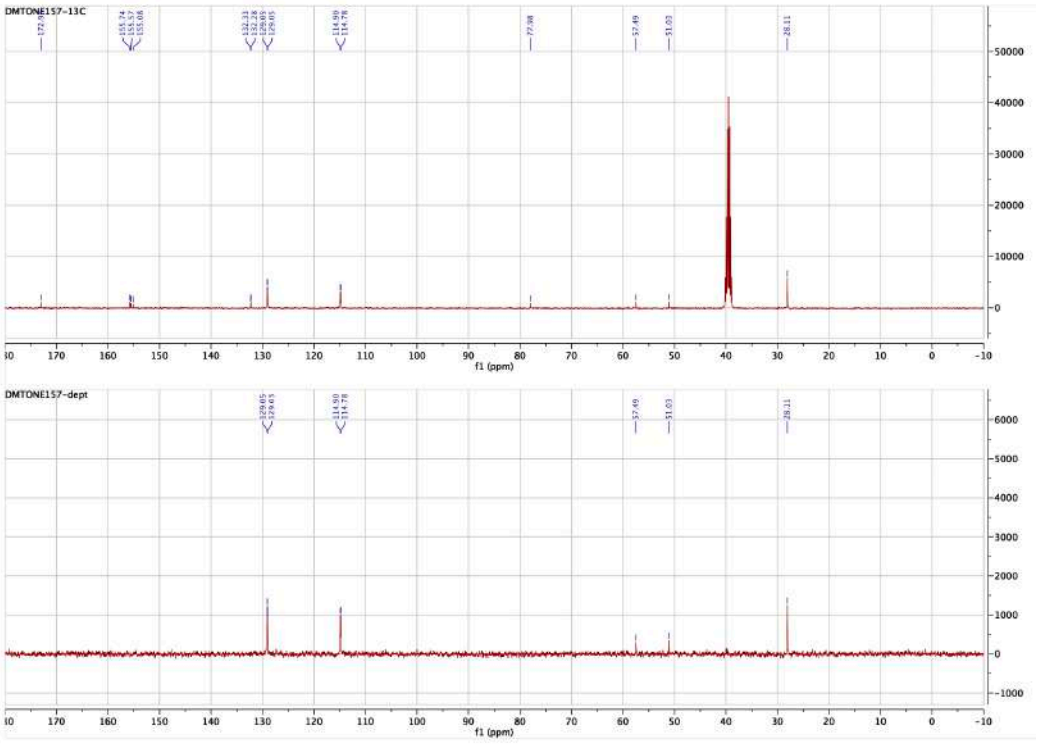

^{13}C and DEPT NMR compound **53**

Compound *(S)-2-((tert-butoxycarbonyl)amino)-3,3-bis(4-hydroxy-3,5-dimethylphenyl)propanoic acid* (**54**):

Yield: 27%

MS (ESI): m/z $[M+H]^+$ 430,51

^{1}H NMR (400 MHz, Chloroform-*d*) δ 6.90 – 6.85 (m, 2H), 6.82 (s, 2H), 4.80 (d, *J* = 8.2 Hz, 1H), 4.21 (d, *J* = 7.9 Hz, 1H), 2.18 (d, *J* = 4.4 Hz, 12H), 1.39 (s, 9H).

^{13}C NMR (101 MHz, Chloroform-*d*) δ 175.06, 155.88, 151.43, 151.28, 132.24, 131.54, 128.65, 128.37, 123.44, 123.18, 80.67, 57.08, 51.30, 28.35, 16.17.

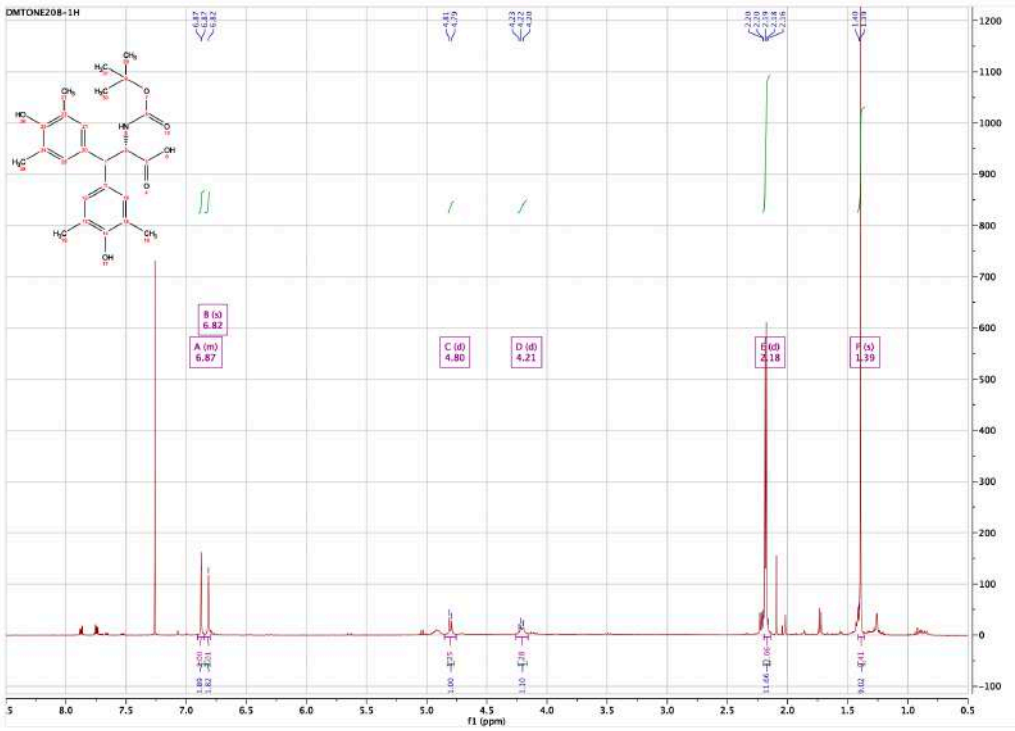

^{1}H NMR compound **54**

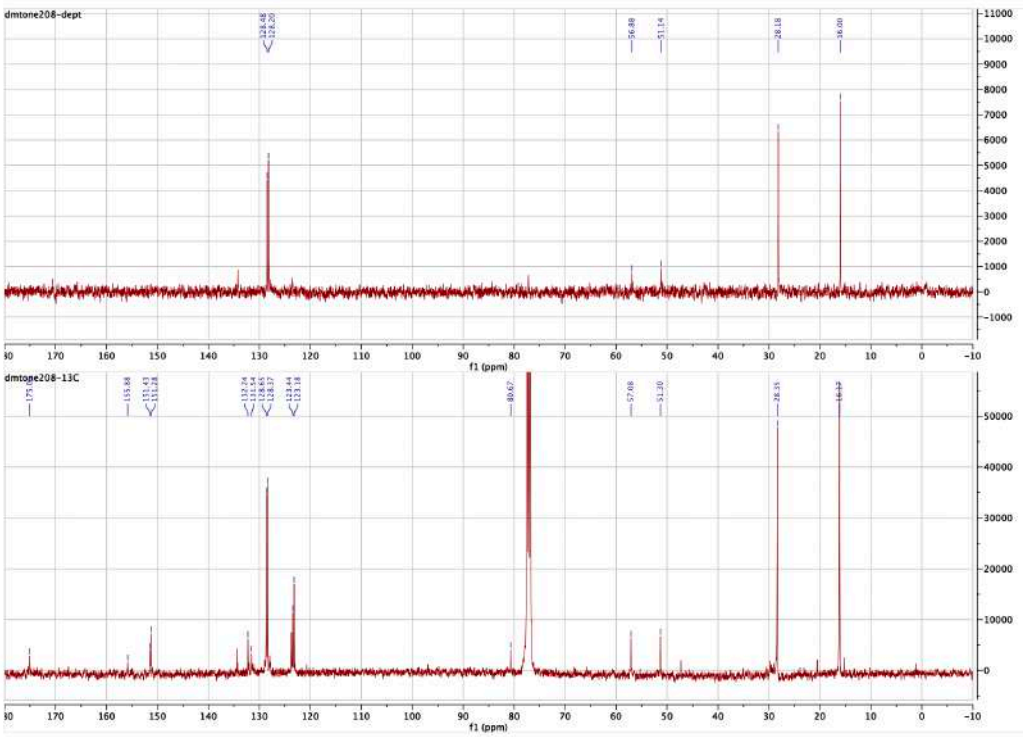

^{13}C and DEPT NMR compound **54**

7.5 Further application of 2,6-Dmt, via peptide welding technology (PWT)

Synthesis of *benzyl tert-butyl ((5R,8S)-12-((R)-2-(((benzyloxy)carbonyl)amino)-6-((tert-butoxycarbonyl)amino)hexanamido)-8-carbamoyl-6-oxododecane-1,5-diyl)dicarbamate* (**63**)

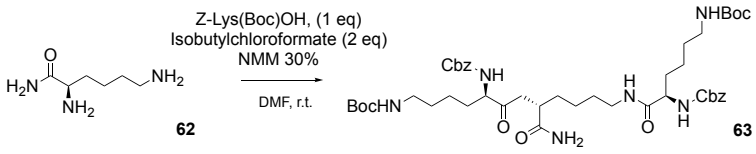

To a solution of Z-Lys(Boc)-OH (1 mmol) in DMF, N-methylmorpholine 30% V/V (5 mmol) and isobutylchloroformate (2.2 mmol) were added at 0 °C. After 5 minutes, (*L*)-Lysinamide **62**, previously dissolved in DMF, was added dropwise. The reaction was warmed to room temperature and left stirring for 4 hours. After this time, the solvent was removed under vacuum then, water was added to the crude residue obtaining a precipitate that was recrystallized from EtOH, affording a white solid.

Compound **63**:
Yield: 56%

^{1}H NMR (DMSO-*d*6, 400 MHz): δ 7.86-7.79 (m, 2H), 7.51-7.41 (m, 2H), 7.38-7.29 (m, 11H), 7.02 (bs, 1H), 6.80-6.77 (m, 2H), 5.04-4.97 (m, 4H), 4.19-4.13 (m, 1H), 3.98-3.85 (m, 2H), 3.03-2.95 (m, 2H), 2.87-2.84 (m, 4H), 1.62-1.46 (m, 5H), 1.40-1.20 (m, 31H).

^{13}C NMR (DMSO-*d*6, 101 MHz): δ 174.01, 173.44, 171.64, 155.96, 155.67, 136.94, 128.27, 127.66, 127.00, 77.28, 65.28, 54.68, 53.85, 52.00, 41.51, 40.29, 31.67, 31.42, 29.78, 29.00, 28.45, 22.66.

MS (ESI): m/z calcd for C44H67N7O11 [M+H]+871.05, found 870.97.

T_R = 19.63

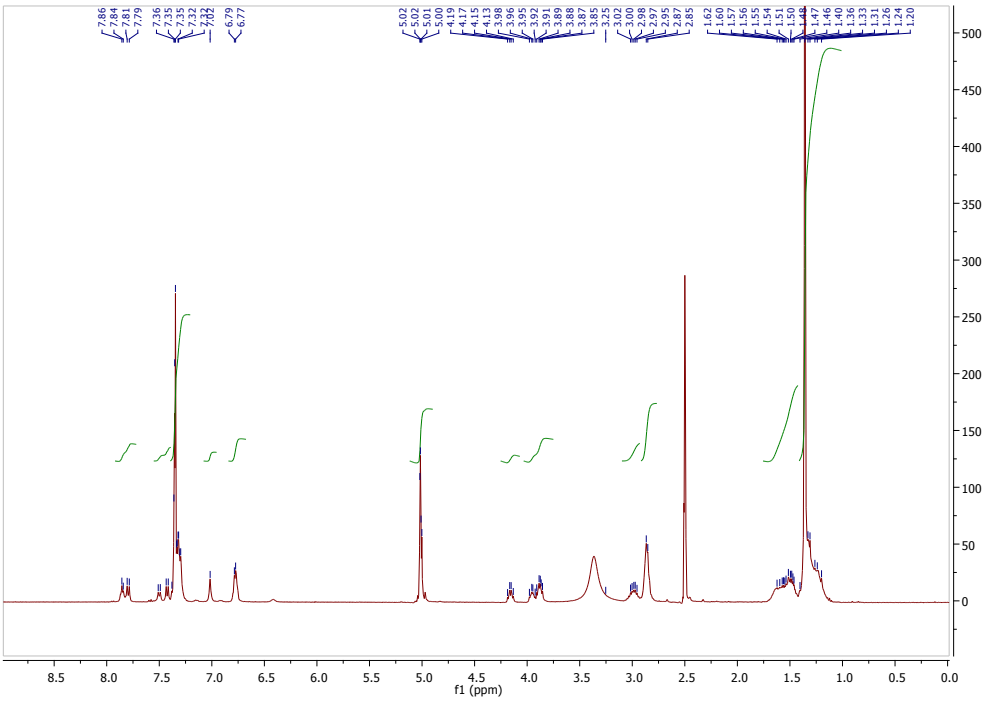

^{1}H NMR compound **63**

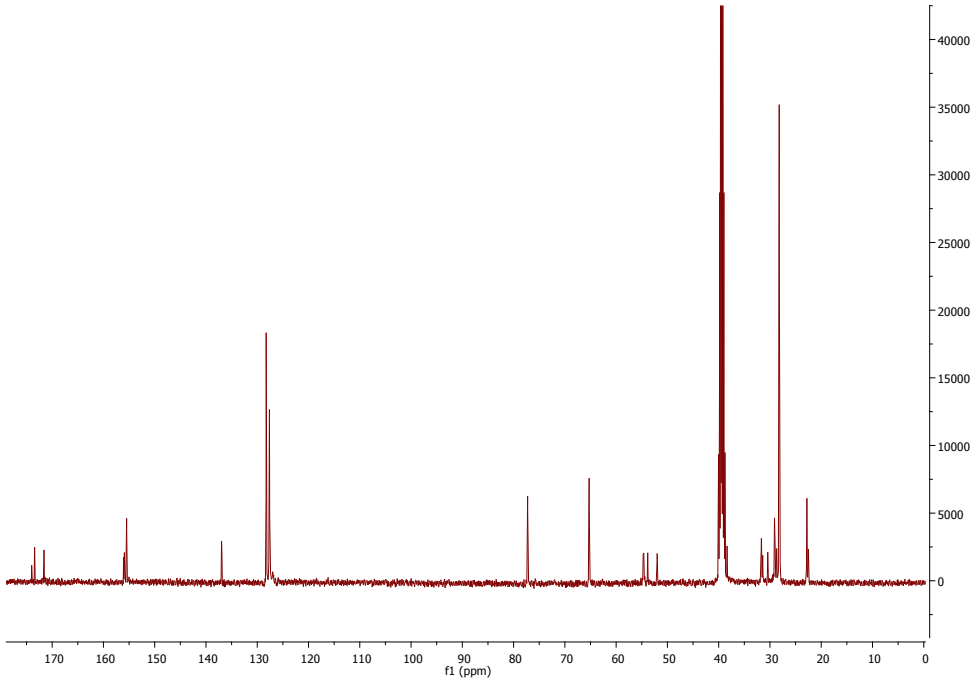

^{13}C NMR compound **63**

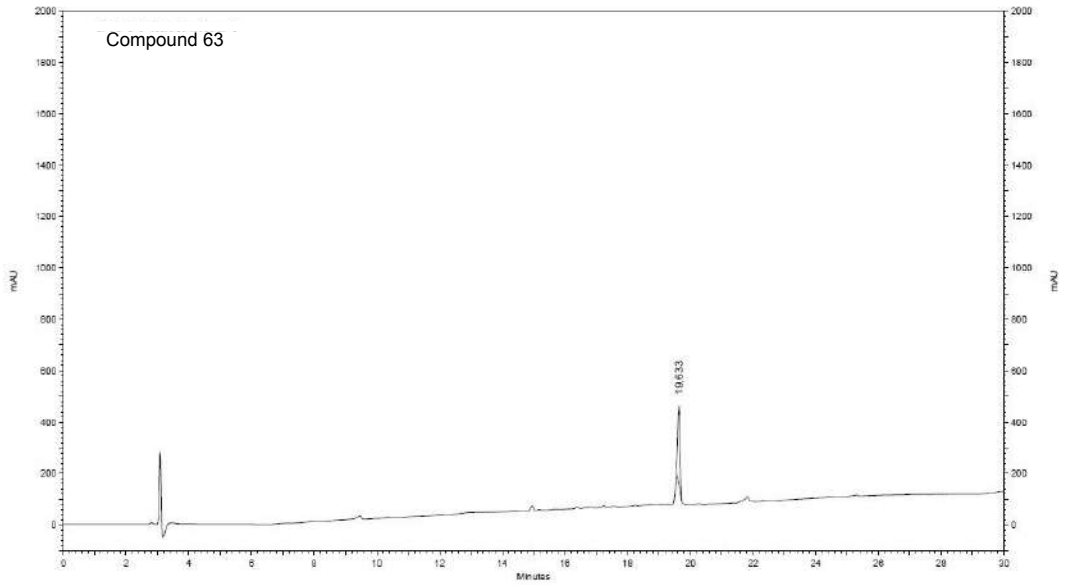

Analytical HPLC compound **63**

Synthesis of *tert-butyl ((10R,13R,20R)-13-carbamoyl-10,20-bis(4-(2,5-dioxo-2,5-dihydro-1H-pyrrol-1-yl)butanamido)-2,2-dimethyl-4,11,19-trioxo-3-oxa-5,12,18-triazatetracosan-24-yl)carbamate* (**64**)

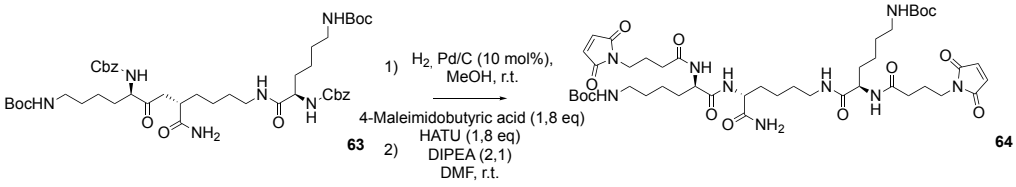

Pd/C (10% mmol) was added to a suspension of **62** (1 mmol) in MeOH and the reaction was stirred overnight under H_2 atmosphere. The mixture was filtered using a celite pad and the filtrate was concentrated under vacuum to obtain an amorphous solid that was suspended in Et_2O and filtered. This was used in the next step without further purification. The solid was added to a solution of 4-maleimidobutyric acid (1.8 mmol), HATU (1.8 mmol) and DIPEA (2.1 mmol) in DMF and the reaction was stirred for 3 hours at room temperature. After the removal of the solvent under vacuum, the desired derivative **64** was obtained via crystallization from AcOEt, as white solid.

Compound **64**:

Yield: 50%

^{1}H NMR (DMSO-*d*$_6$, 400 MHz): δ 7.98-7.96 (m, 1H), 7.89-7.82 (m, 2H), 7.77-7.75 (m, 1H), 7.23 (bs, 1H), 7.03-6.96 (m, 5H), 6.76-6.72 (m, 2H), 4.16-4.07 (m, 3H), 3.03-2.94 (m, 2H), 2.90-2.81 (m, 6H), 2.12-2.08 (m, 6H), 1.71-1.18 (m, 40H).

^{13}C NMR (DMSO-*d*6, 101 MHz): δ 173.47, 171.56, 171.40, 171.15, 171.04, 155.47, 134.40, 77.25, 52.73, 52.41, 52.12, 39.68, 38.32, 36.73, 32.34, 31.88, 31.45, 29.21, 28.69, 28.20, 24.18, 22.72.

MS (ESI): m/z calcd for $C_{44}H_{69}N_9O_{13}$ $[M+H]^+$ 933.08, found 933.05.

T_R =17.97

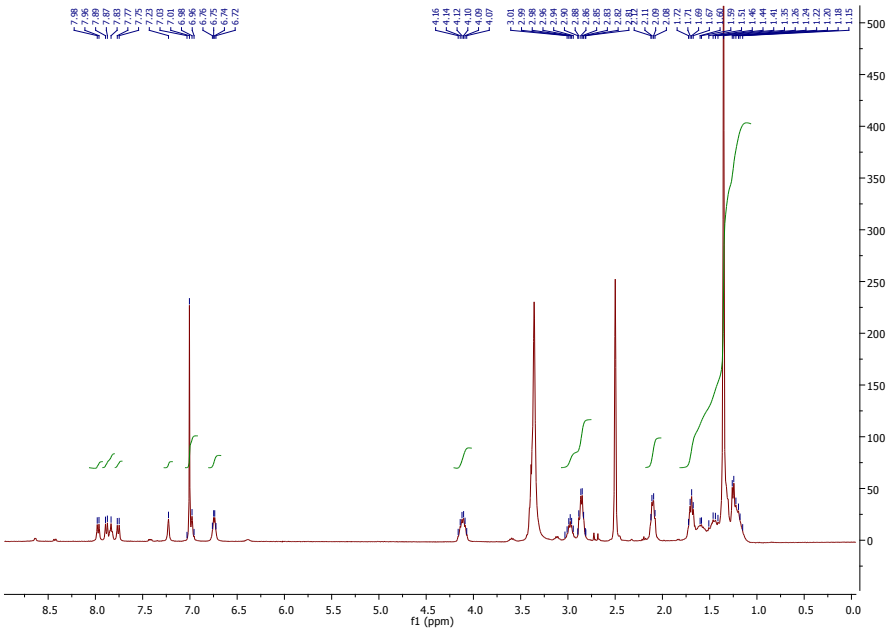

^{1}H NMR compound **64**

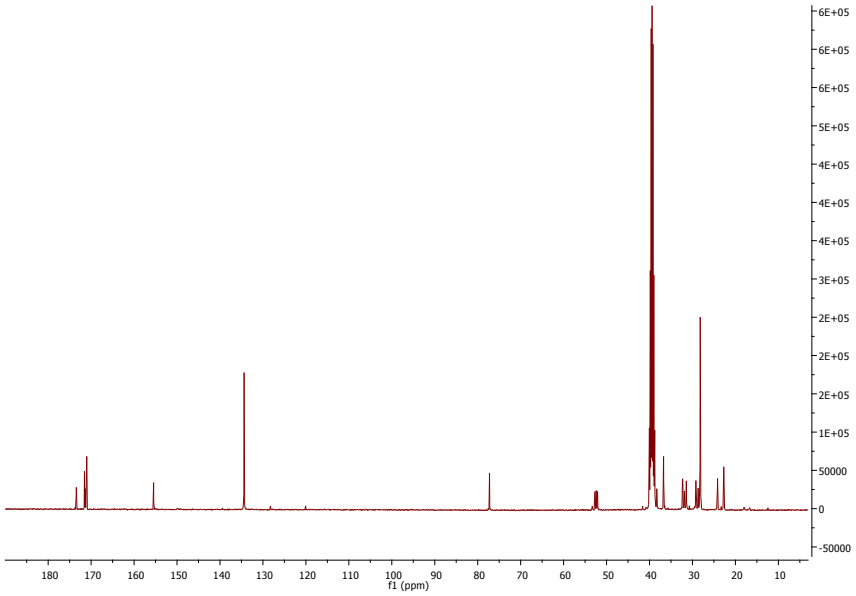

^{13}C NMR compound **64**

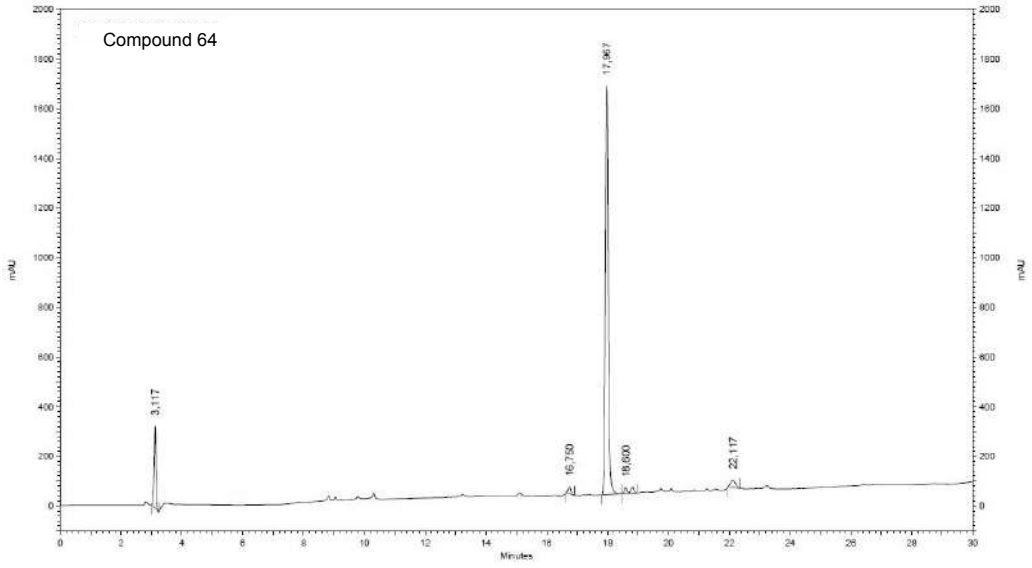

Analytical HPLC compound **64**

Synthesis of *N,N'-((5R,5'R)-(((R)-6-amino-6-oxohexane-1,5-diyl)bis(azanediyl))bis(5-(4-(2,5-dioxo-2,5-dihydro-1H-pyrrol-1-yl)butanamido)-6-oxohexane-6,1-diyl))bis(4-formylbenzamide)* (**65**)

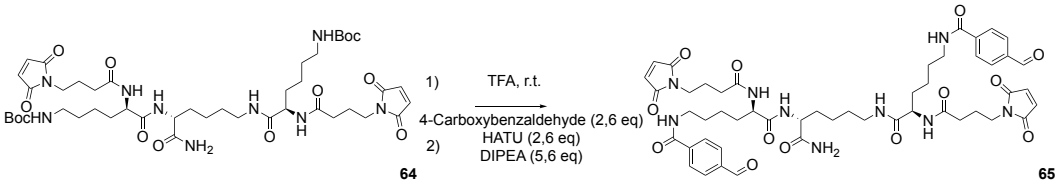

The compound **64** (1 mmol) was dissolved in TFA (5 ml) and the mixture was stirred at room temperature for 2 hours. After removal of all the volatiles under vacuum, the residue was dissolved in a mixture of DMF (5 mL) and DIPEA (3 mmol). The resulting solution was added to a stirring mixture of HATU (2.6 mmol), 4-carboxybenzhaldeyde (2.6 mmol) and DIPEA (2.6 mmol) in DMF (5 mL). The brownish mixture was left stirring overnight at room temperature. After this time, the solvent was removed under vacuum and compound **65** was crystallized from acetone/Et_2O as white solid. The isolated product was used without further purification in the conjugation reaction**.**

Compound **65**:

Yield: 58%

^{1}H NMR (DMSO-*d*$_6$, 400 MHz): δ 10.05 (s, 2H), 8.63-8.59 (m, 2H), 7.97-7.92 (m, 14H), 7.01-6.91 (m, 4H), 4.20-4.04 (m, 3H), 3.62-2.86 (m, 8H with residual water of the deuterated solvent), 2.12-2.05 (m, 6H), 1.74-1.15 (m, 22H).

^{13}C NMR (DMSO-*d*6, 101 MHz): δ 192.79, 173.42, 171.51, 171.34, 171.11, 170.93, 165.14, 139.58, 137.52, 134.32, 129.24, 127.75, 53.18, 52.63, 52.21, 41.51, 38.27, 36.66, 32.24, 31.80, 31.36, 28.61, 24.05, 22.80.

MS (ESI): m/z calcd for $C_{50}H_{61}N_9O_{13}$ $[M+H]^+$ 996.75.

T_R = 17.73

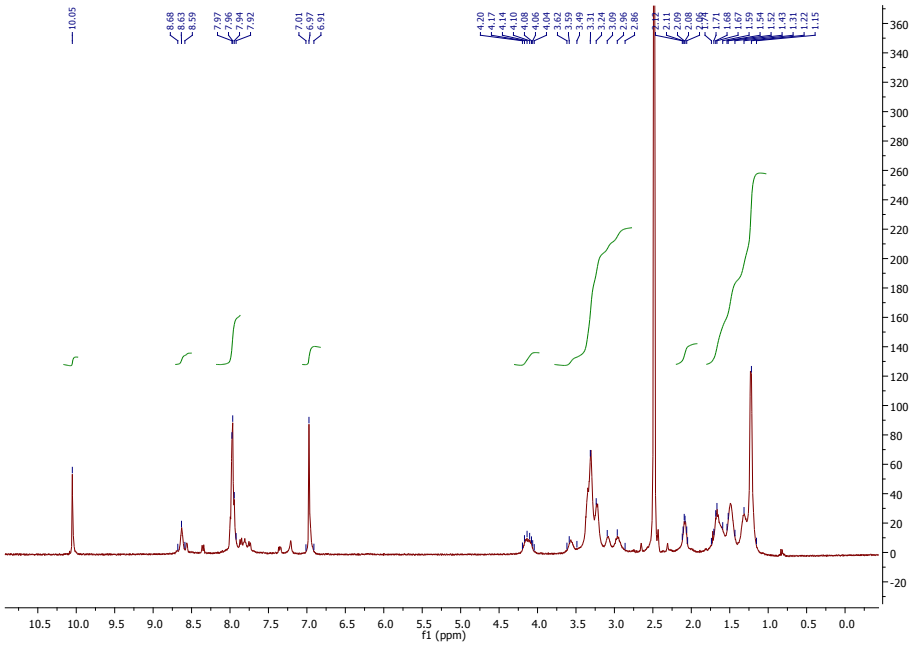

^{1}H NMR compound **65**

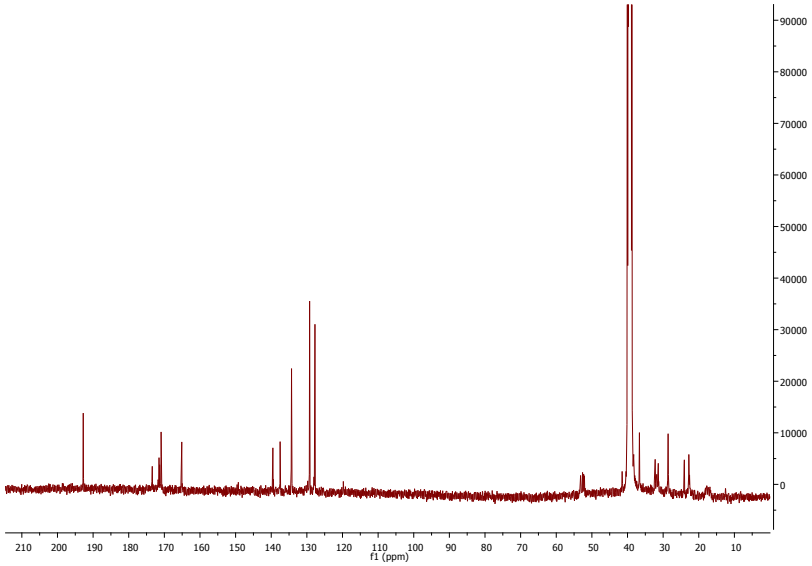

^{13}C NMR compound **65**

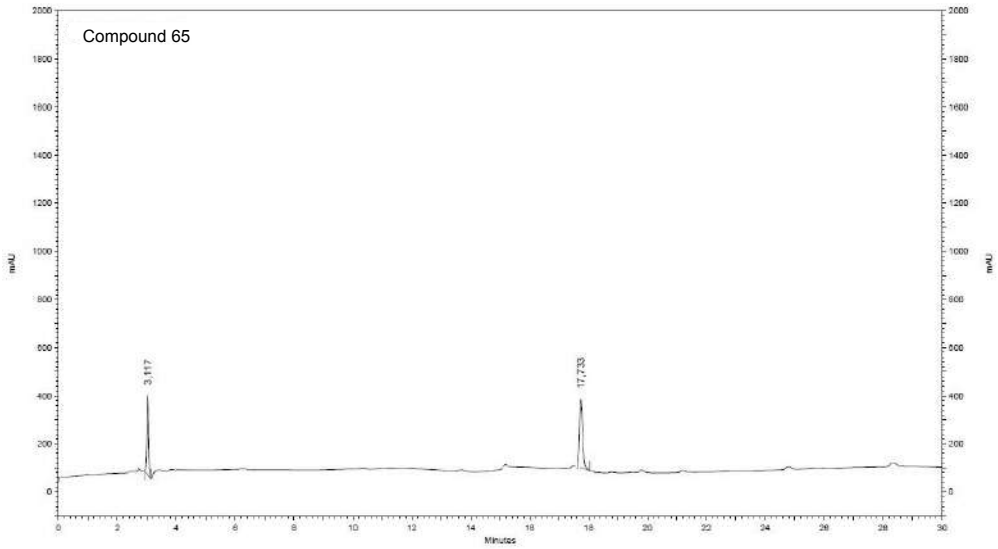

Analytical HPLC compound **65**

General procedure for the synthesis of the hydrazinobenzoic dermorphin derivatives (**69a-c**).

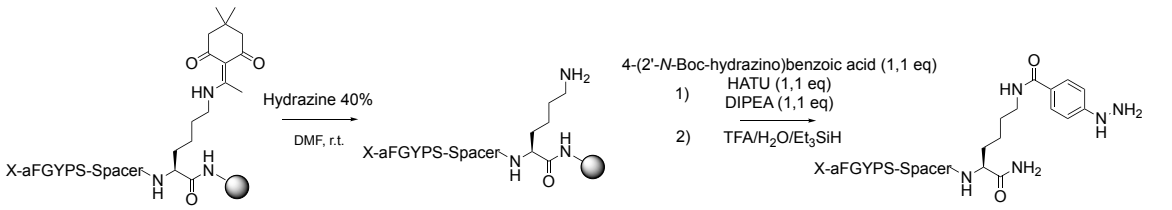

67a: X = Y; Spacer = none
67b: X = Y; Spacer = $(O2Oc)_2$
67c: X = Dmt; Spacer = none

68a: X = Y; Spacer = none
68b: X = Y; Spacer = $(O2Oc)_2$
68c: X = Dmt; Spacer = none

69a: X = Y; Spacer = none
69b: X = Y; Spacer = $(O2Oc)_2$
69c: X = Dmt; Spacer = none

The resin supported peptide derivatives **67a-c** were swelled in DMF for 5 minutes, then a 20% v/v hydrazine solution in DMF was added (3 x 2 mL) and the reaction proceeded for 30 minutes. The resin was washed with DMF, MeOH and finally DCM. A solution of Boc-hydrazinobenzoic acid (1.1 eq), HATU (1.1 eq) and DIPEA (1.1 eq) in DMF (2 mL) was added to the previously swelled resin. This suspension was stirred for 3.5 hours and after this time the resin was washed with DMF, MeOH and DCM. The resin was treated with the cleavage cocktail for 2 hours. The suspension was filtered and the liquid phase was concentrated to give an amorphous pale yellow solid after precipitation from ether. Compounds **69a-c** were finally purified by preparative HPLC (pale yellow solids, yield 58-64 %).

MS (ESI) **69a**: m/z calcd for $C_{53}H_{68}N_{12}O_{12}$ $[M+H]^+$ 1066.19, found 1066.09

T_R = 16.00

MS (ESI) **69b**: m/z calcd for $C_{65}H_{90}N_{14}O_{18}$ $[M+H]^+$ 1356.50, found 1356.40

T_R = 12.52

MS (ESI) **69c**: m/z calcd for $C_{55}H_{72}N_{12}O_{12}$ $[M+H]^+$ 1094.24, found 1093.86

T_R = 12.89

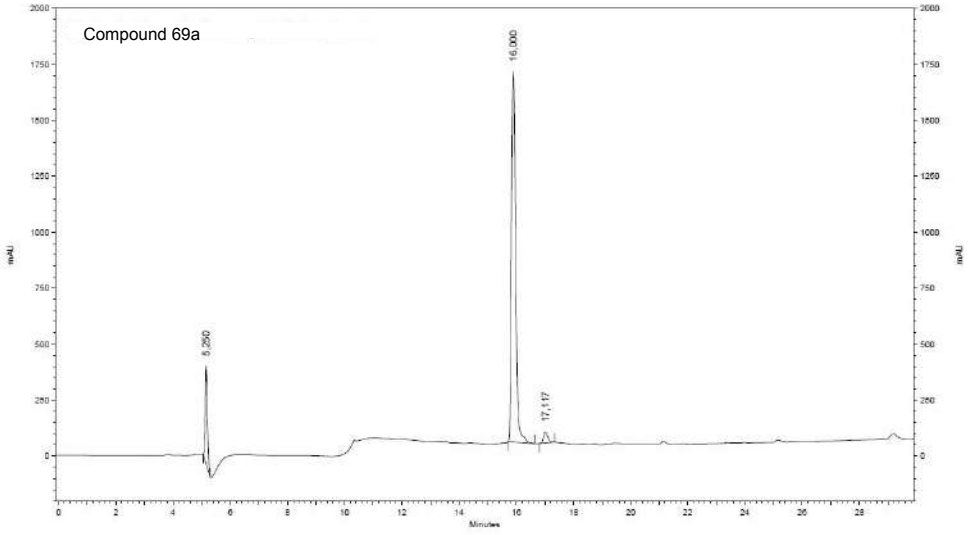

Analytical HPLC compound **69a**

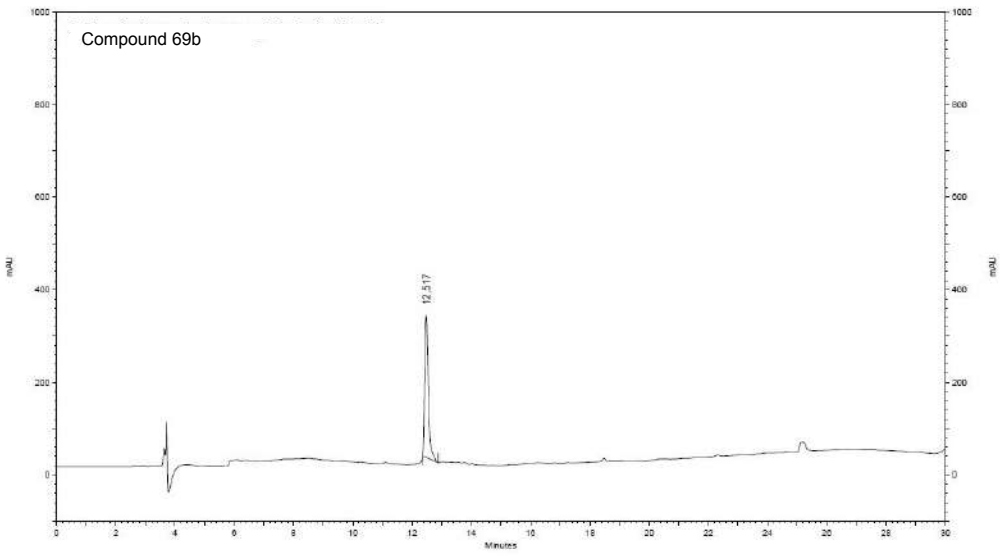

Analytical HPLC compound **69b**

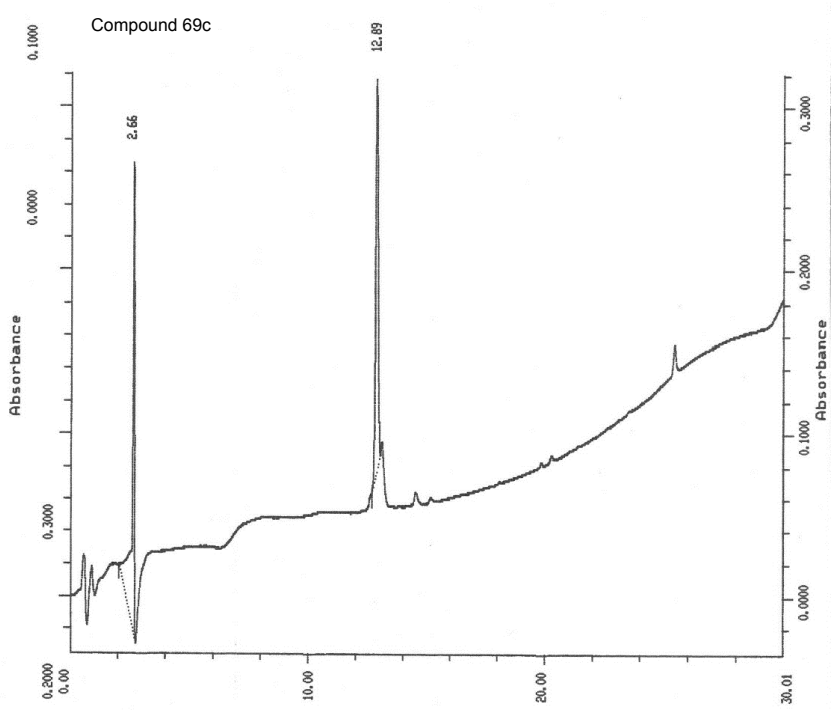

Analytical HPLC compound **69c**

General procedure for the synthesis of the hydrazinobenzoic dermorphin derivatives (**70a-c**).

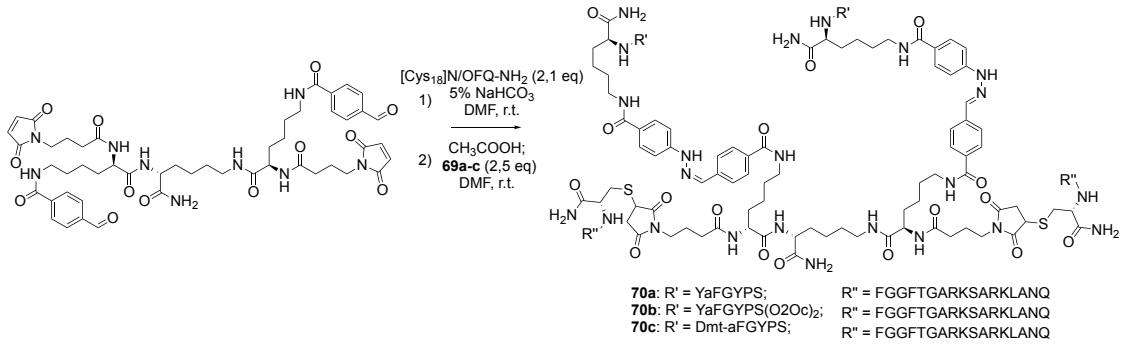

To a solution of **65** (1 μmol) and [Cys^{18}]N/OFQ-NH$_2$ (2.1 eq) in dried DMF (300 μl), 10 μL of a 5% aqueous solution of $NaHCO_3$ were added. After 5 minutes, the ESI-MS spectrum showed the complete consumption of **65**. Then, the pH of the solution was adjusted with CH_3COOH to reach pH 3 and the hydrazinobenzoic derivatives **69a-c** (2.5 eq) were added. The reaction was stirred at room temperature for 30 minutes. After this time, the solvent was removed under vacuum and the residue was purified by preparative HPLC to give **70a-c** (pale yellow solids, yield 20-39%).

MS (ESI) **70a**: m/z calcd for $C_{320}H_{463}N_{91}O_{79}S_2$ $[M+7H]^{7+}$ 988.54, found 988.94.
T_R = 11.57
MS (ESI) **70b**: m/z calcd for $C_{344}H_{507}N_{95}O_{91}S_2$ $[M+8H]^{8+}$ 937.62, found 937.70.
T_R = 13.43
MS (ESI) **70c**: m/z calcd for $C_{324}H_{471}N_{91}O_{79}S_2$ $[M+5H]^{5+}$ 1394.78, found 1394.85.
T_R = 14.82

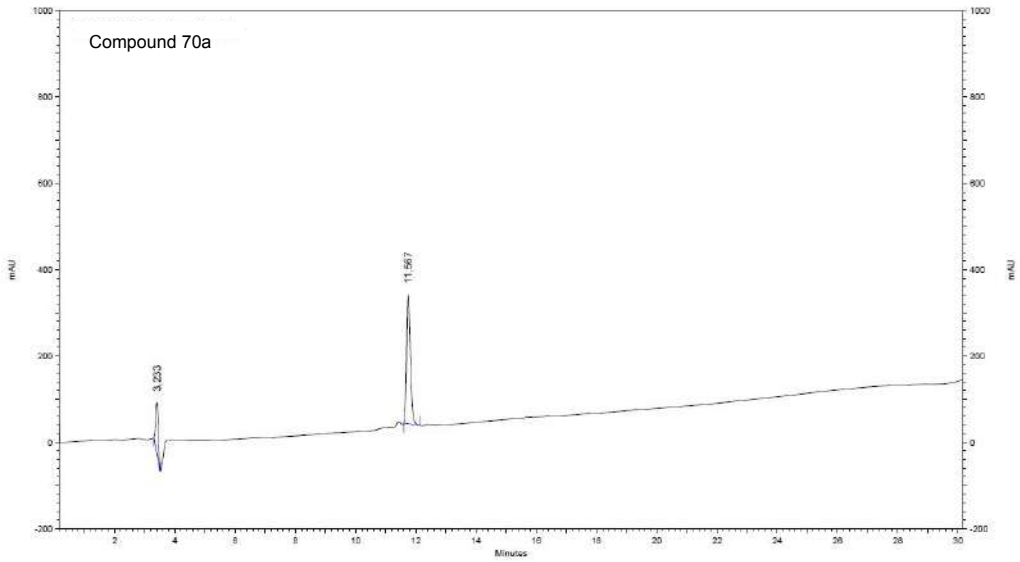

Analytical HPLC compound **70a**

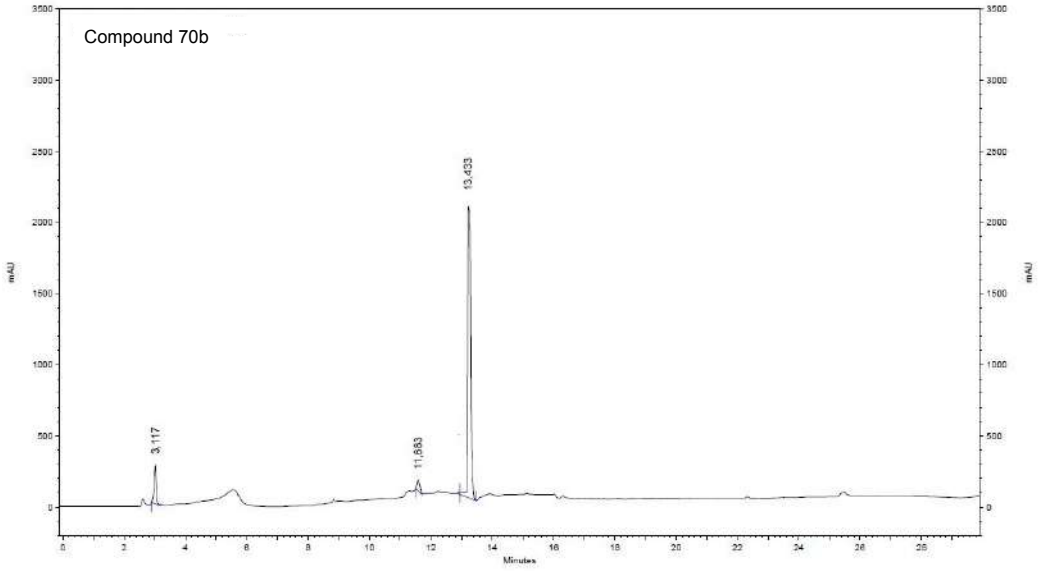

Analytical HPLC compound **70b**

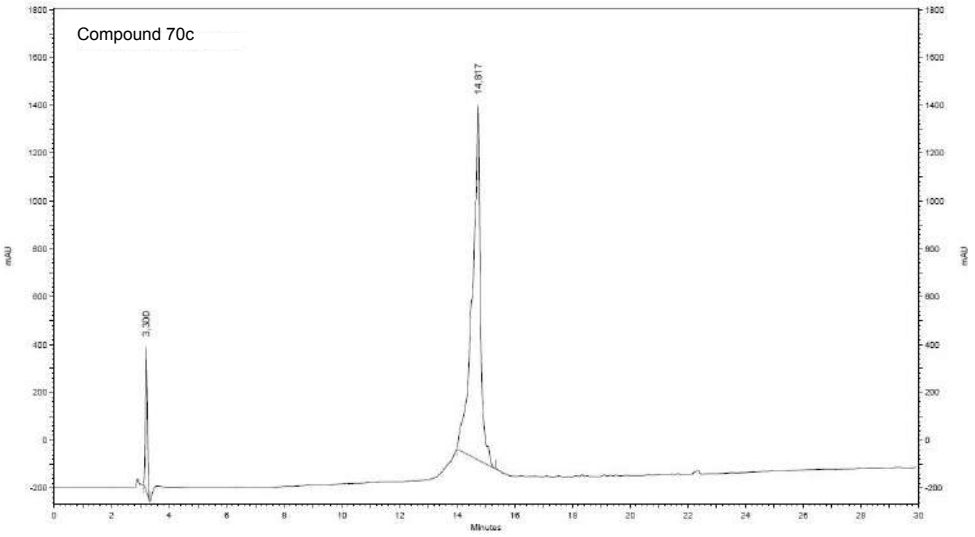

Analytical HPLC compound **70c**

8. References

[1] Janecka A., Fichna J., Janecki T., *Curr. Top. Med. Chem*.; **2004**, 4, (1), 1-17

[2] Corder G., Castro D.C., Bruchas M.R., Scherrer G., *Annu. Rev. Neurosci*.; **2018**, 41, 453-473

[3] Toll L., Ozawa A., Cippitelli A., *Handb. Exp. Pharmacol*.; **2019**, 254, 165-186

[4] Neal C.R., Mansour A., Reinscheid R., Nothacker H.P., Civelli O., *J. Comp. Neurol*.; **1999**, 412, 563-605

[5] Granier S., Manglik A., Kruse A.C., Koblika T.S., Thian F.S. et al., *Nature*; **2012**, 485, 400-404

[6] Manglik A., Kruse A.C., Kobilka T.S., Thian F.S., Mathiesen J.M., *Nature*; **2012**, 485, 321-326

[7] Thompson A.A., Liu W., Chun E., Katritch V., Wu H., et al., *Nature*; **2012**, 485, 395-399

[8] Wu H., Wacker D., Mileni M., Katritch V., Han G.W., et al., *Nature*; **2012**, 485, 327-332

[9] Ahlbeck K., *Curr. Med. Res. Opin*.; **2011**, 27, 439-448

[10] McNicol E., Horowicz-Mehler N., Fisk R.A., Bennett K., Gialeli-Goundas M., Chew P.W., Lau J., Carr D., *J. Pain;* **2003**, 4, 231-256

[11] Morphy R., Rankovic Z., *J. Med. Chem*.; **2005**, 48, 21, 6523–6543

[12] Schiller P.W., *Life Sciences*; **2010**, 86, 598–603

[13] Jenck F., Wichmann J., Dautzenberg F.M., Kilpatrick G. et al., *Proc. Natl. Acad. Sci. U.S.A*.; **2000**, 97, 4938–4943

[14] Dautzenberg F.M., Wichmann J., Higelin J., Py-Lang G., Kratzeisen C., Malherbe P., Kilpatrick G.J., Jenck F., *J. Pharmacol. Exp. Ther*.; **2001**, 298, 812–819

[15] Ko M.C., Woods J.H., Fantegrossi W.E., Galuska C.M., Wichmann J., Prinssen E.P., *Neuropsychopharmacology*; **2009**, 34, 2088–2096

[16] Anand J. P., Kochan K. E., Nastase A. F., Montgomery D., Mosberg H. I. et al., *Br. J. Pharmacol*.; **2018**, 175, 2013−2027

[17] Aceto M.D., Harris L.S., Negus S.S., Banks M.L., Hughes L.D., Akgun E., Portoghese P.S., *Int. J. Med. Chem*.; **2012**, 2012, 1-6

[18] Freye E., Latasch L., Portoghese P.S., *European Journal of Anaesthesiology*; **1992**, 9, 6, 457–462

[19] Greedy B.M., Bradbury F., Thomas M.P., Grivas K., Husbands S. M. et al., *J. Med. Chem*.; **2013**, 56, 3207−3216

[20] Woods J.H., Winger G.,*Drug Alcohol Depend*.; **1987**, 20, 303–315.

[21] Maisonneuve I.M., Archer S., Glick S.D., *Neurosci. Lett*.; **1994**, 181, 1–2, 57–60

[22] Archer S., Glick S.D., Bidlack J.M., *Neurochem. Res*.; **1996**, 21, 11, 1369–1373

[23] Dietis N., Guerrini R., Calo G., Salvadori S., Rowbotham D.J., Lambert D.G., *Br. J. Anaesth*., **2009**, 103, 38–49

[24] Toll L., Bruchas M.R., Calo G., Cox B.M., Zaveri N.T., *Pharmacol. Rev*.; **2016**, 68, 419–457

[25] Cremeans C.M., Gruley E., Kyle D.J., Ko M.C., *J. Pharmacol. Exp. Ther*.; **2012**, 343, 1,72–81

[26] Lin A.P., Ko M.C., *ACS Chem. Neurosci*.; **2013**, 4, 2, 214–224

[27] Günther T., Dasgupta P., Mann A., Miess E., Kliewer A., Fritzwanker S., Steinborn R., Schulz S., *Br. J. Pharmacol*.; **2018**, 175, 14, 2857–2868

[28] Evans R.M., You H., Hameed S., Altier C., Mezghrani A., Bourinet E. et al*., J. Biol. Chem*.; **2010**, 285, 1032–1040

[29] Mollereau C., Parmentier M., Mailleux P., Butour J.L., Moisand C., Chalon P., Caput D., Vassart G., Meunier J.C., *FEBS Lett*.; **1994**, 341, 33-38

[30] Reinscheid R.K, Nothacker H.R, Bourson A., Ardati A., Henningsen R.A., Bunzow J.R., Grandy D.K., Langen H., Monsma F.J.Jr., Civelli O., *Science*; **1995**, 270, 792-794

[31] Kastin A.J., *Handbook of biologically active peptides*; **2013**, 215, 1577-1585

[32] Calo' G., Lambert D.G., Guerrini R., *Handbook of biologically active peptides*; **2013**, 2**,** 1577–1585

[33] Mustazza C., Pieretti S., Marzoli F., *Curr. Med. Chem*.; **2018**, 25, 20, 2353–2384

[34] Calo' G., Guerrini R., *ACS Symp. Ser. Am. Chem. Soc*.; **2013**, 1131, 275–325

[35] Pacifico S., Albanese V., Illuminati D., Trapella C, Preti D., Lo Cascio E., Calò G., Guerrini R. et al. *J. Med. Chem*.; **2021**, 64, 10, 6656-6669

[36] Mollica A., Mirzaie S., Costante R., Carradori S., Macedonio G., Stefanucci A., Dvoracsko S., Novellino E., *J. Enzyme Inhib. Med. Chem*.; **2015**, 31, 6, 953-963

[37] Calo' G., Rizzi A., Bogoni G., Neugebauer V., Salvadori S., Guerrini R., Bianchi C., Regoli D., *Eur. J. Pharmacol*.; **1996,** 311**,** 1**,** 3-5

[38] Dooley C.T., Houghten R.A., *Life Sci*.; **1996**, 59, 1, 23-29

[39] Guerrini R., Calo' G., Rizzi A., Bianchi C., Lazarus L.H., Salvadori S., Temussi P.A., Regoli D., *J. Med. Chem*.; **1997**, 40, 12, 1789-1793

[40] Preti D., Calò G., Guerrini R., *Handb. Exp. Pharmacol*.; **2018**, 254, 17-36

[41] Varani K., Rizzi A., Calo G., Bigoni R., Toth G., Guerrini R., Gessi S., Salvadori S., Borea P.A., Regoli D., *Naunyn-Schmiedeberg's Arch. Pharmacol*.; **1999**, 360, 270-277

[42] Molinari S., Camarda V., Rizzi A., Marzola G., Salvadori S., Marzola E., Molinari P., McDonald J., Ko M.C., Lambert D.G., Calò G., Guerrini R., *Br. J. Pharmacol*.; **2013**, 168, 1, 151-162

[43] Thompson A.A., Liu W., Chun E., Katritch V., Wu H., Vardy E., Huang X.P., Trapella C., Guerrini R., Calo' G., Roth B.L., Cherezov V., Stevens R.C., *Nature*; **2012**, 485,7398, 395-399

[44] Daga P.R., Zaveri N.T., *Proteins*; **2012**, 80, 8, 1948-1961

[45] Calo' G., Guerrini R., Bigoni R., Rizzi A., Bianchi C., Regoli D., Salvadori S., *J. Med. Chem*.; **1998**, 41 (18), 3360-3366.

[46] Guerrini R., Calo' G., Bigoni R., Rizzi D., Rizzi A., Zucchini M., Varani K., Hashiba E., Lambert D.G., Toth G., Borea P.A., Salvadori S., Regoli D*., J. Med. Chem*.; **2001**, 44, 23, 3956-3964

[47] Topham C. M., Mouledous L., Poda G., Maigret B., Meunier J.C., *Protein Eng*.; **1998**, 11, 1163-1179.

[48] Mouledous L., Topham C.M., Moisand C., Mollereau C., Meunier J.C., *Mol. Pharmacol*.; **2000**, 57, 495-502.

[49] Guerrini R., Marzola E., Trapella C., Pacifico S., Cerlesi M.C., Malfacini D., Ferrari F., Bird M.F., Lambert D.G., Salvadori S., Calo' G., *Bioorg. Med. Chem*.; **2015**, 23, 7, 1515-1520.

[50] Okada K., Sujaku T., Chuman Y., Nakashima R., Nose T., Costa T., Yamada Y., Yokoyama M., Nagahisa A., Shimohigashi Y., *Biochem. Biophys. Res. Commun*.; **2000**, 278, 2, 493-498

[51] Okada K., Isozaki K., Li J., Matsushima A., Nose T., Costa T., Shimohigashi Y., *Bioorg. Med. Chem*.; **2008**, 16, 20, 9261-9267

[52] Dygos J.H., Yonan E.E., Scaros M.G., Goodmonson O.J., Getman D.P., Periana R.A., Beck, G.R., *Synthesis*; **1992**, 8, 741-743

[53] Balboni G., Marzola E., Sasaki Y., Ambo A., Marczak E.D., Lazarus L.H., Salvadori S., *Bioorg. Med. Chem*.; **2010**, 18, 6024-6030

[54] Salvadori S., Attila M., Balboni G., Bianchi C., Bryant S.D., Crescenzi O., Guerrini R., Picone D., Tancredi T., Temussi P.A., Lazarus L.H., *Mol. Med*.; **1995**, 1, 678-689.

[55] Bryant S.D., Jinsmaa Y., Okada Y., Lazarus L.H., Salvadori S., *Biopolymers*; **2003**, 71, 86-102

[56] Capasso, A., *Med. Chem*.; **2007**, 3, 480-487

[57] Guerrini R., Capasso A., Sorrentino L., Anacardio R., Bryant S.D., Lazarus L.H., Attila M., Salvadori S., *Eur. J. Pharm.;* **1996**, 302, 37–42

[58] Schiller P.W., Nguyen T.M.-D., Berezowska I., Dupuis S., Weltrowska G., Chung N.N., Lemieux C., *Eur. J. Med. Chem*.; **2000**, 35, 895–901

[59] Shimoyama M., Shimoyama N., Zhao G.-M., Schiller P.W., Szeto H.H., *J. Pharm. Exp. Ther*.; **2001**, 297, 364–371

[60] Sasaki Y., Suto T., Ambo A., Ouchi H., Yamamoto Y., *Chem. Pharm. Bull*.; **1999**, 47, 10, 1506-1509

[61] Mallareddy J.R., Borics A., Keresztes A., Toth G. et al., *J. Med. Chem.;* **2011**, 54, 1462-1472

[62] Schiller P.W., Nguyen T.M.-D., Chung N.N., Lemieux C., *J. Med. Chem.;* **1989**, 32, 3, 698-703

[63] Schiller P.W., Fundytus M.E., Merovitz L., Chung N.N., Coderre T.J. et al., *J. Med. Chem.;* **1999**, 42, 3520-3526

[64] Piekielna-Ciesielska J., Mollica A., Pieretti S., Fichna J., Szymaszkiewicz A., Zielinska M., Kordek R., Janecka A., *J. Enzyme Inhib. Med. Chem*.; **2018**, 33, 1, 560-566

[65] Ambo A., Niizuma H., Sasaki A., Kohara H., Sasaki Y., *Bioorg. Med. Chem. Lett*.; **2002**, 12, 879–881

[66] Sasaki Y., Sasaki A., Niizuma H., Goto H., Ambo A., *Bioorg. Med. Chem. Lett*.; **2002**, 12, 6, 879-881

[67] Sasaki Y., Sasaki A., Niizuma H., Goto H., Ambo A., *Bioorg. Med. Chem. Lett*.; **2003**, 11, 675-678

[68] Sasaki Y., Ambo A., *Int. J. Med. Chem*.; **2012**, 2012, 1-11

[69] Sasaki Y., Hirabuki M., Ambo A., Ouchi H., Yamamoto Y., *Bioorg. Med. Chem. Lett*.; **2001**, 11, 327–329

[70] Soloshonok V.A., Tang X., Hruby V.J., *Tetrahedron*; **2001**, 57, 6375-6382

[71] Balducci D., Contaldi S., Lazzari I., Porzi G., *Tetrahedron: Asymmetry*; **2009**, 20, 1398-1401

[72] Mollica A., Costante R., Mirzaie S., Carradori S., Macedonio G., Stefanucci A., Novellino E., *J. Heterocyclic Chem.;* **2016**, 53, 2106-2110

[73] Abrash H.I., Niemann C., *Biochemistry*; **1963**, 2, 947-953

[74] Dygos J.H., Yonan E.E., Scaros M.G., Goodmonson O.J., Getman D.P., Periana R.A., Beck G.R., *Synthesis*; **1992**, 741

[75] Praquin C.F.B., de Koning P.D., Peach P.J., Howard R.M., Spencer S.L., *Org. Process Res. Dev.;* **2011**, 15, 1124-1129

[76] Bender A.M., Griggs N.W., Gao C., Trask T.J., Traynor J.R., Mosberg H.I., *ACS Med. Chem. Lett.*; **2015**, 6, 1199-1203

[77] Roudesly F., Oble J., Poli G., *J. Mol. Catal. A Chem.*; **2017**, 426, 275-296.

[78] Rogge T., Kaplaneris N., Chatani N., Kim J., Chang S., Punji B., Schafer L.L., Musaev D.G., Wencel-Delord J., Roberts C.A., Sarpong R., Wilson Z.E., Brimble M.A., Johansson M.J., Ackermann L., *Nature Rev. Methods Primers;* **2021**, *1*, 43.

[79] Murahashi S., *J. Am. Chem. Soc.;* **1955**, *77*, 6403-6404

[80] Kleiman J.P., Dubeck M., *J. Am. Chem. Soc.;* **1963**, *85*, 1544-1545

[81] Ryabov A.D., *Chem. Rev.;* **1990**, *90*, 403-424

[82] Albrecht M., *Chem. Rev.;* **2010**, *110*, 576-623

[83] Cope A.C., Siekman R.W., *J. Am. Chem. Soc.;* **1965**, *87*, 3272-3273

[84] Cope A.C., Friedrich E.C., *J. Am. Chem. Soc.;* **1968**, *90*, 909-913

[85] Tremont S.J., Rahman H.U., *J. Am. Chem. Soc.*; **1984**, 106, 5759-5760

[86] McCallum J.S., Gasdaska J.R., Liebeskind L.S., Tremont S.J., *Tetrahedron Lett.;* **1989**, *30*, 4085−4088

[87] Daugulis O., Zaitsev V.G., *Angew. Chem. Int. Ed.;* **2005**, *44*, 4046−4048

[88] Zaitsev V.G., Shabashov D., Daugulis O., *J. Am. Chem. Soc*.; **2005**, 127, 13154–13155

[89] Nadres E.T., Santos I.G., Daugulis D., *J. Org. Chem*.; **2013**, 78, 9689−9714

[90] Sambiagio C., Schönbauer D., Blieck R., Dao-Huy T., Pototschnig G., Schaaf P., Wiesinger T., Zia M.F., Wencel-Delord J., Besset T., Maes B.U.W., Schnürch M., *Chem. Soc. Rev*.; **2018**, 47, 6603–6743

[91] Catellani M., Frignani F., Rangoni A., *Angew. Chem. Int. Ed. Engl.;* **1997**, *36*, 119

[92] Tóth B.L., Monory A., Egyed O., Domján A., Bényei A., Szathury B., Novák Z., Stirling A., *Chem. Sci.;* **2021**, *12*, 5152-5163

[93] Daugulis O., Roane J., Tran L.D., *Acc. Chem. Res.;* **2015**, 48, 1053−1064

[94] Brandhofer T., García Mancheño O., *Eur. J. Org. Chem*.; **2018**, 6050–6067

[95] Yun Y.-l., Yang J., Miao Y.-h., Sun J., Wang X.-j., *Chem. Soc*.; **2020**, 24, 151-185

[96] Li J.-J., Mei T.-S., Yu J.-Q., *Angew. Chem. Int. Ed.;* **2008**, *47*, 6452

[97] Zhang S.-Y., He G., Nack W.A., Zhao Y., Li Q., Chen G., *J. Am. Chem. Soc.;* **2013**, *135*, 2124

[98] Zhao Y., Chen G., *Org. Lett.;* **2011**, *13*, 4850-4853

[99] Wang X., Niu S., Xu L., Zhang C., Meng L., Zhang X., Ma D., *Org: Lett.;* **2017**, 19, 246-249

[100] Gardner Swain C., Rogers R. J., *J. Am. Chem. Soc.;* **1975**, *97*, 799–800

[101] Yu Z.-Q., Lv Y.-W., Yu C.-M., Su W.-K., *Tetrahedron Lett.* **2012**, *54*, 1261–1263.

[102] Xu W.-B., Xu Q.-H., Zhang Z.-F., Li J.-Z., *Asian J. Org. Chem.* **2014**, *3*, 1062–1065.

[103] Wassmundt F.W., Kiesman W.F., *J. Org. Chem.;* **1995**, *60*, 1713–1719.

[104] Voutyritsa E., Theodorou A., Kokotou M.G., Kokotos C.G.; *Green Chemistry;* **2017**, *19*, 1291-1298

[105] Maggiolo A., *J. Am. Chem. Soc*.; **1951**, *73*, 5815–5816

[106] Camarda V., Fischetti C., Anzellotti N., *Naunyn-Schmied Arch. Pharmacol*.; **2009**, 379, 599–607

[107] Camarda V., Calo' G., *Calcium Signaling Protocols*; **2012**, 937, 293-306

[108] McDonald I.A., Nice P.L., Jung M.J., Sabol J.S. et al., *Tetrahedron Lett*.; **1991**, 32, 7, 887-890

[109] Majer P., Slaninova J., Lebl M., *In. J. Peptide Protein Res.*; **1994**, 43, 62-68

[110] Van Bestbrugge J., Doctoral thesis, **1997**

[111] Busto E., Gerstmann M., Tobola F., Dittmann E., Wiltschi B., Kroutil W., *Catal. Sci. Technol.*; **2016**, 6, 8098-8103

[112] Subba Reddy B.V., Rajender Reddy L., Corey E.J., *Org. Lett.*; **2006**, 8, 15, 3391-3394

[113] Wasa M., Chan K.S.L., Zhang X.-G., He J., Miura M., Yu J.-Q., *J. Am. Chem. Soc.*; **2012**, 134, 18570-18572

[114] Chen G., Shigenari T., Jain P., Zhang Z., Jin Z., He J., Mapelli C., Miller M.M., Yu J.-Q. et al., *J. Am. Chem. Soc.*; **2015**, 137, 3338-3351

[115] He J., Li S., Deng Y., Spangler J.E., Yu J.-Q. et al., *Science*; **2014**, 343, 1216-1220

[116] Tran L.D., Daugulis O., *Angew. Chem.*; **2012**, 124, 5278 –5281

[117] Zhang Q., Chen K., Rao W., Zhang Y., Chen F.-J., Shi B.-F., *Angew. Chem. Int. Ed.*; **2013**, 52, 13588 –13592

[118] Chen K., Zhang S.-Q., Xu J.-W., Hu F., Shi B.-F., *Chem. Comm.*; **2014**, 50, 13924-13927

[119] Wang B., Nack W.A., He G., Zhang S.-Y., Chen G., *Chem. Sci.*; **2014**, 5, 3952-3957

[120] Dang Y., Qu S., Nelson J.W., Pham H.D., Wang Z.-X., Wang X., *J. Am. Chem. Soc.*; **2015**, 137, 2006−2014

[121] Chang K.J., Pugh W., Blanchard S.G., McDermed J., Tam J.P., *Proc. Natl. Acad. Sci. U.S.A.*; **1988**, 85, 13, 4929-4933

[122] Bracci L., Falciani C., Lelli B., Lozzi L., Runci Y., Pini A., De Montis M.G., Tagliamonte A., Neri P., *J. Biol. Chem.*; **2003**, 278, 47, 46590-46595

[123] Guerrini R., Marzola E., Trapella C., Pelà M., Molinari S., Cerelesi M.C., Malfacini D., Rizzi A., Salvadori S., Calò G., *Bioorg. Med. Chem.*; **2014**, 22, 3703-3712

[124] Ruzza C., Rizzi A., Malfacini D., Pulga A., Pacifico S., Salvadori S., Trapella C., Reinscheid R.K., Calo G., Guerrini R., *Res. Perspect.*; **2015**, 3, 1−10

[125] Rizzi A., Malfacini D., Cerlesi M.C., Ruzza C., Marzola E., Bird M.F., Rowbotham D. J., Salvadori S., Guerrini R., Lambert D.G., Calo G., *Br. J. Pharmacol.*; **2014**, 171, 4138−4153

[126] Ruzza C., Rizzi A., Malfacini D., Cerlesi M.C., Ferrari F., Marzola E., Ambrosio,C., Gro C., Salvadori S., Costa T., Calo G., Guerrini R., *Br. J. Pharmacol.*; **2014**, 171, 4125−4137

[127] Calò G., Rizzi A., Ruzza C., Ferrari F., Pacifico S., Gavioli E.C., Salvadori S., Guerrini R., *Peptides*; **2018**, 99, 195−204

[128] Xu Z., Jia S., Wang W., Yuan Z., Ravoo B.J., Guo D.-S., *Nature Chemistry*; **2019**, 11, 86-93

[129] Cerelesi M.C., Ding H., Bird M.F., Kiguchi N., Calò G., Guerrini R. et al., *Eur. J. Pharmacol.*; **2017**, 794, 115-126

[130] Marrone G.F., Lu Z., Rossi G., Narayan A., Hunkele A., Marx S., Xu J., Pintar J., Majumdar S., Pan Y.X., Pasternak G.W., *ACS Chem. Neurosci.*; **2016**, 7, 1717−1727

[131] Yamamoto T., Nair P., Largent-Milnes T.M., Jacobsen N.E., Davis P., Ma S., Yamamura H.I., Vanderah T.W., Porreca F., Lai J., Hruby V.J., *J. Med. Chem.*; **2011**, 54, 2029−2038

[132] Bird M.F., Cerlesi M.C., Brown M., Malfacini D., Vezzi V., Molinari P., Micheli L., Di Cesare Mannelli L., Ghelardini C., Guerrini R., Calò G., Lambert D. G., *PLoS. One*; **2016**, 11, 1−22

[133] Pacifico S., Albanese V., Illuminati D., Fantinati A., Calò G., Preti D., Guerrini G., et al., *Bioconjugate. Chem.*; **2019**, 30, 9, 2444-2451

[134] Ding H., Kiguchi N., Yasuda D., Daga P.R., Polgar W.E., Lu J.J., Czoty P.W., Kishioka S., Zaveri N.T., Ko M.C., *Sci. Transl. Med.*; **2018**, 10, 1-11

Abbreviations

αAAs: α amino acids

AC: Adenylate cyclase

AMLA: Ambiphilic metal-ligand activation

AMP: 2-(aminomethyl)pyridine

AQ: 8-aminoquinoline

Boc: *Tert*-butoxy carbonyl

cAMP: Cyclic adenosine monophosphate

Cbz: Benzyloxy carbonyl

CHO cells: Chinese hamster ovary cells

CMD: Concerted metalation deprotonation

CNS: Central nervous system

CT: Charge transfer

DALDA: H-Tyr-*D*-Arg-Phe-Lys-NH_2

DAMGO: H-Tyr^1-*D*-Ala^2-Gly^3-*N*-Me-Phe^4-Gly-ol-Enkephalin

Dde: 1,1′-(2,2-Dichloroethene-1,1-diyl)bis(4-chlorobenzene)

DFT: Density functional theory

DG: Directing group

DIC: N,N-Diisopropylcarbodiimide

DIPEA: Di-*iso*-propyl-ethyl amine

DKP: Diketopiperazine

DMF: Dimethylformamide

Dmp: Dimethyl-phenylalanine

DMR: Dynamic mass redistribution

Dmt: Dimethyl-Tyrosine

DOP: δ-opioid receptor

Dyn: Dynorphin

EA: Electrophilic activation

EDG: Electron donating group

ERK 1/2: Extracellular signal regulated kinase 1 and 2

EM: Endomorphin

EWG: Electron withdrawing group

Fmoc: Fluorenylmethyloxycarbonyl

GDP: Guanosine diphosphate

GPCR: G protein coupled receptor

GTP: Guanosine triphosphate

HFIP: hexa-fluor-*iso*-propanol

HATU: *N*-[(Dimethylamino)-1*H*-1,2,3-triazolo-[4,5-*b*]pyridin-1-ylmethylene]-*N*-methylmethanaminium hexafluorophosphate *N*-oxide

HOBt: 1-Hydroxybenzotriazole

HPLC: High performance liquid chromatography

JNK 1-3: C-Jun N-terminal kinase 1-3

Kir3: Inwardly rectifying potassium channel

KOP: κ-opioid receptor

m: Meta

MAPK: Mitogen-activated protein kinase

MD: Molecular dynamics

Mmt: Mono-methyl-Tyrosine

MOP: μ-opioid receptor

NOP: Nociceptin/orphanin FQ receptor

o: Ortho

OR: Opioid receptor

ORL-1: Opioid receptor like-1

OS: Opioid system

p: Para

PA: Picolinic amide

PD: Pharmacodynamic

Phth: Phthalimide

PK: Pharmacokinetic

Pmc: 2,2,5,7,8-pentamethylcromane-6-sulfonyl

ppN/OFQ: preproN/OFQ

PWT: Peptide welding technology

SAR: Structure-activity relationship

SPhos: 2-Dicyclohexylphosphino-2′,6′-dimethoxybiphenyl

SPPS: Solid phase peptide synthesis

TBDMS: *Tert*-butyl-dimethyl-silyl

tBu: *Tert*-butyl

TCE: 1,1,2,2-tetrachloroethane

TEA: Triethylamine

TFA: Trifluoroacetic acid

Tic: 1,2,3,4-tetrahydroisoquinoline-3-carboxylic acid

TIPP-NH_2: Tyr-Tic-Phe-Phe-NH_2

TM: Transmembrane domain

Trt: Trityl

YRFB: Tyr-*D*-Arg-Phe-βAla-NH_2

Bioconjugate Chemistry

Article

Cite This: *Bioconjugate Chem.* 2019, 30, 2444−2451

pubs.acs.org/bc

Tetrabranched Hetero-Conjugated Peptides as Bifunctional Agonists of the NOP and Mu Opioid Receptors

Salvatore Pacifico,[†] Valentina Albanese,[†] Davide Illuminati,[†] Anna Fantinati,[†] Erika Marzola,[†] Federica Ferrari,[‡] Joaquim Azevedo Neto,[‡] Chiara Sturaro,[‡] Chiara Ruzza,[‡] Girolamo Calò,[‡] Delia Preti,*[,†] and Remo Guerrini[†]

[†]Department of Chemical and Pharmaceutical Sciences, University of Ferrara, Via Luigi Borsari 46, Ferrara 44121, Italy

[‡]Department of Medical Sciences, Section of Pharmacology, University of Ferrara Via Fossato di Mortara 17/19, Ferrara 44121, Italy

Supporting Information

ABSTRACT: The general aim of the work was the validation of a new synthetic methodology designed for obtaining bifunctional heterotetrabranched peptide ligands. Applying an easily accessible synthetic route, we provided a small series of hetero-multimeric peptide conjugates targeting the nociceptin/orphanin FQ (N/OFQ) peptide receptors (NOP) and mu opioid receptors. Among these, H-PWT1-N/OFQ-[Dmt^1]dermorphin demonstrated a similar and high agonist potency at the NOP and mu receptors. The achieved results confirmed the robustness of the approach that is extremely versatile and virtually applicable to different peptide sequences whose pharmacological activity can be combined for generating dual acting multimeric compounds. These innovative pharmacological tools will be extremely helpful for investigating the consequences of the simultaneous activation and/or blockage of different peptidergic receptors.

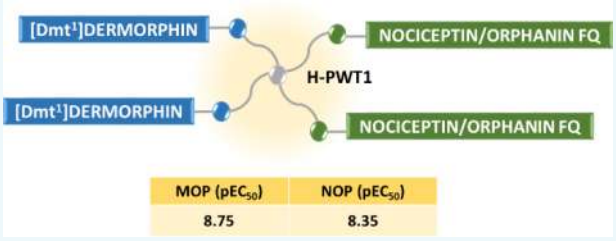

INTRODUCTION

Bioactive peptides obtained from natural sources hold great potential for the development of drugs because of their capability to modulate a broad panel of biological functions excelling in potency and selectivity of action with a usually low toxicity profile. However, as is largely known, peptides suffer from a short duration of action when administered for therapeutic purposes because of their fast degradation by peptidases. Despite this, the number of peptide drugs being placed on the market has been extraordinarily increasing in the last two decades.[1,2] In most cases, this has been made possible by the identification of chemical strategies useful for improving peptide resistance to peptidases. In the past few years, with the development of the so-called peptide welding technology (PWT), we provided evidence that the multimerization of bioactive peptides can be one of the possible approaches to be exploited for extending their limited half-life.[3] The methodology, which is based on a high efficacy chemical synthesis for the generation of tetra-branched peptide conjugates, is of particular interest because it is an elegant way to improve the drug-likeness and pharmacokinetic properties of bioactive peptides in view of their potential therapeutic employment.

All PWT-derivatives reported to date have been efficiently prepared following a convergent synthetic approach based on the conjugation of a clustering core with four linear monomers of the same target peptide after their independent synthesis.[4] Three different cores have been exploited, each of which is strategically functionalized with four reactive maleimide groups as depicted in Figure 1 (PWT1 with a tris-lysine motif, PWT2 with a cyclam-based scaffold, and PWT3 with a symmetric lysine-ethylendiamine derivative).[3] The classical procedure

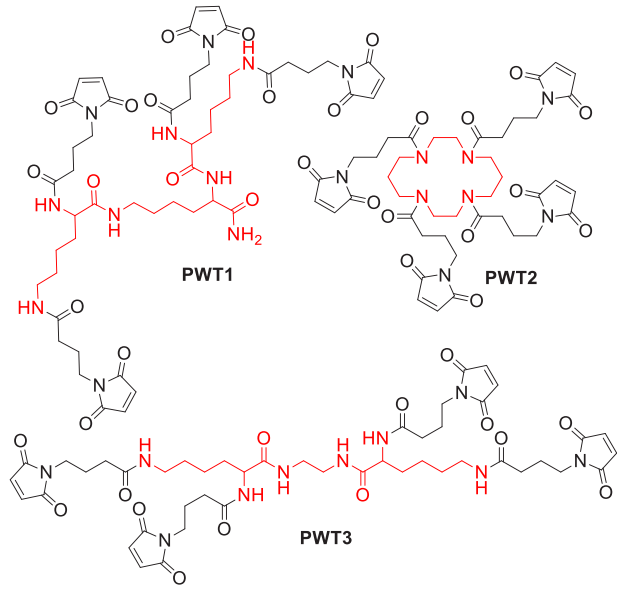

Figure 1. Chemical structures of the clustering cores used for generating PWT peptides.

Received: July 30, 2019
Revised: August 27, 2019
Published: August 28, 2019

DOI: 10.1021/acs.bioconjchem.9b00519
Bioconjugate Chem. 2019, 30, 2444−2451

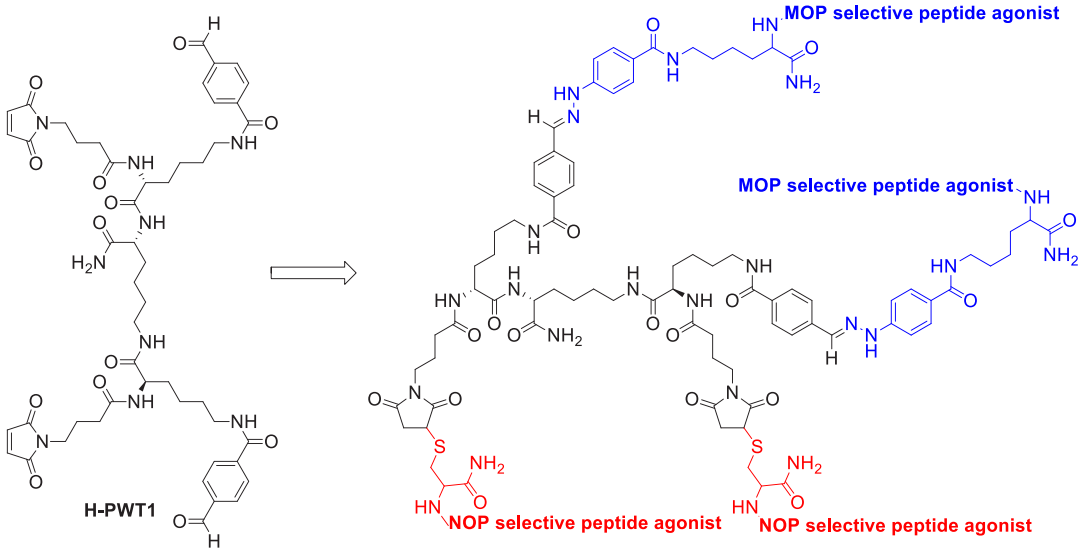

Figure 2. General design for the generation of heterotetrameric H-PWT1 derivatives as NOP/MOP dual acting ligands.

consisted of a thiol-Michael reaction between the central reactive scaffold and the peptide of interest in which a key cysteine residue was conveniently introduced.[4]

Thanks to this highly chemo-selective conjugation, different GPCR-targeting peptides have been homotetramerized such as nociceptin/orphanin FQ (N/OFQ),[5] N/OFQ related peptides,[3] tachykinins,[6] and neuropeptide S.[7] Of note, the resulting multibranched ligands exhibited an in vitro pharmacological profile similar to that of the native peptides. Even more important, a higher potency and a marked prolongation of action in vivo have been generally observed, possibly due to reduced susceptibility to the action of proteolytic enzymes.[8] Thus, the first generation of PWT derivatives has been considered as valuable pharmacological tools suitable for investigating in vivo the effects of the potent, selective, and prolonged stimulation/blocking of a single target in physiopathological conditions.

The innovative purpose of this study is the design, synthesis, and in vitro pharmacological characterization of the first examples of heteromultivalent PWT derivatives of potential interest for the study of multifactorial diseases where the simultaneous modulation of multiple signaling systems can be advantageous as compared to the activation/blocking of a single target. To this aim, we focused on the recent evidence that molecules that are able to modulate multiple opioid receptors (currently classified as MOP/μ, DOP/δ, KOP/κ, and NOP, the opioid related N/OFQ peptide receptor) may result in novel opioid analgesics possibly with reduced side effects.[9] Most progress has been made in the development of NOP/MOP bifunctional agonists that have been demonstrated to relieve some of the side effects of pure MOP agonists, including tolerance, dependence, constipation, and respiratory depression.[9] Of note, NOP receptor is colocalized with the MOP opioid receptor in the pain pathways[10] where they seem to be involved in the formation of heterodimers.[11−13] In addition, the coadministration of N/OFQ and MOP receptor agonists (i.e., morphine, buprenorphine) in nonhuman primates was shown to enhance the antinociceptive effects of classical opioid analgesics reducing their remarkable side effects.[14,15]

Overall, these findings inspired the synthesis of peptide and nonpeptide bifunctional NOP/MOP ligands. Among these, the small molecule agonists BU08028 and SR16435 have emerged for their antihyperalgesic and antiallodynic action in animal models of inflammatory and neuropathic pain with higher potency if compared to selective NOP or MOP ligands.[16] AT-121 is another relevant example of bifunctional NOP/MOP that displayed analgesic properties without opioid side effects in nonhuman primates.[17] Furthermore, the mixed opioid/NOP receptor agonist Cebranopadol is a novel first-in-class analgesic currently in clinical development by the company Grünenthal for the treatment of different acute and chronic pain states.[18,19] In addition, a few peptide-based bifunctional NOP/MOP receptor ligands have been obtained through the generation of chimeric peptides containing an opioid and a N/OFQ receptor-binding pharmacophore that have been merged in a linear sequence.[20−23]

A first attempt to combine the PWT technology to the principles of polypharmacology consisted of the homotetramerization of the peptide [Dmt^1]N/OFQ(1−13)-NH_2 that behaves as a potent agonist for both NOP and classical opioid receptors and elicits robust antinociceptive effects after spinal administration in nonhuman primates.[24] PWT2-[Dmt^1]N/OFQ(1−13)-NH_2 displayed the same potency of the linear parent peptide in vitro and a prolonged action in vivo.[25] Here, we described a new chemical strategy that allowed us to exploit the PWT technology to the obtainment of NOP/MOP bivalent heterotetrameric peptides. In particular, we synthesized a novel PWT core (H-PWT1, depicted in Figure 2) featuring two maleimide and two benzaldehyde groups that have been independently reacted with two chains of N/OFQ, as a native ligand of the NOP receptor, and two chains of dermorphin or dermorphin-related peptides, as MOP agonists.

RESULTS AND DISCUSSION

Chemistry. For the synthesis of the new heterotetrameric PWT derivatives, we employed the same convergent approach previously applied for the classical homotetrameric compounds. This is generally characterized by high efficiency in terms of feasibility, reaction yields, and ease of purification. Thus, we first synthesized in the liquid phase the central core

DOI: 10.1021/acs.bioconjchem.9b00519
Bioconjugate Chem. 2019, 30, 2444−2451

H-PWT1 starting from a residue of Lys-NH_2 as described in Scheme 1. This was coupled with two molecules of *Z*-Lys(Boc)-OH in standard conditions to give the trilysine derivative **1**. After the selective removal of Cbz by catalytic hydrogenation, the resulting Boc protected intermediate was coupled with 4-maleimidobutirryc acid leading to the bis-functionalized core **2**. Boc deprotection followed by a second coupling with 4-formylbenzoic acid then gave the desired heterofunctionalized H-PWT1 (**3**) as the first building block of the convergent synthetic route.

Scheme 1. Synthesis of the Orthogonally Functionalized H-PWT1 Core 3[a]

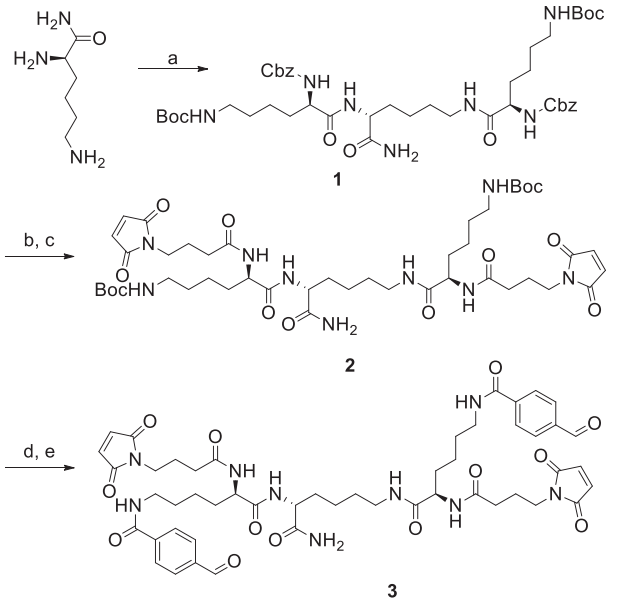

[a]Reagents and conditions: *Z*-Lys(Boc)OH, NMM 30%, isobutyl-chloroformate, DMF; (b) H_2, Pd/C, MeOH; (c) 4-maleimidobutyric acid, HATU, DIPEA, DMF; (d) TFA; (e) 4-carboxybenzaldehyde, HATU, DIPEA, DMF.

The next stage was the synthesis of the target peptides containing an additional anchoring residue in the linear sequence. In this regard, the native sequence of N/OFQ (FGGFTGARKSARKLANQ) with a supplementary cysteine residue at the C-terminal position was synthesized following a classic solid-phase technique as previously described.[4] The thiol residue of [Cys^{18}]N/OFQ-NH_2 has been introduced in view of the possible functionalization of H-PWT1 via a thiol-Michael reaction with the two maleimide moieties. The absence of additional cysteine residues in the sequence of N/OFQ ensured the chemoselectivity of the final conjugation step. Previous SAR studies and crystallographic analysis clearly suggested that the C-terminal region of N/OFQ represents an appropriate attachment point that allows peptide modifications without loss of activity and selectivity.[4]

Dermorphin has been selected for the development of the MOP agonist component of the designed heterotetrameric NOP/MOP dual acting ligands. In one of the investigated examples, the native sequence of the peptide (YaFGYPS-NH_2) was synthesized in solid phase and elongated at the C-terminal position with a lysine(Dde) residue until the obtainment of the resin supported peptide **4a** as depicted in Scheme 2. The selective deprotection of Dde with 20% hydrazine solution in DMF[26] then led to a free amine group on the lysine side chain

Scheme 2. Synthesis of the Hydrazinobenzoic Dermorphin Derivatives 6a−c[a]

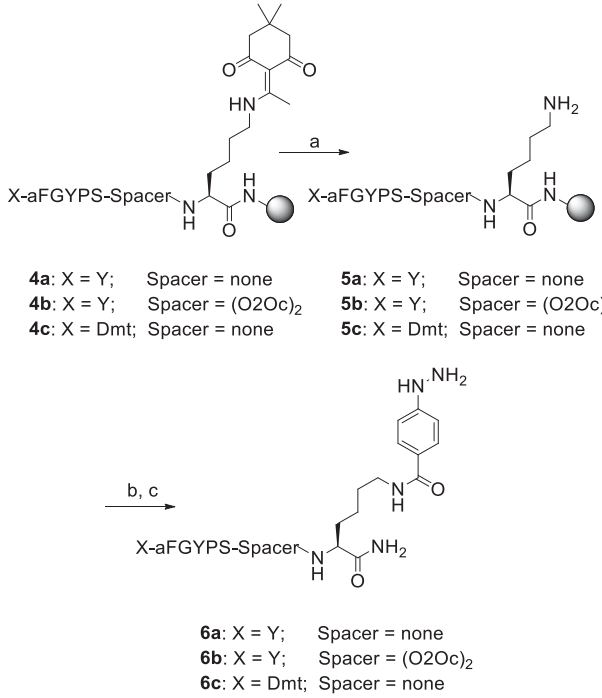

[a]Reagents and conditions: (a) 20% hydrazine, DMF; (b) 4-(2′-*N*-Boc-hydrazino)benzoic acid, HATU, DIPEA, DMF; (c) TFA/H_2O/triisopropylsilane.

(**5a**) that was coupled with 4-(2′-*N*-Boc-hydrazino)benzoic. The final cleavage with a cocktail of TFA/H_2O/triisopropylsilane gave the desired Dermorphin derivative **6a** functionalized with a reactive hydrazine group suitable for the linking to the aldehyde moieties of **3**. As in the case of N/OFQ, the C-terminal derivatization of dermorphin has been shown to be well tolerated for the maintainance of the peptide activity.[20]

In the second dermorphin analogue **6b**, two polyoxyethylene units have been introduced as spacer between the MOP pharmacophore and the C-terminal anchoring residue. This has been made with the aim to improve the water solubility of the resulting tetrabranched derivative and to evaluate the effect of the lengthening of the distance between the message domain and the central core. Finally, we synthesized **6c**, a novel dermorphin derivative in which the Tyr^1 residue has been replaced by the non-natural amino acid 2,6-dimethyl tyrosine (Dmt). Dmt has been extensively exploited for its contribution in increasing the potency and metabolic stability of opioid peptides when introduced instead of Tyr at the first position.[27−30] Nevertheless, to the best of our knowledge, this kind of modification has never been performed before on the message domain of dermorphin. Thus, we decided to adopt this strategy speculating that it could be effective in improving opioid agonist activities in our bivalent tetramers.

In the last step of the synthetic method, the desired heteromultimeric peptide derivatives were obtained via conjugation of **3** with two molecules of [Cys^{18}]N/OFQ-NH_2 and two molecules of **6a**, **6b**, or **6c** following the one-pot, two-step approach depicted in Scheme 3. First, 2 equiv of [Cys^{18}]N/OFQ-NH_2 was reacted with **3**, in mild condition, using $NaHCO_3$ as catalysts for the thiol-Michael addition between the C-terminal cysteine residue and the maleimide

DOI: 10.1021/acs.bioconjchem.9b00519
Bioconjugate Chem. 2019, 30, 2444−2451

Scheme 3. One-Pot, Two-Step Strategy for the Hetero Bioconjugation of Peptides[a]

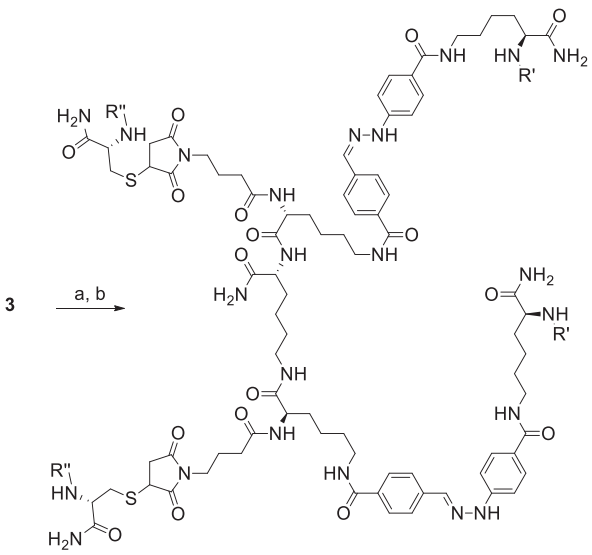

7a: R' = YaFGYPS; R'' = FGGFTGARKSARKLANQ
7b: R' = YaFGYPS(O2Oc)$_2$; R'' = FGGFTGARKSARKLANQ
7c: R' = Dmt-aFGYPS; R'' = FGGFTGARKSARKLANQ

[a]Reagents and conditions: (a) [Cys^{18}]N/OFQ-NH$_2$, 5% NaHCO$_3$, DMF; (b) CH$_3$COOH, **6a−c**, DMF.

functions. After 5 min, UPLC-MS analysis indicated the complete consumption of the starting reagents and the quantitative formation of the corresponding semifunctionalized thiol-ether intermediate. In the second step, the hydrazine group of the dermorphin-related peptides was reacted with the remaining aldehyde functions of the core. The formation of the hydrazone adduct was performed in the same reactor by adding CH$_3$COOH until reaching pH 5 before the addition of **6a−c**. UPLC-MS analysis indicated the quantitative formation of **7a** (H-PWT1-N/OFQ-dermorphin), **7b** (H-PWT1-N/OFQ-dermorphin(O2Oc)$_2$), and **7c** (H-PWT1-N/OFQ-[Dmt^1]dermorphin) within 30 min. The target compounds were then easily purified via preparative HPLC.

In the resulting tetrabranched derivatives, the four peptide chains were stably linked to the central core through thioether or hydrazone bonds in analogy to the strategies currently in use for the generation of chemoimmunoconjugates.[31] To confirm the actual stability of these linkers in the conditions required for the biological assay discussed below, H-PWT1-N/OFQ-dermorphin was dissolved in HBSS supplemented with 20 mM HEPES (pH 7.5) and incubated at 40 °C for a maximum of 4 h. Samples of the solution were taken up after 1 and 4 h and analyzed via RP-HPLC. The resulting chromatograms confirmed that no appreciable degradation of the molecule occurred within the considered times (see Figure S1).

The following linear monomers have been synthesized as internal references in standard solid-phase conditions: N/OFQ, YaFGYPS-NH$_2$ (dermorphin), YaFGYPS(O2Oc)$_2$-NH$_2$ (dermorphin(O2Oc)$_2$-NH$_2$), and Dmt-aFGYPS-NH$_2$ ([Dmt^1]dermorphin). In addition, for comparative reasons, the homo tetrabranched derivatives PWT1-N/OFQ,[5] PWT1-dermorphin, PWT1-dermorphin(O2Oc)$_2$, and PWT1-[Dmt^1]-dermorphin have been prepared in analogy to the previously described approach (HPLC chromatograms and ESI mass spectra have been reported in the Supporting Information).[4]

Pharmacology. The described ligands were assayed in calcium mobilization studies performed in CHO cells coexpressing either the human recombinant NOP or the MOP receptors and the chimeric protein Gα_{qi5}.[32,33] The NOP and MOP agonist potencies of the heterotetramers **7a−c** were expressed as pEC$_{50}$'s and compared to those of the parent peptide monomers and the reference homotetrabranched derivatives investigated under the same experimental conditions (see Table 1). This calcium mobilization assay has been previously validated with a large panel of NOP and opioid ligands,[32,33] and the standard agonists used in the present work (N/OFQ and dermorphin) displayed potencies and selectivity profiles consistent with these studies. In particular, N/OFQ evoked a concentration-dependent stimulation of calcium release in cells expressing the human NOP receptor with high potency (pEC$_{50}$ = 9.52) and maximal effects (308 ± 30% over basal values), while dermorphin was inactive up to micromolar concentrations. Conversely, dermorphin behaved as a potent full agonist of the MOP receptor (pEC$_{50}$ = 8.09;

Table 1. In Vitro Effects of the Synthesized Compounds in Calcium Mobilization Studies Performed on CHO Cells Coexpressing Either the NOP or the MOP Receptor and the Gα_{qi5} Chimeric Protein

	NOP		MOP		
	pEC$_{50}$ (CL$_{95\%}$)	α ± SEM	pEC$_{50}$ (CL$_{95\%}$)	α ± SEM	NOP/MOP
Linear Peptide Monomers					
N/OFQ	9.52 (8.97−10.06)	1	<6		>1000
dermorphin	<6		8.09 (7.44−8.74)	1	<0.01
dermorphin(O2Oc)$_2$NH$_2$	<6		7.74 (7.21−8.27)	0.94 ± 0.06	<0.1
[Dmt^1]dermorphin	<6		8.76 (8.42−9.10)	0.91 ± 0.07	<0.01
Homotetrameric PWT1 Derivatives					
PWT1-N/OFQ	8.44 (8.13−8.75)	1.08 ± 1.07	<6		>100
PWT1- dermorphin	<6		7.53 (7.23−7.84)	0.88 ± 0.05	<0.1
PWT1-dermorphin(O2Oc)$_2$	<6		7.34 (6.81−7.88)	0.80 ± 0.08	<0.1
PWT1-[Dmt^1]dermorphin	<6		9.64 (9.20−10.08)	1.04 ± 0.06	<0.001
Heterotetrameric H-PWT1 Derivatives					
H-PWT1-N/OFQ-dermorphin (**7a**)	8.09 (7.98−8.20)	0.99 ± 0.04	7.13 (6.90−7.37)	0.93 ± 0.03	0.11
H-PWT1-N/OFQ-dermorphin(O2Oc)$_2$ (**7b**)	8.21 (8.03−8.40)	1.09 ± 0.09	7.42 (7.25−7.59)	0.91 ± 0.03	0.16
H-PWT1-N/OFQ-[Dmt^1]dermorphin (**7c**)	8.35 (7.71−8.99)	0.88 ± 0.03	8.75 (8.32−9.19)	1.00 ± 0.04	2.5

DOI: 10.1021/acs.bioconjchem.9b00519
Bioconjugate Chem. 2019, 30, 2444−2451

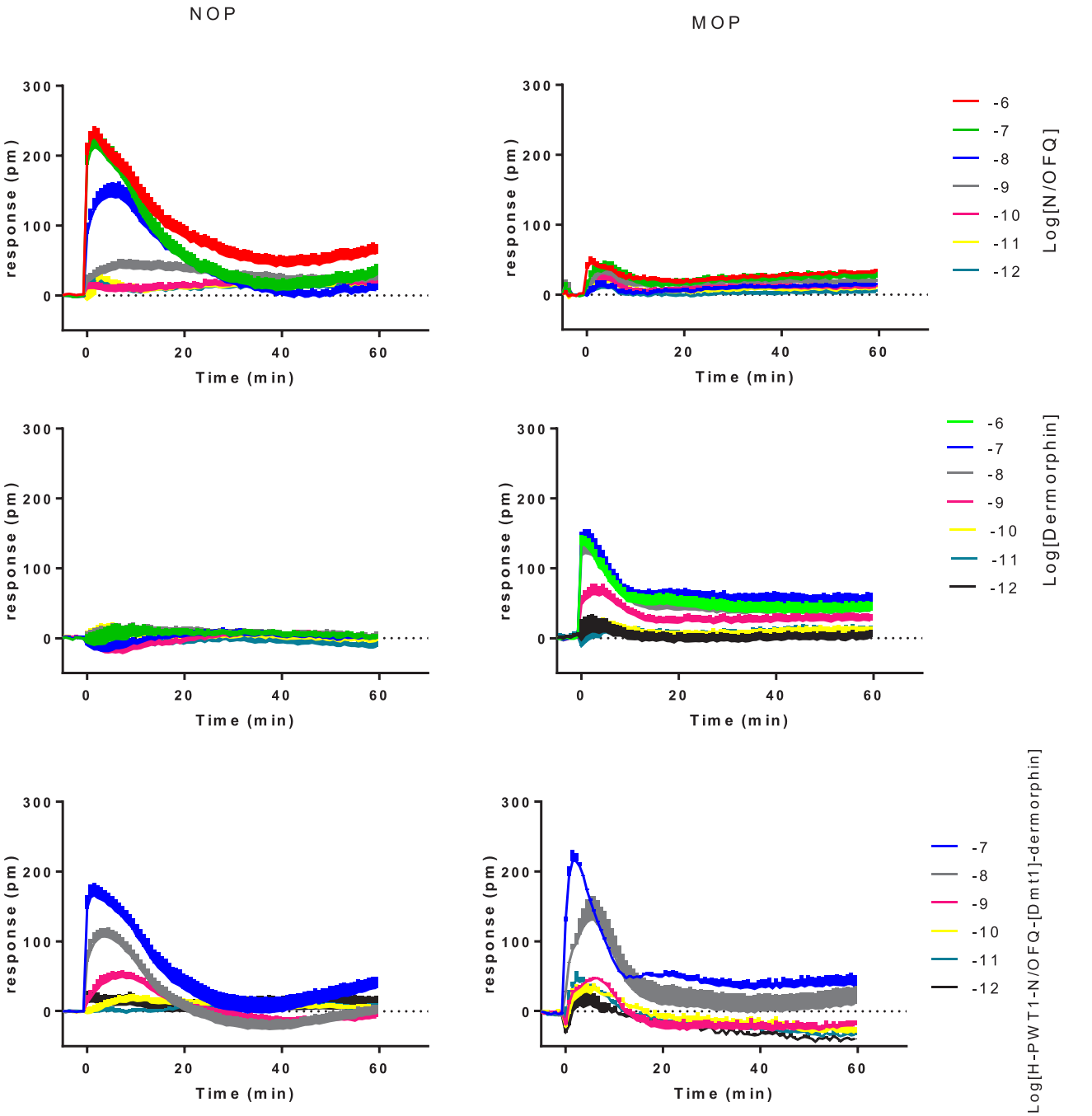

Figure 3. DMR traces of N/OFQ (top panels), dermorphin (middle panels), and H-PWT1-N/OFQ-[Dmt^1]dermorphin (bottom panels) in CHO cells expressing the NOP (left panels) and the MOP (right panels) receptors. Data are the mean ± SEM of four experiments performed in duplicate.

E_{max} 324 ± 18% over basal values) toward which N/OFQ resulted inactive.

In the first instance, the standard opioid agonists N/OFQ and dermorphin have been tetramerized in compound H-PWT1-N/OFQ-dermorphin (**7a**) that elicited a potent stimulatory action both in cells expressing the NOP receptor and in those transfected with the MOP receptor with maximal effects similar to those of the corresponding linear monomers.

These encouraging results demonstrated that the new heteromultimerization strategy did not compromise the pharmacological activity of the starting bioactive peptides, in line with what was previously observed in the same assay for most of PWT-based homotetramers.[3,5−7] Even though H-PWT1-N/OFQ-dermorphin displayed an interesting profile of mixed NOP/MOP full agonist, the potency of the compound in activating the NOP receptor (pEC_{50} = 8.09) was almost 30-fold lower if compared to that of unconjugated N/OFQ. Likewise, **7a** resulted to be 10-fold less potent than dermorphin in stimulating the MOP receptor (pEC_{50} = 7.13). This would indicate that the H-PWT1-based assembling of the analyzed bioactive sequences disfavors to some degree their interaction with the respective biological targets. This effect was also evident from the in vitro pharmacological profile of the homotetrabranched derivatives PWT1-N/OFQ

DOI: 10.1021/acs.bioconjchem.9b00519
Bioconjugate Chem. 2019, 30, 2444−2451

(Table 1)[5] and PWT1-dermorphin that behaved, respectively, as a NOP-selective and a MOP-selective agonist 3−10-fold less potent than the native peptide precursors.

Moreover, the bifunctional profile of **7a** was considered suboptimal in view of the unbalanced NOP/MOP potency, that is, 10-fold higher potency for the NOP receptor. This prompted us to investigate suitable strategies for the structural modification of the dermorphin sequence with the aim to increase the MOP potency of the resulting heterotetrabranched derivatives. First, we designed compound **7b** (H-PWT1-N/OFQ-dermorphin$(O2Oc)_2$) in which the MOP pharmacophore was spaced from the central PWT core through two polyoxyethylene units. The hydrophilic linker was selected because of the low water solubility experienced with the homotetrabranched derivative PWT2-dermorphin previously described.[3] In addition, we speculated about the possibility that a flexible linker of the proper length could facilitate the interaction of the message sequence of dermorphin with the binding pocket of the MOP receptor. As compared to **7a**, H-PWT1-N/OFQ-dermorphin$(O2Oc)_2$ displayed a substantial maintenance of NOP potency (pEC_{50} = 8.21) but only a marginal increase in MOP potency (pEC_{50} = 7.42). However, it has to be considered that the modification of the dermorphin sequence in the derivative dermorphin-$(O2Oc)_2$-NH_2 resulted per se slightly detrimental for MOP potency. Thus, in the case of **7b**, the H-PWT1-derivatization of the dermorphin component did not significantly affect the MOP potency of the linear precursor. This was also confirmed in the homotetrameric derivative PWT1-dermorphin$(O2Oc)_2$ displaying potency similar to that of PWT1-dermorphin.

In the last derivative H-PWT1-N/OFQ-[Dmt^1]dermorphin (**7c**), the dermorphin component was directly linked to the core but modified at the N-terminal portion where the Tyr^1 residue was replaced with a 2,6-dimethyl tyrosine. The corresponding linear precursor [Dmt^1]dermorphin was shown to be 5-fold more potent than the native peptide analogue (pEC_{50} = 8.76), confirming the important effect of this chemical modification in promoting the interaction of opioid peptide ligands with the MOP receptor.[27−30] Surprisingly, and unlike most of the previously reported PWT derivatives, the newly described homotetrabranched PWT1-[Dmt^1]dermorphin exhibited a significantly improved MOP-agonist potency as compared to the parent peptide monomer (pEC_{50} = 9.64). This would suggest that, in the case of compound PWT1-[Dmt^1]dermorphin, the beneficial effect of the introduction of Dmt^1 was amplified by the presence of multiple modified message domains that would cooperate synergistically in MOP receptor binding and activation. It can be speculated that the molecular flexibility and the relatively high distance between the four pharmacophores of the investigated multivalent ligand make possible the concurrent targeting of functional dimers or oligomers of the mu opioid receptor.[34]

Of relevance for the aim of this work, the introduction of a Dmt^1 residue had also a positive impact on the pharmacological profile of compound **7c**. Indeed, the MOP potency of H-PWT1-N/OFQ-[Dmt^1]dermorphin was significantly incremented in comparison with **7a** and **7b** to such an extent that the NOP/MOP potency ratio was reversed (NOP pEC_{50} = 8.35, MOP pEC_{50} = 8.75). Even in this case, the maximal effects of the compound at both of the investigated receptors were comparable to those of the unconjugated peptide precursors with no changes in ligand efficacy. Thus, H-PWT1-N/OFQ-[Dmt^1]dermorphin exhibited a profile of dual acting full agonist with high and balanced potencies for NOP and MOP receptors.

To confirm this result with a different assay, H-PWT1-N/OFQ-[Dmt^1]dermorphin has been investigated in DMR studies performed in CHO cells expressing the human MOP or NOP receptors (Figure 3). DMR is a label-free assay that gives the possibility to measure, in a noninvasive manner, receptor-dependent holistic cellular responses.[35] DMR studies have been performed in recent years investigating the pharmacological profile of several GPCR including classical opioid[36] and NOP[37] receptors. As shown in Figure 3, N/OFQ elicited a concentration-dependent DMR response in cells expressing the NOP receptor (pEC_{50} 9.48, E_{max} 236 ± 33 pm) being inactive in MOP cells. The opposite results were obtained with dermorphin that evoked DMR responses in cells expressing the MOP receptor (pEC_{50} 8.98, E_{max} 152 ± 28 pm) being inactive in NOP cells. Similar results have been previously obtained with both peptides in our laboratories.[37] Importantly, N/OFQ and dermorphin up to 1 μM were inactive in wild-type CHO cells (data not shown). H-PWT1-N/OFQ-[Dmt^1]dermorphin produced similar DMR responses in cells expressing the NOP or the MOP receptors. However, the potency and maximal effects of H-PWT1-N/OFQ-[Dmt^1]dermorphin could not be estimated in these experiments because at 1 μM the tetrameric peptide elicited statistically significant DMR responses in wild-type CHO cells (data not shown). This result was not completely unexpected because similar findings had been previously reported in DMR studies investigating the homomeric PWT derivatives of N/OFQ[37] and neuropeptide S.[38] Corroborating these findings, bioassay studies performed with tissues taken from wild-type and NOP receptor knockout mice demonstrated that PWT-N/OFQ displays reduced selectivity than the parent peptide. The implications of these findings are 2-fold: (i) a certain loss of selectivity as compared to the parent peptide(s) is probably a common feature of both homo and heteromeric PWT derivatives, and (ii) the label-free DMR assay is superior to single end point assays for revealing this aspect. Despite the above-mentioned limitations, DMR experiments confirmed that H-PWT1-N/OFQ-[Dmt^1]-dermorphin behaves as a mixed NOP/MOP agonist able to stimulate the two receptors in the same range of concentrations.

CONCLUSION

With this work, we validated an easily accessible synthetic methodology that allows one to obtain heterotetrameric peptide ligands with a bifunctional pharmacological profile. Overall, the results of this study will allow the scientific community to increase the knowledge regarding the design and synthesis of bivalent ligands for peptidergic receptors. As detailed above, the approach has been successfully applied to the identification of the NOP/MOP mixed full agonist H-PWT1-N/OFQ-[Dmt^1]dermorphin, which exhibited a balanced potency at the investigated targets with EC_{50} values in the low nanomolar range. The available evidence suggests that dual acting NOP/MOP agonists may have therapeutic potential in the treatment of pain as nonaddictive analgesics and possibly as medications to treat drug abuse.[17,23,39]

The newly disclosed compound H-PWT1-N/OFQ-[Dmt^1]-dermorphin can be considered a valuable tool for future in vivo studies aimed at investigating the effects of the simultaneous

DOI: 10.1021/acs.bioconjchem.9b00519
Bioconjugate Chem. 2019, 30, 2444−2451

stimulation of the NOP and MOP receptors in disease models. This will allow the understanding and, possibly, the expansion of the therapeutic potential of opioid bivalent ligands for treating any disease that can likely benefit by multitarget drug treatments. In vivo studies will be useful to establish if the newly described methodology can be exploited to enhance the in vivo potency of the investigated peptides and particularly their duration of action, as previously demonstrated with different examples of homotetrameric PWT derivatives.[3] Of note, the strategy herein described is extremely versatile and virtually applicable to any peptide sequence; thus, this approach could be translated in the future to the development of bivalent compounds targeting other receptor systems. As a consequence, the achieved results could be extremely helpful to explore new therapeutic perspectives and pave the way to innovative pharmacological treatments for diseases in which the concurrent activation or blockade of two different receptors is more effective/safer than the selective modulation of a single target.

■ ASSOCIATED CONTENT

Supporting Information

The Supporting Information is available free of charge on the ACS Publications website at DOI: 10.1021/acs.bioconjchem.9b00519.

Detailed synthetic procedures, HPLC chromatograms and ESI mass spectra of compounds **1**−**3**, **6a**−**c**, **7a**−**c**, PWT1-N/OFQ, PWT1-dermorphin, and PWT1-dermorphin$(O2Oc)_2$PWT1-[Dmt^1]dermorphin, and procedures for biological experiments (PDF)

■ AUTHOR INFORMATION

Corresponding Author

*Phone: +39-532-455501. E-mail: prtdle@unife.it.

ORCID

Delia Preti: 0000-0002-1075-3781

Author Contributions

S.P., V.A., D.I., A.F., and E.M. performed the chemical synthesis; F.F., C.S., J.A.N., and C.R. performed the pharmacological studies; and G.C., R.G., and D.P. designed the experiments, analyzed the data, and wrote the manuscript.

Notes

The authors declare no competing financial interest.

■ ACKNOWLEDGMENTS

D.P. is supported by grants FAR 2018 (Fondo di Ateneo per la Ricerca Scientifica) and FFABR 2017 (Finanziamento delle attività base di ricerca) from the University of Ferrara. G.C. and R.G. are supported by grant PRIN 2015 (Prot. 2015WX8Y5B_002) from the Italian Ministry of Research and Education.

■ REFERENCES

(1) Rafferty, J., Nagaraj, H., McCloskey, A. P., Huwaitat, R., Porter, S., Albadr, A., and Laverty, G. (2016) Peptide therapeutics and the pharmaceutical industry: barriers encountered translating from the laboratory to patients. *Curr. Med. Chem. 23*, 4231−4259.

(2) Henninot, A., Collins, J. C., and Nuss, J. M. (2018) The current state of peptide drug discovery: back to the future? *J. Med. Chem. 61*, 1382−1414.

(3) Calo, G., Rizzi, A., Ruzza, C., Ferrari, F., Pacifico, S., Gavioli, E. C., Salvadori, S., and Guerrini, R. (2018) Peptide welding technology - A simple strategy for generating innovative ligands for G protein coupled receptors. *Peptides 99*, 195−204.

(4) Guerrini, R., Marzola, E., Trapella, C., Pelà, M., Molinari, S., Cerlesi, M. C., Malfacini, D., Rizzi, A., Salvadori, S., and Calò, G. (2014) A novel and facile synthesis of tetra branched derivatives of nociceptin/orphanin FQ. *Bioorg. Med. Chem. 22*, 3703−3712.

(5) Rizzi, A., Malfacini, D., Cerlesi, M. C., Ruzza, C., Marzola, E., Bird, M. F., Rowbotham, D. J., Salvadori, S., Guerrini, R., Lambert, D. G., and Calo, G. (2014) In vitro and in vivo pharmacological characterization of nociceptin/orphanin FQ tetrabranched derivatives. *Br. J. Pharmacol. 171*, 4138−4153.

(6) Ruzza, C., Rizzi, A., Malfacini, D., Cerlesi, M. C., Ferrari, F., Marzola, E., Ambrosio, C., Gro, C., Salvadori, S., Costa, T., Calo, G., and Guerrini, R. (2014) Pharmacological characterization of tachykinin tetrabranched derivatives. *Br. J. Pharmacol. 171*, 4125−4137.

(7) Ruzza, C., Rizzi, A., Malfacini, D., Pulga, A., Pacifico, S., Salvadori, S., Trapella, C., Reinscheid, R. K., Calo, G., and Guerrini, R. (2015) In vitro and in vivo pharmacological characterization of a neuropeptide S tetrabranched derivative. *Pharmacol. Res. Perspect. 3*, 1−10.

(8) Bracci, L., Falciani, C., Lelli, B., Lozzi, L., Runci, Y., Pini, A., De Montis, M. G., Tagliamonte, A., and Neri, P. (2003) Synthetic peptides in the form of dendrimers become resistant to protease activity. *J. Biol. Chem. 278*, 46590−46595.

(9) Gunther, T., Dasgupta, P., Mann, A., Miess, E., Kliewer, A., Fritzwanker, S., Steinborn, R., and Schulz, S. (2018) Targeting multiple opioid receptors - improved analgesics with reduced side effects? *Br. J. Pharmacol. 175*, 2857−2868.

(10) Schroder, W., Lambert, D. G., Ko, M. C., and Koch, T. (2014) Functional plasticity of the N/OFQ-NOP receptor system determines analgesic properties of NOP receptor agonists. *Br. J. Pharmacol. 171*, 3777−3800.

(11) Evans, R. M., You, H., Hameed, S., Altier, C., Mezghrani, A., Bourinet, E., and Zamponi, G. W. (2010) Heterodimerization of ORL1 and opioid receptors and its consequences for N-type calcium channel regulation. *J. Biol. Chem. 285*, 1032−1040.

(12) Pan, Y. X., Bolan, E., and Pasternak, G. W. (2002) Dimerization of morphine and orphanin FQ/nociceptin receptors: generation of a novel opioid receptor subtype. *Biochem. Biophys. Res. Commun. 297*, 659−663.

(13) Wang, H. L., Hsu, C. Y., Huang, P. C., Kuo, Y. L., Li, A. H., Yeh, T. H., Tso, A. S., and Chen, Y. L. (2005) Heterodimerization of opioid receptor-like 1 and mu-opioid receptors impairs the potency of micro receptor agonist. *J. Neurochem. 92*, 1285−1294.

(14) Ko, M. C., and Naughton, N. N. (2009) Antinociceptive effects of nociceptin/orphanin FQ administered intrathecally in monkeys. *J. Pain 10*, 509−516.

(15) Cremeans, C. M., Gruley, E., Kyle, D. J., and Ko, M. C. (2012) Roles of mu-opioid receptors and nociceptin/orphanin FQ peptide receptors in buprenorphine-induced physiological responses in primates. *J. Pharmacol. Exp. Ther. 343*, 72−81.

(16) Sukhtankar, D. D., Zaveri, N. T., Husbands, S. M., and Ko, M. C. (2013) Effects of spinally administered bifunctional nociceptin/orphanin FQ peptide receptor/mu-opioid receptor ligands in mouse models of neuropathic and inflammatory pain. *J. Pharmacol. Exp. Ther. 346*, 11−22.

(17) Ding, H., Kiguchi, N., Yasuda, D., Daga, P. R., Polgar, W. E., Lu, J. J., Czoty, P. W., Kishioka, S., Zaveri, N. T., and Ko, M. C. (2018) A bifunctional nociceptin and mu opioid receptor agonist is analgesic without opioid side effects in nonhuman primates. *Sci. Transl. Med. 10*, 1−11.

(18) Calo, G., and Lambert, D. G. (2018) Nociceptin/orphanin FQ receptor ligands and translational challenges: focus on cebranopadol as an innovative analgesic. *Br. J. Anaesth. 121*, 1105−1114.

(19) Eerdekens, M. H., Kapanadze, S., Koch, E. D., Kralidis, G., Volkers, G., Ahmedzai, S. H., and Meissner, W. (2019) Cancer-related chronic pain: Investigation of the novel analgesic drug candidate

DOI: 10.1021/acs.bioconjchem.9b00519
Bioconjugate Chem. 2019, 30, 2444−2451

cebranopadol in a randomized, double-blind, noninferiority trial. *Eur. J. Pain. 23*, 577−588.
(20) Bird, M. F., Cerlesi, M. C., Brown, M., Malfacini, D., Vezzi, V., Molinari, P., Micheli, L., Di Cesare Mannelli, L., Ghelardini, C., Guerrini, R., Calò, G., and Lambert, D. G. (2016) Characterisation of the novel mixed mu-NOP peptide ligand dermorphin-N/OFQ (DeNo). *PLoS One 11*, 1−22.
(21) Kawano, S., Ito, R., Nishiyama, M., Kubo, M., Matsushima, T., Minamisawa, M., Ambo, A., and Sasaki, Y. (2007) Receptor binding properties and antinociceptive effects of chimeric peptides consisting of a micro-opioid receptor agonist and an ORL1 receptor antagonist. *Biol. Pharm. Bull. 30*, 1260−1264.
(22) Guillemyn, K., Starnowska, J., Lagard, C., Dyniewicz, J., Rojewska, E., Mika, J., Chung, N. N., Utard, V., Kosson, P., Lipkowski, A. W., Chevillard, L., Arranz-Gibert, P., Teixidó, M., Megarbane, B., Tourwé, D., Simonin, F., Przewlocka, B., Schiller, P. W., and Ballet, S. (2016) Bifunctional peptide-based opioid agonist-nociceptin antagonist ligands for dual treatment of acute and neuropathic pain. *J. Med. Chem. 59*, 3777−3792.
(23) Preti, D., Calo, G., and Guerrini, R. (2018) NOP-targeted peptide ligands. *Handb. Exp. Pharmacol. 254*, 17−36.
(24) Molinari, S., Camarda, V., Rizzi, A., Marzola, G., Salvadori, S., Marzola, E., Molinari, P., McDonald, J., Ko, M. C., Lambert, D. G., Calo', G., and Guerrini, R. (2013) [Dmt^1]N/OFQ(1−13)-NH_2: a potent nociceptin/orphanin FQ and opioid receptor universal agonist. *Br. J. Pharmacol. 168*, 151−162.
(25) Cerlesi, M. C., Ding, H., Bird, M. F., Kiguchi, N., Ferrari, F., Malfacini, D., Rizzi, A., Ruzza, C., Lambert, D. G., Ko, M. C., Calo, G., and Guerrini, R. (2017) Pharmacological studies on the NOP and opioid receptor agonist PWT2-[Dmt^1]N/OFQ(1−13). *Eur. J. Pharmacol. 794*, 115−126.
(26) Bycroft, B. W., Chan, W. C., Chhabra, S. R., and Hone, N. D. (1993) A novel lysine-protecting procedure for continuous flow solid phase branched peptides. *J. Chem. Soc., Chem. Commun. 9*, 778−779.
(27) Marrone, G. F., Lu, Z., Rossi, G., Narayan, A., Hunkele, A., Marx, S., Xu, J., Pintar, J., Majumdar, S., Pan, Y. X., and Pasternak, G. W. (2016) Tetrapeptide endomorphin analogs require both full length and truncated splice variants of the mu opioid receptor gene Oprm1 for analgesia. *ACS Chem. Neurosci. 7*, 1717−1727.
(28) Yamamoto, T., Nair, P., Largent-Milnes, T. M., Jacobsen, N. E., Davis, P., Ma, S., Yamamura, H. I., Vanderah, T. W., Porreca, F., Lai, J., and Hruby, V. J. (2011) Discovery of a potent and efficacious peptide derivative for delta/mu opioid agonist/neurokinin 1 antagonist activity with a 2′,6′-dimethyl-L-tyrosine: in vitro, in vivo, and NMR-based structural studies. *J. Med. Chem. 54*, 2029−2038.
(29) Giri, A. K., Apostol, C. R., Wang, Y., Forte, B. L., Largent-Milnes, T. M., Davis, P., Rankin, D., Molnar, G., Olson, K. M., Porreca, F., Vanderah, T. W., and Hruby, V. J. (2015) Discovery of novel multifunctional ligands with mu/delta opioid agonist/neurokinin-1 (NK1) antagonist activities for the treatment of pain. *J. Med. Chem. 58*, 8573−8583.
(30) Bryant, S. D., Jinsmaa, Y., Salvadori, S., Okada, Y., and Lazarus, L. H. (2003) Dmt and opioid peptides: a potent alliance. *Biopolymers 71*, 86−102.
(31) Lu, J., Jiang, F., Lu, A., and Zhang, G. (2016) Linkers having a crucial role in antibody-drug conjugates. *Int. J. Mol. Sci. 17*, 561.
(32) Camarda, V., and Calo, G. (2013) Chimeric G proteins in fluorimetric calcium assays: experience with opioid receptors. *Methods Mol. Biol. 937*, 293−306.
(33) Camarda, V., Fischetti, C., Anzellotti, N., Molinari, P., Ambrosio, C., Kostenis, E., Regoli, D., Trapella, C., Guerrini, R., Severo, S., and Calo, G. (2009) Pharmacological profile of NOP receptors coupled with calcium signaling via the chimeric protein G alpha qi5. *Naunyn-Schmiedeberg's Arch. Pharmacol. 379*, 599−607.
(34) Pascal, G., and Milligan, G. (2005) Functional complementation and the analysis of opioid receptor homodimerization. *Mol. Pharmacol. 68*, 905−915.
(35) Schroder, R., Schmidt, J., Blattermann, S., Peters, L., Janssen, N., Grundmann, M., Seemann, W., Kaufel, D., Merten, N., Drewke, C., Gomeza, J., Milligan, G., Mohr, K., and Kostenis, E. (2011) Applying label-free dynamic mass redistribution technology to frame signaling of G protein-coupled receptors noninvasively in living cells. *Nat. Protoc. 6*, 1748−1760.
(36) Morse, M., Sun, H., Tran, E., Levenson, R., and Fang, Y. (2013) Label-free integrative pharmacology on-target of opioid ligands at the opioid receptor family. *BMC Pharmacol. Toxicol. 14*, 1−18.
(37) Malfacini, D., Simon, K., Trapella, C., Guerrini, R., Zaveri, N. T., Kosyenis, E., and Calo, G. (2018) NOP receptor pharmacological profile - A dynamic mass redistribution study. *PLoS One 13*, 1−20.
(38) Ruzza, C., Ferrari, F., Guerrini, R., Marzola, E., Preti, D., Reinscheid, R. K., and Calo, G. (2018) Pharmacological profile of the neuropeptide S receptor: Dynamic mass redistribution studies. *Pharmacol. Res. Perspect. 6*, 1−11.
(39) Toll, L. (2013) The use of bifunctional NOP/mu and NOP receptor selective compounds for the treatment of pain, drug abuse, and psychiatric disorders. *Curr. Pharm. Des. 19*, 7451−7460.

DOI: 10.1021/acs.bioconjchem.9b00519
Bioconjugate Chem. 2019, 30, 2444−2451

Journal of Medicinal Chemistry

pubs.acs.org/jmc

Article

Novel Mixed NOP/Opioid Receptor Peptide Agonists

Salvatore Pacifico, Valentina Albanese, Davide Illuminati, Erika Marzola, Martina Fabbri, Federica Ferrari, Victor A.D. Holanda, Chiara Sturaro, Davide Malfacini, Chiara Ruzza,* Claudio Trapella, Delia Preti,* Ettore Lo Cascio, Alessandro Arcovito, Stefano Della Longa,* Martina Marangoni, Davide Fattori, Romina Nassini, Girolamo Calò, and Remo Guerrini

Cite This: *J. Med. Chem.* 2021, 64, 6656–6669

Read Online

ACCESS | Metrics & More | Article Recommendations | Supporting Information

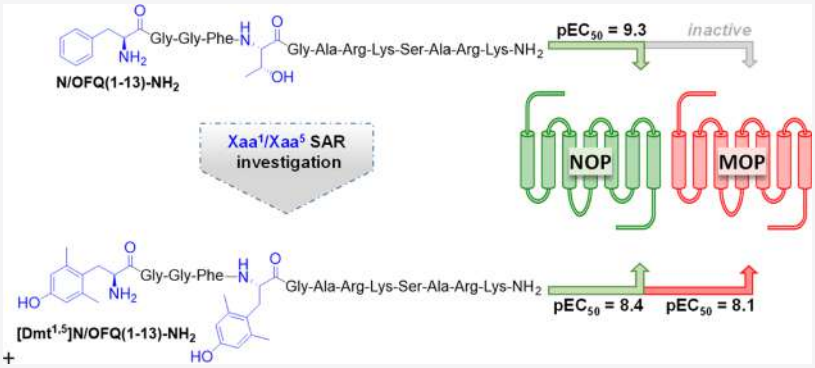

ABSTRACT: The nociceptin/orphanin FQ (N/OFQ)/N/OFQ receptor (NOP) system controls different biological functions including pain and cough reflex. Mixed NOP/opioid receptor agonists elicit similar effects to strong opioids but with reduced side effects. In this work, 31 peptides with the general sequence [Tyr/Dmt[1],Xaa[5]]N/OFQ(1-13)-NH_2 were synthesized and pharmacologically characterized for their action at human recombinant NOP/opioid receptors. The best results in terms of NOP versus mu opioid receptor potency were obtained by substituting both Tyr[1] and Thr[5] at the N-terminal portion of N/OFQ(1-13)-NH_2 with the noncanonical amino acid Dmt. [Dmt[1,5]]N/OFQ(1-13)-NH_2 has been identified as the most potent dual NOP/mu receptor peptide agonist so far described. Experimental data have been complemented by *in silico* studies to shed light on the molecular mechanisms by which the peptide binds the active form of the mu receptor. Finally, the compound exerted antitussive effects in an *in vivo* model of cough.

INTRODUCTION

Nociceptin/orphanin FQ (N/OFQ; FGGFTGARKSAR-KLANQ) is the endogenous ligand of the N/OFQ peptide (NOP) receptor.[1,2] N/OFQ and the NOP receptor display high structural homology with peptides and receptors of the opioid family but distinct pharmacology.[3] The N/OFQ-NOP receptor system controls several biological functions at both central and peripheral levels including pain transmission, mood and anxiety, food intake, learning and memory, locomotion, cough and micturition reflexes, cardiovascular homeostasis, intestinal motility, and immune responses.[4]

The effects of N/OFQ and selective NOP agonists in analgesiometric assays are complex depending on the dose, administration route, type of pain, and animal species.[5,6] On the contrary, strong and consistent experimental evidence suggests that the simultaneous activation of NOP and opioid receptors elicits synergistic analgesic effects.[6,7] On these bases, mixed NOP/opioid receptor agonists (cebranopadol,[8,9] AT-121,[10] BU10038,[11] and BPR1M97[12]) have been developed and investigated for their antinociceptive properties. It was consistently demonstrated that these drugs elicit similar analgesic effects to strong opioids but with substantially reduced side effects including respiratory depression, tolerance, and abuse liability (see the recent review by Kiguchi *et al.*[13]).

Other ligands targeting multiple opioid receptors have been studied.[14] For example, dual-acting mu agonist/delta antagonist peptidomimetics demonstrated to produce antinociception *in vivo* with reduced tolerance liability compared with morphine.[15,16] Moreover, mixed kappa agonist/mu partial agonist ligands have been investigated as potential treatment agents for cocaine and other psychostimulant abuses.[17] Finally, mixed kappa agonist/delta antagonist ligands have been developed as

Received: November 27, 2020
Published: May 17, 2021

https://doi.org/10.1021/acs.jmedchem.0c02062
J. Med. Chem. 2021, 64, 6656–6669

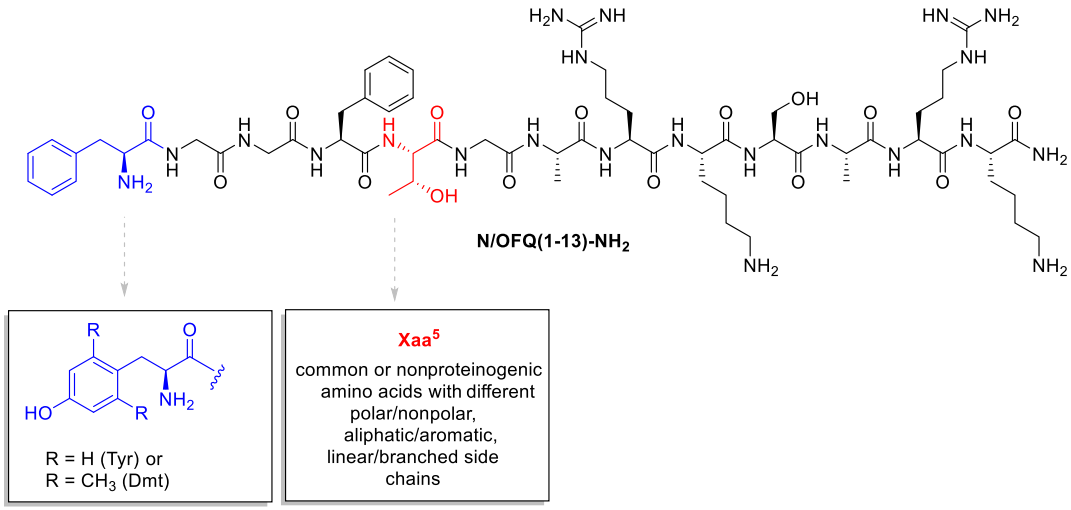

Figure 1. SAR investigation leading to a series of [Tyr/Dmt[1],Xaa[5]]N/OFQ(1-13)-NH_2 peptide derivatives as possible mixed NOP/opioid receptor ligands.

Table 1. Effects of Standard Agonists and a First Series of [Tyr[1],Xaa[5]]N/OFQ(1-13)-NH_2 Derivatives at NOP and mu Opioid Receptors in Calcium Mobilization Studies

		NOP		mu		NOP/mu
		pEC_{50} ($CL_{95\%}$)	E_{max} ± S.E.M.	pEC_{50} ($CL_{95\%}$)	E_{max} ± S.E.M	CR
1	N/OFQ(1-13)NH_2	9.29 (9.12−9.46)	368 ± 11	inactive		<0.001
2	dermorphin	inactive		7.71 (7.35−8.07)	380 ± 15	>50
3	[Tyr[1]]N/OFQ(1-13)-NH_2	9.23 (9.07−9.39)	380 ± 11	crc incomplete; 10 μM: 197 ± 69		0.001
4	[Tyr[1],Asn[5]]N/OFQ(1-13)-NH_2	8.70 (8.26−9.11)	327 ± 15	crc incomplete; 10 μM: 209 ± 29		0.002
5	[Tyr[1],Val[5]]N/OFQ(1-13)-NH_2	8.70 (8.53−8.87)	334 ± 19	crc incomplete; 10 μM: 254 ± 19		0.002
6	[Tyr[1],Lys(Ac)[5]]N/OFQ(1-13)-NH_2	8.55 (7.88−9.22)	370 ± 16	crc incomplete; 10 μM: 161 ± 31		0.003
7	[Tyr[1],Abu[5]]N/OFQ(1-13)-NH_2	8.15 (7.61−8.69)	366 ± 20	crc incomplete; 10 μM: 213 ± 37		0.007
8	[Tyr[1],Lys[5]]N/OFQ(1-13)-NH_2	7.26 (6.74−7.78)	366 ± 6	crc incomplete; 10 μM: 113 ± 35		0.05
9	[Tyr[1],Dap[5]]N/OFQ(1-13)-NH_2	7.20 (6.95−7.45)	367 ± 9	crc incomplete; 10 μM: 144 ± 44		0.06
10	[Tyr[1],Dab[5]]N/OFQ(1-13)-NH_2	6.43 (6.28−6.58)	340 ± 22	crc incomplete; 10 μM: 41 ± 4		0.37
11	[Tyr[1],Leu[5]]N/OFQ(1-13)-NH_2	8.03 (7.46−8.60)	339 ± 24	6.08 (5.95−6.21)	339 ± 25	0.01
12	[Tyr[1],Nle[5]]N/OFQ(1-13)-NH_2	8.77 (8.45−9.09)	375 ± 9	6.74 (6.15−7.33)	323 ± 4	0.01
13	[Tyr[1],Nva[5]]N/OFQ(1-13)-NH_2	8.43 (7.55−9.31)	358 ± 14	6.25 (5.59−6.91)	313 ± 19	0.007
14	[Tyr[1,5]]N/OFQ(1-13)-NH_2	7.07 (6.68−7.46)	332 ± 19	6.76 (6.34−7.18)	357 ± 21	0.49

tools for the characterization of delta and kappa-opioid receptor phenotypes.[18]

With the aim of generating a peptide acting as a nonselective NOP/opioid agonist, we investigated different approaches. On one hand, the peptide [Dmt[1]]N/OFQ(1-13)-NH_2 has been identified as a nonselective agonist for NOP and opioid receptors[19] and its tetrabranched derivative, generated using the peptide welding technology (PWT),[20] was demonstrated to produce a robust analgesic effect after spinal administration in nonhuman primates. However, this action was sensitive to NOP but not opioid receptor antagonists.[21] On the other hand, N/OFQ and dermorphin-related peptides were linked together to generate the hetero-tetrabranched derivative H-PWT1-N/OFQ-[Dmt[1]]dermorphin[22] or the dimeric compound DeNo.[23] Despite its promising *in vitro* pharmacological profile as a mixed NOP/opioid agonist, DeNo was not effective as a spinal analgesic.[23] In the present study, we further investigate the possibility of generating a mixed NOP/opioid agonist based on the following evidence: (i) mixed NOP/kappa ligands can be obtained combining the C-terminal sequence of N/OFQ with the N-terminal of dynorphin A, where amino acids in positions 5 and 6 were particularly important for receptor selectivity;[24] (ii) Thr[5] in N/OFQ(1-13)-NH_2 can be replaced with several different residues without loss of peptide efficacy and potency at the NOP receptor;[25] (iii) the substitution of Phe[1] in N/OFQ with Tyr[26] and particularly with Dmt[19,27,28] increases affinity/potency at classical opioid receptors. Thus, in the present study, 31 peptide derivatives with the general sequence [Tyr/Dmt[1],Xaa[5]]N/OFQ(1-13)-NH_2 were generated and tested for their action at NOP and opioid receptors (Figure 1).

Experimental data have been complemented by an *in silico* study of the binding of [Dmt[1,5]]N/OFQ(1-9)-NH_2 to the mu receptor. This non-natural peptide has been compared with the agonist peptide DAMGO ([D-Ala[2], *N*-MePhe[4], Gly-ol]-enkephalin) and the N-terminal fragment of N/OFQ (N/OFQ(1-9)-NH_2). The starting point of the computational study was the structure of the activated mu receptor in complex with the agonist peptide DAMGO that has been previously reported by X-ray diffraction and cryo-electron microscopy.[29,30] The last structure of the complex DAMGO-mu receptor was used as a model, allowing the setup of the two unknown complexes with the selected peptides by molecular docking. Specifically, docking of a flexible ligand to multiple receptor conformations as already applied to the study of NOP agonists and antagonists[31,32] was

https://doi.org/10.1021/acs.jmedchem.0c02062
J. Med. Chem. 2021, 64, 6656−6669

Table 2. Effects of Standard Agonists and [Tyr^1,Xaa^5]N/OFQ(1-13)-NH$_2$ Derivatives with Different Aromatic Residues as Xaa^5 at NOP and mu Opioid Receptors in Calcium Mobilization Studies

		NOP		mu		NOP/mu
		pEC$_{50}$ (CL$_{95\%}$)	E_{max} ± S.E.M.	pEC$_{50}$ (CL$_{95\%}$)	E_{max} ± S.E.M.	CR
1	N/OFQ(1-13)-NH$_2$	9.40 (9.19−9.61)	288 ± 15	inactive		<0.001
2	dermorphin	inactive		7.83 (7.56−8.11)	306 ± 23	>50
3	[Tyr^1]N/OFQ(1-13)-NH$_2$	9.13 (8.83−9.43)	266 ± 14	crc incomplete; 10 μM: 217 ± 29		0.001
15	[Tyr^1,Phe^5]N/OFQ(1-13)-NH$_2$	7.72 (7.56−7.87)	242 ± 11	6.41 (5.85−6.97)	315 ± 32	0.05
16	[Tyr^1,His^5]N/OFQ(1-13)-NH$_2$	7.39 (7.16−7.62)	249 ± 23	crc incomplete; 10 μM: 230 ± 37		0.05
17	[Tyr^1,Trp^5]N/OFQ(1-13)-NH$_2$	7.27 (7.19−7.35)	288 ± 28	crc incomplete; 10 μM: 193 ± 31		0.07
18	[Tyr^1,hPhe^5]N/OFQ(1-13)-NH$_2$	8.70 (8.24−9.16)	301 ± 26	crc incomplete; 10 μM: 228 ± 29		0.003
19	[Tyr^1,Phg^5]N/OFQ(1-13)-NH$_2$	7.57 (7.12−8.02)	293 ± 31	6.81 (6.33−7.29)	287 ± 48	0.17
20	[Tyr^1,p(OCH$_3$)Phe^5]N/OFQ(1-13)-NH$_2$	7.88 (7.81−7.95)	246 ± 18	crc incomplete; 10 μM: 221 ± 49		0.02
21	[Tyr^1,(pF)Phe^5]N/OFQ(1-13)-NH$_2$	7.31 (6.81−7.81)	311 ± 22	crc incomplete; 10 μM: 256 ± 55		0.06
22	[Tyr^1,(pNO$_2$)Phe^5]N/OFQ(1-13)-NH$_2$	7.31 (6.90−7.72)	305 ± 22	crc incomplete; 10 μM: 192 ± 64		0.06
23	[Tyr^1,Dip^5]N/OFQ(1-13)-NH$_2$	6.61 (6.13−7.09)	240 ± 26	6.78 (6.28−7.27)	331 ± 32	1.48
24	[Tyr^1,Bip^5]N/OFQ(1-13)-NH$_2$	6.93 (6.63−7.22)	272 ± 29	crc incomplete; 10 μM: 151 ± 66		0.15
25	[Tyr^1,1Nal^5]N/OFQ(1-13)-NH$_2$	7.17 (6.82−7.52)	245 ± 16	6.08 (5.67−6.49)	319 ± 31	0.08
26	[Tyr^1,2Nal^5]N/OFQ(1-13)-NH$_2$	6.82 (6.60−7.04)	266 ± 15	crc incomplete; 10 μM: 244 ± 10		0.19
27	[Tyr^1,(pNH$_2$)Phe^5]N/OFQ(1-13)-NH$_2$	7.52 (7.11−7.93)	274 ± 15	6.43 (5.80−7.05)	329 ± 37	0.08
28	[Tyr^1,Dmt^5]N/OFQ(1-13)-NH$_2$	7.75 (7.22−8.27)	251 ± 22	6.71 (6.36−7.07)	301 ± 35	0.09

Table 3. Effects of Standard Agonists and [Dmt^1,Xaa^5]N/OFQ(1-13)-NH$_2$ Derivatives at NOP and mu Opioid Receptors in Calcium Mobilization Studies

		NOP		mu		NOP/mu
		pEC$_{50}$ (CL$_{95\%}$)	E_{max} ± S.E.M.	pEC$_{50}$ (CL$_{95\%}$)	E_{max} ± S.E.M.	CR
1	N/OFQ(1-13)-NH$_2$	9.59 (9.30−9.88)	289 ± 34	inactive		<0.001
2	dermorphin	inactive		8.15 (7.97−8.33)	359 ± 18	>100
3	[Tyr^1]N/OFQ(1-13)-NH$_2$	9.15 (8.48−9.82)	236 ± 13	5.80 (5.22−6.38)	251 ± 34	<0.001
29	[Dmt^1]N/OFQ(1-13)-NH$_2$	8.57 (8.26−8.87)	294 ± 22	7.37 (7.12−7.51)	311 ± 20	0.06
30	[Dmt^1,Tyr^5]N/OFQ(1-13)-NH$_2$	6.91 (6.81−7.01)	304 ± 21	7.81 (7.47−8.15)	410 ± 25	7.94
31	[Dmt^1,Phe^5]N/OFQ(1-13)-NH$_2$	7.25 (6.69−7.81)	277 ± 28	8.19 (7.71−8.66)	335 ± 22	8.71
32	[Dmt^1,Phg^5]N/OFQ(1-13)-NH$_2$	6.95 (6.78−7.12)	282 ± 12	8.54 (8.13−8.96)	339 ± 28	39
33	[Dmt^1,1Nal^5]N/OFQ(1-13)-NH$_2$	7.22 (6.91−7.54)	286 ± 19	7.80 (7.51−8.09)	349 ± 20	3.80
34	[Dmt^1,(pNH$_2$)Phe^5]N/OFQ(1-13)-NH$_2$	7.58 (7.37−7.79)	258 ± 20	7.82 (7.35−8.29)	358 ± 15	1.73
35	[Dmt^{1,5}]N/OFQ(1-13)-NH$_2$	8.39 (8.05−8.72)	270 ± 25	8.08 (7.74−8.42)	354 ± 16	0.49

Table 4. Effects of Standard Agonists and [Dmt^{1,5}]N/OFQ(1-13)-NH$_2$ at NOP and mu Opioid Receptors in DMR Studies

		NOP		mu		mu/NOP
		pEC$_{50}$ (CL$_{95\%}$)	E_{max} ± S.E.M.	pEC$_{50}$ (CL$_{95\%}$)	E_{max} ± S.E.M.	CR
36	N/OFQ	9.37 (8.96−9.79)	209 ± 14	inactive		<0.001
2	dermorphin	inactive		8.92 (8.74−9.10)	151 ± 16	>500
35	[Dmt^{1,5}]N/OFQ(1-13)-NH$_2$	7.71 (6.65−8.76)	223 ± 11	8.64 (8.28−9.01)	202 ± 20	8.51

carried out to provide the best binding pose of the two peptides [Dmt^{1,5}]N/OFQ(1-9)-NH$_2$ and N/OFQ(1-9)-NH$_2$. This docking procedure was further challenged by long-lasting molecular dynamics (MD) simulations and compared with an MD simulation of the DAMGO-mu receptor-G$_i$ protein complex to identify the key interactions necessary for a successful nonselective NOP/opioid agonist. Finally, considering that NOP receptor agonists have demonstrated antitussive effects *in vivo*[33−37] and that opioids are effective drugs currently in use to treat cough,[38] the most potent mixed NOP/opioid agonist has been evaluated *in vivo* for its antitussive effects in guinea pigs.

RESULTS

Chemistry. The peptide derivatives reported in Tables 1−4 were prepared through automated Fmoc/*t*Bu-based solid-phase peptide synthesis (SPPS) on a Rink amide MBHA resin. Commercially available protected amino acids were employed as synthetic precursors of the target peptides except for Fmoc-2′,6′-dimethyl-tyrosine (Fmoc-Dmt-OH) that was instead synthesized in analogy to an approach previously published by Wang *et al.*[39] (Scheme S1 of the Supporting Information). Specifically, H-Tyr-OH was first esterified to H-Tyr-OMe under standard conditions, and then, the phenolic hydroxyl was protected with a *tert*-butyldimethylsilyl ether moiety before the following coupling with picolinic acid. The latter function worked as a directing group for the subsequent Pd(OAc)$_2$-catalyzed C−H alkylation with CH$_3$I and K$_2$CO$_3$ allowing the simultaneous and regioselective introduction of two methyl groups at the ortho-positions of the aromatic ring. Then, full deprotection under strongly acidic conditions, followed by treatment with Fmoc-Cl, led to the desired 2′,6′-dimethyl

https://doi.org/10.1021/acs.jmedchem.0c02062
J. Med. Chem. 2021, 64, 6656−6669

tyrosine scaffold (detailed procedures and analytical characterizations of Fmoc-Dmt-OH and its precursors have been reported in the Supporting Information). The structures of other nonproteinogenic amino acids employed in this work have been depicted in Table S1.

***In Vitro* Structure−Activity Relationship.** N/OFQ(1-13)-NH_2 stimulated calcium mobilization with high potency and maximal effects in cells coexpressing NOP receptors and chimeric G proteins, while being inactive in cells expressing the mu opioid receptor. On the contrary, dermorphin stimulated calcium mobilization with high potency and maximal effects in mu expressing cells, while it was inactive in NOP cells (Table 1). The substitution of Phe^1 with Tyr as in [Tyr^1]N/OFQ(1-13)-NH_2 did not affect NOP potency while promoting a minor increase in mu potency. Thr^5 in [Tyr^1]N/OFQ(1-13)-NH_2 was replaced with a series of both proteinogenic and non-proteinogenic amino acids with different polar/nonpolar, aliphatic/aromatic, linear/branched side chains with the aim to explore the effect of several structural parameters on the biological activity. The substitution of Thr^5 with Asn, Val, Lys(Ac) caused a slight (<10-fold) reduction in NOP potency and no modification of mu potency. The same substitution with Abu, Lys, Dap, and Dab induced a larger loss (>10-fold) of NOP potency. The introduction in position 5 of Leu, Nle, and Nva promoted a moderate decrease in NOP potency associated with a significant increase in mu potency. A similar increase in mu potency was achieved with [$Tyr^{1,5}$]N/OFQ(1-13)-NH_2, which however displayed a larger decrease in NOP potency; thus, the NOP/mu concentration ratio for this peptide was near 1 (Table 1). None of the amino acid substitutions evaluated in Table 1 modified ligand efficacy at both NOP and mu receptors. Based on these results, aromatic residues were selected for further modifications of position 5 of [Tyr^1]N/OFQ(1-13)-NH_2.

As shown in Table 2, 14 compounds with an aromatic residue substituting Thr^5 in [Tyr^1]N/OFQ(1-13)-NH_2 were assayed in NOP and mu receptor expressing cells. The different amino acids did not modify ligand efficacy but produced different effects on NOP and mu potency. In particular, the NOP potency of these derivatives was in the range of 8.70−6.61, while the mu potency of these compounds was <6 with the exceptions of peptides substituted with Phe, Phg, 1Nal, (pNH_2)Phe, and Dmt (range 6.08−6.81). Then, for further investigation, we selected those sequences showing pEC_{50} values >7 for the NOP receptor and >6 for the mu receptor associated with an NOP/mu concentration ratio >0.05. These criteria were matched by [Tyr^1]N/OFQ(1-13)-NH_2 derivatives substituted in position 5 with Tyr, Phe, Phg, 1Nal, (pNH_2)Phe, and Dmt.

The third series of peptides was generated by substituting Tyr^1 with Dmt that is known to increase opioid receptor potency.[40] In fact, as shown in Table 3, [Dmt^1]N/OFQ(1-13)-NH_2 displayed a moderate (10-fold) decrease in NOP potency compared to [Tyr^1]N/OFQ(1-13)-NH_2 associated to a more pronounced increase (approx. 40-fold) in mu potency. The substitution of Thr^5 of [Dmt^1]N/OFQ(1-13)-NH_2 with the above-mentioned amino acids generated results similar to those obtained with [Tyr^1]N/OFQ(1-13)-NH_2, that is, a slight to moderate decrease in NOP potency associated to a large increase in mu potency. The most exciting result has been obtained with [$Dmt^{1,5}$]N/OFQ(1-13)-NH_2 that displayed similar and high potency at both NOP and mu receptors.

[$Dmt^{1,5}$]N/OFQ(1-13)-NH_2 was further evaluated in dynamic mass redistribution (DMR) experiments performed on CHO cells expressing the human NOP and mu receptors. As summarized in Table 4, N/OFQ elicited a concentration-dependent positive DMR signal in cells expressing the NOP receptor being inactive in mu expressing cells. Opposite results were obtained with dermorphin that behaves as a mu-selective agonist. [$Dmt^{1,5}$].N/OFQ(1-13)-NH_2 elicited a robust DMR response in both cell lines with similar maximal effects to standard agonists. [$Dmt^{1,5}$].N/OFQ(1-13)-NH_2 displayed nanomolar potency at both NOP and the mu receptor with a mu/NOP potency ratio of 8.51 (Table 4).

Finally, the agonist properties of [$Dmt^{1,5}$]N/OFQ(1-13)-NH_2 were evaluated at delta and kappa opioid receptors in calcium mobilization experiments. As shown in Figure 2,

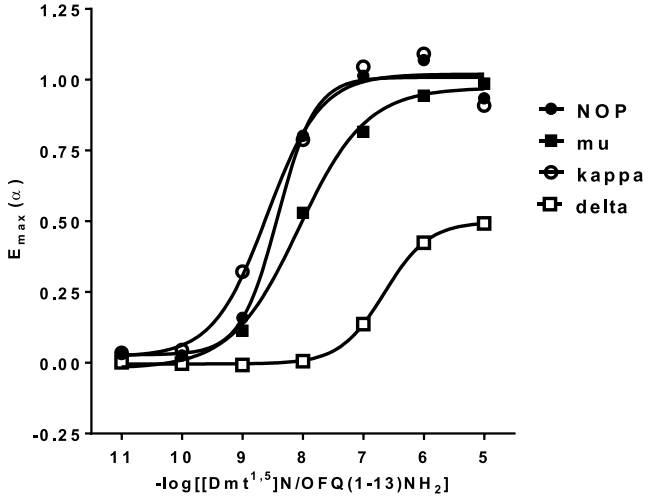

Figure 2. Effects of [$Dmt^{1,5}$]N/OFQ(1-13)-NH_2 at NOP and classical opioid receptors in calcium mobilization studies.

[$Dmt^{1,5}$]N/OFQ(1-13)-NH_2 displayed low potency and efficacy at the delta receptor. On the contrary, the peptide showed at the kappa opioid receptor high potency (pEC_{50} = 8.49) similar to that displayed at NOP (pEC_{50} = 8.39) and mu (pEC_{50} = 8.08) receptors. Thus, [$Dmt^{1,5}$]N/OFQ(1-13)-NH_2 should be classified as a mixed NOP/mu/kappa full agonist.

Molecular Dynamics. As explained in the Experimental Section, MD simulations have been performed setting up nine-residue long peptides (i.e., [Phe/Dmt^1,Thr/Dmt^5]N/OFQ(1-9)-NH_2) due to the fact that longer peptides lack reliable starting conformations by molecular docking. Moreover, in the following, we will focus on the first five residues of the peptides, those entering the mu opioid receptor orthosteric site, as residues 6−9 represent the more flexible part of the peptides along the MD simulation. The results obtained for [$Dmt^{1,5}$]N/OFQ(1-9)-NH_2 were compared with those obtained by similar simulations performed on the mu agonist peptide DAMGO and also on N/OFQ(1-9)-NH_2 as a sort of negative control since this peptide lacks mu receptor affinity.[26]

In Figure 3A, the 3D conformation obtained after docking and MD for [$Dmt^{1,5}$]N/OFQ(1-9)-NH_2 (colored purple) is superimposed to the known one reported for DAMGO (colored yellow, PDB code 6DDF).[30] Subsequent panels (Figure 3B−E) show the main interactions relating to each of the three aromatic residues, that is, Dmt^1, Phe^4, and Dmt^5. Furthermore, a general comparison between the results of MD simulations performed on DAMGO (blue), [$Dmt^{1,5}$]N/OFQ(1-9)-NH_2 (green), and N/OFQ(1-9)-NH_2 (red) is shown in Figure 4. In this figure, patterns of the main receptor-peptide interactions provided are

https://doi.org/10.1021/acs.jmedchem.0c02062
J. Med. Chem. 2021, 64, 6656−6669

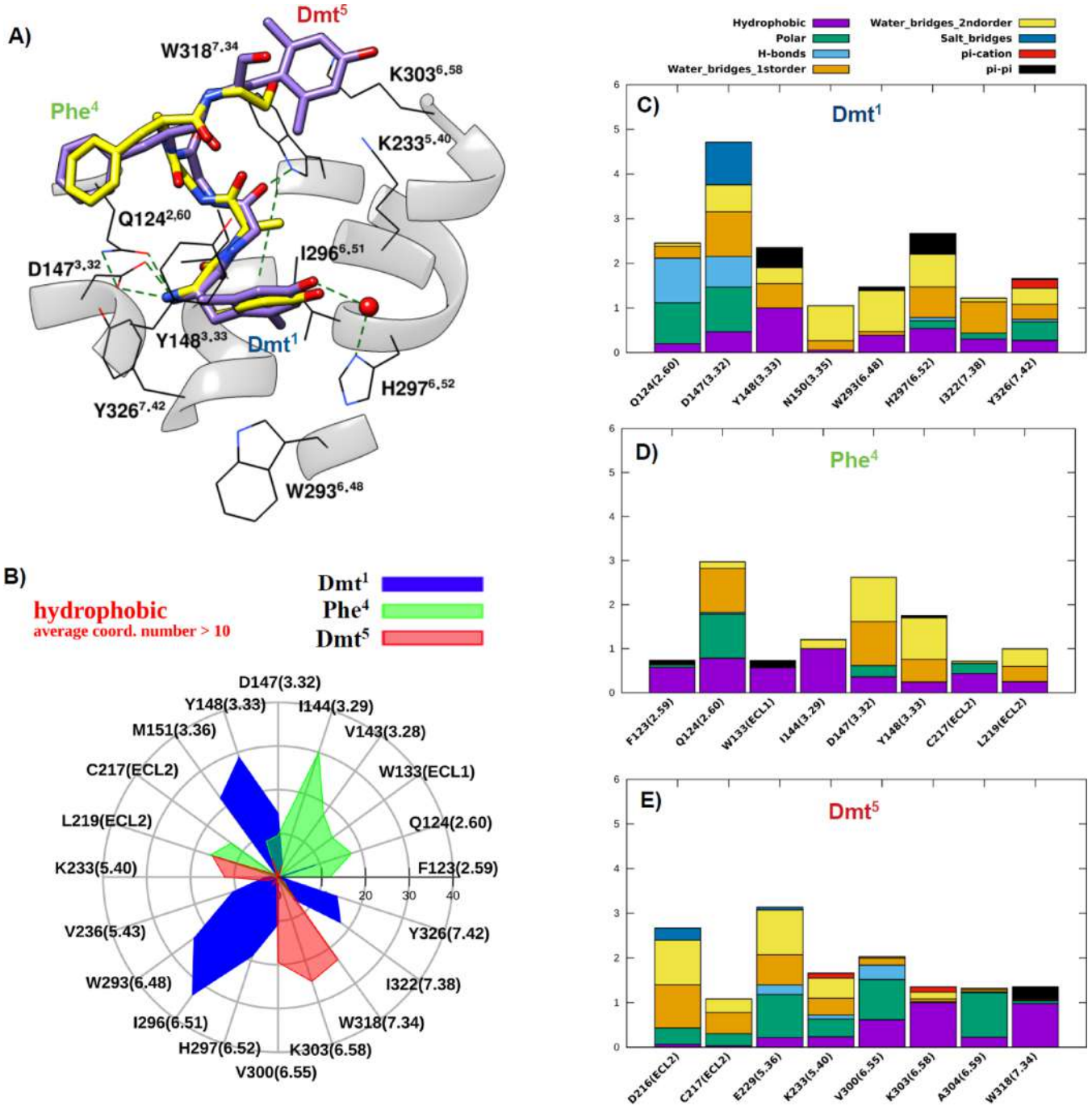

Figure 3. (A) Orthosteric site of [Dmt^{1,5}]N/OFQ(1-9)-NH_2 (colored purple) in the active mu receptor, according to "*in silico*" docking and MD (starting receptor structure from PDB code 6DDF). Only the first five residues are shown. The reported DAMGO conformation (the same PDB code) is superimposed (yellow). (B) Hydrophobic contacts between Dmt^1, Phe^4, and Dmt^5 with their neighboring residues. (C−E) Interaction histograms of residues Dmt^1, Phe^4, and Dmt^5, respectively, including hydrophobic, polar, H-bonds, water bridges of first and second order, salt bridges, and π−cation and π−π stacking as derived from long-lasting MD.

displayed and superimposed, that is, hydrophobic and polar average number of contacts (Figure 4A,B), percentage of formation of hydrogen bonds, and average "strength" of π−π stacking and π−cation interaction (Figure 4C−E, respectively). Accordingly, the representative conformation of [Dmt^{1,5}]N/OFQ(1-9)-NH_2 in the orthosteric site largely overlaps with that of DAMGO (Figure 3A). The N-terminus of Dmt^1 forms salt bridge/hydrogen bond contacts with D^{147} (a residue conserved all along the opioid family) similar to both DAMGO and the morphinan agonist BU72 (PDB code 5C1M).[29] MD simulations show that this important interaction is strongly stabilized by the presence of another conserved residue, Q^{124} (TM2), whose nitrogen and oxygen side-chain atoms reinforce the hydrogen bond network by contacts with both the carboxyl oxygen of D^{147} and the N-terminus of Dmt^1. Moreover, water bridges fill the small remaining volume between the D^{147} and Q^{124} side chains and the backbone donor/acceptors of Dmt^1, Gly^3, and Gly^2, with the latter being in direct H-bond with W^{318} of TM7.

https://doi.org/10.1021/acs.jmedchem.0c02062
J. Med. Chem. 2021, 64, 6656−6669

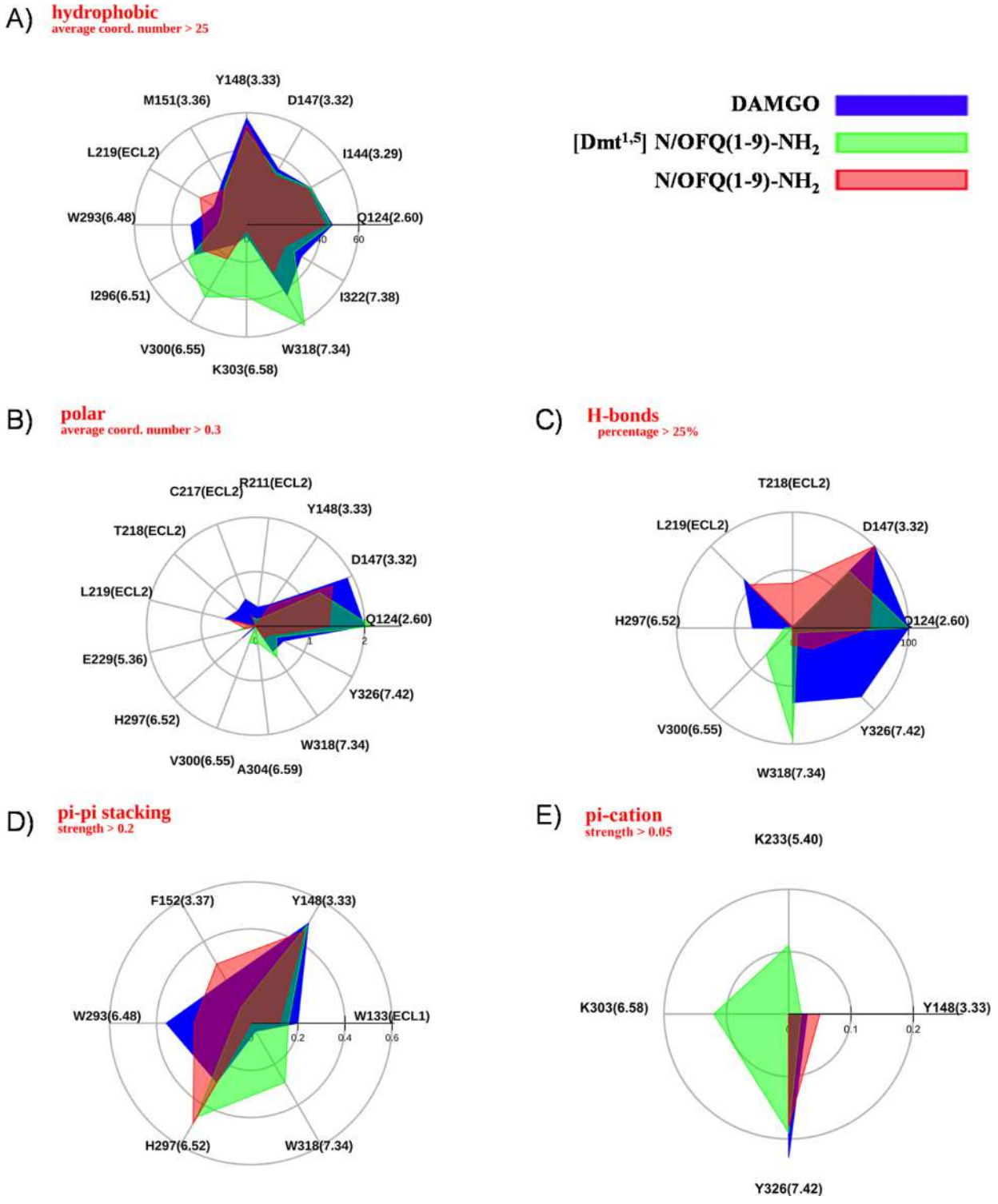

Figure 4. Maps of hydrophobic (A), polar (B), H-bond (C), $\pi-\pi$ stacking (D), and $\pi-$cation (E) interactions between the mu receptor and the studied ligands along MD trajectories. Only residues 1−5 are considered for [$Dmt^{1,5}$]N/OFQ(1-9)-NH_2 and N/OFQ(1-9)-NH_2.

Dmt^1 is also in direct hydrophobic contact with TM6 residues (W^{293}, H^{297}, and especially I^{296}, Figure 3B,C). Along the MD trajectories, its aromatic head moves alternating first- and second-order water bridges with H^{297} of TM6 (Figure 3C). Partial $\pi-\pi$ stacking between the Dmt^1 and H297 rings is also observed during the simulations. Hydrophobic, π-stacking, and water bridge contacts between Dmt^1 and Y^{148} (TM3), H^{297} and W^{293} (TM6) frequently occur (Figure 3C). The latter residue, in the so-called receptor polar cavity, is thought to be very important for the activation mechanism in many class A GPCRs, and these interactions, although not fully stable, could contribute to stabilize the receptor active state.

The formation of alternating second-order water bridges (along 78% of the trajectory) shows that the N-terminus of Dmt^1, together with D^{147}, is also in contact with N^{150} (Figure 3C), an important conserved residue that in the reported high-

https://doi.org/10.1021/acs.jmedchem.0c02062
J. Med. Chem. 2021, 64, 6656−6669

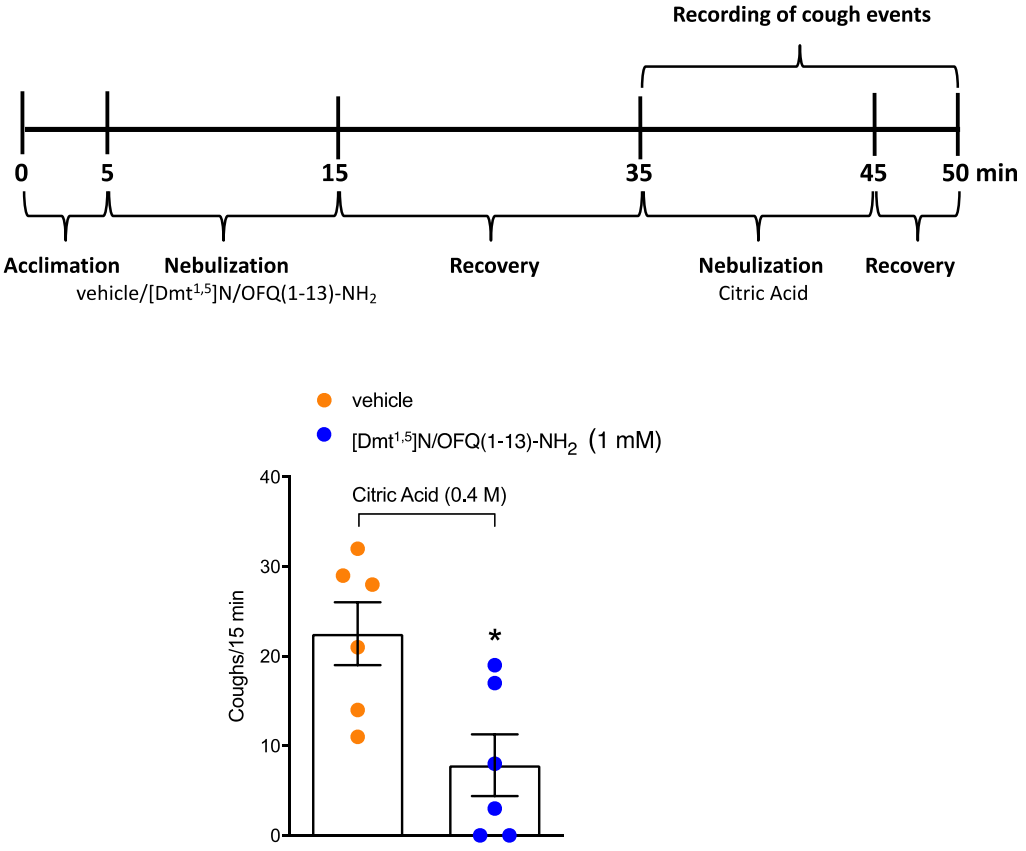

Figure 5. Effect of [Dmt^{1,5}]N/OFQ(1-13)-NH_2 on citric acid-induced cough in conscious guinea pigs. Schematic representation of the experimental procedure for the cough measurement in conscious guinea pigs and pooled data of cough number after [Dmt^{1,5}]N/OFQ(1-13)-NH_2 (1 mM) or vehicle (0.9% NaCl) nebulization, 30 min before the nebulization of the tussive agent, citric acid (0.4 M). Values are the mean ± SEM of the numbers of coughs/15 min, with data points overlaid (n = 6 guinea pigs for each condition). *p < 0.05 vs vehicle, Student's t-test.

resolution structure of the inactive delta receptor[41] is shown to connect the orthosteric site to the sodium pocket in the central part of the receptor.

While Dmt^1 interacts with both TM3 (more than 40 contacts with residues Y^{148} and M^{151}) and TM6 (about 80 contacts with residues W^{293}, I^{296}, and H^{297}), Phe^4 is immersed in the same hydrophobic pocket as the phenyl group of DAMGO between TM2 (residues F^{123} and Q^{124}) and TM3 (residues V^{143} and I^{144}) (Figure 3B,D), still participating with its amidic nitrogen and water bridges to the main hydrogen bond network linking the peptide to D^{147} and Q^{124} (Figure 3D).

The Dmt^5 peptide residue mainly interacts with residues not conserved within the opiate family, that is, E^{229} and K^{233} of TM5, V^{300}, and K^{303} of TM6, and W^{318} of TM7. Movements of this ring allow an alternation of nonpolar interactions with the aliphatic chains of K^{303} (TM6) and K^{233} (TM5) (Figure 3B) and of possible π−cation interactions with the positively charged amine of both the same K residues (Figure 3E). Similarly, the amidic oxygens of Gly^3, Dmt^5, and Gly^6 alternate in H-bond or water bridge contacts with R^{211} (ECL2) and E^{229} (TM5) on two opposite sides of the receptor.

Details on the MD simulations of DAMGO and [Dmt^{1,5}]N/OFQ(1-9)-NH_2 in complex with the mu receptor are given in Figures S1 and S2, reporting the root-mean-square deviation (RMSD) analyses and clustering outcomes for each of the investigated peptides. Moreover, the RMSD analysis (Figure S3) and the representative conformation of residues 1−5 of N/OFQ(1-9)-NH_2 (purple) are shown, compared to DAMGO (yellow). MD shows that the interactions of N/OFQ(1-9)-NH_2 with TM6 are strongly diminished; in addition to the absence of polar contacts and the water density between residues 1−5 of the peptide and TM6, there are only about 20 nonpolar contacts (between Phe^1 and W^{293} and between Phe^1 and F^{236}), while both polar and nonpolar interactions with TM3 increase.

In Figure 4, the maps of hydrophobic, polar, hydrogen bond, π−π stacking, and π−cation interactions for the peptides under study are superimposed for an overall immediate comparison. The hydrophobic and polar interaction maps are widely superimposable on all peptides (Figure 4A,B), attesting the similarity of their conformation inside the orthosteric site, with an increase of nonpolar contacts between [Dmt^{1,5}]N/OFQ(1-9)-NH_2 and TM6 (I^{296}, V^{300}, and K^{303}) essentially due to the aromatic ring of Dmt^5. The N-terminus of all three peptides forms hydrogen bonds with D^{147} and Q^{124} (Figure 4C). More interestingly, according to our simulation, the H-bond contact reported in the crystal structure between the amidic oxygen of Gly^3 of DAMGO and the indole nitrogen of W^{318} is not fully stable; in the same time, the phenolic head of Tyr^1 tends to extend toward the so-called "polar cavity" between Y^{326} and W^{293} in the intracellular side (Figure S1C), with the possibility to form π-stacking with W^{293} (Figure 4D) and a H-bond besides a π−cation contact between its N-terminus and the phenol group of Y^{326}. On the other hand, the H-bond between Gly^2 of [Dmt^{1,5}]N/OFQ(1-9)-NH_2 and W^{318} remains quite stable, as reinforced by partial π-stacking between W^{318} and Dmt^5 (Figures 3E and 4D), while the Dmt^1 phenolic head, sterically hindered by the two methyl groups, does not extend toward the polar cavity. Concerning N/OFQ (1-9)-NH_2, Phe^1 has

https://doi.org/10.1021/acs.jmedchem.0c02062
J. Med. Chem. 2021, 64, 6656−6669

negligible hydrogen and water bond contacts with the inner side of the receptor, and the contacts between Phe^4, Thr^5 of the peptide and T^{218}, L^{219} of extracellular loop 2 (ECL2) are stronger (Figure 4C). The N-terminus of the three peptides can form π−cation interactions with the aromatic ring of Y^{326}, while as mentioned above, π−cation contributions due to interactions of K^{233} and K^{303} are exclusive of [Dmt^{1,5}]N/OFQ(1-9)-NH$_2$ (Figure 4E).

***In Vivo* Experiments: [Dmt^{1,5}]N/OFQ(1-13)-NH$_2$ Effect on Citric Acid-Induced Cough in the Conscious Guinea Pig.** To test the antitussive effect of [Dmt^{1,5}]N/OFQ(1-13)-NH$_2$, we used a model of cough induced by citric acid in guinea pigs. Data showed that the coadministration of [Dmt^{1,5}]N/OFQ(1-13)-NH$_2$ with citric acid did not affect the tussive response (coughs/15 min: vehicle = 17.83 ± 3.95 vs [Dmt^{1,5}]N/OFQ(1-13)-NH$_2$ 17.67 ± 1.73). However, the nebulization with [Dmt^{1,5}]N/OFQ(1-13)-NH$_2$ before (30 min) the challenge with the tussive agent significantly reduced the cough number induced by citric acid (Figure 5).

DISCUSSION

This structure activity investigation was aimed at the identification of novel peptides acting as mixed NOP/mu receptor agonists. To this aim, we substituted Phe^1 of N/OFQ(1-13)-NH$_2$ with amino acids containing a phenol moiety and Thr^5 with several proteinogenic and nonproteinogenic residues. Novel peptides were investigated in calcium mobilization experiments performed in cells expressing the human recombinant receptors and chimeric G proteins. The structure activity investigation led to the identification of the potent mixed agonist [Dmt^{1,5}]N/OFQ(1-13)-NH$_2$ whose NOP and mu agonist properties were confirmed in DMR studies. Moreover, [Dmt^{1,5}]N/OFQ(1-13)-NH$_2$ was also able to potently stimulate kappa but not delta opioid receptors. The capability of this peptide to bind the mu receptor has been also investigated in MD studies that suggested a similar active conformation for [Dmt^{1,5}]N/OFQ(1-13)-NH$_2$ and DAMGO and crucial interactions with D^{147} and H^{297}. Moreover, the binding of [Dmt^{1,5}]N/OFQ(1-13)-NH$_2$ is reinforced by additional polar interactions of Dmt^5 with K^{223} and K^{303}. Finally, [Dmt^{1,5}]N/OFQ(1-13)-NH$_2$ elicited a robust antitussive action *in vivo* in a model of cough induced by nebulization of citric acid in conscious guinea pigs.

Previous studies demonstrated that the substitution of Phe^1 in N/OFQ with Tyr reduces NOP selectivity over opioid receptors[26,42] and that Thr^5 of N/OFQ(1-13)-NH$_2$ can be substituted with different amino acids with no changes in peptide efficacy and relatively little modifications of potency.[25] Thus, we selected a series of amino acids to substitute Thr^5 in [Tyr^1]N/OFQ(1-13)-NH$_2$ in order to increase the mu receptor activity of the peptide derivatives. The results obtained with [Tyr^1]N/OFQ(1-13)-NH$_2$ derivatives were similar to those previously obtained with N/OFQ(1-13)-NH$_2$ derivatives in terms of NOP receptor activity. As far as the mu receptor is concerned, an increase in potency has been obtained with Leu, Nle, Nva, and Tyr. These results are not unexpected since Leu in position 5 is found in naturally occurring opioid ligands (Leu-enkephalin and dynorphin) and Nle (and possibly Nva) may mimic methionine, which is also present in position 5 of other endogenous opioid peptides (Met-enkephalin, beta-endorphin). In addition, the same can be said for Tyr^5, which is found in amphibian opioid peptides such as the mu-selective agonist dermorphin. Moreover, previous studies demonstrated that position 5 of enkephalin can be replaced with aromatic residues[43] or non-natural aliphatic residues[44] with no major changes of bioactivity. Interestingly, [Tyr^{1,5}]N/OFQ(1-13)-NH$_2$ displayed very similar potency at NOP and the mu opioid receptor; thus, with the aim to identify potent mixed NOP/mu agonists, further studies were performed substituting position 5 with aromatic amino acids.

Despite the investigation of 14 chemically different aromatic residues, no clear structure activity information was obtained. In fact, with the exception of hPhe^5, little changes in NOP potency were measured and the same can be said for mu receptor activity. Thus, for further studies, we selected compounds matching the following criteria: pEC$_{50}$ > 7 for the NOP receptor and >6 for the mu receptor, with NOP/mu ratio > 0.05. This let us to select Tyr, Phe, Phg, 1Nal, (pNH$_2$)Phe, and Dmt to be substituted in position 5 of [Dmt^1]N/OFQ(1-13)-NH$_2$.

The opioid receptor binding enhancing properties of Dmt in position 1[19, 27, 28] were confirmed by the present results. In fact, compared to [Tyr^1]N/OFQ(1-13)-NH$_2$, [Dmt^1]N/OFQ(1-13)-NH$_2$ displayed approximately 3-fold reduced potency at NOP associated with almost 100-fold increased potency at the mu receptor. The same pattern of effects, that is, no change or modest reduction of NOP potency associated with a large increase in mu potency was obtained with [Dmt^1]N/OFQ(1-13)-NH$_2$ derivatives substituted in position 5 with Tyr, Phe, Phg, 1Nal, and (pNH$_2$)Phe. [Dmt^{1,5}]N/OFQ(1-13)-NH$_2$ is however the exception to this rule; in fact, this peptide displayed, compared to [Tyr^1,Dmt^5]N/OFQ(1-13)-NH$_2$, increased potency at both NOP and mu receptors. This led to an NOP/mu ratio of potency of [Dmt^{1,5}]N/OFQ(1-13)-NH$_2$ near 1. Interestingly, a very similar NOP/mu ratio was displayed by [Tyr^{1,5}]N/OFQ(1-13)-NH$_2$, which was however approximately 30-fold less potent at both receptors.

The calcium mobilization assay used in the present study has been previously set up[45,46] in our laboratories and then validated by investigating a large number of NOP and opioid receptor ligands.[19,23,47] However, this assay is based on the aberrant signaling generated by the expression of chimeric G proteins; therefore, we reassessed the pharmacological effects of [Dmt^{1,5}]N/OFQ(1-13)-NH$_2$ with the DMR assay. This test measures the physiological G$_i$-dependent signaling of NOP and opioid receptors as demonstrated by its sensitivity to pertussis toxin treatment.[48,49] DMR studies confirmed the mixed mu/NOP full agonist properties of [Dmt^{1,5}]N/OFQ(1-13)-NH$_2$.

Finally, the effects of [Dmt^{1,5}]N/OFQ(1-13)-NH$_2$ at kappa and delta opioid receptors were investigated. At delta receptors, [Dmt^{1,5}]N/OFQ(1-13)-NH$_2$ displayed low potency and efficacy, while it behaved as a potent full agonist at the kappa receptor. Of note, the kappa potency of [Dmt^{1,5}]N/OFQ(1-13)-NH$_2$ was similar to that shown at NOP and mu receptors. These results were not unexpected. In fact, binding experiments performed in guinea-pig brain membranes demonstrated the following rank order of affinity for [Tyr^1]N/OFQ(1-13)-NH$_2$: NOP > mu = kappa > delta.[26] Moreover, similar results have been previously obtained in functional studies performed with human recombinant receptors with [Dmt^1]N/OFQ(1-13)-NH$_2$ that displayed the following rank order of potency: NOP = mu > kappa > delta.[19] Collectively, these findings indicate that modifications of position 1 of N/OFQ such as Tyr and Dmt are sufficient for increasing mu and kappa but not delta receptor binding. Most probably, this is due to the fact that the C-terminal portion of N/OFQ is enriched in positively charged

https://doi.org/10.1021/acs.jmedchem.0c02062
J. Med. Chem. 2021, 64, 6656−6669

residues that may favor mu and kappa interactions but are detrimental for delta receptor binding.[50]

To get insights into the mechanisms by which [Dmt^{1,5}]N/OFQ(1-13)-NH_2 binds the mu receptor, MD studies were performed using the recently solved DAMGO-mu receptor-G_i complex.[30] The results obtained with [Dmt^{1,5}]N/OFQ(1-9)-NH_2 were compared with those of DAMGO and N/OFQ(1-9)-NH_2 used as the positive and negative control, respectively. These studies show that beyond the pivotal and expected interaction between the [Dmt^{1,5}]N/OFQ(1-9)-NH_2 N-terminus and D^{147}, the phenol oxygen of Dmt^1 can make first- or second-order water bridges with H^{297} (Gln in NOP) of TM6 of the mu receptor. This is in good agreement with the observation of a water bridge between the agonist BU72 and H^{297} in the active mu receptor and other small molecules or peptide mimetic agonists of kappa and delta receptors[30] and can account for the reduction of NOP selectivity and the increase of mu potency as simply induced by the presence of the phenol groups of Tyr^1 or Dmt^1 in N/OFQ instead of the phenyl group of Phe^1. Partial $\pi-\pi$ stacking between Dmt^1 (or Tyr^1) and H297 could further contribute to peptide stabilization in the orthosteric site, thus enhancing these effects. Analogous contacts have been reported for cocrystallized mu[51] and delta[52] but not NOP[53] antagonists. Importantly, Phe^1 of the N/OFQ sequence cannot form water bridges with H^{297}, and this is most probably the reason for the lack of mu affinity of the peptide.

Interestingly, as stated above, Dmt^5 mainly interacts with residues that differ within the opiate family, that is, E^{229} (G in NOP, D in kappa and delta) and K^{233} (A in NOP) of TM5, V^{300} (I in kappa), and K^{303} (W, E, and Q in delta, kappa, and NOP receptor, respectively) of TM6, and W^{318} (L in NOP) of TM7. While the carbonyl oxygen of Dmt^5 is in water bridge contact with E^{229}, its aromatic bulky head is stacked between the aliphatic chains of K^{303} and K^{233}, making possible π−cation interactions with the positively charged amine of both lysines (Figure 3B,E). In the reported crystal structure of mu-DAMGO[30] (PDB code 6DDF), the K^{303} positive charge is found at a 3.3 Å distance of the carbonyl oxygen of N(Me)-Phe of DAMGO, compatible with a weak H-bond, whereas K^{233} does not appear to contribute to the stabilization of the mu active state induced by both DAMGO and BU72;[29] the K^{233} amine group is found covalently linked to the antagonist β-funaltrexamine in the crystal structure of the inactive mu receptor.[51] As K^{303} and K^{233} are present in the mu but not the NOP receptor, the above-mentioned interactions between Dmt^5 and the two lysine residues could contribute to explain the mu-selective increase of affinity of [Dmt^{1,5}]N/OFQ(1-13)-NH_2 compared to [Dmt^1]N/OFQ(1-13)-NH_2, thus making [Dmt^{1,5}]N/OFQ(1-13)-NH_2 a mixed mu/NOP agonist. Last, as observed along the MD runs, the indole nitrogen of W^{318} in TM7 does not interact with N/OFQ but can form H-bond contact with Gly^2 of [Dmt^{1,5}]N/OFQ(1-9)-NH_2 as well as with DAMGO (49 and 63% of the trajectory, respectively). Thus, beyond differences in steric hindrance of Tyr^1 and Dmt^1 that may generically contribute to a larger hydrophobic core for the last one, the entity of the interaction between W^{318} and Gly^2 could also contribute to explain the enhanced potency of [Dmt^{1,5}] N/OFQ(1-13)-NH_2. Data obtained from this molecular modeling investigation are in agreement with those reported by recent studies performed on a series of cyclic opioid peptides.[54]

The role of the N/OFQ-NOP receptor system has been widely reported in several biological functions at the central and peripheral levels, including the cough reflex.[4] Previous studies showed that NOP receptor agonists given centrally or peripherally suppress capsaicin and acid inhalation-induced cough in guinea pigs.[33−37] Moreover, opioid drugs are widely used as antitussive agents,[38] and inhalation of encephalin was shown to be effective in reducing cough reflex *in vivo*.[55] The novel mixed NOP/opioid agonist [Dmt^{1,5}]N/OFQ(1-13)-NH_2 showed an inhibitory activity against citric acid-induced cough in guinea pigs, thus demonstrating the *in vivo* activity of the compound. However, further studies are needed to investigate the receptor mechanism involved in the antitussive action of the molecule.

CONCLUSIONS

In this study, starting from the NOP-selective sequence of N/OFQ(1-13)-NH_2, we developed a structure activity investigation focused on positions 1 and 5. Regarding position 1, a phenol moiety is required to increase mu receptor binding, and regarding position 5, aromatic residues generated the best results in terms of similar potency at NOP and mu receptors. This study led to the identification of [Dmt^{1,5}]N/OFQ(1-13)-NH_2 as the most potent mixed peptide agonist for NOP and mu receptors so far described in the literature. MD studies shed light on the molecular mechanisms adopted by this peptide to bind the active form of the mu receptor: some features of the mode of binding of [Dmt^{1,5}]N/OFQ(1-9)-NH_2 are superimposable to those of DAMGO, that is, the ionic bond with D^{147} of TM3 and the H-bond network with H^{297} of TM6, while others are peculiar of [Dmt^{1,5}]N/OFQ(1-9)-NH_2, that is, polar interactions of Dmt^5 with K^{223} and K^{303} of TM5 and TM6, respectively.

[Dmt^{1,5}]N/OFQ(1-13)-NH_2 is a novel mixed agonist for NOP and mu receptors that exerted antitussive effects in an *in vivo* model of cough. The compound will be evaluated in future studies for its antinociceptive properties. In fact, mixed NOP/mu agonists of both peptide and nonpeptide structures have been consistently demonstrated in preclinical studies to promote antinociceptive effects similar to those of morphine being however better tolerated particularly in terms of respiratory depression, tolerance, and abuse liability.[13] Importantly, phase II and III clinical studies performed with the mixed NOP/mu agonist cebranopadol have confirmed this favorable profile in pain patients.[9,56] Nowadays, the availability of safer analgesic drugs is particularly needed for facing the opioid epidemic that leads to a progressive increase of fatal overdoses over the past 2 decades.[57]

EXPERIMENTAL SECTION

Chemistry. *Materials and Methods.* All solvents and reagents were purchased from Sigma-Aldrich and Fisher Scientific. Enantiopure Fmoc-protected amino acids and the resins for SPPS were purchased from AAPPTec. Peptides were synthesized using a standard Fmoc/*t*-butyl strategy[58] with a Syro XP multiple peptide synthesizer (MultiSynTech GmbH, Witten Germany) on a Rink amide MBHA resin (4-(2′,4′-dimethoxyphenyl-Fmoc-aminomethyl)-phenoxyacetamido-norleucyl-MBHA resin; loading 0.55 mmol/g). Fmoc-amino acids were used with a 4-fold excess on a 0.11 mM scale of the resin and coupled to the growing peptide chain using *N*,*N*′-diisopropylcarbodiimide and 1-hydroxybenzotriazole (DIC/HOBt, 4-fold excess) for 1 h at room temperature. Each Fmoc removal step was performed using 40% piperidine in *N*,*N*-dimethylformamide, and all the subsequent couplings were repeated until the desired peptide-bound resin was completed. The cleavage cocktail to obtain the peptides from the resin consisted of 95% trifluoroacetic acid, 2.5% water, and 2.5% triethylsilane, and cleavages were conducted for 3 h at room temperature. After filtration of the resin, diethyl ether was added to

https://doi.org/10.1021/acs.jmedchem.0c02062
J. Med. Chem. 2021, 64, 6656−6669

the filtrate to promote precipitation of the peptide products that were finally isolated by centrifugation. Reverse-phase purification of crude peptides was carried out on a Waters Prep 600 high-performance liquid chromatography (HPLC) system with a Jupiter column C18 (250 × 30 mm, 300 Å, 15 μm spherical particle size) using a gradient, programmed time by time, of acetonitrile/water [with 0.1% trifluoroacetic acid (TFA)] at a flow rate of 20 mL/min. Nonpeptide derivatives were purified through flash column chromatography using a Biotage System Isolera One. Analytical HPLC was performed with a Beckman 116 liquid chromatograph furnished of a UV detector. The purity of peptides in Table 1 was assessed with a Symmetry C18 column (4.6 × 75 mm, 3.5 μm particle size, SYSTEM GOLD) at a flow rate of 0.5 mL/min using a linear gradient from 100% of A (water + 0.1% TFA) to 100% of B (acetonitrile + 0.1% TFA) over a period of 25 min. The purity of peptides in Tables 2 and 3 was assessed with an Agilent Zorbax C18 column (4.6 × 150 mm, 3.5 μm particle size, KARAT32) at a flow rate of 0.7 mL/min using a linear gradient from 100% of A (water + 0.1% TFA) to 100% of B (acetonitrile + 0.1% TFA) over a period of 25 min. All final compounds were monitored at 220 nm showing ≥95% purity, and their molecular weights were confirmed using an ESI Micromass ZQ, Waters (HPLC chromatograms and ESI mass spectra of the final peptide derivatives have been reported in the Supporting Information). ^{1}H and ^{13}C NMR spectra were recorded for nonpeptide derivatives on a Varian 400 MHz instrument, and all experiments were performed in deuterated DMSO using its residual shifts as reference (s: singolet, d: doublet, dd: double doublet, t: triplet, m: multiplet).

***In Vitro* Pharmacological Studies.** *Drugs and Reagents.* [D-Pen^{2},D-Pen^{5}]enkephalin (DPDPE) and naltrexone were purchased from Tocris Bioscience (Bristol, UK). Concentrated solutions (1 mM) were made in bidistilled water and kept at −20 °C until use. The medium and reagents for cell culture were from Euroclone (Milan, Italy). Fluo-4 AM and pluronic acid were from Invitrogen/ThermoFisher Scientific (Waltham, USA). *N*-(2-Hydroxyethyl)piperazine-*N*′-ethanesulfonic acid (HEPES), probenecid, brilliant black, and bovine serum albumin (BSA) fraction V were from Sigma-Aldrich (St. Louis, USA).

Calcium Mobilization Assay. CHO cells stably coexpressing the human NOP or kappa or the mu receptor and the C-terminally modified $G_{\alpha qi5}$ and CHO cells coexpressing the delta receptor and the $G_{\alpha qG66Di5}$ protein were generated and cultured as described previously.[45,46] Cells were maintained in Dulbecco's modified Eagle's medium/nutrient mixture F-12 (DEMEM/F-12) supplemented with 10% FBS, 100 U/mL penicillin and 100 μg/mL streptomycin, 100 μg/mL hygromicin B, and 200 μg/mL G418 and cultured at 37 °C in 5% CO_2 humidified air. Cells were seeded at a density of 50,000 cells/well into 96-well black, clear-bottom plates. The following day, the cells were incubated with Hanks' balanced salt solution (HBSS) supplemented with 2.5 mM probenecid, 3 μM of the calcium-sensitive fluorescent dye Fluo-4 AM, and 0.01% pluronic acid for 30 min at 37 °C. After that time, the loading solution was aspirated and 100 μL/well of HBSS supplemented with 20 mM HEPES, 2.5 mM probenecid, and 500 μM brilliant black was added. Serial dilutions were carried out in HBSS/HEPES (20 mM) buffer (containing 0.02% BSA fraction V). After placing both plates (cell culture and master plate) into the fluorometric imaging plate reader FlexStation II (Molecular Devices, Sunnyvale, CA), fluorescence changes were measured. On-line additions were carried out in a volume of 50 μL/well. To facilitate drug diffusion into the wells, the present studies were performed at 37 °C. Maximum change in fluorescence, expressed as percent over the baseline fluorescence, was used to determine agonist response.

DMR Assay. CHO cells stably expressing the human NOP and mu receptors were kindly provided by D.G. Lambert (University of Leicester, UK). Cells were cultured in DMEM/F-12 medium supplemented with 10% FBS, 100 U/mL penicillin, 100 μg/mL streptomycin, and 2 mmol/L L-glutamine. The medium was supplemented with 400 μg/mL G418 to maintain expression. Cells were cultured at 37 °C in 5% CO_2 humidified air. For DMR measurements, the label-free EnSight Multimode Plate Reader (Perkin Elmer, MA, US) was used. Cells were seeded 15,000 cells/well in a volume of 30 μL onto fibronectin-coated 384-well DMR microplates and cultured for 20 h to obtain confluent monolayers. Cells were starved in the assay buffer (HBSS with 20 mM HEPES, 0.01% BSA fraction V) for 90 min before the test. Serial dilutions were made in the assay buffer. After reading the baseline, compounds were added in a volume of 10 μL; then, DMR changes were recorded for 60 min. Responses were described as picometer (pm) shifts over time (sec) following subtraction of values from vehicle-treated wells. Maximum picometer (pm) modification (peak) was used to generate concentration response curves. All the experiments were carried out at 37 °C.

Data Analysis and Terminology. The pharmacological terminology adopted in this paper is consistent with IUPHAR recommendations.[59] All data are expressed as the mean ± standard error of the mean (SEM) of at least three experiments performed in duplicate. For potency values, 95% confidence limits ($CL_{95\%}$) were indicated. Agonist potencies are given as pEC_{50}, that is, the negative logarithm to base 10 of the molar concentration of an agonist that produces 50% of the maximal effect of that agonist. Concentration-response curves to agonists were fitted to the classical four-parameter logistic nonlinear regression model: $\text{Effect} = \text{Baseline} + (E_{max} - \text{Baseline})/(1 + 10^{(\text{LogEC}_{50} - \text{Log[compound]}) \times \text{Hillslope}})$. Curve fitting was performed using PRISM 6.0 (GraphPad Software Inc., San Diego).

Molecular Dynamics. The setup of an *in silico* model of the nonnatural peptides [Dmt^{1,5}] N/OFQ(1-9)-NH_2 and N/OFQ(1-9)-NH_2 in complex with the human mu receptor has been described in the Supporting Information. Classical MD simulations of these two receptor-peptide complexes were performed and compared with an MD simulation of the experimental system DAMGO-mu receptor-G_i protein complex as derived by the PDB file 6DDF.[30] The GROMACS 2018.3 package[60] was used under the AMBER parm99sb force field[61] at the full atomistic level using a TIP3P water solvent and an explicit preequilibrated phospholipid bilayer of 128 POPC (1-palmitoyl-2-oleoyl-*sn*-glycero-3-phosphocholine) molecules obtained by the Prof. Tieleman website (http://moose.bio.ucalgary.ca). All the MD sessions were performed in a water−membrane system prepared as previously described.[31,32] The receptor-peptide-membrane systems were solvated in a triclinic water box (having basis vector lengths of 7, 7.4, and 9.3 nm) under periodic boundary conditions for a total number of about 45,000 atoms (6400 solvent molecules). The total charge of the system was neutralized by randomly substituting water molecules with Na^+ ions and Cl^- ions to obtain neutrality with a 0.15M salt concentration. Following a steepest descent minimization algorithm, the system was equilibrated under canonical ensemble (*NVT*) conditions for 300 ps using a V-rescale, modified Berendsen thermostat with position restrains for both the receptor-peptide complex and the lipids and thereafter in a isothermal−isobaric ensemble (*NPT*) for 500 ps, applying position restraints to the heavy atoms of the protein-peptide complex, and using a Nose−Hoover thermostat and a Parrinello-Rahman barostat at 1 atm with a relaxation time of 2.0 ps. The MD simulation of the mu receptor-DAMGO-G_i protein was carried out on the whole ternary complex without positional restraints. On the other hand, in order to reduce the computational time, in the two mu receptor-peptide complexes, the G_i protein was not included in the system, but all residues within 5 Å of the G_i protein interface were restrained to the initial structure of the activated receptor using 5.0 kcal mol^{-1} $Å^{-2}$ harmonic restraints applied to non-hydrogen atoms. Using such restraints ensures that the receptor maintains an active conformation throughout the simulation. MD runs were performed under *NPT* conditions at 300 K with a T-coupling constant of 1 ps. van der Waals interactions were modeled using a 6−12 Lennard-Jones potential with a 1.2 nm cutoff. Long-range electrostatic interactions were calculated, with a cutoff for the real space term of 1.2 nm. All covalent bonds were constrained using the LINCS algorithm. The time step employed was 2 fs, and the coordinates were saved every 5 ps for analysis.

The MD analysis of the DAMGO-mu receptor-G_i protein complex (Figure S1) shows an overall stability of the starting configuration (corresponding to the crystal structure) with some motion of the phenolic head toward the intracellular side of the receptor, still conserving the water bridge contact with H^{297}. A non-negligible rearrangement is observed (Figures S2 and S3) along the MD sessions,

https://doi.org/10.1021/acs.jmedchem.0c02062
J. Med. Chem. 2021, 64, 6656−6669

starting from the docked conformations of [Dmt^{1,5}]N/OFQ(1-9)-NH_2 and N/OFQ(1-9)-NH_2, probably due to the limitations of the docking procedures applied to molecules with a large number of torsions, and confirms the importance of performing long-lasting MD sessions. Analysis of MD trajectories was performed using state-of-the-art computational tools, as described in the Supporting Information.

Artwork. 3D images of peptide-receptor structures were obtained by the Chimera software.[62]

***In Vivo* Pharmacological Studies.** *Animals.* Guinea pigs (Dunkin Hartley, male, 400−450 g, Charles River, Milan, Italy) were used. The group size of $n = 6$ animals was determined by sample size estimation using G*Power (v3.1)[63] to detect the size effect in a post-hoc test with type 1 and 2 error rates of 5 and 20%, respectively. Allocation concealment to the vehicle(s) or treatment group was performed using a randomization procedure (http://www.randomizer.org/). The assessors were blinded to the identity (allocation to the treatment group) of the animals. Guinea pigs were housed in a temperature- and humidity-controlled vivarium (12 h dark/light cycle, free access to food and water) for at least 1 week before the start of the experiments. Cough experiments were done in a quiet, temperature-controlled (20−22 °C) room between 9 am and 5 pm and were performed by an operator blinded to the treatment. All experiments were carried out according to the European Union (EU) guidelines for animal care procedures and the Italian legislation (DLgs 26/2014) application of the EU Directive 2010/63/EU. All animal studies were approved by the Animal Ethics Committee of the University of Florence and the Italian Ministry of Health (permit #450/2019-PR) and followed the animal research reporting *in vivo* experiment (ARRIVE) guidelines.

Measurement of Cough in Conscious Guinea Pigs. Cough experiments were performed using a whole-body plethysmography system (Buxco, Wilmington, NC, USA, upgraded version 2018).[64] The apparatus consists of four plethysmographs (four transparent Perspex chambers) ventilated with a constant airflow and each provided by a nebulizing head (Aerogen) and adjustable bias flow rates for acclimation and nebulization. The particle size presents an aerodynamic mass median diameter of 6 μm, and the output of the nebulizing heads can be set in the range between 0 and 0.4 mL per minute. The number of elicited coughs was automatically counted using the instrument. The nebulization rate used in the following experiments was 0.15 mL/min, and the air flows were 1750 mL/min during the acclimation phase and 800 mL/min during nebulization. These rates were previously found in our lab to elicit a significant number of cough events in the citric acid-induced cough model.

On the day of experiments, guinea pigs were individually placed into the chambers and let to acclimate for 10 min. To test the antitussive effect of [Dmt^{1,5}]N/OFQ(1-13)-NH_2, two different protocols were used. Protocol 1: after acclimation, a mixture of [Dmt^{1,5}]N/OFQ(1-13)-NH_2 (1 mM) or its vehicle (0.9% NaCl) and the tussive agent, citric acid (0.4 M), was nebulized for 10 min. During the 10 min of nebulization and for 5 min immediately post challenge (recovery period), the number of elicited coughs was automatically recorded using the BUXCO system. Protocol 2: after acclimation, [Dmt^{1,5}]N/OFQ(1-13)-NH_2 (1 mM) or its vehicle (0.9% NaCl) was nebulized for 10 min. After 20 min of recovery, the tussive agent, citric acid (0.4 M), was delivered by aerosol via a nebulizer for 10 min. During the 10 min of the citric acid challenge and 5 min immediately post challenge (recovery period), the number of elicited coughs was automatically recorded using the BUXCO system.

For the *in vivo* experiment, the statistical significance of differences between groups was assessed using Student's *t*-test.

■ ASSOCIATED CONTENT

Supporting Information

The Supporting Information is available free of charge at https://pubs.acs.org/doi/10.1021/acs.jmedchem.0c02062.

Synthesis of Fmoc-2′,6′-dimethyltyrosine; synthetic procedures for the preparation of Fmoc-2′,6′-dimethyltyrosine; structures of nonproteinogenic amino acids; HPLC chromatograms and ESI mass spectra of the final peptide derivatives; model setup of non-natural peptides for MD; model setup of the mu receptor; model setup of the peptide-mu receptor complexes; and analysis of MD trajectories (PDF)

Molecular formula strings (CSV)

Model coordinates: representative structure of the [Dmt^{1,5}]N/OFQ(1-9)-NH_2-mu receptor complex (PDB)

Model coordinates: representative structure of the N/OFQ(1-9)NH_2-mu receptor complex (PDB)

■ AUTHOR INFORMATION

Corresponding Authors

Chiara Ruzza − *Department of Neuroscience and Rehabilitation, Section of Pharmacology, University of Ferrara, Ferrara 44121, Italy; Technopole of Ferrara, LTTA Laboratory for Advanced Therapies, Ferrara 44121, Italy*; Phone: +39-0532-455220; Email: chiara.ruzza@unife.it

Delia Preti − *Department of Chemical, Pharmaceutical and Agricultural Sciences, University of Ferrara, Ferrara 44121, Italy*; orcid.org/0000-0002-1075-3781; Phone: +39-0532-455501; Email: delia.preti@unife.it

Stefano Della Longa − *Department of Life, Health and Environmental Sciences, University of L'Aquila, L'Aquila 67100, Italy*; orcid.org/0000-0002-8157-9530; Phone: +39-0862-433568; Email: stefano.dellalonga@univaq.it

Authors

Salvatore Pacifico − *Department of Chemical, Pharmaceutical and Agricultural Sciences, University of Ferrara, Ferrara 44121, Italy*; orcid.org/0000-0002-3377-5107

Valentina Albanese − *Department of Chemical, Pharmaceutical and Agricultural Sciences, University of Ferrara, Ferrara 44121, Italy*

Davide Illuminati − *Department of Chemical, Pharmaceutical and Agricultural Sciences, University of Ferrara, Ferrara 44121, Italy*

Erika Marzola − *Department of Chemical, Pharmaceutical and Agricultural Sciences, University of Ferrara, Ferrara 44121, Italy*

Martina Fabbri − *Department of Chemical, Pharmaceutical and Agricultural Sciences, University of Ferrara, Ferrara 44121, Italy*

Federica Ferrari − *Department of Neuroscience and Rehabilitation, Section of Pharmacology, University of Ferrara, Ferrara 44121, Italy*

Victor A.D. Holanda − *Department of Neuroscience and Rehabilitation, Section of Pharmacology, University of Ferrara, Ferrara 44121, Italy*

Chiara Sturaro − *Department of Neuroscience and Rehabilitation, Section of Pharmacology, University of Ferrara, Ferrara 44121, Italy*

Davide Malfacini − *Department of Pharmaceutical and Pharmacological Sciences, University of Padova, Padova 35131, Italy*

Claudio Trapella − *Department of Chemical, Pharmaceutical and Agricultural Sciences, University of Ferrara, Ferrara 44121, Italy; Technopole of Ferrara, LTTA Laboratory for Advanced Therapies, Ferrara 44121, Italy*

Ettore Lo Cascio − *Dipartimento di Scienze Biotecnologiche di Base, Cliniche Intensivologiche e Perioperatorie, Università Cattolica del Sacro Cuore, Roma 00168, Italy*
Alessandro Arcovito − *Dipartimento di Scienze Biotecnologiche di Base, Cliniche Intensivologiche e Perioperatorie, Università Cattolica del Sacro Cuore, Roma 00168, Italy; Fondazione Policlinico Universitario A. Gemelli IRCCS, Roma 00168, Italy*
Martina Marangoni − *Department of Health Sciences, Section of Clinical Pharmacology and Oncology, University of Florence, Florence 50139, Italy*
Davide Fattori − *Department of Health Sciences, Section of Clinical Pharmacology and Oncology, University of Florence, Florence 50139, Italy*
Romina Nassini − *Department of Health Sciences, Section of Clinical Pharmacology and Oncology, University of Florence, Florence 50139, Italy*
Girolamo Calò − *Department of Pharmaceutical and Pharmacological Sciences, University of Padova, Padova 35131, Italy*
Remo Guerrini − *Department of Chemical, Pharmaceutical and Agricultural Sciences, University of Ferrara, Ferrara 44121, Italy; Technopole of Ferrara, LTTA Laboratory for Advanced Therapies, Ferrara 44121, Italy*

Complete contact information is available at: https://pubs.acs.org/10.1021/acs.jmedchem.0c02062

Notes

The authors declare the following competing financial interest(s): S.P., V.A., D.I., C.T., E.M., C.R., D.P., G.C., and R.G. are inventors of the patent application (102020000025972) focused on NOP/mu mixed agonists. G.C. and R.G. are founders of the University of Ferrara spin off company UFPeptides s.r.l., the assignee of such patent application. C.R. is CEO of UFPeptides s.r.l.

■ ACKNOWLEDGMENTS

FAR (Fondo di Ateneo per la Ricerca Scientifica) grants from the University of Ferrara support D.P., C.R., G.C., and R.G. C.R. is supported by an FIR (Fondo per l'Incentivazione alla Ricerca) grant from the University of Ferrara. S.P., F.F., D.P., G.C., and R.G. are supported by the grant PRIN 2015 (Prot. 2015WX8Y5B_002) from the Italian Ministry of Research and Education.

■ ABBREVIATIONS

CHO cells, chinese hamster ovary cells; $CL_{95\%}$, 95% confidence limits; CR, concentration ratio; crc, concentration−response curve; DAMGO, [D-Ala^2, *N*-MePhe^4, Gly-ol]-enkephalin; DIC, *N*,*N*′-diisopropylcarbodiimide; DIPEA, *N*,*N*-diisopropylethylamine; DMEM/F-12, Dulbecco's modified Eagle's medium/nutrient mixture F-12; DMR, dynamic mass redistribution; DPDPE, [D-Pen^2,D-Pen^5]enkephalin; EtOAc, ethyl acetate; FBS, fetal bovine serum; FmocCl, Fmoc chloride; HATU, hexafluorophosphate azabenzotriazole tetramethyl uronium; HBSS, Hanks' balanced salt solution; LINCS, LINear Constraint Solver; MBHA resin, 4-methylbenzhydrylamine resin; N/OFQ, nociceptin/orphanin FQ; *NPT*, isothermal−isobaric ensemble; *NVT*, canonical ensemble conditions; PWT, peptide welding technology; SEM, standard error of the mean; SPPS, solid-phase peptide synthesis

■ REFERENCES

(1) Meunier, J.-C.; Mollereau, C.; Toll, L.; Suaudeau, C.; Moisand, C.; Alvinerie, P.; Butour, J. L.; Guillemot, J. C.; Ferrara, P.; Monsarrat, B.; Mazarguil, H.; Vassart, G.; Parmentier, M.; Costentin, J. Isolation and structure of the endogenous agonist of opioid receptor-like ORL1 receptor. *Nature* **1995**, *377*, 532−535.
(2) Reinscheid, R. K.; Nothacker, H. P.; Bourson, A.; Ardati, A.; Henningsen, R. A.; Bunzow, J. R.; Grandy, D. K.; Langen, H.; Monsma, F. J., Jr.; Civelli, O. Orphanin FQ: a neuropeptide that activates an opioidlike G protein-coupled receptor. *Science* **1995**, *270*, 792−794.
(3) Toll, L.; Bruchas, M. R.; Calò, G.; Cox, B. M.; Zaveri, N. T. Nociceptin/Orphanin FQ receptor structure, signaling, ligands, functions, and interactions with opioid systems. *Pharmacol. Rev.* **2016**, *68*, 419−457.
(4) Lambert, D. G. The nociceptin/orphanin FQ receptor: a target with broad therapeutic potential. *Nat. Rev. Drug Discovery* **2008**, *7*, 694−710.
(5) Schröder, W.; Lambert, D. G.; Ko, M. C.; Koch, T. Functional plasticity of the N/OFQ-NOP receptor system determines analgesic properties of NOP receptor agonists. *Br. J. Pharmacol.* **2014**, *171*, 3777−3800.
(6) Toll, L.; Ozawa, A.; Cippitelli, A. NOP-related mechanisms in pain and analgesia. *Handb. Exp. Pharmacol.* **2019**, *254*, 165−186.
(7) Kiguchi, N.; Ko, M. C. Effects of NOP-related ligands in nonhuman primates. *Handb. Exp. Pharmacol.* **2019**, *254*, 323−343.
(8) Linz, K.; Christoph, T.; Tzschentke, T. M.; Koch, T.; Schiene, K.; Gautrois, M.; Schröder, W.; Kögel, B. Y.; Beier, H.; Englberger, W.; Schunk, S.; De Vry, J.; Jahnel, U.; Frosch, S. Cebranopadol: a novel potent analgesic nociceptin/orphanin FQ peptide and opioid receptor agonist. *J. Pharmacol. Exp. Ther.* **2014**, *349*, 535−548.
(9) Calò, G.; Lambert, D. G. Nociceptin/orphanin FQ receptor ligands and translational challenges: focus on cebranopadol as an innovative analgesic. *Br. J. Anaesth.* **2018**, *121*, 1105−1114.
(10) Ding, H.; Kiguchi, N.; Yasuda, D.; Daga, P. R.; Polgar, W. E.; Lu, J. J.; Czoty, P. W.; Kishioka, S.; Zaveri, N. T.; Ko, M.-C. A bifunctional nociceptin and mu opioid receptor agonist is analgesic without opioid side effects in nonhuman primates. *Sci. Transl. Med.* **2018**, *10*, No. eaar3483.
(11) Kiguchi, N.; Ding, H.; Cami-Kobeci, G.; Sukhtankar, D. D.; Czoty, P. W.; DeLoid, H. B.; Hsu, F.-C.; Toll, L.; Husbands, S. M.; Ko, M.-C. BU10038 as a safe opioid analgesic with fewer side-effects after systemic and intrathecal administration in primates. *Br. J. Anaesth.* **2019**, *122*, e146−e156.
(12) Chao, P. K.; Chang, H. F.; Chang, W. T.; Yeh, T. K.; Ou, L. C.; Chuang, J. Y.; Tsu-An Hsu, J.; Tao, P. L.; Loh, H. H.; Shih, C.; Ueng, S. H.; Yeh, S. H. BPR1M97, a dual mu opioid receptor/nociceptin-orphanin FQ peptide receptor agonist, produces potent antinociceptive effects with safer properties than morphine. *Neuropharmacology* **2020**, *166*, 107678.
(13) Kiguchi, N.; Ding, H.; Ko, M.-C. Therapeutic potentials of NOP and MOP receptor coactivation for the treatment of pain and opioid abuse. *J. Neurosci. Res.* **2020**, DOI: 10.1002/jnr.24624.
(14) Azzam, A. A. H.; McDonald, J.; Lambert, D. G. Hot topics in opioid pharmacology: mixed and biased opioids. *Br. J. Anaesth.* **2019**, *122*, e136−e145.
(15) Anand, J. P.; Kochan, K. E.; Nastase, A. F.; Montgomery, D.; Griggs, N. W.; Traynor, J. R.; Mosberg, H. I.; Jutkiewicz, E. M. In vivo effects of μ-opioid receptor agonist/δ-opioid receptor antagonist peptidomimetics following acute and repeated administration. *Br. J. Pharmacol.* **2018**, *175*, 2013−2027.
(16) Aceto, M. D.; Harris, L. S.; Negus, S. S.; Banks, M. L.; Hughes, L. D.; Akgun, E.; Portoghese, P. S. MDAN-21: a bivalent opioid ligand containing mu-agonist and delta-antagonist pharmacophores and its effects in rhesus monkeys. *Int. J. Med. Chem.* **2012**, *2012*, 327257.
(17) Greedy, B. M.; Bradbury, F.; Thomas, M. P.; Grivas, K.; Cami-Kobeci, G.; Archambeau, A.; Bosse, K.; Clark, M. J.; Aceto, M.; Lewis, J. W.; Traynor, J. R.; Husbands, S. M. Orvinols with mixed kappa/mu opioid receptor agonist activity. *J. Med. Chem.* **2013**, *56*, 3207−3216.

(18) Daniels, D. J.; Kulkarni, A.; Xie, Z.; Bhushan, R. G.; Portoghese, P. S. A bivalent ligand (KDAN-18) containing δ-antagonist and κ-agonist pharmacophores bridges δ2 and κ1 opioid receptor phenotypes†. *J. Med. Chem.* **2005**, *48*, 1713−1716.
(19) Molinari, S.; Camarda, V.; Rizzi, A.; Marzola, G.; Salvadori, S.; Marzola, E.; Molinari, P.; McDonald, J.; Ko, M.; Lambert, D.; Calò, G.; Guerrini, R. [Dmt^1]N/OFQ(1-13)-NH_2: a potent nociceptin/orphanin FQ and opioid receptor universal agonist. *Br. J. Pharmacol.* **2013**, *168*, 151−162.
(20) Guerrini, R.; Marzola, E.; Trapella, C.; Pelà, M.; Molinari, S.; Cerlesi, M. C.; Malfacini, D.; Rizzi, A.; Salvadori, S.; Calò, G. A novel and facile synthesis of tetra branched derivatives of nociceptin/orphanin FQ. *Bioorg. Med. Chem.* **2014**, *22*, 3703−3712.
(21) Cerlesi, M. C.; Ding, H.; Bird, M. F.; Kiguchi, N.; Ferrari, F.; Malfacini, D.; Rizzi, A.; Ruzza, C.; Lambert, D. G.; Ko, M. C.; Calò, G.; Guerrini, R. Pharmacological studies on the NOP and opioid receptor agonist PWT2-[Dmt^1]N/OFQ(1-13). *Eur. J. Pharmacol.* **2017**, *794*, 115−126.
(22) Pacifico, S.; Albanese, V.; Illuminati, D.; Fantinati, A.; Marzola, E.; Ferrari, F.; Neto, J. A.; Sturaro, C.; Ruzza, C.; Calò, G.; Preti, D.; Guerrini, R. Tetrabranched hetero-conjugated peptides as bifunctional agonists of the NOP and mu opioid receptors. *Bioconjugate Chem.* **2019**, *30*, 2444−2451.
(23) Bird, M. F.; Cerlesi, M. C.; Brown, M.; Malfacini, D.; Vezzi, V.; Molinari, P.; Micheli, L.; Mannelli, L. D. C.; Ghelardini, C.; Guerrini, R.; Calò, G.; Lambert, D. G. Characterisation of the novel mixed mu-NOP peptide ligand dermorphin-N/OFQ (DeNo). *PLoS One* **2016**, *11*, No. e0156897.
(24) Lapalu, S.; Moisand, C.; Mazarguil, H.; Cambois, G.; Mollereau, C.; Meunier, J.-C. Comparison of the structure-activity relationships of nociceptin and dynorphin A using chimeric peptides. *FEBS Lett.* **1997**, *417*, 333−336.
(25) Guerrini, R.; Marzola, E.; Trapella, C.; Pacifico, S.; Cerlesi, M. C.; Malfacini, D.; Ferrari, F.; Bird, M. F.; Lambert, D. G.; Salvadori, S.; Calò, G. Structure activity studies of nociceptin/orphanin FQ(1-13)-NH_2 derivatives modified in position 5. *Bioorg. Med. Chem.* **2015**, *23*, 1515−1520.
(26) Varani, K.; Rizzi, A.; Calò, G.; Bigoni, R.; Toth, G.; Guerrini, R.; Gessi, S.; Salvadori, S.; Borea, P. A.; Regoli, D. Pharmacology of [Tyr^1]nociceptin analogs: receptor binding and bioassay studies. *Naunyn-Schmiedeberg's Arch. Pharmacol.* **1999**, *360*, 270−277.
(27) Yamamoto, T.; Nair, P.; Largent-Milnes, T. M.; Jacobsen, N. E.; Davis, P.; Ma, S.-W.; Yamamura, H. I.; Vanderah, T. W.; Porreca, F.; Lai, J.; Hruby, V. J. Discovery of a potent and efficacious peptide derivative for δ/μ opioid agonist/Neurokinin 1 antagonist activity with a 2′,6′-dimethyl-l-tyrosine: In vitro, In vivo, and NMR-Based Structural Studies. *J. Med. Chem.* **2011**, *54*, 2029−2038.
(28) Giri, A. K.; Apostol, C. R.; Wang, Y.; Forte, B. L.; Largent-Milnes, T. M.; Davis, P.; Rankin, D.; Molnar, G.; Olson, K. M.; Porreca, F.; Vanderah, T. W.; Hruby, V. J. Discovery of novel multifunctional ligands with μ/δ opioid agonist/Neurokinin-1 (NK1) antagonist activities for the treatment of pain. *J. Med. Chem.* **2015**, *58*, 8573−8583.
(29) Huang, W.; Manglik, A.; Venkatakrishnan, A. J.; Laeremans, T.; Feinberg, E. N.; Sanborn, A. L.; Kato, H. E.; Livingston, K. E.; Thorsen, T. S.; Kling, R. C.; Granier, S.; Gmeiner, P.; Husbands, S. M.; Traynor, J. R.; Weis, W. I.; Steyaert, J.; Dror, R. O.; Kobilka, B. K. Structural insights into μ-opioid receptor activation. *Nature* **2015**, *524*, 315−321.
(30) Koehl, A.; Hu, H.; Maeda, S.; Zhang, Y.; Qu, Q.; Paggi, J. M.; Latorraca, N. R.; Hilger, D.; Dawson, R.; Matile, H.; Schertler, G. F. X.; Granier, S.; Weis, W. I.; Dror, R. O.; Manglik, A.; Skiniotis, G.; Kobilka, B. K. Structure of the μ-opioid receptor-Gi protein complex. *Nature* **2018**, *558*, 547−552.
(31) Della Longa, S.; Arcovito, A. "In silico" study of the binding of two novel antagonists to the nociceptin receptor. *J. Comput.-Aided Mol. Des.* **2018**, *32*, 385−400.
(32) Della Longa, S.; Arcovito, A. Microswitches for the activation of the nociceptin receptor induced by cebranopadol: hints from microsecond molecular dynamics. *J. Chem. Inf. Model.* **2019**, *59*, 818−831.
(33) McLeod, R. L.; Bolser, D. C.; Jia, Y.; Parra, L. E.; Mutter, J. C.; Wang, X.; Tulshian, D. B.; Egan, R. W.; Hey, J. A. Antitussive effect of nociceptin/orphanin FQ in experimental cough models. *Pulm. Pharmacol. Ther.* **2002**, *15*, 213−216.
(34) McLeod, R. L.; Jia, Y.; Fernandez, X.; Parra, L. E.; Wang, X.; Tulshian, D. B.; Kiselgof, E. J.; Tan, Z.; Fawzi, A. B.; Smith-Torhan, A.; Zhang, H.; Hey, J. A. Antitussive profile of the NOP agonist Ro-64-6198 in the guinea pig. *Pharmacology* **2004**, *71*, 143−149.
(35) McLeod, R. L.; Tulshian, D. B.; Ho, G. D.; Fernandez, X.; Bolser, D. C.; Parra, L. E.; Zimmer, J. C.; Erickson, C. H.; Fawzi, A. B.; Jayappa, H.; Lehr, C.; Erskine, J.; Smith-Torhan, A.; Zhang, H.; Hey, J. A. Effect of a novel NOP receptor agonist (SCH 225288) on guinea pig irritant-evoked, feline mechanically induced and canine infectious tracheobronchitis cough. *Pharmacology* **2009**, *84*, 153−161.
(36) McLeod, R. L.; Parra, L. E.; Mutter, J. C.; Erickson, C. H.; Carey, G. J.; Tulshian, D. B.; Fawzi, A. B.; Smith-Torhan, A.; Egan, R. W.; Cuss, F. M.; Hey, J. A. Nociceptin inhibits cough in the guinea-pig by activation of ORL1 receptors. *Br. J. Pharmacol.* **2001**, *132*, 1175−1178.
(37) Lee, M.-G.; Undem, B. J.; Brown, C.; Carr, M. J. Effect of nociceptin in acid-evoked cough and airway sensory nerve activation in guinea pigs. *Am. J. Respir. Crit. Care Med.* **2006**, *173*, 271−275.
(38) Gibson, P. G.; Ryan, N. M. Cough pharmacotherapy: current and future status. *Expert Opin. Pharmacother.* **2011**, *12*, 1745−1755.
(39) Wang, X.; Niu, S.; Xu, L.; Zhang, C.; Meng, L.; Zhang, X.; Ma, D. Pd-catalyzed dimethylation of tyrosine-derived picolinamide for synthesis of (S)-N-Boc-2,6-dimethyltyrosine and its analogues. *Org. Lett.* **2017**, *19*, 246−249.
(40) Bryant, S. D.; Jinsmaa, Y.; Salvadori, S.; Okada, Y.; Lazarus, L. H. Dmt and opioid peptides: a potent alliance. *Biopolymers* **2003**, *71*, 86−102.
(41) Fenalti, G.; Giguere, P. M.; Katritch, V.; Huang, X.-P.; Thompson, A. A.; Cherezov, V.; Roth, B. L.; Stevens, R. C. Molecular control of δ-opioid receptor signalling. *Nature* **2014**, *506*, 191−196.
(42) Shimohigashi, Y.; Hatano, R.; Fujita, T.; Nakashima, R.; Nose, T.; Sujaku, T.; Saigo, A.; Shinjo, K.; Nagahisa, A. Sensitivity of opioid receptor-like receptor ORL1 for chemical modification on nociceptin, a naturally occurring nociceptive peptide. *J. Biol. Chem.* **1996**, *271*, 23642−23645.
(43) Morley, J. S. Structure-activity relationships of enkephalin-like peptides. *Annu. Rev. Pharmacol. Toxicol.* **1980**, *20*, 81−110.
(44) Ndong, D. B.; Blais, V.; Holleran, B. J.; Proteau-Gagne, A.; Cantin-Savoie, I.; Robert, W.; Nadon, J. F.; Beauchemin, S.; Leduc, R.; Pineyro, G.; Guerin, B.; Gendron, L.; Dory, Y. L. Exploration of the fifth position of leu-enkephalin and its role in binding and activating delta (DOP) and mu (MOP) opioid receptors. *Pept. Sci.* **2019**, *111*, No. e24070.
(45) Camarda, V.; Calò, G. Chimeric G proteins in fluorimetric calcium assays: experience with opioid receptors. *Methods Mol. Biol.* **2013**, *937*, 293−306.
(46) Camarda, V.; Fischetti, C.; Anzellotti, N.; Molinari, P.; Ambrosio, C.; Kostenis, E.; Regoli, D.; Trapella, C.; Guerrini, R.; Severo, S.; Calò, G. Pharmacological profile of NOP receptors coupled with calcium signaling via the chimeric protein Gαqi5. *Naunyn-Schmiedeberg's Arch. Pharmacol.* **2009**, *379*, 599−607.
(47) Rizzi, A.; Cerlesi, M. C.; Ruzza, C.; Malfacini, D.; Ferrari, F.; Bianco, S.; Costa, T.; Guerrini, R.; Trapella, C.; Calò, G. Pharmacological characterization of cebranopadol a novel analgesic acting as mixed nociceptin/orphanin FQ and opioid receptor agonist. *Pharmacol. Res. Perspect.* **2016**, *4*, No. e00247.
(48) Codd, E. E.; Mabus, J. R.; Murray, B. S.; Zhang, S. P.; Flores, C. M. Dynamic mass redistribution as a means to measure and differentiate signaling via opioid and cannabinoid receptors. *Assay Drug Dev. Technol.* **2011**, *9*, 362−372.
(49) Malfacini, D.; Simon, K.; Trapella, C.; Guerrini, R.; Zaveri, N. T.; Kostenis, E.; Calò, G. NOP receptor pharmacological profile - A dynamic mass redistribution study. *PLoS One* **2018**, *13*, No. e0203021.
(50) Schwyzer, R. Molecular mechanism of opioid receptor selection. *Biochemistry* **1986**, *25*, 6335−6342.

https://doi.org/10.1021/acs.jmedchem.0c02062
J. Med. Chem. 2021, 64, 6656−6669

(51) Manglik, A.; Kruse, A. C.; Kobilka, T. S.; Thian, F. S.; Mathiesen, J. M.; Sunahara, R. K.; Pardo, L.; Weis, W. I.; Kobilka, B. K.; Granier, S. Crystal structure of the μ-opioid receptor bound to a morphinan antagonist. *Nature* **2012**, *485*, 321−326.
(52) Granier, S.; Manglik, A.; Kruse, A. C.; Kobilka, T. S.; Thian, F. S.; Weis, W. I.; Kobilka, B. K. Structure of the δ-opioid receptor bound to naltrindole. *Nature* **2012**, *485*, 400−404.
(53) Thompson, A. A.; Liu, W.; Chun, E.; Katritch, V.; Wu, H.; Vardy, E.; Huang, X.-P.; Trapella, C.; Guerrini, R.; Calò, G.; Roth, B. L.; Cherezov, V.; Stevens, R. C. Structure of the nociceptin/orphanin FQ receptor in complex with a peptide mimetic. *Nature* **2012**, *485*, 395−399.
(54) Stefanucci, A.; Dimmito, M. P.; Macedonio, G.; Ciarlo, L.; Pieretti, S.; Novellino, E.; Lei, W.; Barlow, D.; Houseknecht, K. L.; Streicher, J. M.; Mollica, A. Potent, efficacious, and stable cyclic opioid peptides with long lasting antinociceptive effect after peripheral administration. *J. Med. Chem.* **2020**, *63*, 2673−2687.
(55) Adcock, J. J. Peripheral opioid receptors and the cough reflex. *Respir. Med.* **1991**, *85*, 43−46.
(56) Tzschentke, T. M.; Linz, K.; Koch, T.; Christoph, T. Cebranopadol: A novel first-in-class potent analgesic acting via NOP and opioid receptors. *Handb. Exp. Pharmacol.* **2019**, *254*, 367−398.
(57) Volkow, N. D.; Blanco, C. The changing opioid crisis: development, challenges and opportunities. *Mol. Psychiatry* **2021**, *26*, 218−233.
(58) Benoiton, N. L. *Chemistry of Peptide Synthesis*; Taylor & Francis: London, 2006; pp 125−155.
(59) Neubig, R. R.; Spedding, M.; Kenakin, T.; Christopoulos, A. International union of pharmacology committee on receptor nomenclature and drug classification. XXXVIII. Update on terms and symbols in quantitative pharmacology. *Pharmacol. Rev.* **2003**, *55*, 597−606.
(60) Abraham, M. J.; Murtola, T.; Schulz, R.; Páll, S.; Smith, J. C.; Hess, B.; Lindahl, E. GROMACS: High performance molecular simulations through multi-level parallelism from laptops to supercomputers. *SoftwareX* **2015**, *1*−*2*, 19−25.
(61) Hornak, V.; Abel, R.; Okur, A.; Strockbine, B.; Roitberg, A.; Simmerling, C. Comparison of multiple Amber force fields and development of improved protein backbone parameters. *Proteins* **2006**, *65*, 712−725.
(62) Pettersen, E. F.; Goddard, T. D.; Huang, C. C.; Couch, G. S.; Greenblatt, D. M.; Meng, E. C.; Ferrin, T. E. UCSF Chimera? A visualization system for exploratory research and analysis. *J. Comput. Chem.* **2004**, *25*, 1605−1612.
(63) Faul, F.; Erdfelder, E.; Lang, A.-G.; Buchner, A. G*Power 3: a flexible statistical power analysis program for the social, behavioral, and biomedical sciences. *Behav. Res. Methods* **2007**, *39*, 175−191.
(64) Belvisi, M. G.; Patel, H. J.; Freund-Michel, V.; Hele, D. J.; Crispino, N.; Birrell, M. A. Inhibitory activity of the novel CB2 receptor agonist, GW833972A, on guinea-pig and human sensory nerve function in the airways. *Br. J. Pharmacol.* **2008**, *155*, 547−557.

https://doi.org/10.1021/acs.jmedchem.0c02062
J. Med. Chem. 2021, 64, 6656−6669

Inorganic Chemistry

pubs.acs.org/IC

Article

Thermodynamic Stability and Speciation of Ga(III) and Zr(IV) Complexes with High-Denticity Hydroxamate Chelators

Yuliya Toporivska, Andrzej Mular, Karolina Piasta, Małgorzata Ostrowska, Davide Illuminati, Andrea Baldi, Valentina Albanese, Salvatore Pacifico, Igor O. Fritsky, Maurizio Remelli, Remo Guerrini, and Elzbieta Gumienna-Kontecka*

Cite This: *Inorg. Chem.* 2021, 60, 13332−13347

Read Online

ACCESS | Metrics & More | Article Recommendations | Supporting Information

ABSTRACT: Increasing attention has been recently devoted to ^{89}Zr(IV) and ^{68}Ga(III) radionuclides, due to their favorable decay characteristics for positron emission tomography (PET). In the present paper, a deep investigation is presented on Ga(III) and Zr(IV) complexes with a series of tri-(**H_3L1**, **H_3L3**, **H_3L4** and desferrioxamine E, **DFOE**) and tetrahydroxamate (**H_4L2**) ligands. Herein, we describe the rational design and synthesis of two cyclic complexing agents (**H_3L1** and **H_4L2**) bearing three and four hydroxamate chelating groups, respectively. The ligand structures allow us to take advantage of the macrocyclic effect; the **H_4L2** chelator contains an additional side amino group available for a possible further conjugation with a biomolecule. The thermodynamic stability of Ga(III) and Zr(IV) complexes in solution has been measured using a combination of potentiometric and pH-dependent UV−vis titrations, on the basis of metal−metal competition. The Zr(IV)-**H_4L2** complex is characterized by one of the highest formation constants reported to date for a tetrahydroxamate zirconium chelate (log β = 45.9, pZr = 37.0), although the complex-stability increase derived from the introduction of the fourth hydroxamate binding unit is lower than that predicted by theoretical calculations. Solution studies on Ga(III) complexes revealed that **H_3L1** and **H_4L2** are stronger chelators in comparison to DFOB. The complex stability obtained with the new ligands is also compared with that previously reported for other hydroxamate ligands. In addition to increasing the library of the thermodynamic stability data of Ga(III) and Zr(IV) complexes, the present work allows new insights into Ga(III) and Zr(IV) coordination chemistry and thermodynamics and broadens the selection of available chelators for ^{68}Ga(III) and ^{89}Zr(IV).

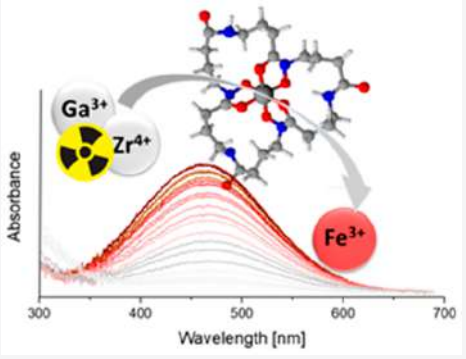

INTRODUCTION

Recent research confirms an increasing interest in the use of gallium and zirconium radioiosotopes for medical diagnostic techniques such as PET or single-photon emission computed tomography (SPECT).[1−8]

The interest in the use of ^{68}Ga ($t_{1/2}$ = 1.13 h, $E_{\beta+avg}$ = 830 keV, 89%) for clinical PET comes from the accessibility of its production via an easily portable and long-lived ^{68}Ge/^{68}Ga generator system.[9] The favorable decay characteristics of ^{89}Zr ($t_{1/2}$ = 78.4 h, $E_{\beta+avg}$ = 395.5 keV, 23%) allow high PET image resolution to be obtained, since the sufficiently long half-life is an optimal match for the pharmacokinetics of most monoclonal antibodies.[10]

To be applied to molecular imaging, the metal isotope must be converted into a radiolabeled probe that can specifically reach the target of interest *in vivo* and remain there long enough to be detected. Therefore, the metal ion must be bound by an efficient chelator to overcome metal hydrolysis and transchelation, and linked to a biologically active targeting molecule, to be properly directed to the desirable molecular target *in vivo*.

To the best of our knowledge, the most widely used chelator for ^{68}Ga is 1,4,7,10-tetraazacyclododecane-1,4,7,10-tetraacetic acid (DOTA).[11] In 2016 the FDA approved a ^{68}Ga-DOTATATE (NETSPOT) kit for the preparation of a ^{68}Ga-DOTATATE injection;[12] clinical trials revealed the superiority of ^{68}Ga-DOTATATE with respect to ^{111}In-pentetreotide in imaging neuroendocrine tumors.[13] Currently, the most successfully used ^{89}Zr(IV) chelator is DFOB, but some decomposition has been observed over time *in vivo*, and ^{89}Zr slowly accumulates in bones.[14−16]

Many chelators have been already suggested for ^{68}Ga and ^{89}Zr on the basis of *in vivo* assays.[14,17−23] While scientists are currently devoting considerable efforts toward the design of

Received: June 2, 2021
Published: August 20, 2021

https://doi.org/10.1021/acs.inorgchem.1c01622
Inorg. Chem. 2021, 60, 13332−13347

Scheme 1. Structures of the Ligands Investigated and Discussed in This Paper

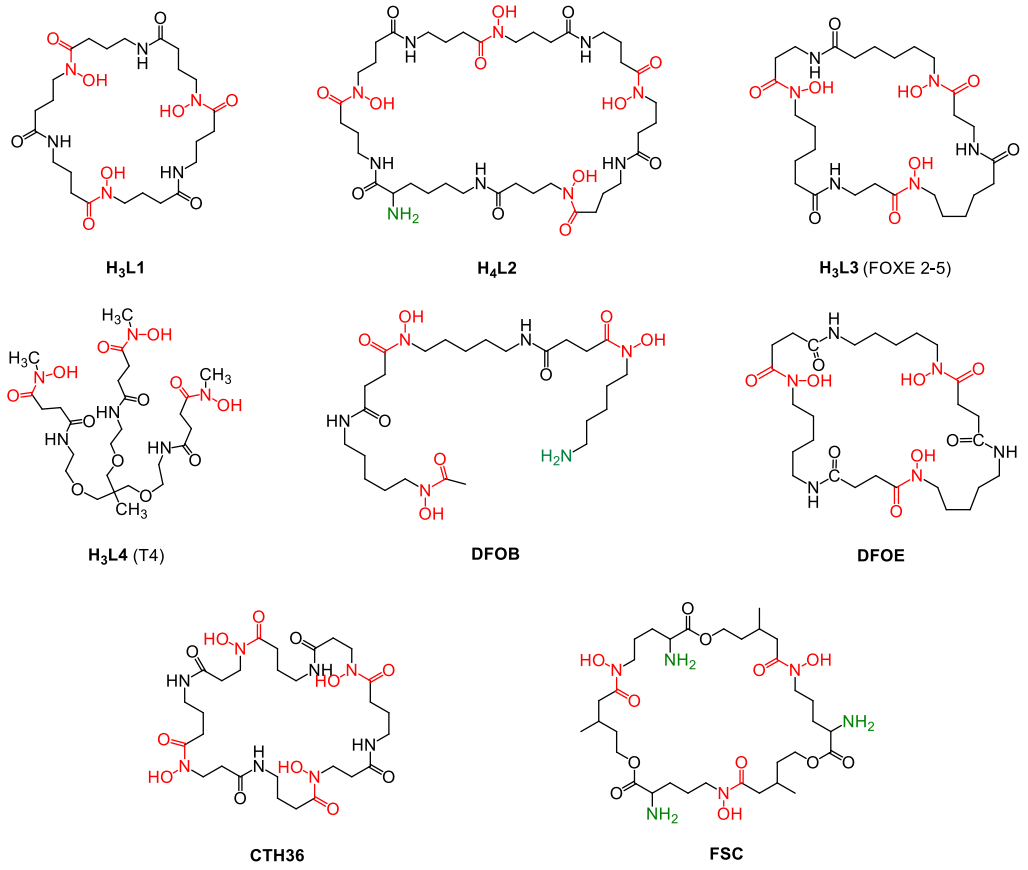

more efficient ^{89}Zr and ^{68}Ga chelators by increasing the *in vivo* stability of the corresponding complexes, the solution equilibrium chemistry, especially of Zr(IV) systems, has still rarely been investigated.[2,24−27] Solution studies on the coordination chemistry and formation constants of Zr(IV) complexes are not trivial for several reasons: an extremely high thermodynamic stability (requiring application of indirect competition methods with the use of other strong ligands with known stability constants), strong hydrolysis (occurring over almost the entire pH range), and the lack of spectral activity of the complexes. On the other hand, knowledge of the speciation of such complexes, especially at physiological pH, could provide information concerning the actual chemical form of the complex in biological media, and this can contribute to both a better understanding of the *in vivo* speciation and an explanation of the differences in the biological activity.

Our laboratory has recently reported the thermodynamic properties of Zr(IV)-DFOB complexes, suggesting the formation of three mononuclear complexes, i.e. $[ZrHL]^{2+}$ $[ZrL]^{+}$, and $[ZrLH_{-1}]$, over the pH range 1−11.[24] The stability constants and pZr value determined for the Zr(IV)-DFOB system place DFOB among the best Zr(IV) chelators, although the formation of six-coordinate unsaturated complexes (i.e., with the coordination sphere of Zr(IV) completed by two water molecules[28] or hydroxide ligands[29]) and the susceptibility of coordinated water molecules to deprotonation were suggested to be the reason for the *in vivo* lability of ^{89}Zr(IV)-DFOB complexes. The thermodynamic stability of Zr(IV)-DFOB complexes is in line with *in vivo* research[15,16,30,31] and also with Holland's recent DFT calculations,[32] indicating that our experimental approach was appropriate.

By capitalizing upon our earlier works on siderophore mimics,[33−36] in this work we have designed, synthesized, and fully characterized tri- and tetrahydroxamic **H_3L1** and **H_4L2** chelators (Scheme 1), analogues of **DFOE**,[37] and their Ga(III) and Zr(IV) complexes. In addition, the physicochemical properties of Zr(IV) complexes with three further trihydroxamic ligands, i.e. **H_3L3** (FOXE 2-5),[38] **H_3L4** (T4),[35] and **DFOE** (Scheme 1), were also investigated for the sake of comparison. The ligands employed here were selected to investigate the influence of some structural elements on the physicochemical properties of Zr(IV) complexes: i.e., (i) the number of binding groups required to complete the coordination sphere of the metal cation; (ii) the possible advantage of the macrocyclic effect; (iii) the size of the ligand cavity, which should be large enough to minimize ring strain; (iv) the symmetry of the ligand, which could limit the probability of a complex challenge. Ga(III) (and Fe(III)) binding to all of these ligands was also performed and will be discussed here, as the relation between the ligand structure and the stability of the complexes has been much more studied and is better understood for trivalent metal ions. Moreover, Fe(III) complexes are used as a tool to determine the thermodynamic stability of Ga(III) and Zr(IV) analogues.

According to DFT studies, to minimize the ring strain, the cyclic tetrahydroxamic ligand should consist of a minimum of 36 atoms, which gives at least 7 chemical groups or 8 bonds.[39,40] The tetrahydroxamic ligand **H_4L2**, designed to completely saturate the oxophilic coordination sphere of Zr(IV), meets this criterion, possessing at least 9 bonds

https://doi.org/10.1021/acs.inorgchem.1c01622
Inorg. Chem. 2021, 60, 13332−13347

Scheme 2. Synthetic Pathway of the Ligand H_3L1[a]

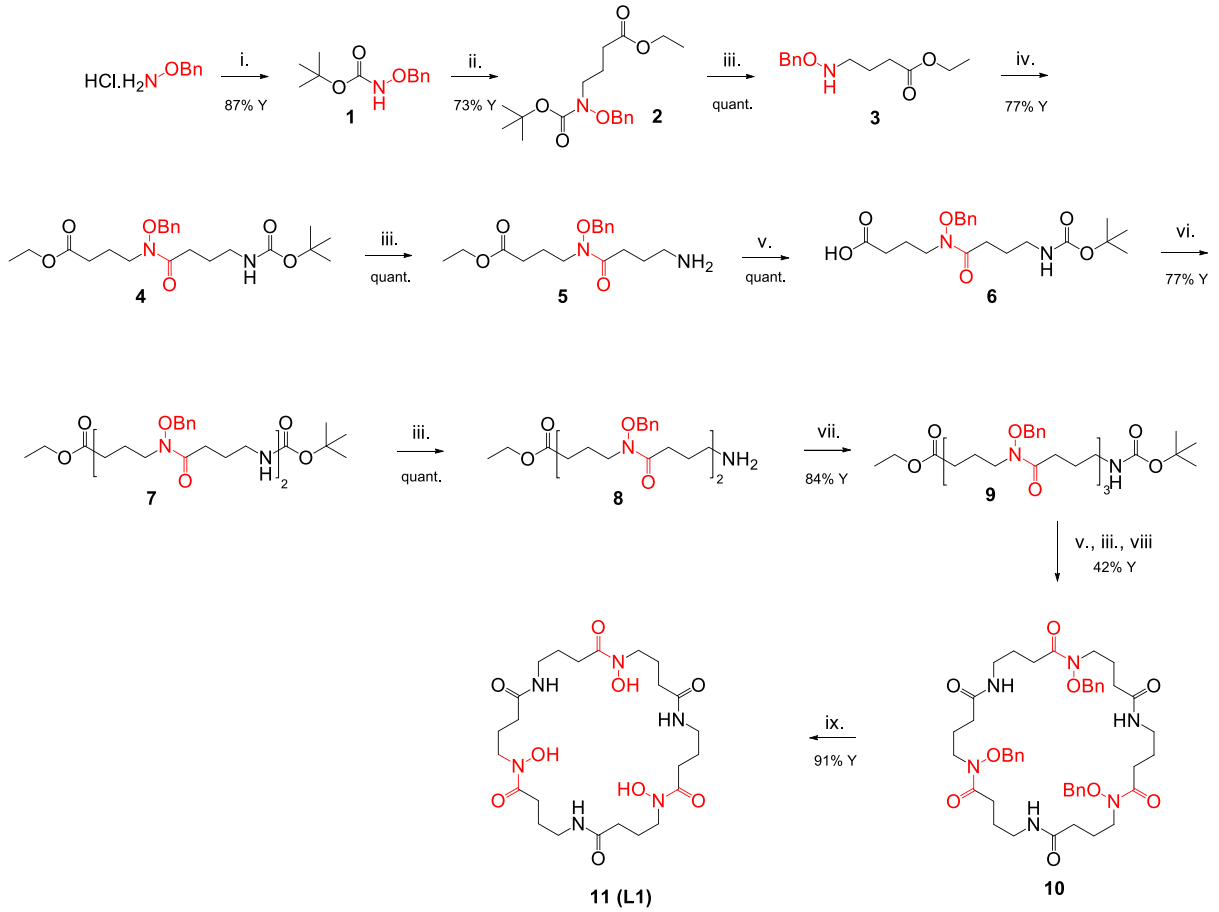

[a]Reagents and conditions: (i) $(Boc)_2O$, K_2CO_3, H_2O/dioxane; (ii) ethyl 4-bromobutyrate, NaH, DMF; (iii) TFA; (iv) Boc-γ-aminobutyric acid, HATU, DIPEA, DMF; (v) LiOH, H_2O/dioxane; (vi) **5**, HATU, DIPEA, DMF; (vii) **6**, HATU, DIPEA, DMF; (viii) HATU, DIPEA, DMF; (ix) H_2, Pd/C, MeOH.

between binding groups. Of note, H_4L2 has been designed with the aim of introducing in the chelator a primary amine group, useful to improve the solubility of the ligand but, primarily, to allow the easy conjugation of the chelator to a targeting molecule for future *in vivo* studies. Trihydroxamic H_3L1 is a symmetrical, macrocyclic ligand, comprising 9 bonds between binding groups; it allows the determination and direct comparison of the influence of the fourth binding group of H_4L2 on Zr(IV) stability. This ligand also reveals the effect of the shortening of the chain in comparison to **DFOE**, H_3L3, and DFOB, all with 10 bonds (Scheme 1). Tripodal H_3L4, used earlier as a good mimic of a ferrichrome siderophore, was investigated here in order to compare its Zr(IV) binding capacity to those of other tri- and tetrahydroxamic ligands.[35] In H_3L1, H_4L2, and H_3L3[38] we have used retrohydroxamic units, with a reversed order with respect to the native hydroxamic moiety.

Until now, the stability constants for tetrahydroxamate Zr(IV) complexes have only been estimated from computational calculations[32] for linear DFO* ($\log \beta_{[Zr(DFO^*)]} = 51.56$) and cyclic CTH36 ($\log \beta_{[Zr(CTH36)]} = 52.84$). DFO*[41] and CTH36[39] possess 10 and 8 bonds between two hydroxamic groups, respectively.

Therefore, an experimental verification of the order of the stability increase between tri- and tetrahydroxamic chelators should be very useful. The same is true for examining the effects of a number of other variable structural elements, such as the symmetry of the structure and the length of the chain between the hydroxamate binding units. Although the thermodynamic formation constants do not predict *in vivo* stability and kinetic inertness, they are very useful and interesting parameters that may allow for a better design of efficient chelators for Zr(IV) ions.

RESULTS AND DISCUSSION

Design and Synthesis of the Ligands. The synthetic approaches for the preparation of H_3L1 and H_4L2 are depicted in Schemes 2 and 3, respectively. The hydroxamate-based monomers protected either at the carboxylic group as an ethyl ester (**5**) or at the amino function with Boc (**6**) were employed as common synthetic precursors of H_3L1 and H_4L2. The building blocks **5** and **6** were synthesized by starting from *O*-benzylhydroxylamine hydrochloride that was first reacted with di-*tert*-butyl dicarbonate to give compound **1** and then alkylated with ethyl 4-bromobutyrate in the presence of NaH to provide compound **2** (Scheme 2). Boc removal with TFA furnished the intermediate **3**, which was coupled with Boc-protected γ-aminobutyric acid using HATU as a coupling reagent. This allowed us to obtain the orthogonally protected **4** as a suitable precursor of both **5** and **6**, which were alternatively isolated after acidic and basic treatments, respectively.

https://doi.org/10.1021/acs.inorgchem.1c01622
Inorg. Chem. 2021, 60, 13332−13347

Scheme 3. Synthetic Pathway of the Ligand H_4L2[a]

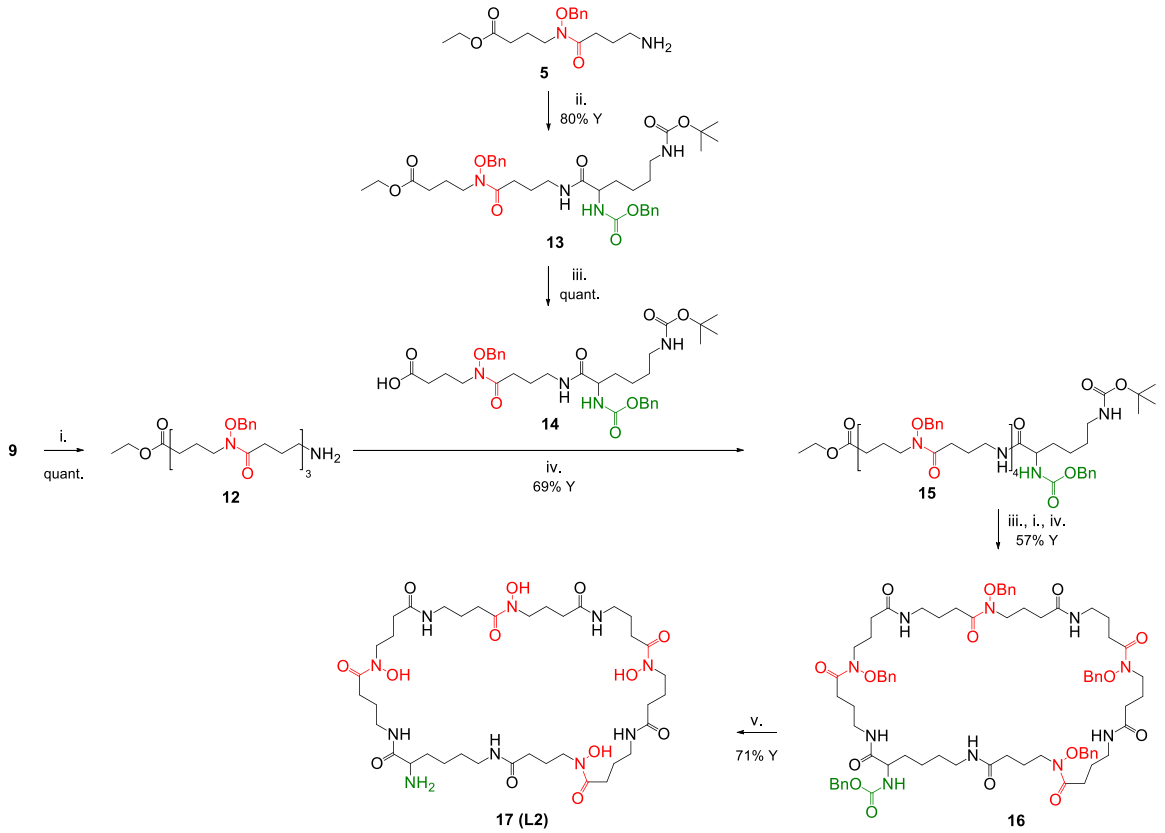

[a]Reagents and conditions: (i) TFA; (ii) Z-Lys(Boc)-OH, HATU, DIPEA, DMF; (iii) LiOH, H_2O/dioxane; (iv) HATU, DIPEA, DMF; (v) H_2, Pd/C, MeOH.

For the synthesis of H_3L1, **5** and **6** were linked together via a standard amide coupling followed by TFA treatment to give **8**. The reaction with another unit of **6** gave **9** as the linear protected precursor of H_3L1. A head−tail HATU-mediated cyclization of **9** was realized under dilute conditions (0.5 mg/mL) after removal of the protection at the C and N terminal positions. A final Pd-catalyzed hydrogenolysis afforded the desired macrocycle H_3L1 in good yields.

For the synthesis of the tetrahydroxamic derivative H_4L2 (Scheme 3), an appropriate hydroxamate-bearing lysine derivative was first prepared as a building block (**14**). This was obtained by a coupling reaction between **5** and a residue of Z-Lys(Boc)-OH followed by saponification of the ester function. The monomeric unit **14** was coupled to **12**, which resulted from TFA-mediated Boc deprotection of **9**. The resulting intermediate **15** underwent head−tail HATU-mediated cyclization after removal of the protections at the C and N terminal positions as described above, leading to **16**. In addition in this case, the final macrocycle was obtained after Pd-catalyzed removal of the benzyl functions from the hydroxamic groups. These conditions led also to CBz cleavage, leaving the free amino group suitable for future bioconjugation strategies.

H_3L1, H_4L2, and their precursors were fully characterized by ^1H and ^{13}C NMR (see the Supporting Information). The degree of purity of the final product was evaluated by analytical HPLC assays (see the Supporting Information), showing a purity of higher than 95%.

Thermodynamic Solution Studies. *Ligand Protonation Constants.* The metal affinity of a ligand depends on its acid−base properties; therefore, the protonation equilibria of H_3L1 and H_4L2 were first investigated. The proton-dissociation processes of the ligands were followed by potentiometric titrations in the pH range 2−11. The hydrolytic stability of the ligands was monitored by a second titration of the same sample with NaOH, following back-acidification of the initially titrated sample. The recorded titration curves were almost exactly superimposed; consequently, the protonation constants calculated from the two consecutive titrations were found to be equal within 0.05 log unit, which indicated that no decomposition occurred.

Data analysis allowed the determination of three protonation constants for H_3L1 and four protonation constants for H_4L2; all of them fall in the pH range 8−10 and can be attributed to the hydroxamate groups (Table 1). For each ligand, the protonation constants were assigned by comparing them with the known protonation constants of hydroxamate ligands.[24,35,37,42] When the changes in temperature, ionic strength, and ligand structures are allowed for, the protonation constants of H_3L1 and H_4L2 are in excellent agreement with the literature values of the cyclic hydroxamate siderophore **DFOE** (log K_1 = 9.89, log K_2 = 9.42, and log K_3 = 8.65) reported by Anderegg et al.[37] The pH-dependent UV−vis titrations of H_3L1 and H_4L2 (Figure S1) revealed the development of a strong band with λ_{max} = 230 nm, when the pH was increased from 7 to 11, which is usually observed for a hydroxamic group deprotonation process.[24,43] The amino group protonation of H_4L2 was not detectable in the

https://doi.org/10.1021/acs.inorgchem.1c01622
Inorg. Chem. 2021, 60, 13332−13347

Table 1. Protonation Constants of Ligands and log β Values of Complexes Formed with Fe(III), Ga(III), and Zr(IV)[a] Ions

	H_3L1		H_4L2		H_3L3 (FOXE 2−5)[38,b]		H_3L4 (T4)[35,c]		DFOE[36,38,b]	
assignt	log β	log K	log β	log K	log β	log K	log β	log K	log β	log K
LH	9.89(1)[d]	9.89[d]	10.06(1)[d]	10.06[d]	9.89	9.89	9.50	9.50	9.89	9.89
LH_2	19.13(1)[d]	9.24[d]	19.65(1)[d]	9.59[d]	19.31	19.31	18.47	8.97	19.31	9.42
LH_3	27.44(1)[d]	8.31[d]	28.59(1)[d]	8.94[d]	27.96	27.96	26.73	8.26	27.96	8.65
LH_4			36.77(1)[d]	8.18[d]						
	H_3L1		H_4L2		H_3L3 (FOXE 2−5)[38,b]		H_3L4 (T4)[35,c]		DFOE[36,38,b]	
	log β	pK_a	log β	pK_a	log β	pK_a	log β	pK_a	log β	pK_a
$[FeH_2L]$			39.96(3)[e]	3.00[d] 3.12[d]						
[FeHL]	31.80(3)[e]	3.21[d] 3.1[d]	36.96(7)[e] 36.82(6)[d]				29.82	2.48		
[FeL]	28.59(2)[e] 28.7(1)[d]				32.43	32.43	27.34		32.43	
$[GaH_2L]$			38.11(3)[f]	2.20[d] 2.15(4)[e]						
[GaHL]	29.44(7)[f]	2.65[d] 2.53(2)[e]	35.91(7)[d]	8.13[d]			27.92(3)[f]	2.36[d] 2.24(1)[e]		
[GaL]	26.79(2)[d]	9.79[d]	27.60(6)[d]		29.79	29.79	25.56(1)[d]		29.79	
[ZrHL]			45.9(3)[f]	2.6[d] 2.2(1)[e]			36.4(5)[f]	2.15[d] 2.2(2)[e]		
[ZrL]	34.8(2)[f]	5.48[d] 5.34(5)[e]	43.3(1)[d]		35.46(5)[f]	7.03[d] 7.2(1)[e]	34.25(5)[d]	5.43[d] 5.5(2)[e]	35.54(9)[f]	
$[ZrLH_{-1}]$	29.32(8)[d]				28.31(7)[d]		28.8(1)[d]			

[a]Charges omitted for clarity. [b]The protonation constants of the ligands together and the stability constants of Fe(III) and Ga(III) complexes were taken from the literature. [c]The protonation constants of the ligands and the stability constants of Fe(III) complexes were taken from the literature. [d]Determined by potentiometric titrations. [e]Determined by pH-dependent UV−vis titrations. [f]Determined by metal−metal competition titrations; all measurements performed at 25 °C and I = 0.1 M $NaClO_4$.

experimental pH range. We are aware that the electron-withdrawing character of both the $-NH_3^+$ and −NHOH groups affects the acidity of the other group in comparison with that in the related nonsubstituted compound **H_3L1**. As was previously reported in the example of α- and β-alanine hydroxamic acids, the amino group may be more acidic than the hydroxamic group, or vice versa. According to the literature, the amino group may be more acidic than hydroxamic one, or vice versa.[44,45] On the basis of the protonation constant of the amino group of DFOB (log K_{amine} = 10.97[24]), we assume for **H_4L2** that it is >11. However, we keep in mind that the deprotonation processes of amino and hydroxamate groups overlap and cannot be distinguished by potentiometry. To elucidate the protonation microequilibria of **H_4L2**, ^{1}H NMR titrations should be carried out. However, such a precise analysis is not needed for the determination of the stability of **H_4L2**-metal complexes and therefore was not performed. The species distribution diagrams of **H_3L1** and **H_4L2** are presented in Figure S2. The protonation constants of **H_3L3** and **H_3L4** were reported elsewhere (Table 1).[35,38]

ESI-MS: Stoichiometry Evaluation. The stoichiometry of the complexes was evaluated by ESI-MS, frequently used as the first step in the determination of metal complex stoichiometry and already previously employed.[35,46,47] When the fact that ESI-MS is not able to distinguish the ionizable protons in the species is taken into account, this method can be successfully applied to evaluate the metal to ligand stoichiometry directly from the m/z values. For all of the investigated systems, an analysis of the ESI-MS data (collected for various metal to ligand molar ratios) revealed only mononuclear complexes (for details see Figure S3 and Table S1 in the Supporting Information).

Determination of Complex Stability. To evaluate the thermodynamic stability of Ga(III) and Zr(IV) complexes of the investigated ligands, the binding properties and speciation of Fe(III) complexes have first been determined (all the details are given in the Supporting Information). There are several reasons for this protocol. First, (i) the electron configuration of Ga(III) (d^{10}) and Zr(IV) (d^0) hinders the attainment of spectral information for most of the complexes. Furthermore, (ii) both metal ions are highly acidic and they are readily hydrolyzed over almost the entire pH range. In addition, (iii) the high charge to size ratio of the Zr(IV) ion implies the formation of complexes with an exceptional thermodynamic stability (already at very low pH); as a consequence, the stability constants cannot be directly determined using standard potentiometric titrations. Thus, the thermodynamic stability constants of the Fe(III)-**H_3L1** and Fe(III)-**H_4L2** systems were first determined (using a combination of potentiometric and pH-dependent UV−vis titrations), followed by Fe(III)−Ga(III) and Fe(III)−Zr(IV) metal−metal competition experiments. Of importance, in order to get accurate results, an experiment where two metal ions compete for a ligand must fulfill two basic requirements: (i) one of the metal chelates should have a strong absorption band in teither he visible or ultraviolet region of the spectrum, with an extinction coefficient much different from that of the free metal ion, while the second metal complex should not absorb in the same region of the spectrum; (ii) the equilibrium constant for the competition reaction must not be too small or too large.

https://doi.org/10.1021/acs.inorgchem.1c01622
Inorg. Chem. 2021, 60, 13332−13347

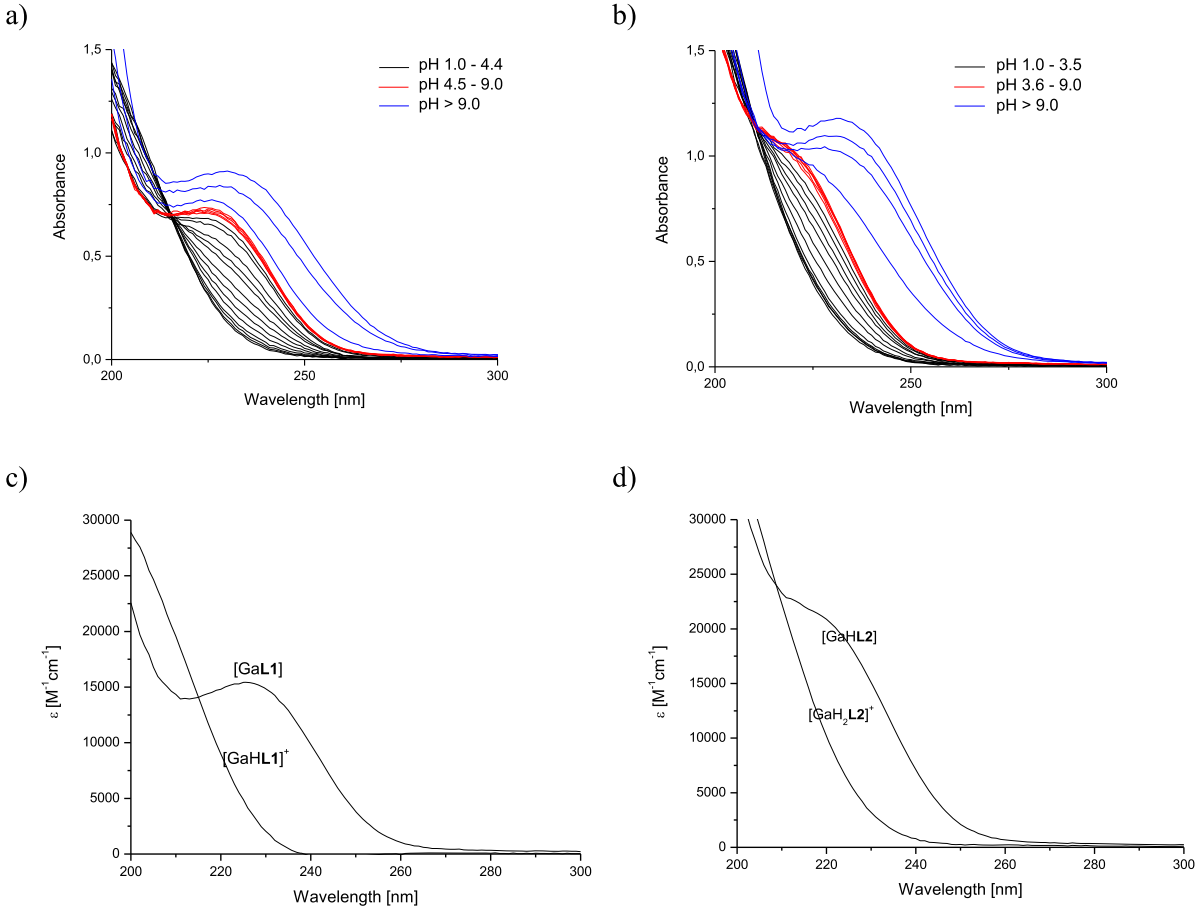

Figure 1. UV spectra of Ga(III)-$\mathbf{H_3L1}$ (a, c) and Ga(III)-$\mathbf{H_4L2}$ (b, d) systems at a metal to ligand molar ratio of 1:1 in the pH range 1.0−11.0. Conditions: c_{L1} = 0.05 mM, c_{L2} = 0.05 mM, 0.1 M $NaClO_4$, T = 25 °C.

These requirements are fulfilled in the competition experiments between Fe(III) and Ga(III) for both ligands. In the case of Fe(III)−Zr(IV) competition, the difference between the stability constants of Fe(III) and Zr(IV) complexes was too high; thus, an additional competitor ligand—nitrilotriacetic acid (NTA)—was used in the titrations.

NTA is one of the most widely investigated and often used chelating agents.[48,49] It was selected for the current studies, as both Zr(IV)-NTA and Fe(III)-NTA complexes remain stable until pH 4, even at a metal to ligand molar ratio of 1:1.[27,48] Moreover, as an additional competing agent, NTA prevents the hydrolysis of the metal ions present in solution and weakens the transchelation observed in the case of $\mathbf{H_3L1}$ and $\mathbf{H_4L2}$ Fe(III) complexes titrated directly by Zr(IV) ions. The accuracy of the metal−metal competition titration with NTA was checked on the Zr(IV)-DFOB system, for which experimental data gave log $\beta_{[ZrHDFOB]}$ = 46.1(2) (see the Supporting Information), in very good agreement with our recently reported data (log $\beta_{[ZrHDFOB]}$ = 47.7, allowing for changes in the ionic strength).[24] Similar competition procedures are widely used for the evaluation of the stability constants of spectroscopically blind metal complexes.[25,50]

Ga(III) Complex Formation Equilibria. The evaluation of thermodynamic stability constants of Ga(III) and Zr(IV) complexes with $\mathbf{H_3L1}$, $\mathbf{H_4L2}$, and $\mathbf{H_3L4}$ started from pH-dependent UV−vis spectrophotometric titrations in the pH range 1−11 (Figure 1 and Figure S7, respectively). The spectral changes in the 200−300 nm range, corresponding to the hydroxamate group protonation state, were monitored.[51] The appearance of a band with a maximum at 225−230 nm with an increase in pH was observed and associated with complex formation.

The pH-dependent UV−vis titration experiments for the Ga(III)-$\mathbf{H_3L1}$ system revealed an increase in a 230 nm transition band starting from pH 1 up to pH 4.4, with pK_a = 2.53(2) (Figure 1 and Table 1). For the Ga(III)-$\mathbf{H_4L2}$ system, the 225 nm band development was observed starting from pH 1 up to pH 3.5, with pK_a = 2.15(4) (Figure 1 and Table 1), while for Ga(III)-$\mathbf{H_3L4}$, it continued to increase up to pH 4.6 with pK_a = 2.36(1) (Figure S7 and Table 1). Similar behavior was observed in the acidic range for Ga(III)-DFOB (and was assigned to two protonation constants of the complex, pK_{a1} = 0.78 and pK_{a2} = 1.10[43]) and Th(IV)-DFOB (with pK_a = 1.9[42]) complexes. For the three investigated systems, UV spectra did not reveal any additional changes up to pH 9, indicating that the fully coordinated complex [Ga**L**], in the case of the Ga(III)-$\mathbf{H_3L1}$ and Ga(III)-$\mathbf{H_3L4}$ systems, and the monoprotonated $[GaH\mathbf{L2}]^+$ complex, in the Ga(III)-$\mathbf{H_4L2}$ system, are the dominant species in solution. When the pH was increased to above 9, an increase in absorbance below 240 nm was observed (Figure 1 and Figure S7). Considering that the spectrophotometric titrations of the free ligands showed the same absorption curves at higher pH, we can suppose that the sharp band at 230−240 nm arises from unbound deprotonated hydroxamate chromophores. Most probably, at higher pH the complex is dissociated, yielding the hydrolyzed gallium species

https://doi.org/10.1021/acs.inorgchem.1c01622
Inorg. Chem. 2021, 60, 13332−13347

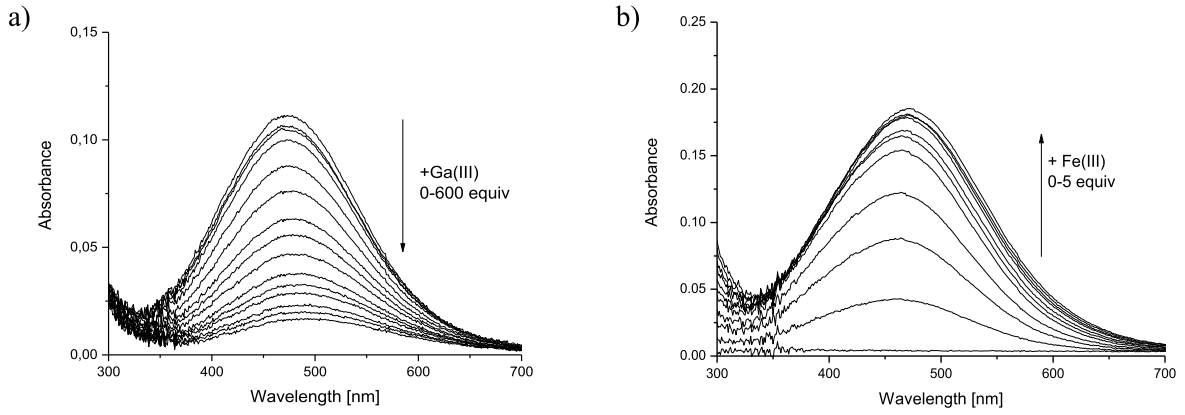

Figure 2. UV−vis metal−metal competition experiment for (a) Fe(III)-$\mathbf{H_3L1}$+Ga(III) ($c_{Fe(III)}$ = 0.075 mM, c_L = 0.075 mM) and (b) Ga(III)-$\mathbf{H_3L1}$+Fe(III) ($c_{Fe(III)}$ = 0.08 mM, c_{L1} = 0.08 mM) systems at pH 1.5, I = 0.1 M ($NaClO_4$), and T = 25 °C.

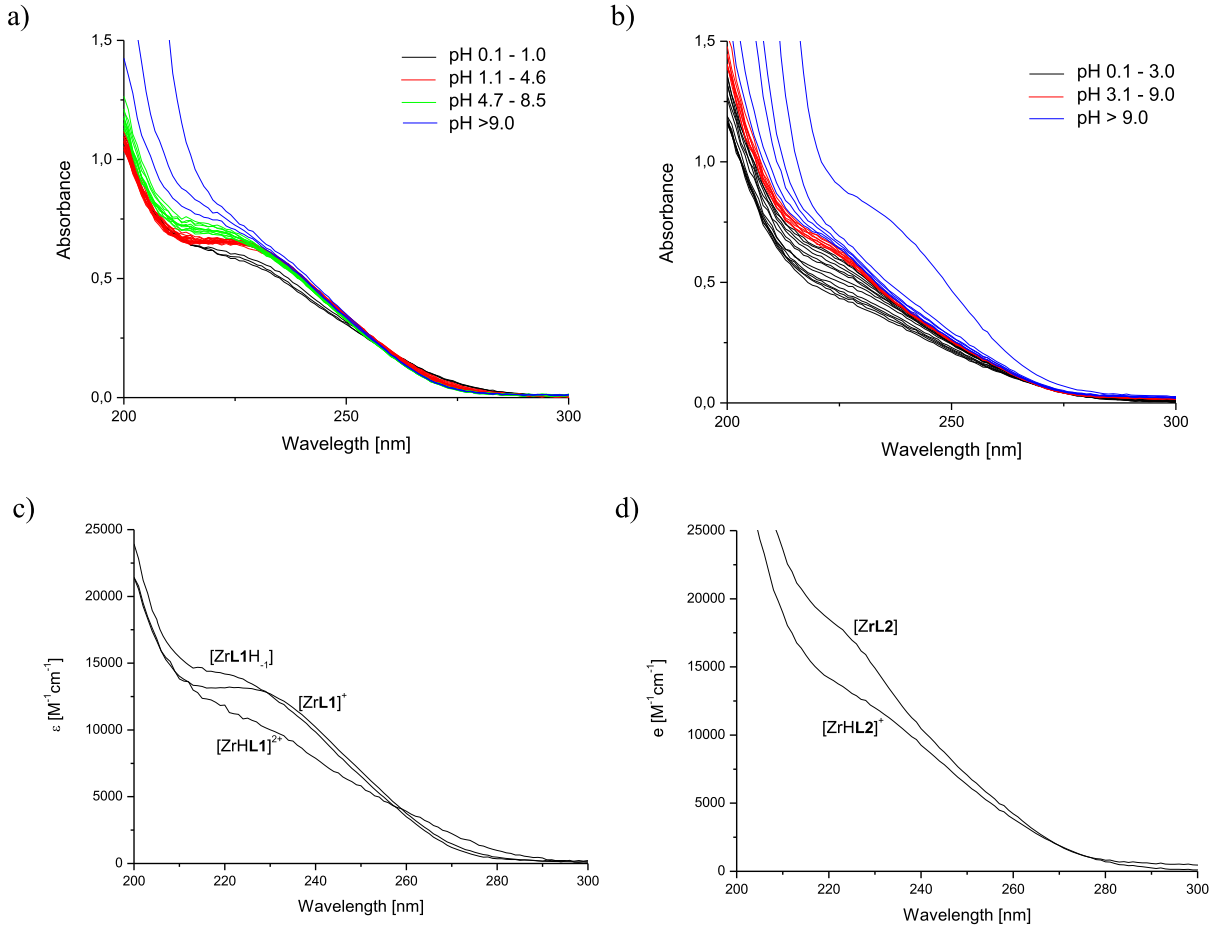

Figure 3. UV spectra of the Zr(IV)-$\mathbf{H_3L1}$ (a, c) and Zr(IV)-$\mathbf{H_4L2}$ (b, d) systems at a metal to ligand molar ratio of 1:1 in the pH range 0.1−11 Conditions: c_{L1} = 0.05 mM, c_{L2} = 0.037 mM, 0.1 M $NaClO_4$.

$[Ga(OH)_4]^-$. A similar observation has already been noted for hydroxamate ligands.[43,52]

Assuming the domination of the $[GaH\mathbf{L1}]^+$ complex below pH 2, its stability was determined by metal−metal competition titrations, (i) Fe(III)-$\mathbf{H_3L1}$ + Ga(III) and (ii) Ga(III)-$\mathbf{H_3L1}$ + Fe(III), both performed at pH 1.5. This pH was chosen in order to prevent the hydrolysis of the free metal ions and decomposition of the ligand, which is common for hydroxamic acids at a very acidic pH.[37,51] Upon addition of Ga(III) (up to 600 equiv) to the Fe(III)-$\mathbf{H_3L1}$ solution, the UV−vis band of $[FeH\mathbf{L1}]^+$ (λ_{max} = 470 nm, Figure 2a) slowly disappeared as a result of the $[GaH\mathbf{L1}]^+$ complex formation. In the next competition experiment, the appearance of an LMCT transition band (λ_{max} = 470 nm) upon addition of Fe(III) to the Ga(III)-$\mathbf{H_3L1}$ solution was observed (Figure 2b). The data refinement using $\mathbf{H_3L1}$ protonation constants (Table 1), Fe(III)-$\mathbf{H_3L1}$ stability constants (Table 1), and stability constants of hydroxocomplexes of both metals (see the Experimental Section) yielded a log $\beta_{[GaHL1]^+}$ value of 29.44(7) for Fe(III)-$\mathbf{H_3L1}$ + Ga(III) (Table 1) and of

https://doi.org/10.1021/acs.inorgchem.1c01622
Inorg. Chem. 2021, 60, 13332−13347

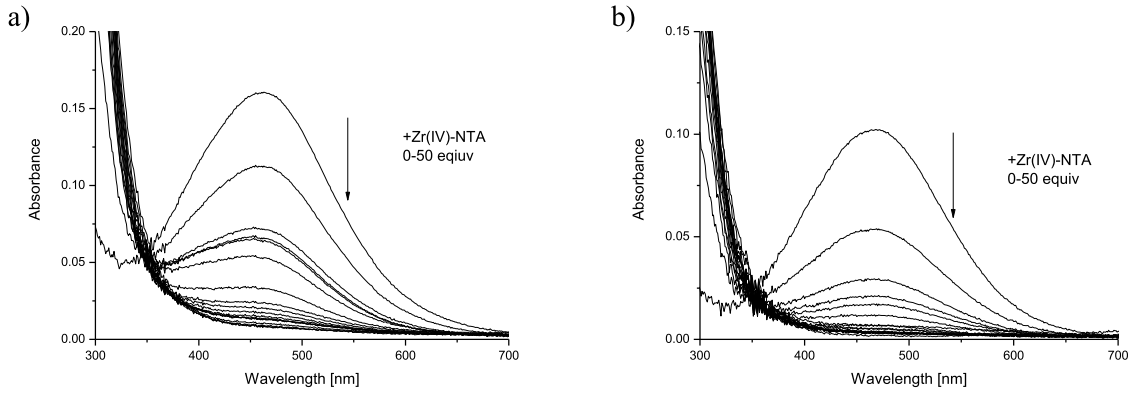

Figure 4. UV−vis spectra of competition titrations of the Fe(III)-$\mathbf{H_3L1}$ + Zr(IV)-NTA ($c_{Fe(III)}$ = 0.098 mM, c_{L1} = 0.098 mM) (a) and Fe(III)-$\mathbf{H_4L2}$ + Zr(IV)-NTA ($c_{Fe(III)}$ = 0.055 mM, c_{L2} = 0.055 mM) (b) systems at pH 1.5 with 0.1 M $NaClO_4$.

28.3(6) in the case of Ga(III)-$\mathbf{H_3L1}$ + Fe(III) competition titrations.

For the Ga(III)-$\mathbf{H_4L2}$ system, $[GaH_2\mathbf{L2}]^+$ was assumed to be the most abundant species at pH 1.5, and its stability was again determined via (i) Fe(III)-$\mathbf{H_4L2}$ + Ga(III) and (ii) Ga(III)-$\mathbf{H_4L2}$ + Fe(III) titrations (Figure S8). The refinement of the titration data yielded log $\beta_{[GaH_2L2]^+}$ = 38.11(3) and 39.06(4) for Fe(III)-$\mathbf{H_4L2}$ + Ga(III) and Ga(III)-$\mathbf{H_4L2}$ + Fe(III) competition titrations, respectively.

For the Ga(III)-$\mathbf{H_3L4}$ system, $[GaH\mathbf{L4}]^+$ was assumed to be the major complex at pH 1.5, and its stability was determined via an Fe(III)-$\mathbf{H_3L4}$ + Ga(III) competition titration (Figure S9). The refinement of the titration data yielded log $\beta_{[GaHL4]^+}$ = 27.92(3).

For the Ga(III)-$\mathbf{H_3L1}$ and Ga(III)-$\mathbf{H_4L2}$ systems, the constants obtained with the two types of titrations are not far from each other but are significantly different. Most likely, the constants measured by means of Ga(III)-$\mathbf{H_3L1}$/$\mathbf{H_4L2}$ + Fe(III) competition experiments are endowed with a greater error, attributable to the overlapping absorption of free iron, present in excess. Therefore, we retained the constants obtained from the Fe(III)-$\mathbf{H_3L1}$/$\mathbf{H_4L2}$ + Ga(III) competition experiments (log $\beta_{[GaHL1]^+}$ = 29.44(7) and log $\beta_{[GaH_2L2]^+}$ = 38.11(3)) as fixed values in the subsequent potentiometric data calculations. The best-fitted speciation model for Ga(III)-$\mathbf{H_3L1}$ and Ga(III)-$\mathbf{H_3L4}$ systems revealed the presence of one additional complex, [Ga**L**], with log β values of 26.79(2) and 25.56(1), respectively (pK_{a1} = 2.65 for Ga(III)-$\mathbf{H_3L1}$ and 2.36 for Ga(III)-$\mathbf{H_3L4}$; Table 1). For the Ga(III)-$\mathbf{H_4L2}$ system, in addition to $[GaH_2\mathbf{L2}]^+$, $[GaH\mathbf{L2}]$ and $[Ga\mathbf{L2}]^-$ complexes were found with log $\beta_{[GaHL2]}$ = 35.91(7) and log $\beta_{[GaL2]^-}$ = 27.60(6) (pK_{a1} = 2.20 and pK_{a2} = 8.13; Table 1). The pK_{a2} value of 8.13 is in good agreement with the pK_a values of the free ligand (Table 1) and could be assigned to the deprotonation of an unbound hydroxamate group.

Zr(IV) Complex Formation Equilibria. The UV−vis titrations of Zr(IV)-$\mathbf{H_3L1}$ equimolar solution over the pH range 0.1−11 (Figure 3a,c) showed a well-defined absorbance band in the 200−300 nm range. The significant changes and the presence of an isosbestic point observed when the pH was increased from 0.1 to 0.9, allowed us to calculate a pK_{a1} value of 0.4(2); afterward, the observed 230 nm shoulder remained stable up to pH 4.6. When the pH was increased to 7.0, the development of a 220 nm shoulder with an isosbestic point at 230 nm was observed, characterized by pK_{a2} = 5.34(5). From pH 7.0, the spectra do not reveal any significant changes until pH 9.0, where the hydrolysis probably started. Since information about hydrolysis of the hydroxamate ligands at acidic pH has beenwidely described in the literature,[51,52] pK_{a1} = 0.4 indicates that the three hydroxamate groups are dissociated and therefore most probably bound to the Zr(IV) ion, already at pH <2.0. Assuming the formation of only monomeric complexes, the stability of $[Zr\mathbf{L1}]^+$ was determined via UV−vis competition batch experiments, using a Zr(IV)-NTA solution as a competing system for the Fe(III)-$\mathbf{H_3L1}$ complex (Figure 4a). The large LMCT band centered at 470 nm characteristic of dihydroxamate $[FeH\mathbf{L1}]^+$ species decreased gradually, and the refinement of the titration data, using the Fe(III)-$\mathbf{H_3L1}$ stability constants (Table 1) together with the Fe(III) and Zr(IV) hydrolysis constants, yielded a log $\beta_{[ZrL1]^+}$ value of 34.8(2).

The UV−vis titration data of the Zr(IV)-$\mathbf{H_4L2}$ system (Figure 3b,d) showed the development of a 230 nm shoulder upon an increse in pH from 0.1 to 3.0 and allowed us to calculate a pK_a value of 2.2(1). Further, the spectra did not reveal any significant changes over the pH range 3.1−9.0, wherethe hydrolysis probably started. $[ZrH\mathbf{L2}]^+$ was assumed to be the major complex at pH 1.5, and its stability was determined via Fe(III)-$\mathbf{H_4L2}$ + Zr(IV)-NTA (Figure 4b) competition titrations. The refinement of the titration data yielded log $\beta_{[ZrHL2]^+}$ = 45.9(3).

The UV−vis spectra of the Zr(IV)-$\mathbf{H_3L3}$ and Zr(IV)-$\mathbf{H_3L4}$ systems were very similar to the spectra described above (Figure S11); at a pH of around 7 a slight blue shift of the 230 nm band appeared together with the isosbestic point, allowing us to calculate pK_a = 7.2(1) for Zr(IV)-$\mathbf{H_3L3}$ and 5.5(2) for Zr(IV)-$\mathbf{H_3L4}$ (Table 1). For Zr(IV)-$\mathbf{H_3L4}$, an additional pK_a = 2.2(2) was calculated, probably corresponding to the formation of the three-hydroxamate complex (Table 1). An evaluation of the competition titration data for Fe(III)-$\mathbf{H_3L3}$ + Zr(IV)-NTA revealed log $\beta_{[ZrL3]^+}$ = 35.46(5), while for Fe(III)-$\mathbf{H_3L4}$ + Zr(IV)-NTA log $\beta_{[ZrHL4]^{2+}}$ = 36.4(5) (Figure S12 and Table 1). Additionally, we have performed the same kind of titration for Fe(III)-**DFOE** + Zr(IV)-NTA, which gave log $\beta_{[ZrDFOE]^+}$ = 35.54(9) (Figure S12 and Table 1). It is worth noting that, during the competition titrations for the $\mathbf{H_3L3}$ ligand and **DFOE**, a decrease in the 430 nm (typical for three-hydroxamate iron complexes) band was observed, confirming that all three hydroxamate groups are bound already at pH <2.[38]

https://doi.org/10.1021/acs.inorgchem.1c01622
Inorg. Chem. 2021, 60, 13332−13347

Using the constants obtained from competition titrations (log $\beta_{[ZrL1]^+}$ = 34.8(2) and log $\beta_{[ZrHL2]^+}$ = 45.9(3)) as fixed values, the potentiometric data were processed. The best-fitted speciation models revealed the presence of one additional complex for the Zr(IV)-**H_3L1** system ([Zr**L1**H_{-1}], log $\beta_{[ZrL1H_{-1}]}$ = 29.32(8)) and one additional complex for the Zr(IV)-**H_4L2** system ([Zr**L2**], log $\beta_{[ZrL2]}$ = 43.3(1)) (Table 1).

The $[ZrL1]^+$ complex dominates the solution from pH 3 up to pH ∼5, where its deprotonation to [Zr**L1**H_{-1}] occurs, with pK_a = 5.48 (Figure S13a). These results are in line with the spectroscopic data (pK_a = 5.34(5)) and could be ascribed to the dissociation of a water molecule from the coordination sphere of the Zr(IV) ion. For the Zr(IV)-EDTA system, the pK_a attributed to the deprotonation of a water molecule is 6.2,[27] while for Zr(VI)-DFOB it is 6.36.[24]

The stability constants calculated for the Zr(IV)-**H_4L2** system reveal pK_a = 2.6, which is in good agreement with the spectroscopic data (pK_a = 2.2(1)) and could be assigned to the deprotonation of the hydroxamic group and the formation of a fully coordinated tetrahydroxamate complex. The [Zr**L2**] complex dominates the solution from pH 3 up to pH ∼9, when the dissociation of the complex probably occurs (Figure S13b).

An evaluation of the potentiometric data of Zr(IV)-**H_3L3** (with log $\beta_{[ZrL3]}$ = 35.46 fixed) revealed the presence of an additional complex, [Zr**L3**H_{-1}] (log $\beta_{[ZrL3H_{-1}]}$ = 28.35(5)) (Figure S13c), while for Zr(IV)-**H_3L4** (with log $\beta_{[ZrHL4]}$ = 36.4 fixed), there are two additional complexes, [Zr**L4**] (log $\beta_{[ZrL4]}$ = 34.25(5)) and [Zr**L4**H_{-1}] (log $\beta_{[ZrL4H_{-1}]}$ = 28.8(1)) (Figure S13d). For both systems, the pK_a values calculated from potentiometric experiments are in excellent agreement with those from the pH-dependent UV−vis titrations (Table 1) and match the data obtained for the whole series of hydroxamate-based ligands. Of importance, the pK_a value attributed to the deprotonation of a water molecule in the Zr(IV)-**H_3L3** system (pK_a = 7.2) is higher than those for Zr(VI)-DFOB (pK_a = 6.36)[24] and Zr(IV)-**H_3L1** (pK_a = 5.48), suggesting that a longer linker between the binding groups is advantageous. In Zr(IV)-**H_3L4**, this process is not observed, as all the coordinating positions of the Zr(IV) ion are occupied by four hydroxamate ligands.

Ligand Sequestering Ability. Despite a large variety of PET chelators synthesized and tested in order to provide strong coordination of Ga(III) and Zr(IV) *in vivo*, until now it is has been hard to avoid the release of these metal ions in the body. Here we report two new Ga(III) and Zr(IV) hydroxamate chelators, designed to achieve an efficient sequestering of these metal ions but also to understand how the cyclization and the introduction of an additional hydroxamate group influences the stability of Zr(IV) complexes. Therefore, it is important to evaluate and compare the Ga(III)- and Zr(IV)-sequestering abilities of **H_3L1** and **H_4L2** with those of other chelators. However, the direct comparison of the stability constants of metal complexes is not straightforward, and other tools taking into account all the physicochemical properties of the ligands, i.e. their denticity, coordination modes, and acid−base properties, should be used.[52] In order to reliably compare the chelating abilities of **H_3L1** and **H_4L2** toward Ga(III) and Zr(IV) ions, the pM values were calculated. pFe was originally introduced by Raymond for the comparison of iron-siderophore systems;[53] pGa = −log[$Ga(III)_{free}$] and pZr = −log[$Zr(IV)_{free}$] were calculated at pH 7.4 with c_L = 10 μM and $c_{Ga(III)/Zr(IV)}$ = 1 μM (Table 2).

Table 2. pGa and pZr Values for Various Synthetic and Natural Chelators[a]

ligand	pGa	pZr	chelating groups and ligand geometry
H_3L1	22.5	32.4	3 hydroxamate groups in a cyclic arrangement
H_4L2	22.3	37.0	4 hydroxamate groups in a linear arrangement
H_3L3	25.4	31.5	3 hydroxamate groups in a cyclic arrangement
H_3L4	21.9	32.6	3 hydroxamate groups in a linear arrangement
DFOB	21.6[43]	32.2[24]	3 hydroxamate groups in a linear arrangement
DFOE	25.2[38]	31.0	3 hydroxamate groups in a cyclic arrangement
DOTA	20.5[11]		4 macrocyclic amine groups and 4 carboxylate pendant arms
NOTA	27.4[54]		3 macrocyclic amine groups and 3 carboxylate pendant arms
H_2hox	28.4[55]		2 8-hydroxyquinoline groups and 2 amino groups in a linear arrangement
PrP9	23.1[56]		3 macrocyclic amine groups and 3 carboxylate pendant arms
HBED	28.0[57]		2 hydroxyaromatic donor groups and 2 carboxylate pendant arms
THPN		42.7[2]	4 3-hydroxy-4-pyridinone pendant arms
3,4,3-LI-HOPO		44.0[25,58]	4 1-hydroxy-2-pyridinonates in a linear arrangement
DTPA		32.3[25,59]	3 amino groups in linear arrangement and 4 carboxylate pendant arms

[a]Values (re)calculated at pH 7.4 and c_L = 10 μM and $c_{Ga(III)/Zr(IV)}$ = 1 μM, on the basis of the protonation and stability constants given in original publications. The hydrolysis constants of Ga(III) and Zr(IV) ions were taken from the literature[60] and are given in the Experimental Section.

The pGa values for Ga(III)-**H_3L1** and Ga(III)-**H_4L2** systems are on the same order of magnitude as those of the well-known gallium chelators DFOB and PRP9 but are higher than that of the clinically used DOTA (Table 2). On the other hand, H_2hox,[55] NOTA,[54] and HBED[57] present much higher Ga(III) chelating efficacy. The observed effect reflects the differences in the number and type of chelating groups present in the ligands (and therefore the number and type of donor atoms), as well as the ligand dimensions. Of importance, there is only about a 1 order of magnitude increase between pGa values for the linear trihydroxamate ligand DFOB and the cyclic tri- and tetrahydroxamates **H_3L1** and **H_4L2**, respectively. This indicates that the cyclization of the structure only slightly influences the complex stability. It is worth underlining that **H_3L1** has shorter spacers between the hydroxamate groups (9 bonds) in comparison to those in DFOB and **DFOE** (10 bonds). In **H_3L3**, the spacers have the same length of 10 bonds and the Ga(III) complexes reach the stability of **DFOE**.[38] Additionally, there is almost no difference in complex stability between Ga(III)-**H_3L1** and Ga(III)-**H_4L2**, even though the cavity of **H_4L2** is much larger than that of **H_3L1**, allowing higher flexibility and entropy of the complex structure.

For the Zr(IV) complexes of trihydroxamate **H_3L1**, **H_3L3**, and **H_3L4** systems, the pZr value is on the same order as those for DFOB[24] and DTPA[25] chelators. This suggests that ligand cyclization does not provide any increase in complex stability with respect to its linear analogue; for **H_3L3** and **DFOE** one

https://doi.org/10.1021/acs.inorgchem.1c01622
Inorg. Chem. 2021, 60, 13332−13347

may even claim a slight decrease in relation to DFOB. A similar conclusion was drawn from the comparison of Zr(IV) complexes of DFOB with fusarinine C (FCS, Scheme 1), where only minor differences in complex stability were observed in *in vivo* studies.[61] An elongation of the chain between hydroxamate binding units from 9 bonds in $\mathbf{H_3L1}$ to 10 in $\mathbf{H_3L3}$ is not reflected in the corresponding pZr values. The flexibility of the tripodal $\mathbf{H_3L4}$ ligand does not produce a higher stability of Zr(IV) complexes. Of importance, the pZr value for the tetrahydroxamate analogue $\mathbf{H_4L2}$ is >4 units higher than the values calculated for Zr(IV)-DFOB and Zr(IV)-$\mathbf{H_3L1}$ systems, reflecting the higher affinity of tetrahydroxamate $\mathbf{H_4L2}$ for Zr(IV), as expected. This feature was already observed in biological studies of other tetrahydroxamate chelators.[4,39,41] The high thermodynamic stability is certainly the result of the involvement of the fourth hydroxamate coordinating group of the ligand moiety.

The $\mathbf{H_3L1}$ and $\mathbf{H_4L2}$ ligands are very good examples to directly compare the stability of Zr(IV) complexes formed with tri- and tertrahydroxamate compounds. For these two ligands, we observe an increase in log β of 8.5 orders of magnitude for the Zr(IV)-$\mathbf{H_4L2}$ complex with respect to Zr(IV)-$\mathbf{H_3L1}$ (Table 1). However, this increase is lower than that predicted from the computational calculations performed by Holland[32] for tri- and tetrahydroxamate chelators: i.e., DFOB (log $\beta_{[Zr(DFOB)]}$ = 41.20) versus linear DFO*[41] (log $\beta_{[Zr(DFO*)]}$ = 51.56) and cyclic CTH36[39] (log $\beta_{[Zr(CTH36)]}$ = 52.84). Also, log $\beta_{[ZrL2]}$ = 43.3(1) does not reach the values predicted from the above calculations for eight-coordinate Zr(IV)-DFO* and Zr(IV)-CTH36. Of note, the log $\beta_{[ZrH(DFOB)OH]}$ value previously determined by us for DFOB (40.04)[24] matches very well the computationally predicted log $\beta_{[Zr(DFOB)]}$ value (41.20).[32] Still, in the $[ZrH(DFOB)OH]^+$ complex, dominating at pH 6.5−10.5, we have suggested the presence of an unbound protonated amino group and a hydrolyzed water molecule bound to Zr(IV). For the cyclic trihydroxamate ligand $\mathbf{H_3L1}$, characterized by 9-bond linkers between its hydroxamate units (Scheme 1), log $\beta_{[ZrL1]}$ = 34.8(2) is not far from the value estimated for the trihydroxamate cyclic siderophore FSC,[7,62] log $\beta_{[Zr(FSC)]}$ = 38.92;[32] this difference can be ascribed to the alterations in geometry and dimensions of the ligands. Zirconium is known to form complexes with a complicated geometry of a dodecahedron or square antiprism,[63,64] and numerous DFT studies have revealed that minor variations in ligand geometry (such as a pendant arm elongation or a modification of the ligand cavity size) could result in significant changes in the stability of Zr(IV) complexes.[39,65,66] $\mathbf{H_4L2}$ presented in this work possesses four hydroxamate units and amide units in the linker, but a larger cavity size and a significant asymmetry (coming from one much longer linker and with two amides and amino group) with respect to CTH36 (Scheme 1).[32,39] These structural alterations are most probably the reason for the lower thermodynamic stability of $\mathbf{H_4L2}$ complexes, as the coordination sphere might not be uniformly closed around the central ion. Unfortunately, the thermodynamic characterization of Zr(IV)-CTH36 complexes has not yey been reported; thus, the pZr value cannot be quantified. Another cyclic hydroxamic ligand, $PPDDFOT_1$, that possesses four hydroxamic groups in a symmetrical arrangement and a cavity size even larger than that of $\mathbf{H_4L2}$ (11 bonds between hydroxamic groups) showed superior stability vs DFOB in EDTA challenging assays.[67] These results confirm that the Zr(IV) complex stability is strongly dependent on the ligand geometry and emphasize the demand for a thermodynamic solution study in order to understand this dependence. Other octadentate hydroxy-pyridinone chelators, such as THPN[2] and 3,4,3-LI-HOPO,[25] form the strongest complexes (Table 2). The reason could be not only the type of chelating groups present in the ligands but also the ligand architecture and dimensions.

CONCLUSIONS

In the present work we have developed new chelating agents for the complete saturation of the coordination spheres of Ga(III) and Zr(IV) metals. The trihydroxamic ($\mathbf{H_3L1}$) and tetrahydroxamic ($\mathbf{H_4L2}$) ligands were successfully synthesized, and the thermodynamic properties of their Ga(III) and Zr(IV) complexes were evaluated. In addition, a series of other synthetic ($\mathbf{H_3L3}$, $\mathbf{H_3L4}$) and natural (**DFOE**) compounds was investigated. $\mathbf{H_3L1}$ proved to be an efficient Ga(III) chelator, but the stability of its Zr(IV) complexes is about 1 order of magnitude lower than that reported for the Zr(IV)-DFOB system. $\mathbf{H_4L2}$ is the first tetrahydroxamate ligand for which the formation constants and speciation with Zr(IV) were experimentally determined. Of importance, it revealed an enhanced stability of 8.5 orders of magnitude (log $\beta_{[ZrL2]}$ = 43.3, pZr = 37.0) with respect to Zr(IV)-$\mathbf{H_3L1}$ (log $\beta_{[ZrL1]}$ = 34.8, pZr = 32.4), as a consequence of the introduction of a fourth hydroxamate binding unit. However, the stability increase is lower than that predicted by computational calculations for the tetrahydroxamate chelators DFO* (log $\beta_{[Zr(DFO*)]}$ = 51.56) and CTH36 (log $\beta_{[Zr(CTH36)]}$ = 52.84), and this effect can be ascribed to the structural alterations of the $\mathbf{H_4L2}$ ligand.

Overall, the determination of the thermodynamic stability of metal complexes coupled with a suitable chelator design will help further developments of optimal chelators for PET imaging applications. However we are aware that there are still a great number of tests to do in order for these ligands to be used as a PET chelators, such as radiolabeling and kinetics studies, biodistribution assays, etc. Current efforts are focused on the design and studies of tetrapodal hydroxamate ligands, to interrogate how their shape and size tune the thermodynamic stability of Zr(IV) complexes.

According to the literature, the ^{89}Zr radiolabeling strategies for hydroxamate ligands is usually simple, robust, and relatively rapid. They are performed under mild pH conditions, at room temperature, and take around 1 h for DFOB derivatives on their own without being attached to any targeting vectors and 1−3 h for DFO derivatives attached to targeting vectors, such as trastuzumab.[14,68,69] Cyclic hydroxamate ligands such as C7[40] and CTH36[39] (both with 8 bonds between hydroxamate groups) have demonstrated excellent complexation abilities at ambient temperature (>99% complexation after 120 min for C7 and >90% of the activity within 5 min reaction time for CTH36, respectively). The slightly smaller ligands C6 and C5, reported by Guerard et al.,[40] appear to be less suitable for radiolabeling, with higher temperatures being required to obtain high complexation yields. The cyclic ligands reported in this paper possess a larger cavity size, with at least 9 bonds between hydroxamate groups, which allows us to assume that the radiolabeling process will be highly efficient and performed under mild conditions. Preliminary radiolabeling of artificial FOXE siderophores with ^{68}Ga, represented here by FOXE 2−5, was achieved after 10 min at room temperature with

https://doi.org/10.1021/acs.inorgchem.1c01622
Inorg. Chem. 2021, 60, 13332−13347

moderate yields and high specific activities of ^{68}Ga.[38] Further characterization is ongoing.

EXPERIMENTAL SECTION

Synthesis. *General Considerations.* Unless stated otherwise, all commercially available reagents and solvents were of analytical grade. For the synthesis of **H_3L1** and **H_4L2**, solvents and reagents were purchased from Bachem, BLDpharm, and Fluka. Crude products were purified via flash column chromatography on silica gel (Merck, 230–400 Mesh) or, for compounds **10**, **11**, **16**, and **17**, by semipreparative RP-HPLC using a Waters Prep 600 system equipped with a C18 Jupiter column (250 × 30 mm, 300 Å, 15 μm spherical particle size). Gradients were established each time by considering the analytical HPLC profile of the crude product. The column was perfused at a flow rate of 20 mL/min over 30 min with a binary system of solvent A (H_2O + 0.1% v/v TFA) and solvent B (60% CH_3CN in water +0.1% v/v TFA). Analytical RP-HPLC analyses were performed on a XBridge C18 column (4.6 × 150 mm, 5 μm particle size) using a flow rate of 0.7 mL/min and a linear gradient of acetonitrile (and 0.1% TFA) in water (and 0.1% TFA) from 0% to 100% over 25 min. The mass spectra were recorded on an ESI-Micromass ZMD 2000 instrument. TLC was performed on precoated plates of silica gel F254 (Merck, Darmstadt, Germany). ^{1}H NMR analyses were obtained using a Varian spectrometer (400 MHz) and were referenced to residual ^{1}H signals of the deuterated solvents (δ(^{1}H) 7.26 for $CDCl_3$; δ(^{1}H) 2.50 for DMSO). The following abbreviations are used to describe the shape of the peaks: s, singlet; d, doublet; dd, doublet of doublets; t, triplet; m, multiplet.

*Synthesis of tert-Butyl(benzyloxy)carbamate (**1**).* To an ice-cooled solution of *O*-benzylhydroxylamine·HCl (4.00 g, 25 mmol) in a 1,4-dioxane/H_2O mixture (60 mL, 1/1 v/v) was added K_2CO_3 (10.37 g, 75 mmol). Boc_2O (8.18 g, 37.5 mmol), previously dissolved in dioxane, was then added dropwise, and the reaction mixture was stirred at room temperature overnight. The solvent was removed under vacuum, and the crude product extracted using ethyl acetate (30 mL) and water (3 × 15 mL). The organic phase was dried over Na_2SO_4, filtered, and evaporated. Compound **1** (4.86 g, 87% yield) was obtained as a colorless oil, which was used without any further purification. NMR data match those reported in the literature (PMID: 11906271). ESI-MS: calcd for $C_{12}H_{18}NO_3$, 224.28 [M + H]$^+$; found, 224.13 [M + H]$^+$. T_R = 19.70 min.

*Synthesis of Ethyl 4-((Benzyloxy)(tert-butoxycarbonyl)amino)-butanoate (**2**).* To a solution of **1** (4.86 g, 21.79 mmol) in DMF (15 mL) was added NaH (60% dispersion in mineral oil, 1.20 g, 23.94 mmol). The mixture was initially stirred at rt for 30 min, and then the reaction mixture was warmed to 60 °C and ethyl 4-bromobutyrate was added dropwise. At the completion of the reaction, the solvent was removed, and the residue was extracted with ethyl acetate and water (3 × 30 mL), dried over Na_2SO_4, and concentrated under vacuum. The product (**2**) was obtained as a yellowish oil (5.36 g, 73% yield). The NMR data correspond to those in the literature (PMID: 28715615). MS (ESI): calcd for $C_{18}H_{28}NO_5$, 338.20 [M + H]$^+$; found, 360.18 [M + Na]$^+$, 697.37 [2M + Na]$^+$. T_R = 23.51 min.

*Synthesis of Ethyl 4-(N-(Benzyloxy)-4-((tert-butoxycarbonyl)-amino)butanamido)butanoate (**4**).* Compound **2** (5.36 g, 15.90 mmol) was dissolved in trifluoroacetic acid (TFA, 6 mL), and the mixture was stirred at room temperature for 2 h. The reaction mixture was monitored by MS (ESI) before being concentrated under vacuum. The deprotected amino ester **3** was used without further purification in the next step. To an ice-cold solution of Boc-γ-aminobutiric acid (2.7 g, 13.45 mmol) in DMF (20 mL) were added 1-[bis(dimethylamino)methylene]-1*H*-1,2,3-triazolo[4,5-*b*]-pyridinium 3-oxide hexafluorophosphate (HATU, 5.6 g, 14.75 mmol) and DIPEA (2.6 mL, 14.75 mmol). A portion of **3** (3.5 g, 14.75 mmol) was dissolved in DMF (10 mL), and this solution was added dropwise to the first one. Then the reaction mixture was warmed to room temperature and stirred for 1 h. After removal of the solvent, the residue was dissolved in ethyl acetate and washed with a 5% aqueous solution of citric acid, a 10% aqueous solution of $NaHCO_3$, and brine. The crude product was purified by column chromatography using ethyl acetate/petroleum ether (from 1/4 to 1/1 by volume) as an eluent mixture. Compound **4** was obtained as a slightly yellowish oil (4.35 g, 76.6% yield). ESI-MS: calcd for $C_{22}H_{35}N_2O_6$, 423.53 [M + H]$^+$; found, 423.25 [M + H]$^+$, 445.23 [M + Na]$^+$, 867.47 [2M + Na]$^+$. T_R = 21.11 min. ^{1}H NMR (400 MHz, $CDCl_3$): δ 7.44–7.32 (m, 5H), 4.80 (s, 2H), 4.11 (qd, *J* = 7.1, 2.9 Hz, 2H), 3.70 (t, *J* = 6.8 Hz, 2H), 3.12 (t, *J* = 6.6 Hz, 2H), 2.42 (t, *J* = 7.2 Hz, 2H), 2.32 (t, *J* = 7.3 Hz, 2H), 1.99–1.91 (m, 2H), 1.80–1.73 (m, 2H), 1.42 (s, 9H), 1.26–1.20 (m, 3H).^{13}C NMR ($CDCl_3$): δ 172.9, 156.0, 134.3, 129.2, 129.0, 128.7, 79.1, 60.4, 44.6, 40.3, 31.4, 29.6, 28.4, 24.7, 22.3, 14.2.

*Synthesis of Ethyl 10,20-Bis(benzyloxy)-2,2-dimethyl-4,9,14,19-tetraoxo-3-oxa-5,10,15,20-tetraazatetracosan-24-oate (**7**).* The Boc-deprotected derivative **5** (3.40 g, 7.8 mmol) was used as previously described for **3**. Compound **6** was synthesized by dissolving the ethyl ester **4** (3.0 g, 7.1 mmol) in a 1,4-dioxane/H_2O mixture in the presence of LiOH (1 M aqueous solution, 12.5 mmol). The mixture was stirred at rt for 20–30 min. Once the reaction was complete, dioxane was evaporated and the crude product was acidified using 1 M HCl to reach pH 6. Then, the aqueous phase was extracted using ethyl acetate. Compound **6** (0.91 g, 2.31 mmol) was used in the next step without further purification. The coupling reaction was conducted as previously described for **4**, and derivative **7** was obtained as a yellowish oil (1.24 g, 77% yield) after column chromatography. ESI-MS: calcd for $C_{37}H_{55}N_4O_9$, 699.87 [M + H]$^+$; found, 699.96 [M + H]$^+$. T_R = 21.18 min. ^{1}H NMR (400 MHz, $CDCl_3$): δ 7.50–7.31 (m, 10H), 7.04 (bs, 1H), 4.81 (d, *J* = 5.3 Hz, 4H), 4.12 (q, *J* = 7.1 Hz, 2H), 3.71–3.69 (m, 4H), 3.26 (dd, *J* = 11.9, 6.2 Hz, 2H), 3.17–3.09 (m, 2H), 2.53–2.39 (m, 4H), 2.33 (t, *J* = 7.3 Hz, 2H), 2.20 (t, *J* = 6.8 Hz, 2H), 1.98–1.92 (m, 4H), 1.84–1.73 (m, 4H), 1.42 (s, 9H), 1.24 (t, *J* = 7.1 Hz, 3H). ^{13}C NMR ($CDCl_3$): δ 174.7, 173.3, 173.0, 134.2, 129.3, 129.1, 129.1, 128.8, 60.5, 44.7, 44.3, 40.0, 39.6, 33.1, 31.4, 30.0, 29.4, 28.5, 24.8, 23.9, 23.2, 22.3, 14.3.

*Synthesis of Ethyl 10,20,30-Tris(benzyloxy)-2,2-dimethyl-4,9,14,19,24,29-hexaoxo-3-oxa-5,10,15,20,25,30-hexaazatetratria-contan-34-oate (**9**).* Compound **9** was synthesized under the same coupling conditions used for **4** by starting from the acid derivative **6** (0.91 g, 2.31 mmol) and the amino derivative **8** (1.81 g, 2.54 mmol). The desired product was obtained as a colorless oil (1.89 g, 84% yield) after column chromatography. ESI-MS: calcd for $C_{52}H_{75}N_6O_{12}$, 976.20 [M + H]$^+$; found, 975.94 [M + H]$^+$. T_R = 17.83.^{1}H NMR (400 MHz, $CDCl_3$): δ 7.39–7.35 (m, 15H), 5.05 (bs, 3H), 4.83–4.77 (m, 6H), 4.11 (q, *J* = 7.1 Hz, 2H), 3.72–3.67 (m, 6H), 3.34–3.19 (m, 4H), 3.16–3.11 (m, 2H), 2.49–2.45 (m, 6H), 2.32 (t, *J* = 7.3 Hz, 2H), 2.25–2.12 (m, 4H), 2.02–1.89 (m, 6H), 1.87–1.72 (m, 6H), 1.42 (s, 9H), 1.24 (t, *J* = 7.1 Hz, 3H). ^{13}C NMR ($CDCl_3$): δ 175.3, 174.1, 172.5, 157.3, 135.4, 128.9, 128.3, 128.2, 80.7, 73.8, 61.2, 48.6, 41.2, 40.4, 35.2, 31.8, 31.5, 28.4, 24.1, 21.7, 18.5, 14.7.

*Synthesis of 1,11,21-Tris(benzyloxy)-1,6,11,16,21,26-hexaazacy-clotriacontane-2,7,12,17,22,27-hexaone (**10**).* Compound **9** was Boc-deprotected as described for **3**. Then, the ethyl group was hydrolyzed by LiOH as for **6**. To a dilute solution of the fully deprotected trimer (1.92 g, 2.0 mmol) in DMF (100 mL) were added HATU (0.84 g, 2.2 mmol) and DIPEA (0.38 mL, 2.2 mmol) dropwise at 0 °C. The reaction mixture was stirred for 3 h. Then, the solvent was removed, and the residue was extracted with ethyl acetate and an aqueous solution of citric acid (10%), a solution of $NaHCO_3$ (5%), and brine. The crude product was purified via semipreparative HPLC, giving the desired product as a colorless oil (0.70 g, 42% yield). ESI-MS: calcd for $C_{45}H_{61}N_6O_9$, 830.02 [M + H]$^+$; found, 829.90 [M + H]$^+$. T_R = 21.47 min. ^{1}H NMR (400 MHz, $CDCl_3$): δ 7.39–7.31 (m, 18H), 4.77 (s, 6H), 3.69–3.67 (m, 6H), 3.25–3.23 (m, 6H), 2.46 (t, *J* = 6.7 Hz, 6H), 2.19 (t, *J* = 7.0 Hz, 6H), 1.97–1.91 (m, 6H), 1.85–1.70 (m, 6H). ^{13}C NMR ($CDCl_3$): δ 174.9, 173.8, 133.8, 129.3, 128.8, 44.2, 39.4, 33.0, 29.5, 23.7, 23.2.

*Synthesis of 1,11,21-Trihydroxy-1,6,11,16,21,26-hexaazacyclo-triacontane-2,7,12,17,22,27-hexaone (**11**, **H_3L1**).* To a solution of the benzyl-protected derivative **10** (0.70 g, 0.84 mmol) in MeOH (30 mL) was added glacial acetic acid (1 mL). The mixture was treated with a catalytic amount (0.084 mmol) of palladium on activated

https://doi.org/10.1021/acs.inorgchem.1c01622
Inorg. Chem. 2021, 60, 13332–13347

charcoal (10% Pd basis) under a hydrogen atmosphere. After 24 h, the reaction mixture was filtered through Celite, concentrated under reduced pressure, diluted with water, and alkalinized with saturated sodium bicarbonate. The aqueous phase was extracted with ethyl acetate (4 × 10 mL), and the combined organic layers were dried over Na_2SO_4, filtered, and concentrated under vacuum. Compound **11** was obtained as a light yellow oil after preparative HPLC purification (0.43 g, 91% yield). ESI-MS: calcd for $C_{24}H_{43}N_6O_9$, 559.64 $[M + H]^+$; found, 559.79 $[M + H]^+$. T_R = 15.79 min. ^{1}H NMR (400 MHz, $CDCl_3$): δ 9.59 (bs, 3H), 7.83−7.81 (m, 3H), 3.53−3.38 (m, 6H), 3.15−2.93 (m, 6H), 2.40−2.24 (m, 5H), 2.20−2.16 (m, 2H), 2.02 (t, J = 7.1 Hz, 5H), 1.76−1.70 (m, 6H), 1.64−1.50 (m, 6H). ^{13}C NMR ($CDCl_3$): δ 174.5, 173.0, 172.2, 169.5, 158.9, 158.5, 129.9, 50.5, 47.3, 47.1, 38.7, 38.6, 33.0, 31.5, 31.2, 30.3, 29.7, 24.9, 24.8, 23.0, 22.3, 19.7. HR-ESI-MS m/z 559.30894; calcd for $C_{24}H_{43}N_6O_9$ ($[M + H]^+$) 559.30860. Anal. Calcd for $C_{24}H_{42}N_6O_9$: C, 51.6; H, 7.6; N, 15.0. Found: C, 51.4; H, 7.5; N, 14.9.

*Synthesis of Ethyl 17-(Benzyloxy)-10-(((benzyloxy)carbonyl)-amino)-2,2-dimethyl-4,11,16-trioxo-3-oxa-5,12,17-triazahenicosan-21-oate (**13**).* Compound **13** was synthesized under the same coupling conditions used for compounds **4** and **9** bystarting from Z-Lys(Boc)-OH (1.05 g, 2.75 mmol) and the amino derivative **5** (1.09 g, 2.50 mmol). The desired product was obtained as a yellowish oil (1.40 g, 80% yield) after column chromatography. ESI-MS: calcd for $C_{36}H_{53}N_4O_9$, 685.84 $[M + H]^+$; found, 685.73 $[M + H]^+$. T_R = 26.16 min. ^{1}H NMR (400 MHz, $CDCl_3$): δ 7.37−7.35 (m, 5H), 7.31−7.26 (m, 5H), 6.99 (s, 1H), 5.85 (d, J = 7.7 Hz, 1H), 5.13−4.96 (m, 2H), 4.76 (s, 2H), 4.07 (q, J = 7.1 Hz, 2H), 3.73−3.59 (m, 2H), 3.28−3.13 (m, 2H), 3.03−2.97 (m, 2H), 2.47−2.40 (m, 2H), 2.28 (t, J = 7.3 Hz, 2H), 1.94−1.88 (m, 2H), 1.84−1.69 (m, 3H), 1.62−1.58 (m, 1H), 1.39 (s, 11H), 1.31 (dd, J = 19.1, 12.2 Hz, 2H), 1.19 (t, J = 7.1 Hz, 3H). ^{13}C NMR ($CDCl_3$): δ 13C NMR (101 MHz, cdcl3) δ 174.3, 172.9, 172.0, 156.2, 136.2, 134.1, 129.2, 128.9, 128.6, 128.4, 128.0, 127.9, 78.9, 76.2, 66.8, 60.4, 54.8, 44.4, 39.9, 39.2, 38.5, 32.2, 31.2, 29.7, 29.4, 28.3, 23.7, 22.4, 22.1, 14.1.

*Synthesis of Ethyl 17,27,37,47-Tetrakis(benzyloxy)-10-(((benzyloxy)carbonyl)amino)-2,2-dimethyl-4,11,16,21,26,31,36,41,46-nonaoxo-3-oxa-5,12,17,22,27,32,37,42,47-nonaazahenpentacontan-51-oate (**15**).* The tetramer **15** was synthesized under the same coupling conditions used for compounds **4**, **9**, and **13** by starting from the acid derivative **14** (0.61 g, 0.93 mmol) and the amino derivative **12** (0.90 g, 1.02 mmol). The desired product was obtained as a colorless oil (0.97 g, 69% yield) after column chromatography. ESI-MS: calcd for $C_{81}H_{113}N_{10}O_{18}$, 1514.85 $[M + H]^+$; found, 1514.16 $[M + H]^+$, 775.95 $[M + 2H]^{2+}$. T_R = 25.88 min. ^{1}H NMR (400 MHz, $CDCl_3$): δ 7.47−7.28 (m, 25H), 5.13−4.96 (m, 2H), 4.86−4.65 (m, 8H), 4.09 (dd, J = 13.8, 6.8 Hz, 3H), 3.80−3.53 (m, 8H), 3.32−3.10 (m, 7H), 3.04−3.00 (m, 2H), 2.54−2.34 (m, 7H), 2.29 (t, J = 7.0 Hz, 2H), 2.23−2.05 (m, 6H), 1.96−1.90 (m, 8H), 1.82−1.68 (m, 8H), 1.66−1.53 (m, 2H), 1.40 (s, 12H), 1.25−1.19 (m, 4H), 0.94−0.85 (m, 2H). ^{13}C NMR ($CDCl_3$): δ 174.5, 172.9, 136.2, 134.0, 129.2, 129.1, 128.8, 128.5, 128.2, 128.0, 67.0, 60.5, 55.0, 44.1, 39.4, 39.0, 32.9, 32.0, 31.3, 29.8, 29.7, 29.5, 28.4, 23.9, 23.0, 22.5, 22.2, 14.2.

*Synthesis of Benzyl (6,16,26,36-Tetrakis(benzyloxy)-2,7,12,17,22,27,32,37,42-nonaoxo-1,6,11,16,21,26,31,36,41-nonaazacycloheptatetracontan-43-yl)carbamate (**16**).* Compound **15** was Boc-deprotected as described for **3**. Then, the ethyl group was hydrolyzed by LiOH as for **6**. To a dilute solution of the fully deprotected tetramer (0.55 g, 0.367 mmol) in DMF (40 mL) were added HATU (0.154 g, 0.40 mmol) and DIPEA (0.07 mL, 0.40 mmol) dropwise at 0 °C. The reaction mixture was stirred for 3 h. Then, the solvent was removed, and the residue was extracted with ethyl acetate and an aqueous solution of citric acid (10%), a solution of $NaHCO_3$ (5%), and brine. The crude product was purified via semipreparative HPLC, giving the desired product as a colorless oil (0.29 g, 57% yield). ESI-MS: calcd for $C_{74}H_{99}N_{10}O_{15}$, 1368.66 $[M + H]^+$; found, 1368.36 $[M + H]^+$, 684.74 $[M+2H]^{2+}$. T_R = 25.73 min. ^{1}H NMR (400 MHz, DMSO-d_6): δ 7.96−7.63 (m, 6H), 7.56−7.13 (m, 25H), 5.06−4.89 (m, 2H), 4.85−4.71 (m, 8H), 4.00−3.76 (m, 3H), 3.09−2.88 (m, 10H), 2.84−2.61 (m, 1H), 2.43−2.25 (m, 8H), 2.09−1.93 (m, 9H), 1.75−1.71 (m, 9H), 1.59−1.53 (m, 8H), 1.39−1.08 (m, 7H), 1.07−0.76 (m, 2H). ^{13}C NMR (DMSO-d_6): δ 171.8, 156.4, 135.2, 129.8, 129.1, 128.9, 128.7, 128.2, 128.1, 75.7, 65.8, 55.1, 44.5, 38.5, 33.0, 29.5, 24.7, 23.2.

*Synthesis of (S)-43-Amino-6,16,26,36-tetrahydroxy-1,6,11,16,21,26,31,36,41-nonaazacycloheptatetracontane-2,7,12,17,22,27,32,37,42-nonaone (**17**, **H_4L2**).* Compound **17** was synthesized as previously described for **11** by starting from derivative **16** (0.13 g, 71% yield). ESI-MS: calcd for $C_{38}H_{69}N_{10}O_{13}$, 874.03 $[M + H]^+$; found, 873.75 $[M + H]^+$. T_R = 21.28 min. ^{1}H NMR (400 MHz, DMSO-d_6): δ 9.64−9.59 (m, 3H), 8.07−8.04 (m, 2H), 7.86−7.71 (m, 4H), 3.47−3.44 (m, 9H), 3.04−2.99 (m, 10H), 2.42−2.22 (m, 8H), 2.04−2.00 (m, 8H), 1.76−1.49 (m, 20H), 1.47−1.16 (m, 5H). ^{13}C NMR (DMSO-d_6): δ 172.9, 172.2, 168.7, 158., 56.5, 52.7, 47.2, 38.7, 33.0, 31.2, 29.7, 29.1, 24.8, 24.5, 23.0, 22.1. HR-ESI-MS m/z 873.50488; calcd for $C_{38}H_{69}N_{10}O_{13}$ ($[M + H]^+$) 873.50401. Anal. Calcd for $C_{38}H_{68}N_{10}O_{13}$: C, 52.3; H, 7.9; N, 16.0. Found: C, 52.3; H, 7.8; N, 16.1.

Thermodynamic Solution Studies. *General Considerations.* Unless otherwise stated, all commercially available reagents and solvents were of analytical grade, were purchased from commercial suppliers (Sigma-Aldrich, Titripur, Merck, Fisher Scientific, Fluka), and were used as received without further purification. All solutions were prepared in doubly distilled water. A stock solution of Fe(III) was prepared immediately before use from $Fe(ClO_4)_3{\cdot}xH_2O$ in 0.01 M $HClO_4$ and standardized by an inductively coupled plasma−optical emission spectrometer (ICP-OES; iCAP 7400 Duo ICP-OES) along with spectrophotometric determination, on the basis of the molar extinction coefficient ε = 4160 M^{-1} cm^{-1} at 240 nm.[70,71] Stock solutions of Ga(III) and Zr(IV) were prepared immediately before use from $Ga(ClO_4)_3{\cdot}xH_2O$ and anhydrous $ZrCl_4$, respectively, in 0.1 M $HClO_4$ to prevent hydrolysis and standardized by ICP-OES (iCAP 7400 Duo ICP-OES) along with direct titration with ethylenediaminetetraacetic acid (EDTA).[72,73] The $HClO_4$ solutions were titrated with standardized NaOH (0.1 N). The carbonate-free NaOH solution was standardized by titration with potassium hydrogen phthalate (KHP). All stock solutions were prepared using a R200D Sartorius analytical balance (with 0.01 mg precision).

All measurements were performed at 0.1 M $NaClO_4$ ionic strength, which was chosen instead of 1.0 M $NaClO_4$ ionic strength in order to increase the solubility of the investigated ligands and their complexes. We are aware that some measurements were performed at a very acidic pH (<1), where the ionic strength 0.1 M is not enough to keep the ionic activity stable, but due to the decomposition of hydroxamate ligands in strong acids,[43,51] all measurements performed below pH 1 were assumed to be endowed with a large error and (i) were not taken into account during data evaluation or (ii) precluded from the discussion.

Electrospray Ionization Mass Spectrometry (ESI-MS). ESI-MS data were recorded on a Bruker Q-FTMS spectrometer. The instrumental parameters were as follows: scan range, m/z 200−1600; dry gas, nitrogen; temperature, 170 °C; capillary voltage, 4500 V; ion energy, 5 eV. The capillary voltage was optimized to the highest signal to noise ratio. The spectra were recorded in the positive mode. Compounds were dissolved in a MeOH/H_2O solution (80/20 by weight); the same solvent mixture was used to dilute the matrix solutions to the concentration range of 0.01 mM. The Fe(III), Ga(III), and Zr(IV) and stock solutions were prepared as described previously and added to the ligand solutions in 1/1, 2/1 and 1/3 mixtures for Fe(III) and Ga(III) and 1/1 and 1/3 mixtures for Zr(IV), all at pH 3 (the pH was adjusted by using acetic acid). The free hydrogen ion concentration was measured with a Mettler-Toledo InLab Semi-Micro combined glass electrode filled with NaCl in MeOH/H_2O (80/20 by weight). Potential differences were measured with a Beckman ϕ72 pH meter, standardized according to the classical methods with buffers prepared according to reported procedures in MeOH/H_2O solvent (80/20 by weight).[74,75]

Potentiometric Titrations. The potentiometric titrations of ligands and their complexes were carried out using a Titrando 905

https://doi.org/10.1021/acs.inorgchem.1c01622
Inorg. Chem. 2021, 60, 13332−13347

(Metrohm) automatic titrator system, equipped with a combined glass electrode (Mettler Toledo, InLab Semi-Micro, with XEROLYT EXTRA Polymer filling) and a 800 Dosino dosing system, equipped with a a 2 mL micro buret. The ionic strength was fixed at I = 0.1 M with $NaClO_4$. The electrode was calibrated daily in terms of hydrogen ion concentration using $HClO_4$ (0.1 M) with CO_2-free NaOH solutions (0.1 M).[76] A stream of high-purity argon, presaturated with water vapor, was passed over the surface of the solution cell, the cell was filled with 50 mL of the studied solution, and the system was thermostated at 25.0 ± 0.2 °C. At least three titrations were performed for each system, with a starting concentration of the ligand of 1 mM and a 1:1 metal to ligand molar ratio with a 10% excess of the ligand in the pH range 2−11. The purity and exact concentration of the ligand solutions were determined using the Gran method.[77] Special care was taken to ensure that complete equilibration was attained. The titration curves were carefully checked and did not display any pH fluctuations that often accompany the precipitation of metal hydroxides. The potentiometric data were refined with the SUPERQUAD[78] and HYPERQUAD[79] programs, which use nonlinear least-squares methods. The successive protonation constants of the ligand were calculated from the cumulative constants determined with the program and defined by eqs 1 and 2 (charges are omitted for clarity).

$$H_{n-1}L + H \leftrightarrows H_nL \quad (1)$$

$$K_n^H = \frac{[H_nL]}{[H_{n-1}L][H]} \quad (2)$$

The stability constants calculated for metal complexes are defined by eqs 3 and 4:

$$pM + qH + rL \leftrightarrows M_pH_qL_r \quad (3)$$

$$\beta_{M_pH_qL_r} = \frac{[M_pH_qL_r]}{[M]^p[H]^q[L]^r} \quad (4)$$

The uncertainties in the log K values correspond to the added standard deviations in the cumulative constants.

pH-Dependent UV−Vis Titrations. The pH-dependent UV−vis spectrophotometric experiments for the Fe(III)-**H_3L1**, Fe(III)-**H_4L2**, Ga(III)-**H_3L1**, Ga(III)-**H_4L2**, Ga(III)-**H_3L4**, Zr(IV)-**H_3L1**, Zr(IV)-**H_4L2**, Zr(IV)-**H_3L3**, and Zr(IV)-**H_3L4** systems were carried out as a function of concentration with a Varian Cary 300 Bio spectrophotometer in the 300−700 nm range for iron complexes and 200−300 nm range for gallium and zirconium solutions using Hellma quartz optical cells with a 1 cm path length. To calculate the stability constants for investigated systems, two sets of pH-dependent UV−vis titrations were carried out: in the pH ranges (i) 0.1−2 and (ii) 2−11. In the (i) series, the experiments were performed by making 20 samples, differing by 0.1 pH unit, with a constant total volume of 0.7 mL and concentration of metal ion of ∼0.05−0.1 mM and metal to ligand molar ratio of 1:1; for all samples, the ionic strength was adjusted to 0.1 M by the addition of $NaClO_4$ and the pH (range 0.1−2.0) was controlled by the concentration of $HClO_4$. After preparation, each solution was allowed to equilibrate for about 1 h, and then its UV−vis spectrum was recorded. This was necessary to minimize the effects of hydroxamate ligand hydrolysis, which occurs in strong acid.[43,51] In the (ii) set of experiments, 3 mL of a solution containing a 1:1 Fe(III):ligand molar ratio, where the ferric concentration was around 0.20 mM, was introduced into a cell and the pH was adjusted by adding the proper microvolume of $HClO_4$; the solutions were allowed to equilibrate (up to 30 min) and checked with a Mettler Toledo Super Easy pH meter with an accuracy of ±0.01, and then the spectra were recorded.

Metal Competition Batch UV−Vis Titrations. In order to calculate the stability constants of the investigated complexes, several competitive titrations were performed. All of them were carried out as a function of concentration with a Varian Cary 300 Bio spectrophotometer in the 300−650 nm range (with 1 nm precision) using Hellma quartz optical cells with a 1 cm path length. Spectrophotometric titrations were performed on samples with a concentration of the ligand of ∼0.05−0.1 mM and I = 0.1 M (completed by adding $NaClO_4$), at 25.0 ± 0.1 °C; pH 1.5 or 2.0 was adjusted by adding the proper volume of $HClO_4$. In general, the stock solution of the starting complex (Fe(III)-L, Ga(III)-L, or Zr(IV)-L, respectively) was divided into several aliquots to which an excess of titrant (Ga(III), Fe(III), or Zr(IV)-NTA, respectively) was added. After preparation, each solution was allowed to equilibrate for about 1 h, and then its UV−vis spectrum was recorded. The vials were kept in the dark, and the absorbance was measured again after 24, 48, and 120 h. Changes were observed only between the spectra collected after 1 and 24 h, indicating that an equilibrium was attained.

In order to determine the log β values of $[GaHL]^+$ for **H_3L1** and **H_3L4** and of $[GaH_2L2]^+$, competition experiments at pH 1.5 of (i) Fe(III)-**H_3L** + Ga(III) and (ii) Ga(III)-**L** + Fe(III) were performed. For (i) 15 samples with a constant concentration of Fe(III) ions and **L** (1:1) were titrated by up to 600 equiv of Ga(III) ions; for Ga(III)-**L** + Fe(III), 18 samples with a constant concentration of Ga(III) ions and **H_3L** (1:1) were titrated by up to 4 equiv of Fe(III) ions.

In order to determine the log β values of $[ZrL]^+$ for **H_3L1**, **H_4L2**, **H_3L3**, **H_3L4**, and **DFOE** and for $[ZrHL2]^+$, competition experiments at pH 1.5 or 2, Fe(III)-**L** + Zr(IV)-NTA, were performed. In each experiment 18 samples with a constant concentration of Fe(III) ions and ligands were titrated by up to 50 equiv of a Zr(IV)-NTA solution with a metal to ligand molar ratio of 1:3, starting from 0 equiv.

Data Treatment. In the calculations of complex stability constants, the protonation constants of free ligands (Table 1) and the constants were related to hydrolytic species being taken into account: Ga(III),[60] $Ga(OH)^{2+}$ log $\beta_{GaH_{-1}}$ = −3.11, $Ga(OH)_2^+$ log $\beta_{GaH_{-2}}$ = −7.66, $Ga(OH)_3$ log $\beta_{GaH_{-3}}$ = −11.94, $Ga(OH)_4^-$ log$\beta_{GaH_{-4}}$ = −15.66, to Fe(III),[80] $Fe(OH)^{2+}$ log $\beta_{FeH_{-1}}$ = −2.56, $Fe(OH)_2^+$ log $\beta_{FeH_{-2}}$ = −6.2, $Fe(OH)_3$ log $\beta_{FeH_{-3}}$ = −11.44, $Fe(OH)_4^-$ log $\beta_{FeH_{-4}}$ = −21.88, $Fe(OH)_5^{2-}$ log $\beta_{FeH_{-5}}$ = −2.74, $Fe(OH)_6^{3-}$, and Zr(IV),[60] $Zr(OH)^{3+}$ log $\beta_{ZrH_{-1}}$ = −0.56, $Zr(OH)_2^{2+}$ log $\beta_{ZrH_{-2}}$ = −1.44, $Zr(OH)_4$ log $\beta_{ZrH_{-4}}$ = −8.85, $Zr(OH)_6^{2-}$ log $\beta_{ZrH_{-6}}$ = −30.6, $Zr_3(OH)_4^{8+}$ log $\beta_{Zr_3H_{-4}}$ = −6.96, $Zr_4(OH)_8^{8+}$ log $\beta_{Zr_4H_{-8}}$ = 6.52, $Zr_3(OH)_9^{3+}$ log $\beta_{Zr_3H_{-9}}$ = 12.19. The Zr(IV) hydrolysis constants for the species $Zr(OH)^{3+}$, $Zr(OH)_2^{2+}$, $Zr(OH)_4$, and $Zr_3(OH)_4^{8+}$ were recalculated for 0.1 M $NaClO_4$ ionic strength according to literature parameters.[60] The pK_w value used in the calculation at the 0.1 M $NaClO_4$ ionic strength was −13.77.[81]

The UV−vis data were refined to obtain the overall binding constant using SPECFIT/32 software[82−84] that adjusts the absorptivity and the stability constants of the species formed at equilibrium. Specfit uses factor analysis to reduce the absorbance matrix and to extract the eigenvalues prior to the multiwavelength fit of the reduced data set according to the Marquardt algorithm.[82−84] Uncertainties in log β were calculated from the standard deviation.

The competition data were refined to obtain the overall binding constant using SPECFIT/32 software.[82−84] The protonation constants of ligands and formation constants for iron complexes (Table 1 and the literature[24]) were used as fixed parameters during data analysis. The concentration of iron complexes was calculated from the absorbance spectra (collected in the 300−700 nm range). Hydrolytic forms of the ferric ion in the studied pH range are characterized by an absorption band with a λ_{max} value of below 300 nm, and therefore they are beyond the experimental wavelength window. However, the spectrum of Fe(III) in solution at the pH of the experiment was fixed in the calculations.[85,86] The stability constants of the Fe(III)-NTA[48] and Zr(IV)-NTA[27] complexes were taken from the literature and were used as fixed constants during the evaluation of the stability constants of the zirconium complexes.

The competition equilibrium is described by eqs 5 and 6:

$$FeL + ZrNTA \rightleftarrows ZrL + FeNTA \quad (5)$$

$$K = \frac{[FeL][ZrNTA]}{[FeNTA][ZrL]} \quad (6)$$

https://doi.org/10.1021/acs.inorgchem.1c01622
Inorg. Chem. 2021, 60, 13332−13347

The molecular charges are omitted for clarity. The data were processed using Origin 7.0. The species distribution diagrams were computed with the HYSS program.[79]

■ ASSOCIATED CONTENT

Supporting Information

The Supporting Information is available free of charge at https://pubs.acs.org/doi/10.1021/acs.inorgchem.1c01622.

ESI-MS spectra and UV−vis spectroscopic data from solution studies, detail of the Fe(III) complex solution study, and $^{1}H/^{13}C$ NMR spectra and chromatograms of the synthesized compounds (PDF)

■ AUTHOR INFORMATION

Corresponding Author

Elzbieta Gumienna-Kontecka − *University of Wroclaw, Faculty of Chemistry, 50-383 Wrocław, Poland;* orcid.org/0000-0002-9556-6378; Email: elzbieta.gumienna-kontecka@chem.uni.wroc.pl

Authors

Yuliya Toporivska − *University of Wroclaw, Faculty of Chemistry, 50-383 Wrocław, Poland*

Andrzej Mular − *University of Wroclaw, Faculty of Chemistry, 50-383 Wrocław, Poland*

Karolina Piasta − *University of Wroclaw, Faculty of Chemistry, 50-383 Wrocław, Poland;* orcid.org/0000-0003-0160-6920

Małgorzata Ostrowska − *University of Wroclaw, Faculty of Chemistry, 50-383 Wrocław, Poland*

Davide Illuminati − *University of Ferrara, Dipartimento di Scienze Chimiche, Farmaceutiche ed Agrarie, 44121 Ferrara, Italy*

Andrea Baldi − *University of Ferrara, Dipartimento di Scienze Chimiche, Farmaceutiche ed Agrarie, 44121 Ferrara, Italy*

Valentina Albanese − *University of Ferrara, Dipartimento di Scienze Chimiche, Farmaceutiche ed Agrarie, 44121 Ferrara, Italy;* orcid.org/0000-0002-1947-2644

Salvatore Pacifico − *University of Ferrara, Dipartimento di Scienze Chimiche, Farmaceutiche ed Agrarie, 44121 Ferrara, Italy*

Igor O. Fritsky − *Taras Shevchenko National University of Kyiv, Department of Chemistry, 01601 Kyiv, Ukraine;* orcid.org/0000-0002-1092-8035

Maurizio Remelli − *University of Ferrara, Dipartimento di Scienze Chimiche, Farmaceutiche ed Agrarie, 44121 Ferrara, Italy*

Remo Guerrini − *University of Ferrara, Dipartimento di Scienze Chimiche, Farmaceutiche ed Agrarie, 44121 Ferrara, Italy*

Complete contact information is available at: https://pubs.acs.org/10.1021/acs.inorgchem.1c01622

Notes

The authors declare no competing financial interest.

■ ACKNOWLEDGMENTS

This contribution is based upon work from COST Action CA18202, NECTAR−Network for Equilibria and Chemical Thermodynamics Advanced Research, supported by COST (European Cooperation in Science and Technology). We acknowledge the Polish National Science Centre (NCN, UMO 2015/19/B/ST5/00413) for financial support. A.M. was supported by the NCN (UMO-2017/26/A/ST5/00363).

■ REFERENCES

(1) Heskamp, S.; Raave, R.; Boerman, O.; Rijpkema, M.; Goncalves, V.; Denat, F. Zr-89-Immuno-Positron Emission Tomography in Oncology: State-of the-Art Zr-89 Radiochemistry. *Bioconjugate Chem.* **2017**, *28* (9), 2211−2223.

(2) Buchwalder, C.; Jaraquemada-Pelaez, M. D.; Rousseau, J.; Merkens, H.; Rodriguez-Rodriguez, C.; Orvig, C.; Benard, F.; Schaffer, P.; Saatchi, K.; Hafeli, U. O. Evaluation of the Tetrakis(3-Hydroxy-4-Pyridinone) Ligand THPN with Zirconium(IV): Thermodynamic Solution Studies, Bifunctionalization, and in Vivo Assessment of Macromolecular Zr-89-THPN-Conjugates. *Inorg. Chem.* **2019**, *58* (21), 14667−14681.

(3) Buchwalder, C.; Rodriguez-Rodriguez, C.; Schaffer, P.; Karagiozov, S. K.; Saatchi, K.; Hafeli, U. O. A new tetrapodal 3-hydroxy-4-pyridinone ligand for complexation of (89)zirconium for positron emission tomography (PET) imaging. *Dalton Trans.* **2017**, *46* (29), 9654−9663.

(4) Raave, R.; Sandker, G.; Adumeau, P.; Jacobsen, C. B.; Mangin, F.; Meyer, M.; Moreau, M.; Bernhard, C.; Da Costa, L.; Dubois, A.; Goncalves, V.; Gustafsson, M.; Rijpkema, M.; Boerman, O.; Chambron, J.-C.; Heskamp, S.; Denat, F. Direct comparison of the in vitro and in vivo stability of DFO, DFO* and DFOcyclo* for Zr-89-immunoPET. *Eur. J. Nucl. Med. Mol. Imaging* **2019**, *46* (9), 1966−1977.

(5) Alnahwi, A. H.; Ait-Mohand, S.; Dumulon-Perreault, V.; Dory, Y. L.; Guerin, B. Promising Performance of 4HMS, a New Zirconium-89 Octadendate Chelator. *ACS Omega* **2020**, *5* (19), 10731−10739.

(6) Kaeopookum, P.; Petrik, M.; Summer, D.; Klinger, M.; Zhai, C.; Rangger, C.; Haubner, R.; Haas, H.; Hajduch, M.; Decristoforo, C. Comparison of Ga-68-labeled RGD mono- and multimers based on a clickable siderophore-based scaffold. *Nucl. Med. Biol.* **2019**, *78*−*79*, 1−10.

(7) Zhai, C. Y.; He, S. Z.; Ye, Y. J.; Rangger, C.; Kaeopookum, P.; Summer, D.; Haas, H.; Kremser, L.; Lindner, H.; Foster, J.; Sosabowski, J.; Decristoforo, C. Rational Design, Synthesis and Preliminary Evaluation of Novel Fusarinine C-Based Chelators for Radiolabeling with Zirconium-89. *Biomolecules* **2019**, *9* (3), 91−105.

(8) Pandey, A.; Savino, C.; Ahn, S. H.; Yang, Z. Y.; Van Lanen, S. G.; Boros, E. Theranostic Gallium Siderophore Ciprofloxacin Conjugate with Broad Spectrum Antibiotic Potency. *J. Med. Chem.* **2019**, *62* (21), 9947−9960.

(9) Velikyan, I. Prospective of Ga-68-Radiopharmaceutical Development. *Theranostics* **2014**, *4* (1), 47−80.

(10) Holland, J. P.; Williamson, M. J.; Lewis, J. S. Unconventional Nuclides for Radiopharmaceuticals. *Mol. Imaging* **2010**, *9* (1), 1−20.

(11) Kubicek, V.; Havlickova, J.; Kotek, J.; Gyula, T.; Hermann, P.; Toth, E.; Lukes, I. Gallium(III) Complexes of DOTA and DOTA-Monoamide: Kinetic and Thermodynamic Studies. *Inorg. Chem.* **2010**, *49* (23), 10960−10969.

(12) NETSPOT (kit for the preparation of gallium Ga 68 DOTATATE injection); https://www.accessdata.fda.gov/drugsatfda_docs/nda/2016/208547Orig1s000TOC.cfm (accessed April 1, 2018).

(13) Calais, J.; Fendler, W.; Eiber, M.; Wolin, E.; Slavik, R.; Barrio, M.; Gupta, P.; Quon, A.; Schiepers, C.; Auerbach, M.; Czernin, J.; Herrmann, K. High degree of implementation of intended management changes after Ga-68-DOTATATE PET/CT imaging in patients with neuroendocrine tumors. *J. Nucl. Med.* **2017**, *58*, 172−178.

(14) Dilworth, J. R.; Pascu, S. I. The chemistry of PET imaging with zirconium-89. *Chem. Soc. Rev.* **2018**, *47* (8), 2554−2571.

(15) Deri, M. A.; Abou Diane, S.; Francesconi, L. C.; Lewis, J. C. Physical, chemical, and biological insights into Zr-89 -DFO. *J. Labelled. Comp. Radiopharm* **2013**, *56*, S216.

(16) Holland, J. P.; Divilov, V.; Bander, N. H.; Smith-Jones, P. M.; Larson, S. M.; Lewis, J. S. Zr-89-DFO-J591 for ImmunoPET of

Prostate-Specific Membrane Antigen Expression In Vivo. *J. Nucl. Med.* **2010**, *51* (8), 1293−1300.
(17) Boros, E.; Packard, A. B. Radioactive Transition Metals for Imaging and Therapy. *Chem. Rev.* **2019**, *119* (2), 870−901.
(18) Kostelnik, T. I.; Orvig, C. Radioactive Main Group and Rare Earth Metals for Imaging and Therapy. *Chem. Rev.* **2019**, *119* (2), 902−956.
(19) Li, L. L.; Jaraquemada-Pelaez, M. D.; Sarden, N.; Kuo, H. T.; Sarduy, E. A.; Robertson, A.; Kostelnik, T.; Jermilova, U.; Ehlerding, E.; Merkens, H.; Radchenko, V.; Lin, K.-S.; Benard, F.; Engle, J.; Schaffer, P.; Orvig, C. New bifunctional chelators for theranostic applications. *Nucl. Med. Biol.* **2019**, *62*, S36−S42.
(20) Nurchi, V. M.; Jaraquemada-Pelaez, M. D.; Crisponi, G.; Lachowicz, J. I.; Cappai, R.; Gano, L.; Santos, M. A.; Melchior, A.; Tolazzi, M.; Peana, M.; Medici, S.; Zoroddu, M.-A. A new tripodal kojic acid derivative for iron sequestration: Synthesis, protonation, complex formation studies with Fe^{3+}, Al^{3+}, Cu^{2+} and Zn^{2+}, and in vivo bioassays. *J. Inorg. Biochem.* **2019**, *193*, 152−165.
(21) Richardson-Sanchez, T.; Tieu, W.; Gotsbacher, M. P.; Telfer, T. J.; Codd, R. Exploiting the biosynthetic machinery of Streptomyces pilosus to engineer a water-soluble zirconium(IV) chelator. *Org. Biomol. Chem.* **2017**, *15* (27), 5719−5730.
(22) Brown, C. J. M.; Gotsbacher, M. P.; Codd, R. Improved Access to Linear Tetrameric Hydroxamic Acids with Potential as Radiochemical Ligands for Zirconium(IV)-89 PET Imaging. *Aust. J. Chem.* **2020**, *73* (10), 969−978.
(23) Sarbisheh, E. K.; Salih, A. K.; Raheem, S. J.; Lewis, J. S.; Price, E. W. A High-Denticity Chelator Based on Desferrioxamine for Enhanced Coordination of Zirconium-89. *Inorg. Chem.* **2020**, *59* (16), 11715−11728.
(24) Toporivska, Y.; Gumienna-Kontecka, E. The solution thermodynamic stability of desferrioxamine B (DFO) with Zr(IV). *J. Inorg. Biochem.* **2019**, *198*, 110753−110758.
(25) Sturzbecher-Hoehne, M.; Choi, T. A.; Abergel, R. J. Hydroxypyridinonate Complex Stability of Group (IV) Metals and Tetravalent f-Block Elements: The Key to the Next Generation of Chelating Agents for Radiopharmaceuticals. *Inorg. Chem.* **2015**, *54* (7), 3462−3468.
(26) Intorre, B. I.; Martell, A. E. Zirconium complexes in aqueous solution. 1. Reaction with multidentate ligands. *J. Am. Chem. Soc.* **1960**, *82* (2), 358−364.
(27) Intorre, B. J.; Martell, A. E. Zirconium complexes in aqueous solution. 3. Estimation of formation constants. *Inorg. Chem.* **1964**, *3* (1), 81−87.
(28) Racow, E. E.; Kreinbih, J. J.; Cosby, A. G.; Yang, Y.; Pandey, A.; Boros, E.; Johnson, C. J. General Approach to Direct Measurement of the Hydration State of Coordination Complexes in the Gas Phase: Variable Temperature Mass Spectrometry. *J. Am. Chem. Soc.* **2019**, *141* (37), 14650−14660.
(29) Summers, K. L.; Sarbisheh, E. K.; Zimmerling, A.; Cotelesage, J. J. H.; Pickering, I. J.; George, G. N.; Price, E. W. Structural Characterization of the Solution Chemistry of Zirconium(IV) Desferrioxamine: A Coordination Sphere Completed by Hydroxides. *Inorg. Chem.* **2020**, *59* (23), 17443−17452.
(30) Holland, J. P.; Sheh, Y. C.; Lewis, J. S. Standardized methods for the production of high specific-activity zirconium-89. *Nucl. Med. Biol.* **2009**, *36* (7), 729−739.
(31) Holland, J. P.; Vasdev, N. Charting the mechanism and reactivity of zirconium oxalate with hydroxamate ligands using density functional theory: implications in new chelate design. *Dalton Trans.* **2014**, *43* (26), 9872−9884.
(32) Holland, J. P. Predicting the Thermodynamic Stability of Zirconium Radiotracers. *Inorg. Chem.* **2020**, *59* (3), 2070−2082.
(33) Szebesczyk, A.; Olshvang, E.; Shanzer, A.; Carver, P. L.; Gumienna-Kontecka, E. Harnessing the power of fungal siderophores for the imaging and treatment of human diseases. *Coord. Chem. Rev.* **2016**, *327*, 84−109.
(34) Kornreich-Leshem, H.; Ziv, C.; Gumienna-Kontecka, E.; Arad-Yellin, R.; Chen, Y.; Elhabiri, M.; Albrecht-Gary, A. M.; Hadar, Y.; Shanzer, A. Ferrioxamine B analogues: Targeting the FoxA uptake system in the pathogenic Yersinia enterocolitica. *J. Am. Chem. Soc.* **2005**, *127* (4), 1137−1145.
(35) Olshvang, E.; Szebesczyk, A.; Kozlowski, H.; Hadar, Y.; Gumienna-Kontecka, E.; Shanzer, A. Biomimetic ferrichrome: structural motifs for switching between narrow- and broad-spectrum activities in P. putida and E. coli. *Dalton Trans.* **2015**, *44* (48), 20850−20858.
(36) Besserglick, J.; Olshvang, E.; Szebesczyk, A.; Englander, J.; Levinson, D.; Hadar, Y.; Gumienna-Kontecka, E.; Shanzer, A. Ferrichrome Has Found Its Match: Biomimetic Analogues with Diversified Activity Map Discrete Microbial Targets. *Chem. - Eur. J.* **2017**, *23* (53), 13181−13191.
(37) Anderegg, G.; Leplatte, F.; Schwarzenbach, G. Hydroxamatkomplexe. 3. Eisen(iii)-austausch zwischen sideraminen und komplexonen - diskussion der bildungskonstanten der hydroxamatkomplexe. *Helv. Chim. Acta* **1963**, *46* (4), 1409−1422.
(38) Mular, A.; Shanzer, A.; Kozłowski, H.; Decristoforo, C.; Gumienna-Kontecka, E. Unpublished results.
(39) Seibold, U.; Wangler, B.; Wangler, C. Rational Design, Development, and Stability Assessment of a Macrocyclic Four-Hydroxamate-Bearing Bifunctional Chelating Agent for Zr-89. *ChemMedChem* **2017**, *12* (18), 1555−1571.
(40) Guerard, F.; Lee, Y. S.; Brechbiel, M. W. Rational Design, Synthesis, and Evaluation of Tetrahydroxamic Acid Chelators for Stable Complexation of Zirconium(IV). *Chem. - Eur. J.* **2014**, *20* (19), 5584−5591.
(41) Patra, M.; Bauman, A.; Mari, C.; Fischer, C. A.; Blacque, O.; Haussinger, D.; Gasser, G.; Mindt, T. L. An octadentate bifunctional chelating agent for the development of stable zirconium-89 based molecular imaging probes. *Chem. Commun.* **2014**, *50* (78), 11523−11525.
(42) Whisenhunt, D. W.; Neu, M. P.; Hou, Z. G.; Xu, J.; Hoffman, D. C.; Raymond, K. N. Specific sequestering agents for the actinides. 29. Stability of the thorium(IV) complexes of desferrioxamine B (DFO) and three octadentate catecholate or hydroxypyridinonate DFO derivatives: DFOMTA, DFOCAMC, and DFO-1,2-HOPO. Comparative stability of the plutonium(IV) DFOMTA complex. *Inorg. Chem.* **1996**, *35* (14), 4128−4136.
(43) Borgias, B.; Hugi, A. D.; Raymond, K. N. Isomerization and solution structures of desferrioxamine-B complexes of aluminium (3+) and galium (3+). *Inorg. Chem.* **1989**, *28* (18), 3538−3545.
(44) Farkas, E.; Kiss, T.; Kurzak, B. Microscopic dissociation processes of alaninehydroxamic acids. *J. Chem. Soc., Perkin Trans. 2* **1990**, No. 7, 1255−1257.
(45) Tegoni, M.; Ferretti, L.; Sansone, F.; Remelli, M.; Bertolasi, V.; Dallavalle, F. Synthesis, solution thermodynamics, and x-ray study of Cu-II 12 metallacrown-4 with GABA hydroxamic acid: An unprecedented crystal structure of a 12 MC-4 with a gamma-aminohydroxamate. *Chem. - Eur. J.* **2007**, *13* (4), 1300−1309.
(46) Piasta, K.; Dzielak, A.; Mucha, A.; Gumienna-Kontecka, E. Non-symmetrical bis(aminoalkyl) phosphinates: new ligands with enhanced binding of Cu(II) ions. *New J. Chem.* **2018**, *42* (10), 7737−7745.
(47) Ostrowska, M.; Toporivska, Y.; Golenya, I. A.; Shova, S.; Fritsky, I. O.; Pecoraro, V. L.; Gumienna-Kontecka, E. Explaining How alpha-Hydroxamate Ligands Control the Formation of Cu(II)-, Ni(II)-, and Zn(II)-Containing Metallacrowns. *Inorg. Chem.* **2019**, *58* (24), 16642−16659.
(48) Sanchiz, J.; Esparza, P.; Dominguez, S.; Brito, F.; Mederos, A. Solution studies of complexes of iron(III) with iminodiacetic, alkyl-substituted iminodiacetic and nitrilotriacetic acids by potentiometry and cyclic voltammetry. *Inorg. Chim. Acta* **1999**, *291* (1−2), 158−165.
(49) Motekaitis, R. J.; Martell, A. E. The iron(III) and iron(II) complexes of nitrilotriacetic acid. *J. Coord. Chem.* **1994**, *31* (1), 67−78.
(50) Deblonde, G. J. P.; Sturzbecher-Hoehne, M.; Abergel, R. J. Solution Thermodynamic Stability of Complexes Formed with the Octadentate Hydroxypyridinonate Ligand 3,4,3-LI(1,2-HOPO): A

Critical Feature for Efficient Chelation of Lanthanide(IV) and Actinide(IV) Ions. *Inorg. Chem.* **2013**, *52* (15), 8805−8811.
(51) Schwarzenbach, G.; Schwarzenbach, K. Hydroxamatkomplexe. 1. Die stabilitat der eisen(iii)-komplexe einfacher hydroxamsauren und des ferrioxamins B. *Helv. Chim. Acta* **1963**, *46* (4), 1390−1399.
(52) Evers, A.; Hancock, R. D.; Martell, A. E.; Motekaitis, R. J. Metal-ion recognition in ligands with negatively charged oxygen donor groups - complexation of Fe(III), Ga(III), In(III), Al(III), and other highly charged metal-ions. *Inorg. Chem.* **1989**, *28* (11), 2189−2195.
(53) Harris, W. R.; Carrano, C. J.; Raymond, K. N. Coordination chemistry of microbial iron transport compounds. 16. Isolation, characterization, and formation-constants of ferric aerobactin. *J. Am. Chem. Soc.* **1979**, *101* (10), 2722−2727.
(54) Clarke, E. T.; Martell, A. E. Stabilities of the Fe(III), Ga(III) and In(III) chelates of N,N′,N″-triazacyclononanetriacetic acid. *Inorg. Chim. Acta* **1991**, *181* (2), 273−280.
(55) Wang, X. Z.; Jaraquemada-Pelaez, M. D.; Cao, Y.; Pan, J. H.; Lin, K. S.; Patrick, B. O.; Orvig, C. H_2hox: Dual-Channel Oxine-Derived Acyclic Chelating Ligand for Ga-68 Radiopharmaceuticals. *Inorg. Chem.* **2019**, *58* (4), 2275−2285.
(56) Notni, J.; Hermann, P.; Havlickova, J.; Kotek, J.; Kubicek, V.; Plutnar, J.; Loktionova, N.; Riss, P. J.; Rosch, F.; Lukes, I. A. Triazacyclononane-Based Bifunctional Phosphinate Ligand for the Preparation of Multimeric Ga-68 Tracers for Positron Emission Tomography. *Chem. - Eur. J.* **2010**, *16* (24), 7174−7185.
(57) Motekaitis, R. J.; Sun, Y.; Martell, A. E.; Welch, M. J. Stabilities of gallium(III), iron(III), and indium(III) chelates of hydroxyaromatic ligands with different overall charges. *Inorg. Chem.* **1991**, *30* (13), 2737−2740.
(58) Abergel, R. J.; D'Aleo, A.; Leung, C. N. P.; Shuh, D. K.; Raymond, K. N. Using the Antenna Effect as a Spectroscopic Tool: Photophysics and Solution Thermodynamics of the Model Luminescent Hydroxypyridonate Complex $[Eu^{III}$(3,4,3-LI(1,2-HOPO))$]^-$. *Inorg. Chem.* **2009**, *48* (23), 10868−10870.
(59) Anderegg, G.; Arnaud-Neu, F.; Delgado, R.; Felcman, J.; Popov, K. Critical evaluation of stability constants of metal complexes of complexones for biomedical and environmental applications (IUPAC Technical Report). *Pure Appl. Chem.* **2005**, *77* (8), 1445−1495.
(60) Brown, P. L.; Ekberg, C. *Hydrolysis of Metal Ions*; Wiley: 2016.
(61) Summer, D.; Garousi, J.; Oroujeni, M.; Mitran, B.; Andersson, K. G.; Vorobyeva, A.; Lofblom, J.; Orlova, A.; Tolmachev, V.; Decristoforo, C. Cyclic versus Noncyclic Chelating Scaffold for Zr-89-Labeled ZEGFR:2377 Affibody Bioconjugates Targeting Epidermal Growth Factor Receptor Overexpression. *Mol. Pharmaceutics* **2018**, *15* (1), 175−185.
(62) Zhai, C. Y.; Summer, D.; Rangger, C.; Franssen, G. M.; Laverman, P.; Haas, H.; Petrik, M.; Haubner, R.; Decristoforo, C. Novel Bifunctional Cyclic Chelator for Zr-89 Labeling-Radiolabeling and Targeting Properties of RGD Conjugates. *Mol. Pharmaceutics* **2015**, *12* (6), 2142−2150.
(63) Wadas, T. J.; Wong, E. H.; Weisman, G. R.; Anderson, C. J. Coordinating Radiometals of Copper, Gallium, Indium, Yttrium, and Zirconium for PET and SPECT Imaging of Disease. *Chem. Rev.* **2010**, *110* (5), 2858−2902.
(64) Burdett, J. K.; Hoffmann, R.; Fay, R. C. Eigth-coordination. *Inorg. Chem.* **1978**, *17* (9), 2553−2568.
(65) Rousseau, J.; Zhang, Z. X.; Wang, X. Z.; Zhang, C. C.; Lau, J.; Rousseau, E.; Colovic, M.; Hundal-Jabal, N.; Benard, F.; Lin, K. S. Synthesis and evaluation of bifunctional tetrahydroxamate chelators for labeling antibodies with Zr-89 for imaging with positron emission tomography. *Bioorg. Med. Chem. Lett.* **2018**, *28* (5), 899−905.
(66) Boros, E.; Holland, J. P.; Kenton, N.; Rotile, N.; Caravan, P. Macrocycle-Based Hydroxamate Ligands for Complexation and Immunoconjugation of (89)Zirconium for Positron Emission Tomography (PET) Imaging. *ChemPlusChem* **2016**, *81* (3), 274−281.
(67) Tieu, W.; Lifa, T.; Katsifis, A.; Codd, R. Octadentate Zirconium(IV)-Loaded Macrocycles with Varied Stoichiometry Assembled From Hydroxamic Acid Monomers using Metal-Templated Synthesis. *Inorg. Chem.* **2017**, *56* (6), 3719−3728.
(68) Zeglis, B. M.; Mohindra, P.; Weissmann, G. I.; Divilov, V.; Hilderbrand, S. A.; Weissleder, R.; Lewis, J. S. Modular Strategy for the Construction of Radiometalated Antibodies for Positron Emission Tomography Based on Inverse Electron Demand Diels-Alder Click Chemistry. *Bioconjugate Chem.* **2011**, *22* (10), 2048−2059.
(69) Price, E. W.; Orvig, C. Matching chelators to radiometals for radiopharmaceuticals. *Chem. Soc. Rev.* **2014**, *43* (1), 260−290.
(70) Bastian, R.; Weberling, R.; Palilla, F. Determination of iron by ultraviolet spectrophotometry. *Anal. Chem.* **1956**, *28* (4), 459−462.
(71) Szebesczyk, A.; Olshvang, E.; Besserglick, J.; Gumienna-Kontecka, E. Influence of structural elements on iron(III) chelating properties in a new series of amino acid-derived monohydroxamates. *Inorg. Chim. Acta* **2018**, *473*, 286−296.
(72) Babko, A. K.; Gridchina, G. I. Vliyanie sostoyaniya tsirkoniya v rastvore na ego vzaimodeistvie s organicheskimi reaktivami. *Zhur. Neorg. Khim.* **1962**, *7* (4), 889−893.
(73) Enyedy, E. A.; Primik, M. F.; Kowol, C. R.; Arion, V. B.; Kiss, T.; Keppler, B. K. Interaction of Triapine and related thiosemicarbazones with iron(III)/(II) and gallium(III): a comparative solution equilibrium study. *Dalton Trans.* **2011**, *40* (22), 5895−5905.
(74) Alfenaar, M.; Deligny, C. L. Universal ph-scale in methanol and methanol-water mixtures. *Recl. Trav. Chim. Pays-Bas* **1967**, *86* (11), 1185−1190.
(75) Gelsema, W. J.; Deligny, C. L.; Remijnse, A. G.; Blijleve, H. pH-measurements in alcohol-water mixtures using aqueous standard buffer solutions for calibration. *Recl. Trav. Chim. Pays-Bas* **1966**, *85* (7), 647−660.
(76) Gans, P.; O'Sullivan, B. GLEE, a new computer program for glass electrode calibration. *Talanta* **2000**, *51* (1), 33−37.
(77) Gran, G.; et al. Determination of the equivalent point in potentiometric titrations. *Acta Chem. Scand.* **1950**, *4* (4), 559−577.
(78) Gans, P.; Sabatini, A.; Vacca, A. Superquad - an improved general program for computation of formation-constants from potentiometric data. *J. Chem. Soc., Dalton Trans.* **1985**, No. 6, 1195−1200.
(79) Alderighi, L.; Gans, P.; Ienco, A.; Peters, D.; Sabatini, A.; Vacca, A. Hyperquad simulation and speciation (HySS): a utility program for the investigation of equilibria involving soluble and partially soluble species. *Coord. Chem. Rev.* **1999**, *184*, 311−318.
(80) Baes, C. F.; Mesmer, R. E. The thermodynamics of cation hydrolysis. *Am. J. Sci.* **1981**, *281* (7), 935−962.
(81) Zdyb, K.; Plutenko, M. O.; Lampeka, R. D.; Haukka, M.; Ostrowska, M.; Fritsky, I. O.; Gumienna-Kontecka, E. Cu(II), Ni(II) and Zn(II) mononuclear building blocks based on new polynucleating azomethine ligand: Synthesis and characterization. *Polyhedron* **2017**, *137*, 60−71.
(82) Gampp, H.; Maeder, M.; Meyer, C. J.; Zuberbuhler, A. D. Calculation of equilibrium-constants from multiwavelength spectroscopic data. 1. Mathematical considerations. *Talanta* **1985**, *32* (2), 95−101.
(83) Gampp, H.; Maeder, M.; Meyer, C. J.; Zuberbuhler, A. D. Calculation of equilibrium-constants from multiwavelength spectroscopic data. 2. Specfit - 2 user-friendly programs in basic and standard fortran-77. *Talanta* **1985**, *32* (4), 257−264.
(84) Rossotti, F. J.; Rossotti, H. S.; Whewell, R. J. Use of electronic computing techniques in calculation of stability constants. *J. Inorg. Nucl. Chem.* **1971**, *33* (7), 2051−2065.
(85) Milburn, R. M.; Vosburgh, W. C. A spectrophotometric study of the hydrolysis of iron(iii) ion 0.2. Polynuclear species. *J. Am. Chem. Soc.* **1955**, *77* (5), 1352−1355.
(86) Milburn, R. M. A spectrophotometric study of the hydrolysis of iron(iii) ion 0.3. Heats and entropies of hydrolysis. *J. Am. Chem. Soc.* **1957**, *79* (3), 537−540.

https://doi.org/10.1021/acs.inorgchem.1c01622
Inorg. Chem. 2021, 60, 13332−13347

Bioorganic Chemistry 119 (2022) 105518

Contents lists available at ScienceDirect

Bioorganic Chemistry

journal homepage: www.elsevier.com/locate/bioorg

Synthesis and biological evaluation of novel rhodanine-based structures with antiviral activity towards HHV-6 virus

Valentina Gentili [1], Giulia Turrin [1], Paolo Marchetti, Sabrina Rizzo, Giovanna Schiuma, Silvia Beltrami, Virginia Cristofori, Davide Illuminati, Greta Compagnin, Claudio Trapella [*], Roberta Rizzo [*], Daria Bortolotti [1], Anna Fantinati [1]

University of Ferrara, Department of Chemical, Pharmaceutical and Agricultural Sciences, Via Fossato di Mortara, 17, 44121 Ferrara, Italy

A B S T R A C T

An increased awareness of diseases associated with Human herpesvirus 6 (HHV-6) infection or reactivation has resulted in a growing interest in the evaluation of the best treatment options available for the clinical management of HHV-6 disease. However, no compound has yet been approved exclusively for HHV-6 infection treatment. For this reason, the identification of anti-HHV6 compounds provides a valuable opportunity for developing efficient antiviral therapies. A possible target for antiviral drugs is the virus-cell fusion step. In this study, we synthetized potential fusion intermediates inhibitors based on the rhodanine structure. The obtained derivatives were tested for cytotoxicity and for antiviral activity in human cells infected with HHV6. Level of infection was monitored by viral DNA quantification at different time points up to 7 days post infection. Among the synthetized derivatives, **9e** showed a significative inhibitory effect on viral replication that lasted over 7 days, probably attributable to the particular combination of hydrophilic and hydrophobic substituents to the rhodanine moiety. Our results support the use of these amphipathic fusion inhibitors for the treatment of HHV-6 infections.

1. Introduction

Most of available antiviral drugs are design to target specific viral proteins [1,2]. However, this therapeutic approach determines a selection for resistance [3], and also display a limited spectrum of action. In view of this, novel antivirals are therefore needed.

In the last years, several studies were focused on the identification of new antiviral targets based on the interference with viral fusion on cell membrane [4]. In fact, fusion of enveloped virus with the host cell is crucial in viral infectivity. Viral fusion is a process driven by specialized protein expressed on viral envelope that, after conformational modifications due to their binding to specific cellular receptors, leads to envelope-cell membrane fusion and the consequent release of the nucleocapsid into the cytoplasm.

The steps of the viral fusion process evidenced two possible moments on which fusion inhibitors could be effective: *i.* pre-fusion step, which involved the engagement of the cellular receptor during the viral adsorption and *ii.* fusion intermediates step, in which a physical fusion occurs between the lipid bilayers of both envelope and cytoplasmic membrane [5].

Various molecules are proposed in literature as membrane fusion inhibitors that affect the viral attachment through cell receptor, disturbing the viral adsorption phase [5]. Essentially, these molecules exert their function by blocking the cognate virus-receptor interaction via competition for the entry receptors, representing the classical inhibitors of virus entry [5]. The use of this strategy is exemplified by Maraviroc (Selzentry; Pfizer), a competitive molecule for the virus co-receptor CC-chemokine receptor 5 (CCR5) that inhibits HIV-1 entry [6]. However, despite the potential efficacy of these competitors as antivirals, the development of receptor-specific entry inhibitors for the great majority of viral pathogens is limited by the identification of the actual receptors. In this view, the design of new antivirals, capable of inhibiting cell entry of enveloped viruses by blocking the formation of fusion intermediates seems to represent the most convenient approach. In fact, these molecules could act independently from the cellular receptor involved during viral entry, thus no specific receptor structure is required.

Fusion intermediates inhibitors work mainly by modifying the lipidic structure of both virus and host cell membrane, in order to avoid the release of the nucleocapsid inside the cells. Among antiviral mechanisms of action against the entry of enveloped viruses, the most studied include the induction of cholesterol depletion [7] and the alteration of membrane components that modify membrane fluidity [8] or cause virolysis.

* Corresponding authors at: University of Ferrara, Department of Chemical, Pharmaceutical and Agricultural Sciences, Via Luigi Borsari 46, 44121 Ferrara, Italy (R. Rizzo). University of Ferrara, Department of Chemical, Pharmaceuticaland Agricultural Sciences, Via Fossato di Mortara, 17 44121 Ferrara, Italy (C. Trapella).
E-mail addresses: trap@unife.it (C. Trapella), rbr@unife.it (R. Rizzo).
[1] These authors contributed equally to the research.

https://doi.org/10.1016/j.bioorg.2021.105518
Received 3 June 2021; Received in revised form 4 October 2021; Accepted 23 November 2021
Available online 26 November 2021

This, for instance, is observed in treatment with rigid amphipathic fusion inhibitors (RAFIs) [9-12].

Other molecules displaying a broad-spectrum of antiviral activity through a selective action on enveloped viruses are rhodanine and thiobarbituric derivatives. Their activity is due to lipid oxidation ability, which affects the fluidity of the lipid bilayer and interferes with virus-cell fusion. Recently, polyrhodanine nanostructure has been reported as antiviral, anticancer and bacteriostatic [13]

Fusion intermediate inhibitors are promising antiviral drugs since they exert their function in the early phase of infection, namely before damages have occurred to cells [14,15]. The advantage of using this kind of antivirals includes the broad spectrum of enveloped viruses that could be inhibited without the risk of developing resistance. Some of these antivirals have been described to be effective on different human viruses, such as the respiratory syncytial virus (RSV) [16], Hepatitis B (HBV) [17] and C (HCV) viruses [18,19].

Considering enveloped viruses associated to different human pathological conditions, herpesviruses are among the most studied. In particular, these viruses are characterized by the ability to develop a latency phase after the primary infection, causing as a consequence the onset of symptoms throughout the life span.

The Herpesiviridae family includes nine components that infect humans and can be divided into three subfamilies: alpha-, beta- and gamma-herpesvirus according to their different cell tropism and symptomatology.

Human Herpes Virus-6 (HHV-6) is a beta-herpesvirus with a worldwide distribution that exists in two different species characterized by peculiar biological differences [20]: HHV-6A and HHV-6B. HHV-6B is the etiologic agent of roseola (*exanthema subitum*), while the disease associated with HHV-6A infection is still not clearly identified. These differences could be attributed to a different engagement of cell receptors by the two viruses. In fact, while HHV-6B recognizes CD134, expressed on *T*-cells, HHV-6A uses CD46, expressed on all nucleated cells [21], subtending its ability to infect a wide range of tissues, as confirmed by the recent association of HHV-6A infection with several diseases, including Multiple Sclerosis (MS) [22], Alzehimer's Disease (AD) [23,24] and infertility [25,26]. Importantly, to date, the treatment for HHV-6 infection consists only in antivirals that are already used to treat other herpetic infections and that target specific viral protein in order to inhibit viral replication and gene expression [27,28]. Moreover, HHV-6 establishes a latent infection in the target tissues and it could be reactivated several times during life, thus it requires several treatments with antivirals which can increase the risk of resistances [29,30]. In light of this, the use of fusion intermediates inhibitors to threat HHV-6 infection may represent an efficient strategy to improve infection control and decrease resistance onset.

The data available in literature on the use of fusion inhibitors to control herpetic infections report mainly the effect of some compounds in affecting the pre-fusion phase, by interfering with glycoprotein B interaction and cellular-membrane lipid rafts formation [31-33]. On the other hand, concerning the inhibition of the fusion intermediate formation, Cagno et al. described the antiviral activity of rhodanine derivatives on enveloped viruses including HSV-2 acyclovir resistant strain [34] and Boresnstein et al. recently reported the effect of ginkgolic acid on several herpes viruses, including EBV, HSV-1 and HCMV [35].

Conversely, no data are available on the use of fusion intermediates inhibitors for this particular type of infection.

In this study, we have synthesized ten potential fusion intermediates inhibitors based on rhodanine structure, potentially active on HHV-6 infection. We tested the compounds on human cell lines, to determine their toxicity and effectiveness in controlling the HHV-6 infection, in order to identify the most safe and active compound.

2. Results and discussion

2.1. Chemistry

Recently different works has been published on the synthesis of antiviral molecule based on rhodanine heterocycle [34], acting as disrupting molecules for the enveloped viruses such as HSV-2, Influenza A virus, Zika.

Referring to the work of Cagno et al. [34] we chose the rhodanine-based compound **1** as reference compound to develop a SAR study focused on the modification of its hydrophilic head and lipophilic chain (Fig. 1). Different specific modifications have been made, considering RAFIs and their mechanism of action as starting point for this study [36].

The synthesis of the rhodanine scaffold was focused on the introduction of several aromatic rings, starting from different primary chiral and achiral amines, in order to build a small library of compounds bearing a series of substituents attached to the nitrogen atom (Scheme 1).

The synthesis of rhodanine derivatives has been achieved in a one-pot reaction between bromo-acetyl bromide (**2**) and the corresponding primary amine **3a-f** in carbon disulfide, to obtain in moderate to good yield the rhodanine core **4a-f**. Then, as shown in Scheme 2, to insert structural modifications of the polar head of the compound **1** (Fig. 1), we used a palladium catalyzed Suzuki reaction as a key step for the formation of the carbon–carbon bond between the iodo derivatives **5a-e** and the five-membered heterocycles, **6a-b** (furane or thiophene). Due to the instability of the rhodanine scaffold in basic conditions [37], we decided to work with the corresponding methyl ester derivatives **5a-e** to obtain the aldehydic compounds **7a-e** with higher yields. Then, we removed the ester function in the next step through lithium hydroxide hydrolysis, to afford compounds **8a-d**.

Once obtained the derivatives **8a-d**, we could bind them with the rhodanine scaffold trough a Knowenagel condensation [38], to obtain the desired products **9a**. Starting from **9a** we conceptualized new compounds with different lipophilic tails (**9b-f)** or different hydrophilic heads (**10a-d)** as depicted in Scheme 3.

2.2. Biological evaluation

2.2.1. Evaluation of cytotoxicity of *9a* and derivate compounds with different lipophilic tails

9a-f cytotoxicity was assayed in human lymphocytic cell lines by MTT assay, after 24 h treatment at 100 μM, 10 μM and 1 μM. As shown in Fig. 2, all the compounds did not affect cell viability at the concentrations of 1μM and 10 μM, while the concentration of 100 μM showed a high cytotoxic effect ($p < 0.0001$, Student T test). The anti-viral efficacy was evaluated for the concentrations of 1 and 10 μM, that are hundred-ten times lower than the cytotoxic concentration and ensure a safe use as

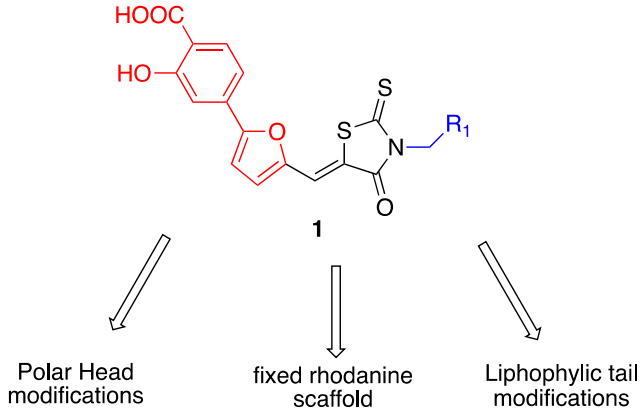

Fig. 1. Structure of the rhodamine-based reference compound.

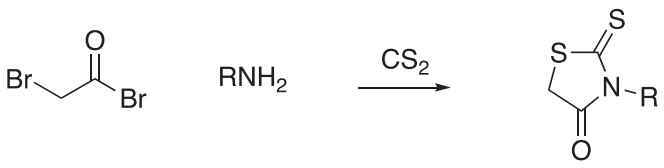

2 **3a-f**

4a = $(CH_2)_2Ph$
4b = $(CH_2)_3Ph$
4c = CH_2-4-MePh
4d = CH_2-3,4-dimethoxyphenyl
4e = (*R*)-$CH_2CH(CH_3)Ph$
4f = (*S*)-$CH_2CH(CH_3)Ph$

Scheme 1. Synthesis of rhodanine derivatives with modifications at lipophilic tail.

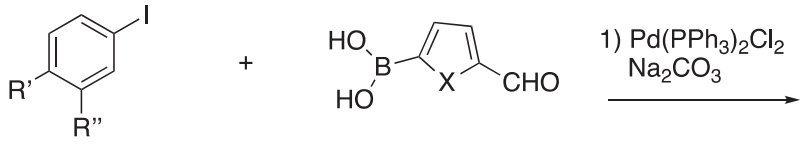

5a: R'=COOMe, R"=OH
5b: R'=COOMe, R"=H
5c: R'=H, R"= OH
5d: R'=OH, R"=COOMe

6a: X=O
6b: X=S

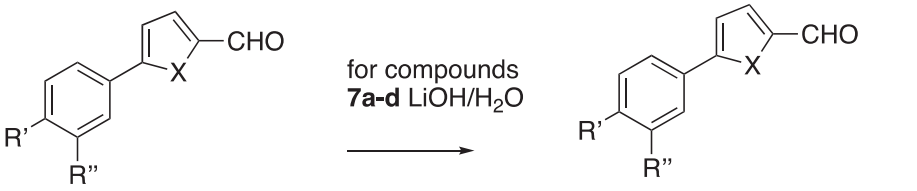

7a: R'=$COOCH_3$,R"=OH, X=O
7b: R'=$COOCH_3$,R"=OH, X=S
7c: R'=OH,R"=$COOCH_3$, X=O
7d: R'=$COOCH_3$,R"=H, X=O
7e: R'=H, R"=OH, X=O

8a: R'=COOH,R"=OH, X=O
8b: R'=COOH,R"OH, X=S
8c: R'=OH,R"=COOH, X=O
8d: R'=COOH,R"=H, X=O

Scheme 2. Synthesis of polar head bearing the aldehyde moiety.

a drug. The absence of cytotoxicity in the 1 and 10 μM range of concentration could be explained by the fact that cellular membranes are metabolically active and are characterized by a regenerative activity, that is absent in viromes.

2.2.2. *Anti-HHV-6 activity of **9a** and derivate compounds with different lipophilic tails*

The antiviral activity of **9a-f** compounds was tested on HHV-6A infected J-Jhan cells and HHV-6B SupT1 infected cells. The compounds were added to infected cell cultures at the concentration of 1 and 10μM and pellet cell samples were collected at 24, 48, 72 h (hpi) and 7 days post infection (dpi) for HHV-6 DNA quantification by real time PCR. Results are reported as percentage compared to untreated infected control.

9a-9d molecules did not affect viral replication when used at the concentration of 1 μM (Fig. 3a, b), while **9e** and **9f** molecules were able to decrease viral replication in a significant level ($p < 0.0001$, Student T test) (Fig. 3a, b).

The treatment at 10μM was more effective in reducing HHV-6A and HHV-6B replication (Fig. 3c, d). In particular, the highest antiviral effect was observed in presence of **9a, 9e** and **9f** treatment, which significantly decreased viral replication at all the time points considered, showing a decrease of 90–75% of viral load already after 24 hpi compared to untreated control ($p < 0.01$, Student T test), followed by a complete drop of the viral infection till 7 dpi for **9a** and **9e** ($p < 0.0001$, Student T test) (Fig. 3c, d). On the contrary, in presence of **9b**, **9c** and **9d** treatment we observed no effect on viral load at 24 hpi, while there was a drop in both HHV-6A and HHV-6B replication at 48 hpi that is maintained until 7dpi ($p < 0.0001$, Student T test) (Fig. 3c, d).

2.2.3. *Evaluation of cytotoxicity and antiviral activity of **9a** derivatives with modified hydrophilic head*

MTT assay was performed to assess the **10a**, **10b** and **10c** derivatives cytotoxicity on human lymphocyte cell lines after treatment for 24 h at the concentration of 1 and 10μM. The results showed that **10a**, **10b** and **10d** did not affect cell viability, while **10c** resulted in a significant cytotoxic effect (Fig. 4, $p < 0.05$ Student T test). We hypothesize that the toxicity of compound 10c might be due to the lack of the phenol OH that is involved in the hydrogen bond with the carboxylic moiety. In fact, both 10b and 10d are not toxic, where the OH group of 10b makes a

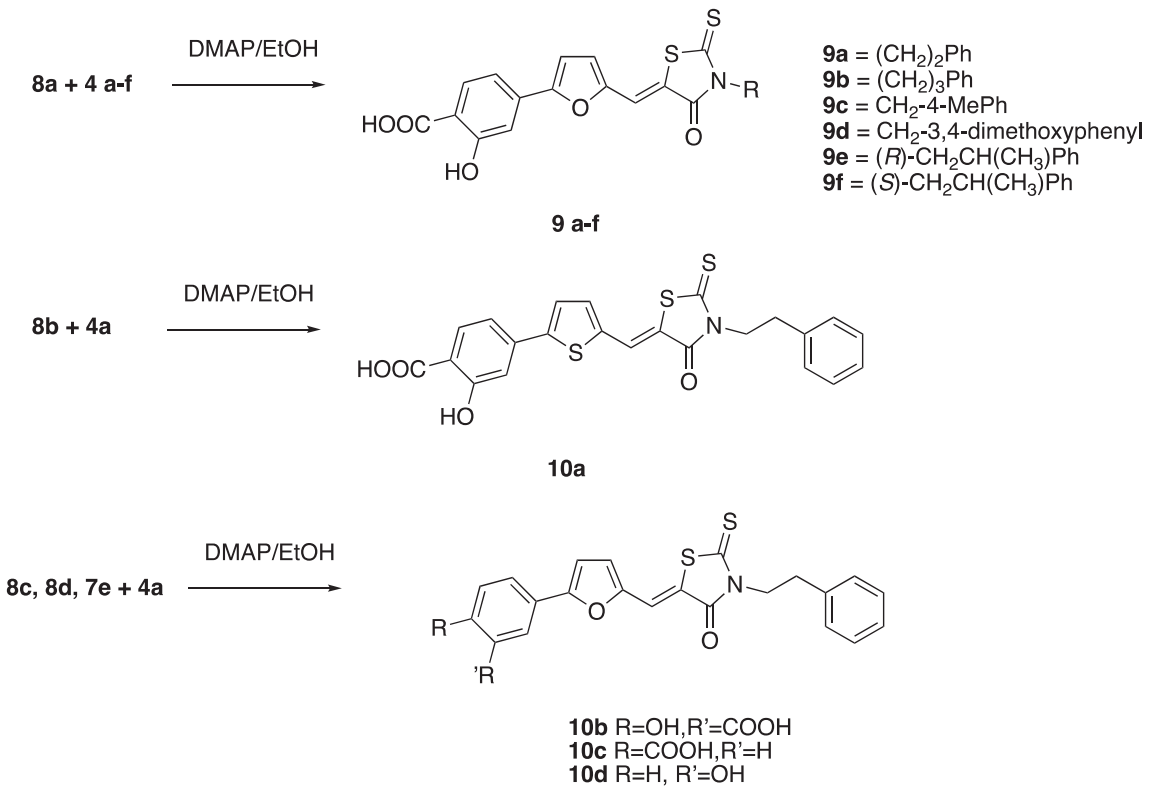

Scheme 3. Synthesis of the final rhodanine scaffold bearing different polar heads and lipophylic tails.

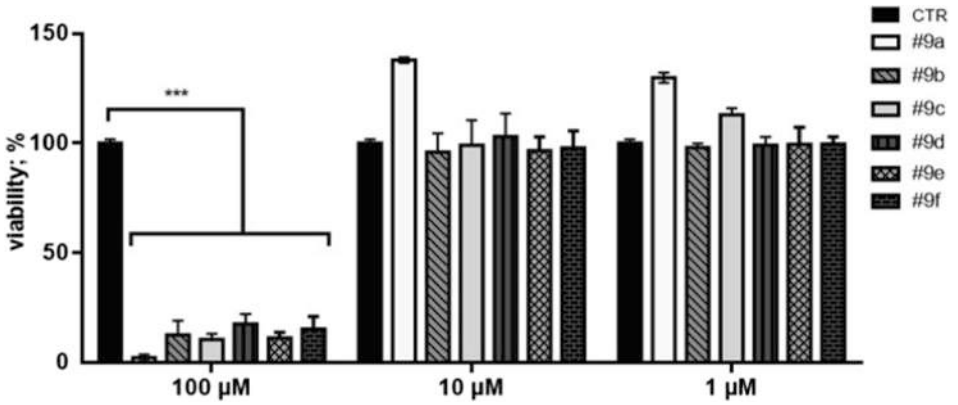

Fig. 2. Cell viability analysis by MTT assay in human lymphocyte cell lines after 24 h treatment with #**9a-9f** at the concentrations of 1, 10 and 100 µM. Values are reported as mean ± SD of 3 independent experiments.

hydrogen bond with the carboxylic moiety, 10d lacks the COOH function, supporting that the toxicity of 10c might be related to this acidic function when it's not involved in the hydrogen bond due to the lack of hydroxyl group. Basing on this result, **10c** was not considered for further analysis.

Antiviral activity of **10a, 10b and 10d** compounds was evaluated. As shown in Fig. 5, the HHV-6A and HHV-6B viral load was reduced of 52 and 54% ($p = 0.0016$, Student T test) and 90 and 89% ($p = 0.0002$, Student T test), respectively, after 72hpi and 7dpi after treatment with **10b**. **10a** treatment reduced the viral load of 52% ($p = 0.0046$, Student T test) and 49% ($p = 0.0044$, Student T test), at 48hpi and 72hpi, respectively, but the anti-HHV-6A and HHV-6B effect was lost after 7dpi (Fig. 5). **10d** treatment reduced the viral load of 90% ($p < 0.0001$, Student T test) at 24hpi and 48hpi, but the anti-HHV-6A and HHV-6B effect was lost after 72hpi (Fig. 5).

This data confirmed that the modification of **9a** polarity obtained in these derivatives does not improve its inhibition of the viral replication, suggesting that this moiety participates only partially at the antiviral effect.

3. Conclusion

Despite the increasing evidence reporting HHV-6A and HHV-6B association with different diseases [22-26], there are no specific antiviral drugs available acting against this specific virus. The present study explores the antiviral effects of rhodanine-based fusion intermediate inhibitors on HHV-6 infection in human cells. Since HHV-6 is an enveloped virus, we synthesized potential fusion intermediate inhibitors [14,15], characterized by the presence of a rhodanine scaffold, with the aim of blocking the virion-cell fusion. We obtained different derivatives by substitution and bioisosteric replacements of hydrophilic head and lipophilic tail of the molecules tested for their cytotoxicity and antiviral

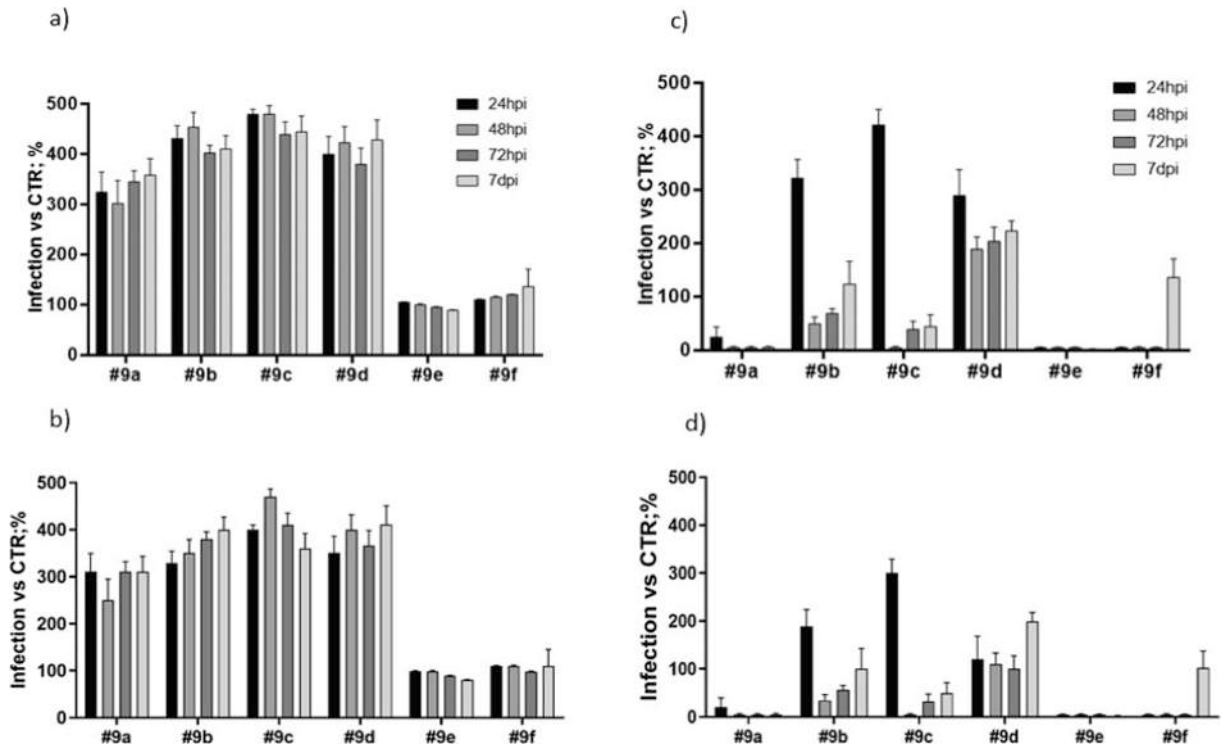

Fig. 3. Infection percentage compared to the untreated infected control (CTR) after treatment at 1 μM (a, b) and 10 μM (c, d) with #**9a-9f** compounds 24, 48 and 72 h and 7 days post infection with HHV-6A (a, c) and HHV-6B (b, d). HHV-6 genomes were quantified by real time-PCR and normalized for housekeeping RNaseP gene. Data were reported as mean percentage ± SD obtained from 3 independent experiments compared to untreated infected cells.

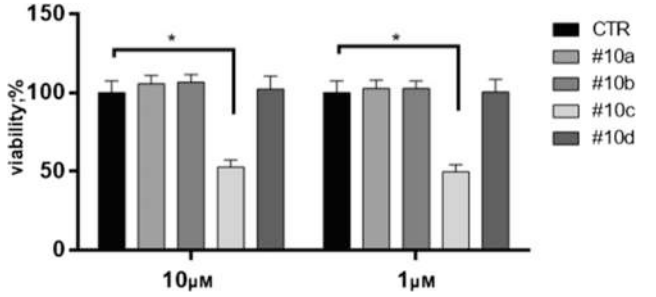

Fig. 4. Cell viability analysis by MTT assay in human lymphocyte cell lines after 24 h treatment with #**10a**, #**10b**, #**10c** and #**10d** at the concentration of 1 and 10 μM, compared to untreated control (CTR). Values are reported as mean ± SD of 3 independent experiments. *$p < 0.05$ Student T test.

effect on HHV-6A and HHV-6B replication. Experimental results identified the **9a** derivative as the lead compound, showing a complete reduction of HHV-6 viral load 48 h after infection, when used at 10uM, without showing any cytotoxicity. In order to improve the antiviral effect of the lead compound **9a**, we worked on the modification of the hydrophilic head or the lipophilic tail to increase the amphipacity of the molecule, obtaining different derivatives. Among these, compound **9e** at the concentration of 10uM, showed the highest antiviral activity, with a complete abatement of the viral load after 24 h and no cytotoxicity. The improved efficacy of compound **9e** could be attributed to its peculiar combination of hydrophilic and hydrophobic substituents to the rhodanine moiety, that possibly allowed a better interaction with the viral envelope. The insertion into the viral envelop might induce envelope structure destabilization and virolysis that inhibit virion fusion and infection of the target cell. These results support the use of amphipathic fusion intermediate inhibitors based on rhodanine structure to treat HHV-6A and HHV-6B infection. Despite the two viruses engage different cellular receptors, we observed a comparable inhibitory effect by treating with inhibitors based on rhodanine structure. This could be ascribable to the amphipathic nature of the compounds, which disorganize the viral envelope structure, avoiding the viral fusion with the host cell membranes, without engaging specific viral structures. In fact, enveloped viruses as HHV-6, gain their external membrane during virions release directly from cell surface. Anyway, while cell membranes are metabolically active, viral envelopes are not. In this way, rhodanine derivatives could induce virolysis and interfere with envelope-cell fusion process by intercalating in the viral outer phospholipidic bilayer without inducing critical cell membrane alteration, as proved by the absence of cytotoxicity observed after treating cells with antiviral concentrations.

This characteristic might avoid the onset of resistance in the new viral progeny, that usually observed with repeated treatments with common antiviral drugs.

4. Experimental section

4.1. Chemistry

Reagents were purchased from commercial suppliers and used without further purification. ^{1}H and ^{13}C NMR spectra were recorded, in deuterated DMSO or $CDCl_3$ solution, respectively, at 400 and 100 MHz on a Varian Mercury Plus 400, and peak positions are given in parts per million and were referenced to residual ^{1}H signals of the deuterated solvents respectively ($\delta^{1}H$ 7.26 for $CDCl_3$, δ ^{1}H 2.50 for DMSO-d_6). J values are expressed in Hertz. Positive-ion electrospray ionization (ESI) mass spectra were recorded on ESI Micromass ZQ 2000 instrument. Thin layer chromatography (TLC) was carried out using Merck precoated silica gel F-254 plates. Flash chromatography was done using Merck silica gel 60 (0.063–0.200 mm). Solvents were dried according to standard procedures, and reactions requiring anhydrous conditions were performed under argon. Solutions containing the final products were dried with Na_2SO_4, filtered, and concentrated under reduced

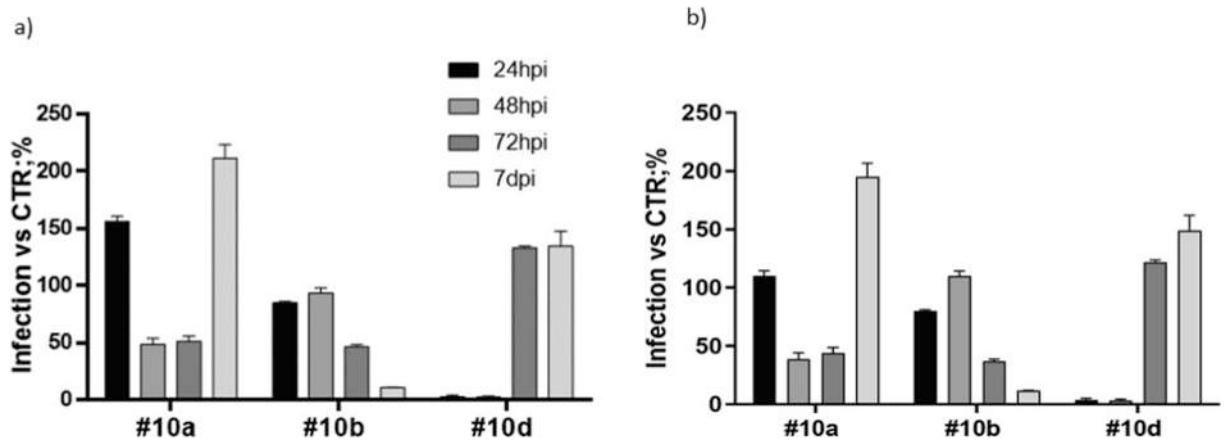

Fig. 5. Infection percentage compared to the untreated infected control after treatment with 10 μM **10a**, **10b** and **10d** compounds 24, 48 and 72 h and 7 days post infection with HHV-6A (a) and HHV-6B (b) . HHV-6 genomes were quantified by real time-PCR and normalized for housekeeping RNaseP gene. Data were reported as mean percentage ± SD obtained from 3 independent experiments compared to untreated infected cells.

pressure using a rotatory evaporator. The purity of the tested compounds was determined by combustion elemental analyses conducted by the Microanalytical Laboratory of the Chemistry Department of the University of Ferrara, Italy, with a Yanagimoto MT-5 CHN recorder elemental analyzer. All tested compounds yielded data consistent with a purity of at least 95% compared with the theoretical values. Melting points were determined on a Reichert-Kofler apparatus and are uncorrected.

*4.1.1. General procedure for the synthesis of rhodanines **4a-f***

Bromoacetyl bromide (1 mmol) was added, drop by drop, to a mixture of the pertinent amine (1 mmol) in CS_2 (5 mL) at 0–2 °C. The reaction mixture was allowed to warm up to room temperature and then heated at 100 °C for 3 h. After this time, AcOEt (25 mL) was added and the mixture was washed with H_2O (3 × 7 mL). After evaporation of the solvent the resulting crude product (brown–red oil) was purified by column chromatography using as eluent mixtures of solvents in the proportions indicated for each compound.

*4.1.2. General procedure for the synthesis of compounds **7a-e***

Methyl-4-iodosalycilate **5a-e** (1.00 mmol) and 5-formyl-2-furan boronic acid **6a, b** (1.30 mmol) were dissolved in EtOH (10 mL) and DMF (5 mL) mL. The reaction mixture was stirred for 10 min under Argon at room temperature, then $Pd(PPh_3)_2Cl_2$ (0.1 mmol) and a 2 M solution of Na_2CO_3 (4 mL) were added. After 1 h, to the resultant orange suspension was added H_2O (20 mL) and 2 N HCl till pH = 4–5 and then extracted with EtOAc (3 × 20 mL). When necessary, the mixture was stirred until organic and aqueous layers become clear. The combined organic layers were washed with brine (2 × 10 mL), dried over Na_2SO_4, filtered, and evaporated to give a crude product that was purified by flash chromatography with the opportune eluent to yield the desired product **7a-e** as brown-orange solids.

*4.1.3. General procedure for the synthesis of compounds **8a-d***

LiOH (10 mmol) was added to a solution of compounds **7a-e** (1 mmol) in CH_3OH (10 mL) and H_2O (5 mL). The reaction mixture was refluxed till ester disappeared in TLC (~1h), acidified with HCl 2 N till pH 4–5 and extracted with AcOEt (3 × 25 mL). The combined organic layers were washed with a $NaHCO_3$ saturated solution (2 × 20 mL) and brine (2 × 20 mL). The desired products **8a-e** were obtained as brown–red solid after evaporation of the solvent.

*4.1.4. General procedure for the synthesis of final compounds **9a-f**, **10** and **10a-c***

A solution of compounds **8a-8d** (1 mmol), **4a-f** (1 mmol) and DMAP (0.2 mmol) in EtOH (10 mL) was refluxed overnight. The resulting suspension was filtered and the filtrate washed with cooled isopropanol to give the product as an orange-red solid that was purified by column chromatography using as eluent mixtures of solvents in the proportions indicated for each compound.

*4.1.5. **(4a)** 3-(2-phenylethyl)-2-thioxo-1,3-thiazolidin-4-one*

Oil, Yield 59%. ^{1}H NMR ($CDCl_3$) d: 2.92–2.96 (m, 2H), 3.92 (s, 2H), 4.18–4.22 (m, 2H), 7.25–7.31 (m, 5H). ^{13}C NMR ($CDCl_3$) d: 35.7, 35.3, 45.7, 126.8, 128.6, 128.9, 137.4, 173.5, 200.9. M.p.: 106–8 °C. R_f AcOEt/P 1/4: 0.51.

*4.1.6. **(4b)** 3-(3-phenylpropyl)-2-thioxo-1,3-thiazolidin-4-one*

Oil, Yield 55%. ^{1}H NMR ($CDCl_3$) d: 1.98–2.04 (m, 2H), 2.69 (t, 2H, J = 10.2), 3.74 (s, 2H), 4.01–4.06 (m, 2H), 7.18–7.27 (m, 5H) 126.4, 128.5, 128.7, 141.0, 174.1, 200.6. ^{13}C NMR ($CDCl_3$) d: R_f AcOEt/P 1/6: 0.46.

*4.1.7. **(4c)** 3-(4′-methylphenylmethyl)-2-thioxo-1,3-thiazolidin-4-one*

Solid, Yield 65 %. ^{1}H NMR ($CDCl_3$) d: 2.33 (s, 3H), 3.98 (s, 2H), 5.16 (s, 2H), 7.13 (d, 2H, J = 8), 7.35 (d, 2H, J = 8). ^{13}C NMR ($CDCl_3$) d: 21.4, 35.5, 47.5, 129.2, 129.3, 131.8, 138.1, 173.9, 201.1. M.p.: 71–2 °C. R_f AcOEt/P 1/10: 0.25.

*4.1.8. **(4d)** 3-(3′,4′-dimethoxyphenylmethyl)-2-thioxo-1,3-thiazolidin-4-one*

Oil, Yield 53 %. ^{1}H NMR (DMSO) d: 3.71 (s, 3H), 3.72 (s, 3H), 4.33 (s, 2H), 5.00 (s, 2H), 6.80–6.86 (m, 1H), 6.87 (d, 1H J = 8), 6.95 (d, 1H, J = 2). ^{13}C NMR (DMSO) d: 35.8, 46.6, 55.3, 55.4, 111.5, 112.0, 120.2, 127.3, 148.2, 148.4, 174.4, 203.1. R_f AcOEt/P 1/1: 0.523.

*4.1.9. **[(R)-4e]** (R)-3-(2-phenylpropyl)-2-thioxo-1,3-thiazolidin-4-one*

Oil, Yield 62%. ^{1}H NMR ($CDCl_3$) d: 1.31 (d, 3H, J = 7.2), 3.47–3.57 (m, 1H), 3.79 (d, 1H, J = 22), 3.88 (d, 1H, J = 22), 4.10–4.17 (m, 2H) 7.24–7.33 (m, 5H). ^{13}C NMR ($CDCl_3$) d: 17.6, 34.5, 36.1, 50.4, 126.4, 126.8, 127.9, 142.0, 173.1, 200.8. R_f AcOEt/P 1/6: 0.3.

*4.1.10. **[(S)-4f)]** (S)-3-(2-phenylpropyl)-2-thioxo-1,3-thiazolidin-4-one*

Oil, Yield 56%. ^{1}H NMR ($CDCl_3$) d: 1.31 (d, 3H, J = 7.2), 3.47–3.57 (m, 1H), 3.79 (d, 1H, J = 22), 3.88 (d, 1H, J = 22), 4.10–4.17 (m, 2H) 7.24–7.33 (m, 5H). ^{13}C NMR ($CDCl_3$) d: 17.6, 34.5, 36.1, 50.4, 126.4, 126.8, 127.9, 142.0, 173.1, 200.8. R_f AcOEt/P 1/6: 0.3.

*4.1.11. **(7a)** 4-(5-formylfuran-2-yl)-2-hydroxybenzoate methyl ester*

Solid, Yield: 65% ^{1}H NMR (DMSO) d 3.90 (s, 3H), 7.45–7.47 (m, 3H),

7.67 (d, 1H, J = 3.6), 7.88 (d, 1H, J = 8), 9.65 (s, 1H), 10.6 (s, 1H). ^{13}C NMR (CDMSO) d: 52.4, 111.1, 113.0, 113.8, 115.7, 124.7, 131.0, 134.4, 152.1, 156.1, 159.9, 168.3, 178.2. $[M + H]^+$: 247.4. M.p.: 155–7 °C R_f AcOet/Pet 1/2: 0.43.

*4.1.12. **(7b)** 4-(5-formylthiophen-2-yl)-2-hydroxybenzoate methyl ester*

Solid, Yield: 70 %. ^{1}H NMR ($CDCl_3$) d:3.98 (s, 3H), 7.17–7.19 (m, 1H), 7.29 (d, 1H, J = 2), 7.48 (d, 1H, J = 4), 7.75 (d, 1H, J = 4), 7.87–7.89 (m, 1H), 9.9 (s, 1H), 10.8 (s, 1H), ^{13}C NMR ($CDCl_3$) d: 52.5, 112.8, 114.9, 117.2, 125.6, 130.8, 137.0, 139.7, 143.7, 152.1, 161.8, 170.0, 182.8. $[M + H]^+$: 263.8. M.p.: 123–25 °C. R_f AcOEt/Pet 1/2: 0.5

*4.1.13. **(7c)** 3-(5-formylfuran-2-yl)-4-hydroxybenzoate methyl ester*

Colorless solid, Yield: 72%. ^{1}H NMR ($CDCl_3$) d 4.00 (s, 3H), 6.75 (d, 1H, J = 3.6), 7.06 (d, 1H, J = 8.8), 7.31 (d, 1H, J = 3.6), 7.88 (m, 1H), 8.32 (d, 1H, J = 2.4), 9.6 (s, 1H), 11.0 (s, 1H). ^{13}C NMR ($CDCl_3$) d: 52.6, 106.7, 112.8, 118.5, 120.7, 127.1, 132.5, 151.8, 158.6, 162.6, 170.1, 176.9. $[M + H]^+$: 247.3. M.p.: 130–2 °C. R_f AcOet/Pet 1/2: 0.2.

*4.1.14. **(7d)** 4-(5-formylfuran-2-yl)benzoate methyl ester*

Colorless solid, Yield: 83%. ^{1}H NMR ($CDCl_3$) d: 3–96 (s, 3H), 6.97 (d, 1H, J = 3.6), 7.35 (d, 1H, J = 3.6), 7.89 (m, 1H), 8.12 (m, 1H), 9.70 (s, 1H). ^{13}C NMR ($CDCl_3$) d: 52.4, 109.4, 123.1, 125.1, 130.3, 130.8, 132.9, 152.6, 158.0, 166.5, 177.6. $[M + H]^+$: 231.3. M.p.: 143–5 °C. R_f AcOet/Pet 1/2: 0.4.

*4.1.15. **(7e)** 5-(3-hydroxyphenyl)furan-2-carboxaldehyde*

Colorless solid, Yield: 90%. ^{1}H NMR ($CDCl_3$) d: 6.82 (d, 1H, J = 3.6), 6.92 (m, 1H), 7.26–7.38 (m, 4H), 9.61 (s, 1H). ^{13}C NMR ($CDCl_3$) d: 108.1, 112.1, 117.1, 117.8, 130.2, 130.3, 151.8, 156.4, 159.5, 177.4. $[M + H]^+$: 189.2. M.p.: 128–30 °C. R_f AcOet/Pet 1/2: 0.3.

*4.1.16. **(8a)** 4-(5-formylfuran-2-yl)-2-hydroxybenzoic acid*

Solid. Yield: 95%. ^{1}H NMR (DMSO) d 7.39–7.45 (m, 3H), 7.65 (d, 1H, J = 3.6), 7.86–7.89 (m, 1H), 9.63 (s, 1H).^{13}C NMR (DMSO) d: 111.6, 112.9, 114.2, 116.1, 124.9, 131.0, 135.1, 152.7, 157.0, 162.0, 171.4, 178.8. $[M + H]^+$: 243.2. M.p.: 230 °C (Dec.). R_f CH_2Cl_2/MeOH 4/1: 0.3.

*4.1.17. **(8b)** 4-(5-formylthiophen-2-yl)-2-hydroxybenzoic acid*

Solid, Yield: 89%. ^{1}H NMR (DMSO) d: 7.04–7.07 (m, 2H), 7.71 (d, 1H, J = 4), 7.77 (d, 1H, J = 8), 8.02 (d, 1H, J = 4), 9.89 (s, 1H), 11.5 (br. s., 1H). ^{13}C NMR (DMSO) d: 113.4, 114.0, 117, 127, 131.3, 138.7, 138.8, 143.0, 150.3, 161.3, 171.2, 184.2. $[M + H]^+$: 259.7. M.p.: 203–5 °C (Dec.). R_f CH_2Cl_2/MeOH 3/1: 0.35.

*4.1.18. **(8c)** 3-(5-formylfuran-2-yl)-4-hydroxybenzoic acid*

Solid, Yield: 91%. ^{1}H NMR (DMSO) d: 6.94 (d, 1H, J = 12), 7.12 (d, 1H, J = 4), 7.55–7.60 (m, 2H), 7.86 (m, 1H), 8.20 (d, 1H, J = 2.4), 9.5 (s, 1H). ^{13}C NMR (DMSO) d: 107.3, 116.7, 118.4, 119.1, 127.3, 131.5, 151.6, 159.0, 164.0, 171.4, 177.6, 206.9. $[M + H]^+$: 243.5. M.p.: 213–15 °C. R_f CH_2Cl_2/MeOH 4/1: 0.3.

*4.1.19. **(8d)** 4-(5-formylfuran-2-yl)benzoic acid*

Solid, Yield: 96%. ^{1}H NMR ($CDCl_3$) d 7.43 (d, 1H, J = 3.6), 7.67 (d, 1H, J = 3.6), 7.66–8.04 (m, 4H), 9.64 (s, 1H), 13.18 (br s, 1H). ^{13}C NMR ($CDCl_3$) d: 111.0, 125.4, 130.6, 131.7, 132.8, 152.6, 157.3, 167.1, 178.7, 206.9. $[M + H]^+$: 217.8. M.p.: 130–2 °C. R_f CH_2Cl_2/MeOH 4/1: 0.4.

*4.1.20. **(9a)** 2-Hydroxy-4-{5-[4-oxo-3-phenethyl-2-thioxothiazolidin-5-ylidenemethyl]furan-2-yl}benzoic acid*

Orange solid, Yield 78%. ^{1}H NMR ($CDCl_3$) d 2.95–2.99 (m, 2H), 4.11–4.14 (m, 2H), 7.17–7.38 (m, 9H), 7.61 (s, 1H), 7.82 (d, 1H, J = 8.2). ^{13}C NMR ($CDCl_3$) d: 32.6, 45.7, 111.7, 112.1, 113.8, 118.7, 119.1, 123.5, 127.1, 129.0, 129.1, 131.5, 132.6, 138.1, 149.8, 158.1, 163.2, 166.7, 171.8, 194.1. $[M + H]^+$: 452.4. M.p.: 118–20 °C. R_f CH_2Cl_2/MeOH 8/1: 0.33

*4.1.21. **(9b)** 2-Hydroxy-4-{5-[4-oxo-3-phenylpropyl-2-thioxothiazolidin-5-ylidenemethyl]furan-2-yl}benzoic acid*

Orange solid, Yield 81%. ^{1}H NMR (DMSO) d 1.94–1.98 (m, 2H), 2.65 (t, 2H, J = 7.6), 4.05 (t, 2H, J = 7.6), 6.90 (d, 1H, J = 8.4), 7.14–736 (m, 7H), 7.65 (s, 1H), 7.83 (d, 1H, J = 8.2), 8.21 (d, 1H, J = 8.4). ^{13}C NMR (DMSO) d: 27.7, 32.2, 43.9, 106.7, 110.6, 111.4, 112.5, 118.1, 118.5, 122.9, 125.8, 128.1, 128.2, 130.8, 131.3, 140.7, 149.1, 158.0, 163.2, 166.5, 171.0, 193.8. $[M + H]^+$: 466.6. M.p.: 188–190 °C. R_f CH_2Cl_2/MeOH 10/1: 0.3.

*4.1.22. **(9c)** 2-Hydroxy-4-{5-[4-oxo-3-(4′methylphenylmethyl)-2-thioxothiazolidin-5-ylidenemethyl]furan-2-yl}benzoic acid*

Orange solid, Yield 82%. ^{1}H NMR (DMSO) d 2.24, (s, 3H), 5.18 (s, 2H), 7.12 (d, 2H, J = 8), 7.19–7.23 (m, 4H), 7.36 (s, 2H), 7.69 (s, 1H), 7.85 (d, 1H, J = 8). ^{13}C NMR (DMSO) d: 20.6, 46.7, 111.4, 111.6, 113.4, 118.5, 123.2, 127.6, 129.0, 131.0, 131.9, 136.8, 149.4, 157.6, 162.5, 166.5, 171.2, 193.7. $[M + H]^+$: 452.3. M.p.: 267 °C (Dec.). R_f CH_2Cl_2/MeOH 8/1: 0.28.

*4.1.23. **(9d)** 2-Hydroxy-4-{5-[4-oxo-3-(3′,4′-dimethoxyphenyl)methyl]-2-thioxothiazolidin-5-ylidenemethyl]furan-2-yl}benzoic acid*

Orange solid, Yield 75%. ^{1}H NMR (DMSO) d 3.00 (s, 3H), 3.69 (s, 3H), 4.10–4.12 (m, 2H), 5.16 (s, 1H), 6.70 (d, 1H J = 7.6), 6.84–6.87 (m, 1H), 7.10–7.13 (m 1H), 7.28–7.34 (m, 1H), 7.66–7.68 (m, 2H), 7.78 (d, 1H, J = 8), 8.12 (d, 1 h, J = 6.8). ^{13}C NMR (DMSO) d: 55.8, 67.8, 107.2, 111.2, 112.1, 112.4, 112.9, 119.1, 120.6, 123.8, 129.1, 132.0, 132.1, 146.0, 148.8, 149.0, 167.4, 171.3, 194.4. $[M + H]^+$: 498.0. M.p.: 226–28 °C. R_f CH_2Cl_2/MeOH/Tol 17/2/1: 0.22.

*4.1.24. **(9e)** (R)-2-Hydroxy-4-{5-[4-oxo-3-(2-phenylpropyl)methyl]-2-thioxothiazolidin-5-ylidenemethyl]furan-2-yl}benzoic acid*

Orange solid, Yield 91%. ^{1}H NMR (DMSO) d 1.23 (d, 1H, J = 7.2), 3.40–3.45 (m, 1H), 4.14 (d, 2H, J = 7.6), 7.13–7.31 (m, 9H), 7.58 (s, 1H), 7.82 (d, 1H, J = 8.4). ^{13}C NMR (DMSO) d: 18.7, 37.0, 51.0, 111.3, 112.0, 113.2, 118.6, 118.8, 121.0, 123.6, 127.2, 127.6, 128.9, 131.4, 131.9, 143.2, 149.6, 158.6, 163.7, 167.0, 171.7, 194.5. $[M + H]^+$: 466.8. M.p.: 227–30 °C. R_f CH_2Cl_2/MeOH 6/1: 0.25.

*4.1.25. **(9f)** (S)-2-Hydroxy-4-{5-[4-oxo-3-(2-phenylpropyl)methyl]-2-thioxothiazolidin-5-ylidenemethyl]furan-2-yl}benzoic acid*

Orange solid, Yield 88%. ^{1}H NMR (DMSO) d 1.23 (d, 1H, J = 7.2), 3.40–3.45 (m, 1H), 4.14 (d, 2H, J = 7.6), 7.13–7.31 (m, 9H), 7.58 (s, 1H), 7.82 (d, 1H, J = 8.4). ^{13}C NMR (DMSO) d: 18.7, 37.0, 51.0, 111.3, 112.0, 113.2, 118.6, 118.8, 121.0, 123.6, 127.2, 127.6, 128.9, 131.4, 131.9, 143.2, 149.6, 158.6, 163.7, 167.0, 171.7, 194.5. $[M + H]^+$: 466.8. M.p.: 227–30 °C. R_f CH_2Cl_2/MeOH 6/1: 0.25.

*4.1.26. **(10a)** 2-Hydroxy-4-{5-[4-oxo-3-phenethyl-2-thioxothiazolidin-5-ylidenemethyl]tiophen-2-yl}benzoic acid*

Orange solid, Yield 65%. ^{1}H NMR (DMSO) d 2.92–2.96 (m, 2H), 4.19–4.23 (m, 2H), 7.04 7.08 (m, 2H), 7.20–7.31 (m, 5H), 7.71–7.75 (m, 3H), 8.03 (s, 1H). ^{13}C NMR (DMSO) d: 32.6, 46.0, 11.4, 113.8, 119.8, 126.6, 127.1, 129.0, 129.1, 131.4, 136.0, 137.0, 138.3, 138.1, 152.3, 163.8, 166.8, 171.4, 192.4. $[M + H]^+$: 468.7. M.p.: 190–192 °C (dec.). R_f CH_2Cl_2/MeOH 4/1: 0.32.

*4.1.27. **(10b)** 2-Hydroxy-5-{5-[4-oxo-3-phenethyl-2-thioxothiazolidin-5-ylidenemethyl]furan-2-yl}benzoic acid*

Orange solid, Yield 79%. 1H NMR (DMSO) d 3.93–397 (m, 2H), 4.02–4.24 (m, 2H), 6.81 (d, 1H, J = 8.4), 7.05 (d, 1H, J = 4), 7.58 (s, 1H), 7.67–7.70 (m, 1H), 8.18–8.20 (m, 1H). ^{13}C NMR (DMSO) d: 32.0, 45.1, 106.8, 107.3, 115.6, 116.0, 117.5, 118.4, 120.1, 124.4, 126.5, 126.7, 128.4, 128.6, 137.6, 140.0, 147.8, 156.5, 160.1, 166.2, 170.3, 193.4. $[M + H]^+$: 452.2. M.p.: 230–2 (dec.) °C. R_f CH_2Cl_2/MeOH 8/1:

0.2.

4.1.28. (10c) 4-{5-[4-oxo-3-phenethyl-2-thioxothiazolidin-5-ylidenemethyl]furan-2-yl}benzoic acid

Yellow-orange solid, Yield 65%. ^{1}H NMR (DMSO) d 2.94–2.98 (m, 2H), 4.21–4.25 (m, 2H), 7.64 (s, 1H), 7.23–7.46 (m, 7H), 7.92–7.94 (m, 2H), 8.07–8.09 (m, 2H), 13.19 (br s, 1H). ^{13}C NMR (DMSO) d: 32.0, 45.1, 112.0, 118.0, 119.2, 122.9, 124.2, 126.5, 128.4, 128.6, 130.2, 131.9, 137.5, 149.9, 159.7, 166.1, 166.7, 193.5. $[M + H]^+$: 436.5. M.p.: 270 °C (dec.). R_f CH_2Cl_2/MeOH 2/1: 0.7.

4.1.29. (10d) 5-[[5-(4-hydroxyphenyl)-2-furanyl]methylene]-2-thioxo-3-phenethyl-4-thiazolidinone,

Orange solid, Yield 66%. ^{1}H NMR (DMSO) d 3.00–3.04 (m, 2H), 4.33–4.37 (m, 2H), 5.20 (br s, 1H), 6.84 (d, 1H, J = 3.6), 6.85–6.92 (m, 1H), 6.93 (d, 1H, J = 3.6), 7.26–7.36 (m, 8H), 7.44 (s, 1H). ^{13}C NMR (DMSO) d: 33.0, 45.7, 109.3, 111.3, 116.5, 117.4, 117.9, 119.8, 121.4, 126.7, 128.6, 129.0, 130.3, 130.5, 137.6, 149.4, 156.1, 158.5, 167.3, 194.2. $[M + H]^+$: 408.4. M.p.: 194–6 °C. AcOet/Pet 1/3: 0.2.

4.2. Biological evaluation

4.2.1. Cell culture and treatment

The human T cell line J-Jhan and Sup-T1 were cultured in RPMI-1640 (Gibco BRL, Invitrogen Corporation, Carlsbad, CA, USA) with 10% FCS supplemented with 100 U/ml each of penicillin and streptomycin and maintained at 37 °C in humidified atmosphere of 5% CO_2. J-Jhan and Sup-T1 have been selected since are known to represent cell lines of choice which allow HHV-6A and HHV-6B replication, respectively. Both cell lines were seeded into 24-well plate at the cell density of 0.5×10^6 /ml and treated with synthetized HHV-6 inhibitors at concentration of 1, 10 and 100 μM, for 24 h.

4.2.2. Cell viability analysis by MTT assay

Cell viability was determined by MTT test (3-(4,5-dimethilthiazol-2yl)-2,5-diphenyl tetrazolium bromide) colorimetric assay (Roche Diagnostics Corporation, Indianapolis, IN, USA) following the manufacturer's instructions as previously described [39]. Cell viability was determined by treating human lymphocyte cell lines with different concentration of HHV-6 inhibitors, 10-fold serially diluted from 0 to 100 μM, for 24 h. Afterwards, MTT assay was performed, and absorbance was read at 570 nm.

4.2.3. HHV-6 infection

J-Jhan cells were infected with a HHV-6A (U1102 strain) cell-free inoculum and Sup T1 cells were infected with a HHV-6B (Z29 strain) cell-free inoculum as previously described [24] at a 100:1 multiplicity of infection (MOI, virus genomes:cell ratio). Virus adsorption was carried out in a 1% FBS medium for 3 h, then the excess virus was eliminated by centrifugation and washing in PBS, and cells were finally seeded at 0.5×10^6 cells/ml in complete medium with high FBS concentration. Control cells were treated with the same procedure but uninfected. At 1, 2, 3, and 7 days post-infection (d.p.i.) cell samples were collected by centrifugation at 1000 × g for 5 min at 4 °C. Cell pellets were then washed in PBS, and analyzed for viral DNA presence by Real Time PCR.

4.2.4. Analysis of HHV-6 replication inhibition

The inhibitory effect on HHV-6 replication was determined by analyzing viral DNA from J-Jhan HHV-6A infected cells and Sup T1 HHV-6B infected cells. Total DNA was extracted from cell pellets collected from both infected or uninfected cell lines by a commercial kit (Exgene Cell SV kit, GeneAll, Seoul, Korea), and quantified by spectrophotometric reading at 260 and 280 nm. 100 ng of total extracted DNA was analyzed by specific qPCR targeting U42 gene of HHV-6 in duplicate, as previously described [40]. Briefly, a standard curve ranging from 10^7 to 10 copies of U42 gene was used to quantify the infection by interpolation and normalized to the human RNaseP housekeeping gene (TaqMan™ Copy Number Reference Assay, human, RNase P, ThermoFisher Scientific, USA) used as a control.

4.2.5. Statistical analysis

Results obtained ad mean ± SD from 3 independent experiments were evaluated for statistical significance by Student T test using GraphPad Prism9 software.

Declaration of Competing Interest

The authors declare that they have no known competing financial interests or personal relationships that could have appeared to influence the work reported in this paper.

Acknowledgement

We thank Dr. Erika Marzola for HPLC analysis, Dr. Alberto Casolari for the acquisition of proton and carbon NMR spectra and Dr Ercolina Bianchini for the elemental analysis. We thank Iva Pivanti and Dr Mercedes Fernandez for technical support and Alessandro Sofia for statistical analysis. This study was supported by HHV-6 foundation grant and FISM – Fondazione Italiana Sclerosi Multipla – cod. 2019/R-Single/004 and financed or co-financed with the '5 per mille' public funding.

Appendix A. Supplementary material

Supplementary data to this article can be found online at https://doi.org/10.1016/j.bioorg.2021.105518.

References

[1] E. De Clercq, A. Brancale, A.V. Hodge, H.J. Field, Antiviral chemistry and chemotherapy's current antiviral agents Fact File 2006 (1st edition), Antivir. Chem. Chemother. 17 (2006) 113–166, https://doi.org/10.1177/095632020601700302.
[2] E. De Clercq, Three decades of antiviral drugs, Nat. Rev. Drug Discov. 6 (2007) 941, https://doi.org/10.1038/nrd2485.
[3] D. Pillay, The priorities for antiviral drug resistance surveillance and research, J. Antimicrob. Chemother. 60 (Suppl 1) (2007) i57–i58, https://doi.org/10.1093/jac/dkm159.
[4] G.P. Pattnaik, H. Chakraborty, Entry Inhibitors: Efficient Means to Block Viral Infection, J. Membr. Biol. 253 (5) (2020) 425–444, https://doi.org/10.1007/s00232-020-00136-z.
[5] F. Vigant, N.C. Santos, B. Lee, Broad-spectrum antivirals against viral fusion, Nat. Rev. Microbiol. 13 (7) (2015) 426–437, https://doi.org/10.1038/nrmicro3475.
[6] T.J. Henrich, D.R. Kuritzkes, HIV-1 entry inhibitors: recent development and clinical use, Curr. Opin. Virol. 3 (1) (2013) 51–57, https://doi.org/10.1016/j.coviro.2012.12.002.
[7] S. Pollock, N.B. Nichita, A. Böhmer, C. Radulescu, R.A. Dwek, N. Zitzmann, Polyunsaturated liposomes are antiviral against hepatitis B and C viruses and HIV by decreasing cholesterol levels in infected cells, PNAS 107 (40) (2010) 17176–17181, https://doi.org/10.1073/pnas.1009445107.
[8] F. Vigant, A. Hollmann, J. Lee, N.C. Santos, M.E. Jung, B. Lee, The rigid amphipathic fusion inhibitor dUY11 acts through photosensitization of viruses, J. Virol. 88 (3) (2014) 1849–1853, https://doi.org/10.1128/JVI.02907-13.
[9] H. Badani, R.F. Garry, W.C. Wimley, Peptide entry inhibitors of enveloped viruses: the importance of interfacial hydrophobicity, BBA 1838 (9) (2014) 2180–2197, https://doi.org/10.1016/j.bbamem.2014.04.015.
[10] H. Jenssen, P. Hamill, R.E.W. Hancock, Peptide antimicrobial agents, Clin. Microbiol. Rev. 19 (3) (2006) 491–511, https://doi.org/10.1128/CMR.00056-05.
[11] G. Cheng, A. Montero, P. Gastaminza, C. Whitten-Bauer, S.F. Wieland, M. Isogawa, B. Fredericksen, S. Selvarajah, P.A. Gallay, M.R. Ghadiri, F.V. Chisari, A virocidal amphipathic α-helical peptide that inhibits hepatitis C virus infection in vitro, PNAS 105 (2008) 3088–3093, https://doi.org/10.1073/pnas.0712380105.
[12] C.J. Sample, K.E. Hudak, B.E. Barefoot, M.D. Koci, M.S. Wanyonyi, S. Abraham, H. F. Staats, E.A. Ramsburg, A mastoparan-derived peptide has broad-spectrum antiviral activity against enveloped viruses, Peptides 48 (2013) 96–105, https://doi.org/10.1016/j.peptides.2013.07.014.
[13] S.M. Mousavi, M. Zarei, S.A. Hashemi, A. Babapoor, A.M. Amani, A conceptual review of rhodanine: current applications of antiviral drugs, anticancer and antimicrobial activities, Artif. Cells Nanomed. Biotechnol. 47 (1) (2019) 1132–1148, https://doi.org/10.1080/21691401.2019.1573824.
[14] N.A. Meanwell, Hepatitis C virus entry: an intriguing challenge for drug discovery, Curr. Opin. Invest. Drugs 7 (2006) 727–732.

[15] J.P. Yang, D. Zhou, F. Wong-Staal, Screening of small-molecule compounds as inhibitors of HCV entry, Methods Mol. Biol. 510 (2009) 295–304, https://doi.org/10.1007/978-1-59745-394-3_22.
[16] M.J. Brooks, J.J. Sasadeusz, G.A. Tannock, Antiviral chemotherapeutic agents against respiratory viruses: where are we now and what's in the pipeline? Curr. Opin. Pulm. Med. 10 (3) (2004) 197–203, https://doi.org/10.1097/00063198-200405000-00009.
[17] Y.S. Boriskin, I.A. Leneva, E.I. Pecheur, S.J. Polyak, Arbidol: a broadspectrum antiviral compound that blocks viral fusion, Curr. Med. Chem. 15 (2008) 997–1005, https://doi.org/10.2174/092986708784049658.
[18] C.C. Colpitts, A.V. Ustinov, R.F. Epand, R.M. Epand, V.A. Korshun, L.M. Schang, 5-(Perylen-3-yl)ethynyl-arabino-uridine (aUY11), an arabino-based rigid amphipathic fusion inhibitor, targets virion envelope lipids to inhibit fusion of influenza virus, hepatitis C virus, and other enveloped viruses, J. Virol. 87 (7) (2013) 3640–3654, https://doi.org/10.1128/JVI.02882-12. Epub 2013 Jan 2.
[19] Y.S. Boriskin, E.-I. Pécheur, S.J. Polyak, Arbidol: a broad-spectrum antiviral that inhibits acute and chronic HCV infection, Virol J 3 (1) (2006), https://doi.org/10.1186/1743-422X-3-56.
[20] R. Rizzo, D. Di Luca, Human herpesvirus 6A and 6B and NK cells, Acta Microbiol. Immunol. Hung. 65 (2) (2018) 119–125, https://doi.org/10.1556/030.65.2018.010. Epub 2018 Mar 7.
[21] E. Caselli, M. D'Accolti, F. Caccuri, I. Soffritti, V. Gentili, D. Bortolotti, A. Rotola, E. Cassai, S. Fiorentini, A. Zani, A. Caruso, R. Rizzo, D. Di Luca, The U94 Gene of Human Herpesvirus 6: A Narrative Review of Its Role and Potential Functions, Cells 9 (12) (2020) 2608, https://doi.org/10.3390/cells9122608.
[22] R. Rizzo, V. Gentili, I. Casetta, E. Caselli, R. De Gennaro, E. Granieri, E. Cassai, D. Di Luca, A. Rotola, Altered natural killer cells' response to herpes virus infection in multiple sclerosis involves KIR2DL2 expression, J. Neuroimmunol. 251 (1–2) (2012) 55–64, https://doi.org/10.1016/j.jneuroim.2012.07.004. Epub 2012 Aug 5.
[23] R. Rizzo, D. Bortolotti, V. Gentili, A. Rotola, S. Bolzani, E. Caselli, M.R. Tola, D. Di Luca, T. Fülöp, KIR2DS2/KIR2DL2/HLA-C1 Haplotype Is Associated with Alzheimer's Disease: Implication for the Role of Herpesvirus Infections, J. Alzheimers Dis. 67 (4) (2019) 1379–1389, https://doi.org/10.3233/JAD-180777.
[24] D. Bortolotti, V. Gentili, A. Rotola, E. Caselli, R. Rizzo, HHV-6A infection induces amyloid-beta expression and activation of microglial cells, Alzheimers Res. Ther. 11 (1) (2019), https://doi.org/10.1186/s13195-019-0552-6.
[25] R. Marci, V. Gentili, D. Bortolotti, G. Lo Monte, E. Caselli, S. Bolzani, A. Rotola, D. Di Luca, R. Rizzo, Presence of HHV-6A in Endometrial Epithelial Cells from Women with Primary Unexplained Infertility, PLoS One 11 (7) (2016) e0158304, https://doi.org/10.1371/journal.pone.0158304, eCollection 2016.
[26] D. Bortolotti, V. Gentili, A. Rotola, R. Cultrera, R. Marci, D. Di Luca, R. Rizzo, HHV-6A infection of endometrial epithelial cells affects immune profile and trophoblast invasion, Am. J. Reprod. Immunol. 82 (4) (2019) e13174, https://doi.org/10.1111/aji.13174. Epub 2019 Aug 17.
[27] S.H. James, N.B. Price, C.B. Hartline, E.R. Lanier, M.N. Prichard, Selection and recombinant phenotyping of a novel CMX001 and cidofovir resistance mutation in human cytomegalovirus, Antimicrob. Agents Chemother. 57 (7) (2013) 3321–3325, https://doi.org/10.1128/AAC.00062-13. Epub 2013 May 6.
[28] E. De Clercq, L. Naesens, In search of effective anti-HHV-6 agents, Rev. J. Clin. Virol. 37 (Suppl 1) (2006) S82–S86, https://doi.org/10.1016/S1386-6532(06)70017-8.
[29] P. Bonnafous, L. Naesens, S. Petrella, A. Gautheret-Dejean, D. Boutolleau, W. Sougakoff, H. Agut, Different mutations in the HHV-6 DNA polymerase gene accounting for resistance to foscarnet, Antivir. Ther. 12 (6) (2007) 877–888.
[30] Y. Isegawa, C. Matsumoto, K. Nishinaka, K. Nakano, T. Tanaka, N. Sugimoto, A. Ohshima, PCR with quenching probes enables the rapid detection and identification of ganciclovir-resistance-causing U69 gene mutations in human herpesvirus 6, Mol. Cell. Probes 24 (4) (2010) 167–177, https://doi.org/10.1016/j.mcp.2010.01.002. Epub 2010 Jan 18.
[31] N. Maeda, A. Furukawa, K. Kakita, M. Anada, S. Hashimoto, S. Matsunaga, K. Kuroki, T. Ose, A. Kato, J. Arii, Y. Kawaguchi, H. Arase, K. Maenaka, Rapid Screening by Cell-Based Fusion Assay for Identifying Novel Antivirals of Glycoprotein B-Mediated Herpes Simplex Virus Type 1 Infection, Biol. Pharm. Bull. 39 (11) (2016) 1897–1902, https://doi.org/10.1248/bpb.b16-00533.
[32] G.A. Wudiri, S.M. Schneider, A.V. Nicola, Herpes Simplex Virus 1 Envelope Cholesterol Facilitates Membrane Fusion, Front. Microbiol. 8 (2017) 2383, https://doi.org/10.3389/fmicb.2017.02383.
[33] H. Tang, A. Kawabata, M. Takemoto, K. Yamanishi, Y. Mori, Human herpesvirus-6 infection induces the reorganization of membrane microdomains in target cells, which are required for virus entry, Virology 378 (2) (2008) 265–271, https://doi.org/10.1016/j.virol.2008.05.028.
[34] V. Cagno, C. Tintori, A. Civra, R. Cavalli, M. Tiberi, L. Botta, A. Brai, G. Poli, C. Tapparel, D. Lembo, M. Botta, Novel broad spectrum virucidal molecules against enveloped viruses, PLoS One 13 (12) (2018) e0208333, https://doi.org/10.1371/journal.pone.0208333, eCollection 2018.
[35] R. Borenstein, B.A. Hanson, R.M. Markosyan, E.S. Gallo, S.D. Narasipura, M. Bhutta, O. Shechter, N.S. Lurain, F.S. Cohen, L. Al-Harthi, D.A. Nicholson, Ginkgolic acid inhibits fusion of enveloped viruses, Sci. Rep. 10 (1) (2020) 4746, https://doi.org/10.1038/s41598-020-61700-0.
[36] S. Speerstra, A.A. Chistov, G.V. Proskurin, A.V. Aralov, E.A. Ulashchik, P. P. Streshnev, V.V. Shmanai, V.A. Korshun, L.M. Schang, Antivirals acting on viral envelopes via biophysical mechanism of actions, Antiviral Res. 149 (2018) 164–173, https://doi.org/10.1016/j.antiviral.2017.11.018.
[37] D. Kaminskyy, D. Khyluk, O. Vasylenko, R. Lesyk, An efficient method for the transformation of 5-ylideneRhodanines into 2,3,5-trisubstituted-4-thiazolidinones, Tetrahedron Lett. 53 (5) (2012) 557–559, https://doi.org/10.1016/j.tetlet.2011.11.095.
[38] A.R. Katritzky, S.R. Tala, H. Lu, A.V. Vakulenko, Q.-Y. Chen, J. Sivapackiam, K. Pandya, S. Jiang, A.K. Debnath, Design, Synthesis, and Structure−Activity Relationship of a Novel Series of 2-Aryl 5-(4-Oxo-3-phenethyl-2-thioxothiazolidinylidenemethyl)furans as HIV-1 Entry Inhibitors, J. Med. Chem. 52 (23) (2009) 7631–7639, https://doi.org/10.1021/jm900450n.
[39] D. Bortolotti, J. LeMaoult, C. Trapella, D. Di Luca, E.D. Carosella, R. Rizzo, Pseudomonas aeruginosa Quorum Sensing Molecule N-(3-Oxododecanoyl)-l-Homoserine-Lactone Induces HLA-G Expression in Human Immune Cells, Infect. Immun. 83 (2015) 3918–3925, https://doi.org/10.1128/IAI.00803-15.
[40] R. Rizzo, I. Soffritti, M. D'Accolti, D. Bortolotti, D. Di Luca, E. Caselli, HHV-6A/6B infection of NK cells modulates the expression of miRNAs and transcription factors potentially associated to impaired NK activity, Front. Microbiol. 8 (2017) 2143, https://doi.org/10.3389/fmicb.2017.02143.

JOC The Journal of Organic Chemistry

pubs.acs.org/joc Article

Synthesis of 2,6-Dimethyltyrosine-Like Amino Acids through Pinacolinamide-Enabled C−H Dimethylation of 4-Dibenzylamino Phenylalanine

Davide Illuminati,‡ Anna Fantinati,‡ Tiziano De Ventura, Daniela Perrone, Chiara Sturaro, Valentina Albanese, Erika Marzola, Virginia Cristofori, Julie Oble, Giovanni Poli,* and Claudio Trapella*

Cite This: https://doi.org/10.1021/acs.joc.1c02527 Read Online

ACCESS | Metrics & More | Article Recommendations | Supporting Information

ABSTRACT: The synthesis of a small library of *NH*-Boc- or *NH*-Fmoc-protected L-phenylalanines carrying methyl groups at positions 2 and 6 and diverse functionalities at position 4 has been achieved. The approach, which took advantage of a Pd-catalyzed directed C−H dimethylation of picolinamide derivatives, allowed the electronic and steric properties of the resulting amino acid derivatives to be altered by appending a variety of electron-withdrawing, electron-donating, or bulky groups.

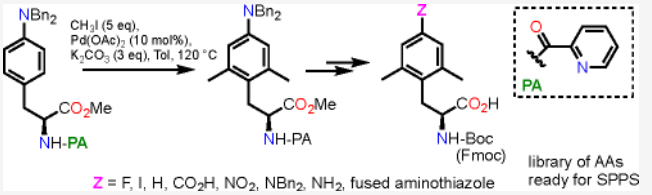

INTRODUCTION

The aromatic moiety in the *N*-terminal message domain of opioid peptides, commonly represented by Tyr,[1] Phe,[1] and Phe,[4] is fundamental in the binding and activation processes of opioid receptors.[1] In particular, 2,6-dimethyl-L-tyrosine (Dmt) has become one of the most popular non-natural amino acids for replacing tyrosine in synthetic opioid peptides.[2] Indeed, the conformational restriction imparted by the two extra methyl groups affects the receptor affinity as well as the selectivity and bioactivity of peptides that incorporate this modified amino acid.[3] In particular, peptides incorporating Dmt[1] in lieu of Tyr[1] in the message domain had lower selectivity profiles as MOP and NOP agonists in addition to increased biological activities and stabilities. The coactivation of MOP/NOP or MOP/DOP receptors, in fact, tends to be characterized by a strong analgesic potential associated with low or no undesired effects, which are normally expressed by a single-receptor activation.[4]

The important role of Dmt is underlined by the number of reported syntheses of tyrosine derivatives carrying two symmetrically disposed methyl groups on the aromatic ring.[5] So far, three conceptually different approaches have been developed for preparing (*S*)-2,6-dimethyltyrosine and its derivatives. One approach is based on the enantio- or diastereoselective alkylation of glycine equivalents (Scheme 1, path a),[6] while a second one is based on the asymmetric hydrogenation of (*Z*)-2-amido-3-(4-acetoxy-2,6-dimethylphenyl)-2-propenoates (path b).[7]

A third and more recent approach is based on the Pd-catalyzed dimethylation of tyrosine derivatives at positions 2 and 6 of the aromatic ring, as recently reported by Zhang and Ma (Scheme 1, path c).[8] This elegant nonracemizing C−H activation protocol has its roots in the pioneering work of Tremont on the Pd-promoted alkylation of acetanilides,[9]

Scheme 1. Approaches to (*S*)-2,6-Dimethyltyrosine and Its Derivatives

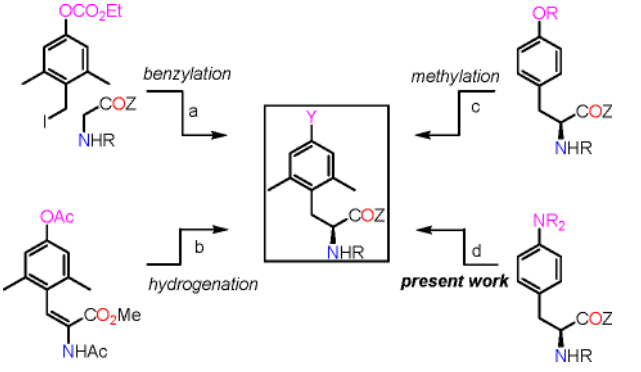

which laid the foundation for the picolinamide-based strategy to achieve the Pd-catalyzed γ- and δ-C−H activation of amines that was reported by Daugulis[10] more than 20 years later.[11] This chemistry was further extended by Chen[12] in the alkylation of γ-*ortho*-C(sp^2)−H bonds of benzylamides.[13]

Inspired by the above works, we envisioned extending the study of the Pd-catalyzed δ-*ortho*-C(sp^2)−H activation strategy to differently 4-substituted L-phenylalanine picolinamides (path d) so as to obtain a small library of 2,6-dimethylated

Received: October 15, 2021

https://doi.org/10.1021/acs.joc.1c02527
J. Org. Chem. XXXX, XXX, XXX−XXX

derivatives ready for incorporation in solid-phase peptide synthesis (SPPS).

RESULTS AND DISCUSSION

We started our study by converting commercially available 4-fluorophenyl-L-alanine **1** into the corresponding methyl ester, which was subsequently submitted to a standard amidation protocol with picolinic acid to afford the fluorinated picolinamide **2** (Scheme 2). Commercially available 4-nitro-

Scheme 2. Synthesis of the Functionalized Phenylalanine Picolinamide Methyl Ester[a]

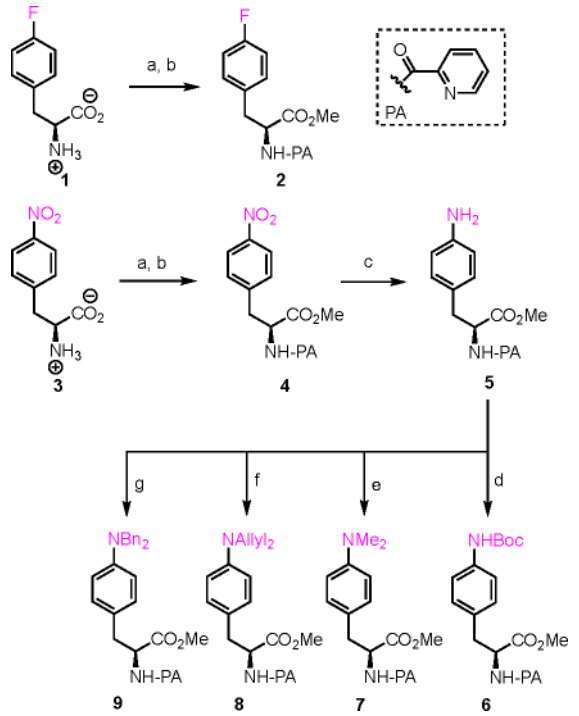

[a]Conditions are as follows: (a) $SOCl_2$ and MeOH at 65 °C (99% from **1** and 99% from **3** without purification); (b) picolinic acid, DIPEA, HATU, and DCM at r.t. (91% from **1** Me ester and 91% from **3** Me ester); (c) Pd/C (10%) and AcOEtat 55 °C and H_2 20 bar under flow conditions (97%); (d) Boc_2O, NaOH (2 N), and H_2O/1,4-dioxane at r.t. (75%); (e) MeI, K_2CO_3, and CH_3CN at 80 °C (87%); (f) AllylBr, K_2CO_3, and CH_3CN at 120 °C (80%); and (g) BnBr, K_2CO_3 and CH_3CN at 120 °C (82%).

L-phenylalanine **3** was analogously converted into the corresponding methyl ester picolinamide **4**. The treatment of **4** under hydrogen atmosphere in the presence of Pd/C (10%) in flow conditions afforded the corresponding aniline **5**. The latter was in turn converted into the *NH*-Boc derivative **6**, the *N,N*-dimethyl derivative **7**, the *N,N*-diallyl derivative **8**, and the *N,N*-dibenzyl derivative **9**.

The study of the key dimethylation reaction was tackled next (Table 1). On the one hand, submitting the 4-fluoro, 4-nitro, 4-*NH*-Boc, 4-*N*-Me_2, and 4-*N*-$Allyl_2$ derivatives **2**, **4**, **6**, **7**, and **8**, respectively, to the same reaction conditions reported by Zhang and Ma[8] (CH_3I, $Pd(OAc)_2$, (10 mol %), K_2CO_3 and toluene at 120 °C) gave none of the expected methylated products. On the other hand, to our satisfaction treating the *N,N*-dibenzyl derivative **9** with the same reaction conditions reported above gave the expected 2,6-dimethylated product **10** in a 72% yield, even if this step needed to be repeated three

Table 1. Tests of the Pd-Catalyzed Dimethylation[a]

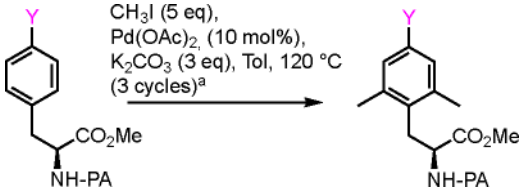

Y	substrate	product	isolated yield (%)
F	**2**		
NO_2	**4**		
NHBoc	**6**		
NMe_2	**7**		
$NAllyl_2$	**8**		
NBn_2	**9**	**10**	72%

[a]All substrates (**2**, **4**, **6**, **7**, **8**, and **9**) were treated with the same conditions, as reported.

times to obtain only the dimethylated product (from 18.30 mmol **9**).

These results reveal that the electronic situation of the aromatic ring of the picolinamide substrates is the key for the success of the reaction. In particular, it is likely that the C−H activation[14] step at the *δ-ortho*-C(sp^2)−H position (Figure 1A) and the subsequent MeI oxidative addition step in the catalytic cycle are viable only when the aromatic ring is rich enough to enrich the palladium atom in turn (Figure 1B).

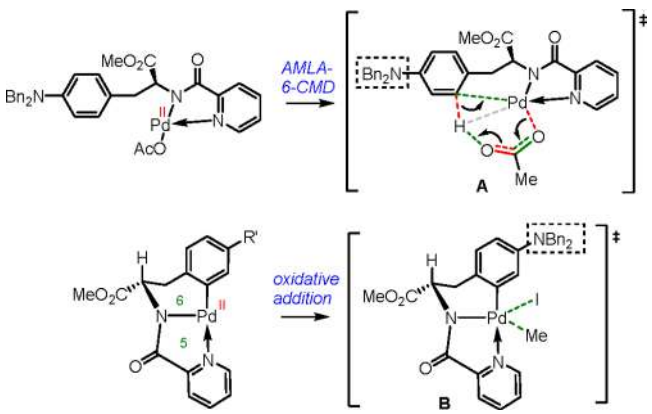

Figure 1. Postulated transition states for (A) the *δ*-ortho C(sp^2)−H palladation step and (B) the MeI oxidative addition step in the dimethylation of **9** to **10**. Green dashed bonds refer to forming bonds, red dashed bonds refer to breaking bonds, and the gray dashed bonds refers to an agostic interaction. A full catalytic cycle is proposed in the SI.

With the key 2,6-dimethylated aniline **10** in hand, we turned our attention to its conversion to a number of non-natural L-phenylalanine derivatives by exploiting the rich chemistry of anilines (Scheme 3). Accordingly, the debenzylation of **10** gave the primary aniline **11**. The latter could be further transformed into the fluoride **13**,[15] the iodide **14**, the protodeaminated product **15**,[16] as well as the nitrile **16**[17] passing through the common diazonium tetrafluoroborate intermediate **12**. Treating the four intermediates **13**−**16** with a 6 N HCl solution allowed ester and amide hydrolysis, and the resulting amino acid hydrochlorides were subsequently protected as *N-tert*-butyloxycarbonyl (*NH*-Boc) synthons to afford the building blocks **17**−**20**. As expected, the acidic treatment of nitrile **16**

https://doi.org/10.1021/acs.joc.1c02527
J. Org. Chem. XXXX, XXX, XXX−XXX

Scheme 3. Conversion of the Key Intermediate 10 to the Selectively Functionalized *NH*-Boc and *NH*-Fmoc 2,6-Dimethyl-L-phenylalanine building blocks 17−22[a]

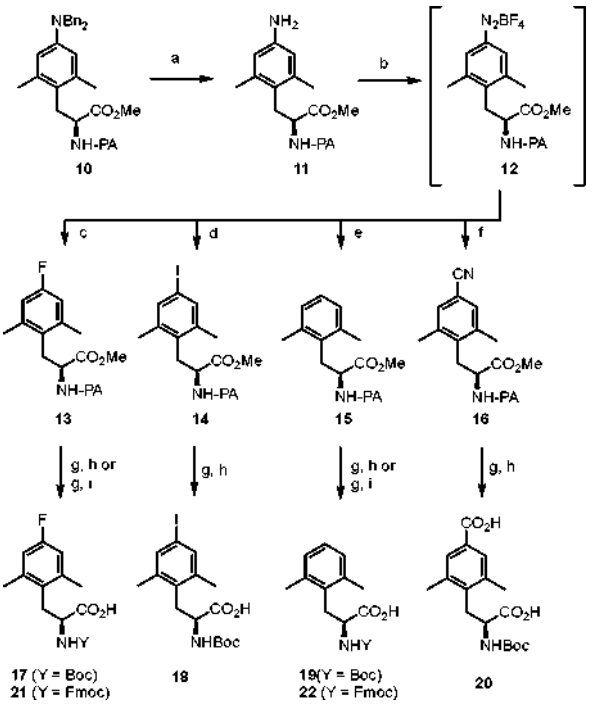

[a]Conditions are as follows: (a) Pd/C (10%), and AcOEt at 80 °C and H_2 (45 bar) under flow conditions (quantitative yield); (b) HBF_4, isoamyl nitrite, and THF at −10 °C (without purification and isolation); (c) THF at 70 °C, MW (70%); (d) KI, CuI, and acetone at 120 °C, MW (35%); (e) $FeSO_4$ and DMF at r.t. (39%); (f) TMSCN, Cu_2O, and CH_3CN at 55 °C (without isolation); (g) HCl (6 N) at 110 °C (without purification); (h) Boc_2O, NaOH (2 N), and H_2O/1,4-dioxane at r.t. (**17**, 72%; **18**, 70%; **19**, 75%; **20**, 10%); and (i) FmocCl, NaOH (2 N), and H_2O/1,4-dioxane at r.t. (**21**, 75%; **22**, 80%).

brought also about the hydrolysis of the nitrile function into the corresponding carboxylic acid. An alternative *NH*-Fmoc protection was also carried out on the amino acids derived from **13** and **15** to afford the *N*-fluorenylmethyloxycarbonyl-protected (*NH*-Fmoc) modified amino acids **21** and **22**, respectively.

Furthermore, the direct mild hydrolysis of the key intermediate **10**, followed by the standard Boc protection of the amine function, afforded the *N,N*-dibenzyl 2,6-dimetylated *NH*-Boc-protected amino acid **23**, and subsequent catalytic hydrogenation gave the debenzylated aniline **24** (Scheme 4).

Finally, the hydrogen peroxide oxidation[18] of aniline **11** led to the corresponding nitro derivative **25**, which reversed the electron demand of the aromatic nucleus. Furthermore, the anellation of **11** by treatment with potassium thiocyanate and bromine in acetic acid gave the corresponding amino-benzothiazole **27**, whose structure was reminiscent of the important Aba-Gly opioid scaffold shape.[19] Once again, a standard two-step protocol allowed the two picolinamides **25** and **27** to be converted to the corresponding *NH*-Boc derivatives **26** and **28** (Scheme 5).

PRELIMINARY BIOLOGICAL EVALUATIONS

We started the biological part of this project with the SPPS-mediated insertion of the newly synthesized amino acids **21** and **22** into N/OFQ(1−13)-NH_2, the shorter active fragment of nociceptin.[20] The resulting Osuitably methylated peptides [(*p*-F)Dmp[4]](N/OFQ(1−13)-NH_2) and [Dmp[4]](N/OFQ-(1−13)-NH_2)[21] were then compared with the corresponding nondimethylated ones. Our preliminary results are disclosed below.[22] Specifically, these compounds were evaluated in an intracellular Ca^{2+} mobilization assay on CHO cells, which were transfected to express the recombinant NOP receptor and coupled to the chimeric protein Gαqi5.[23] The results obtained are represented by the dose−response curves in Figure 2. All the examined peptides showed full-agonist behavior. In particular, the beneficial effect of [*p*-EWG[4]] and the loss of potency due to the presence of [Dmp[4]] have to be noticed.[24] Noteably, [(*p*-F)Dmp[4]] showed a balanced potency profile due to the presence of both the *p*-EWG group and the 2,6-dimethyl groups.

Scheme 4. Synthesis of the *N,N*-Dibenzyl and Free Aniline *NH*-Boc Derivatives[a]

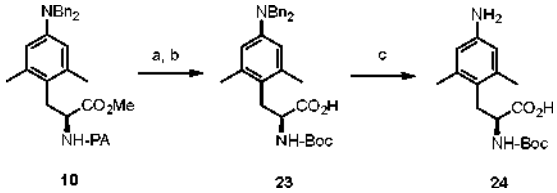

[a]Conditions are as follows: (a) HCl (3 N) at 60 °C for 1 week (without isolation); (b) Boc_2O, NaOH (2 N), and H_2O/dioxane at r.t. (70%); and (c) H_2, Pd/C (10%), and AcOEt at r.t. (70%).

Scheme 5. Conversion of Intermediate 11 into Selectively Functionalized *NH*-Boc 2,6-Dimethyl-L-phenylalanine Building Blocks 26 and 28[a]

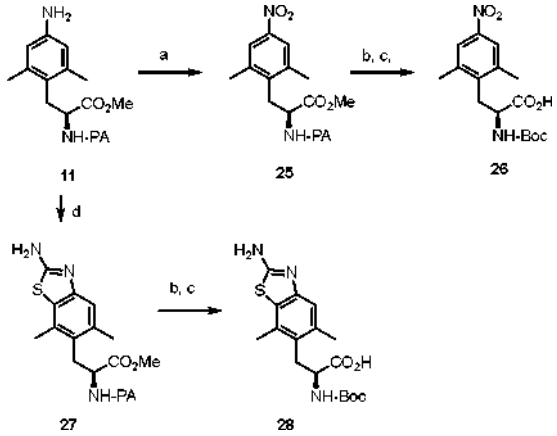

[a]Conditions are as follows: (a) EDTA, K_2CO_3, H_2O_2 (30%), and CH_3CN at r.t. (56%); (b) HCl (6 N) at 110 °C; (c) Boc_2O, NaOH (2 N), and H_2O/1,4-dioxane at r.t. (**26**, 67%; **28**, 70%); and (d) KSCN, Br_2, and AcOH at r.t. (30%).

CONCLUSION

In summary, starting from 4-nitro-L-phenylalanine[26] we achieved the late-stage synthesis of a small library of Dmt-like *NH*-Boc- or *NH*-Fmoc-protected L-phenylalanines whose aromatic rings were methylated at positions 2 and 6 and carried diverse functionalities at position 4. The appended groups can be strong or mild electron-withdrawing and electron-donating ones or bulky (such as p-*N,N*-dibenzyl) and can also have extended aromaticity (such as the

https://doi.org/10.1021/acs.joc.1c02527
J. Org. Chem. XXXX, XXX, XXX−XXX

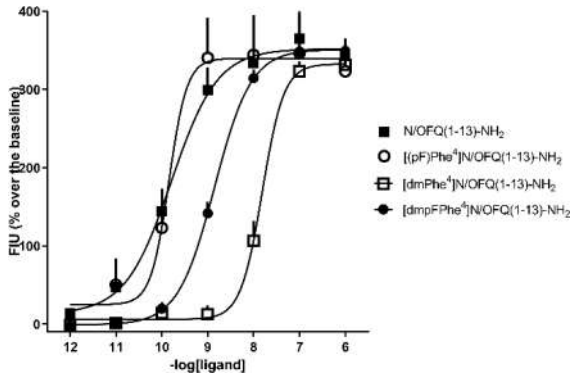

Figure 2. Calcium mobilization assay in $CHO_{NOP+G\alpha qi5}$ cells. Concentration−response curves to N/OFQ(1−13)−NH_2 and N/OFQ(1−13)−NH_2 analogues. N/OFQ(1−13)−NH_2 behaved as a NOP agonist with a high potency (pEC_{50} = 9.77 (9.36−10.18)) and efficacy (E_{max} = 352 ± 15).[25]

aminothiazole fused ring). This goal, which has evident medicinal chemistry implications, was achieved by merging the powerful picolinamide-enabled Pd-catalyzed C−H 2,6-dimethylation of 4-dibenzylamino phenylalanine with the rich chemistry of anilines. As mentioned above, we started the biological phase of this project by inserting two of the newly synthesized amino acids into the message domain of an active peptide fragment via SPPS for the biological assessment of their opioid-like properties.[27] More in-depth results will be published elsewhere.

■ EXPERIMENTAL SECTION

Chemistry. *General Information. Reagents.* All commercial materials were purchased from Fluorochem and Sigma-Aldrich and used as received unless otherwise noted. $Pd(OAc)_2$ (>98%, Fluorochem) was used in the Pd-catalyzed reactions. Reagents as 4-fluorophenyl-L-alanine **1** (CAS no. 64231-54-5) and 4-nitro-L-phenylalanine **3** (CAS no. 949-99-5) were purchased from Fluorochem (Hadfield, Derbyshire, UK).

Instruments. Analytical RP-HPLC analyses were performed on a XBridge C18 column (4.6 × 150 mm, 5 μm particle size) with a flow rate of 0.5 mL/min using a linear gradient of acetonitrile (0.1% TFA) in water (0.1% TFA) from 0% to 100% in 25 min. Retention times (t_r) from analytical RP-HPLC analyses are reported in minutes. When necessary, compounds were purified on a reverse-phase Waters Prep 600 HPLC system equipped with a Jupiter column C18 (250 × 30 mm, 300 Å, 15 μm spherical particle size). Gradients used consisted of A (H_2O and 0.1% TFA) and B (40% H_2O in CH_3CN and 0.1% TFA) at a flow rate of 20 mL/min. The UV detection wavelength for semipreparative HPLC was 220 nm. All final products showed a degree of purity >95% at 220 and 254 nm. The mass spectra were recorded with a MICROMASS ZMD 2000 instrument. TLC was performed on precoated plates of silica gel F254 (Merck, Darmstadt, Germany). ^{1}H NMR and ^{13}C DEPT NMR spectra were obtained at ambient temperature using a Varian 400 MHz spectrometer and were referenced to residual ^{1}H signals of the deuterated solvents (δ ^{1}H 7.26 for $CDCl_3$, δ ^{1}H 2.50 for DMSO-d_6, and δ ^{1}H 3.31, 4.87 for CD_3OD); the following abbreviations were used to describe the shapes of the peaks: s, singlet; d, doublet; dd, double doublet; t, triplet; and m, multiplet. Optical rotations were analyzed on a Jasco P-2000 polarimeter instrument with a path length of 1 dm (589 nm) and reported as follows: $[\alpha]_T^D$ (c in grams per 100 mL of solvent). The infrared analyses were performed with a Spectrum 100 FT-IR spectrometer (PerkinElmer Inc., Waltham, Massachusetts, USA). The hydrogenation reaction in AcOEt was performed under continuous-flow conditions in an H-Cube Pro setup (Thalesnano, Hungary) equipped with a module for the automatic control of operational parameters (reaction temperature in degrees Celsius, pressure in bar, flow rates of the liquid feed in milliliters per minute, and hydrogen). All microwave reactions were carried out using a Biotage Initiator +TM 2.0 apparatus (Biotage Sweden).The system can process reaction volumes between 0.2 and 20 mL at temperatures between 40 and 300 °C. The sealed vial is inserted into the microwave cavity and closed with the cavity lid, then high frequency microwaves (2.45 GHz) generated by a magnetron heat the reaction mixture. The reactor has an automated power control so that a constant reaction temperature can be automatically maintained throughout the reaction. Indeed, the system has an external probe that measures the average temperature of reaction, which is given by the constant stirring of the mixture. After processing, the reaction mixture is immediately cooled with pressurized air.

*(S)-Methyl-3-(4-fluorophenyl)-2(picolinamido)propanoate (**2**).* To a solution of 4-fluoro-L-phenylalanine (2.28 mmol, 0.500 g) in anhydrous MeOH (20 mL) was added $SOCl_2$ (2.50 mmol, 0.182 mL) in a dropwise manner. The reaction mixture was heated using an oil bath at reflux overnight. The volatile substances were removed under vacuum to give the crude methyl-4-fluoro-phenylalanine hydrochloride, which was washed with 10 mL of an aqueous saturated sodium bicarbonate solution (to pH ∼ 8) and extracted with DCM. The organic layers were combined and evaporated under vacuum to give the corresponding ester as a white solid (0.525 g, 99% yield), which was used directly for the next step.

A mixture of the previous crude amino product, picolinic acid (2.70 mmol, 0.333 g), HATU (2.70 mmol, 1.02 g), and DIPEA (5.64 mmol, 0.98 mL) in DCM (40 mL) was stirred at room temperature overnight. Then, the reaction was quenched with an aqueous saturated NH_4Cl solution, and the two layers were separated. The aqueous layer was extracted with DCM (three times), and the organic layers were combined, dried over Na_2SO_4, filtered, and concentrated in vacuum. The residue was purified by flash chromatography (1:1 petroleum ether/AcOEt) to afford the compound **2** (0.618 g, 91% yield) as a white oil. HRMS *m/z:* $[M + H]^+$ calcd for $C_{16}H_{16}N_2O_3F$ 303.1139, found 303.1137. ^{1}H NMR (400 MHz, $CDCl_3$) δ 8.56 (ddt, J = 4.8, 1.8, 0.9 Hz, 1H), 8.48 (d, J = 8.4 Hz, 1H), 8.15 (dt, J = 7.8, 1.1 Hz, 1H), 7.84 (td, J = 7.7, 1.7 Hz, 1H), 7.43 (ddd, J = 7.6, 4.8, 1.2 Hz, 1H), 7.18−7.10 (m, 2H), 6.96 (dd, J = 9.2, 8.3 Hz, 2H), 5.05 (dt, J = 8.4, 6.1 Hz, 1H), 3.73 (d, J = 0.9 Hz, 3H), 3.25 (dd, J = 13.9, 7.2 Hz, 1H), 3.17 (dd, J = 13.9, 7.2 Hz, 1H). ^{13}C{^{1}H} NMR (101 MHz, $CDCl_3$) δ 171.8, 164.1, 163.4, 160.9, 149.3, 148.4, 137.5, 131.9, 130.9, 126.6, 122.4, 115.7, 115.5, 53.6, 52.5, 37.6. ^{19}F NMR (376 MHz, $CDCl_3$) δ −115.8. IR 3384, 1740, 1673, 1506, 1218 cm^{-1}. $[\alpha]_D^{22}$ = −37.22 (c = 0.039, MeOH).

*(S)-Methyl-3-(4-nitrophenyl)-2-(picolinamido)propanoate (**4**).* To a solution of 4-nitro-L-phenylalanine (23.81 mmol, 5.00 g) in anhydrous MeOH (100 mL) was added $SOCl_2$ (26.19 mmol, 1.91 mL) in a dropwise manner. The reaction mixture was heated using an oil bath at reflux overnight. The volatile substances were removed under vacuum to give the crude methyl-4-nitro-phenylalanine hydrochloride, which was washed with 30 mL of an aqueous saturated sodium bicarbonate solution (to pH ∼ 8) and extracted with DCM. The organic layers were combined and evaporated under vacuum to give the corresponding ester as yellowish solid (6.17 g, 99% yield), which was used directly for the next step.

A mixture of the previous crude amino product, picolinic acid (28.56 mmol, 3.51 g), HATU (28.56 mmol, 10.86 g), and DIPEA (59.52 mmol, 10.37 mL) in DCM (150 mL) was stirred at room temperature overnight. Then, the reaction was quenched with an aqueous saturated NH_4Cl solution, and the two layers were separated. The aqueous layer was extracted with DCM, and the organic layers were combined, dried over Na_2SO_4, filtered, and concentrated in vacuum. The residue was purified by flash chromatography (1:1 petroleum ether/AcOEt) to afford the compound **4** (7.12 g, 91% yield) as a yellowish oil. HRMS *m/z:* $[M + H]^+$ Calcd for $C_{16}H_{16}N_3O_5$ 330.1084, found 330.1087. ^{1}H NMR (400 MHz, $CDCl_3$) δ 8.57−8.54 (m, 1H), 8.51 (d, J = 8.4 Hz, 1H), 8.22−8.03 (m, 3H), 7.85 (td, J = 7.7, 1.7 Hz, 1H), 7.49−7.41 (m, 1H), 7.35 (d, J = 8.7 Hz, 2H), 5.12 (dt, J = 8.4, 6.2 Hz, 1H), 3.76 (s, 3H), 3.41 (dd, J

https://doi.org/10.1021/acs.joc.1c02527
J. Org. Chem. XXXX, XXX, XXX−XXX

= 13.8, 5.8 Hz, 1H), 3.30 (dd, J = 13.8, 6.5 Hz, 1H). $^{13}C\{^1H\}$ NMR (101 MHz, $CDCl_3$) δ 171.3, 164.1, 148.4, 144.1, 137.7, 130.4, 126.8, 123.9, 122.6, 53.2, 52.8, 38.2. IR 3373, 1739, 1671, 1512, 1343 cm^{-1}. $[\alpha]_D^{23}$ = −23.14 (c = 0.028, MeOH).

*(S)-Methyl-3-(4-aminophenyl)-2-(picolinamido)propanoate (**5**).* The compound **4** was dissolved in AcOEt (150 mL, 0.15 M) and set up in continuous-flow hydrogenator reactor H-Cube Pro Thales-Nano at a temperature of 55 °C, a pressure of 20 bar and a flow of 0.3 mL/min with Pd/C (10 mol %) as the catalyst. When the reaction was complete, as monitored via mass spectrometry, the solvent was concentrated in vacuum to obtain the crude product **5** (6.70 g, 97% yield) as a red-orange oil. HRMS *m/z:* $[M + H]^+$ Calcd for $C_{16}H_{18}N_3O_3$ 300.1342, found 300.1341. ^1H NMR (400 MHz, DMSO-d6) δ 8.79−8.55 (m, 2H), 8.07−7.89 (m, 2H), 7.67−7.51 (m, 1H), 6.83 (d, J = 8.4 Hz, 2H), 6.45 (d, J = 8.4 Hz, 2H), 4.90 (s, 2H), 4.68 (ddd, J = 8.1, 7.1, 6.0 Hz, 1H), 3.65 (s, 3H), 3.05−2.92 (m, 2H). $^{13}C\{^1H\}$ NMR (101 MHz, DMSO) δ 171.8, 163.6, 149.1, 148.7, 147.3, 138.0, 129.6, 127.0, 123.5, 122.0, 114.0, 53.8, 52.1, 35.9. IR 3350, 1734, 1668, 1516, 831 cm^{-1}. $[\alpha]_D^{22}$ = +3.98 (c = 0.034, MeOH).

*(S)-Methyl-3-(4-((tert-butoxycarbonyl)amino)phenyl)-2-(picolinamido)propanoate (**6**).* The compound **5** (1.13 mmol, 0.340 g) was solubilized in a water/dioxane (1:2) solution (6 mL). The mixture was basified with an aqueous NaOH (2 N) solution until pH 10 or 11 was reached at 0 °C. To the solution was added Boc_2O (1.25 mmol, 0.273 g), and the reaction mixture was left stirring at r.t. for 12 h. The completion of the reaction was monitored by ESI mass spectrometry and TLC. The dioxane was removed under vacuum, and an aqueous HCl (1 N) solution was added at 0 °C to pH 1. The mixture was extracted with ethyl acetate (three times), and the combined organic phases were dried over Na_2SO_4 and concentrated under vacuum. The crude was purified by flash chromatography (1:1 AcOEt/petroleum ether/1% acetic acid) and crystallized with 2:1 Et_2O/petroleum ether to obtain the compound **6** as a white solid (0.340 g, 75% yield). HRMS *m/z:* $[M + H]^+$ Calcd for $C_{21}H_{26}N_3O_5$ 400.1867, found 400.1866. ^1H NMR (400 MHz, $CDCl_3$) δ 8.55 (ddd, J = 4.8, 1.7, 0.9 Hz, 1H), 8.48 (d, J = 8.4 Hz, 1H), 8.15 (dt, J = 7.8, 1.1 Hz, 1H), 7.83 (td, J = 7.7, 1.7 Hz, 1H), 7.43 (ddd, J = 7.6, 4.8, 1.2 Hz, 1H), 7.27 (d, J = 8.3 Hz, 2H), 7.09 (d, J = 8.5 Hz, 2H), 6.47 (s, 1H), 5.03 (dt, J = 8.4, 6.0 Hz, 1H), 3.72 (s, 3H), 3.24−3.13 (m, 2H), 1.50 (s, 9H). $^{13}C\{^1H\}$ NMR (101 MHz, $CDCl_3$) δ 171.9, 164.0, 152.9, 149.4, 148.4, 137.5, 130.7, 130.0, 126.5, 122.4, 118.7, 80.6, 53.7, 52.5, 37.7, 28.5, 27.6. IR 3315, 1721, 1667, 1515, 1155 cm^{-1}. MP 65−67 °C. $[\alpha]_D^{23}$ = +5.255 (c = 0.0355, MeOH).

*(S)-Methyl-3-(4-(dimethylamino)phenyl)-2-(picolinamido)-propanoate (**7**).* To a solution of the aniline **5** (1.67 mmol, 0.500 g) in CH_3CN (20 mL) were added methyl iodide (4.17 mmol, 0.26 mL) and potassium carbonate (3.34 mmol, 0.46 g). The mixture was stirred and heated using an oil bath at 80 °C overnight. Then, the solvent was removed under vacuum, and the residue was dissolved in AcOEt and washed with water. Once the layers were separated, the solvent was removed under vacuum. The crude mixture was purified by flash chromatography (2:3 AcOEt/petroleum ether) to afford **7** as a yellowish oil (0.47 g, 87% yield). HRMS *m/z:* $[M + Na]^+$ Calcd for $C_{18}H_{21}N_3O_3Na$ 350.1475, found 350.1473. ^1H NMR (400 MHz, $CDCl_3$) δ 8.56 (ddd, J = 4.8, 1.7, 0.9 Hz, 1H), 8.53−8.39 (m, 1H), 8.16 (dt, J = 7.8, 1.1 Hz, 1H), 7.83 (td, J = 7.7, 1.7 Hz, 1H), 7.42 (ddd, J = 7.6, 4.7, 1.3 Hz, 1H), 7.14−6.96 (m, 2H), 6.69 (d, J = 8.2 Hz, 2H), 5.00 (dt, J = 8.3, 6.0 Hz, 1H), 3.73 (s, 3H), 3.15 (d, J = 6.0 Hz, 2H), 2.92 (s, 6H). $^{13}C\{^1H\}$ NMR (101 MHz, $CDCl_3$) δ 172.17, 164.12, 149.57, 148.44, 137.35, 130.11, 126.42, 122.38, 113.09, 53.85, 52.40, 40.96, 37.48. IR 3381, 1736, 1673, 1509, 1344 cm^{-1}. $[\alpha]_D^{22}$ = +0.978 (c = 0.015, MeOH).

*(S)-Methyl-3-(4-(diallylamino)phenyl)-2-(picolinamido)-propanoate (**8**).* To a solution of the aniline **5** (1.67 mmol, 0.500 g) in CH_3CN (20 mL) were added allyl bromide (4.17 mmol, 0.36 mL) and potassium carbonate (3.34 mmol, 0.46 g). The mixture was stirred and heated using an oil bath at 120 °C overnight. Then, the solvent was removed under vacuum, and the residue was dissolved in AcOEt and washed with water. Once the layers were separated, the solvent was removed under vacuum. The crude mixture was purified by flash chromatography (2:3 AcOEt/petroleum ether) to afford **8** as a yellowish oil (0.50 g, 80% yield). HRMS *m/z:* $[M + Na]^+$ Calcd for $C_{22}H_{25}N_3O_3Na$ 402.1788, found 402.1774. ^1H NMR (400 MHz, $CDCl_3$) δ 8.55 (ddt, J = 4.8, 1.9, 1.0 Hz, 1H), 8.46 (d, J = 8.2 Hz, 1H), 8.15 (dq, J = 7.8, 1.3 Hz, 1H), 7.90−7.75 (m, 1H), 7.46−7.38 (m, 1H), 7.01 (d, J = 8.1 Hz, 2H), 6.62 (s, 2H), 5.82 (d, J = 14.2 Hz, 2H), 5.21−5.09 (m, 4H), 4.98 (dt, J = 8.6, 6.0 Hz, 1H), 3.88 (d, J = 5.0 Hz, 4H), 3.72 (d, J = 2.0 Hz, 3H), 3.13 (d, J = 5.9 Hz, 2H). $^{13}C\{^1H\}$ NMR (101 MHz, $CDCl_3$) δ 172.15, 164.13, 149.57, 148.43, 148.28, 137.34, 134.19, 130.13, 126.42, 123.40, 122.37, 116.25, 112.68, 53.81, 52.89, 52.40, 37.47. IR 3387, 2979, 1741, 1674, 1509 cm^{-1}. $[\alpha]_D^{22}$ = +1.52 (c = 0.014, MeOH)

*(S)-Methyl-3-(4-(dibenzylamino)phenyl)-2-(picolinamido)-propanoate (**9**).* To a solution of the aniline **5** (22.40 mmol, 7.32 g) in CH_3CN (150 mL) were added benzyl bromide (56.02 mmol, 6.66 mL) and potassium carbonate (44.81 mmol, 6.19 g). The mixture was stirred and heated using an oil bath at 120 °C overnight. The crude mixture was purified by flash chromatography (2:3 AcOEt/petroleum ether) to afford **9** as a yellowish orange solid (8.76 g, 82% yield). HRMS *m/z:* $[M + H]^+$ calcd for $C_{30}H_{30}N_3O_3$ 480.2281, found 480.2288. ^1H NMR (400 MHz, $CDCl_3$) δ 8.54 (ddd, J = 4.8, 1.7, 0.9 Hz, 1H), 8.46 (d, J = 8.3 Hz, 1H), 8.15 (dt, J = 7.8, 1.1 Hz, 1H), 7.83 (td, J = 7.7, 1.7 Hz, 1H), 7.41 (ddd, J = 7.6, 4.8, 1.3 Hz, 1H), 7.35−7.28 (m, 4H), 7.27−7.20 (m, 6H), 6.98 (d, J = 8.7 Hz, 2H), 6.67 (d, J = 8.4 Hz, 2H), 4.97 (dt, J = 8.3, 6.0 Hz, 1H), 4.61 (s, 4H), 3.70 (s, 3H), 3.17−3.05 (m, 2H). $^{13}C\{^1H\}$ NMR (101 MHz, $CDCl_3$) δ 171.9, 164.1, 149.5, 148.4, 137.4, 130.3, 130.1, 128.9, 128.8, 128.3, 127.9, 127.6, 127.1, 126.5, 122.4, 56.1, 53.7, 52.4, 37.5. IR 3374, 1725, 1665, 1516, 837, 737 cm^{-1}. MP 104−106 °C. $[\alpha]_D^{23}$ = −4.095 (c = 0.0155, MeOH).

*(S)-Methyl-3-(4-(dibenzylamino)-2,6-dimethylphenyl)-2-(picolinamido)propanoate (**10**).* To a solution of compound **9** (18.30 mmol, 9.28 g) in toluene (150 mL) were added K_2CO_3 (54.86 mmol, 7.5 g), CH_3I (91.53 mmol, 5.69 mL), and $Pd(OAc)_2$ (1.83 mmol, 0.41 g). The mixture was stirred and heated using an oil bath at 120 °C overnight. After 24 h the reaction was cooled to r.t., filtered through a Celite pad, and washed with AcOEt (50 mL). The filtrate was concentrated under vacuum to obtain the crude product, which was then used for two other catalytic reactions at the same conditions. The final crude product was purified by flash chromatography (3:7 AcOEt/petroleum ether) to afford **10** (6.76 g, 72% yield) as a yellowish solid. HRMS *m/z:* $[M + H]^+$ calcd for $C_{32}H_{34}N_3O_3$ 508.2594, found 508.2597. ^1H NMR (400 MHz, $CDCl_3$) δ 8.56 (ddd, J = 4.7, 1.7, 0.9 Hz, 1H), 8.13 (d, J = 7.8 Hz, 1H), 7.83 (td, J = 7.7, 1.7 Hz, 1H), 7.42 (ddd, J = 7.6, 4.8, 1.3 Hz, 1H), 7.33−7.26 (m, 4H), 7.26−7.20 (m, 6H), 6.44 (s, 2H), 4.89 (m, J = 7.9 Hz, 1H), 4.57 (s, 4H), 3.66 (s, 3H), 3.19−3.02 (m, 2H), 2.29 (s, 6H). $^{13}C\{^1H\}$ NMR (101 MHz, $CDCl_3$) δ 173.0, 164.1, 149.5, 148.4, 148.0, 138.9, 138.1, 137.4, 128.9, 128.7, 128.2, 126.9, 126.4, 122.3, 112.6, 53.8, 52.7, 52.4, 32.4, 20.8. IR 3384, 1738, 1676, 1602, 1494, 731, 700 cm^{-1}. MP 77−79 °C. $[\alpha]_D^{22}$ = −8.82 (c = 0.0085, MeOH).

*(S)-Methyl-3-(4-amino-2,6-dimethylphenyl)-2-(picolinamido)-propanoate (**11**).* The compound **10** was dissolved in AcOEt (186 mL, 0.05 M) and set up in continuous-flow hydrogenator reactor H-Cube Pro Thales-Nano at a temperature of 80 °C, a pressure of 45 bar, and flow 1 mL/min with Pd/C (10 mol %) as the catalyst. When the reaction was complete, as monitored via mass spectrometry, the solvent was concentrated in vacuum to afford the crude product, which was purified by flash chromatography (1:1 AcOEt/petroleum ether) to obtain **11** (3.05 g, quantitative yield) as a yellowish oil. HRMS *m/z:* $[M + H]^+$ calcd for $C_{18}H_{22}N_3O_3$ 328.1655, found 328.1657. ^1H NMR (400 MHz, DMSO) δ 8.78 (d, J = 8.2 Hz, 1H), 8.67 (dt, J = 4.9, 1.2 Hz, 1H), 8.05−7.93 (m, 2H), 7.62 (tdd, J = 4.8, 2.5, 0.8 Hz, 1H), 6.19 (s, 2H), 4.72 (s, 2H), 4.61 (td, J = 8.4, 6.6 Hz, 1H), 3.61 (s, 3H), 3.19−2.03 (m, 2H), 2.14 (s, 6H). $^{13}C\{^1H\}$ NMR (101 MHz, DMSO) δ 173.7, 165.6, 149.9, 149.3, 145.7, 139.4, 138.7, 128.5, 124.1, 123.3, 116.5, 53.6, 53.6, 31.5, 20.8. IR 3360, 2952, 1734, 1670, 1511, 749 cm^{-1}. $[\alpha]_D^{23}$ = −17.97 (c = 0.011, MeOH).

*(S)-4-(3-Methoxy-3-oxo-2-(picolinamido)propyl)-3,5-dimethylbenzenediazonium Tetrafluoroborate (**12**).* To a solution of

https://doi.org/10.1021/acs.joc.1c02527
J. Org. Chem. XXXX, XXX, XXX−XXX

compound **11** (2.41 mmol, 0.79 g) dissolved in anhydrous THF (15 mL) and cooled to −10 °C were added isoamyl nitrite (4.83 mmol, 0.643 mL) and HBF_4 (9.66 mmol, 1.31 mL). The reaction mixture was stirred for 4 h at −10 °C until a yellow precipitate formed, which was directly used as the wet crude for the next step. An IR analysis and a diazocopulation assay were performed on compound **12** with positive results. IR peaks referable to the diazonium salt are as follows: 2274 cm^{-1}.

*(S)-Methyl-3-(4-fluoro-2,6-dimethylphenyl)-2-(picolinamido)-propanoate (**13**).* Compound **12** (2.41 mmol, 1.02 g) was used directly as the crude dissolved in anhydrous THF (15 mL) in a sealed 10−20 mL reaction vessel. The mixture was heated to 70 °C for 5 min under microwave irradiation. The resulting brown solution was evaporated under vacuum, and the crude was solubilized in AcOEt and washed with H_2O and a saturated aqueous solution of $NaHCO_3$. The solvent of the organic phase was then removed under vacuum to give a crude product, which was purified by flash chromatography (2:3 AcOEt/petroleum ether). The purified product **13** was obtained as a white solid (0.556 g, 70% yield). HRMS *m/z:* $[M + H]^+$ calcd $C_{18}H_{20}N_2O_3F$ 331.1452, found 331.1455. ^1H NMR (400 MHz, $CDCl_3$) δ 8.62−8.51 (m, 2H), 8.10 (dt, J = 7.8, 1.1 Hz, 1H), 7.83 (td, J = 7.7, 1.7 Hz, 1H), 7.43 (ddd, J = 7.6, 4.8, 1.3 Hz, 1H), 6.70 (d, J = 9.4 Hz, 2H), 5.04−4.92 (m, 1H), 3.68 (s, 3H), 3.25−3.15 (m, 2H), 2.39 (d, J = 0.6 Hz, 6H). $^{13}C\{^1H\}$ NMR (101 MHz, $CDCl_3$) δ 172.6, 164.0, 161.3 (d, J = 244.2 Hz), 149.3, 148.4, 139.4 (d, J = 9 Hz), 137.5, 129.0, 126.5, 122.4, 114.9 (d, J = 21 Hz), 52.5, 52.0, 32.6, 20.5. ^{19}F NMR (376 MHz, $CDCl_3$) δ −117.20 (t, J = 9.4 Hz). IR 3365, 2956, 1731, 1658, 1514, 1018 cm^{-1}. MP 117−119 °C. $[\alpha]_D^{23}$ = −17.22 (c = 0.01, MeOH).

*(S)-Methyl-3-(4-iodo-2,6-dimethylphenyl)-2-(picolinamido)-propanoate (**14**).* To a solution of crude compound **12** (0.704 mmol, 0.300 g) in anhydrous acetone (10 mL) in a sealed 10−20 mL reaction vessel were added CuI (0.070 mmol, 13.4 mg) and KI (1.76 mmol, 0.292 g). The mixture was heated to 120 °C for 30 min under microwave irradiation. The resulting brown mixture was filtered through a Celite pad and washed with acetone. The solvent was removed under vacuum until a dark solid was obtained, which was purified by flash chromatography (2:3 AcOEt/petroleum ether) to obtain compound **14** as a white oil (0.11 g, 35% yield). HRMS *m/z:* $[M + H]^+$ calcd for $C_{18}H_{20}N_2O_3I$ 439.0513, found 439.0514. ^1H NMR (400 MHz, $CDCl_3$) δ 8.70−8.51 (m, 2H), 8.11 (d, J = 7.9 Hz, 1H), 7.91−7.78 (m, 1H), 7.50−7.43 (m, 1H), 7.35 (s, 2H), 4.98 (q, J = 8.1 Hz, 1H), 3.69 (s, 3H), 3.23−3.09 (m, 2H), 2.35 (s, 6H). $^{13}C\{^1H\}$ NMR (101 MHz, $CDCl_3$) δ 172.4, 164.3, 149.0, 148.4, 139.5, 137.7, 137.1, 133.1, 126.8, 122.6, 92.7, 52.7, 51.9, 32.9, 19.9. IR 3380, 2952, 1739, 1674, 1511, 1170 cm^{-1}. $[\alpha]_D^{23}$ = −18.67 (c = 0.0165, MeOH).

*(S)-Methyl-3-(2,6-dimethylphenyl)-2-(picolinamido)propanoate (**15**).* To a solution of Fe_2SO_4 (0.884 mmol, 0.246 g) in 6 mL of DMF was added dropwise compound **12** (0.884 mmol, 0.3 g) solubilized in DMF (1.51 mL). The reaction mixture was stirred at r.t. overnight. The solvent was removed under vacuum, and the residue was dissolved in DCM. The organic layer was washed with water, dried over Na_2SO_4, filtered, and concentrated under vacuum. The crude orange oil was purified by flash chromatography (2:3 AcOEt/petroleum ether) to obtain compound **15** as a yellow solid (0.107 g, 39% yield). HRMS *m/z:* $[M + H]^+$ calcd for $C_{18}H_{21}N_2O_3$ 313.1546, found 313.1544. ^1H NMR (400 MHz, $CDCl_3$) δ 8.58 (ddd, J = 4.8, 1.8, 1.0 Hz, 2H), 8.11 (dt, J = 7.8, 1.1 Hz, 1H), 7.82 (td, J = 7.7, 1.7 Hz, 1H), 7.43 (ddd, J = 7.6, 4.8, 1.3 Hz, 1H), 7.06−6.94 (m, 3H), 5.00 (q, J = 8.1 Hz, 1H), 3.67 (s, 3H), 3.32−3.21 (m, 2H), 2.41 (s, 6H). $^{13}C\{^1H\}$ NMR (101 MHz, $CDCl_3$) δ 172.8, 164.0, 149.4, 148.4, 137.4, 137.2, 133.3, 128.5, 126.9, 126.5, 122.4, 52.5, 52.1, 33.1, 20.3. IR 3389, 1736, 1673, 1508, 746 cm^{-1}. MP 94−96 °C. $[\alpha]_D^{23}$ = −18.19 (c = 0.0085, MeOH).

*(S)-4-(2-((tert-Butoxycarbonyl)amino)-2-carboxyethyl)-3,5-dimethylbenzoic Acid (**20**).* To a solution of compound **12** (1.76 mmol, 0.750 g) in acetonitrile (100 mL) were added trimethylsilyl-cyanide (1.76 mmol, 0.220 mL) and Cu_2O (0.704 mmol, 0.100 g). The reaction mixture was heated using an oil bath at 55 °C for 12 h, leading to a crude orange solution. The solution was cooled to r.t, filtered through a Celite pad, and washed with DCM. The filtrate was concentrated under vacuum to yield an orange oil (**16**). The crude product was directly hydrolyzed with an aqueous HCl (6 N) solution at 110 °C to give the corresponding carboxylic acid. The crude was directly solubilized in a water/dioxane (1:2) solution (30 mL), and basified with an aqueous NaOH (2 N) solution until pH 10 or 11 was reacyhed at 0 °C. To the solution was added Boc_2O (2.11 mmol, 0.460 g), and the reaction mixture was left stirring at r.t. for 12 h. The completion of the reaction was monitored by ESI mass spectrometry and TLC. The dioxane was removed under vacuum, and an aqueous HCl (1 N) solution was added to the solution at 0 °C to pH 1. The mixture was extracted with ethyl acetate (three times), and the organic phases were dried over Na_2SO_4 and concentrated under vacuum. The crude was purified per flash chromatography (1:1 AcOEt/petroleum ether/1% acetic acid) and crystallized with 2:1 Et_2O/petroleum ether to obtain compound **20** as a white solid (0.059 g, yield 10%). t_r: 15.92 min. HRMS *m/z:* $[M - H]^-$ calcd for $C_{17}H_{22}NO_6$ 336.1453, found 336.1456. ^1H NMR (400 MHz, CD_3OD) (rotameric mixture) δ 7.65 (s, 2H), 4.40 (dd, J = 9.5, 5.6 Hz, 1H), 3.30−3.02 (m, 2H), 2.43 (s, 6H), 1.34 (s, 7H), 1.18 (s, 2H). $^{13}C\{^1H\}$ NMR (101 MHz, CD_3OD) (mixture of rotamers) δ 175.4, 170.2, 157.6, 141.4, 138.8, 130.4, 129.6, 80.5, 54.4, 33.6, 28.6, 28.1, 20.5. IR 2924, 1687, 1163. MP 80−82 °C. $[\alpha]_D^{22}$ = −33.1 (c = 0.0145, MeOH).

*(S)-Methyl-3-(2,6-dimethyl-4-nitrophenyl)-2-(picolinamido)-propanoate (**25**).* The amino compound **11** (4.78 mmol, 1.56 g) was solubilized in CH_3CN (3.5 mL). An aqueous buffer solution of K_2CO_3 (0.6 M, 1.05 mmol, 0.14 g) and EDTA disodium salt (4×10^{-4} M, 0.7×10^{-3} mmol, 2.6×10^{-4} g) in 1.75 mL of H_2O was prepared and added to the mixture. Subsequently, to the mixture was added 1.35 mL of H_2O_2 (30%). The reaction mixture was stirred at r.t. overnight, and the formation of a yellow precipitate was observed. CH_3CN was removed under vacuum, and the residue was dissolved in AcOEt. The organic layer was washed with water (10 mL × 3), dried over Na2SO4, filtered, and concentrated under vacuum. The crude was purified by flash chromatography (1:1 AcOEt/petroleum ether) to obtain **25** (0.955 g, 56% yield) as a yellowish solid. HRMS *m/z:* $[M + H]^+$ calcd for $C_{18}H_{20}N_3O_5$ 358.1397, found 358.1393. ^1H NMR (400 MHz, $CDCl_3$) δ 8.63 (d, J = 8.8 Hz, 1H), 8.61−8.54 (m, 1H), 8.07 (dt, J = 7.8, 1.1 Hz, 1H), 7.88−7.78 (m, 3H), 7.45 (ddd, J = 7.6, 4.7, 1.3 Hz, 1H), 5.07 (q, J = 8.2 Hz, 1H), 3.71 (s, 3H), 3.36−3.25 (m, 2H), 2.51 (s, 6H). $^{13}C\{^1H\}$ NMR (101 MHz, $CDCl_3$) δ 172.0, 164.0, 149.0, 148.4, 146.4, 141.3, 139.1, 137.6, 126.7, 123.0, 122.5, 52.8, 51.4, 33.5, 20.6. IR 3389, 1737, 1637, 1508, 1342, 745 cm^{-1}. MP 132−134 °C. $[\alpha]_D^{23}$ = −50.94 (c = 0.0195, MeOH).

*(S)-Methyl-3-(2-amino-5,7-dimethylbenzo[d]thiazol-6-yl)-2-(picolinamido)propanoate (**27**).* To a solution of compound **11** (1.07 mmol, 0.353 g) in AcOH (10 mL) were added KSCN (4.31 mmol, 0.419 g) and Br_2 (1.07 mmol, 55.6 μL). The reaction mixture was stirred for 48 h at room temperature. The solvent was removed under vacuum, yielding to an orange compound that was extracted with saturated $NaHCO_3$ and AcOEt (three times). The organic phases were collected, dried over Na_2SO_4, filtered, and concentrated under vacuum. The crude was purified by preparative HPLC to obtain the compound **27** (0.123 g, 30% yield) as a white solid. HRMS *m/z:* $[M + H]^+$ calcd for $C_{19}H_{21}N_4O_3S$ 385.1328, found 385.1329. ^1H NMR (400 MHz, DMSO) δ 8.94 (d, J = 8.3 Hz, 1H), 8.66 (dt, J = 4.8, 1.4 Hz, 1H), 8.06−7.89 (m, 2H), 7.62 (ddd, J = 6.8, 4.8, 2.0 Hz, 1H), 6.97 (s, 1H), 4.73 (td, J = 8.4, 5.8 Hz, 1H), 4.39 (s, 2H), 3.65 (s, 3H), 3.32−3.11 (m, 2H), 2.31 (s, 3H), 2.27 (s, 3H). $^{13}C\{^1H\}$ NMR (101 MHz, DMSO) δ 171.6, 166.7, 163.7, 163.6, 149.1, 148.6, 137.9, 129.7, 129.2 (2CQ), 126.9, 126.6, 122.9, 122.0, 53.1, 52.1, 33.5, 17.9, 17.4. IR 2984, 1742, 1660, 1193, 1135 cm^{-1}. MP 83−85 °C. $[\alpha]_D^{22}$ = −2.67 (c = 0.001, MeOH).

*(S)-2-((tert-Butoxycarbonyl)amino)-3-(4-(dibenzylamino)-2,6-dimethylphenyl)propanoic Acid (**23**).* Compound **10** (1.97 mmol, 1.0 g) was hydrolyzed in a milder way than the acidic hydrolysis described in the hydrolysis general procedure (as reported below). It was solubilized in an aqueous HCl (3 N, 11 mL) solution and

https://doi.org/10.1021/acs.joc.1c02527
J. Org. Chem. XXXX, XXX, XXX−XXX

maintained under reflux at 60 °C for 1 week using an oil bath. The solution was concentrated under vacuum to reduce the volume (about 3 mL), and the crude was used for the protection of the amine as Boc. The previous amine hydrochloride solution was diluted in a water/dioxane (1:2) solution (21 mL). The solution was basified with an aqueous NaOH (2 N) solution to reach pH 10 at 0 °C. To the solution was added Boc_2O (2.36 mmol, 0.516 g), and the reaction mixture was stirred at r.t. for 12 h. The completion of the reaction was monitored by ESI mass spectrometry and TLC, and the dioxane was removed under vacuum. An aqueous HCl (1 N) solution was added at 0 °C to reach pH 1, then the mixture was extracted with ethyl acetate (three times). The combined organic phases were dried over Na_2SO_4 and concentrated under vacuum. The crude was purified per flash chromatography (1:1 AcOEt/petroleum ether/1% acetic acid) and crystallized with 2:1 Et_2O/petroleum ether to afford **23** as a paleyellow solid (0.576 g, 70% yield). t_r: 22.67 min. HRMS *m/z*: $[M - H]^-$ calcd for $C_{30}H_{35}N_2O_4$ 487.2602, found 487.2606. ^1H NMR (400 MHz, DMSO) (mixture of rotamers) δ 7.36−7.27 (m, 4H), 7.26−7.17 (m, 6H), 7.04 (d, J = 8.6 Hz, 1H), 6.35 (s, 2H), 4.58 (s, 4H), 3.97 (td, J = 8.4, 5.2 Hz, 1H), 2.96−2.69 (m, 2H), 2.12 (s, 6H), 1.31 (s, 7H), 1.13 (s, 2H). $^{13}C\{^1H\}$ NMR (101 MHz, DMSO) δ 173.9, 155.3, 146.5, 139.3, 137.2, 128.4, 126.7, 122.9, 112.1, 77.9, 53.9, 53.6, 30.6, 28.2, 27.6, 20.5. ^1H NMR (300 MHz, DMSO at 120 °C) δ 7.34−7.13 (m, 7H), 6.46 (s, 2H), 4.55 (s, 4H), 4.19−4.03 (m, 1H), 3.05−2.75 (m, 2H), 2.18 (s, 6H), 1.31 (s, 9H). IR 2980, 1713, 1603, 1494, 1158 cm^{-1}. MP 82−84 °C. $[\alpha]_D^{23}$ = −133.6 (c = 0.0515, MeOH).

*(S)-3-(4-Amino-2,6-dimethylphenyl)-2-((tert-butoxycarbonyl)-amino)propanoic Acid (**24**).* The benzyl removal reaction was performed by solubilizing compound **23** (0.246 mmol, 0.118 g) in AcOEt (10 mL) with Pd/C (10%) at r.t. under a H_2 atmosphere. The reaction mixture was left stirring until the starting material was completely consumed, as controlled by ESI mass spectrometry. A yellow crude oil was obtained, purified by flash chromatography (4:1 AcOEt/petroleum ether), then crystallized with 2:1 diethyl ether/petroleum ether to obtain compound **24** as a white powder (0.052 g, 70% yield). t_r: 12.60 min. HRMS *m/z*: $[M - H]^-$ calcd for $C_{16}H_{23}N_2O_4$ 307.1663, found 307.1666. ^1H NMR (400 MHz, DMSO) (mixture of rotamers) δ 7.03 (d, J = 8.4 Hz, 1H), 6.18 (s, 2H), 3.94 (q, J = 7.6 Hz, 1H), 2.99−2.62 (m, 2H), 2.12 (s, 6H), 1.33 (s, 7H), 1.20 (s, 2H). $^{13}C\{^1H\}$ NMR (101 MHz, DMSO) (mixture of rotamers) δ 174.0, 155.3, 146.3, 136.9, 122.1, 113.9, 77.9, 54.1, 30.6, 28.2, 27.7, 20.0. IR 3361, 2984, 1694, 1363, 1171 cm^{-1}. MP 160−162 °C. $[\alpha]_D^{21}$ = +43.2 (c = 0.009, MeOH).

General Procedure for Acidic Hydrolysis Deprotection. Once purified, the compound was dissolved in an aqueous HCl (6 N) solution (17 equiv) and heated using an oil bath at 110 °C for 24 h. The obtained hydrolyzed crude product was concentrated under vacuum to reduce the volume, and the crude solution was used directly for the subsequent protection step.

General Procedure for Boc Protection (17−19, 26, and 28). The previously synthesized HCl salt was directly used as the crude and diluted in a water/dioxane (1:2) solution (0.2 M). The mixture was basified with an aqueous NaOH (2 N) solution until a pH value of 10 or 11 was reached at 0 °C. To the solution was added Boc_2O (1.2 equiv), and the reaction mixture was left stirring at r.t. for 12 h. The completion of the reaction was monitored by ESI mass spectrometry and TLC. The dioxane was removed under vacuum, and an aqueous HCl (1 N) solution was added to the mixture at 0 °C to pH 1. The mixture was extracted with ethyl acetate (three times), and the organic phases combined were dried over Na_2SO_4 and concentrated under vacuum. Each crude was purified by flash chromatography as reported below.

*(S)-2-((tert-Butoxycarbonyl)amino)-3-(4-fluoro-2,6-dimethylphenyl)propanoic Acid (**17**).* The crude was purified by flash chromatography (3:2 AcOEt/petroleum ether/1% acetic acid) and crystallized with 2:1 Et_2O/petroleum ether to afford the product **17** as a white solid (0.376 g, 72% yield). t_r: 20.05 min. HRMS *m/z*: $[M - H]^-$ calcd for $C_{16}H_{21}FNO_4$ 310.1460, found 310.1459. ^1H NMR (400 MHz, DMSO) (mixture of rotamers) δ 12.61 (s, 1H), 7.16 (d, J = 8.7 Hz, 1H), 6.80 (d, J = 9.8 Hz, 2H), 4.06 (td, J = 8.8, 6.1 Hz, 1H), 3.07−2.80 (m, 2H), 2.28 (s, 6H), 1.31 (d, J = 4.3 Hz, 8H), 1.15 (s, 1H). $^{13}C\{^1H\}$ NMR (101 MHz, DMSO) δ 173.5, 160.1 (d, J = 240 Hz), 155.2, 139.4, 131.1, 114.0 (d, J = 20 Hz), 78.0, 53.3, 30.7, 28.1, 27.6, 19.9. ^{19}F NMR (376 MHz, DMSO) δ −118.24 (t, J = 9.7 Hz). ^1H NMR (300 MHz, DMSO at 120 °C) δ 6.76 (d, J = 9.8 Hz, 2H), 4.17 (td, J = 8.6, 6.4 Hz, 1H), 3.18−2.85 (m, 2H), 2.32 (s, 6H), 1.32 (s, 9H). IR 2974, 1721, 1651, 1164, 1021 cm^{-1}. MP 133−135 °C. $[\alpha]_D^{23}$ = −30.4 (c = 0.025, MeOH).

*(S)-2-((tert-Butoxycarbonyl)amino)-3-(4-iodo-2,6-dimethylphenyl)propanoic Acid (**18**).* The crude was purified by flash chromatography (3:2 AcOEt/petroleum ether/1% acetic acid) and crystallized with 2:1 Et_2O/petroleum ether to afford the product **18** as a white solid (0.073 g, 70% yield). t_r: 22.60 min. HRMS *m/z*: $[M - H]^-$ calcd for $C_{16}H_{21}INO_4$ 418.0521, found 418.0524. ^1H NMR (400 MHz, DMSO) (mixture of rotamers) δ 12.53 (s, 1H), 7.34 (s, 2H), 7.15 (d, J = 8.6 Hz, 1H), 4.04 (q, J = 8.0, 7.5 Hz, 1H), 3.07−2.80 (m, 2H), 2.24 (s, 6H), 1.30 (s, 8H), 1.15 (s, 1H). $^{13}C\{^1H\}$ NMR (101 MHz, DMSO) δ 173.4, 155.2, 139.6, 136.1, 135.1, 92.0, 78.0, 53.0, 31.0, 28.1, 19.3. IR 3355, 2963, 1726, 1686, 1018, 793 cm^{-1}. MP 128−130 °C. $[\alpha]_D^{21}$ = −82.7 (c = 0.022, MeOH).

*(S)-2-((tert-Butoxycarbonyl)amino)-3-(2,6-dimethylphenyl)-propanoic Acid (**19**).* The crude was purified by flash chromatography (1:1 AcOEt/petroleum ether/1% acetic acid) and crystallized with 2:1 Et_2O/petroleum ether to afford the product **19** as a white solid (0.075 g, 75% yield). t_r: 22.03. HRMS *m/z*: $[M - H]^-$ calcd for $C_{16}H_{22}NO_4$ 292.1543, found 292.1554. ^1H NMR (400 MHz, DMSO) (mixture of rotamers) δ 12.55 (s, 1H), 7.15 (d, J = 8.6 Hz, 1H), 6.96 (d, J = 1.7 Hz, 3H), 4.07 (td, J = 8.6, 6.1 Hz, 1H), 3.11−2.85 (m, 2H), 2.28 (s, 6H), 1.31 (s, 8H), 1.14 (s, 1H). $^{13}C\{^1H\}$ NMR (101 MHz, DMSO) (mixture of rotamers) δ 173.7, 155.3, 136.7, 135.0, 127.9, 126.0, 78.0, 53.4, 31.3, 28.1, 27.6, 19.9. IR 3301, 2973, 1723, 1656, 1366, 1163, 765 cm^{-1}. MP 65−67 °C. $[\alpha]_D^{23}$ = +0,855 (c = 0.0055, MeOH).

*(S)-2-((tert-Butoxycarbonyl)amino)-3-(2,6-dimethyl-4-nitrophenyl)propanoic Acid (**26**).* The crude was purified by flash chromatography (7:3 AcOEt/petroleum ether/1% acetic acid) and crystallized with 2:1 Et_2O/petroleum ether to afford the product **26** as a pale yellow solid (0.605 g, 67% yield). t_r: 19.52 min. HRMS *m/z*: $[M - H]^-$ calcd for $C_{16}H_{21}N_2O_6$ 337.1405, found 337.1405. ^1H NMR (400 MHz, DMSO) (mixture of rotamers) δ 12.75 (s, 1H), 7.87 (s, 2H), 7.26 (d, J = 8.6 Hz, 1H), 4.16 (td, J = 9.1, 5.6 Hz, 1H), 3.19−2.97 (m, 2H), 2.42 (s, 6H), 1.27 (s, 7H), 1.13 (s, 2H). $^{13}C\{^1H\}$ NMR (101 MHz, DMSO) (mixture of rotamers) δ 173.0, 155.2, 145.4, 143.8, 139.3, 122.1, 78.1, 52.6, 31.6, 28.0, 27.5, 19.8. ^1H NMR (300 MHz, 120 °C, DMSO) δ 7.82 (s, 2H), 6.53 (s, 1H), 4.25 (q, J = 8.2 Hz, 1H), 3.31−3.02 (m, 2H), 2.45 (s, 6H), 1.37−1.25 (m, 9H). IR 3250, 2980, 1716, 1639, 1510, 1341, 1160 cm^{-1}. MP 170−172 °C. $[\alpha]_D^{23}$ = −164.2 (c = 0.05, MeOH).

*(S)-3-(2-Amino-5,7-dimethylbenzo[d]thiazol-6-yl)-2-((tert-butoxycarbonyl)amino)propanoic Acid (**28**).* The crude was purified by flash chromatography (4:1 AcOEt/petroleum ether/1% acetic acid) and crystallized with 2:1 Et_2O/petroleum ether to afford the product **28** as a white soli, (0.082 g, 70% yield). t_r: 13.64 min. HRMS *m/z*: $[M - H]^-$ calcd for $C_{17}H_{22}N_3O_4S$ 364.1336, found 364.1339. ^1H NMR (400 MHz, CD_3OD) (mixture of rotamers) δ 7.08 (s, 1H), 4.35 (dd, J = 9.1, 6.0 Hz, 1H), 3.29−2.99 (m, 2H), 2.43 (s, 3H), 2.42 (s, 3H), 1.33 (s, 7H), 1.11 (s, 2H). $^{13}C\{^1H\}$ NMR (101 MHz, CD_3OD) (mixture of rotamers) δ 175.8, 169.4, 157.6, 149.6, 137.0, 130.9, 130.0, 129.6, 118.1, 80.4, 55.2, 33.3, 28.6, 28.1, 20.9, 19.6. IR 2927, 1692, 1513, 1158 cm^{-1}. MP 190−192 °C. $[\alpha]_D^{23}$ = −41.1 (c = 0.009, MeOH).

General Procedure for Fmoc Protection (21 and 22). The previously synthesized HCl salt was used as the crude. It was diluted in a water/dioxane (1:2) solution (0.2 M) and basified with an aqueous NaOH (2 N) solution until pH 10 or 11 was reachedat 0 °C. To the solution was added FmocCl (0.9 equiv), and the reaction mixture was left stirring at r.t. for 2 h. The reaction was monitored by ESI mass spectrometry and TLC until the complete consumption of starting material. The dioxane was then removed under vacuum, and

https://doi.org/10.1021/acs.joc.1c02527
J. Org. Chem. XXXX, XXX, XXX−XXX

an aqueous HCl (1 N) solution was added at 0 °C to pH 1. The mixture was extracted with ethyl acetate (three times), and the organic phases combined were dried over Na_2SO_4 and concentrated under vacuum. Each crude was purified by flash chromatography as reported below.

*(S)-2-((((9H-Fluoren-9-yl)methoxy)carbonyl)amino)-3-(4-fluoro-2,6-dimethylphenyl)propanoic Acid (**21**).* The crude was purified by flash chromatography (3:7 AcOEt/petroleum ether/1% acetic acid) and crystallized with 2:1 Et_2O/petroleum ether to afford **21** as a white solid (0.393 g, 75% yield). t_r: 23.33 min. HRMS *m/z:* $[M + H]^+$ calcd for $C_{26}H_{25}NO_4F$ 434.1762, found 434.1762. ^1H NMR (400 MHz, CD_3OD) δ 7.79 (d, J = 7.5 Hz, 2H), 7.60 (d, J = 4.2 Hz, 2H), 7.38 (t, J = 6.9 Hz, 2H), 7.30 (q, J = 6.9 Hz, 2H), 6.70 (d, J = 9.6 Hz, 2H), 4.42−4.36 (m, 1H), 4.26 (dd, J = 10.3, 6.9 Hz, 2H), 4.14 (t, J = 6.7 Hz, 1H), 3.28−2.90 (m, 2H), 2.35 (s, 6H). $^{13}C\{^1H\}$ NMR (101 MHz, CD_3OD) δ 175.3, 162.4 (d, J = 243 Hz), 158.3, 145.2, 142.5, 140.8, 131.5, 128.7, 128.1, 126.2, 120.9, 115.4 (d, J = 21 Hz), 67.9, 55.2, 46.9, 32.6, 20.5. IR 3313, 1716, 1696, 1533, 730 cm^{-1}. MP 197−199 °C. $[\alpha]_D^{22}$ = −3.32 (c = 0.006, MeOH).

*(S)-2-((((9H-Fluoren-9-yl)methoxy)carbonyl)amino)-3-(2,6-dimethylphenyl)propanoic Acid (**22**).* The crude was purified by flash chromatography (7:3 AcOEt/petroleum ether/1% acetic acid) and crystallized with 2:1 Et_2O/petroleum ether to afford the product **22** as a white solid (0.109 g, 80% yield). t_r: 23.30 min. HRMS *m/z:* $[M - H]^-$ calcd for $C_{26}H_{24}NO_4$ 414.1711, found 414.1715. $[2M - H]^-$ calcd for $C_{52}H_{49}N_2O_8$ 829.3494, found 829.3503. ^1H NMR (400 MHz, DMSO) δ 12.65 (s, 1H), 7.88 (d, J = 7.6 Hz, 2H), 7.83 (d, J = 8.8 Hz, 1H), 7.72−7.61 (m, 2H), 7.49−7.36 (m, 2H), 7.32 (td, J = 7.5, 1.2 Hz, 2H), 6.98−6.89 (m, 3H), 4.24−4.07 (m, 4H), 3.16−2.91 (m, 2H), 2.30 (s, 6H). $^{13}C\{^1H\}$ NMR (101 MHz, DMSO) δ 173.5, 155.9, 143.8, 140.7, 136.7, 134.9, 128.0, 127.6, 127.0, 126.1, 125.3, 120.1, 65.7, 53.9, 46.5, 31.3, 19.9. IR 3319, 2962, 1726, 1702, 1258, 1016, 794, 737 cm^{-1}. MP 153−155 °C. $[\alpha]_D^{23}$ = −284.7 (c = 0.04, MeOH).

Biology. *Calcium Mobilization Assay.* CHO cells stably coexpressing the human NOP and the C-terminal-modified $G\alpha_{qi5}$ protein were used for calcium mobilization experiments. Cells were generated and cultured as described previously.[28] Cells were maintained in a DEMEM/F-12 medium supplemented with 10% FBS, 100 U/ml penicillin, 100 μg/mL streptomycin, 100 μg/mL hygromicin B, and 200 μg/mL G418 and cultured at 37 °C in 5% CO_2 humidified air. Cells were seeded at a density of 50 000 cells per well into black clear-bottom 96-well plates. The following day, the cells were incubated with a medium supplemented with 2.5 mM probenecid, 3 μM Fluo-4 AM (a calcium-sensitive fluorescent dye), and 0.01% pluronic acid for 30 min at 37 °C. After that time, the loading solution was aspirated, and 100 μL/well HBSS supplemented with 20 mM HEPES, 2.5 mM probenecid, and 500 μM Brilliant Black (Sigma-Aldrich) was added to the wells. Concentrated solutions (1 mM) of N/OFQ(1−13)-NH_2 and analogues were made in bidistilled water and kept at −20 °C. Peptide serial dilutions were carried out in HBSS/HEPES (20 mM) buffer (containing 0.02% bovine serum albumin fraction V). After placing both plates (cell culture and master plate) into the fluorometric imaging plate reader of a FlexStation II system (Molecular Devices, Sunnyvale, CA), fluorescence changes were measured. Online additions of the peptides were carried out in a volume of 50 μL/well. To facilitate drug diffusion into the wells, the present study was performed at 37 °C. The maximum change in fluorescence, expressed as percent over the baseline fluorescence, was used to determine the agonist response. All data are expressed as the mean ± standard error of the mean (sem) of three experiments. Concentration−response curves to agonists were fitted to the classical four-parameter logistic nonlinear regression model as follows: effect = baseline + (E_{max} − baseline)/(1 + $10^{(\text{Log } EC_{50} - \text{Log[compound]}) \times \text{Hill slope}}$). Curves fitting were performed using PRISM 6.0 (GraphPad Software In., San Diego, CA).

■ ASSOCIATED CONTENT

Supporting Information

The Supporting Information is available free of charge at https://pubs.acs.org/doi/10.1021/acs.joc.1c02527.

Further experimental procedures and compound characterization (PDF)

■ AUTHOR INFORMATION

Corresponding Authors

Claudio Trapella − *Department of Chemical, Pharmaceutical and Agricultural Sciences, University of Ferrara, 44121 Ferrara, Italy;* orcid.org/0000-0002-6666-143X; Email: trpcld@unife.it

Giovanni Poli − *Faculté des Sciences et Ingénierie, CNRS, Institut Parisien de Chimie Moléculaire, IPCM, Sorbonne Université, 75005 Paris, France;* orcid.org/0000-0002-7356-1568; Email: giovanni.poli@sorbonne-universite.fr

Authors

Davide Illuminati − *Department of Chemical, Pharmaceutical and Agricultural Sciences, University of Ferrara, 44121 Ferrara, Italy; Faculté des Sciences et Ingénierie, CNRS, Institut Parisien de Chimie Moléculaire, IPCM, Sorbonne Université, 75005 Paris, France;* orcid.org/0000-0002-0321-1941

Anna Fantinati − *Department of Environmental and Prevention Sciences, University of Ferrara, 44121 Ferrara, Italy;* orcid.org/0000-0003-0437-5670

Tiziano De Ventura − *Department of Chemical, Pharmaceutical and Agricultural Sciences, University of Ferrara, 44121 Ferrara, Italy;* orcid.org/0000-0003-0534-9087

Daniela Perrone − *Department of Environmental and Prevention Sciences, University of Ferrara, 44121 Ferrara, Italy*

Chiara Sturaro − *Department of Neuroscience and Rehabilitation, Section of Pharmacology, University of Ferrara, Ferrara 44121, Italy*

Valentina Albanese − *Department of Chemical, Pharmaceutical and Agricultural Sciences, University of Ferrara, 44121 Ferrara, Italy;* orcid.org/0000-0002-1947-2644

Erika Marzola − *Department of Chemical, Pharmaceutical and Agricultural Sciences, University of Ferrara, 44121 Ferrara, Italy*

Virginia Cristofori − *Department of Chemical, Pharmaceutical and Agricultural Sciences, University of Ferrara, 44121 Ferrara, Italy;* orcid.org/0000-0002-6837-6042

Julie Oble − *Faculté des Sciences et Ingénierie, CNRS, Institut Parisien de Chimie Moléculaire, IPCM, Sorbonne Université, 75005 Paris, France*

Complete contact information is available at: https://pubs.acs.org/10.1021/acs.joc.1c02527

Author Contributions

‡These authors contributed equally: D.I. and A.F.

Notes

The authors declare no competing financial interest.

https://doi.org/10.1021/acs.joc.1c02527
J. Org. Chem. XXXX, XXX, XXX−XXX

■ ACKNOWLEDGMENTS

J.O. and G.P. would like to acknowledge CNRS and Sorbonne Université for financial support. Support through the Marie Skłodowska-Curie Innovative Training Network European Training Networks (ITN-ETN) C−H Activation for Industrial Renewal is also gratefully acknowledged. C.T. would like to thank FAR 2020 University of Ferrara (Fondo di Ateneo per la Ricerca 2020). The authors thank Dr. Alberto Casolari and Giorgia Macedonio for NMR analysis.

■ REFERENCES

(1) (a) Williams, D. A.; Roche, V. F.; Roche, E. B. Central Analgesics. In *Foye's Principles of Medicinal Chemistry*, 7th ed.; Lemke, T. L., Williams, D. A., Roche, V. F., Zito, S. W., Eds.; Wolters Kluwer Health Aids: 2013; pp 658−699. (b) Lipkowski, A. W.; Carr, D. B.; Bonney, I.; Kosson, P. Chapter 216 - Opioid-Substance P Chimeric Peptides In *Handbook of biologically active peptides*, 2nd ed., Vol. 7; Kastin, A. J., Ed.; Academic Press: San Diego, CA, 2013; pp 1586−1591. (c) Egleton, R. D.; Witt, K. A.; David, T. P. Chapter 232 - Opioid Peptides. In *Handbook of biologically active peptides*, 2nd ed., Vol. 7; Kastin, A. J., Ed.; Academic Press: San Diego, CA, 2013; pp 1696−1701. (d) Janecka, A.; Fichna, J.; Janecki, T. Opioid receptors and their ligands. *Curr. Top. Med. Chem.* **2004**, *4*, 1−17.

(2) Neumeyer, J. L.; Peng, X.; Knapp, B. I.; Bidlack, J. M.; Lazarus, L. H.; Salvadori, S.; Trapella, C.; Balboni, G. New opioid designed multiple ligand from Dmt-Tic and morphinan pharmacophores. *J. Med. Chem.* **2006**, *49*, 5640−5643.

(3) (a) Bryant, S. D.; Jinsmaa, Y.; Salvadori, S.; Okada, Y.; Lazarus, L. H. Dmt and opioid peptides: a potent alliance. *Biopolymers* **2003**, *71*, 86−102. (b) Balboni, G.; Marzola, E.; Sasaki, Y.; Ambo, A.; Marczak, E. D.; Lazarus, L. H.; Salvadori, S. Role of 2′,6′-dimethyl-L-tyrosine (Dmt) in some opioid lead compounds. *Bioorg. Med. Chem.* **2010**, *18*, 6024−6030. (c) Sasaki, Y.; Suto, T.; Ambo, A.; Ouchi, H.; Yamamoto, Y. Biological properties of opioid peptides replacing Tyr in position 1 by 2,6-Dimethyl-Tyr1. *Chem. Pharm. Bull.* **1999**, *47*, 1506−1509. (d) Sasaki, Y.; Ambo, A. 2′,6′-Dimethylphenylalanine: A Useful Aromatic Amino Acid Surrogate for Tyr or Phe Residue in Opioid Peptides. *Int. J. Med. Chem.* **2012**, *2012*, 498901.

(4) (a) Pacifico, S.; Carotenuto, A.; Brancaccio, D.; Novellino, E.; Marzola, E.; Ferrari, F.; Cerlesi, M. C.; Trapella, C.; Preti, D.; Salvadori, S.; Calò, G.; Guerrini, R. Structure- and conformation-activity studies of nociceptin/orphanin FQ receptor dimeric ligands. *Sci. Rep* **2017**, *7*, 45817. (b) Yamamoto, T.; Nair, P.; Largent-Milnes, T. M.; Jacobsen, N. E.; Davis, P.; Ma, S.; Yamamura, H. I.; Vanderah, T. W.; Porreca, F.; Lai, J.; Hruby, V. J. Discovery of a Potent and Efficacious Peptide Derivative for δ/μ Opioid Agonist/Neurokinin 1 Antagonist Activity with a 2′,6′-Dimethyl-L-Tyrosine, in vitro, in vivo and NMR-Based Structural studies. *J. Med. Chem.* **2011**, *54*, 2029−2038. (c) Capasso, A. Bioactivity of New Mu and Delta Opioid Peptides. *Med. Chem.* **2007**, *3*, 480−487.

(5) Bender, A. M.; Griggs, N. W.; Gao, C.; Trask, T. J.; Traynor, J. R.; Mosberg, H. I. Rapid Synthesis of Boc-2′,6′-dimethyl-L-tyrosine and Derivatives and Incorporation into Opioid Peptidomimetics. *ACS Med. Chem. Lett.* **2015**, *6*, 1199−1203.

(6) For a selection, see: (a) He, K.; Zhu, F.; Li, H.; Tang, J.; Zhang, X. An Efficient and Highly Asymmetric Synthesis of (*S*)-2′,6′-Dimethyltyrosine. *Org. Prep. Proced. Int.* **2020**, *52*, 510−516. (b) Tang, X.; Soloshonok, V. A.; Hruby, V. J. Convenient asymmetric synthesis of enantiomerically pure 2′,6′-dimethyltyrosine (DMT) via alkylation of chiral equivalent of nucleophilic glycine. *Tetrahedron: Asymmetry* **2000**, *11*, 2917−2925. (c) Balducci, D.; Contaldi, S.; Lazzari, I.; Porzi, G. A highly efficient stereocontrolled synthesis of (S)-2′,6′-dimethyltyrosine [(S)-DMT]. *Tetrahedron: Asymmetry* **2009**, *20*, 1398−1401.

(7) (a) Imamoto, T.; Tamura, K.; Zhang, Z.; Horiuchi, Y.; Sugiya, M.; Yoshida, K.; Yanagisawa, A.; Gridnev, I. D. Rigid P-Chiral Phosphine Ligands with tert-Butylmethylphosphino Groups for Rhodium-Catalyzed Asymmetric Hydrogenation of Functionalized Alkenes. *J. Am. Chem. Soc.* **2012**, *134*, 1754−1769. (b) Praquin, C. F. B.; de Koning, P. D.; Peach, P. J.; Howard, R. M.; Spencer, S. L. Development of an Asymmetric Hydrogenation Route to (S)-N-Boc-2,6-dimethyltyrosine. *Org. Process Res. Dev.* **2011**, *15*, 1124−1129.

(8) Wang, X.; Niu, S.; Xu, L.; Zhang, C.; Meng, L.; Zhang, X.; Ma, D. Pd-Catalyzed dimethylation of Tyrosine-derived Picolinamide for synthesis of (S)-N-Boc-2,6-dimethyltyrosine and its analogues. *Org. Lett.* **2017**, *19*, 246−249.

(9) Tremont, S. J.; Rahman, H. U. Ortho-Alkylation of acetanilides using alkyl halides and palladium acetate. *J. Am. Chem. Soc.* **1984**, *106*, 5759−5760.

(10) (a) Zaitsev, V. G.; Shabashov, D.; Daugulis, O. Highly Regioselective Arylation of sp^3 C−H Bonds Catalyzed by Palladium Acetate. *J. Am. Chem. Soc.* **2005**, *127*, 13154−13155. (b) Nadres, E. T.; Santos, G. I. F.; Shabashov, D.; Daugulis, O. Scope and Limitations of Auxiliary-Assisted, Palladium-Catalyzed Arylation and Alkylation of sp^2 and sp^3 C−H Bonds. *J. Org. Chem.* **2013**, *78*, 9689−9714.

(11) For an excellent review, see: Sambiagio, C.; Schönbauer, D.; Blieck, R.; Dao-Huy, T.; Pototschnig, G.; Schaaf, P.; Wiesinger, T.; Zia, M. F.; Wencel-Delord, J.; Besset, T.; Maes, B. U. W.; Schnürch, M. A comprehensive overview of directing groups applied in metal-catalysed C−H functionalisation chemistry. *Chem. Soc. Rev.* **2018**, *47*, 6603−6743.

(12) Zhao, Y.; Chen, G. Palladium-Catalyzed Alkylation of *ortho*-C(sp^2)−H Bonds of Benzylamide Substrates with Alkyl Halides. *Org. Lett.* **2011**, *13*, 4850−4853.

(13) (a) Brandhofer, T.; García Mancheño, O. Site-Selective C−H Bond Activation/Functionalization of Alpha-Amino Acids and Peptide-Like Derivatives. *Eur. J. Org. Chem.* **2018**, *2018*, 6050−6067. (b) Yun, Y.-l.; Yang, J.; Miao, Y.-h.; Sun, J.; Wang, X.-j. Recent advances in Palladium(II)-catalyzedactivation of aromatic ring C−H bonds. *J. Saudi Chem. Soc.* **2020**, *24*, 151−185.

(14) (a) Gensch, T.; Hopkinson, M. N.; Glorius, F.; Wencel-Delord. Mild metal-catalyzed C−H activation: examples and concepts. *J. Chem. Soc. Rev.* **2016**, *45*, 2900−2936. (b) Roudesly, F.; Oble, J.; Poli, G. Metal-catalyzed CH activation/functionalization: The fundamentals. *J. Mol. Catal. A* **2017**, *426*, 275−296.

(15) (a) Swain, C. G.; Rogers, R. J. Mechanism of formation of aryl fluorides from arenediazonium fluoborates. *J. Am. Chem. Soc.* **1975**, *97*, 799−800. (b) Yu, Z.-Q.; Lv, Y.-W.; Yu, C.-M.; Su, W.-K. Continuous flow reactor for Balz−Schiemann reaction: a new procedure for the preparation of aromatic fluorides. *Tetrahedron Lett.* **2013**, *54*, 1261−1263.

(16) Wassmundt, F. W.; Kiesman, W. F. Efficient Catalysis of Hydrodediazoniations in Dimethylformamide. *J. Org. Chem.* **1995**, *60*, 1713−1719.

(17) Xu, W.-B.; Xu, Q.-H.; Zhang, Z.-F.; Li, J.-Z. Copper(I)-Oxide-Mediated Cyanation of Arenediazonium Tetrafluoroborates with Trimethylsilyl Cyanide: A Method for Synthesizing Aromatic Nitriles. *Asian J. Org. Chem.* **2014**, *3*, 1062−1065.

(18) Voutyritsa, E.; Theodorou, A.; Kokotou, M. G.; Kokotos, C. G. Organocatalytic oxidation of substituted anilines to azoxybenzenes and nitro compounds: mechanistic studies excluding the involvement of a dioxirane intermediate. *Green Chem.* **2017**, *19*, 1291−1298.

(19) (a) Maggiolo, A. The Reaction of Thiocyanogen with Nitrogen Heterocycles; Pyridines, Pyrimidines and Quinolines. *J. Am. Chem. Soc.* **1951**, *73*, 5815−5816. (b) Zhang, A.; van Vliet, S.; Neumeyer, J. L. Synthesis of aminothiazole derived morphinans. *Tetrahedron Lett.* **2003**, *44*, 6459−6462. (c) Ballet, S.; Salvadori, S.; Trapella, C.; Bryant, S. D.; Jinsmaa, Y.; Lazarus, L. H.; Negri, L.; Giannini, E.; Lattanzi, R.; Tourwé, D.; Balboni, G. New 2′,6′-dimethyl-L-tyrosine (Dmt) opioid peptidomimetics based on the Aba-Gly scaffold. Development of unique μ-opioid receptor ligands. *J. Med. Chem.* **2006**, *49*, 3990−3993.

(20) Guerrini, R.; Calo', G.; Rizzi, A.; Bianchi, C.; Lazarus, L. H.; Salvadori, S.; Temussi, P. A.; Regoli, D. Address and Message Sequences for the Nocicpetin Receptor: A Structure-Activity Study of

https://doi.org/10.1021/acs.joc.1c02527
J. Org. Chem. XXXX, XXX, XXX−XXX

945 Nocicpetin-(1−13)-peptide amide. *J. Med. Chem.* **1997**, *40* (12),
946 1789−1793.
947 (21) Marastoni, M.; Trapella, C.; Scotti, A.; Fantinati, A.; Ferretti,
948 V.; Marzola, E.; Eleonora, G.; Gavioli, R.; Preti, D. Naphtoquinone
949 amino acid derivatives, synthesis and biological activity as proteasome
950 inhibitors. *J. Enzyme Inhib. Med. Chem.* **2017**, *32*, 865−877.
951 (22) The pharmacological assay was performed by the research
952 group directed by Prof. G. Calò at the Department of Medical
953 Sciences of the University of Ferrara.
954 (23) Camarda, V.; Calo, G. Chimeric G Proteins in Fluorimetric
955 Calcium Assays: Experience with Opioid Receptors. *Calcium Signaling*
956 *Protocols.* **2013**, *937*, 293−306.
957 (24) Camarda, V.; Fischetti, C.; Anzellotti, N.; Molinari, P.;
958 Ambrosio, C.; Kostenis, E.; Regoli, D.; Trapella, C.; Guerrini, R.;
959 Severo, S.; Calò, G. Pharmacological profile of NOP receptors
960 coupled with calcium signaling via the chimeric protein $G\alpha_{qi5}$.
961 *Naunyn-Schmied Arch. Pharmacol* **2009**, *379*, 599−607.
962 (25) Similar results were obtained with the [(pF)Phe4]N/OFQ(1−
963 13)-NH_2 analogue (with commercial reagent CAS no. 169243-86-1).
964 [dmpFPhe4]N/OFQ(1−13)-NH_2 (with compound **21**) and
965 [dmPhe4]N/OFQ(1−13)-NH_2 (with compound **22**) displayed
966 similar potencies but lower efficacies (pEC50 = 8.86 (8.65−9.06)
967 and 7.85 (7.63−8.07), respectively) compared to N/OFQ(1−13)-
968 NH_2. Data are the mean ± sem of three separate experiments
969 performed in duplicate.
970 (26) Additional studies to asses if we could obtain the *o*,*o*-
971 dimethylated aniline derivative **10** not only from 4-nitro-L-phenyl-
972 alanine **3** but also from the less expensive L-tyrosine were also
973 undertaken. In particular, we envisioned that a Buchwald−Hartwig
974 (BH) aromatic amination strategy from an appropriate tyrosine
975 derivative might have enabled a second way to access **10**. However,
976 the BH couplings between *N*,*N*-dibenzylamine and *O*-triflyl L-tyrosine
977 methyl ester PA (*o*,*o*-dimethylated at the aromatic ring or not) met
978 with failure, very likely due to an incompatibility between the BH
979 coupling and the PA group.
980 (27) (a) Guerrini, R.; Calo, G.; Bigoni, R.; Rizzi, D.; Rizzi, A.;
981 Zucchini, M.; Varani, K.; Hashiba, E.; Lambert, D. G.; Toth, G.;
982 Borea, P. A.; Salvadori, S.; Regoli, D. Structure-Activity Studies of the
983 Phe^4 Residue of Nociceptin(1−13)-NH_2: Identification of Highly
984 Potent Agonists of the Nociceptin/Orphanin FQ Receptor. *J. Med.*
985 *Chem.* **2001**, *44*, 3956−3964. (b) Balboni, G.; Salvadori, S.; Guerrini,
986 R.; Negri, L.; Giannini, E.; Jinsmaa, Y.; Bryant, S. D.; Lazarus, L. H.
987 Potent δ-Opioid Receptor Agonists Containing the Dmt-Tic
988 Pharmacophore. *J. Med. Chem.* **2002**, *45*, 5556−5563. (c) Sasaki,
989 Y.; Sasaki, A.; Ariizumi, T.; Igari, Y.; Sato, K.; Kohara, H.; Niizuma,
990 H.; Ambo, A. 2′,6′-Dimethylphenylalanine (Dmp) can mimic the N-
991 terminal Tyr in opioid peptides. *Biol. Pharm. Bull.* **2004**, *27*, 244−247.

https://doi.org/10.1021/acs.joc.1c02527
J. Org. Chem. XXXX, XXX, XXX−XXX